Author:
McConnell, Brian James

Title:
Factors controlling sandstone strength and deformability in uniaxial compression.

FACTORS CONTROLLING SANDSTONE STRENGTH AND DEFORMABILITY IN UNIAXIAL COMPRESSION

by

Brian James McConnell

A thesis submitted to the University of Bristol in accordance with the requirements for the degree of Doctor of Philosophy in the Faculty of Science, Department of Geology.

June 1989

ABSTRACT

Sandstones constitute approximately one quarter of the surface bedrock of the British Isles and hence they form a major founding strata for civil engineering structures. Thirty-seven varieties of sandstones, collected from many parts of the British Isles, and ranging in age from Precambrian to Cretaceous, provide samples with all significant lithological variations for inclusion in the testing programme.

Strength and deformability of the sandstone samples under uniaxial compression have been examined. A computer-based monitoring system has been developed for recording stress and strain during testing. Measured values of dry strength varied from 7MPa for the Greensand to 298MPa for the Crackington Sandstone. Strong relationships were observed between uniaxial compressive strength and various static properties of the sandstones, particularly dry bulk density. This good correlation may allow the use of dry bulk density as an index for the rapid estimation of sandstone strength.

In the presence of moisture, the strength of the sandstones decreases by up to 78%, the highest recorded reduction occurring in the Greensand. With the exception of the weakest varieties, the most pronounced loss occurs at low moisture contents, generally below 1%. In sandstones, two dominant processes are active in moisture content related strength reduction, namely clay softening and fracture energy reduction. The relative importance of these two processes varies depending on the mineralogy of the sandstone; fracture energy reduction is significant in mature sandstones but is less important in the argillaceous varieties.

Three principal modes of failure have been observed. Sandstones which fail at stresses greater than 180MPa consistently display axial cleavage, while those weaker than 37MPa fail in cataclasis. Shear failure is an intermediate mode which tends to occur in conjunction with the two end members. SEM examination of pre- and post-failure samples has revealed variations of fracture morphology between different sandstone types. The style of microfracture initiation and propagation is an important control on macroscopic failure mode.

The majority of sandstones deform non-elastically. In the strongest varieties where porosity is low, there is little difference between the Young's modulus measured in Stages I and II of the stress-strain curve. The weakest sandstones show relatively straight stress-strain curves due to their cataclastic mode of deformation.

A system was developed to measure radial strain during sandstone deformation in uniaxial compression. This apparatus is considered to give a more representative value of radial strain as better surface contact with the specimen is achieved. In general the measured Poisson's ratio was less than 0.4. The Ashdown Sandstone was anomalous, having a ratio of 0.9. Examination of the sedimentological characteristics indicated that this sandstone behaved in a manner similar to a locked sand.

A microfabric analysis and regression model have indicated that the main observed variation within uniaxial compressive strength of sandstones is related to porosity, 2-dimensional packing density and the degree of cementation, as expressed by the cement index.

DECLARATION

The material presented in this thesis is the result of my own independent research carried out in the Department of Geology, University of Bristol, under the supervision of Dr. A.B. Hawkins. Any previously published or unpublished work used is given full acknowledgement.

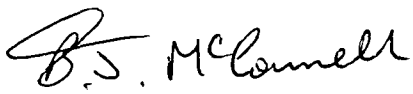

Brian J. McConnell
June 1989

ACKNOWLEDGEMENTS

I would like to thank Dr. Brian Hawkins for his supervision and encouragement throughout the research period and in particular for his invaluable assistance during the latter stages.

Professor D.L. Dineley is acknowledged for the provision of facilities and equipment within the Geology Department.

The assistance of the technical support staff in the Department of Geology is fully acknowledged, particularly Mike Overs, Ian Avent, Gary Webber, Tony Kemp, Simon Powell, Richard Lewis and Stuart Waterman. Andrew Hook and Derek Telling are also thanked for their help with the high speed photography.

The Department of Education for Northern Ireland is acknowledged for the postgraduate award over the last three years which allowed me to carry out the research, especially Mrs. Brown who was most helpful with travel and expenses claims.

The encouragement and friendship of my fellow postgraduates at Bristol has helped to make the past few years both rewarding and enjoyable and it is important that they are each mentioned here: Simon Todd, Iain Stewart, Duncan Wade, Jon Redfern, Greg Pinches, Stuart Wilson, Chris McDonald, Dave Lloyd, Steve Hawkins, Craig Brown, Robbie Narbett and Rod Sloan. In particular I would like to thank Simon, Iain, Rod, Craig and Robbie for their invaluable editing during the final throws of writing up.

The majority of the samples were collected from small isolated working quarries and I feel indebted to the quarry owners who not only provided me with large samples free of charge but who also took a keen interest in my research.

Of the people at home in Northern Ireland I would like to thank my mother Mrs. R.E. McConnell and my brother John for their financial and moral support throughout the past three years.

Mr. Tony Lee of Coleraine Inst. is someone to whom I owe a great deal since it was he who gave me the initial interest and enthusiasm for the subject of geology.

Finally, I would like to thank Jayne Lloyd without whose help and encouragement I would not have finished this thesis.

TABLE OF CONTENTS

LIST OF FIGURES

LIST OF PLATES

LIST OF TABLES

CHAPTER 1

INTRODUCTION

1.1 Definition of Sandstones

The term sandstone is defined geologically as a detrital sedimentary rock whose component particles fall between the grain size diameter limits of 0.0625 and 2.0mm. This definition, although restricting the rock to the stated limits, actually encompasses a huge range in grain sizes. The definition gives sand a 32-fold range in diameter. Volume however, which must be the truest measure of size, when calculated from the upper and lower limits has a range of almost 35000-fold.

A number of variations on the grain size limits have been proposed by various authorities; these are summarised in Fig. 1.1. The commonly used limits of 0.0625 and 2.0mm allow the sandstones to be divided into five units at one phi intervals on the Wentworth scale as proposed in 1933 - from very fine sand to very coarse sand as shown in Fig. 1.2.

The logarithmic scale of the phi system accounts for the fact that grain size changes at the lower end of the scale are much more significant than the same change at larger grain sizes. The recommendation of BS 5930 as shown in the figure are limits of 0.06 and 2.0 mm. The grain size range is divided into three groups, again on a logarithmic scale -

Sub-division	Range	Class Size
coarse sand	0.6 - 2.0 mm	1.4mm
medium sand	0.2 - 0.6 mm	0.4mm
fine sand	0.06 - 0.2 mm	0.14mm

The alteration from Wentworth's lower limit is merely to remove the decimal places considered unnecessary for the identification and analysis of sands. It is considered that three divisions are sufficient for normal engineering appreciation, especially when working in the field, but greater precision is desirable when studying materials under modern research conditions.

It is important to decide whether the average, median or modal sizes of the material designated 'sand' fall within the sand fraction or what proportion of over- or

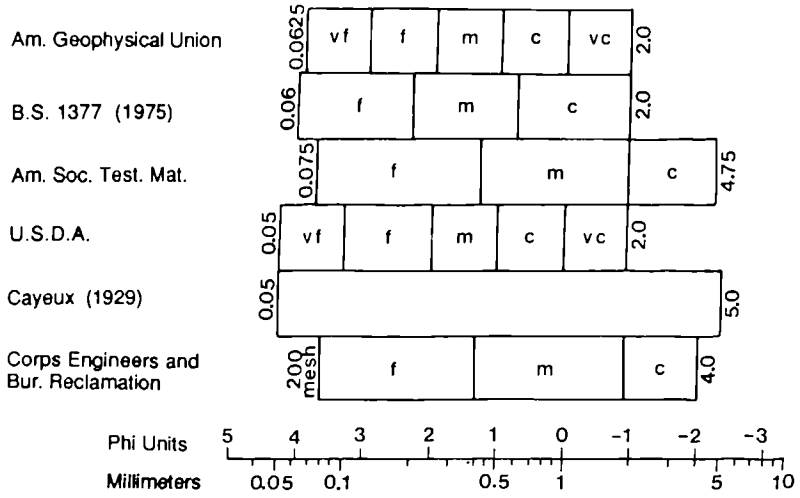

Figure 1.1 Various definitions of the grain size boundaries for sands.

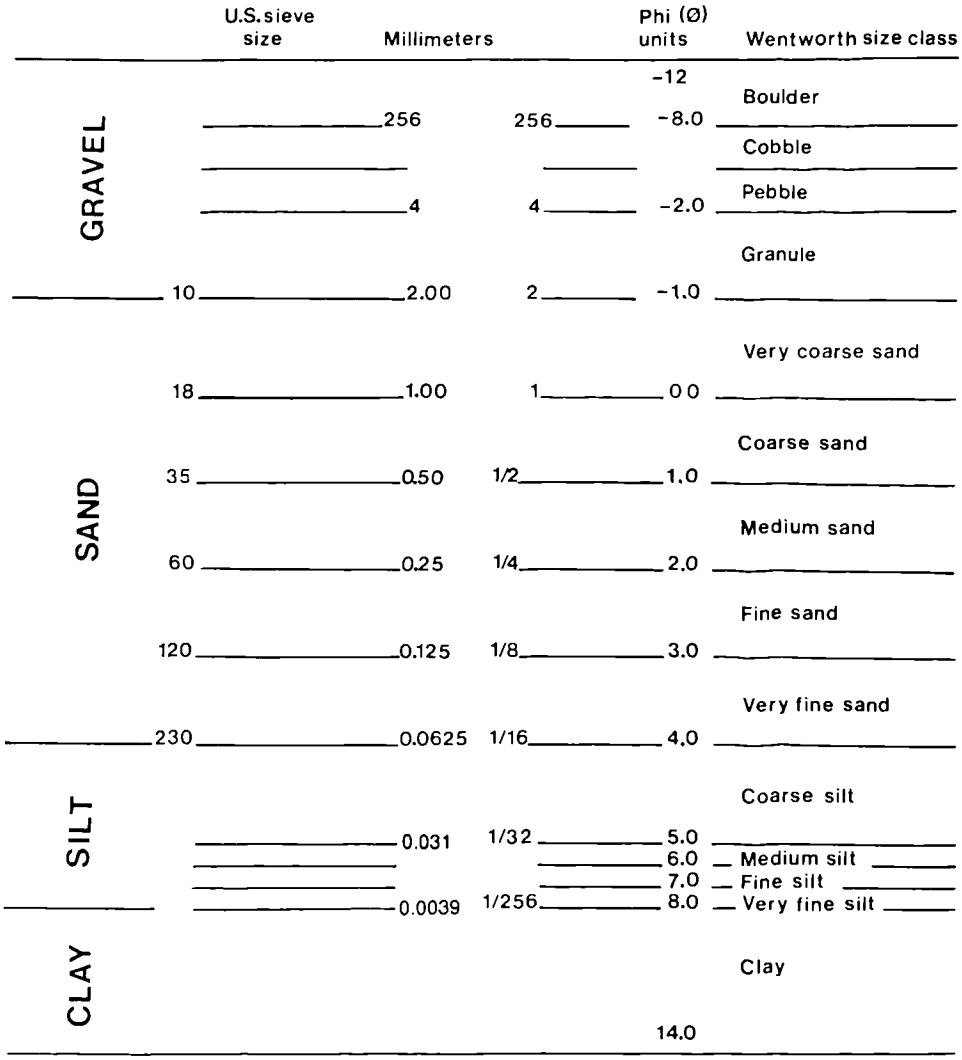

Figure 1.2 The Wentworth grade scale for size classification of sediments.

under-sized grains can be included within a sand/sandstone material. In order to attain descriptive precision, end member triangles have been used. Unfortunately their value is diminished by a lack of agreement as to which is the most suitable, so that one scheme may differ considerably from another. Figure 1.3 illustrates a number of schemes. These triangles allow qualifying terms to be used such as silty SAND or clayey SAND. This terminology is not normally used for sandstones, but the end member triangle principle can be applied to determine whether a particular rock is a sandstone or otherwise as determined from a grain size analysis.

The BS 5930: 1981 recommendation for the description of unconsolidated sediments differs markedly from the value of 50%, normally used by geologists. A 65% limit is recommended as the minimum amount of coarse material (i.e. greater than 0.06 mm) required for a sediment to be termed a sand. This recommendation is based on the fact that relatively low percentages of fines i.e. clays and silt will give the soil cohesive properties while relatively high proportions of sands and gravels are needed to create a non-cohesive granular material. The boundaries are taken at 35 % and 65 % respectively.

Bagnold, (1941) places the lower limit of sand as that at which the terminal velocity is less than the upward eddy currents and the upper limit as the size at which a grain resting on the surface ceases to be moveable either by direct pressure of the fluid or by the impact of the moving grains. The size limits thus defined agree approximately with those set by Wentworth.

Definitions of sandstones as deposits are diverse and no generally accepted usage is apparent from a review of the literature. Indeed very few actually infer anything about the composition or genesis of the sediment. Generally further terms such as desert sand or turbidite sandstone are used to imply more information on composition or origin.

Definitions of sandstones as used by rock mechanicians are generally similar to that given by Jumikis, (1983). "Sandstone is a consolidated, porous and pervious rock composed mainly of sand particles - quartz grains - cemented together by clayey, siliceous, calcareous or limonitic material which fills the spaces between the grains." He goes on to describe the variations in strength and dynamic properties produced by variations in cement type.

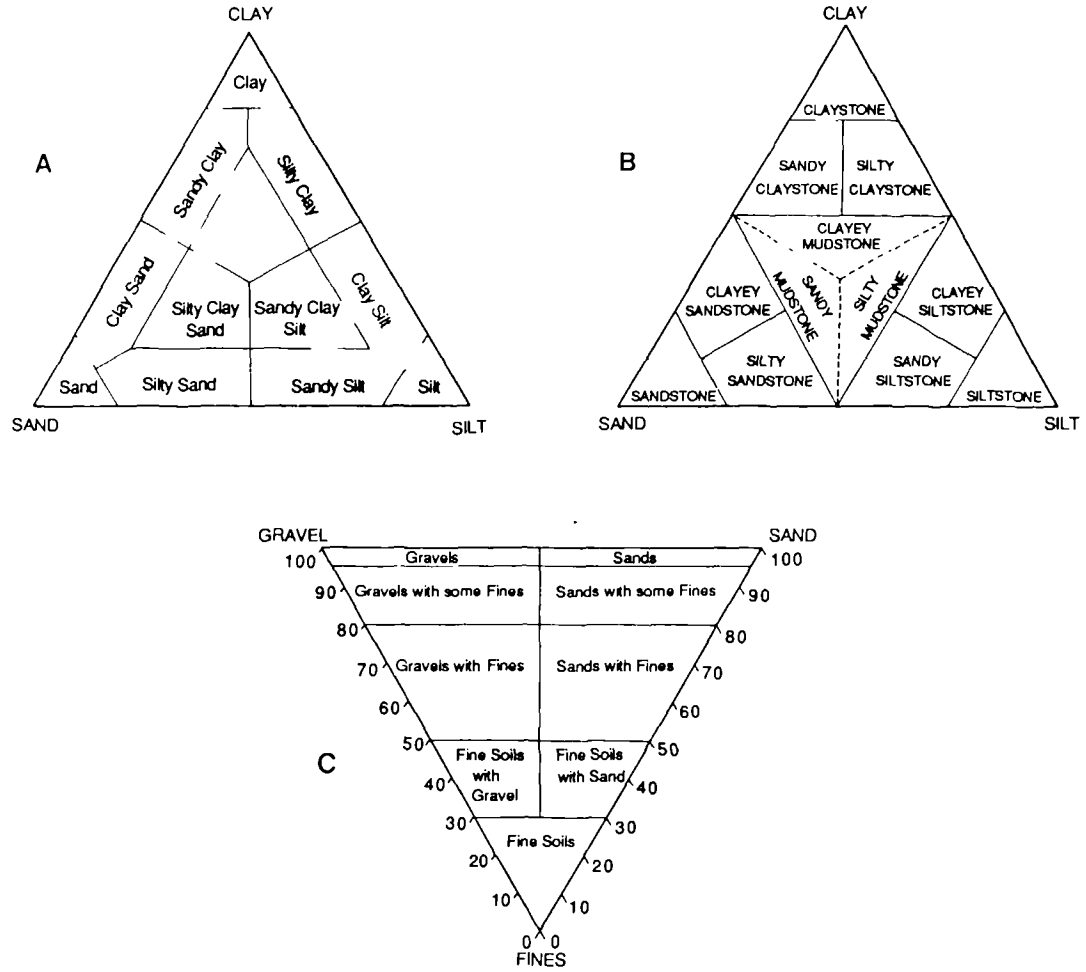

Figure 1.3 Various ternary systems for classification of mixed clastic sediments and rocks.
A. After Shepard, (1954).
B. After Picard, (1971).
C. After Dumbleton, (1968).

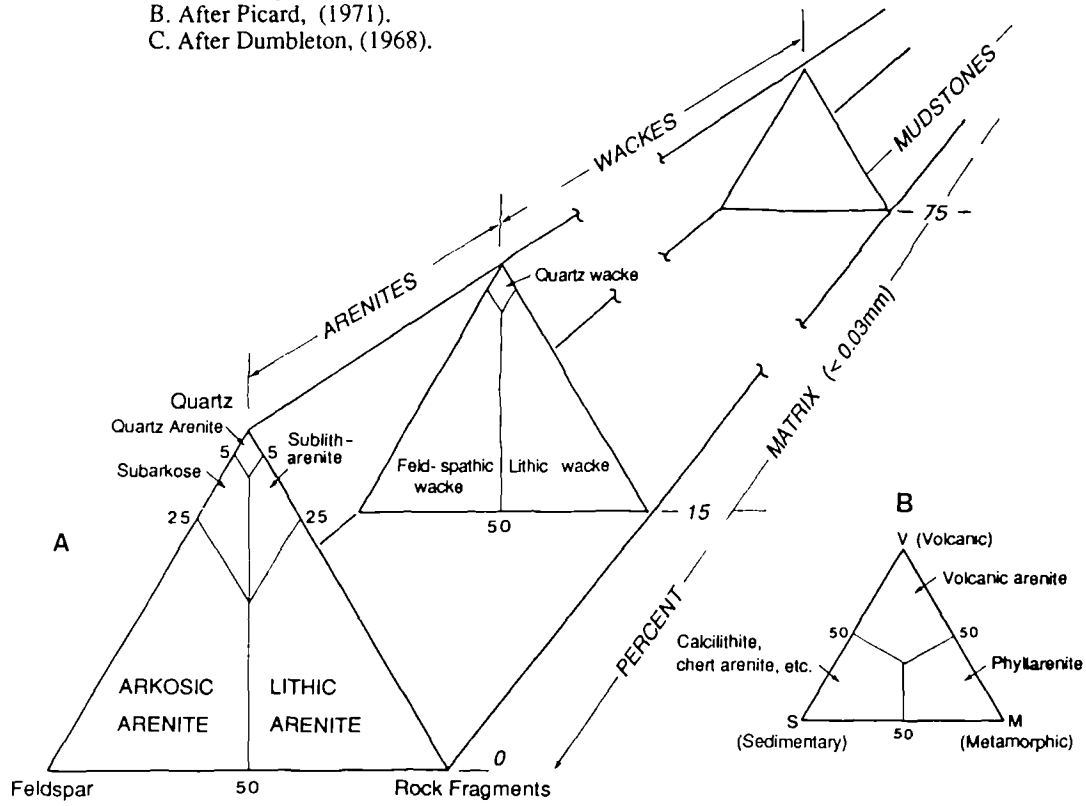

Figure 1.4 A: Classification of terrugineous sandstones, (modified from Dott, 1964)
B: subdivision of lithic arenites, (after Folk, 1968).

1.2 The Sand - Sandstone Boundary

The delineation of the sand/sandstone boundary is of fundamental importance to the rock mechanician or engineering geologist since an unconsolidated, unindurated sand will behave in a drastically different way from a cemented sandstone.

It is generally accepted by traditional soil mechanicians that the limit for distinguishing sand soil from rock is that the soils, which consist of loose non-particles, disintegrate when immersed in water and subjected to agitation.

Rocha (1975) pointed out that the cohesion of soil when present, is deliquescent and that the cohesion of rocks is not destroyed in the presence of water. This is not strictly true for rocks since loss of cohesion does occur on saturation of sandstones but it is not sufficient to cause their total disintegration as suffered by sands.

Dobereiner (1984), used a slightly more specific approach for determining the lower strength limit for sandstones. He defined it as the material that does not disintegrate when saturated by water under vacuum. For weak sandstones this lies at approximately 0.5 MPa of uniaxial compressive strength. He argued that agitation was not necessary and that full saturation gives more reliable results.

The effects of vacuum on the weak sandstones was not considered by Dobereiner; indeed it may be the case that the negative pressure treatment created by the vacuum, caused the disintegration of some samples.

The literature fails to give a clear distinction between sand and sandstone. The recommendation of the Working Party Report, (Anon 1972) is that any sample with a uniaxial compressive strength significantly less than 1.25 MPa should be described and tested as a soil. Clearly it is not easy in a non-cohesive material to have a precise figure since so much will depend on the significance of the contained matrix.

The position of the boundary between sands and sandstones is complicated by what have been termed 'locked sands'. The term was introduced in 1979 by Dusseault and Morgenstern to differentiate some geological materials from dense sands and sandstones. Compaction and the subsequent formation of quartz overgrowths has resulted in these deposits having a locked but uncemented character. The overgrowths are not enough to weld the rock together but sufficient to cause the grains to interlock, resulting in higher strengths than normal dense sands. Dusseault and Morgenstern reported unconfined compressive strengths of greater than 1.0 MPa in many cases.

1.3 Classification of Sandstones

In any classification it is essential to create classes into which sample varieties will fall. This requires the definition of appropriate parameters. An example of a simple 3-fold classification for sandstones is one which divides sandstones into terrigenous, carbonate and pyroclastic varieties. This three-fold classification, although simple and fitting readily into our ordinary geological thinking, is not internally consistent since it is based on a variety of concepts: terrigenous sands are those classified by their source, carbonate sands by their composition and pyroclastic sands by their agent of formation, volcanism.

For the sedimentologist, the ultimate question is one of origin and therefore the defining parameters should be as genetically significant as possible. A simple inventory of the mineral species present in a sandstone contributes little - what is really required is that they be arranged in meaningful genetic groups. A reservoir geologist on the other hand wishes to discriminate between the original detrital components, the minerals introduced as cements and those resulting from post depositional diagenesis or weathering. A classification suitable for engineering geologists would not rely so heavily on genetic controls but on parameters which directly affected the geomechanical properties. This will be discussed in a later chapter.

Numerous sedimentological classifications have been proposed for sandstones using various parameters and limits. The most commonly used system is a modified version of that proposed by Dott (1964) and later modified by Folk, (1968). (Fig 1.4).

The modified Dott classification is a dual one based upon both modal composition of grains and texture. It is relatively simple and is considered to be appropriate to both modern sands and ancient sandstones. Compositions of sandstone cements are therefore not relevant in this approach but clearly may be described by an adjectival prefix, e.g. calcareous sandstone for calcite-cemented sandstone. Composition is described on a triangular graph by the three main components: quartz, feldspar and rock fragments, (Dott 1964, Pettijohn et al. 1972). Arenites are the major clan of sandstones having less than 15 % fine-grained matrix material. Arkosic, lithic and quartz arenites are rich in feldspar, rock fragments and quartz respectively. Quartz arenites (synonymous with ortho-quartzites) are the most mature sandstone group and are frequently multicyclic deposits. It is possible to subdivide lithic arenites further, depending on the compositions of the rock fragments involved.

The second major clan of sandstones are the wackes, which have greater than 15 % matrix. Greywacke is an outdated general term used to describe wackes as a whole. Wackes are divided into feldspar, lithic and quartz types, which are, respectively, rich in feldspar, rock fragments and quartz. Further subdivision of the

lithic wackes is possible depending on the composition of the rock fragments involved. With increasing content of fine-grained matrix the wackes grade into sandy mudrocks(> 50 % matrix) and hence into mudrocks (>75 % matrix).

As the classification is based in part on the percentage matrix present, it is important to consider the grain size limits of the matrix. Some authors would restrict the term to clay-sized particles, i.e. <4μm, (Wentworth scale), (B.S.5930: <2μm). Others set the upper size limit to matrix higher, mostly around 20-30μm, i.e. in the silt range. The latter size range is probably better, since the mean grain size of mudrocks is about medium silt on the Wentworth scale, and the modified Dott's classification allows for intergradation between wackes and mudrocks.

Very little work has been carried out on classifying sandstones from a rock mechanics viewpoint. A number of rock classification systems have been developed for engineering purposes but these cover all rock types and in many cases lithological type is not considered. For example the "Rock Mass Rating (RMR) system, (Geomechanics Classification)" proposed by Bieniawski in 1979, does not require the rock type to be identified, it being based on the following parameters:

1. uniaxial compressive strength of rock material
2. rock quality designation, RQD
3. spacing of discontinuities
4. condition of discontinuities
5. groundwater conditions
6. orientations of discontinuities

Whilst these properties may be the controlling factors, the fact that sandstone rock masses can show great internal variability is not considered in such a rock mass classification. Other classification systems such as the Rock Structure Rating (RSR) model of Skinner (1988) do take rock type into consideration but only to the extent of whether it is sedimentary, igneous or metamorphic.

The only attempts at geotechnical classification of sandstones has been that by Dobereiner, (1984), but this is restricted to weak sandstones, (i.e. less than 20 MPa as defined by ISRM: 1981).

Considering a rock mechanics classification for sandstones in the context of the three prerequisites proposed by Pincus, (1988), it is understandable why a comprehensive system does not exist.

1.4 Occurrence and abundance of sandstones in Great Britain and their importance in engineering.

Various worldwide estimates for the abundance of sandstones relative to the other common sedimentary rocks have been presented by workers such as Kuenen (1941) and Poldervaart (1955).These estimates give averages of 28% sandstone in the continental shield areas and 36% in the sediments of the mobile belts and shelf. The weighted average has been calculated as 34 %.

Figure 1.5 shows the outcrop of the main British and Irish sedimentary sequences which contain abundant sandstones. Since the shaded areas do not consist completely of sandstones, an estimate of 25% sandstone outcrop is proposed. This value is predominantly made up of the main arenaceous units:

Cretaceous - Greensands
Jurassic - Lr Jurassic Sands
Permo-Triass - New Red Sandstone
Carboniferous- Millstone Grit and Coal Measures
Siluro-Devonian - Old Red Sandstone
Precambrian - Torridonian

1.4.1 Scotland

The oldest arenaceous deposits in Scotland and indeed in Great Britain are late Proterozoic in age. These unmetamorphosed sediments are considered to be the equivalent of the Scottish Moinian metamorphics and are termed the Torridonian. Torridonian rocks are found along the western coast of Scotland where they form many of the prominent mountains and also on several Hebridean islands such as Rhum, Skye and Rona.

The most significant sequence of sandstones in Scotland are the Old Red Sandstone deposits, cropping out extensively in the Midland Valley graben and in the Scottish Border area to the south. The sequence attains a maximum thickness in the region of 10 km of continental red beds. Old Red Sandstone sediments also outcrop extensively in the north-east of Scotland around The Moray Firth, at Caithness and in The Shetlands where a thickness of up to 10 km is estimated to be present.

The base of the Carboniferous in Scotland is marked by a conformable upward change from fluviatile red beds of Old Red Sandstone type to the early Dinantian

Figure 1.5 Outcrop of the main British and Irish sedimentary sequences containing significant proportions of sandstone.

Cementstone Group in the western outcrops of the Midland Valley. The Cementstone Group consists of sandstones with some limestones, calcareous mudstones and dolomitic limestones. Major sequences of Carboniferous sandstones of the Millstone Grit (Namurian) and Coal Measures (Westphalian) dominate the geology of the southern Midland Valley. Large outcrops occur in the area to the east of Glasgow, to the north of the Firth of Forth and in the Edinburgh area. These outcrops are coal bearing and constitute the central Scottish Coalfield.

Permian and Triassic sandstones occur as isolated and largely unfossiliferous outcrops generally along the western side of Scotland but also in the north-east at Elgin and Goldspie, (Craig 1965). These outcrops have been equated with a number of depositional Permo-Triassic basins.

1.4.2 England and Wales

Whilst sandstones occur in the Proterozoic and lower Palaeozoic strata such as the lower Cambrian of the Harlech Dome, these are of limited outcrop.

Extensive Old Red Sandstone outcrops occur in the Welsh Borders and in southern and central Ireland forming the Anglo Welsh - Irish Basin. A virtually complete succession of marine Devonian is present in the south-west of England with intercalations of Old Red Sandstone.

The passage between the Devonian and Carboniferous is conformable and transitional in SW England and considered to take place within the Pilton Beds where no obvious facies break occurs. In northern Britain, a marked unconformity occurs, with the lower beds of the Carboniferous frequently absent. The Carboniferous period includes extensive marine and terrestrial sandstone deposits. The Namurian (Millstone Grit) deposits form a deltaic sequence of over 2000m of clastics in the south Pennines while the coarse sandstones of the Millstone Grit in the central Pennines Basin have been attributed to braided fluvial systems.

The Westphalian deposits which include the main coal-bearing strata of the British Isles, generally rest conformably on the Namurian. Thick sequences of coal-bearing sandstones and mudstones were deposited, as summarized below:

Midland Valley of Scotland	1060m
Lancashire - N.Staffordshire	3050m
S.Wales	2440m
Kent	760m

The main sandstone horizons in the Coal Measures are referred to as the Pennant Series in the South Wales and Bristol coalfields.

A large sequence of upper Carboniferous rocks previously called 'The Culm Measures' outcrops in the Culm Basin of SW England. Thick sandstone sequences occur, interbedded with mudstones and shales comprising the Crackington, Bideford and Bude Formations. These deposits are considered to be turbiditic in the case of the Crackington Formation, becoming more deltaic in the younger beds.

During Permian and Triassic times, extensive red-bed deposition took place in molasse troughs and desert basins. These deposits now form large outcrops in Britain. In the north-west of England Permo-Triassic sandstones form a thick red-bed sequence in Cumbria and include the Bunter and Keuper. A Permian aeolian sequence forms the Penrith Sandstone which outcrops along the Vale of Eden.

Extensive tracts of Permo-Triassic red-beds, (mudstones and sandstones) occur in the east and west Midlands flanking the Pennine ridge and continue south-westwards to Bristol. To the south in Devon these become more arenaceous to form the thickly bedded sandstones in the Exeter/Dawlish area.

Jurassic sandstones do not form a significant proportion of sandstone outcrop in the British Isles. The main sandstones of Jurassic age are found in N.W Scotland, Yorkshire and southern England. A major diachronous sequence outcrops in S.W. England from the Cotswolds to the Dorset coast and includes the Cotteswold Sands, Midford Sands, Yeovil Sands and the Bridport Sands.

Cretaceous sandstones outcrop in the south and south-east of England. Late Jurassic to early Cretaceous earth movements caused sandy non-marine sequences to develop widely over NW Europe. Such facies are often termed the 'Wealden' after the Sussex-Kent area where they have been most extensively studied. The Wealden Sandstones were deposited in a fluvial fan delta environment generating alluvial sand plains. During Albian and Aptian times the Lower and Upper Greensands were deposited in a shallow marine environment. These glauconitic sandstones form extensive outcrops in Wiltshire, Dorset, Kent and Sussex.

1.4.3 Northern Ireland

With the Dalradian metamorphics in the west of the Province and the Antrim basalts in the north and east, the percentage outcrop of sandstones in Northern Ireland is relatively low. A number of Devonian and Permian sandstones outcrop along the Antrim coast at Cushendall and Belfast and extend along the Lagan Valley. The largest outcrop in the province is situated in south Tyrone and Fermanagh where a thick Devonian sequence is present.

The Donegal Quartzite of Dalradian age is the only other arenaceous deposit in the North of Ireland, these sediments having however been metamorphosed to greenschist facies.

1.4.4 General Summary

With sandstones forming approximately 25-30 % of the exposed and sub-drift lithologies of the British Isles they are extremely important as founding strata for many important engineering structures. The Nuclear Reprocessing Plant at Sellafield for instance is founded on the St. Bees Sandstone of Permo-Triassic age. In addition numerous tunnels and underground structures and coal mines are formed within arenaceous host rocks.

With increased demand for land for both transport and factories the need for underground excavations will increase and inevitably many will be constructed within sandstone rock masses. The more information available on the geomechanical properties and behaviour of such rocks, the more likely that the correct design of structures will be formulated.

1.5 Past Research

1.5.1 Past Research on Sandstones

The scientific investigation of sands and sandstones goes back nearly two centuries. The earliest work was largely descriptive with the object of distinguishing sandstones from other rock types. They were considered largely as stratigraphic entities - formations in a geological column. Names such as Millstone Grit, the Old Red Sandstone and the Buntsandstein appeared in the early literature and bear witness to the earliest field studies involving sandstones. Interpretations of their origin were based largely on field observations of sedimentary structures such as ripple marks, and on the contained fossils if any.

Not until thin section techniques were available was there any serious study of the fabric and composition of sandstones and use made of their microscopical characteristics to elucidate the natural history of the rock. One of the earliest papers on the petrography of sandstones was a paper by Henry Clifton Sorby (1859). With the exception of the work on the Tertiary sandstones of the Paris Basin by Cayeux, (1906), little work was carried out on sandstones until their importance as oil bearing strata was fully realised.

The use of heavy minerals in stratigraphic correlation, especially for oil field exploration and development, led to widespread interest in sandstone mineralogy. This

interest culminated in the appearance of H.B. Milner's "Introduction to Sedimentary Petrography" in 1922.

Apart from Hadding's work on the sandstones of Sweden, (1929), there have been few monographic studies of sandstones. There have however been noteworthy classical studies of particular sandstone formations, for example Gilligan's study of the Millstone Grit, (1920).

A different approach concerned the study of the "mechanical" composition of sandstones. Grain size analysis and later measurement of grain shape and roundness led to an era of "quantitative sedimentology" and to the study of sandstones as gross particulate systems. A major contribution to the approach was a paper by J.A. Udden in 1914 entitled, "Mechanical Constitution of Clastic Sediments". Statistical analyses began to be used for sandstone grain population with the pioneering work of Wentworth (1929) and Trask (1932) resulting in the publication of many influential works such as those of Krumbein, (beginning in 1936).

Geochemical analyses by workers such as Clarke (1924) studied the chemical compositions and related these to sediment maturity and to different groups of sandstones such as arkoses and wackes.

The past 30 years have seen the widespread development of facies studies. Analysis of vertical sections has been used to give information on the environments of deposition and basin reconstruction. The role of tectonics in sandstone deposition and composition was realised as early as 1945 by Krynine.

Though the focus of sandstone sedimentology continues to be on provenance and environment, the diagenesis of sandstones has received new and intense interest, especially from those interested in oil and gas or diagenetic mineral deposits. The diagenetic histories of sandstones are cast in terms of primary depositional input and the subsequent burial regime. Extensive work has been carried out on mechanisms of pore fluid migration and geochemical evolution in arenaceous deposits that produce cement and authigenic mineral precipitation or alterations.

Many attempts have been made to relate physical properties such as intergranular permeability, sonic transmissivity, tensile strength and thermal conductivity to the grain size distribution, Krumbein and Graybill, (1965) and Till, (1974). Only moderate success has been achieved in the past since in general any aggregate physical property is a complex function of grain size, shape, fabric and composition of both framework grains and cement. 'Sensitive' properties especially, such as permeability are subject to these problems and require the use of regression analysis to determine relationships.

1.5.2 Past Research on the Rock Mechanics of Sandstones

For the most part, European engineers and geologists in the last thirty years are credited with the development of the principles of rock mechanics. These include the methods and techniques of in-situ rock testing in connection with applications to a significant number of underground power plants and arch-dams in Austria, France, Germany, Norway, Sweden, Switzerland, Portugal and Italy, (Jumikis, 1983).

Use of rock mechanics in the United States was mainly limited to mining engineering until the early 1960's. At that time, geotechnical engineers found rock mechanics useful in hard-rock problems. This is somewhat comparable to the application of soil mechanics to problems of earthworks and foundation engineering. Rock mechanics was first recognised as a distinct discipline only since about 1950, with its specialist journal, the Journal of Rock Mechanics, being first published in 1964.

Little work has been reported purely on the rock mechanics of sandstones. In general they have been studied to a limited extent by workers researching a number of rock types and in the past there has been a danger of implying that all sandstones behave in the same way. Many publications quote average values of strength and elastic constants for sandstone implying not only a uniformity of geomechanical properties for all types, but that no variation will occur within the same rock type.

A number of notable papers have been published on the rock mechanics of specific sandstone lithologies. e.g. Hadizadeh and Rutter, (1982) on the cataclastic deformation of quartzite; West, (1979) on the strength properties of the Bunter Sandstone.

Misra, (1972) carried out research on a number of rock types including several sandstones in an attempt to correlate drilling and cutting machine performance with rock properties.

The work of Dobereiner, (1984) was restricted to the geotechnical properties of 'weak sandstones', defined by the International Society of Rock Mechanics as those with uniaxial compressive strength of less than 20 MPa. Seven varieties of weak sandstones were studied in terms of static properties, uniaxial and triaxial compressive strength . His proposed classification for weak sandstones has been discussed earlier.

The research carried out by Priest and Selvakumar, (1982) under the auspices of the Transport and Road Research Laboratory considered the strength properties of a Carboniferous and a Triassic sandstone. Their properties were related to those of a number of limestones; the rocks being assessed as to their performance for tunneling.

Following the introduction of the term 'locked sand' by Dusseault and Morgenstern, (1979) work has been carried out on Tertiary compacted sands by Barton et al, (1985, 1986 and 1989). The research has concentrated on the effects of

relative densities of greater than 100 % on the geotechnical properties of the various sands.

From a review of the literature, it appears that no-one has carried out a monographic rock mechanics study of a number of sandstones from the strongest and most competent to the weakest and most deformable.

1.6 Objectives of the Research

As described above, the term 'sandstone' covers a wide range of rock types both compositionally and texturally. This variation implies that different sandstones are likely to behave in different geomechanical ways when subjected to external stresses. The purpose of the research was to elucidate this behavioural variation within the materials loosely described as sandstones. The main objectives can be outlined as follows:

1. To study the geomechanical variation of a number of sandstones. The samples studied would be taken from a large number of sequences and vary in terms of age, composition, texture and fabric. The geomechanical behaviour would be measured in terms of stresses imposed and the resultant strains.

2. To design a testing and monitoring system which could be used in conjunction with a rock mechanics compression machine to determine sandstone 'strength' by loading samples to failure and produce accurate stress-strain curves to describe their behaviour.

3. To examine the failure processes in sandstones and develop a yield criterion in terms of microfracture formation related to observed strains/dilatancy.

4. To study the effect of moisture on sandstone strength. This would involve the quantification of the influence of different moisture contents on the measured stresses and strains from the totally dry to the saturated state. The objective of this aspect of the research would be to attempt to explain the process or processes involved in the strength reduction observed in porous sedimentary rocks.

5. To determine the bulk and microfabric properties of the sandstones studied and attempt to quantify microfabric on the basis of a number of parameters.

6. To establish relationships between sandstone microfabric and the strength and elastic properties . This would be carried out by regression analysis to determine the factors of greatest influence in controlling sandstone behaviour.

7. To examine the relationship between the accepted geological classification of sandstones and the variation in geomechanical behaviour. Special emphasis will be placed on the position of the boundary between weak and strong sandstones.

No.	NAME	CODE	AGE
1.	Applecross	A	Torridonian
2.	Donegal Quartzite	DQ	Dalradian
3.	Basal Quartzite	BQ	Cambrian
4.	Brownstones	LORS	Siluro-Devonian
5.	Pilton (Type A)	PiA	Lower Carboniferous
6.	Pilton (Type B)	PiB	Lower Carboniferous
7.	Upper Cromhall	UCS	Lower Carboniferous
8.	Millstone Grit (Type A)	MGA	Upper Carboniferous
9.	Millstone Grit (Type B)	MGB	Upper Carboniferous
10.	Millstone Grit (Type C)	MGC	Upper Carboniferous
11.	Millstone Grit (Type D)	MGD	Upper Carboniferous
12.	Holcombe Brook Grit (Type A)	HBGA	Upper Carboniferous
13.	Holcombe Brook Grit (Type B)	HBGB	Upper Carboniferous
14.	Siliceous Sandstone	SS	Upper Carboniferous
15.	Elland Flags	EF	Upper Carboniferous
16.	Thornhill Rock (Type A)	TRA	Upper Carboniferous
17.	Thornhill Rock (Type B)	TRB	Upper Carboniferous
18.	Middle Coal Measures	MCM	Upper Carboniferous
19.	Crackington Formation	CF	Upper Carboniferous
20.	Pennant (Type A)	PnA	Upper Carboniferous
21.	Pennant (Type B)	PnB	Upper Carboniferous
22.	Pennant (Type C)	PnC	Upper Carboniferous
23.	Pennant (Type D)	PnD	Upper Carboniferous
24.	Annan Sandstone	An	Permian
25.	Penrith (Type A)	PrA	Permo-Triass
26.	Penrith (Type B)	PrB	Permo-Triass
27.	Penrith (Type C)	PrC	Permo-Triass
28.	Penrith (Type D)	PrD	Permo-Triass
29.	Penrith (Type E)	PrE	Permo-Triass
30.	Redcliffe	R	Triassic
31.	St. Bees	StB	Triassic
32.	Midford Sands	MS	Jurassic
33.	Ardingly Sandstone (Type A)	ArdA	Lower Cretaceous
34.	Ardingly Sandstone (Type B)	ArdB	Lower Cretaceous
35.	Ashdown Sands	AS	Lower Cretaceous
36.	Greensand (Type A)	G	Upper Cretaceous
37.	Greensand (Type B - Dogger)	D	Upper Cretaceous

Table 1.1 Names, code abbreviations and ages for the sandstones studied.

1.7 The Sandstones Studied

The sandstones studied are listed in Table 1.1. As outlined in the previous section, an effort was made to collect samples from as many different stratigraphic units as possible in order to give a wide spread of sandstone types. In total thirty-seven different types were collected. Where a lithological variation was obvious within an exposure, samples were collected to represent each type. It was considered that any minor variations within basically the same sandstone would help to isolate the factors affecting sandstone strength.

Samples were collected from wherever fresh sandstones were known to be available. The sampling localities throughout Great Britain are shown in Fig 1.6. The ages of the lithologies sampled are shown in Table 1.1. The number of rock types from each major geological era are given in Table 1.2.

Cretaceous	5
Jurassic	1
Permo-Triass	8
Carboniferous	19
Siluro-Devonian	1
Cambro-Ordovician	1
Precambrian	2

Table 1.2 Number of sandstones sampled from each major geological era.

Each major age group is considered in turn and the respective sandstones which were studied, are described below:

1.7.1 Precambrian

The majority of sedimentary rocks in Great Britain deposited during this period have undergone high grade regional metamorphism. However, a number of sequences containing arenaceous deposits remain unaltered or show only low grade alterations. Samples were studied from two periods within the Proterozoic - the Torridonian and the Dalradian.

Figure 1.6 Sampling localities for the sandstones studied.
(Numbers refer to sandstones listed in Table 1.1)

(i) The Torridonian

The "Torridonian" is used as an informal term for the largely continental red clastic rocks of western Scotland. Torridonian rocks are found along the western Scottish coast where they form many of the prominent mountains and also outcrop on several of the Hebridean islands. The rocks can be divided into two units, the Torridon Group and the Stoer Group.

Within the Torridon Group is the basal Applecross Formation which is predominantly fluviatile, (Selley 1970). The sandstones contain remarkably fresh feldspars which suggest that the erosion of the source rocks was controlled by mechanical rather than by chemical factors. The Torridonian sandstone studied was taken from the Applecross Formation:

Name: Applecross Sandstone

Sample locality: North of Glen Boveraig, Isle of Skye

Grid Reference: NG 605 182

Sample type: Block

Hand specimen appearance: The sandstone is a light reddish brown colour with darker specks of a mafic mineral. Fine to medium grained with poorly developed internal cross-bedding. In situ, the sandstone is thinly to medium bedded and discontinuities are widely spaced.

Depositional environment: The red-bed sequence of the Applecross Formation is thought to have been deposited in braided streams on two large alluvial fans building southeastwards from a fault scarp, (Williams. 1966)

(ii) The Dalradian

The Dalradian has been included here totally within the Precambrian on the basis of recent dating work on the Scottish Dalradian by Halliday et al (1989). This work indicates that most or all of the Dalradian is Precambrian in age which is contrary to the normally accepted age for the Dalradian of late Precambrian to Cambrian.

The two main arenaceous deposits of the Dalradian are the Donegal Quartzite and its Scottish equivalent, the Jura Quartzite. The Dalradian rocks sampled were from the Donegal Quartzite:

Name: Donegal Quartzite. (Ards Quartzite)
Sampling locality: Altclogh Quarry, Near Killybegs.
Co. Donegal.
Grid Reference: G 61 81 (Irish Grid)
Sample type: Block

Hand specimen appearance: The quartzite is creamy grey in colour and is thinly to very thinly bedded; the bedding planes display a concentration of biotite and muscovite mica which causes the rock to split relatively easily parallel to bedding. Also visible on the bedding is a slight lineation indicative of low grade metamorphism. The Donegal Quartzite could therefore be termed a metaquartzite.

Depositional environment: Sedimentological interpretations for the Dalradian deposits are sparse, but general features of the sediments, (common cross-bedding and ripple marks) are consistent with shelf to marginal marine environments, (Harris et al. 1978). The polymodal palaeocurrents recorded by Hickman, (1975) imply a tidal-shelf origin for these mineralogically mature deposits. It is considered by Anderton, (1980a) that the sediment was derived from a largely sedimentary source area to the northwest of the present outcrop.

1.7.2 Cambrian and Ordovician

The Cambro-Ordovician sequence in the NW Highlands occupies a narrow band (up to 20km across) from Durness to the Isle of Skye and consists of a lower arenaceous and argillaceous sequence and an upper carbonate suite. The Eriboll Sandstone comprises the lower member with polymodal cross-bedding orientation and the Pipe Rock member. The samples of Cambrian sandstone were taken from this sequence:

Name: Basal (False-bedded) Quartzite
Sampling Locality: North of Glen Boveraig, Isle of Skye
Grid Reference: NG 610 182
Sample type: Block

Hand specimen appearance: This very to extremely strong quartzite is greyish white in colour. The lithology is termed the "False-bedded" Quartzite, so-called because of its ubiquitous sets of cross-laminae. (Cowie 1974).

Depositional Environment: Palaeocurrent directions within the quartzites tend to be bi-polar and their highly mature nature is indicative of deposition in a shallow sub-tidal or inter-tidal environment. (Swett et al 1971).

1.7.3 Silurian and Devonian

The two main Old Red Sandstone outcrops in Britain span between the mainland and Ireland - the Anglo Welsh-Irish and the Scottish Midland Valley - Northern Ireland areas. These possess thick sequences of red-bed clastics. Lower Old Red Sandstone deposits were sampled from the Welsh Border area:

Name: Brownstones -Lower Old Red Sandstone
Sampling Locality: Red Wilderness Quarry,
Forest of Dean
Grid Reference: SO 672 185
Sample type: Block

Hand specimen appearance: The sandstone is fine to medium grained, light pinkish red in colour with small greenish-grey reduction patches and occasional small red mudstone rip-up clasts. Internal cross-bedding is sometimes visible.The outcrop is thinly to medium bedded.

Depositional environment: The Lower Old Red Sandstone deposits of the Welsh Borderland were formed along a south-migrating, low-energy strandline of beaches and barriers with sheltered lagoonal or tidal flat deposits. Behind this coastline were extensive alluvial plains with river channels and low flood plains, (Allen, 1974a).

1.7.4 Carboniferous

The wide range of Carboniferous arenaceous deposits of Great Britain provided the main source of samples for the research, from the extremely strong fine-grained varieties of the lowest Carboniferous, Pilton Formation, to the weak and very weak sandstones of the Millstone Grit Series in Durham.

The main divisions of the Carboniferous are as follows:

Upper Carboniferous:	Coal Measures (Westphalian)
	Millstone Grit Series (Namurian)
Lower Carboniferous:	Carboniferous Limestone Series (Dinantian)

In total, twenty samples of Carboniferous sandstone were collected. These are divided into three groups on the basis of the main divisions of the Carboniferous. The depositional environment for each division is outlined.

(i) Lower Carboniferous

Three sandstone types were sampled from the Lower Carboniferous:

a) **Name:** Pilton Beds (Type A)

Sampling Locality: Bond's Pit, South Molton.
North Devon.

Grid Reference: SS 687 340

Sample type: Block

Hand specimen appearance: The Pilton sandstone is a dense, fine-grained dark grey rock of low porosity. Mica concentrations occur along many of the bedding planes. The lithology is thinly to very thickly bedded.

Depositional environment: Goldring, (1955) confirmed that in north-west Devon the base of the Carboniferous occurs in the Pilton Beds. These deposits form part of the Transition Series which are considered to have been deposited in a shelf sea environment, where turbidity currents played an important role.

b) **Name:** Pilton Beds (Type B)

Sampling Locality: Roadford Reservoir

Grid Reference: SX 434 920

Sample type: Block

Hand specimen appearance: This variety of the Pilton Series is very fine-grained. It is dark grey in colour with occasional thin quartz-filled veins and is thinly to medium bedded.

Depositional environment: As above

c) **Name:** Upper Cromhall Sandstone
Hotwells Group,
Carboniferous Limestone Series

Sampling Locality: Avon Gorge, Bristol

Grid Reference: ST 564 734

Sample Type: Borehole and block samples

Hand specimen appearance: The Upper Cromhall sandstone is a deep pinkish-red colour, fine to medium-grained with low porosity. The rock has a high calcium carbonate content indicated by a strong reaction with weak acid.

Depositional environment: This lithology is interbedded with limestone and mudstones as part of the Cromhall Series of the Hotwells Group. The sand facies was deposited in a high energy intertidal zone which saw recurring rises in sea level and influxes of terrigenous material.

ii) Millstone Grit Series

The environment of deposition of the Millstone Grit Series can be regarded as transitional between the marine - estuarine conditions of the Carboniferous Limestone Series to the deltaic lagoon-swamp conditions of the Coal Measures. The facies are essentially of two types. First, there is a 'Yoredale' facies consisting of repetitive sequences of limestones, marine shales and thin subordinate sandstones. Secondly there is a 'Millstone Grit' or more arenaceous facies, characterised by thick, coarse-grained cross-bedded sandstones together with fine grained sandstones, siltstones and mudstones in which marine intercalations are comparatively thin.

Seven samples were taken from the Millstone Grit facies:

a) **Name:** Millstone Grit (Type A)
Sampling locality: Dunhouse Quarry, Bishop Auckland. Co. Durham.
Grid Reference: NZ 141 183
Sample type: Block
Hand Specimen appearance: Light buff coloured, medium-grained sandstone with abundant brown, organic material in the form of thin, (<1mm) bedding-parallel lenses and specks which show signs of dissolution.

b) **Name:** Millstone Grit (Type B)
Sampling locality: Cat Castle Quarry, Lartington, Barnard Castle, Co. Durham.
Grid Reference: NZ 010 164
Sample type: Block
Hand specimen appearance: The sandstone is grey/buff and coarse-grained with occasional fine to medium gravel sized clasts. The rock has a visibly high porosity and a light yellow clay matrix. Internal bedding is clearly visible due to the associated changes in grain size.

c) **Name:** Millstone Grit (Type C)
Sampling locality: Ladycross Quarry, Slaley Forest, near Hexham, Northumberland.
Grid Reference: NY 945 555
Sample type: Block
Hand specimen appearance: This variety of the Millstone Grit is a brownish-grey, medium-grained, very thinly bedded to laminated sandstone with dark brown fines concentrated along the bedding planes. Liesegang rings are often present.

d) **Name:** Millstone Grit (Type D)
Sampling locality: Shipley Quarry, Marwood,
Barnard Castle, Co. Durham.
Grid Reference: NY 015 209
Sample type: Block
Hand specimen appearance: Slightly yellowish grey in colour and fine to medium-grained with occasional small, dark grey flecks

e) **Name:** Holcombe Brook Grit (Type A)
-Millstone Grit (Type E)
Sampling locality: Cartworth Moor, Near Huddersfield
West Yorkshire.
Grid Reference: SE 134 067
Sample type: Block
Hand specimen appearance: The Holcombe Brook Grit is a light grey coloured medium grained uniform sandstone.

f) **Name:** Holcombe Brook Grit (Type B)
-Millstone Grit (Type F)
Sampling locality: As above
Grid Reference: As above
Sample type: Block
Hand specimen appearance: This variety of the Holcombe Brook Grit has the same visible texture as that of the grey type but is light buff in colour. The alteration of the grey sandstone occurs in situ on the outer areas of large blocks bounded by widely spaced discontinuities and is related to ground water flow.

g) **Name:** Siliceous Sandstone
Quartzitic Sandstone Group
-Millstone Grit (Type G)
Sampling locality: Hotwell Road, Bristol
Grid Reference: ST 577 725
Sample type: Block
Hand specimen appearance: The Siliceous Sandstone is a light purple colour and is fine to medium grained. The rock is extremely dense, with low porosity, and does not show an acid reaction like the Carboniferous sandstones sampled in the Avon Gorge.

(iii) Coal Measures

The Westphalian is the major coal bearing stage in Britain. Sections through the Coal Measure rocks reveal a variable cyclicity of lithologies. These include two main sandstone types - coarsening-up and fining-up sequences.

The coarsening-up sandstone units may be interpreted as due to the gradual infilling of an on-delta lake body by a nearby or delta distributary channel or by minor crevasse-splay from the partly breached bank of a major channel. The sharply based fining-up sandstone units (1-20m thick) sometimes occupy channel forms or define ribbon-shaped outcrops, often showing cross-stratification.

The Coal Measures of northern England and Scotland were deposited in a subsiding gulf while the Coal Measures of the Bristol and S. Wales area formed in a basin into which rivers drained from both north and south.

Nine sandstone types were sampled from the Coal Measure deposits:

a) **Name:** Elland Flags
- Lower Coal Measures

Sampling locality: Crossley's Quarry, Southowram, Halifax, West Yorkshire

Grid Reference: SE 107 238

Sample type: Block

Hand specimen appearance: Greenish-grey, medium-grained with abundant fine-grains of muscovite, especially along bedding planes.

b) **Name:** Thornhill Rock (Type A)
- Middle Coal Measures

Sampling locality: Morley, Leeds, West Yorkshire

Grid Reference: SE 268 263

Sample type: Block

Hand specimen appearance: Light greenish-grey, fine to medium-grained sandstone with some unstable grains oxidizing to a rust brown colour.

c) **Name:** Thornhill Rock (Type B)
- Middle Coal Measures

Sampling Locality: As above

Grid Reference: As above

Sample Type: Block

Hand specimen appearance: Medium greenish-grey fine to medium grained sandstone with some internal cross-bedding.

d) **Name:** Middle Coal Measures
Sampling locality: Springwell, Gateshead, Tyne and Wear
Grid Reference: NZ 284 587
Sample type: Block
Hand specimen appearance: The rock is medium-grained and light buff in colour. The majority of the rock contains many grains which show oxidation to a rust brown colour. Liesegang rings are widely developed and where present, the 'rusted' grains have been removed and the iron concentrated in the Liesegang rings.

e) **Name:** Crackington Formation
Sampling locality: Bideford Bypass, Bideford, North Devon
Grid Reference: SS 455 296
Sample type: Block
Hand specimen appearance: The sandstone is fine to medium and grey when fresh but weathers to a light brown colour.
Depositional environment: The Crackington Formation was deposited in a marine sedimentary basin on whose floor unconsolidated sediments were periodically disturbed by turbidity currents which formed the sandstone beds in areas of deeper water.

f) **Name:** Pennant (Type A) - Upper Coal Measures
Sampling locality: Mine Train Quarry, Parkend, Glos.
Grid Reference: SO 604 101
Sample type: *Block*
Hand specimen appearance: The sandstone is medium-grained and reddish grey in colour. Many of the individual grains have a deep red colour. This variety is the most apparently iron-rich of the three types collected from the Forest of Dean.

g) **Name:** Pennant (Type B) - Upper Coal Measures
Sampling locality: As above
Grid Reference: As above
Sample type: Block
Hand specimen appearance: Medium-grained, grey sandstone with large pores indicative of solution of unstable minerals.

h) **Name:** Pennant (Type C)
- Upper Coal Measures

Sampling locality: As above

Grid Reference: As above

Sample type: Block

Hand specimen appearance: Type C is a pinkish-grey, medium-grained sandstone with patches of deep red, iron-rich material concentrated along bedding planes and discontinuities. This variety is intermediate between the grey and reddish-grey varieties exposed in Mine Train Quarry.

i) **Name:** Pennant (Type D)
- Upper Coal Measures

Sampling locality: Warmley, Bristol

Grid Reference: ST 656 738

Sample type: Borehole samples

Hand specimen appearance: The Bristol Pennant is bluish-grey and medium-grained with a low porosity. The sandstone contains many thin coal laminae and fragments of carbonaceous material. Internal cross-bedding is occasionally visible and many quartz-filled veins are present.

1.7.5 Permian and Triassic

The Permian and Triassic periods are often considered together as the New Red Sandstone era during which the deposition of extensive red beds occurred throughout Great Britain. The lower Permian era, as over most of Europe was mostly a time of subaerial erosion, with the newly uplifted regions being deeply dissected, (Smith et al, 1974). During this erosional phase, reddening of both the sediments and the eroded surfaces took place under semi-arid conditions.

Early sediments consisted of coarse red water-lain breccias and conglomerates composed of locally derived materials - a molasse facies. These basins were often fringed by desert dune fields giving rise to the extensive Permian desert red-beds.

The great bulk of the coarse grained facies of the Triassic consists of conglomerates and cross-bedded sandstone arranged in fining-up cyclothems, representing streamflood and braided stream deposits in which the pebbles were derived from locally outcropping sources; such sequences conform well with those from modern alluvial fans. (Tucker, 1978).

a) **Name:** Annan Sandstone
Sampling locality: Annan, Dumfriesshire, Scotland
Grid Reference: NY 207 703
Sample type: Block

Hand specimen appearance: This sandstone is deep pinkish-red and fine to medium-grained with occasional small areas where fine grains have been oxidised to a rust brown colour.

Depositional environment: The Annan sandstone is a northern extension of the important sequence of the Carlisle Basin and Vale of Eden. It rests unconformably on lower Palaeozoic rocks in the River Annan Valley and shows the large scale trough cross-bedding characteristic of aeolian red bed deposits.

b) **Name:** Penrith Sandstone (Type A)
Sampling locality: Stoneraise Quarry, Near Penrith, Cumbria
Grid Reference: NY 533 358
Sample type: Block

Hand specimen appearance: Pink, medium to coarse-grained sandstone composed predominantly of well-rounded quartz grains. Finer grains occur in thin gradational bands.

Depositional environment: The Penrith Sandstone of lower Permian age is a continental red bed sandstone deposited as 'barchan' dunes in a hot arid desert environment. It is considered that the source of the sediment was the area of the present Lake District, which formed an elevated tract through much of the Permian and Triassic, with periodic uplift and rejuvenation.

c) **Name:** Penrith Sandstone (Type B)
Sampling locality: As above
Grid Reference: As above
Sample type: Block

Hand specimen appearance: Deep brownish-red, medium to coarse-grained sandstone with high intergranular porosity. Little cement present, with grains welded together by quartz.

d) **Name:** Penrith Sandstone (Type C)
Sampling locality: As above
Grid Reference: As above
Sample type: Block

Hand specimen appearance: Light pink, coarse-grained variety of the Penrith Sandstone with lower porosity and an apparently high degree of cementation.

e) **Name:** Penrith Sandstone (Type D)
Sampling locality: Lazonby Fell Quarry, near Penrith
Cumbria
Grid Reference: NY 517 380
Sample type: Block
Hand specimen appearance: Pinkish-red sandstone with medium to coarse well-rounded grains and medium porosity. No internal bedding visible.

f) **Name:** Penrith Sandstone (Type E)
Sampling locality: Shawk Quarry, Near Thursby, Cumbria.
Grid Reference: NY 344 484
Sample type: Block
Hand specimen appearance: Pink in colour and much finer grained than the other varieties of the Penrith Sandstone. Some signs of internal cross-bedding.

g) **Name:** Redcliffe Sandstone - Keuper
Sampling locality: Bedminster, Bristol
Grid Reference: ST 565 701
Sample type: Borehole and block samples
Hand specimen appearance: Deep red in colour, medium-grained clay-rich sandstone with greenish-grey reduced areas and occasional fine to medium angular gravel clasts.
Depositional environment: By Bunter times the Mendips and Bristol Coalfield formed a mountainous tract which bounded sedimentary basins to the north and south. Adjacent to these mountains, alluvial fans deposited coarse detrital material while in more distal parts, sandstones and mudstones were laid down by wind or flash flood. The Keuper sandstones of the Bristol area represent these distal fan deposits.

h) **Name:** St. Bees Sandstone
Sampling Locality: Sellafield Nuclear Reprocessing
Plant, Cumbria
Grid Reference: NY 025 035
Sample Type: Borehole samples
Hand specimen appearance: The St. Bees sandstone is a highly variable

deposit as proven from extensive boreholes constructed in the area. It varies from being deep brownish-red, fine to medium, to pinkish-red, very fine-grained and laminated. The degree of cementation and hence porosity are also highly variable.

Depositional environment: The sequence is estimated as 335m thick. It was deposited on alluvial fans which were shed westwards from the upland massif of the present Lake District area. The sandstones are interfingered with evaporite deposits to the west and thick continental breccias to the west.

1.7.6 Jurassic

Limestone and marl lithologies are typical of the early Lias over most of south and central Britain, but in the Mendips and Glamorgan areas, sequences are condensed and in places comprise oolitic calcarenites.

The middle Jurassic opened with the development of a regressive phase. Fluvio-deltaic environments spread southwards into Britain while at times central England and western Scotland became the site of lagoons. In Yorkshire, sandstones produced by these fluvio-deltaic episodes are dominantly mature subarkoses and quartz arenites, (Nami, 1976). North-west Scotland received abundant terrigenous clastic sediments throughout the middle Jurassic. Much of the sequence was deposited in a shallowing high energy marine environment. Upper Jurassic times saw a diminution in the availability of coarse-grained terrigenous clastic material due to the culmination of the Jurassic sedimentation.

The only Jurassic sandstones sampled were from the Liassic Midford Sands of south-west Britain:

Name: Midford Sands
Sampling locality: Beechen Cliff, Bath
Grid Reference: ST 750 641
Sample type: Block

Hand specimen appearance: The Midford Sands are a weakly cemented, light buff coloured, fine to medium grained, slightly iron-stained sandstone. Segregation nodules are present but poorly developed.

1.7.7 Cretaceous

Cretaceous strata dominate the geology of south-east England. These include the lower Cretaceous sandstones and clays and the Upper Cretaceous Greensands and Chalk. The considerable arenaceous deposits laid down during Cretaceous times crop out from Kent in the east to Dorset and Wiltshire in the West. They are typically rich in glauconite but show low degrees of induration.

The Hastings Beds Group forms the main arenaceous deposit of the lower Cretaceous reaching a maximum thickness of approximately 400m in the Weald. Allen, (1975) has identified three cyclothems within the sequence, in which claystones and mudstones coarsen upwards into cross-bedded sandstones with a capping of frequently bone-rich gravels. Until recently, (Allen, 1975), the Hastings Beds cycles were interpreted as deltaic sequences with the deltas prograding southwards from an uplifted London-Brabant Massif. The muddier facies were interpreted as the prodelta environment and the more sandy sequences as delta shoreface and distributary channel deposits. However, signs of exposure or very shallow water exist in all lithologies throughout the Weald. The latest model reinterprets the mud facies as lagoonal to lacustrine mudswamp deposits and the coarsening sequence as fault-controlled, alluvial braidplain advances into the mudswamp area.

The major Greensand deposits of the Aptian and Albian stages are interpreted as having been laid down in shallow marine and shoreline environments. The presence of abundant glauconite is indicative of not only slow rates of deposition, but also of water depths of greater than approximately fifty metres. (cf. Hancock, 1975).

Five Cretaceous sandstones were studied:

a) **Name:** Ardingly Sandstone - Hastings Beds (Type A)
Sampling locality: West Hoathly, East Grinstead, West Sussex
Grid Reference: TQ 355 323
Sample type: Block
Hand specimen appearance: Light green, glauconitic, very fine-grained, laminated sandstone with internal *cross-bedding.*

b) **Name:** Ardingly Sandstone - Hastings Beds (Type B)
Sampling locality: As above
Grid Reference: As above
Sample type: Block
Hand specimen appearance: Light yellowish-green, glauconitic very fine-grained thinly bedded sandstone.

c) **Name:** Ashdown Sandstone - Hastings Beds
Sampling Locality: Great Wallis Farm, Rotherfield, near Tunbridge Wells, Sussex.

Grid Reference: TQ 583 284

Sample type: Block

Hand specimen appearance: Fine to medium-grained yellowish-white sandstone with green glauconitic grains and small fragments of carbonaceous material on the laminae.

d) **Name:** Upper Greensand (Type A)

Sampling locality: Devizes, Wiltshire

Grid Reference: SU 004 614

Sample type: Block.

Hand specimen appearance: Light green, fine-grained sandstone with a high percentage of clay/silt sized material. The rock weathers to a light brownish-green with abundant iron-staining.

e) **Name:** Upper Greensand (Type B)

Sampling locality: As above

Grid Reference: As above

Sample type: Block

Hand specimen appearance: These segregation nodules which are contained within the Upper Greensand, are grey in colour and much denser, (with lower porosity) than the surrounding material. Many contain fossils at their centres. They are highly calcareous.

Depositional environment: The segregration nodules found within many of the glauconitic sandstones of southern Britain are considered to be of significant engineering importance and were hence sampled as a distinct sandstone type. They form as post-deposition, early diagenetic features by a process of migration of calcium carbonate, (or other ions) towards centres of nucleation, (Allison, 1987). These centres of nucleation are normally decomposing organisms or death assemblages which alter the chemistry of the immediately surrounding sediment.

CHAPTER 2

THE STATIC PROPERTIES OF SANDSTONES AND THEIR METHODS OF DETERMINATION.

2.1 Introduction

Static properties are here defined as those general physical, non-dynamic properties specific to a particular rock type which distinguish it from any other rock type with different lithological characteristics. These include characteristics such as mineralogy, texture and density, all of which can change within a rock until the time of sampling, due to weathering, ground water flow or changes in the stress regime. Dobereiner, (1982) described static properties as those properties not measured by their response to a potential gradient.

In any rock mechanics study, the relationship between the static properties of a rock and its geomechanical behaviour is important. In research where an attempt is made to determine what actually controls rock strength and deformability, the determination and appreciation of the interaction of the static properties of the rock is fundamental.

The static properties which produce the fingerprint characterising a particular sandstone depend on the geological history of the rock. In the formation of any arenaceous rock each of the following six basic processes will have occurred to a greater or lesser degree: source rock weathering; erosion; transportation; deposition; diagenesis and;subsequent weathering.

The sandstone fingerprint is therefore produced by the original source materials and the nature and duration of the six geological processes. Since the work of Sorby (1879), sedimentologists have used this principle in working backwards from the nature of the sandstone to determine its provenance, maturity, depositional environment and for classification purposes, Folk (1974).

The engineering geologist is less interested in the information regarding the past history of the sandstone and leans more towards how the static properties can be used for geological and geotechnical descriptions and classifications.

The static properties of sandstones are as follows:

1) Mineralogy - The detrital constituents
- Chemical minerals
- Organic matter

2) Texture
- Grain size
- Grain shape
- Grain contacts and packing
- Grain orientation and cleavage
- Porosity

3) Density
- Dry bulk density
- Saturated bulk density
- Grain density

4) Macroscale sedimentary features
- Current structures- bedding
- Deformational structures
- Biogenic structures
- Chemically formed structures

2.2 Mineralogy

Sandstones are mixtures of mineral grains and rock fragments derived from naturally disaggregated products of erosion of all types of rock. In theory therefore, the number of of mineral species to be found in all sandstones is as large as the total number of mineral species known. In reality however this is not the case , for the abundant minerals of sandstones belong to very few groups. The processes of weathering, transport and diagenesis alter the chemical and physical nature of certain minerals creating conditions where they deteriorate or are modified considerably.

Detailed studies of weathering, (Ollier,1969; Loughnan, 1962) have quantified the degree to which certain minerals will be totally destroyed or altered chemically while others are little affected. Feldspars may alter to kaolinite or an intermediate product; pyroxenes and amphiboles may simply dissolve and be transported as dissolved ions. In contrast, some minerals such as quartz are only very slightly soluble in typical fluvial and marine conditions and will be eroded from the source area and transported unchanged in amount or character.

Abrasion during transport of sediment causes the softer/weaker minerals to decrease in size and become more rounded relative to the harder/more homogeneous minerals. Many minerals may be so soft as to not survive the rigorous transportation as sand sized grains and will then find their place in silts or muds.

Finally the mineral composition of sandstone may be drastically altered during

diagenesis. Unstable minerals which may have just survived the weathering and transportation processes may finally be removed completely or change their mineralogical state by very low grade metamorphism. In addition, new minerals may be precipitated from solution or deposited by percolating fluids. (Kesseler, 1978; Siebert et al, 1984; Burley, 1985).

For the purposes of any detailed study of microfabric it is important to distinguish between detrital and authigenic components. Many mineral species present in sandstones however, exist as both detrital and authigenic constituents e.g. quartz, feldspars and clays.

2.2.1. The Detrital Constituents

Detrital constituents are those forming the sediment at the time of deposition. They exist as monomineralic grains or as polymineralic grains i.e. rock fragments.

i) The Silica Minerals

Quartz is the most common mineral in sandstones and occurs as the only crystalline polymorph of SiO_2 which is thermodynamically stable - low quartz. (Frondel 1962).

A number of amorphous silica varieties such as opal-A and siliceous sinter occur in modern sandstones but for older 'volcanic' and most non-volcanic sandstones it is only necessary to consider chert in addition to quartz. Krynine (1940) described ten different varieties of quartz occurring in sandstones based on inclusions and shapes of grains as well as whether they are mono- or polycrystalline in nature. Numerous workers have looked at the nature of straining within the quartz grains and debated the usefulness of this property in identifying source rocks. From the point of view of strength and deformability, sandstones containing a high percentage of strained grains could possess lower strengths than those with unstrained quartz.

There has also been some study of quartz types by chemical methods, although they are generally slower and more difficult than optical ones.

ii) Feldspars

All varieties of feldspars have been noted as detrital minerals in sandstones. In the past however, relatively few petrographic analyses gave a breakdown of feldspar varieties: in the average sandstone , K-feldspar (orthoclase and microcline) is the most abundant and sodic plagioclase far outweigh calcic ones. (Smith,1974). Potassium feldspar especially microcline, is a characteristic feldspar of arkoses and feldspathic sandstones, while sodic plagioclases are the only feldspar in many greywackes. Microcline has been suggested to be the most abundant species, by many workers who

do not quote quantitative data. In cases where the alkali feldspars have been distinguished quantitatively, orthoclase is shown to be the most plentiful.

In general, the amount of untwinned k-feldspar is probably underestimated relative to plagioclase, since it is the most difficult feldspar to identify as such in thin section, unless staining techniques are used. It is also known that many different feldspar compositions may occur in the same thin section but without electroprobe analysis it is difficult to distinguish between the various types.

The average feldspar content in sandstones is reported by Leith and Mead, (1915) to be approximately 8.45%, based on observational analysis. This can be compared to the average bulk chemical composition which implies a feldspar fraction of about 11.5%. (Clarke, 1924). Actual modal analyses however, show that some sandstones are essentially feldspar free whereas in others, such as arkoses, feldspar constitutes over 90% of the framework fraction.

iii) Micas, Chlorites and Clay Minerals.

The chemical compositions of these minerals are similar, being hydrous aluminosilicates with sheet structures, and can therefore be considered together. Muscovite, biotite and chlorite occur in sandstones as large detrital grains. They may be either fresh or altered and can be readily identified under the microscope. In most sandstones they are a minor constituent, except along fine grained partings and some shaly sandstones where they are abundant. Because they form platy shaped grains they have a relatively low settling velocity and hence are deposited in lower energy conditions than those in which medium to coarse quartz and feldspar grains are laid down. (i.e. in fine sands or during lulls in deposition- along bedding planes. e.g. The Donegal Quartzite. (Doyle et al 1968).

Muscovite is much more resistant to chemical weathering than biotite or chlorite, but there is not enough data to permit an evaluation of the stability of biotite relative to the several varieties of chlorite during weathering. There appears to be a greater tendency of chlorite to degrade to finer particles than biotite. Chlorite is therefore frequently lumped with the fine clay fraction in sandstones. The alteration of biotite to chlorite in place is also common.

The fine fraction found in some sandstones as the essential constituent of matrix and argillaceous rock fragments includes all the major groups of clays: the kaolin group (kaolinite, dickite, halloysite), the micas (muscovite, illite, glauconite), the smectite group(montmorillonite, nontronite, saponite and many others), the chlorite group, and the mixed-layer group (corrensite and others).(Carroll 1970; Brindley and Brown 1980).

The division of clay mineral groups is primarily on a structural rather than a

compositional basis but it is not within the scope of this thesis to discuss the structural make-up of different clay species. Suffice to say that the behaviour of the different clay types is controlled ultimately by their chemistry and physical structure.

The major origin of clay minerals is as sub-aerial weathering products of silicate minerals. All of the major clay groups are found in weathered residues and soils. Which clays will be found depends on the interaction of climate, geomorphology and parent rock. Humid climates and well drained topographies lead to extensive weathering of feldspars and their silicates to kaolinite. Lower rainfall and poorer drainage may result in the formation of smectite from the same parent material. Mafic silicates in many climates will go to smectites while illite products may form in intermediate to humid climates.

Clay minerals are probably the most susceptible of the sandstone minerals to processes of change from the time of deposition to petrological examination. Thin-section and scanning electron microscope studies which have suggested the probability of precipitation of clay minerals from aqueous solutions at low temperatures and pressures, have been confirmed in laboratory experiments. (Siffert, 1962). In addition, laboratory experiments have shown that under certain conditions, clay minerals will partly dissolve and alter within hours or days.(Mackenzie and Garrels 1965; Siever 1968).

iv) Heavy minerals.

Various heavy silicates and oxides are found in small quantities in sandstones, but rarely total more than one percent of the rock. One major review of heavy minerals has been given by Parfenoff et al (1970) who included study methods, interpretation and mineral descriptions.

The main heavy minerals occurring in sandstones include tourmaline, zircon and rutile. Although these do not occur in large quantities in any source rock, it is their resistance to mechanical and chemical attack which allows them to accumulate as detrital grains. Oxides such as magnetite may persist in a transporting medium and consequently, although they become rounded, often form the opaque minerals in many sandstones.

Heavy mineralogy has in the past been most valuable in establishing petrographic provinces and source types rock but clearly their presence, particularly when abundant, will influence the geomechanical properties of the sandstone.

v) Rock Fragments.

The major types of rock fragments which occur in sandstones are (1) the argillaceous group including shale, slate and phyllite, (2) volcanic rocks, (3) the silica group including quartz derived from metamorphic rocks and cherts. Of lesser importance but locally important are the carbonate rock fragments. A sandstone derived from a carbonate upland massive with high relief undergoing rapid erosion and an arid climate will be most likely to contain a high percentage of carbonate rock fragments. e.g. The Keuper Sandstone of the Bristol area.

During diagenesis however, rock fragments may become deformed and in that state they are difficult to determine as discrete fragments and are easily misidentified as monocrystalline grains. Argillaceous rock fragments of sand size for example are probably not identified as such in many older sandstones because they may be squashed, deformed and moulded during loading, about the more competent grains so that they blend into or appear as clay matrix. (Allen 1962). Where mud flakes of greater than sand size occur, such as in the Old Red Sandstone, they normally become flattened perpendicular to the direction of σ_1 (usually the lithological loading). These features may have a localised effect on the mechanical properties of the sandstone.

Volcanic material, including pyroclastic debris, are abundant in some sandstones. In fact, they can form the dominant constituent of some. When altered diagenetically, such rocks are likely to contain zeolite minerals and devitrification of glasses within the sandstones may lead to the production of opal cement. (Pettijohn et al,1987).

The rock fragment content is governed by several factors: (1) provenance, (2) grain size, (3) maturity and (4) age. In general the rock fragment content is a function of grain size - the coarser the sandstone, the higher the rock fragment content, other things being equal. (Shiki, 1959; Allen,1962).

vi) Carbonate Minerals

Detrital carbonate grains may be abundant in calcareous sandstones formed mainly from skeletal fragments and ooliths. Their presence generally indicates deposition proximal to the source area. Such debris may also be admixed in varying but usually minor amounts in terrigenous sandstones. Scholle, (1978) provides a guide to the recognition of skeletal debris in thin section. Potter, (1978) found the greatest occurrence of detrital carbonate grains in two sand types: big river sands of semi-arid and arid climates and sands derived from Pleistocene glacial drift eroded from carbonate bedrock. The solubility of carbonate together with its softness and cleavage all decrease its probability of survival during stream transport.

2.2.2. The Chemical Minerals.

The chemical minerals are those which form in the rock by processes of precipitation or alteration after the deposition of the rock. They are often termed authigenic - "developing in place during or after deposition". The group includes many of the mineral varieties normally considered detrital, such as quartz, feldspar and clays. Carbonate minerals, as mentioned earlier occur both as detrital and chemical constituents but unlike the others which have a dual role, chemically precipitated carbonates are by far predominant over detrital varieties.

i) Carbonates - Calcite and Dolomite

These are abundant in sandstones as pore-filling and replacements of post-depositional origin. Grains of detrital and primary dolomite have also been identified by Sabins, (1962). Some pore-filling cement may be recrystallized from originally detrital carbonate or may be a precipitate from an aqueous solution in an original empty pore space. Dolomite however appears almost always as a replacement of a calcite precursor.

In general the calcite and dolomite formed during late stage diagenetic events in sandstones are relatively pure with no excess magnesium in the calcite and no excess calcium in the dolomite.

The iron-rich carbonates are less common than calcite and dolomite in most sandstones but abundant constituents of some; (Goldsmith et al 1962). Of the various minerals in the Ca-Mg-Fe-CO_2 system, the ones of importance in sandstones are siderite and iron-rich dolomites (ankerite). Iron and magnesium carbonate cements often enrich sandstones selectively to form bands or concretions as seen in the Bridport and Folkestone Sands. Several theories have been put forward concerning the formation of these concretionary nodules, notably by Allison (1988). These will be discusssed in Chapter 3.

ii) Sulphates and Sulphides.

Gypsum, anhydrite and barite are the three common sulphates found as cementing agents in sandstones which have accumulated in arid and semi-arid environments. The sulphate of these cements is ultimately derived from that dissolved in seawater or in subsurface brines. Shearman, (1978) suggested that much of the gypsum and anhydrite has been derived from broad supra-tidal sabkha flats and deposited in pore spaces of pre-existing sediments below the flats.

The nature of the sulphates, (i.e. gypsum or anhydrite) will depend on the age and depth of burial, being related to pressure, temperature and salinity. (Hardie, 1967). (Fuchtbauer, 1974).

Barite occurs as concretions as well as cement and its origin is related to sea-floor volcanism. It is not common but is localised with respect to marine volcanic provinces.

Pyrite is the principle sulphide found in sandstones and appears to be almost entirely diagenetic in origin, though Precambrian deposits such as the Witwatersrand uranium deposits of South Africa have large amounts of apparently detrital rounded pyrite grains. The mineral is genetically related to a more or less amorphous common mineral FeS- mackinawite, which is found in modern sediments under reducing conditions. FeS forms first by the bacterial reduction of sulphate in seawater and during early diagenesis is converted to FeS_2, pyrite, (Berner 1980). Thus when pyrite is present as an intragranular cement it is presumptive evidence of at least locally reducing conditions. In sandstones it is likely that it is the presence of large amounts of organic matter on tidal flats that is responsible for the reduction.

iii) Other Minerals.

The other minerals of chemical origin which occur in sandstones are phosphates, iron silicates (e.g. glauconite), the zeolites and the iron and titanium oxides.

a) Phosphate

Phosphate precipitation as cement in some sandstones appears to be related to the dissolution of calcium phosphate present in the sediment as bones or shells. In others it appears as an authigenic precipitate or replacement of carbonate formed during early diagenesis in anoxic or suboxic interstitial water environments.(Cook, 1976). The chemistry of the phosphates is complex, the most common mineral being carbonate fluorapatite, $Ca_5(PO4)_3(F,CO_3)$. It is highly variable in composition with substitution of Mg, Sr, and Na for Ca and some SO_4 for PO_4.

The phosphatic minerals often occur as concretionary nodules. e.g. the Hythe Beds of S.E. England.

b) Iron silicates

The iron silicates can be considered to be special varieties of clay minerals that are iron rich. Glauconite is the most common of such minerals throughout the geological column. Simple, spheroidal and ovoidal glauconite pellets occur in quartz arenites and lithic arenites and to a lesser extent in feldspathic and other types of sandstones. The Cretaceous Greensand deposits of S.E. England and Northern Ireland have abundant glauconite giving the rocks a light brownish green colour- hence the name.

Glauconite is a mica related to illite in structure, but with a great deal of both ferrous and ferric iron; (Burst, 1958). The glauconites appear to be associated with mildly reducing conditions perhaps locally induced by the presence of abundant organic matter, related to relatively near shore and shallow environments, (Velde, 1977). Thus a general picture emerges of glauconite forming in sedimentary environments in which biogenic activity is high and sedimentation rates are low, the mineral forming as a penecontemporaneous or early diagenetic mineral. It may be reworked and transported; some sands contain both transported and allocthonous glauconite grains e.g. The sandstones of the Weald.

c) Iron and Titanium oxides

The same general scheme of origin inferred for the iron silicates has been suggested for the haematitic and limonitic iron oxide coatings of red sandstones. Evidence from modern stream sediment loads makes it doubtful that much of this iron was transported as detrital haematite or limonite. Two main theories have been suggested:

1) ferric hydroxide colloid which originated in soils is transported in rivers and near shore environments as a dilute suspension or adsorbed on the surfaces of clay minerals. After deposition, the ferric hydroxides spontaneously dewater to form limonite or if complete hydration occurs, haemetite; *(Houten, 1973).*

2) Walker, (1974) and Walker et al, (1978) have argued convincingly that many red sandstones of desert and more humid environments owe their haematite to precipitation by soil or groundwater. The iron is thought to be derived from the weathering of iron rich primary silicates such as pyroxenes and amphiboles.

Both processes may be at work in one or another situation. Both involve the diagenetic precipitation of the iron oxide.

d) Zeolites

These minerals occur usually in sandstones associated with volcaniclastics in subduction zone environments and have been used to an increasing degree by sedimentologists in provenance studies. There are more than thirty naturally occurring zeolite minerals but only four are common in sandstones: analcine, laumonite, clinoptilolite and mordenite.

They are most common in Cenozoic rocks, much less common in Mesozoic rocks and are virtually absent from early Palaeozoic and Precambrian strata.. It appears that with time, zeolites disappear by diagenesis or metamorphism. In many sandstones zeolite minerals are closely linked to the presence of volcanic glass and it appears that they form as early decomposition products of the weathering of these glasses.

2.2.3. Organic matter

Organic matter occurs in sandstones either as a biochemical precipitate or as organic detritus. In both cases the material is profoundly altered by diagenesis.

Sandstones in general are characterised by extremely small amounts of organic matter, less than 0.1%. Some greywackes are an exception and may contain up to several percent organic matter; (Pettijohn et al 1987). The organic matter native to sandstones is dominantly detrital, but even in tidal flat sandstones where organic productivity is high, only a relatively small residue of organic matter is left after the early biological diagenetic processes have taken place.

The organic end products are derived from the breakdown of plant and animal tissues in the sedimentary environment - the end product depending ultimately on the complex diagenetic history of the sediment. Sandstones such as those of S.E. England which have not undergone extensive diagenetic changes contain plant debris in the form of brownish translucent material which still shows remnant structure. The Pennant series of the Bristol and South Wales coalfields has on the other hand undergone marked diagenesis and contains abundant fine coal partings and black carbonaceous grains.

The decomposition products may become dissolved, transported and reprecipitated during stages of diagenesis. Most of the fluid organic matter, i.e. oil and gas has however been introduced into the sandstone after deposition by migration from beds in which the organic matter was indigenous.

2.2.4 Determination of mineralogy.

It is not within the scope of this thesis to fully describe the methods available for the determination of sandstone mineralogy. A brief outline is presented of the methods used during this research and the reader is referred to a number of useful texts:

i) Thin section microscopy

Thin section microscopy is the most useful tool for the determination of rock mineralogy and texture and when combined with point counting methods, allows the quantification of mineralogy. A Nikon Optiphot binocular polarizing microscope was used during this research for the examination of mineralogy and texture. The mangifications normally used were x40, x100 and x200. In addition, for the coarsest grained sandstone varieties, a x2 objective lens was obtained to give a low magnification of x20, (x2 objective lense and a x10 eye piece).

A plethera of useful texts have been published on the subject of optical microscopy. Two of the most useful texts are "The Atlas of Sedimentary Rock Forming Minerals in Thin Section", by Adams et al, (1984) and "Colour Guide to

minerals and cements of sandstones and associated rocks", by Scholle, (1979).

ii) Scanning electron microscopy

With scanning electron microscopy, (SEM) geologists are able to go one step beyond thin section analysis - to look into pores, identify the smallest minerals , and examine the distribution of these minerals within the pores. Other advantages are the ease of sample preparation, greater depth of field and resolution and a significantly higher magnification range. (most SEM analysis of rocks involves magnifications between 10x to 20,000x).

The SEM micrographs presented in this thesis were taken using a Cambridge 250 Mk III scanning electron microscope. SEM's can be used in a number of different ways. The method used during this research is termed Secondary Electron Imaging.

Minerals were identified with the aid of two publications: "SEM Petrology Analysis", AAPG, (1984) and "Electron Micrographs of Clay Minerals", Sudo et al , (1981).

iii) X-ray diffraction

The X-ray diffraction analyses (XRD) carried out during the research were undertaken by scanning samples with a Philips PW 1730/10 diffractometer operated by an Apple microcomputer system. Material prepared for the XRD analysis was either representative of the whole sample and termed 'whole rock', or was segregated to consist of fine material, largely clay minerals and termed 'clay smears'.

Identification of clay minerals on the XRD traces was performed following the procedures of Brindley and Brown, (1980).

2.3 Texture

The texture of a sandstone includes all the descriptors of the geometry, size and shape of particles and pores that together form the rock - and their spatial interrelationships. Sedimentologists normally study sandstone texture from the point of view of identification of the environment of deposition. The approach of a rock mechanician as in this research looks at the texture of the sandstone from the point of view of influencing the behaviour of the rock when subjected to external stresses. The previous section described the constituent elements of sandstone framework while this section examines the physical features of those elements and how they are linked to form a complete geomaterial.

2.3.1 Grain Size

Sandstones, according to engineering geological definition, have grain sizes ranging from 0.06mm to 2mm. This comprises a huge range in sizes: a spherical grain 2mm in diameter has a volume of about 4.18mm^3 while a grain 0.06mm in diameter has a volume of about 0.000113 mm^3. It is reasonable therefore to assume that a fine grained sandstone will behave in a markedly different way from a coarse sandstone when subjected to external stresses.

The definition of the term size when applied to irregularly shaped objects such as sand grains depends on the method of measurement. The numerous methods of measurement and their associated definitions of grain size have been reviewed by Allen, (1981). One of the most common measurements of grain size limits is based on sieve analysis . In this method the limiting factor is the minimum square aperture through which the particle will pass; (BS 1377; 1975). This method is the preferred one for unconsolidated sands and friable sandstones but is impractical for well cemented sandstones. Very weak to weak sandstones can be broken down carefully and then sieved but disaggregation of stronger samples would pulverise some grains while leaving others larger than their original size due to the adhesion of cements of overgrowths.

Thin section analysis is the normal method for estimating the grain size of completely cemented sandstones. There are however problems with thin section analysis:

i) It is not possible to observe the maximum size of all the grains (and pores) in a thin section since the plane through which the section is cut will not cross through all the grain diameters.

ii) Sieve analysis cannot be correlated with thin section estimates without the application of correction factors. The problem is now better understood since the work of Harrell and Eriksson in 1979. In a later paper Harrell (1980) suggests that other errors can occur in grain size measurement due to the thickness of the slide. (normally 30 microns).

Thin section analysis remains however the standard way of determining grain size in cemented rocks. Scanning electron microscopy can be useful due to the greater depth of field and resultant 3-dimensional view of rock texture. This is especially useful in "clean" sandstones where the grains are not obscured by clay minerals.

In geotechnics, the range of particle size in sandstones has been divided into 3 size grades which do not correspond directly to the scale used by geologists; the two grade scales are compared in Figures 1.1 and 1.2. It approximates to the log scale devised by Wentworth, (1922) and Krumbein, (1934) to compensate for the fact that a difference of 1 mm between sand grains is significant but between boulders is trivial.

2.3.2 Grain shape

Grain shape and roundness are functions of the grain geometry and mineralogy of the initial grains. Certain morphological changes will take place to these grains by the process of transportation during which the detritus will suffer abrasion, solution and current sorting. The extent to which these occur depends on the mineralogy, transport process and other geological controls such as relief which influences the energy of the transporting medium. Shape is defined by various ratios of the axes of a particle - long (L), intermediate (I), and short (S). Two aspects of shape have been identified: sphericity and form. Sphericity is a quantitative parameter measuring the departure of a body from equidimensionality. Sneed and Folk, (1958) suggested the maximum projection sphericity which is the ratio of the cross-sectional area of a sphere of the same volume as the particle divided by its maximum projection area; this is quantitatively defined as:

$$\Psi_p = \frac{\sqrt[3]{S^2}}{LI} \qquad (2.1)$$

where S = short axis

L = long axis

I = intermediate axis

Form describes the geometrical shape to which the grain approximates, be it a cube, cuboid, pyramid, etc. It is important to note that these aspects of grain shape are relatively easy to determine in sands (Sneed and Folk, 1958) but cannot be applied directly to the 2-dimensional image formed by thin section analysis. It is suggested that thin sections cut parallel to bedding will normally give information about the long and intermediate axes while sections cut perpendicular to bedding will show two axes, one of which will be the short axis (S). This is based on the fact that grains will settle, during deposition in a position which brings their centre of gravity closest to the substrate on which it rests i.e. where the intermediate and short axes differ markedly, the grain will topple or roll into a position of lower potential energy. This may not however be the case in sandstones which contain cross-bedding or other internal sedimentary structures.

Roundness is geometrically distinct from shape and is concerned with the curvature of grain corners. It is quantitatively defined as:

$$\sum_{i=1}^{n} \frac{r_i / R}{n} \qquad (2.2)$$

Where r_i is the radius of the circle inscribed in the ith corner of the grain, n is

the number of corners of a grain and R is the smallest radius that will circumscribe the grain.(Waddel, 1935)

Generally however, standard sets of images are used to estimate roundness from angular to well rounded as quantitatively defined. (Krumbein, 1934). Since any one corner of a particular grain will be subjected to the same intensity and degree of rounding, and likewise for edges, it is pertinent to assume that a 2-dimensional image of a grain, such as in thin section will give a good approximation to the actual 3-dimensional roundness. Therefore the quantitative roundness equation (2.2) can be applied more directly to thin section analysis than the maximum projection sphericity equation of Sneed and Folk.

Grain shape and size are known to affect the electrical formation factor (ratio of resistivity of a porous medium to the resistivity of the pore fluid) of sandstones. (Jackson et al, 1978) i.e. different shapes of framework grains alter the geometry of the pore system and thus alter the electrical resistance.

Despite having received little attention in the past, it is considered that grain shape will have a profound effect on the failure characteristics of a particular sandstone. This will be discussed further in Chapter 5.

2.3.3 Grain contacts and packing

Grain to grain relationships as seen in thin section are described by a combination of qualitative terms and quantitative indices, both of which attempt to infer 3-dimensional relationships in the plane of the thin section.

Pettijohn et al (1987) have suggested that sedimentology lacks a systematic knowledge of the spatial distribution of fabric types in a sandstone body. The main impediment to this is lack of reliable instumentation that could determine grain to grain relationships more quickly than grain-by-grain microscopic counting methods and perhaps do so in 3-dimensions as well.

Another difficulty in mapping fabric type is that fabric is highly variable - much like the permeability as can be seen in many single thin sections. Some of this variation is linked to primary deposition, subtle differences in original grain-to-grain relationships being characteristic of each lamination and bed. Figure 2.1 shows the main types of contact observed in sandstones. The term 'triple point' is here introduced to describe the feature observed in some highly indurated sandstones where three grains are welded together, (usually quartz) with no pore space between them. It is suggested that the presence of these triple points will inhibit relative movement of the grains and hence increase strength. The term is analagous to its usage in tectonics. Table 2.1 lists some of the qualitative and quantitative terms defined by various workers to specify sandstone fabric:

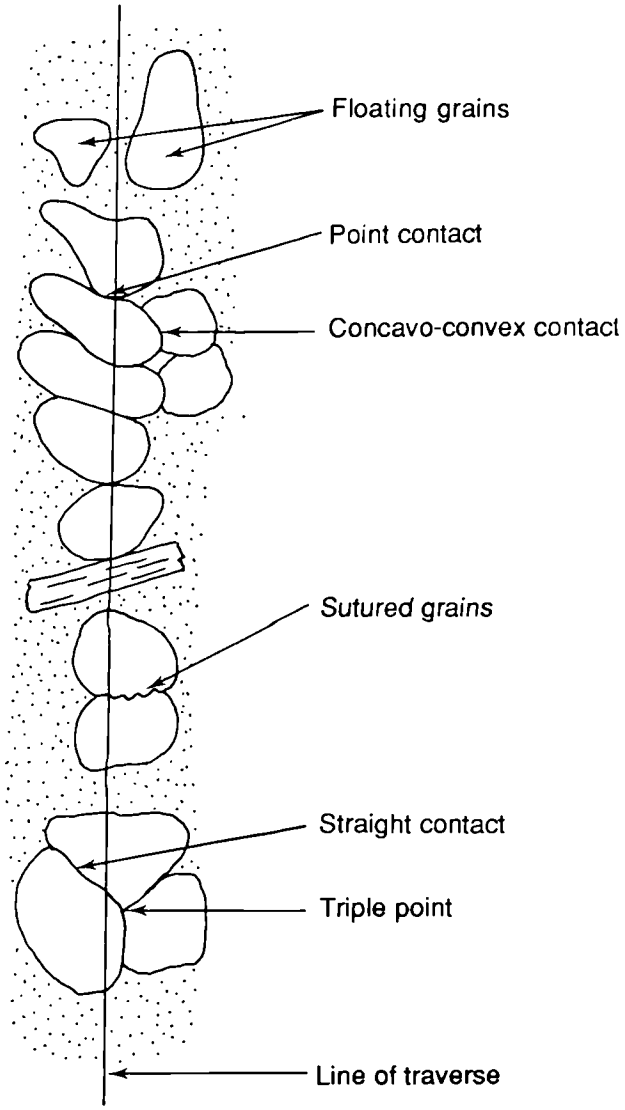

Figure 2.1 Idealised representation of grain contact types observed in sandstones. (Modified after Pettijohn et al, 1987).

QUALITATIVE	QUANTITATIVE
Concavo-convex contact	Condensation index
Contact strength	Contact index
Framework fraction	Packing density
Long contact	Packing index
Sutured contact	Packing proximity
Tangential contact	Weighted contact packing

Table 2.1 Various terms used to specify sandstone fabric.

Cathodo-luminesence is reported to be of more use in the study of grain contact types than is the petrographic microscope. (Nickel, 1978).

An exceptional example of the relationship between grain fabrics and rock behaviour is the flexible sandstone called itacolumites - whose fabrics have been analysed by Dusseault (1980).

2.3.4.Grain orientation

Grain orientation is primarily related to the depositional regime. Hiscott and Middleton, (1980) studied whether grain orientation is related to a unimodal current direction or is it totally random as a result of bioturbation or mass flow.

Apparent grain orientations can also be related to flattening of grains due to tectonic stress e.g. as in the Old Red Sandstone deposits of the Dingle Peninsula.

Sedimentologists have however neglected studies on grain orientation because paleocurrent data is more readily obtained from sedimentary structures. Shape fabrics can be measured directly by apparent long axis in oriented thin sections (or from photographs of them), by photometric methods using thin sections, by magnetic susceptibility and by anisotropic electrical conductivity. Taira and Lienert (1979) compared the different methods and found good correlation.

Grain orientation has been found to be related to permeability. No rock mechanics correlation between loading direction and grain orientation has been reported but it is considered that a cleaved sandstone could have a high strength anisotropy.

2.3.5 Porosity

i) Total porosity.

Total porosity is defined as:

$$\text{Total porosity} = \frac{\text{bulk volume - solid volume}}{\text{bulk volume}} \times 100 \qquad (2.3)$$

Four distinct types of porosity have been identified which together constitute the total porosity of a sandstone:

1) intergranular (interparticulate)
2) intragranular (intraparticulate)
3) fracture porosity
4) solution porosity

see Figure 2.2.

Figure 2.2(a) Photomicrograph of Penrith Sandstone (type A) in plane polarized light. Porosity is shown by the blue resin impregnation. Scale 50 divisions : 1.25mm

Figure 2.2(b) Sketch drawn from photomicrograph illustrating the various types of porosity occurring in sandstones.

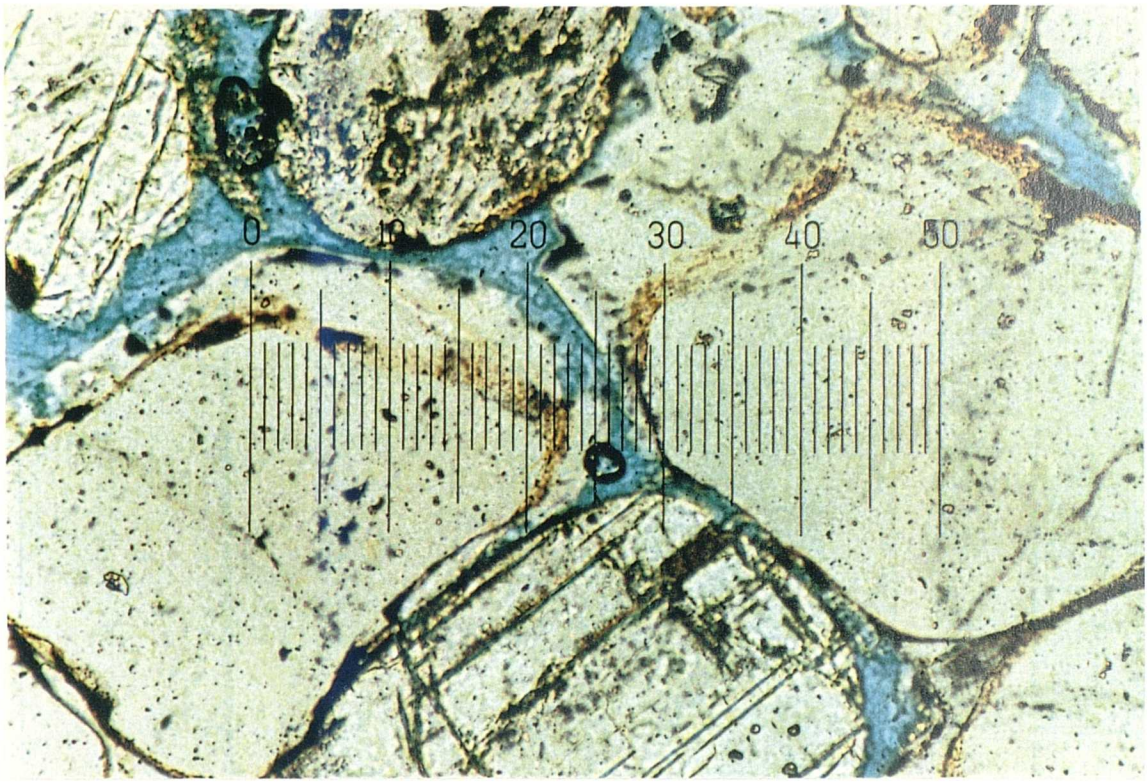
0
10
20
30
40
50

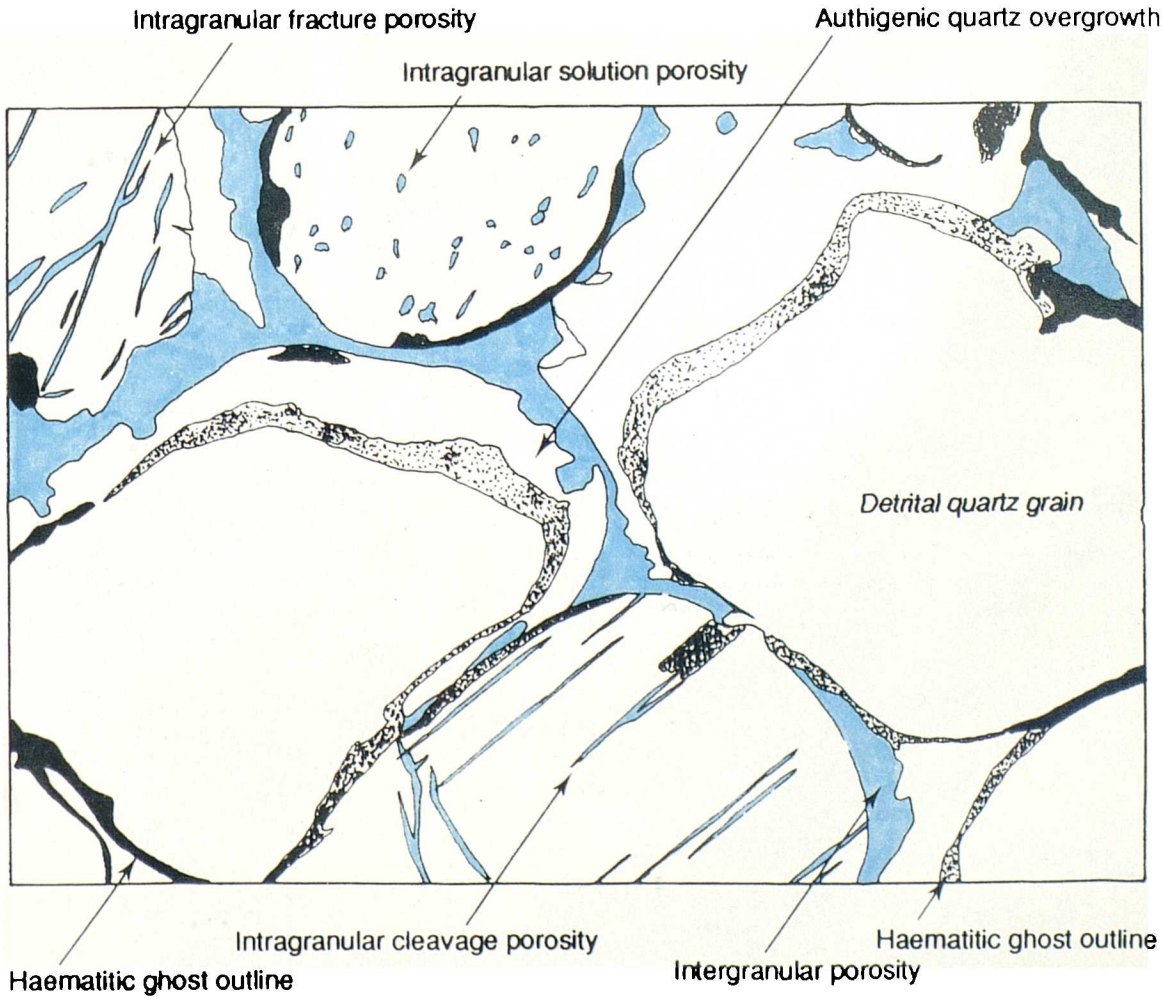
Intragranular fracture porosity
Authigenic quartz overgrowth
Intragranular solution porosity
Detrital quartz grain
Intragranular cleavage porosity
Haematitic ghost outline
Haematitic ghost outline
Intergranular porosity

Intergranular porosity consists of the voids between framework grains, small detrital grains and/or dense authigenic minerals. (quartz and calcite overgrowths). In newly deposited sands, the primary intergranular porosity is high, greater than 40% in some cases. The pores are connected, pore apertures are large and permeability is high. Work by Graton and Fraser, (1935) on equal sized spheres showed that a cubic packing system produces an intergranular porosity of 47.6% while a rhombohedral packing arrangement gives 25.9%. These theoretical maxima bear little significance to sandstones since the latter consist of non-spherical framework grains of mixed sizes and during diagenesis are subjected to pore filling cements and the influx of interstitial clays.

Intragranular porosity is formed within grains such as lithic rock fragments and in most authigenic clays. Clays such as smectite and kaolinite can absorb up to 40% water by volume therefore a sandstone containing a high proportion of detrital and/or authigenic clay will have a high intragranular porosity. The term microporosity is used to describe the type of porosity in clays since the apertures are generally less than 0.5 microns. Permeability of clay rich sandstones is low as a result.

Fractures formed on a micro- and macro- scale during tectonic rock deformation produce fracture porosity. They may pass through both framework and cement and in many cases will link previously unconnected pores. Isolated microfractures which follow grain boundaries must also be included within this category.

Solution porosity is related to the solution of framework or cements. The latter is also included within secondary porosity.

Secondary porosity is a term used to describe the origin of particular porosity types. It refers to porosity formation during diagenesis by the following processes:(1) mesogenetic leaching of carbonate minerals; (2) fracturing; and, (3) shrinkage. (Schmidt and McDonald, 1979).

The only method for determining total porosity is by the disaggregation method. The volume of a dry sample is measured by mercury displacement or by measurement of dimensions if the sample is of regular shape. The rock is then ground to a fine powder and the solid volume determined by liquid displacement or by use of a compression chamber.

ii) Effective porosity

During compaction and later stage diagenesis, some of the pores within a sandstone will become isolated from their neighbours due to pore throats becoming filled with authigenic overgrowths or interstitial clays. The effective porosity refers to

the volume of interconnected pores within a rock and is defined as:

$$\text{Effective porosity} = \frac{\text{interconnected pore volume}}{\text{bulk volume}} \times 100 \qquad (2.4)$$

The effective porosity is invariably less than the total porosity but is normally taken as the porosity of the rock . For the reservoir geologist or hydrogeologist the effective porosity is of prime importance since it controls the transmissivity, storage coefficient and potential discharge of fluid from a reservoir or aquifer. Work by Beard and Weyl, (1973) has shown that grain size and sorting affect porosity and permeability in different ways depending on the environment of deposition. Generally, however for sandstones the permeability increases with effective porosity.

The rock mechanician, interested in the strength and deformability of a sandstone is more concerned with the total porosity rather than the effective porosity. The higher the volume of pores whether connected or unconnected, the less rock framework is present and the more easily deformed the rock. As described above however, total porosity is extremely difficult to measure.

Pirson, (1958) and Monicard, (1980) reviewed the many different laboratory techniques used to determine porosity.

Effective porosity of sandstones can be determined by a number of methods: the two methods used in this research are the mercury porometer and the resaturation technique.

1. Mercury porometer

The mercury porometer manufactured by Ruska Instrument Corporation is widely used for the effective porosity of consolidated rock specimens. It lends itself to use by two methods: the Kobe or Boyle's Law method and the mercury injection method.

The porometer consists of a 100cc volumetric mercury pump to which a pycnometer is attached. The chamber of the pycnometer admits cores up to 30mm long and 37mm diameter. The micrometer dial scales provide direct readings of volumes to 0.01cc. For porosity measurements where accuracy is the prime factor, the Boyle's Law method is commonly used. In this method a fixed volumes of air from 40cc to 16cc are compressed to an indicated volume at a reference pressure, usually 207 kPa, (30psi). This procedure is a preliminary calibration to give a graphical relationship of the apparatus to various grain volumes which facilitates future grain volume measurements. The procedure is then repeated with the core specimen in the pycnometer, providing data from which the core grain volume is readily calculated. The bulk volume of the core is measured by mercury displacement in the pycnometer

and read directly from the volume scale. Following the application of a correction factor for variation in atmospheric pressure, the porosity is calculated by :

$$n = 1 - \frac{VG}{VB} \times 100 \qquad (2.5)$$

where VG = grain volume
VB = bulk volume

Since the sample is penetrated only by air, it can be used for additional core analysis tests.

The mercury injection method is quicker but is not as accurate as the Boyle's Law method and also leaves the sample contaminated with mercury. Bulk volume is obtained in the usual way and the pore volume is obtained by measuring the volume of mercury forced into the pore spaces at high pressures. (4900 kPa).

Table 2.2 lists the advantages and disadvantages of the two methods. Clearly, the Boyle's Law method, despite being slow, is preferable over the mercury injection method.

	Advantages	Disadvantages
Mercury injection Method	Rapid	Mercury contamination Error due to capillary effects Correction factor compensate for air entrapped in the pore spaces
Boyle's Law Method	Accurate Core can be used for further analysis Only air injected into the specimen so no capillary action or entrapment correction required.	Slow

Table 2.2 Comparison between the two porometer methods.

The Boyle's Law method for the determination of effective porosity was used throughout this research, the results of which are presented in Chapter 3.

2) The Resaturation Technique.

The resaturation technique basically measures the weight of water in a sample when saturated. The stages are as follows:

i) Sample preparation
ii) Volume calculation
iii) Oven dried at a temperature of 50°C
iv) Cooled in a dessicator
v) Weighed
vi) Saturated
vii) Reweighed

$$\text{Effective porosity, } n = \frac{Vv}{V} = \frac{(sw - dw)}{w.V} \times 100 \qquad (2.6)$$

where Vv = volume of interconnected voids
V = total sample volume
sw = saturated weight
dw = dry weight
w = density of deionised water

The samples from each sandstone type were prepared as cylindrical specimens measuring 136.8 ±0.2mm long by 54.7 ±0.1mm diameter. The volume of each sample was easily calculated using the formula $\pi r^2 h$.

Samples were oven dried at 50°C and when constant weight was attained, allowed to cool in a dessicator over $CaCO_3$. The dry samples were then weighed accurate to 0.1g. The next stage involved the saturation of the samples; a number of techniques were attempted:

i) Samples were soaked in deionised water at atmospheric pressure for periods of up to two months in an attempt to attain constant weights. High porosity sandstones reached constant weights after periods ranging from two weeks to 1 month while samples with lower porosities (< 10%) often did not achieve constant weight even after two months. On fracturing some of these samples such as the Pennant of the Bristol area, the inner area of the specimens were seen to be dry.

ii) In an effort to increase saturation rates in the high porosity/ permeability sandstones, a vacuum system was designed. (Figure 2.3). Dobereiner (1982) recommended the

use of vacuum saturation on weak sandstones. It was realised that higher suctions or longer durations of treatment would be required for many of the lower porosity sandstones studied in this research. The vacuum pump used was a rotary type capable of creating a negative pressure of up to 200 kPa.

A number of samples were tested in the oven-dry state and a number which had been soaking for 1 month. A summary of the results of vacuum saturation are shown in Table 2.3.

The results demonstrate that the benefits of using this type of saturation are not great, especially for the low porosity sandstones, where in some cases the degree of saturation actually decreased from the soaked state.

Porosity (n)	Sample Conditions	Effect of vacuum saturation.	Results
< 10%	Oven-dry	Resulting weight after 2 hours equal to 2 months normal soaking.	More rapid saturation.
	Soaked	No increase in weight after vac. saturation.	No benefit.
> 10%	Oven-dry	Weight equivalent to or slightly less than 2 months soaking.	No benefit/ detrimental
	Soaked	Weight often less than that for 2 months soaking.	Detrimental to satn. in samples of low n.

Table 2.3 Results of vacuum treatment of sandstone specimens.

iii) A pressurising system was designed and constructed for use on the cored samples. Figure 2.4 and Plates 2.1 and 2.2. The pressure cell was machined from HE30 TE aluminium alloy with wall thickness calculated to be able to withstand internal positive pressures of up to 5500kPa with a factor of safety against failure of 3.

An automatic pressure release safety valve was fitted to the cell and set at a release pressure of 1400kPa. The cell was designed to take NX sized cores with an

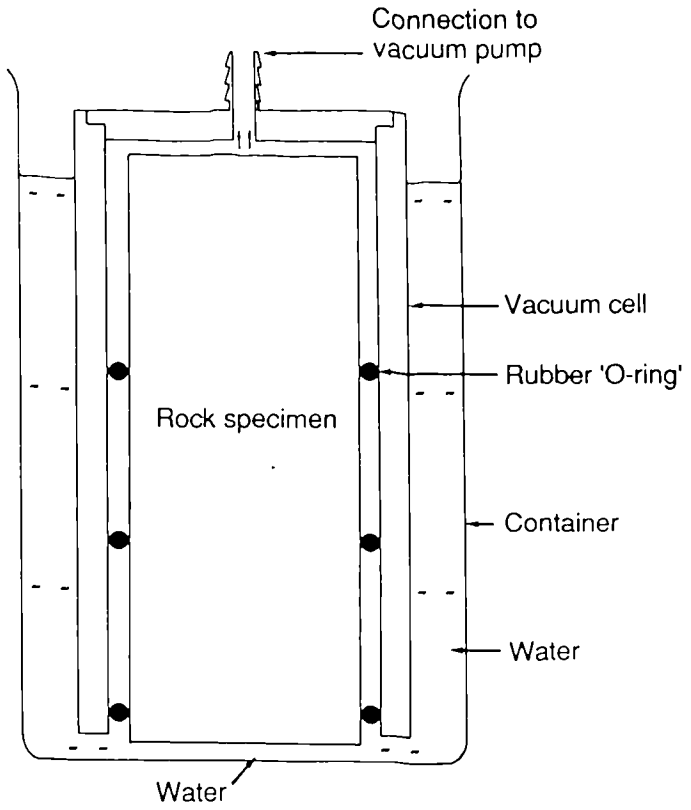

Figure 2.3 Vacuum system used for attempted saturation of sandstone specimens. (Rock specimen is 136.9mm long).

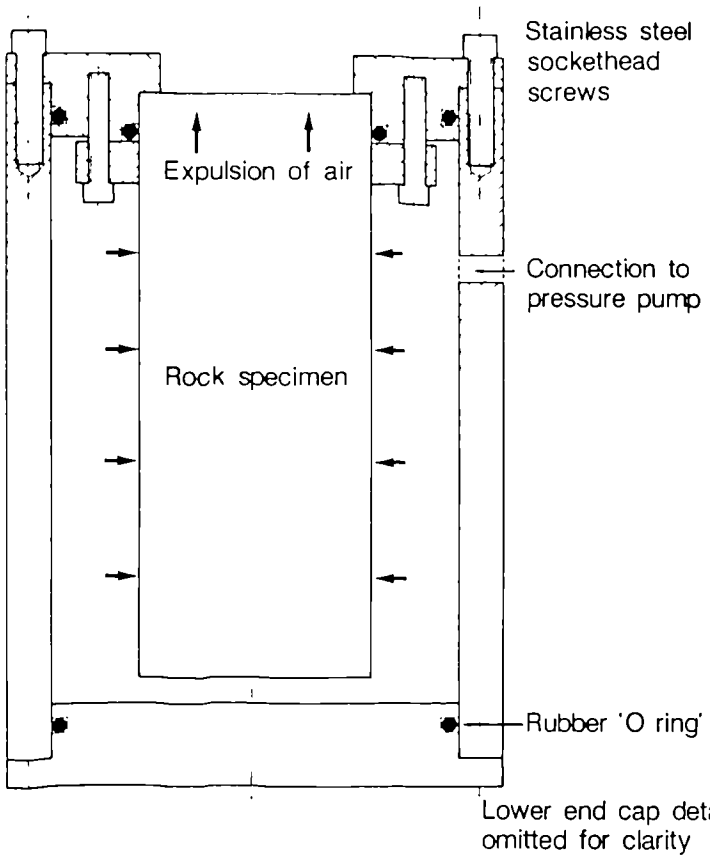

Figure 2.4 Pressure cell designed for saturation of sandstone specimens. (Rock specimen is 136.9mm long).

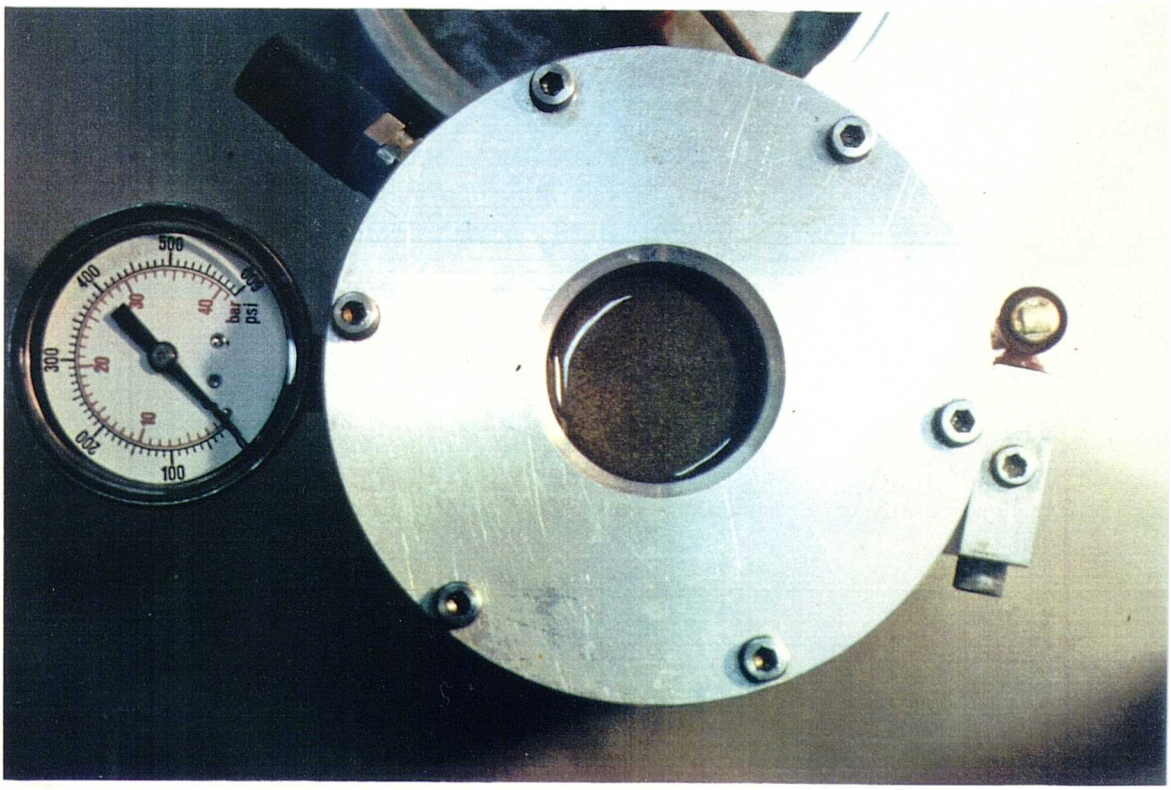

Plate 2.1 Pressure cell used for saturation of sandstone specimens.
(a) Specimen clamped into lid prior to closure of cell. (Specimen is 54.75mm diameter).
(b) Plan view of cell during saturation.

aspect ratio of 2.5:1. The arrangement for sealing the samples into the cell can be seen in Figure 2.4. The upper end of the sample remains open to the atmosphere while the remainder of the surface area is subject to all round hydrostatic pressure. The sample is sealed by a system of rubber O-rings which prevents any pressure dissipation along the rock surface, forcing pressure differential to occur between the open end surface and the rock pores.

The cell itself is deaired by filling both it and the pump reservoir with deionised water and lowering the lid, with the clamped sample, into the water. The system is then bled to remove all air and the valve closed. The pressure is increased to the required level and maintained by means of a high pressure pump and non return valve.

From the dry state, water begins to emerge from the top end of the specimen. As the portal fills with water, steams of air bubbles can be seen issuing from some of the pores. In lower porosity rocks air is forced from the sample rather more slowly and forms tiny bubbles on the rock surface.

The system gave good results over relatively short periods of treatment. Penrith Sandstone (type A) for example, with an effective porosity of 12% reached maximum recorded saturation after 30 minutes; this value being higher than any achieved by normal soaking of this sandstone for 1 month.

Doubts were voiced about the effects of high pressure treatment on the sandstone microfabric,, based on the fact that sandstones will hydrofracture when the hydrostatic fluid pressure exceeds the confining pressure. (Jaeger and Cook, 1976). This will only happen however when a stress gradient exists, across the rock body, which is greater than the tensile strength of the rock framework. Since the water pressure was acting inwards and not confined by any rock material, it was not considered that pressure treatment would have any detrimental effect on the sandstone microfabric.

One possible failure mechanism might be the collapse of previously unconnected pores due to external pressure in neighbouring pores. However, a pressure of 1400kPa is highly unlikely to cause the collapse of such pores whose cross-sectional area would be in the region of 0.03mm2.

2.4 Density

Density is defined as mass per unit volume. The mass of a unit volume of rock in its natural state is different from the mass of the same volume of rock consisting only of its solid phase. The terms dry bulk density, saturated bulk density and grain density are therefore used.

2.4.1 Dry bulk Density

The bulk density is defined as the mass of a unit volume of a rock. It depends on the mineralogical composition, porosity, amount of water and amount of air present in the pores. If the volume of the specimen is Vb (i.e. pore volume Vp + grain volume Vg) and the bulk specimen mass is mb (mass of grains mg + mass of water in the pores mw), then

$$\text{bulk density, } \rho = \frac{mb}{Vb} \tag{2.7}$$

$$= \frac{mg + mw}{Vp + Vg} \tag{2.8}$$

If the rock is completely dry, then the dry bulk density of the rock is given by:

$$\rho d = \frac{mg}{Vp + Vg} \tag{2.9}$$

The dry bulk density was determined using the 'Method of measurements', whereby the volume of the regularly spaced cylinders is calculated. This was carried out using a Vernier caliper measuring the specimens both at the two ends and at the middle twice at right angles to each other, and measuring the heights at four points (ends of two diameters at 90° to each other drawn on flat ends). The average values were then inserted into the equation:

$$Vb = \pi r^2 h \tag{2.10}$$

The air was then removed from the rock samples by forced drying in an oven at a temperature of 50° C for a period of two weeks. After cooling in a dessicator the specimens were weighed and the dry bulk density calculated from equation 2.9.

2.4.2 Saturated bulk density

If a rock is saturated with water, then the saturated bulk density, ρs is calculated from the equation:

$$\rho s = \frac{mg + (Vp \times \text{density of water})}{Vp + Vg} \tag{2.11}$$

The saturation of each specimen was achieved using the pressurising cell produced for porosity measurements. (Section 2.3.5). Volume is calculated in the same way as for dry bulk density.

2.4.3 Grain density.

The grain density of a sandstone ρg is the mass of a unit volume of the grains (i.e. solid phase of mineral skeleton) of a rock:

$$\rho g = \frac{mg}{Vg} \tag{2.12}$$

where mg = mass of grains, and
Vg = volume of grains.

The grain density of a rock is wholly dependant on the density of the minerals forming it and is calculated by the formula:

$$\rho g = \sum_{i=1}^{i=n} \rho i.Vi \tag{2.13}$$

where n = number of minerals forming the rock
ρi = grain density of each mineral, and
Vi = volume of each mineral.

The densities of the sandstone-forming minerals and rock fragments are given in Table 2.4. From the table it can be seen that a huge range of densities exists among the sandstone-forming minerals. For the main framework grains the densities fall between 2.54-3.10. It is important to know the relationship between grain density and porosity for a particular sandstone since two sandstones could have the same densities but different porosities due to their constituent minerals and therefore have markedly different geomechanical properties. This will be discussed further in Chapter 5.

In theory, the formula for calculating grain density is the correct one but in practice it is difficult to apply since many sandstone-forming minerals show a range in densities. Since it is impossible to determine the exact densities of the constituents, a simpler approximation to grain density is given by:

$$\rho g = \frac{mg}{Vb-Vp} \tag{2.14}$$

where Vb = bulk volume
Vp = volume of pores, (porosity)

Mineral or Rock Fragment	Sp. Gr.	Moh's Scale
quartz	2.65	7
chert	2.64-2.75	7
microcline	2.54-2.57	6
orthoclase	2.57	6
plagioclase	2.62-2.76	6
biotite	2.8-3.2	2.5-3
muscovite	2.8-2.9	2.76-3.1
chlorite	2.6-2.9	2-2.5
clays	2.60-2.63	2-2.5
tourmaline	3.0-3.25	7
zircon	4.68	7.5
rutile	4.18-4.25	6-6.5
shale	2.06-2.66	-
slate	2.72-2.84	-
mudstone	1.76-2.40	-
phyllite	2.20-2.40	-
schists	2.70-3.03	-
basalt	2.21-2.77	-
andesite	2.53-2.62	-
carbonate rock	2.37-2.75	-
calcite	2.71	2.5-3..5
dolomite	2.75-2.85	3.5-4
gypsum	2.32	2
anhydrite	2.89-2.98	3-3.5
barite	4.5	3-3.5
pyrite	5.02	6-6.5
phosphate	3.15-3.20	5
glauconite	2.70	2
haemetite	4.8-5.3	5.5-6.5
limonite	4.0	3-5.5
organics	-	-
magnetite	5.2-6.99	6

Table 2.4. Specific gravities and hardnesses of the main sandstone forming components. (Sources; Hoek and Bray, 1974; Jumikis, 1983; Hurlbut and Klein, 1977; Deer, Howie and Zussman, 1982).

2.5 Macroscale Sedimentary Features

Like texture and composition, bedding and sedimentary structures are inherent in sedimentary rocks. Both are made visible by variations in grain size and mineralogy, (especially in chemically formed structures). These features normally manifest themselves on a macroscopic scale and therefore microscopic examinations are inappropriate.

For this reason, like discontinuities, they influence the behaviour of the rock mass rather than the rock material itself. Macroscale sedimentary features are therefore not covered in great detail in this research.

There are four broad types of sedimentary structures: (1) current structures; (2) deformational structures, (formed shortly after deposition); (3) biogenic structures; and (4) chemical structures.

2.5.1 Current Structures

These are formed by currents of water, air or ice as sediment is transported and deposited. The features produced can be described as various forms of bedding. The basic properties of a bed are an upper and lower bounding surface - the bedding planes, thickness and lateral continuity. Various classifications of bedding plane types and thickness have been proposed; BS 5930 presents a classification based purely on the basis of bed thickness, ranging from very thickly bedded, (> 2m) to thinly laminated, (< 6mm). It is also important to note however whether the rock possesses distinct bedding planes or internal, less well developed bedding which is seen purely as a colour or slight grain size change.

Well developed bedding planes are produced by cessations in deposition during which grains of lower settling velocity are laid down. e.g. Mica along the bedding planes of Donegal Quartzite. The rock generally splits by stress relief along these planes during unloading.

Internal bedding does not provide planes of weakness on a macroscale since they are produced by periods of less than normal deposition. They therefore alternating layers of differing grain sizes and mineralogy.

Cross-bedding, common in many sandstones exists as both external and internal features within beds. The internal planar cross-sets in the Old Red Sandstone of The Forest of Dean are functions of mineralogy and may affect deformability on the microscale.

Graded bedding found in many turbidites is defined by an upward decline in grain size within a bed. This will produce a non-uniformity of geomechanical behaviour within a bed as a function of grain size variation.

Finally, currents can produce irregularities and sole markings within and on the base of beds. These may be important in providing asperities considered during slope stability analysis.

2.5.2 Deformational Structures

Various deformational structures are found in sediment following deposition or concurrent with it. these include ball-and-pillow structures, dish structures and load casts which are the most common. These form by:(1) convection cells with a loss of strength due to material becoming thixotropic; (2) instability due to oversteepening of depositional slopes producing a rapid slump or slide; (3) pseudoliquefaction of the sand producing a 'quicksand' capable of injection as sills and dykes. e.g. New Red Sandstone of north-east Ireland; and (4) collapse around melted ice blocks e.g. in glacial outwash deposits.

The resulting structures upset any planar uniformity within the deposits and may in fact, following diagenesis, produce rocks with less preferred weakness orientations and overall stronger nature.

2.5.3 Biogenic Structures

Biogenic structures are those formed as tracks, trails and burrows or by plants. They generally have only a very localized extent and associated geomechanical effect. Where extensive burrowing has taken place, the sediment becomes bioturbated causing a mixing of layers and disruption of planar bedding.

2.5.4 Chemically formed structures

This category of structure is more important to the subject of rock mechanics than deformational or biogenic structures since they include concretionary nodules which can be of great lateral extent and have markedly different strength properties. Also included are stylolites and Liesegang banding.

The Jurassic and Cretaceous strata of southern England are well known for their concretionary nodules and bands e.g. The Bridport Sands and the Upper Greensand. These nodules can be up to three metres long and are generally spherical or ellipsoidal, being flattened parallel to bedding. Where their nucleii are closely spaced they can link to form a continuous bed. e.g. Potterne Rock of Devizes in Wiltshire. Their mode of origin has been the subject of much debate resulting in a plethera of published work; notably Allison, (1987).

They are widely considered to have formed on the sea floor, their position in the stratigraphic sequence being related to the presence of decomposing organisms which provide the raw material for their formation.

CHAPTER 3

THE STATIC PROPERTIES OF THE SANDSTONES STUDIED

The previous chapter outlines the static properties of sandstones in general and describes the most suitable methods for their determination. In this chapter, the static properties are described for each of the sandstones studied.

3.1. Mineralogy and Texture

Mineralogy was determined using standard thin section petrography, X-ray diffraction and scanning electron microscopy, as outlined in the last chapter. Mineralogy was quantified using standard point counting methods, over a sample population of 300 grains, (Carver, 1970), the results being expressed as a number frequency percentage. It is important to note that the percentage pore spaces determined from point counting is always an underestimate of true porosity since it is virtually impossible to detect microporosity using normal petrographic techniques. It has been shown that most errors tend to overestimate grain and cement volume and underestimate pore volume, (Halley, 1976).

X-ray diffraction processes and scanning electron microscopy were used to a limited extent for mineralogical work to identify specific mineral species which proved difficult to identify using normal microscopy.

Thin section photomicrographs in both plane polarized light and under crossed polars are included to demonstrate the various mineralogical and textural properties specific to each sandstone. They are included as good representations of the rock's petrology and texture as determined from a number of thin sections cut in planes both parallel and perpendicular to bedding. The photomicrographs show a fifty-division scale superimposed on them for grain size measurement. This was achieved by fitting a special graticule into the projection lens of a Nikon binocular polarizing microscope at the focal point of the lens so that it would always appear in focus with the subject. The graticule was then calibrated for different objective lenses using a stage mounted graticule and the result is that three different scales are used: 50 divisions to 2.5mm; 50 divisions to 1.25mm and 50 divisions to 0.5mm. Grain size measurements are quoted as the apparent size as determined from thin sections. These measurements are for the original detrital grains and do not include authigenic overgrowths.

During the examination of the sandstones in thin section, it was found that grain shapes and contacts could often be more clearly seen by reducing the angle

between the analyser and polarizer from the standard 90°. The other obvious effect of this action is to change the observed interference colours of the contained minerals, (e.g. quartz tends to a brown colour when the polarizing angle is less than 90°), but provided that other photographs are taken, the minerals can be identified correctly. Where photomicrographs have been taken with a reduced angle between analyser and polarizer it is denoted by 'P/A angle = 70°'.

Each sandstone is described below in terms of mineralogy and texture. The order used is one of geological age as in Chapter 1. In each case, the respective photomicrographs are included on the facing pages to the rock descriptions. Point counting results are presented in list form and a plot is included to show the position of each rock type on a quartz-feldspar-lithic rock fragment ternary diagram. Each deposit is named on the basis of its mineralogy using the Dott-Folk classification.

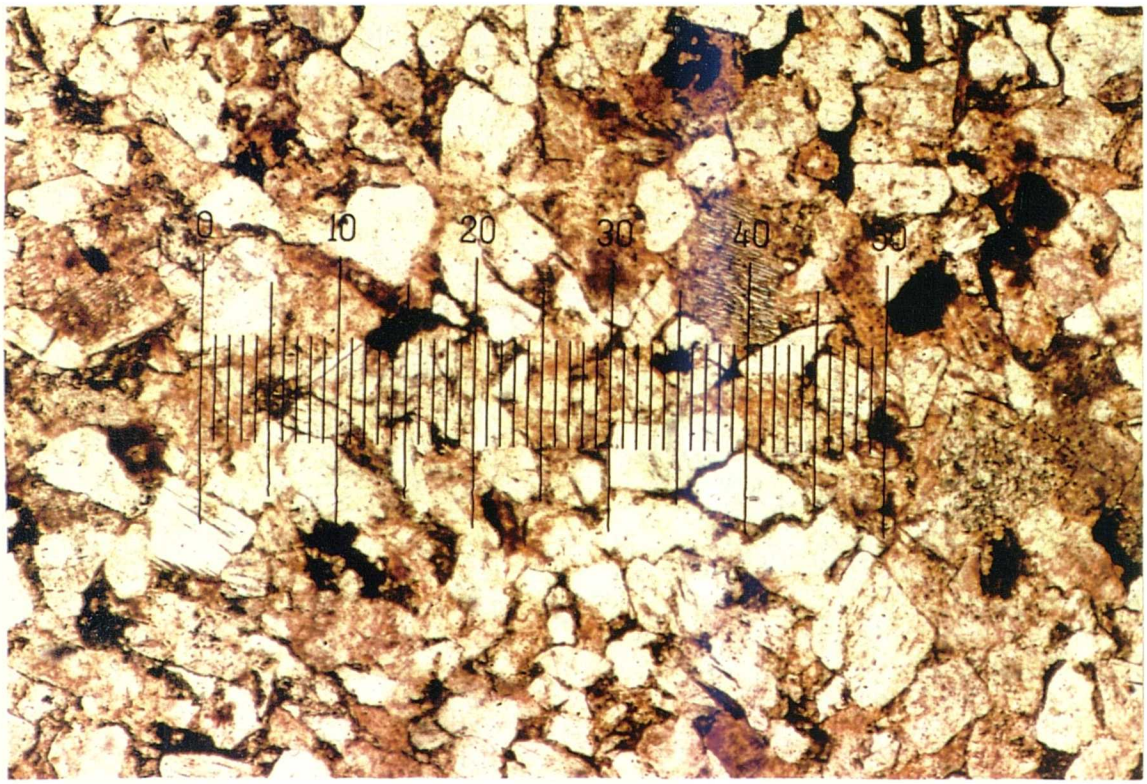

Plate 3.1 Applecross Sandstone. Section perpendicular to bedding under plane polarized light showing haematite cementation and immature texture.
Scale 50 divisions : 1.25mm.

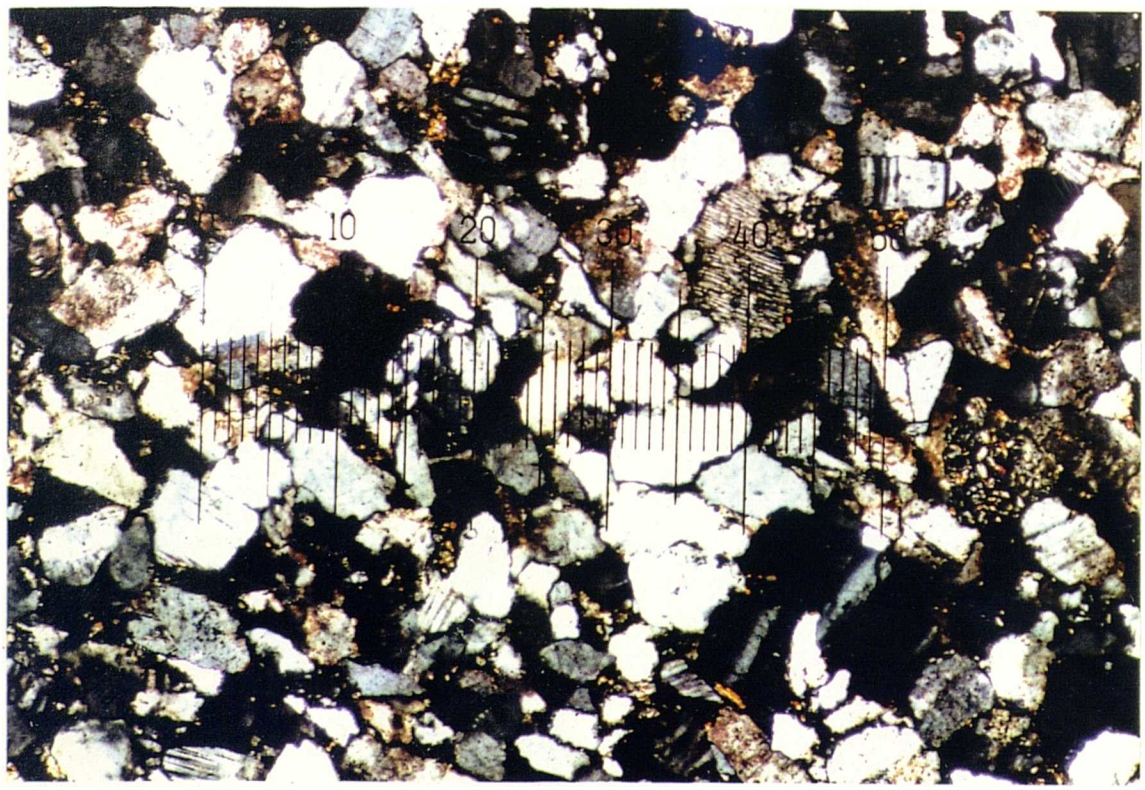

Plate 3.2 Applecross Sandstone under crossed polars showing abundant fresh feldspars.
Scale 50 divisions : 1.25mm

1. Applecross Sandstone (A)

Mineralogy:	%
Quartz	20.0
Alkali feldspar	44.3
Plagioclase feldspar	8.0
SRF's	1.3
MRF's	1.0
IRF's	1.0
Chlorite	8.0
Haematite	13.3
Clay minerals	3.0

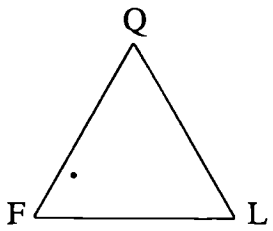

This variety of sandstone is mineralogically immature, with alkali and plagioclase feldspars being the most abundant minerals.The feldspars are remarkably fresh, showing little sign of seritization or kaolinisation. The framework grains are cemented by authigenic chlorite and haematite.

Grain size: The detrital grains are moderately well sorted, with a modal size range of 0.08 to 0.3mm, (fine sand).

Grain shape: Texturally immature. Grains are subangular to subrounded and of low sphericity.

Packing density: Vertical: 87.2 %
Horizontal: 83.0 %

Contacts: Concavo-convex with occasional sutured contacts.

Grain orientation: Little preferred orientation of grains.

Classification: *Arkose.*

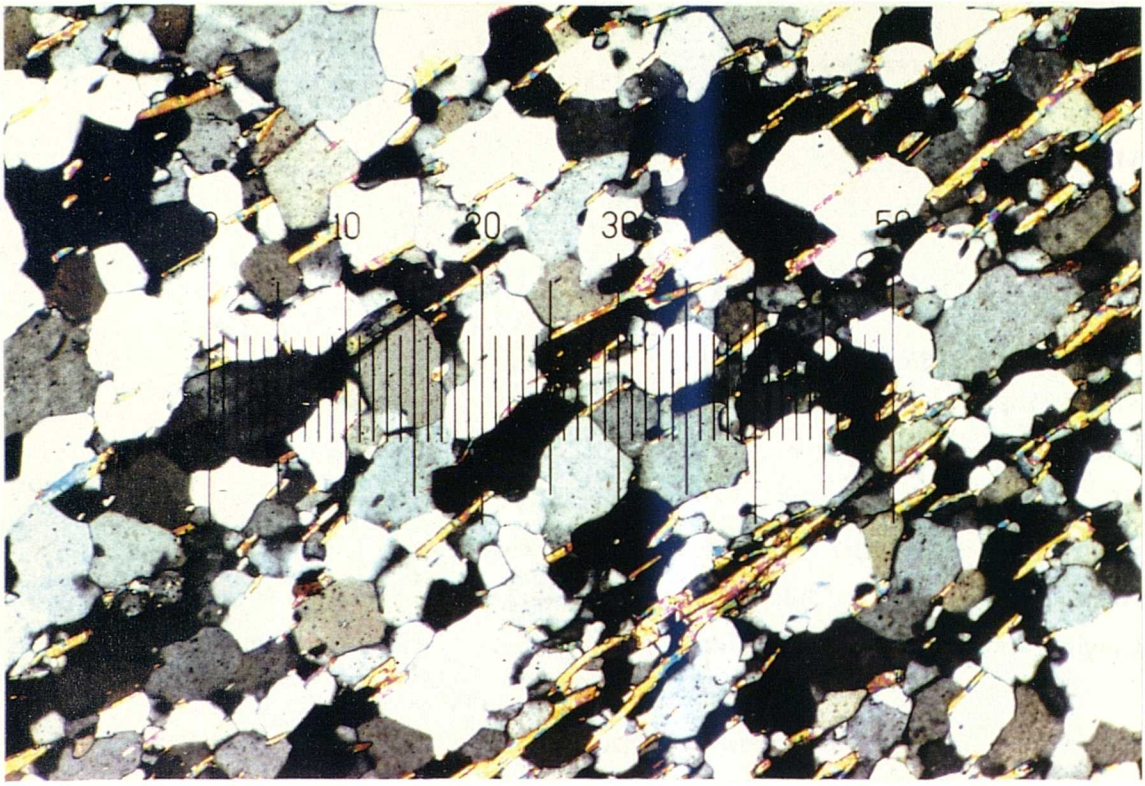

Plate 3.3 Donegal Quartzite. Section perpendicular to bedding under crossed polars. Muscovite flakes are aligned parallel to bedding. Elongated quartz grains also show some bedding-parallel alignment. Scale 50 divisions : 1.25mm.

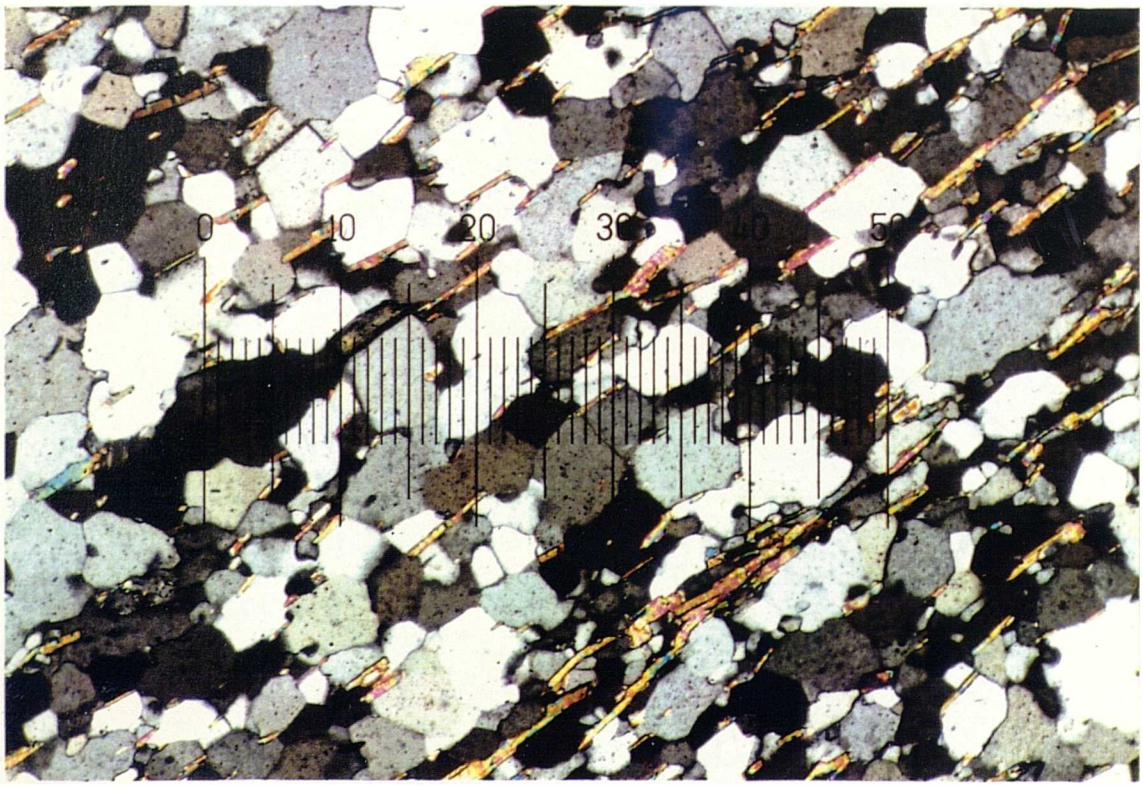

Plate 3.4 Donegal Quartzite under crossed polars with P/A angle = 70°. Straight and concavo-convex contacts are clearly visible. Scale 50 division : 1.25mm.

2. Donegal Quartzite (DQ)

Mineralogy:	%
Quartz	88.7
Alkali feldspar	0.5
Plagioclase feldspar	1.0
MRF's (low grade)	2.5
Muscovite mica	7.3

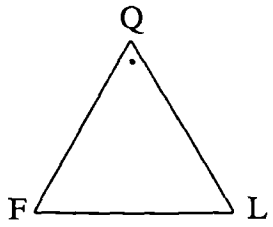

The rock is composed predominantly of quartz with secondary muscovite mica. The mica is concentrated in planes, aligned parallel to bedding. This is a metamorphic feature since it cuts through and across the quartz grains. Low grade, chlorite-rich metamorphic rock fragments are also present.

Grain size: The quartzite is well sorted, with the majority of grains in the range 0.1 - 0.25mm, (fine sand). The muscovite grains reach a maximum of 0.25mm long.

Grain shape: The quartz grains are generally of high sphericity and probably originally well rounded but have been deformed to produce an angular interlocking texture.

Packing density: Vertical: 99.0 %
Horizontal: 98.0 %

Contacts: Straight and concavo-convex contacts dominate and the high packing density has produced multiple triple points.

Grain orientation: Low sphericity quartz grains are generally aligned parallel to bedding. The mica grains give the rock a high preferential mineral alignment parallel to bedding.

Classification: *Quartz arenite (Quartzite).*

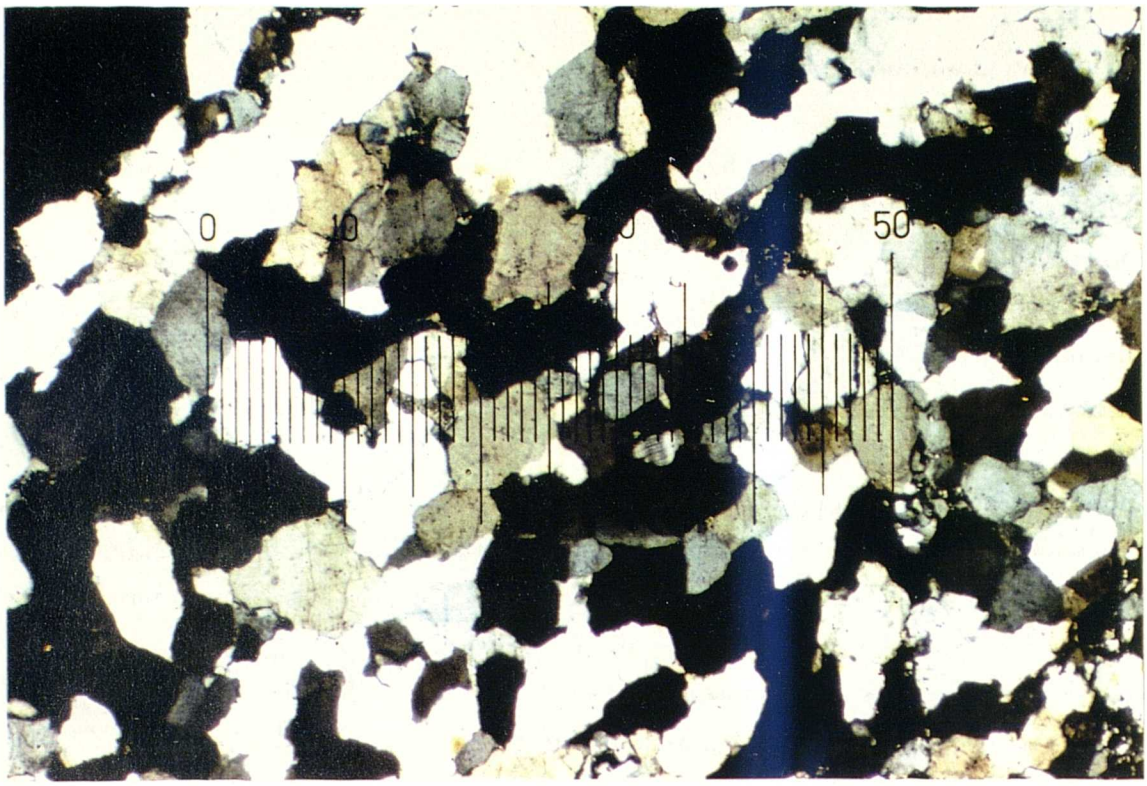

Plate 3.5 Basal Quartzite. Section perpendicular to bedding under crossed polars showing extremely pure quartz mineralogy and high packing density.
Scale 50 divisions : 2.5mm.

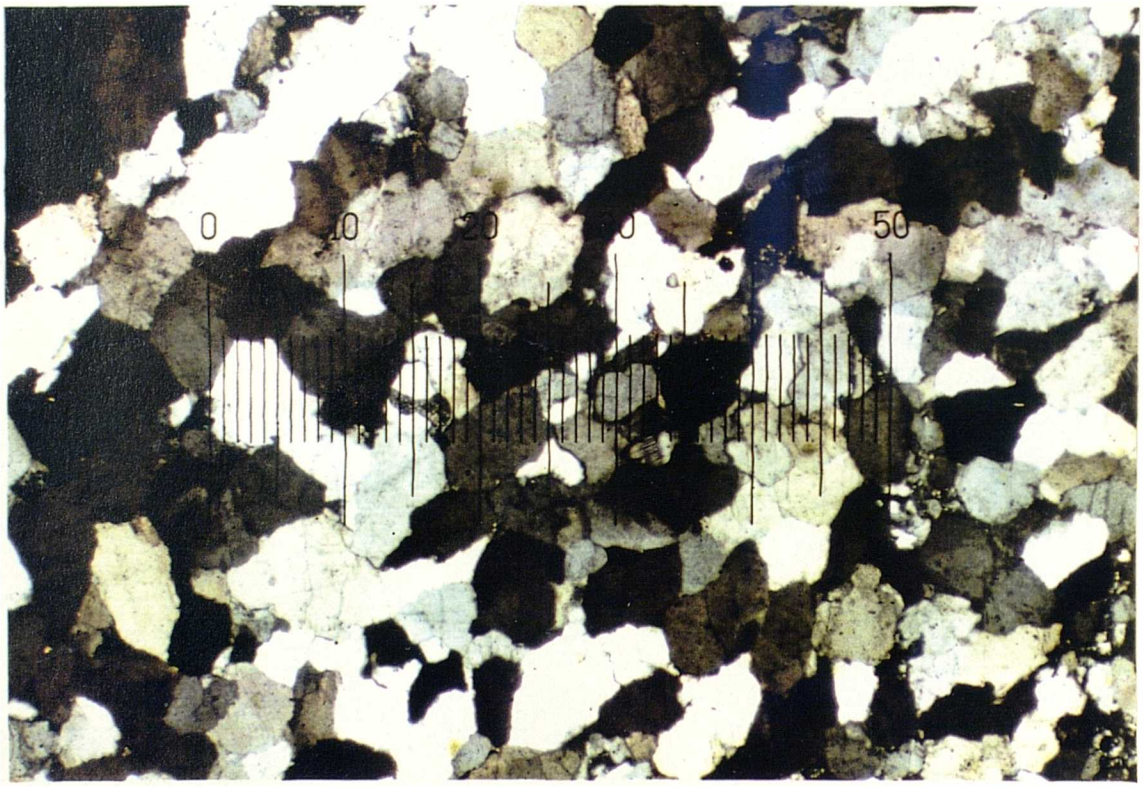

Plate 3.6 Basal Quartzite under crossed polars with P/A angle = 70°. Recrystallization of grain boundaries has produced sutured contacts and an interlocking texture.
Scale 50 division : 2.5mm

3. Basal Quartzite (BQ)

Mineralogy:	%
Quartz	78.0
Microcrystalline quartz	15.3
Alkali feldspar	4.7
Plagioclase feldspar	1.0
Pores	1.0

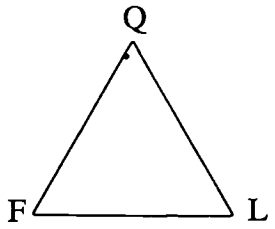

The quartzite is extremely pure, with a total quartz content of approximately 93%. Quartz overgrowths are rare but porosity has been occluded by microcrystalline quartz which was probably introduced authigenically.

Grain size: The rock is poorly sorted; grains range in size from 0.1 - 1.2mm, with a modal size range of 0.25 - 0.6mm, (medium to coarse sand).

Grain shape: Generally of high sphericity but grains have been deformed diagenetically to produce an angular interlocking texture.

Packing density: Vertical: 95.0 %
Horizontal: 93.0 %

Contacts: Abundant sutured contacts and triple points.

Grain orientation: No preferential grain alignment.

Classification: *Subarkose (Subarkosic quartzite).*

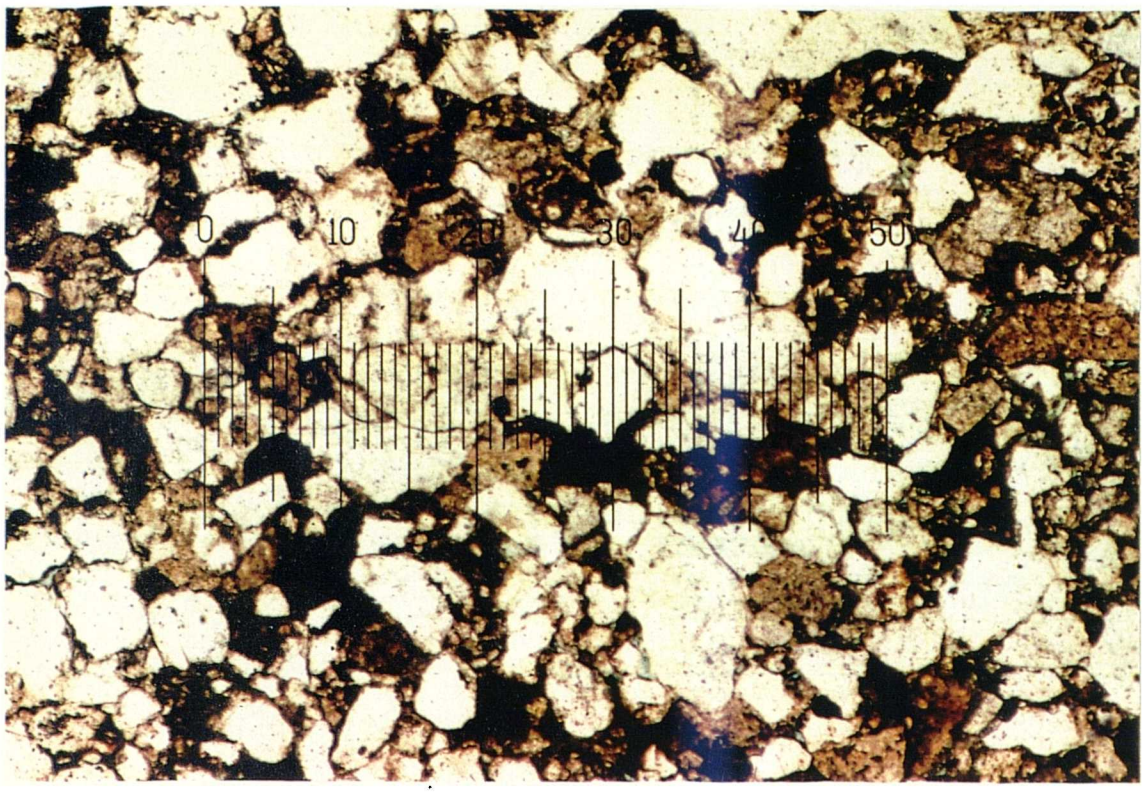

Plate 3.7 Brownstones. Section perpendicular to bedding in plane polarized light showing highly immature mineralogy and texture.
Scale 50 divisions : 1.25mm.

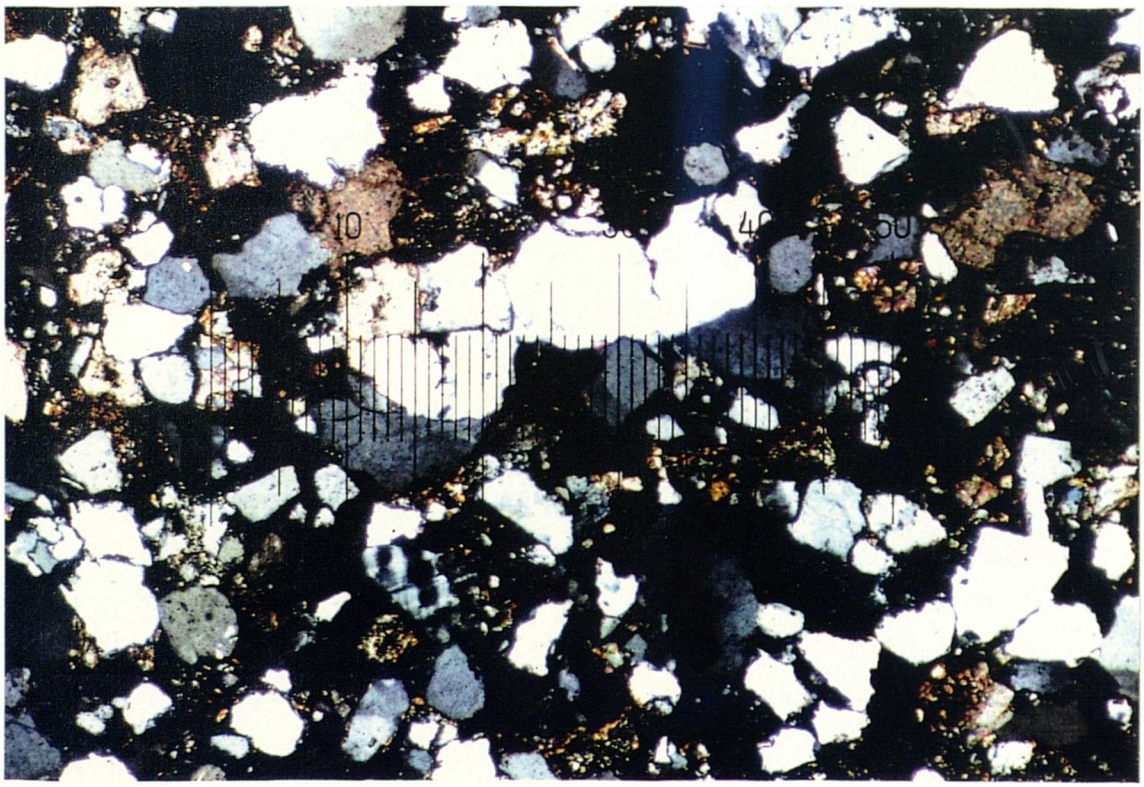

Plate 3.8 Brownstones under crossed polars showing slight calcite cementing on left.
Scale 50 division : 1.25mm.

4. Brownstones (LORS)

Mineralogy:	Red Sandstone %	Green reduction patches %
Quartz	40.0	51.0
Alkali feldspar	5.0	8.0
Plagioclase feldspar	2.0	0.0
SRF's	13.0	5.0
MRF's	5.0	8.0
IRF's	2.3	2.0
CRF's	6.0	1.3
Muscovite mica	0.7	0.0
Biotite mica	0.7	0.0
Haematite	12.7	4.0
Calcite cement	4.3	12.7
Clays	3.0	8.3
Pores	2.3	0.0
Opaques	2.0	7.7
Heavy minerals	1.0	0.0

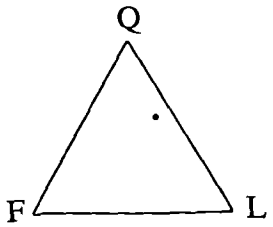

RED

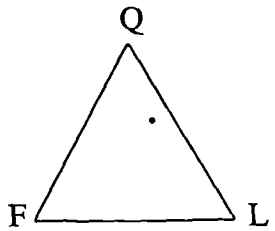

GREEN

The sandstone is mineralogically immature, containing abundant rock fragments and other labile constituents. Quartz grains show poorly developed quartz overgrowths and haematite ghost outlines. Occasional carbonate rock fragments show calcite overgrowths.The normal purple sandstone is cemented by haematite and contains abundant detrital haematite grains. The rock contains abundant greenish-grey 'reduction' patches in which the haematite is replaced by opaque iron oxides and calcite. The mineralogy of the green reduction patches is outlined above. Sedimentary rock fragments also decrease in abundance in these areas while clays increase.

Grain size: The rock is extremely poorly sorted, with detrital grains ranging in size from clay to 0.5mm diameter quartz grains. The majority of grains are in the size range 0.1 - 0.3mm, (fine to medium sand).

Grain shape: Most of the detrital grains are angular to subangular and of low to intermediate sphericity. Soft sedimentary rock fragments show a higher degree of rounding.

Packing density: Vertical: 84.0 %
Horizontal: 83.1 %

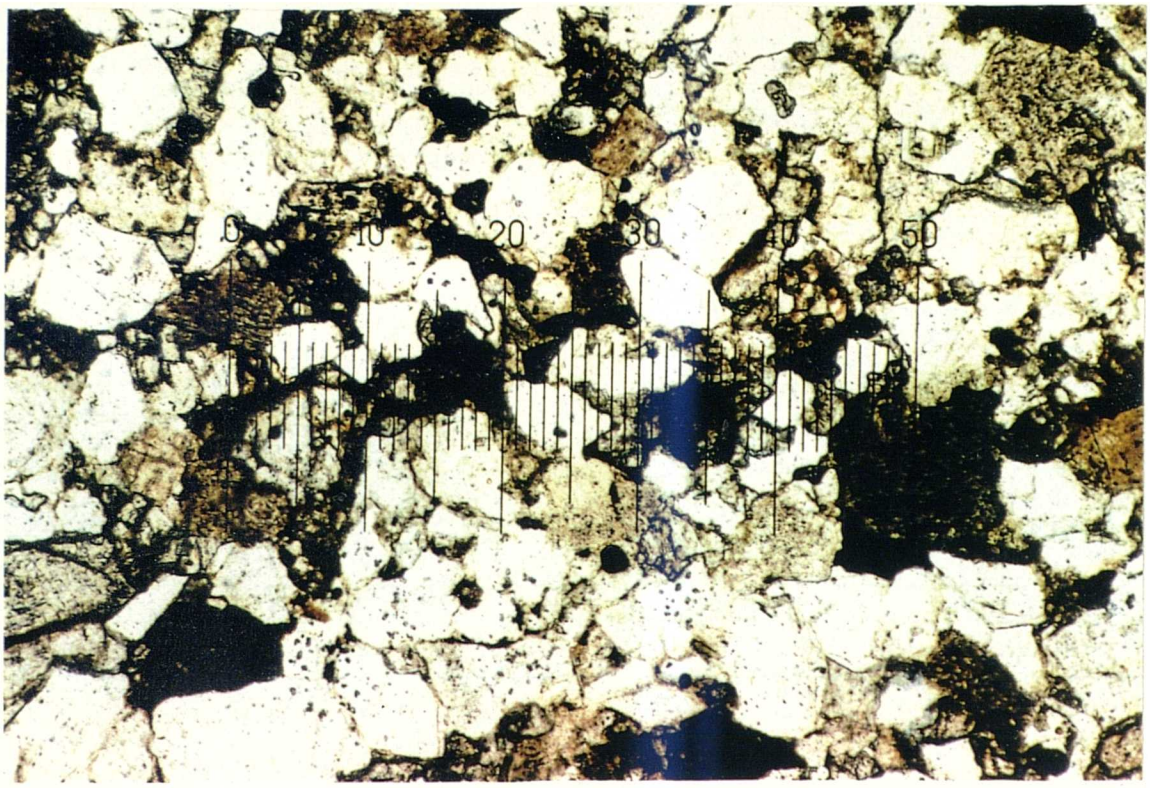

Plate 3.9 Brownstones (reduced area). Section perpendicular to bedding in plane polarized light showing conversion of Fe^{3+} minerals to Fe^{2+} minerals. Scale 50 divisions : 1.25mm.

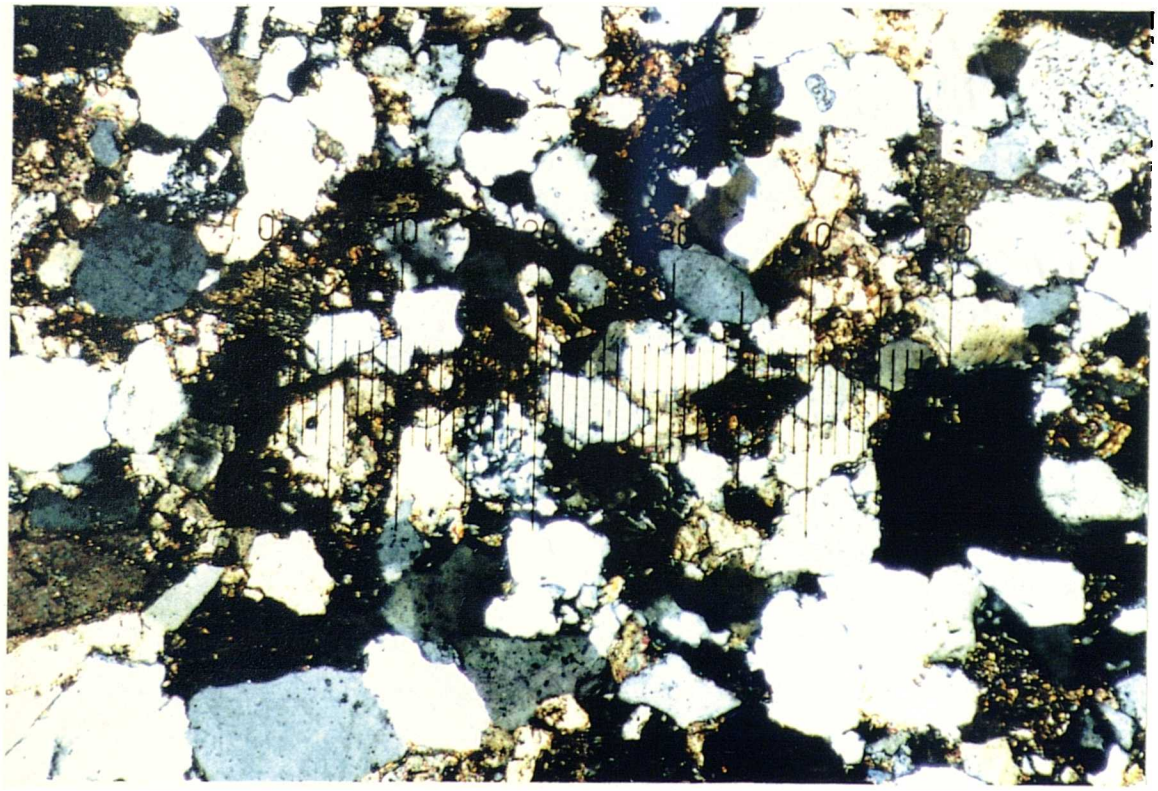

Plate 3.10 Brownstones (reduced area) under crossed polars showing higher degree of calcite cementing than in the normal haematite-rich areas of the rock. Scale 50 division : 1.25mm.

Contacts: Many contacts between quartz grains are sutured but the fabric is dominated by concavo-convex contacts.

Grain orientation: The rock possesses well-developed internal cross-bedding and grains of aspect ratio greater than two are generally aligned parallel to the bedding surfaces.

Classification: *Lithic arenite (sedarenite).*

Reduction patches are classed Sublitharenite.

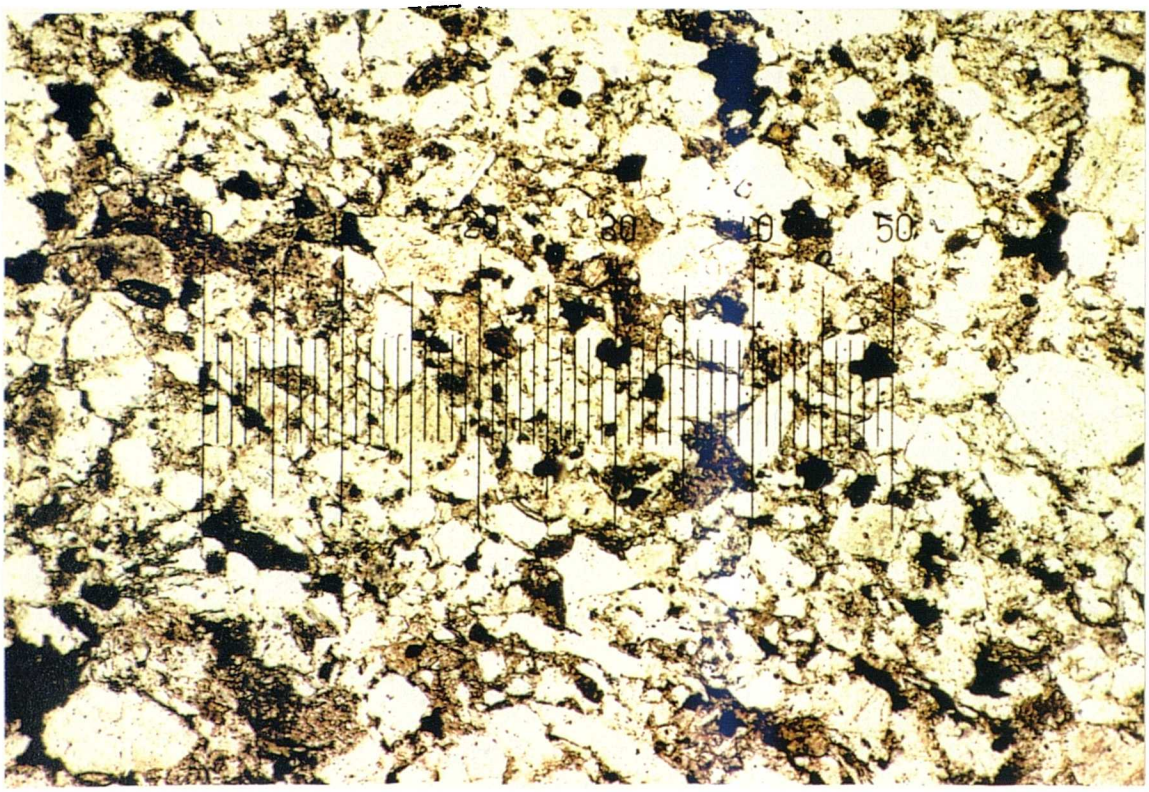

Plate 3.11 Pilton Sandstone (type A). Section perpendicular to bedding in plane polarized light. The rock is fine-grained with abundant clay minerals. Scale 50 divisions : 1.25mm.

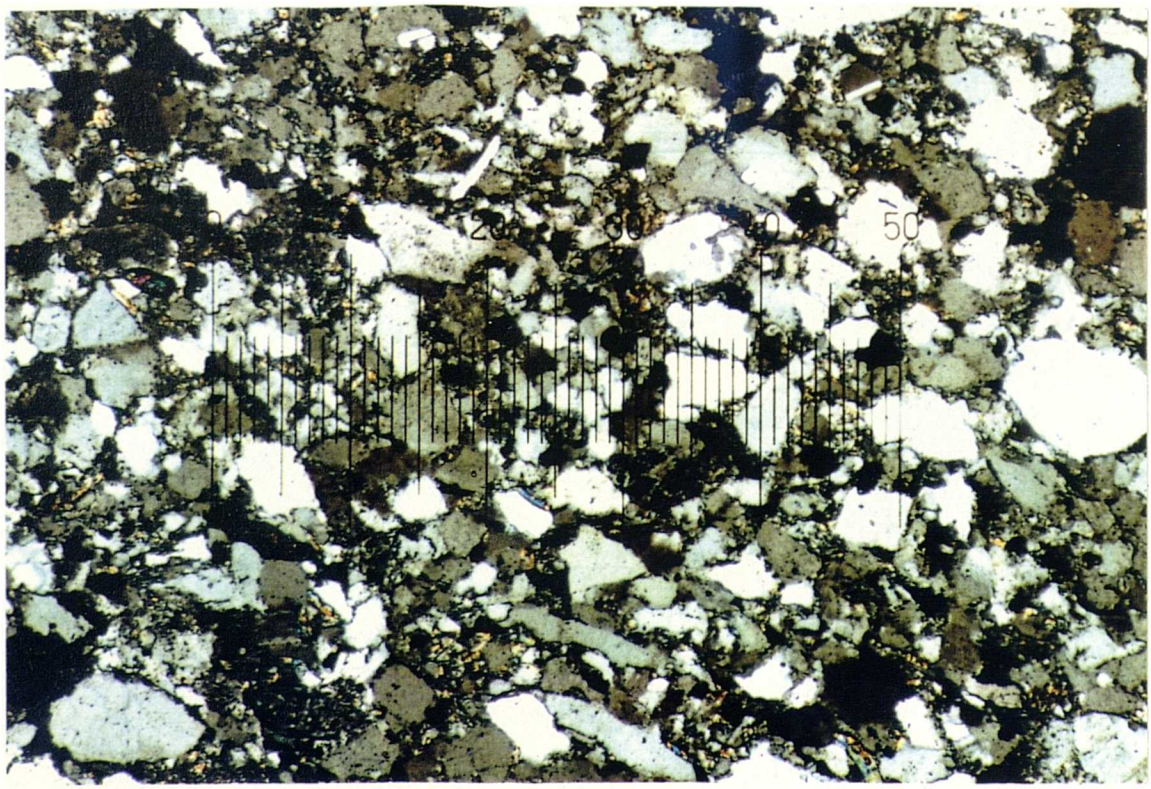

Plate 3.12 Pilton Sandstone (type A) under crossed polars with P/A angle = 70°. Grain contacts show a high degree of suturing and the clay minerals have been recrystallized. Scale 50 division : 1.25mm.

5. Pilton - Type A (PiA)

Mineralogy:	%
Quartz	54.0
Microcrystalline quartz	9.3
Alkali feldspar	3.7
Plagioclase feldspar	0.3
SRF's	4.0
MRF's	6.0
Opaques	3.7
Clays	19.0
Pores	0.0

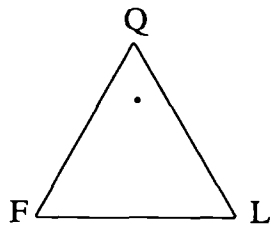

This sandstone is extremely dense with no intergranular porosity visible under the microscope. The mineralogy is dominated by detrital and authigenic quartz and highly birefringent clay minerals including sericite, probably produced as a weathering product of feldspars. Overgrowths can be seen on some quartz grains, with silt-sized quartz infilling the pores.

Grain size: Extremely poorly sorted, fine-grained sandstone. Detrital framework grains range from 0.02 to 0.3mm, (very fine to fine sand).

Grain shape: Grains are very angular and of low sphericity.

Packing density: Vertical: 85.2 %
Horizontal: 85.0 %

Contacts: Sutured and concavo-convex are common with occasional point contacts.

Grain orientation: Orientation of high aspect ratio grains parallel to internal cross-bedding.

Classification: *Lithic wacke.*

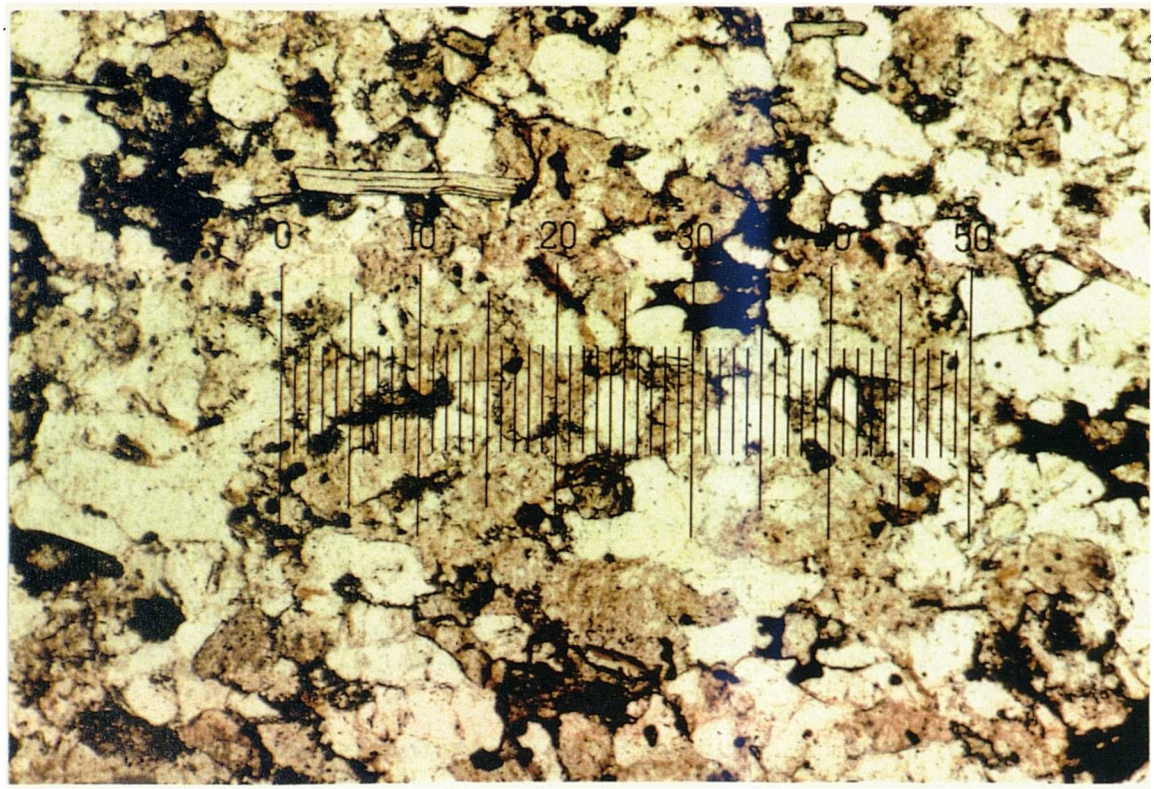

Plate 3.13 Pilton Sandstone (type B). Section perpendicular to bedding in plane polarized light. The rock is fine-grained with elongated muscovite flakes aligned parallel to bedding. Scale 50 divisions : 1.25mm.

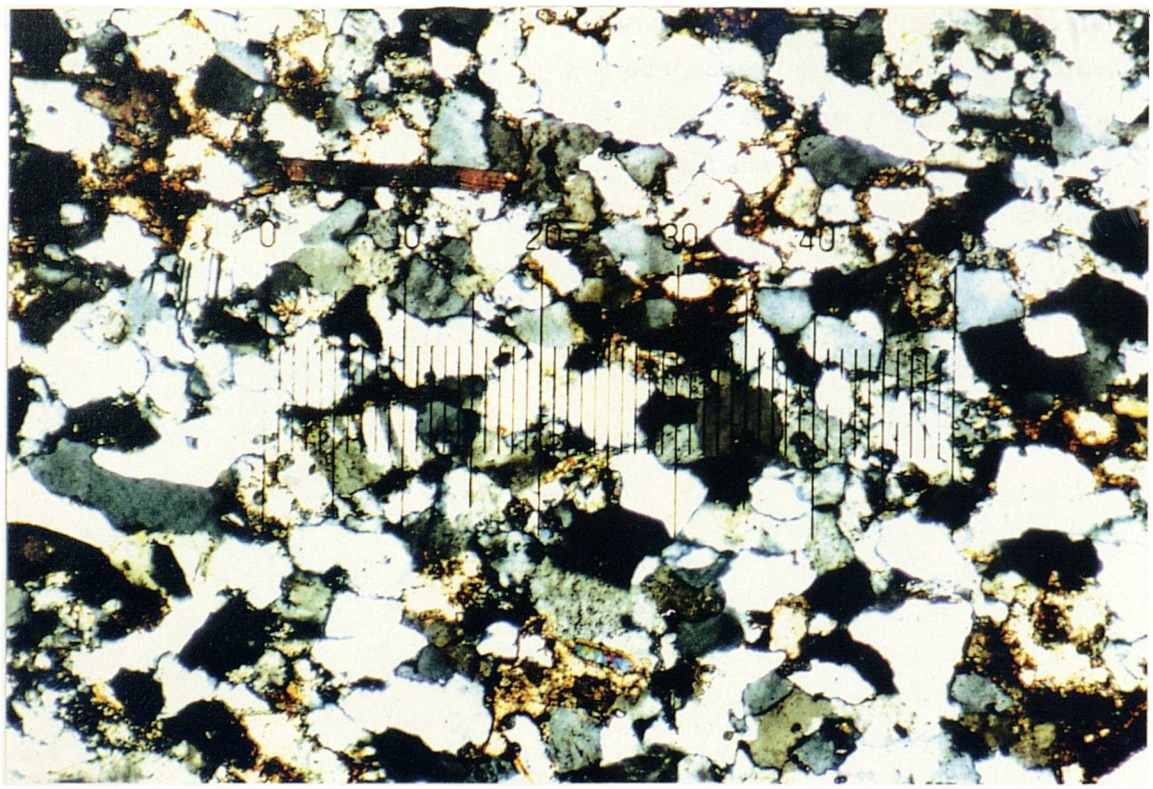

Plate 3.14 Pilton Sandstone (type B) under crossed polars. Grain contacts show a high degree of suturing and interlocking. Secondary calcite cement fills many of the pores giving the rock a low porosity. Scale 50 division : 1.25mm.

6. Pilton - Type B (PiB)

Mineralogy:	%
Quartz	61.3
Alkali feldspar	6.7
Plagioclase feldspar	3.3
SRF's	0.7
MRF's	4.7
Muscovite mica	4.0
Calcite cement	5.3
Haematite	9.7
Clays	4.3

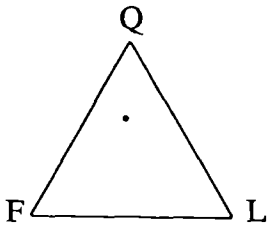

The most abundant mineral is quartz which occurs as detrital sand and silt-sized grains which have been welded together during lithification. Metamorphic rock fragments are abundant as well as alkali and plagioclase feldspars. In addition to quartz welding, the rock is cemented by haematite and calcite. The haematite predates the formation of the calcite cement.

Grain size: Most grains are between 0.05 and 0.2mm long axis, (very fine to fine sand). The photo-micrographs show a muscovite flake 0.4mm long.

Grain shape: Detrital grains are highly angular and of low sphericity.

Packing density: Vertical: 87.6 %
Horizontal: 82.1 %

Contacts: Quartz welding has produced abundant concavo-convex and sutured contacts. Triple points are also abundant.

Grain orientation: Muscovite flakes and high aspect ratio quartz grains are aligned parallel to bedding.

Classification: *Subarkose*.

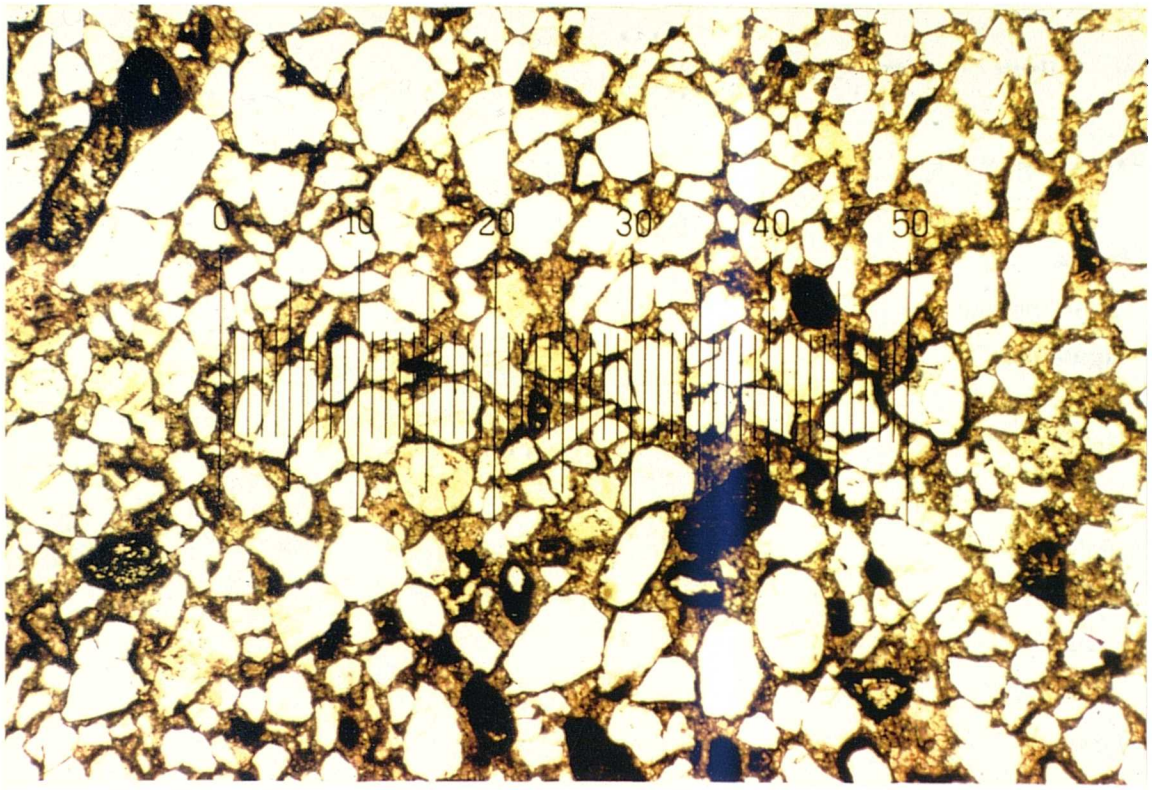

Plate 3.15 Upper Cromhall Sandstone. Section parallel to bedding in plane polarized light. The rock has a low packing density with point contacts predominating. Scale 50 divisions : 2.5mm.

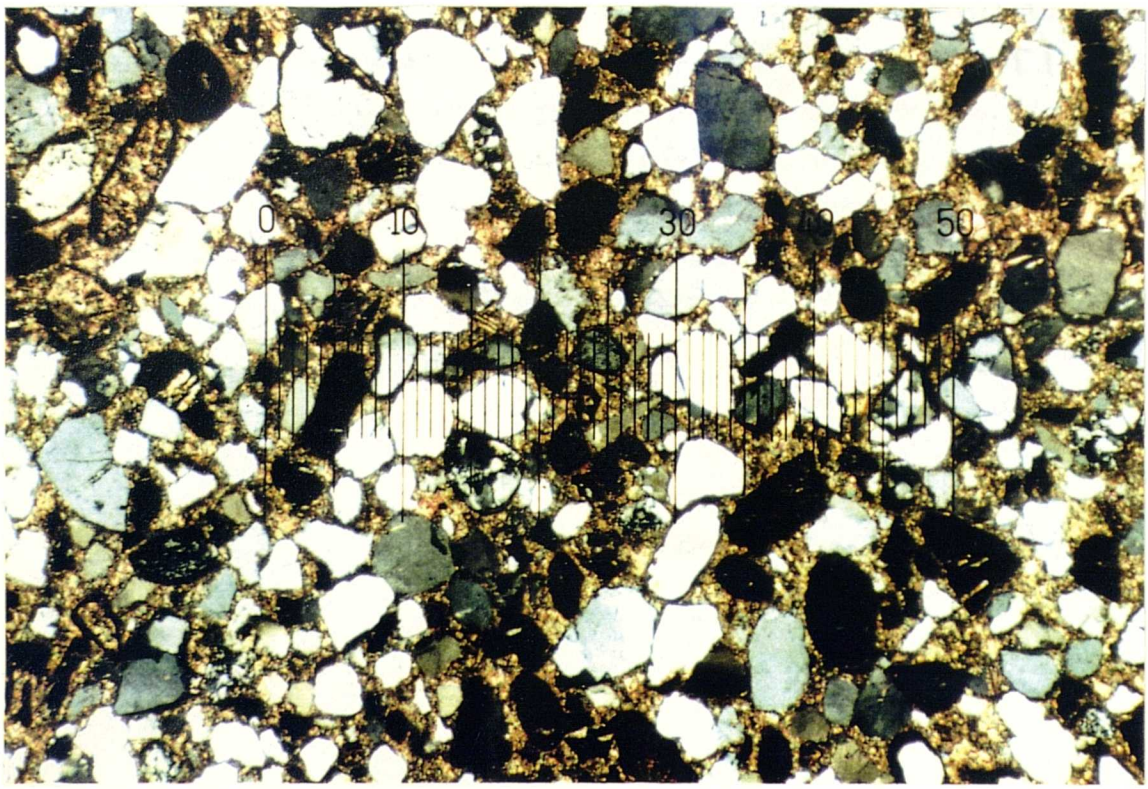

Plate 3.16 *Upper Cromhall Sandstone* under crossed polars. Micritic matrix is abundant with some CRF's having been dissolved leaving remnant haematite rims. Scale 50 division : 2.5mm.

7. Upper Cromhall Sandstone (UCS)

Mineralogy:	%
Quartz	37.0
Alkali feldspar	1.0
Plagioclase	0.0
SRF's	3.0
MRF's	4.0
IRF's	5.3
CRF's	3.7
Pores	0.0
Carbonate mud	31.3
Calcite cement	10.7
Ooliths	3.7
Opaques	0.3

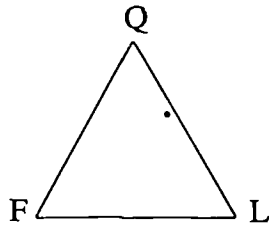

The sandstone is highly calcareous, with almost all the porosity having been occluded by micrite and sparry calcite cement. Corrosion has occurred around many of the detrital quartz grains, most of which contain microfractures vertical and subvertical to bedding. These have all been filled with calcite indicative of formation by tectonic stresses after deposition and lithification. Replacement of some carbonate rock fragments has occurred, leaving iron oxide rims floating in a calcite cement.

Grain size: Most quartz grains and rock fragments are between 0.1 and 0.4mm long axis, (fine to medium sand).

Grain shape: Detrital grains are generally of high sphericity but variable in degree of rounding from well rounded to subangular.

Packing density: Vertical: 63.9 %
Horizontal: 62.4 %

Contacts: The abundance of carbonate mud means that most of the grains appear matrix supported or have a number of point contacts.

Grain orientation: No preferential orientation of any grains.

Classification: *Lithic wacke.*

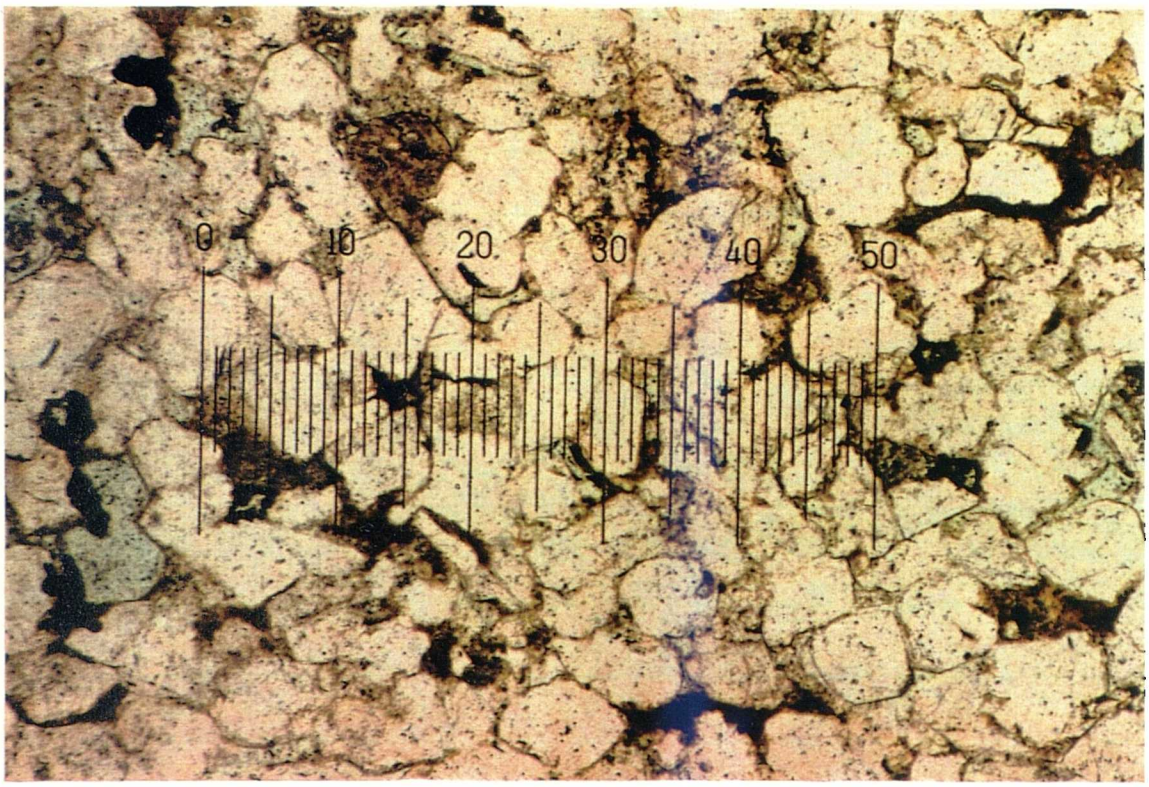

Plate 3.17 Millstone Grit (type A). Section perpendicular to bedding showing predominantly concavo-convex contacts between quartz grains. Pores are shown by blue impregnated epoxy resin. Scale 50 divisions : 1.25mm.

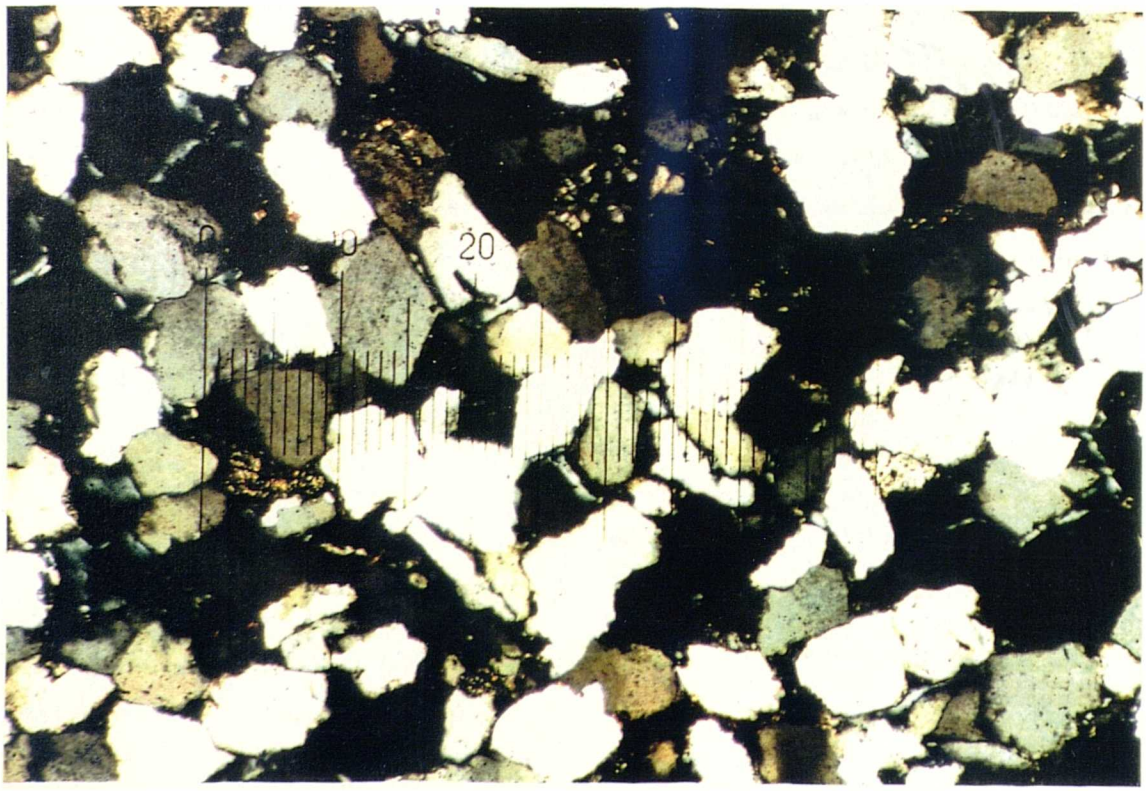

Plate 3.18 *Millstone Grit* (type A) under crossed polars showing occasional sutured contacts. Scale 50 division : 1.25mm.

8. Millstone Grit - Type A (MGA)

Mineralogy:	%
Quartz	70.0
Alkali feldspar	2.3
Plagioclase feldspar	0.3
SRF's	0.7
MRF's	3.7
Kaolinite	7.7
Other clays	5.3
Pores	6.0
Opaques	2.0
Muscovite	2.0

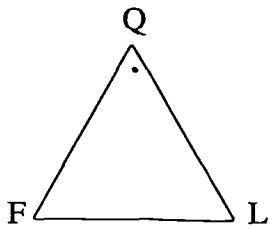

The quartz grains are welded together by sporadically developed quartz overgrowths and the pores filled with authigenic clay minerals - mostly kaolinite.

Grain size: The sandstone is well sorted, with most grains in the range 0.15 to 0.25mm, (fine sand).

Grain shape: Grains are subrounded to subangular and generally of high sphericity.

Packing density: Vertical: 81.0 %
Horizontal: 79.7 %

Contacts: Predominantly straight and concavo-convex with occasional sutured contacts between quartz grains.

Grain orientation: No preferred orientation of grains.

Classification: *Sublitharenite.*

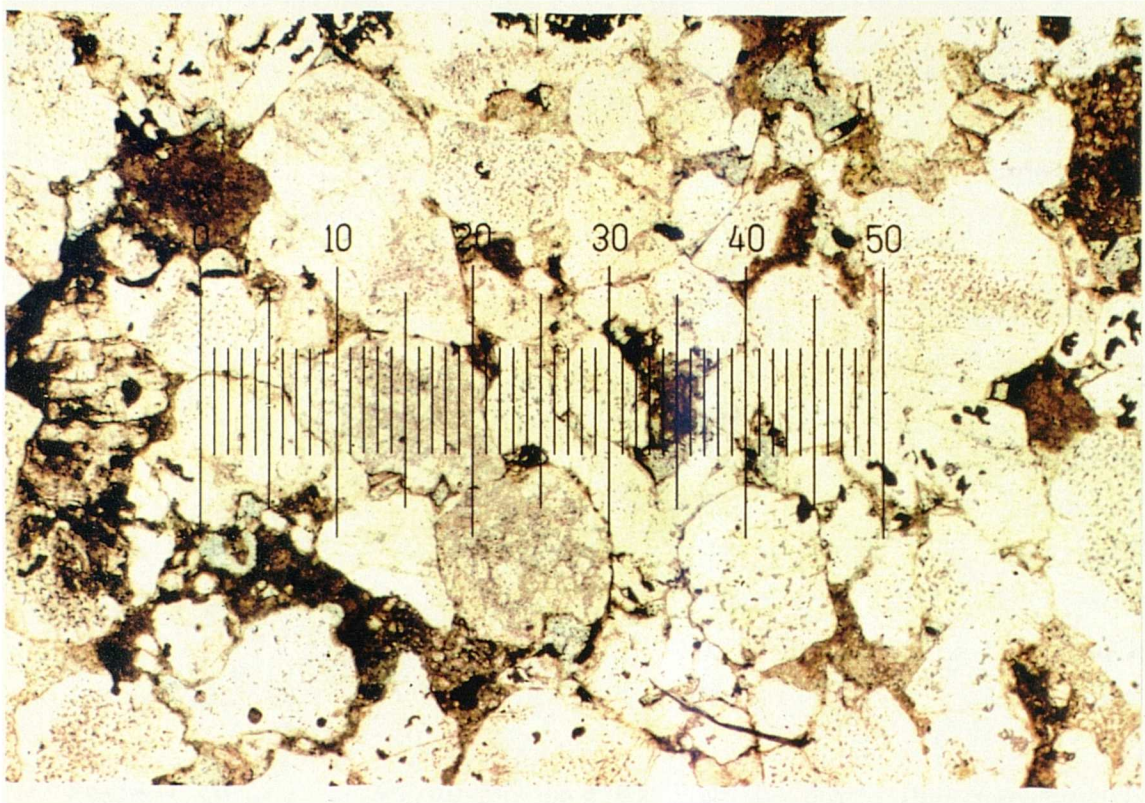

Plate 3.19 Millstone Grit (type B). Section perpendicular to bedding in plane polarized light showing coarse, well rounded grains and large pore spaces partially occluded by kaolinite. Scale 50 divisions : 2.5mm.

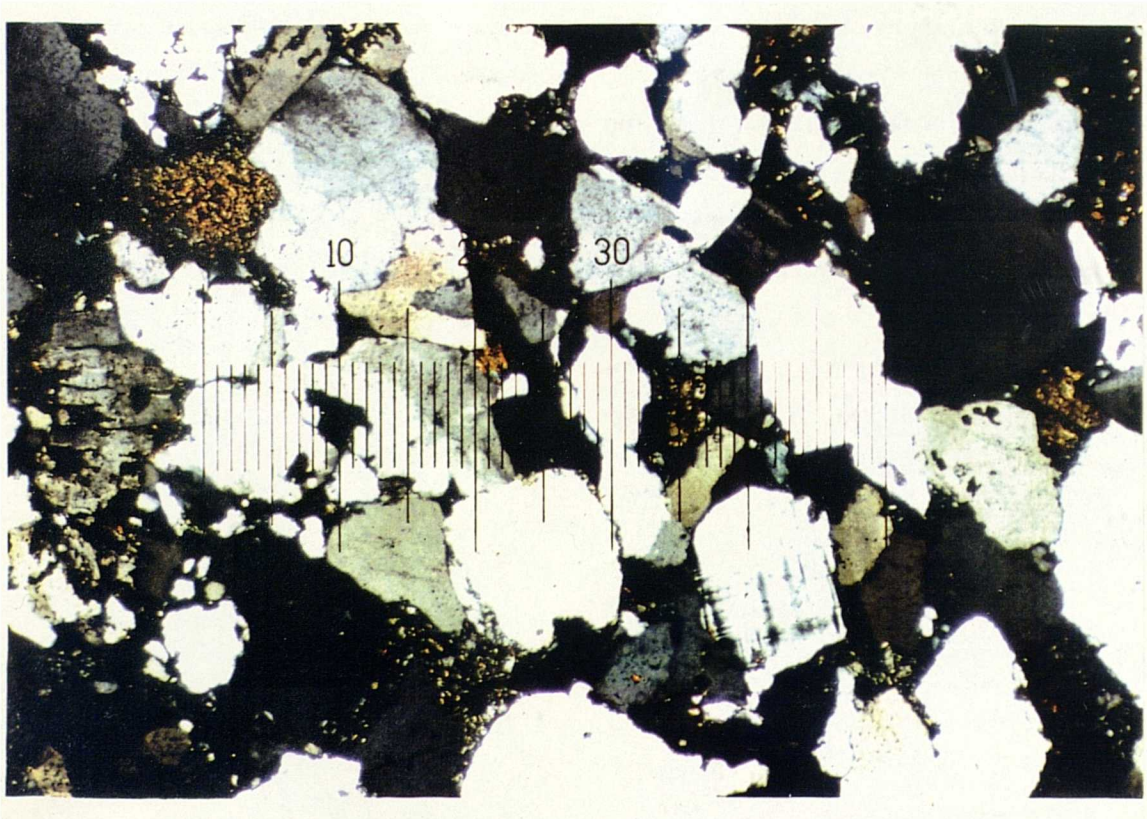

Plate 3.20 Millstone Grit (type B) under crossed polars showing presence of microcline and plagioclase feldspars. Recrystallization at grain contacts has taken place producing concavo-convex and sutured contacts.
Scale 50 division : 2.5mm.

9. Millstone Grit - Type B (MGB)

Mineralogy:	%
Quartz	65.3
Alkali feldspar	8.7
Plagioclase feldspar	1.0
SRF's	1.3
MRF's	5.0
Kaolinite	7.7
Other clays	3.7
Pores	5.3
Opaques	1.0
Muscovite	1.0

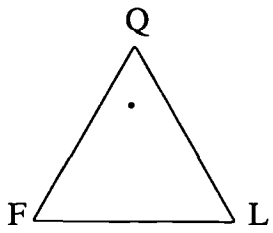

Overgrowths occur on many of the detrital quartz grains, evident by the very fine ghost clay outlines. Alkali feldspars are relatively abundant, occurring often as large well-rounded microcline grains. The sandstone is also cemented by kaolinite, which in many cases totally occludes the pore spaces. It is characterised by its first order grey birefringence and platey book-like structure.

Grain size: This sandstone is the coarsest-grained variety which was studied, with the majority of grains greater than 0.5mm long axis, (coarse to very coarse sand). Occasional grains occur up to 10mm long axis but these constitute a minor proportion of the sediment.

Grain shape: Subrounded to subangular and of high to intermediate sphericity.

Packing density: Vertical: 79.1 %
Horizontal: 87.1 %

Contacts: Generally concavo-convex and sutured.

Grain orientation: No preferential grain alignment.

Classification: *Subarkose.*

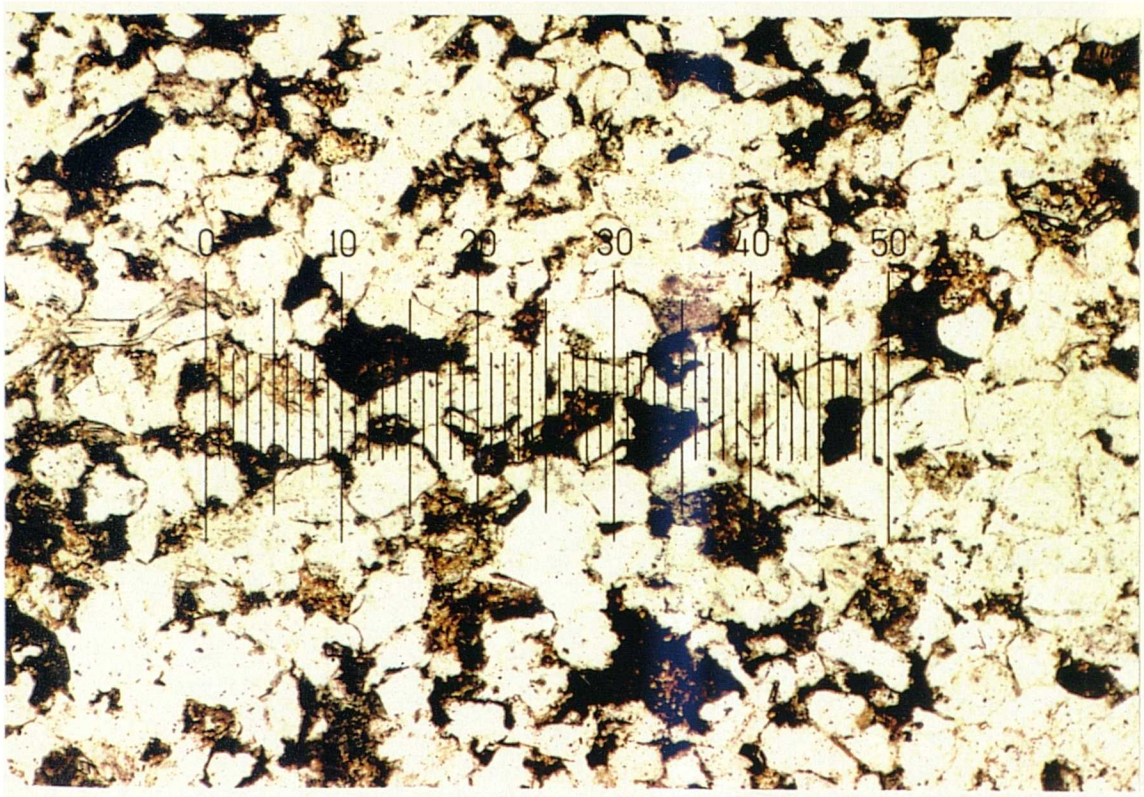

Plate 3.21 Millstone Grit (type C). Section perpendicular to bedding in plane polarized light. The rock is composed predominantly of fine, angular quartz grains with abundant clay minerals. Scale 50 divisions : 1.25mm.

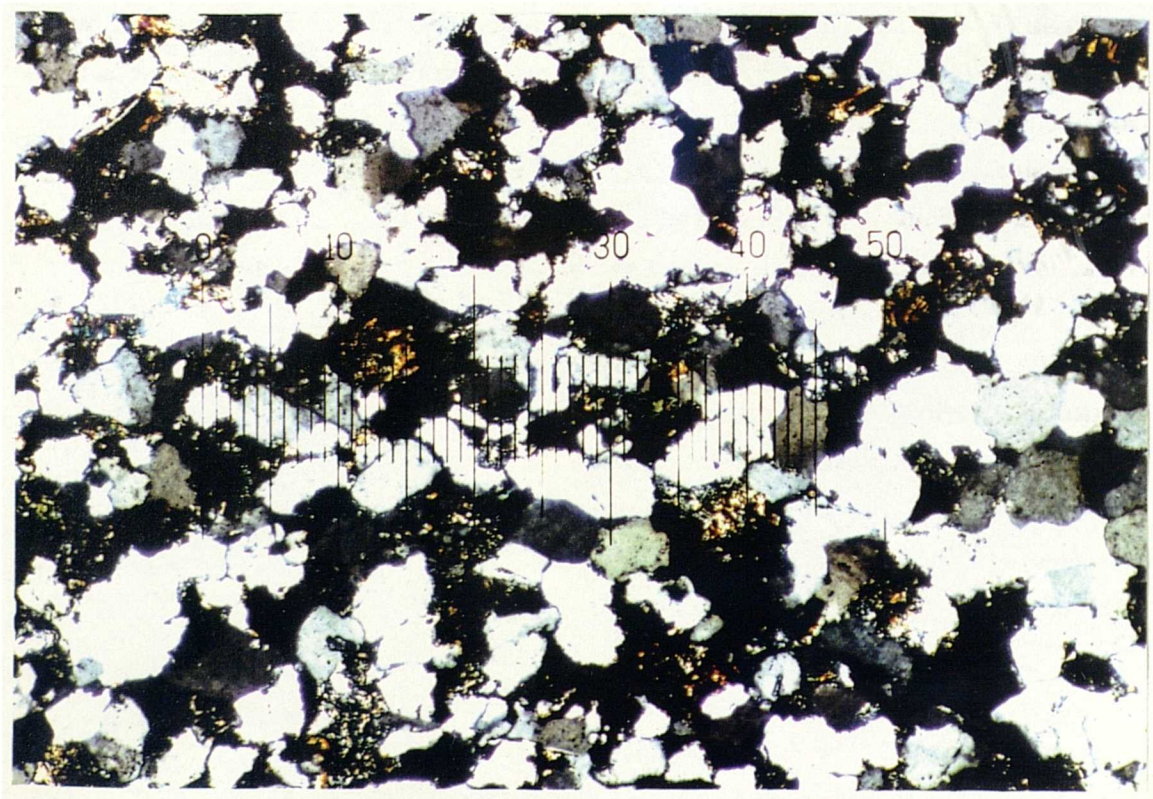

Plate 3.22 Millstone Grit (type C) under crossed polars showing suturing of quartz grains and signs of recrystallization of clays. XRD analysis proved the abundance of kaolinite. Scale 50 division : 1.25mm.

10. Millstone Grit - Type C (MGC)

Mineralogy:	Normal	Stained areas
	%	%
Quartz	73.7	65.7
Alkali feldspar	5.3	3.3
Plagioclase feldspar	0.0	0.0
SRF's	2.0	1.7
MRF's	1.0	1.0
Muscovite mica	1.0	1.0
Haematite	0.0	10.3
Kaolinite	10.3	2.0
Other clays	2.3	12.3
Pores	0.7	0.0
Opaques	0.7	1.7
Authigenic calcite	2.7	0.7
Heavy minerals	0.3	0.7
Glauconite	0.0	0.3

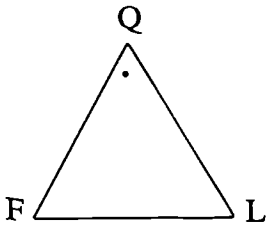

Normal

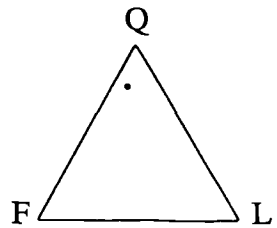

Stained

The abundant quartz grains have been welded together during diagenesis. Clay minerals occasionally infill pore spaces and form a weak secondary cement. In the stained areas the calcite has been reduced while a haematite-rich clay matrix has been introduced.

Grain size: The rock is moderately well sorted with most of the grains in the range 0.1 to 0.2mm, (very fine to fine sand).

Grain shape: Angular to subangular and of low to intermediate sphericity.

Packing density: Vertical: 82.1 %
Horizontal: 75.2 %

Contacts: Concavo-convex and sutured contacts are the most common, with multiple triple points between quartz grains.

Grain orientation: No preferential grain alignment.

Classification: *Subarkose.*

Stained areas are classed Quartz arenite.

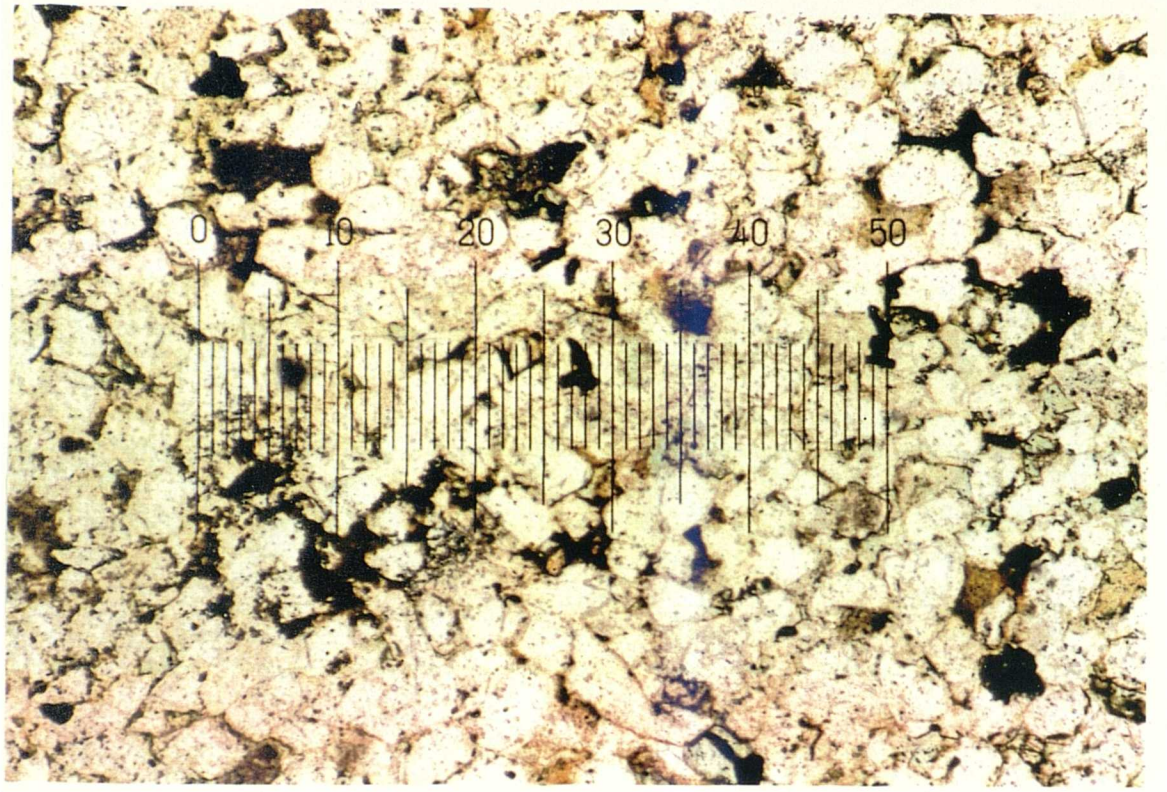

Plate 3.23 Millstone Grit (type D). Section perpendicular to bedding in plane polarized light. The rock is cemented by quartz and clay minerals. Small pores are visible by the blue epoxy resin. Scale 50 divisions : 1.25mm.

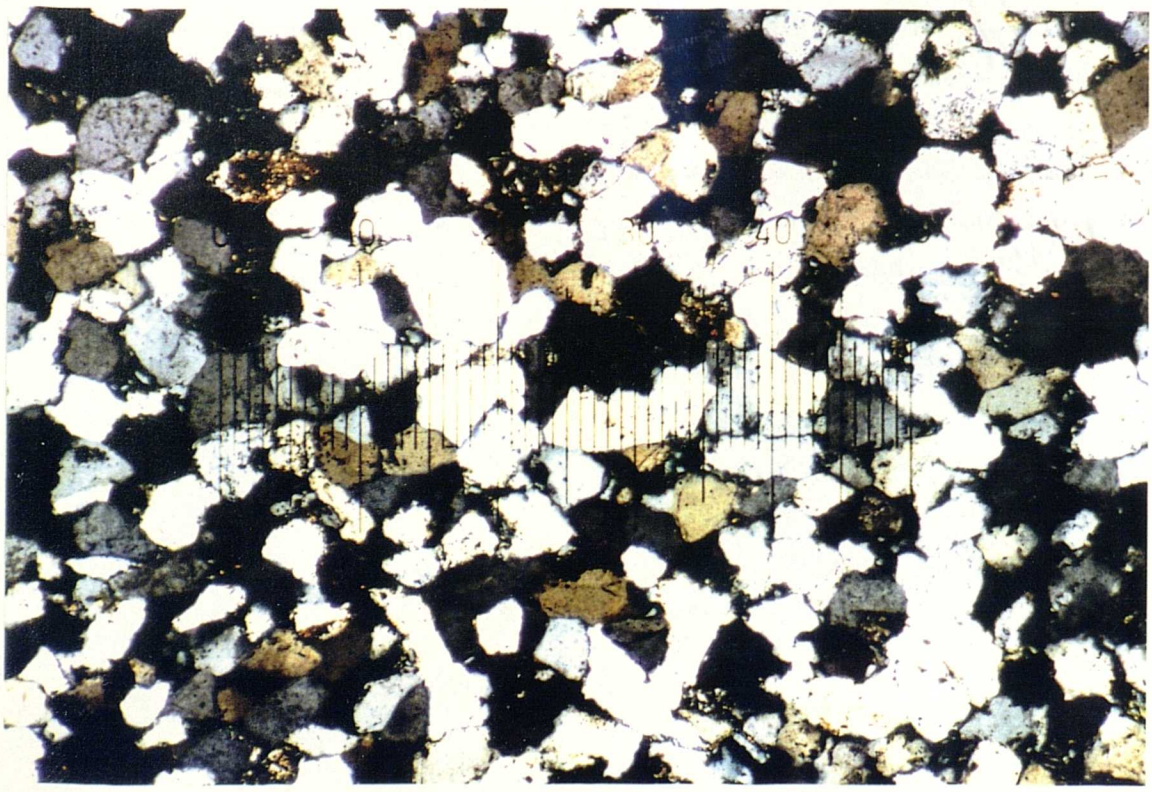

Plate 3.24 Millstone Grit (type D) under crossed polars. Quartz overgrowths have formed on many of the grains. Contacts are generally straight and concavo-convex. Scale 50 divisions : 1.25mm.

11. Millstone Grit - Type D (MGD)

Mineralogy:	%
Quartz	75.3
Alkali feldspar	2.3
Plagioclase feldspar	1.0
SRF's	1.7
MRF's	0.3
Haematite	3.3
Kaolinite	1.0
Other clays	7.7
Pores	5.7
Opaques	0.7
Muscovite mica	1.0

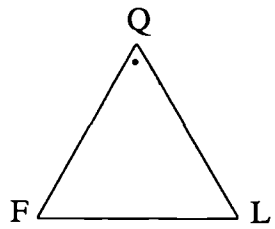

Quartz overgrowths are abundant and in addition to clay minerals, occlude much of the original porosity.

Grain size: Most grains are between 0.08 and 0.15mm long axis, (very fine to fine sand).

Grain shape: Subrounded to subangular and of high to intermediate sphericity.

Packing density: Vertical: 81.4%
Horizontal: 80.7%

Contacts: Generally straight and concavo-convex.

Grain orientation: No preferential grain alignment.

Classification: *Quartz arenite.*

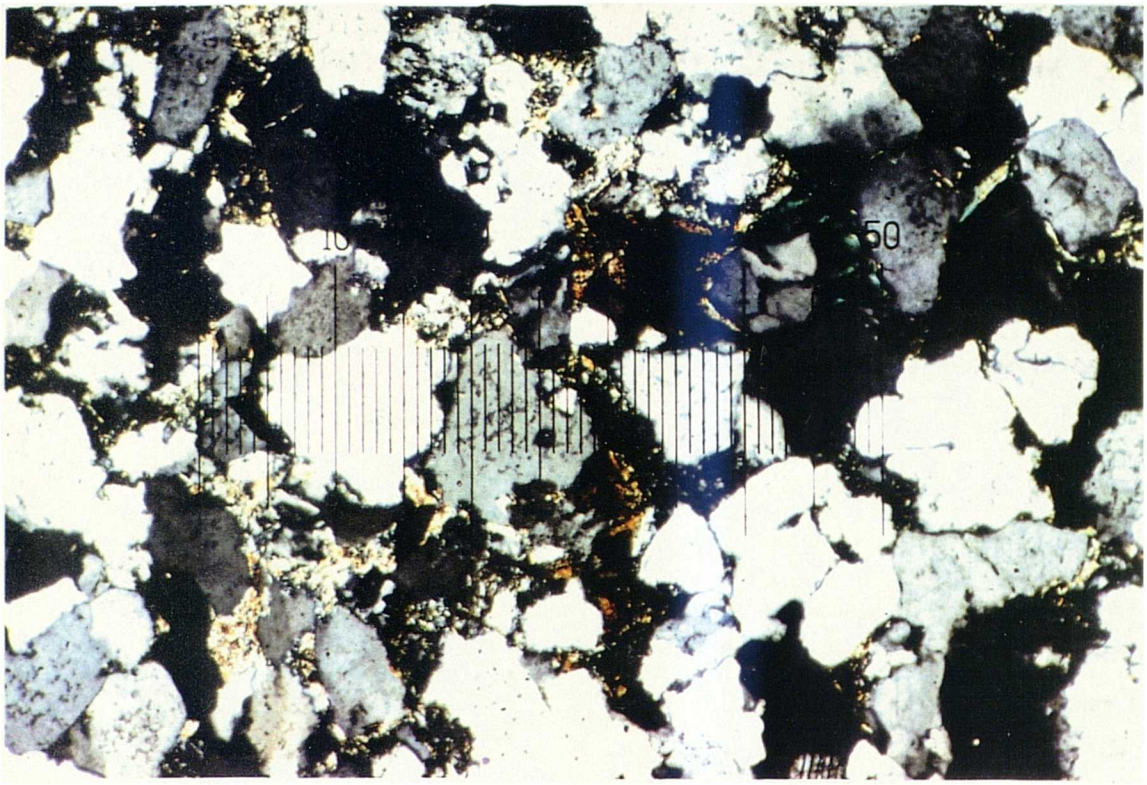

Plate 3.25 Holcombe Brook Grit (type A). Section parallel to bedding under crossed polars. Quartz overgrowths are sporadically developed indicating that the surrounding clay minerals are authigenic. Scale 50 divisions : 1.25mm.

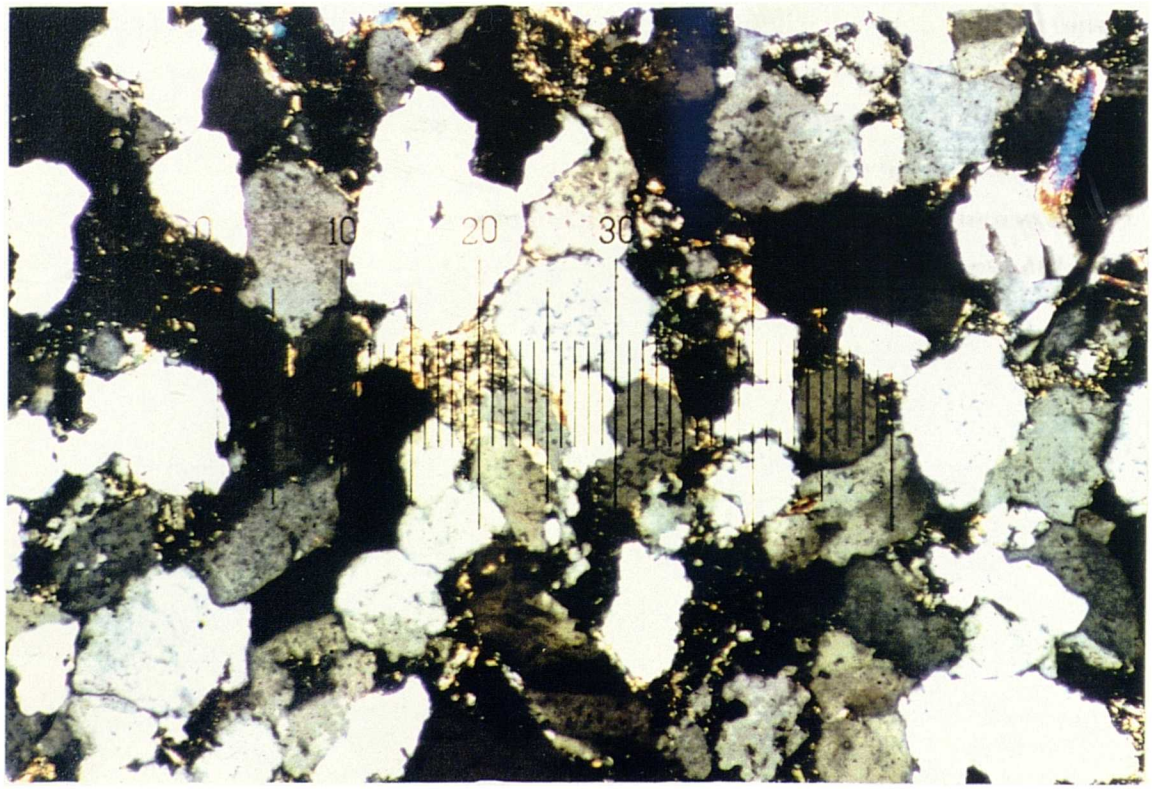

Plate 3.26 Holcombe Brook Grit (type A). Section parallel to bedding under crossed polars with P/A angle = 70°. Extensive suturing has occurred between detrital quartz grains. Scale 50 divisions : 1.25mm.

12. Millstone Grit - Type E. Holcombe Brook Grit - Type A (HBGA)

Mineralogy:	%
Quartz	65.3
Alkali feldspar	7.7
Plagioclase feldspar	2.0
SRF's	1.7
MRF's	2.3
Muscovite	2.0
Kaolinite	6.0
Other clays	8.7
Pores	3.3
Opaques	1.0

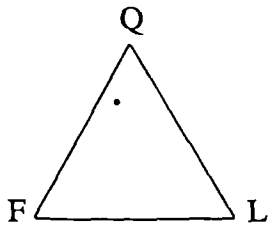

Detrital quartz grains are welded together by sporadically developed overgrowths. Many feldspar grains show a high degree of sericitisation and kaolinisation, resulting in a high secondary intragranular porosity.

Grain size: Most grains are in the range 0.1 to 0.3mm, (fine to medium sand).

Grain shape: Subrounded to subangular and generally of high sphericity.

Packing density: Vertical: 83.9%
Horizontal: 82.7%

Contacts: Many of the contacts between quartz grains show suturing. Concavo-convex contacts are most common.

Grain orientation: No preferential grain alignment.

Classification: *Subarkose.*

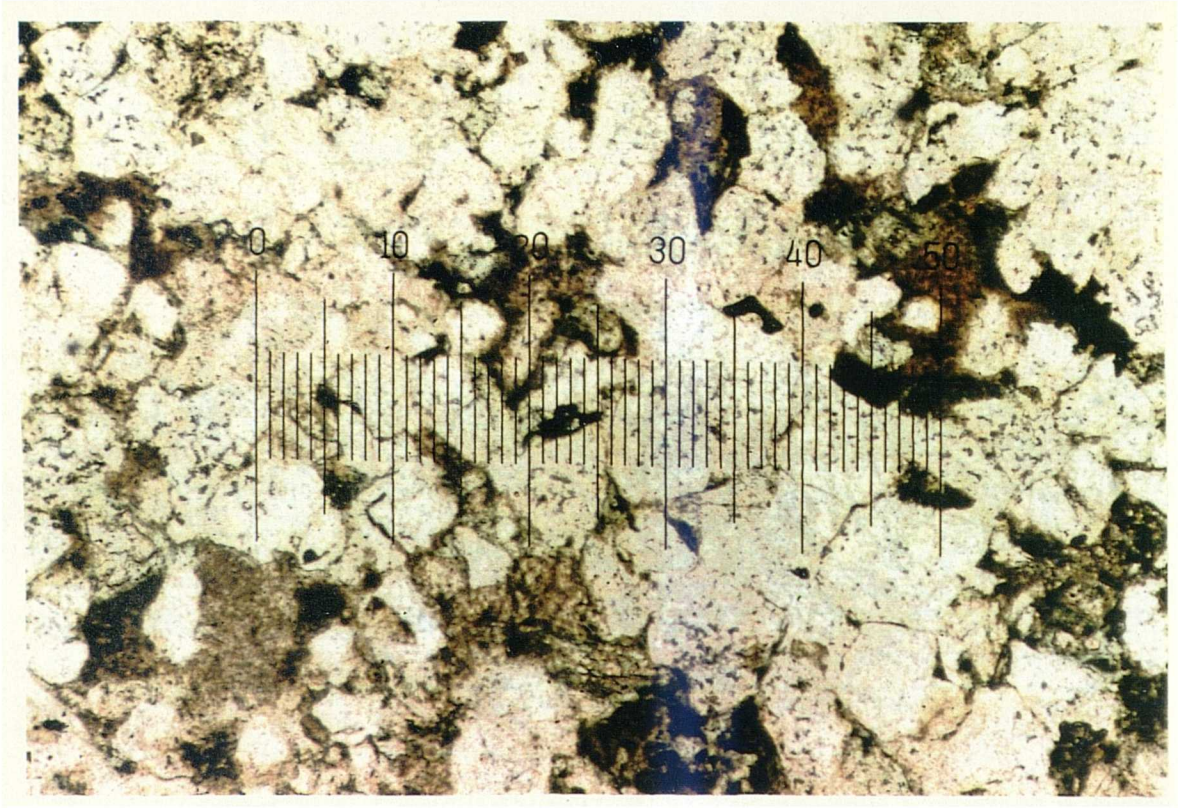

Plate 3.27 Holcombe Brook Grit (type B). Section parallel to bedding in plane polarized light. Grain packing is highly variable with some areas showing abundant pores. Scale 50 divisions : 1.25mm.

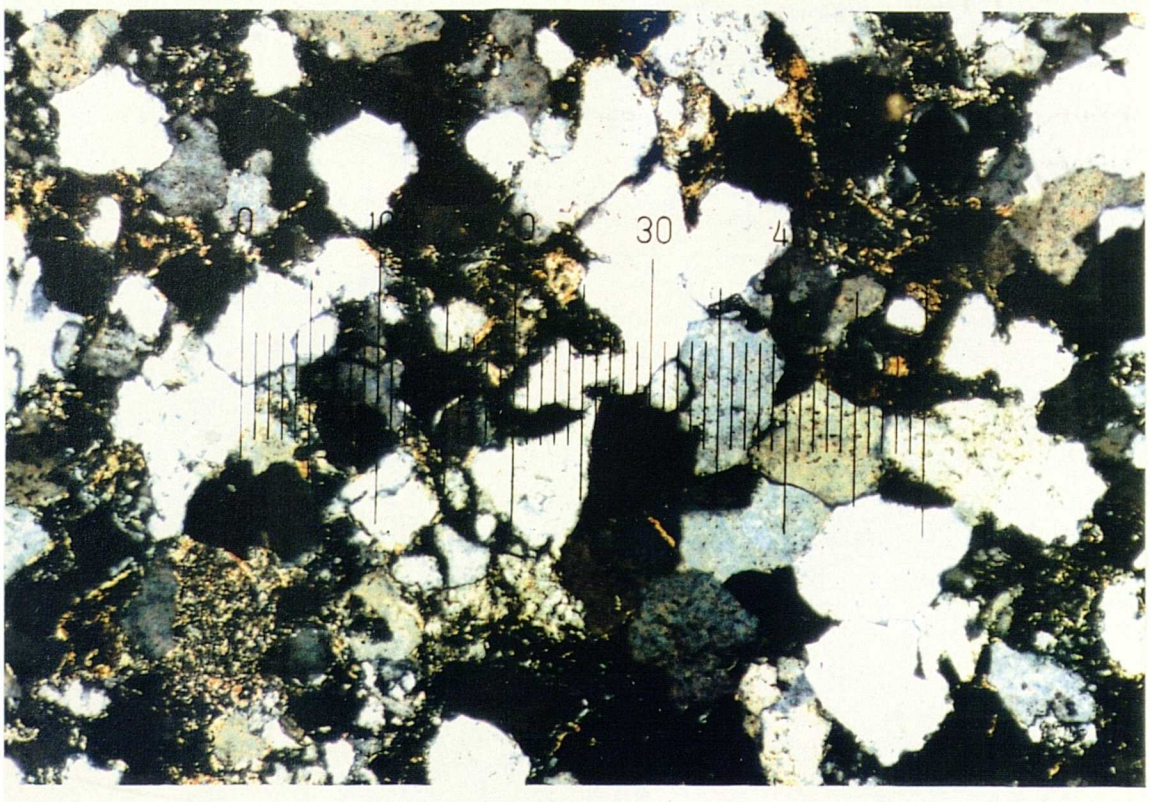

Plate 3.28 Holcombe Brook Grit (type B). Section parallel to bedding under crossed polars. Authigenic clay minerals are abundant. Scale 50 divisions : 1.25mm.

13. Millstone Grit - Type F. Holcombe Brook Grit - Type B (HBGB)

Mineralogy:	%
Quartz	70.3
Alkali feldspar	2.0
Plagioclase feldspar	4.0
SRF's	3.0
Muscovite	2.0
Kaolinite	2.7
Other clays	13.7
Pores	2.0
Opaques	0.3

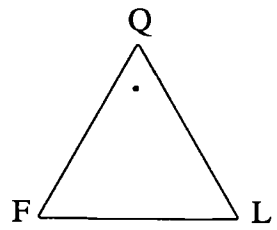

This variety of the Holcombe Brook Grit shows a marked increase in clay minerals as a direct result of weathering of alkali feldspars. In addition, quartz overgrowths are much more developed.

Grain size: Size range is similar to Type G, (0.1-0.3mm, fine to medium sand).

Grain shape: Subrounded to subangular and generally of high sphericity.

Packing density: Vertical: 85.7%
Horizontal: 85.0%

Contacts: Straight and concavo-convex with some suturing.

Grain orientation: No preferential grain orientation.

Classification: *Arkosic wacke.*

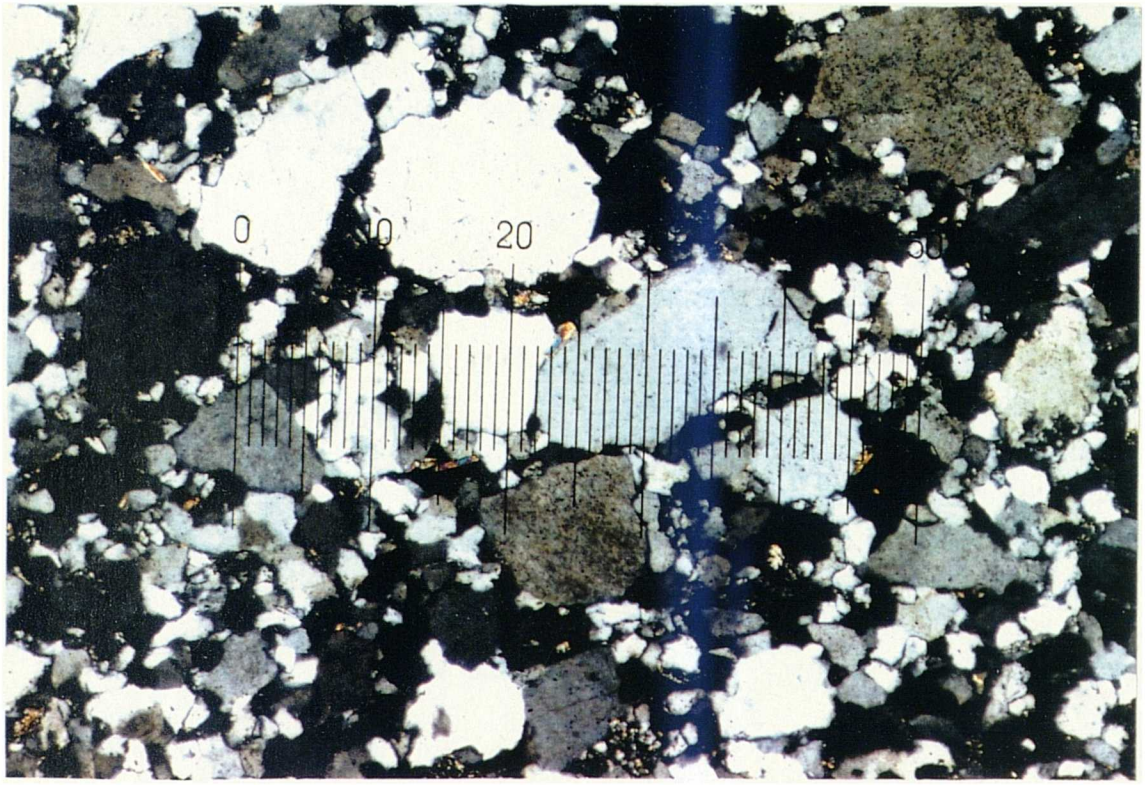

Plate 3.29 Siliceous Sandstone. Section perpendicular to bedding under crossed polars showing bimodality of grain size. Scale 50 divisions : 1.25mm.

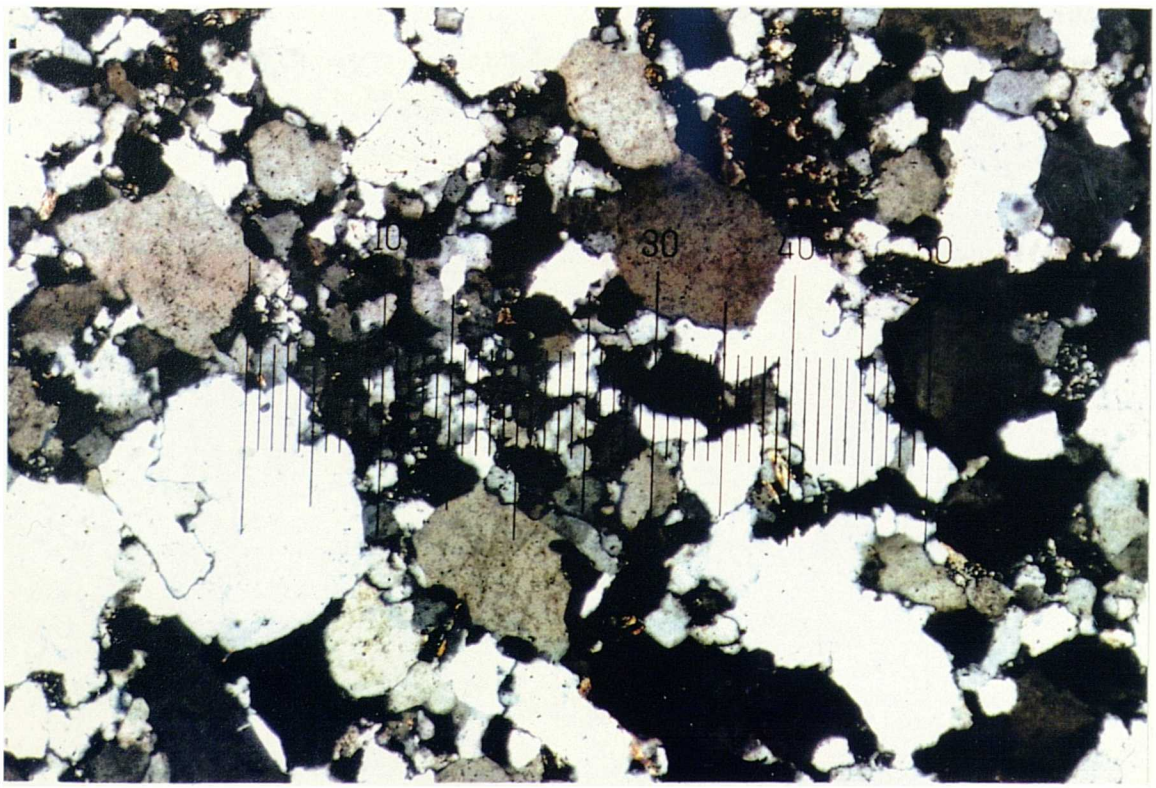

Plate 3.30 Siliceous Sandstone. Section parallel to bedding under crossed polars with P/A angle = 70°. A high degree of grain suturing is evident.
Scale 50 divisions : 1.25mm.

14. Millstone Grit - Type G. Siliceous Sandstone (SS)

Mineralogy:	%
Quartz	82.6
Alkali feldspar	2.6
Plagioclase feldspar	1.0
SRF's	1.0
MRF's	3.3
Muscovite	0.3
Haematite	0.6
Clays	3.0
Opaques	2.6
Heavy minerals	0.6

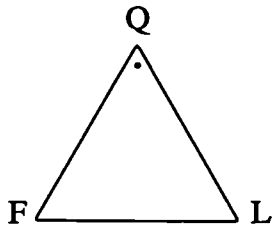

The rock is composed predominantly of quartz. Minor amounts of rock fragments and muscovite are also present. The grains are cemented by quartz welding.

Grain size: The sandstone shows a strong grain size bimodality. The finer grains are in the range 0.05 - 0.125mm while the coarser grains have a modal size range of 0.25 - 0.3mm.

Grain shape: Grains are angular to subangular due to recrystallization but sphericity is high.

Packing density: Vertical: 91.5%
Horizontal: 91.2%

Contacts: Sutured contacts and triple points are abundant.

Grain orientation: Little preferential grain alignment due to high sphericity of grains.

Classification: *Quartz arenite (quartzite).*

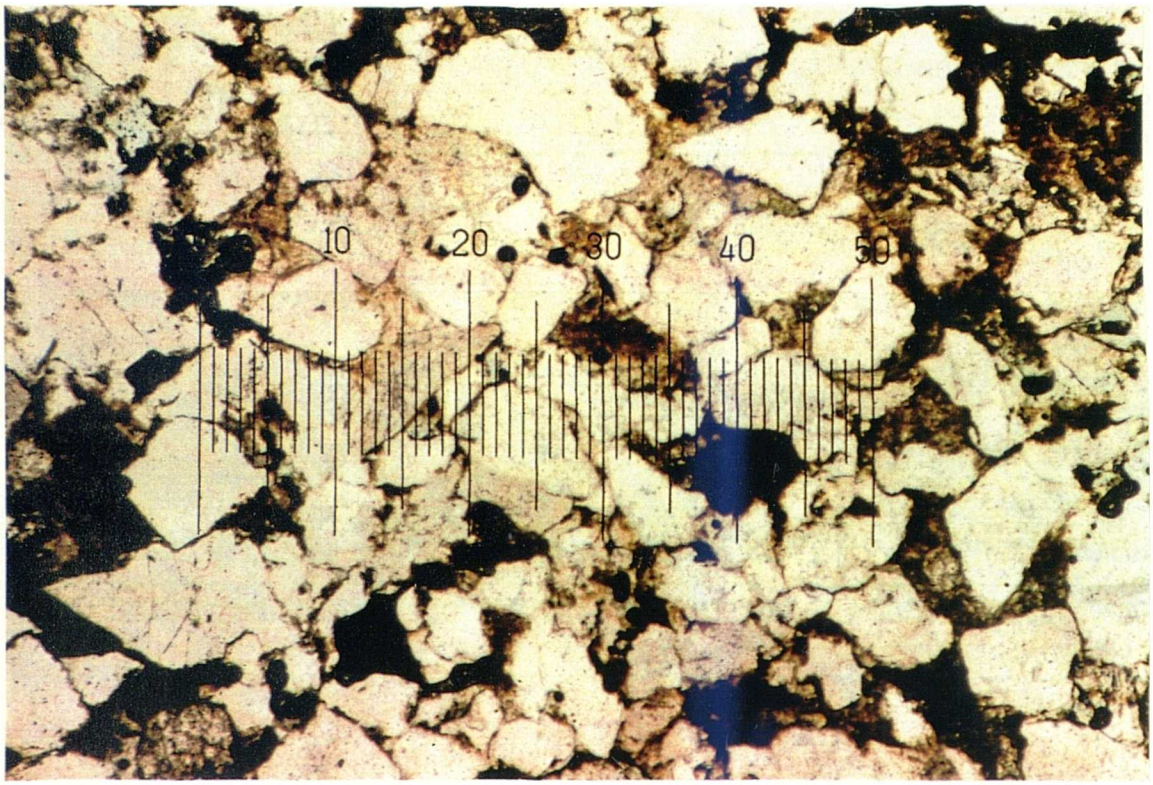

Plate 3.31 Elland Flags. Section perpendicular to bedding in plane polarized light. The angular to subangular grains are cemented by quartz and haematite. Scale 50 divisions : 1.25mm.

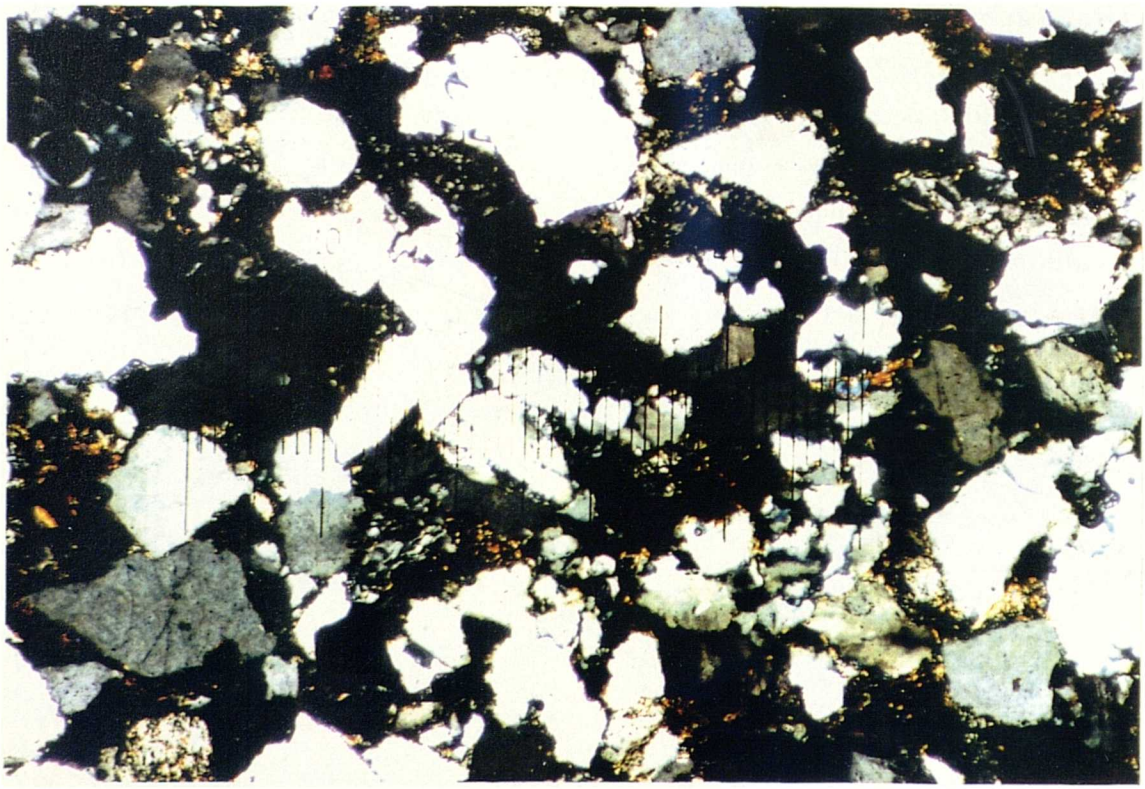

Plate 3.32 Elland Flags under crossed polars. Many of the detrital grains are MRF's and show internal suturing. The abundant SRF's have been deformed around the more competent grains. Scale 50 divisions : 1.25mm.

15. Elland Flags (EF)

Mineralogy:	%
Quartz	52.7
Alkali feldspar	5.0
Plagioclase feldspar	3.3
SRF's	8.3
MRF's	10.0
IRF's	0.7
Muscovite	3.0
Haematite	2.0
Clays	12.3
Pores	2.0
Opaques	0.7

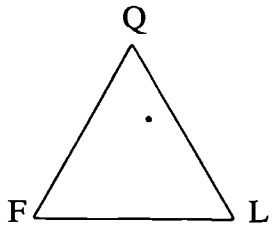

The sandstone contains abundant sedimentary and metamorphic rock fragments. the softer, less competent sedimentary rock fragments having been deformed around the strong quartz grains and metamorphic rock fragments. The rock is generally quartz cemented, with clays infilling many of the pores. Some of the feldspars possess high intragranular porosity.

Grain size: The rock is poorly sorted. Modal size range is 0.1 to 0.3mm, (fine to medium sand).

Grain shape: Angular to subangular and of low to intermediate sphericity.

Packing density: Vertical: 78.9 %
Horizontal: 79.2 %

Contacts: Straight and concavo-convex between quartz grains and rock fragments. Some grain boundaries are totally surrounded by clays.

Grain orientation: No preferential grain alignment.

Classification: *Sublitharenite.*

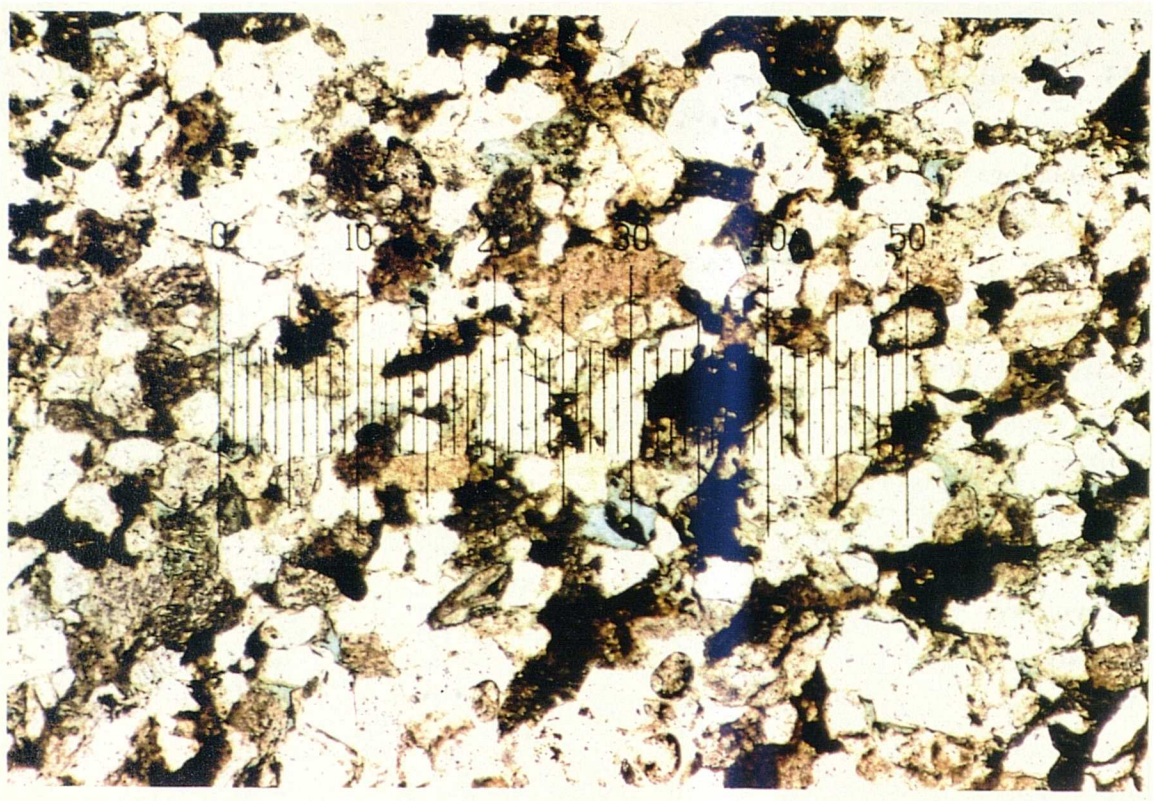

Plate 3.33 Thornhill Rock (type A). Section perpendicular to bedding in plane polarized light. The rock is cemented by quartz and clay minerals but porosity has remained relatively high. Scale 50 divisions : 1.25mm.

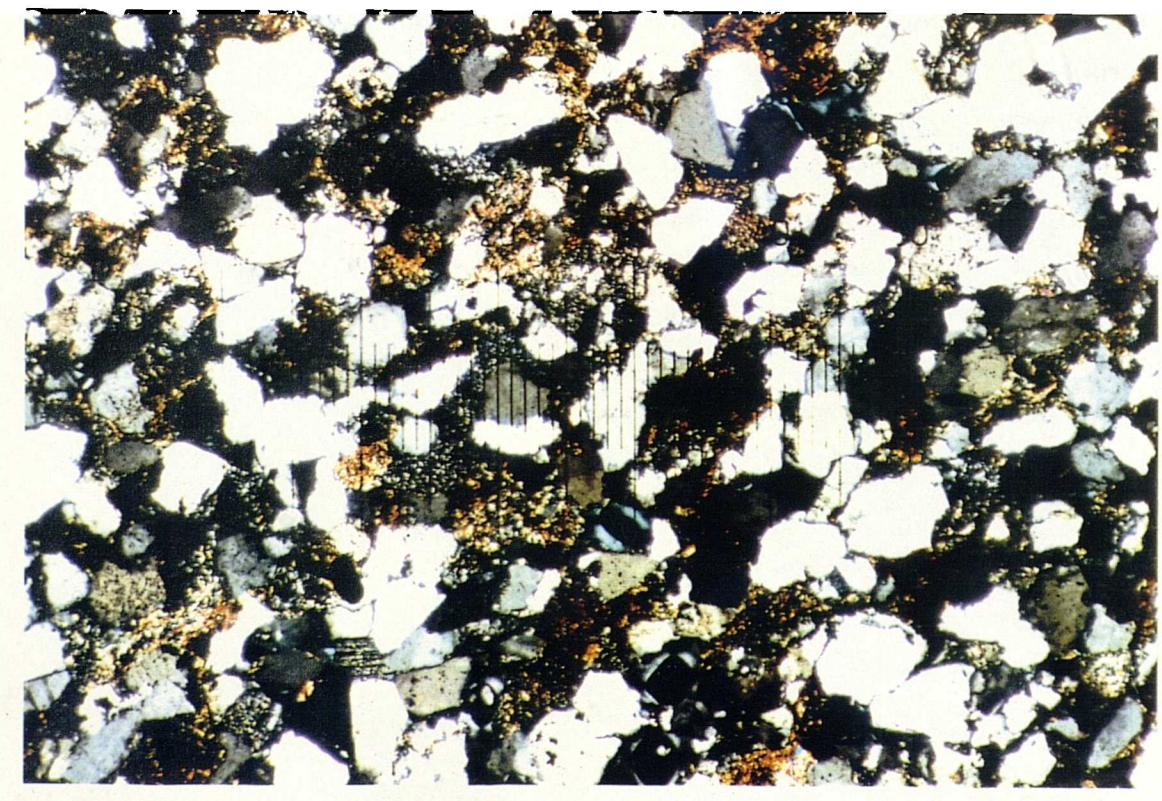

Plate 3.34 Thornhill Rock (type A) under crossed polars. SRF's are abundant and have been highly deformed. Authigenic overgrowths are present on many of the quartz grains. Scale 50 divisions : 1.25mm.

16. Thornhill Rock - Type A (TRA)

Mineralogy:	%
Quartz	52.3
Quartz overgrowths	1.3
Alkali feldspars	4.7
Plagioclase feldspar	2.0
SRF's	21.3
MRF's	6.7
Muscovite	0.7
Clays	5.7
Opaques	2.3
Pores	3.0

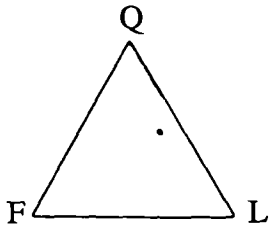

Rock fragments are abundant, especially metamorphic and haematite-rich sedimentary grains. Many of the sedimentary rock fragments show a high degree of deformation into available pore space. Grains are cemented predominantly by quartz but additionally by clay minerals. Authigenic quartz overgrowths are sporadically developed.

Grain size: Modal size of framework grains is 0.06 to 0.15mm, (very fine to fine sand).

Grain shape: Angular to subangular. Grain sphericity is variable from low to high.

Packing density: Vertical: 83.1 %
Horizontal: 85.2 %

Contacts: Many quartz and feldspar grains show straight, concavo-convex and occasional sutured contacts while others are matrix supported.

Grain orientation: No preferential grain alignment.

Classification: *Lithic arenite (sedarenite).*

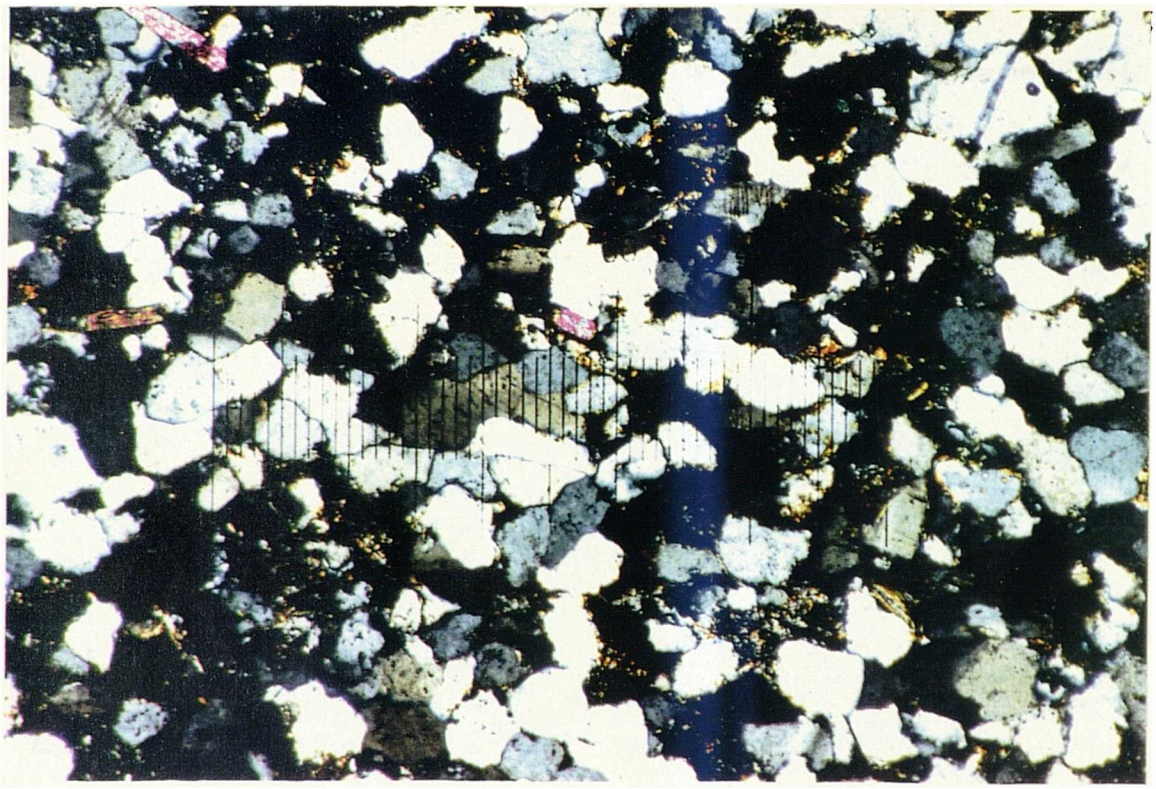

Plate 3.35 Thornhill Rock (type B). Section perpendicular to bedding under crossed polars. Muscovite mica is more abundant in this variety while SRF's are less abundant. Scale 50 divisions : 1.25mm.

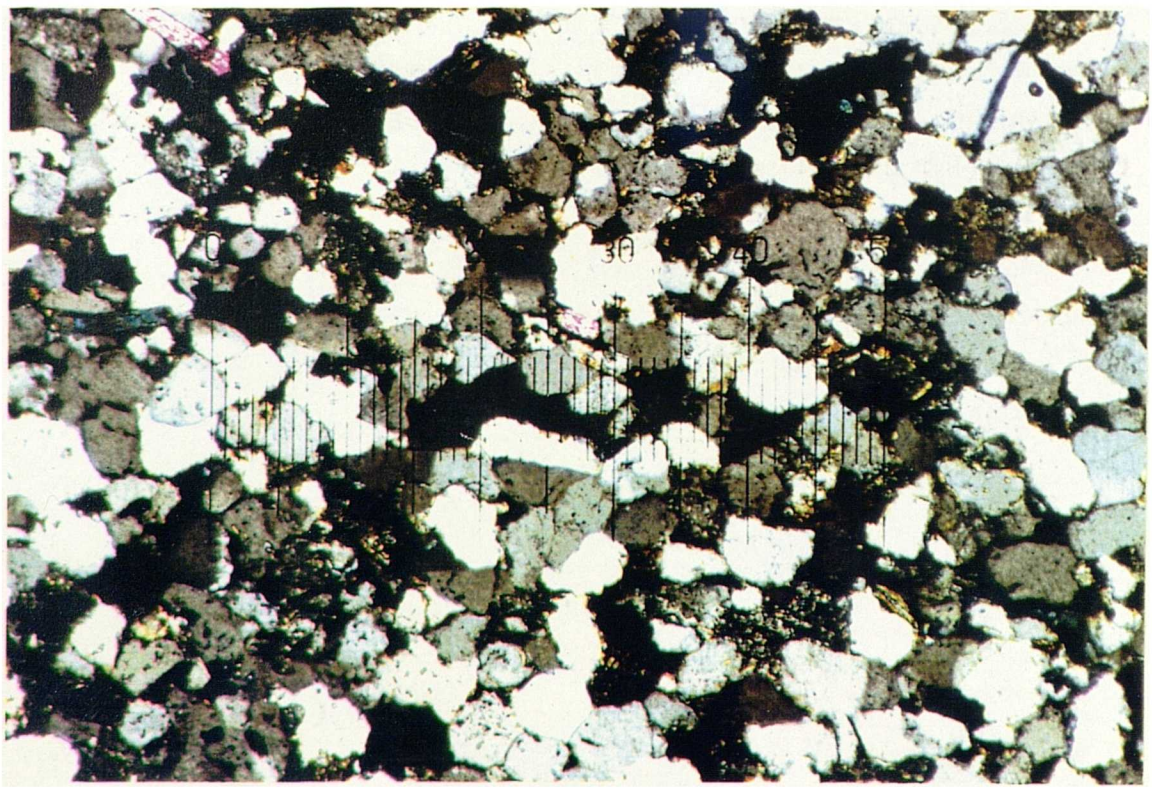

Plate 3.36 Thornhill Rock (type B) under crossed polars with P/A angle = 70° showing abundant concavo-convex and occasional sutured contacts. Quartz overgrowths are sporadically developed. Scale 50 divisions : 1.25mm.

17. Thornhill Rock - Type B (TRB)

Mineralogy:	%
Quartz	70.7
Alkali feldspar	8.3
Plagioclase feldspar	0.0
SRF's	2.0
Muscovite	1.3
Kaolinite	8.3
Other clays	5.7
Pores	3.0
Opaques	0.7

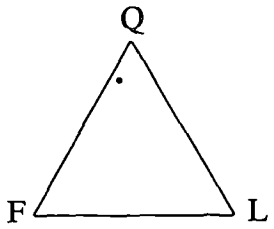

This sandstone variety is quartz cemented, with clays infilling many of the pores. Remnants of highly weathered feldspars remain in a sericite-rich clay matrix.

Grain size: Most grains are in the range 0.05 to 0.15mm, (very fine to fine sand).

Grain shape: Detrital grains are subrounded to subangular and of moderate to high sphericity.

Packing density: Vertical: 71.9%
Horizontal: 83.4%

Contacts: Abundant concavo-convex and occasional sutured contacts.

Grain orientation: No preferential grain alignment.

Classification: *Subarkose.*

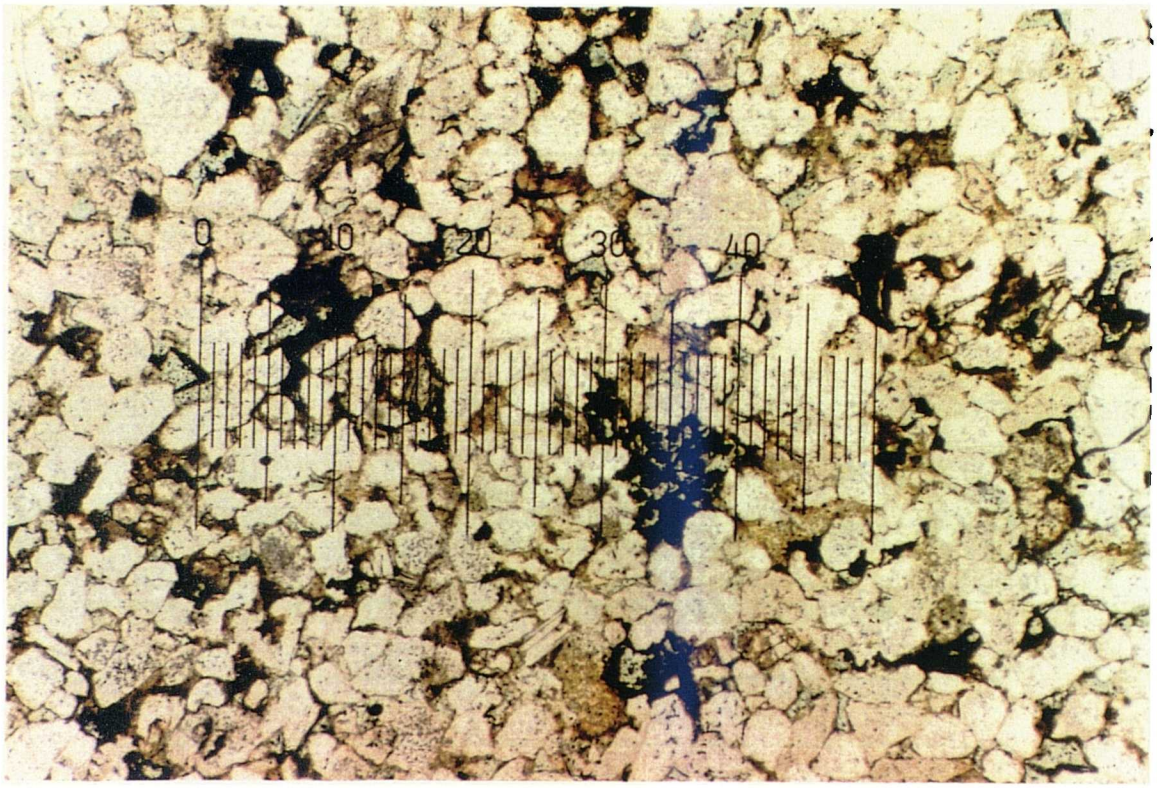

Plate 3.37 Middle Coal Measures. Section perpendicular to bedding in plane polarized light showing high porosity and relative abundance of opaques. Scale 50 divisions : 2.5mm.

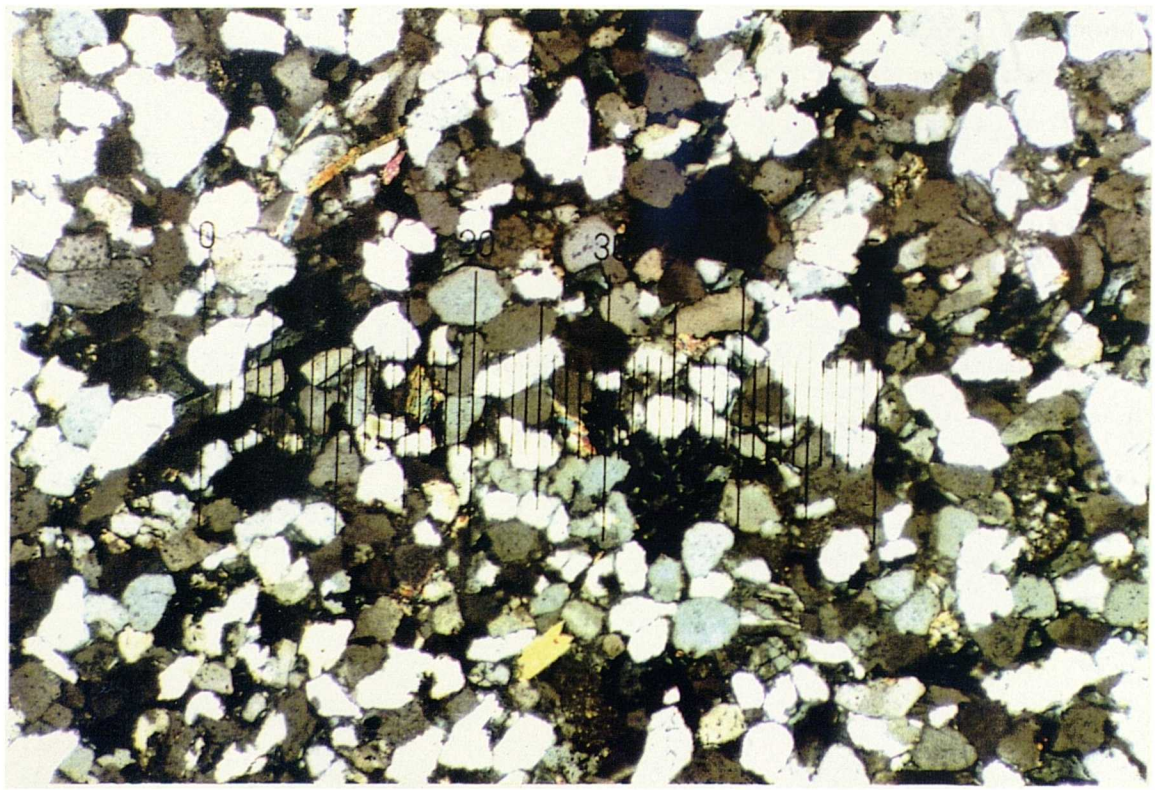

Plate 3.38 Middle Coal Measures under crossed polars with P/A angle = 70°. Point, straight and concavo-convex contacts are all present but packing density is relatively low. Scale 50 divisions : 2.5mm.

18. Middle Coal Measures (MCM)

Mineralogy:	%
Quartz	54.7
Quartz cement	4.3
Alkali feldspar	12.3
Plagioclase feldspar	1.3
SRF's	1.0
MRF's	1.0
IRF's	2.7
Muscovite	1.3
Haematite	2.3
Clays	8.7
Pores	7.7
Opaques	2.7

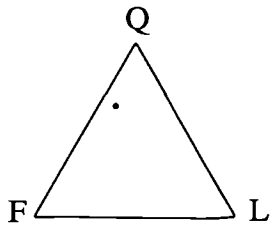

The sandstone is submature with abundant feldspars and clay minerals. Grains are cemented by quartz and clays. Porosity is relatively obvious, occurring as large intergranular clay-lined pores. Chlorite and sericite are the most abundant clay minerals.

Grain size: The rock is moderately sorted. Modal size range is 0.1 to 0.25mm, (fine sand).

Grain shape: Rounded to subrounded and of high sphericity.

Packing density: Vertical: 71.9 %
Horizontal: 78.1 %

Contacts: Mostly point and concavo-convex with occasional sutured contacts.

Grain orientation: No preferential grain alignment.

Classification: *Subarkose.*

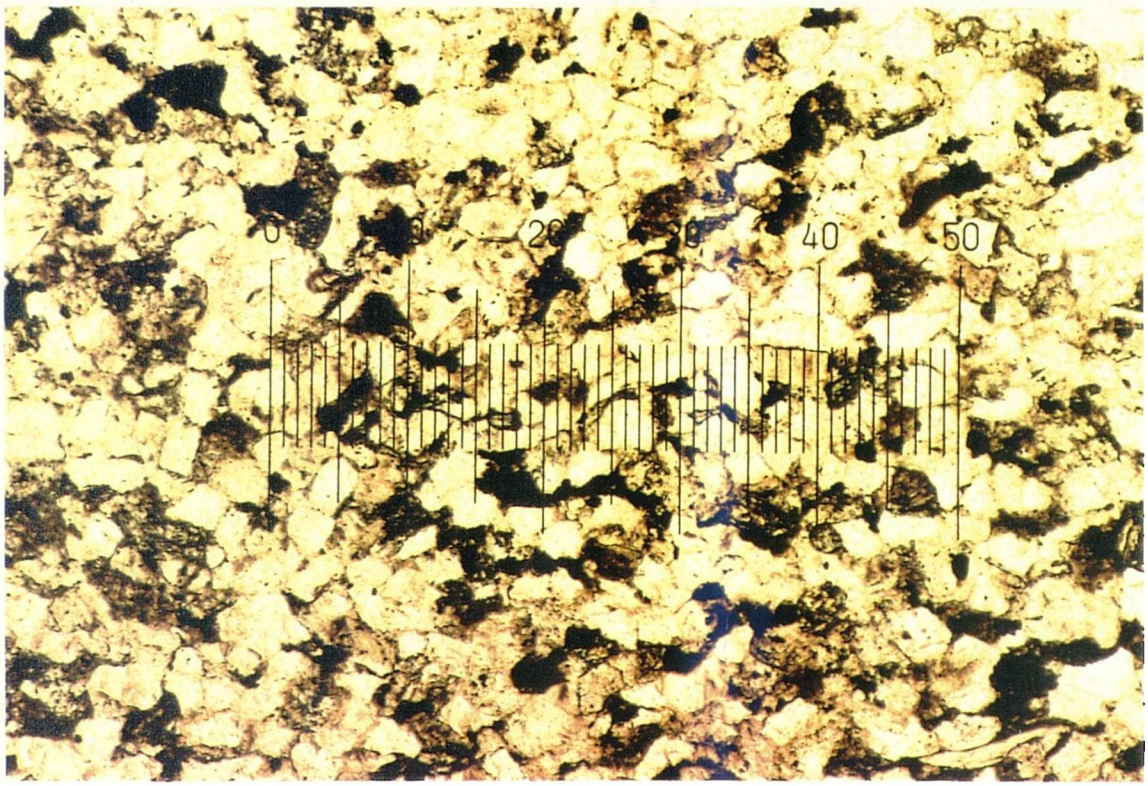

Plate 3.39 Crackington Sandstone. Section perpendicular to bedding in plane polarized light. SRF's and clay minerals are abundant, infilling pores and occluding much of the original porosity. Scale 50 divisions : 1.25mm.

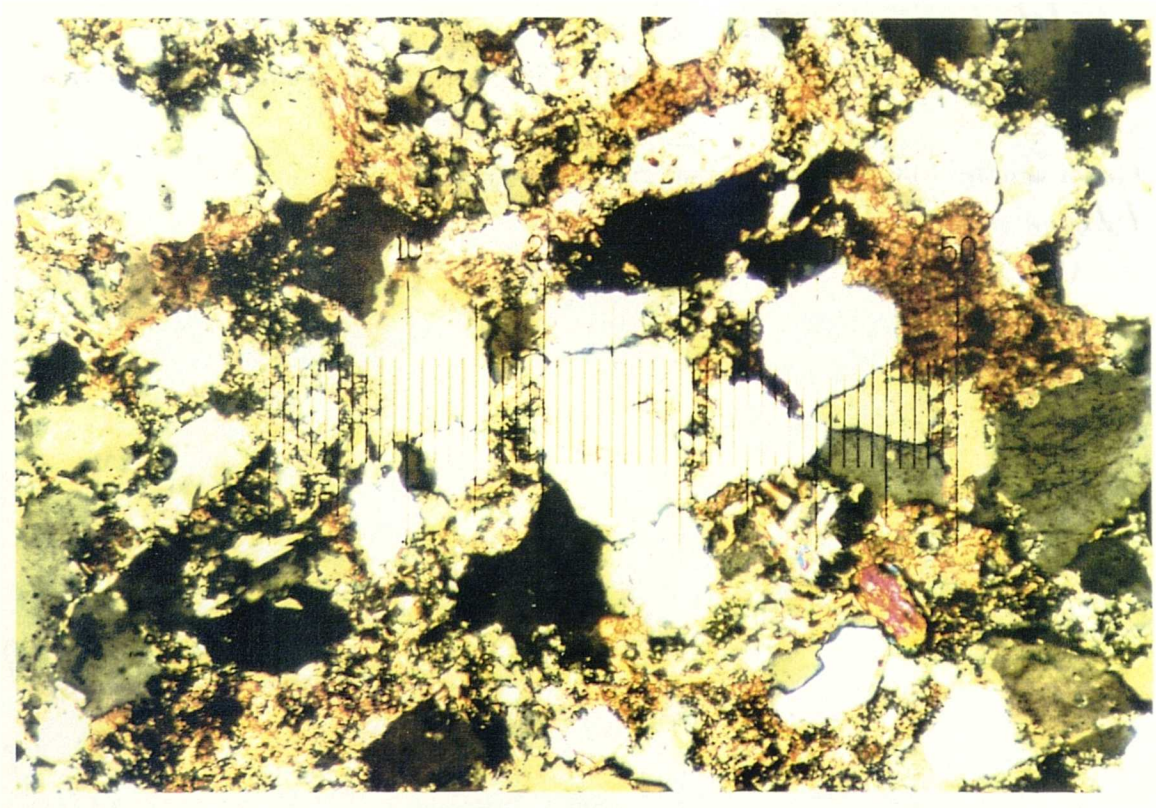

Plate 3.40 Crackington Sandstone. Section perpendicular to bedding under crossed polars with P/A angle = 70°. The rock microfabric indicates a high degree of lithification with most grain contacts being sutured. The abundant clay minerals have been recrystallized. Scale 50 divisions : 0.5mm.

19. Crackington Sandstone (CF)

Mineralogy:	%
Quartz	62.3
Alkali feldspar	2.0
SRF's	9.7
MRF's	6.3
Muscovite	0.7
Haematite	1.0
Clays	15.3
Calcite cement	2.0
Heavy minerals	0.7

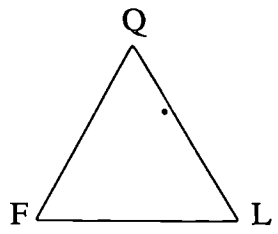

The detrital grains are cemented predominantly by quartz and also by clay minerals. These highly birefringent clay minerals have been recrystallized and infill practically all the pores; hence no porosity is recognisable.

Grain size: Modal size range is 0.06 to 0.12mm, (very fine sand).

Grain shape: Grains are very angular and of low to intermediate sphericity.

Packing density: Vertical: 81.1 %
Horizontal: 83.6 %

Contacts: Abundant suturing and triple point formation between quartz grains and rock fragments.

Grain orientation: No preferential grain alignment.

Classification: *Lithic wacke.*

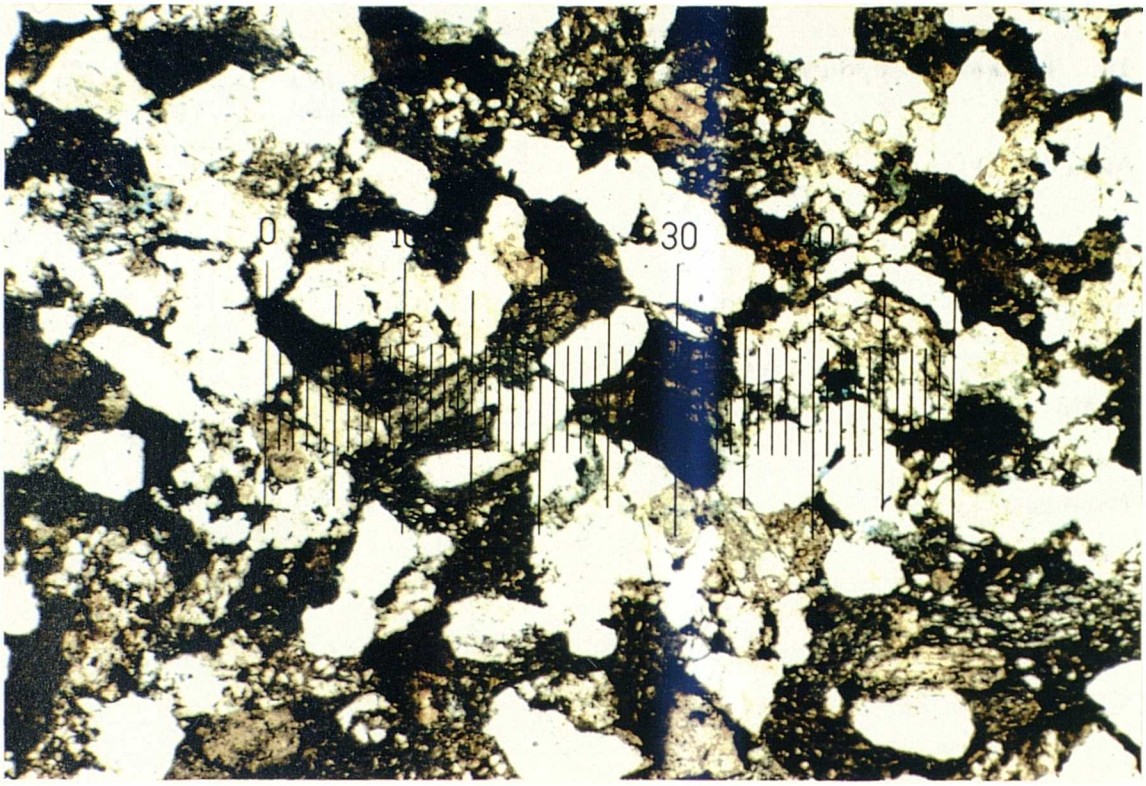

Plate 3.41 Pennant (type A). Section perpendicular to bedding in plane polarized light. The rock contains abundant opaques both as authigenic cement and within many of the SRF's. Scale 50 divisions : 2.5mm.

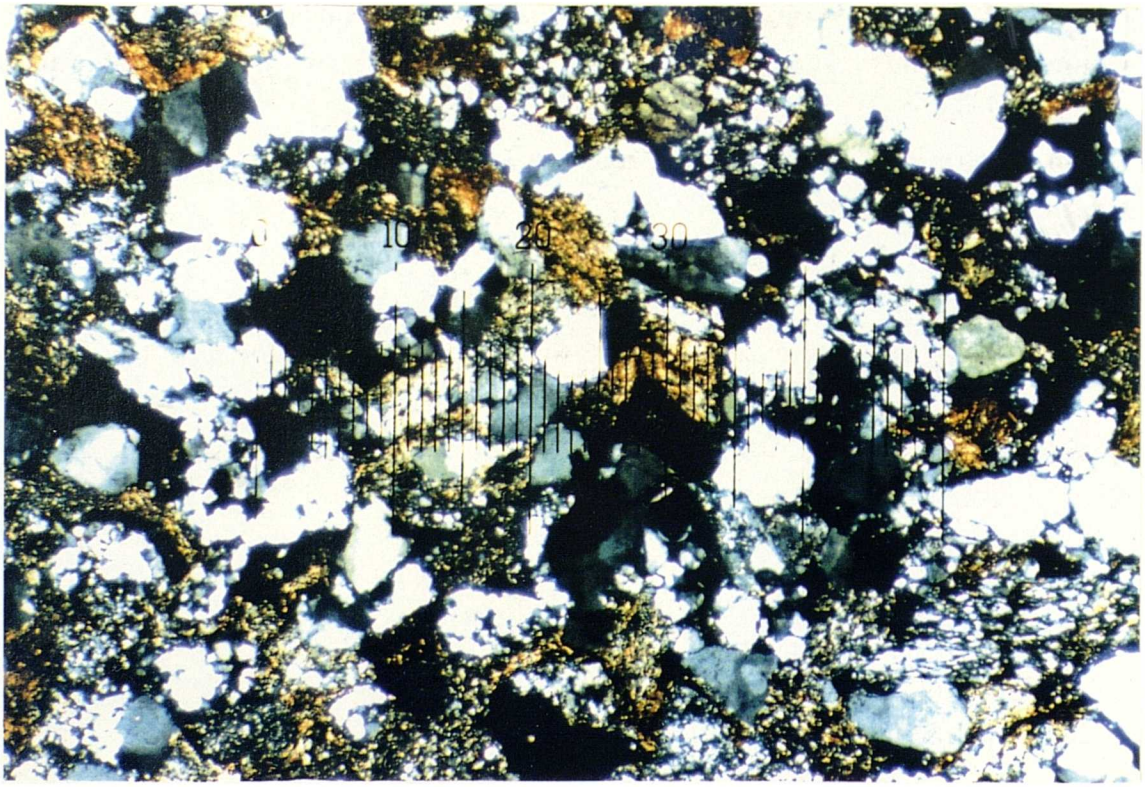

Plate 3.42 Pennant (type A). Section perpendicular to bedding under crossed polars. MRF's and SRF's are abundant, the latter being deformed around the more competent grains. Scale 50 divisions : 2.5mm.

20. Pennant - Type A (PnA)

Mineralogy:	%
Quartz	28.3
Alkali feldspar	3.0
Plagioclase feldspar	0.0
SRF's	18.7
MRF's	25.0
Phyllitic RF's	7.3
Muscovite	0.7
Haematite	3.0
Opaques	11.7
Clays	2.3

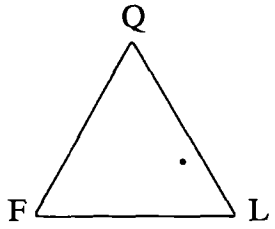

The rock is highly immature - all the quartz grains, sedimentary rock fragments and metamorphic rock fragments are angular although many of the less competent rock fragments have been deformed during diagenesis. Opaque iron oxides are abundant, occurring as secondary pore-filling and cementing materials; in some cases large pores produced by the removal of unstable grains have been totally filled by authigenic iron oxides. Haematite is also present but is subsidiary to other oxides.

Grain size: Many of the phyllitic rock fragments are up to 0.6mm long, but the modal size range is 0.2 to 0.4mm, (medium sand).

Grain shape: Framework grains are higly angular and of low to intermediate sphericity.

Packing Density: Vertical: 91.8 %
Horizontal: 90.7 %

Contacts: Generally concavo-convex, with the less competent rock fragments deformed around the more competent framework grains.

Grain orientation: High aspect ratio grains are aligned parallel to bedding.

Classification: *Phyllarenite.*

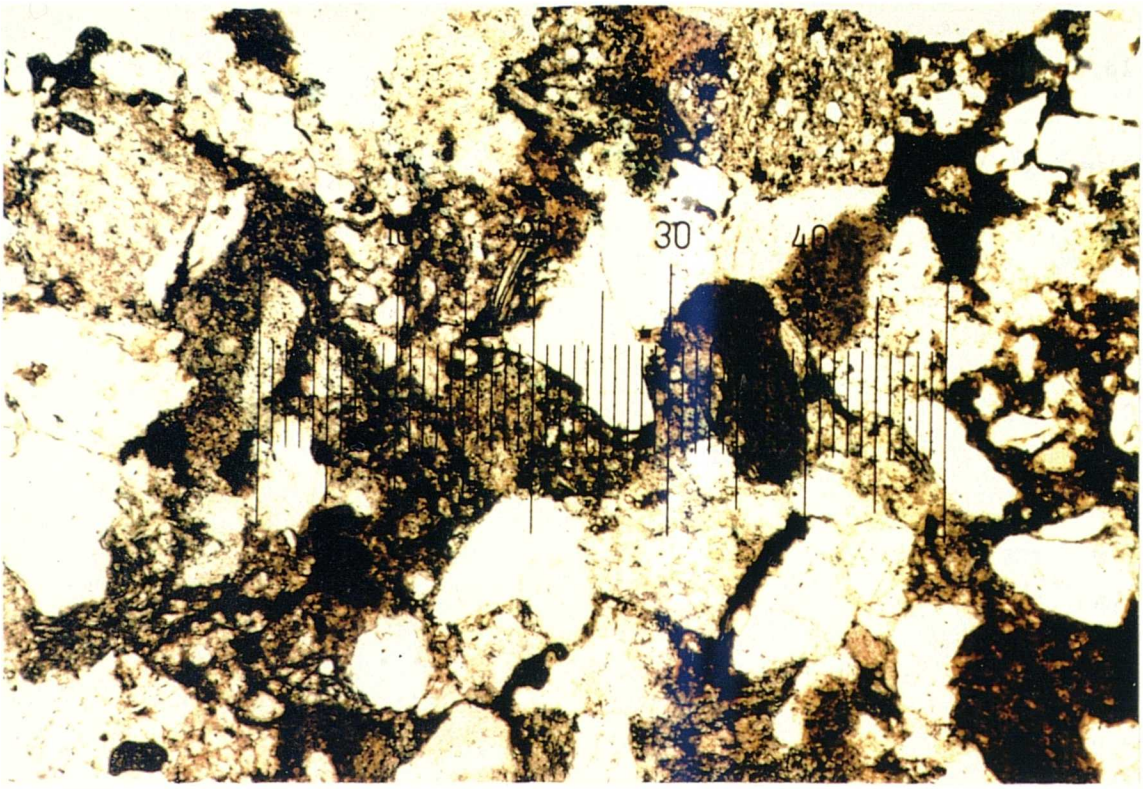

Plate 3.43 Pennant (type B). Section perpendicular to bedding in plane polarized light. Opaques are much less abundant than in type A while phyllitic rock fragments are more frequent. Scale 50 divisions : 1.25mm.

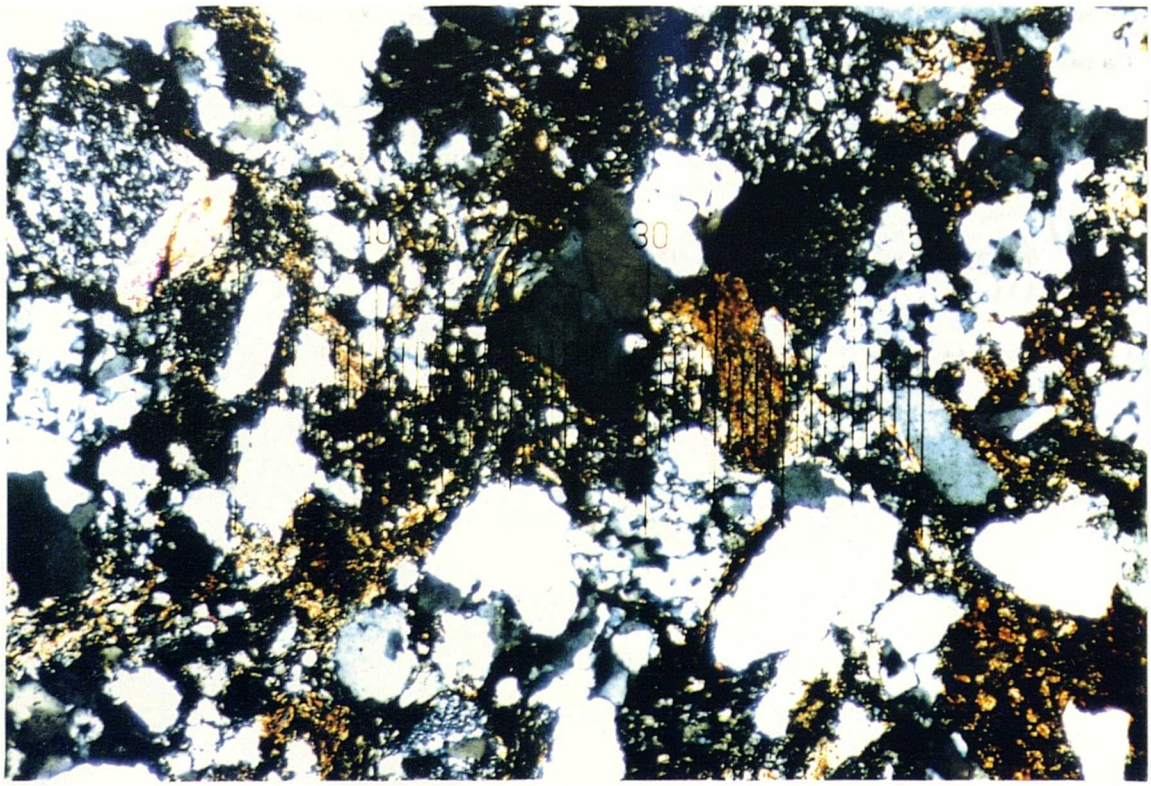

Plate 3.44 Pennant (type B). Section perpendicular to bedding under crossed polars. MRF's are extremely abundant and show some suturing with detrital quartz grains. Scale 50 divisions : 1.25mm.

21. Pennant - Type B (PnB)

Mineralogy:	%
Quartz	30.3
Alkali feldspar	2.0
Plagioclase	0.7
SRF's	17.7
MRF's	28.3
Phyllitic RF's	9.0
Muscovite	0.0
Haematite	0.0
Opaques	1.3
Clays	7.7
Pores	3.0

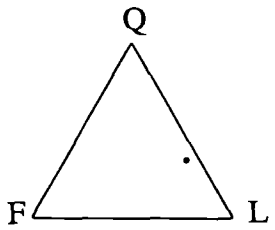

This variety of Pennant sandstone does not contain as much iron oxide as Type A but is again highly immature. Metamorphic rock fragments are more abundant and porosity is higher.

Grain size: Modal size range is 0.1 to 0.4mm, (fine to medium sand).

Grain shape: Angular to subrounded and of low to intermediate sphericity.

Packing density: Vertical: 89.7 %
Horizontal: 85.0 %

Contacts: Generally concavo-convex with occasional sutured contacts between quartz grains.

Grain orientation: Slight alignment of high aspect ratio rock fragments parallel to bedding.

Classification: *Phyllarenite.*

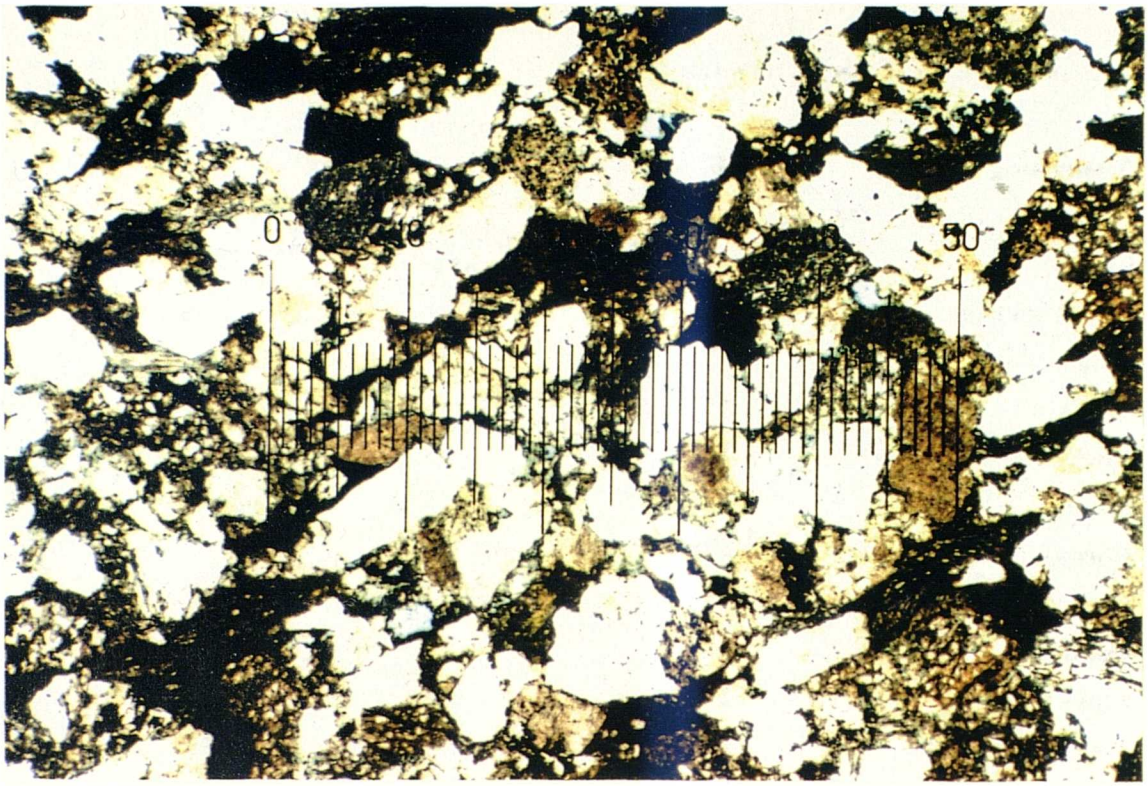

Plate 3.45 Pennant (type C). Section perpendicular to bedding in plane polarized light. Both haematite and opaques are rare in this sandstone. Elongated phyllitic rock fragments are abundant and are aligned generally parallel to bedding. Scale 50 divisions : 2.5mm.

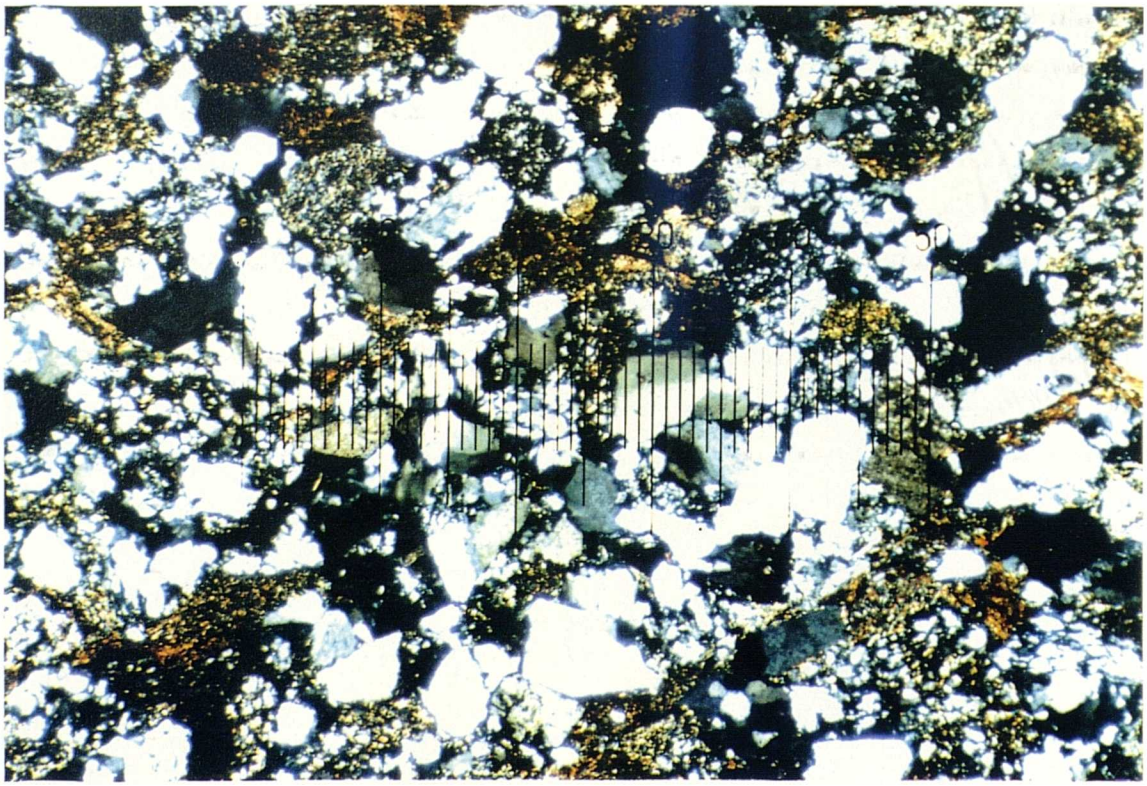

Plate 3.46 Pennant (type C). Section perpendicular to bedding under crossed polars. Phyllitic RF's show distortion around the quartz grains and MRF's. Scale 50 divisions : 2.5mm.

22. Pennant - Type C (PnC)

Mineralogy:	%
Quartz	29.3
Alkali feldspar	2.0
Plagioclase feldspar	0.0
SRF's	8.7
MRF's	30.0
Phyllitic RF's	24.7
Muscovite	1.0
Haematite	0.0
Opaques	1.3
Clays	2.0
Pores	1.0

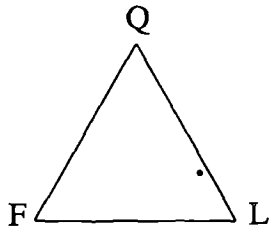

The mineralogy of this variety differs from the other samples in the abundance of elongate phyllitic rock fragments. These have been highly deformed by the more competent quartz grains and metamorphic rock fragments. Type C contains more opaques than Type B but some porosity is evident. Many of the coarser sedimentary rock fragments contain opaques which indicates a primary detrital source.

Grain size: Modal size range is 0.2 to 0.4mm, (medium sand).

Grain shape: Angular to subrounded and of low to intermediate sphericity.

Packing density: Vertical: 86.2 %
Horizontal: 86.8 %

Contacts: Generally concavo-convex with occasional sutured grains. Phyllitic rock fragments show a high degree of accommodation.

Grain orientation: General alignment of phyllitic rock fragments parallel to bedding but diagenetic loading has distorted many grains.

Classification: *Phyllarenite.*

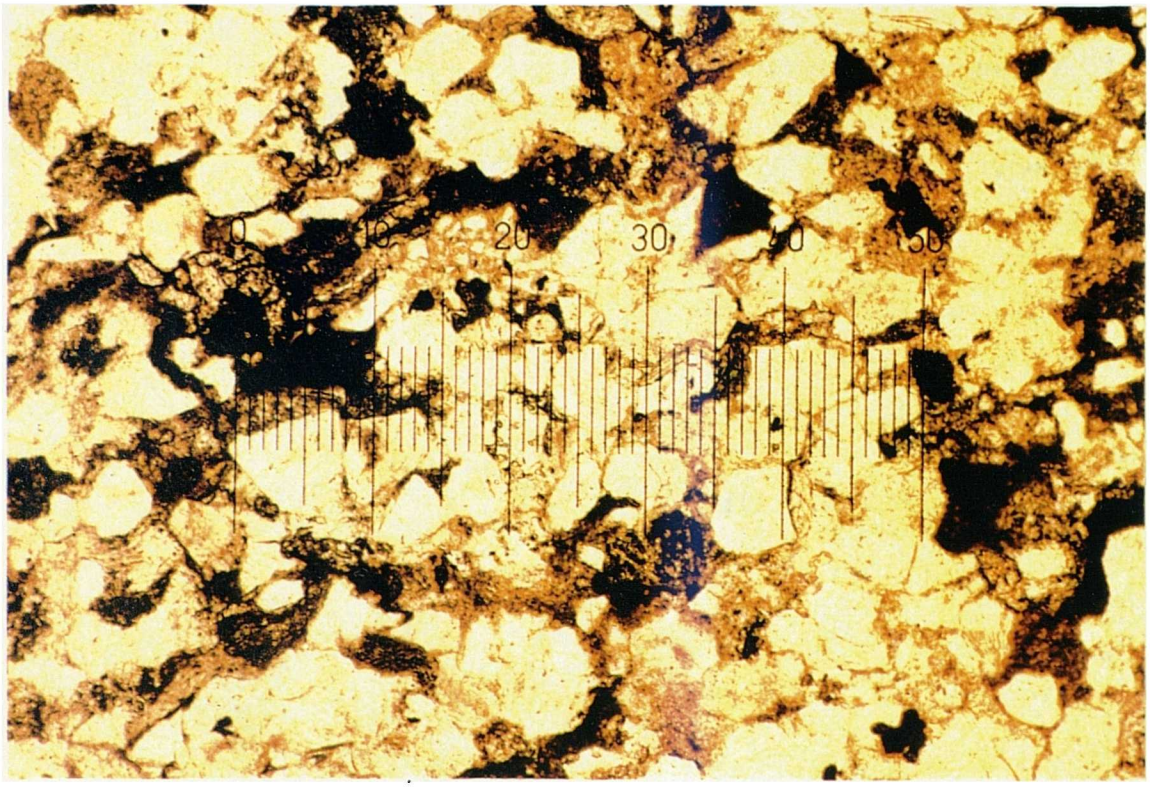

Plate 3.47 Pennant (type D). Section perpendicular to bedding in plane polarized light. Lithic rock fragments and clay minerals are abundant. The majority of the detrital grains are angular and of low sphericity.
Scale 50 divisions : 1.25mm.

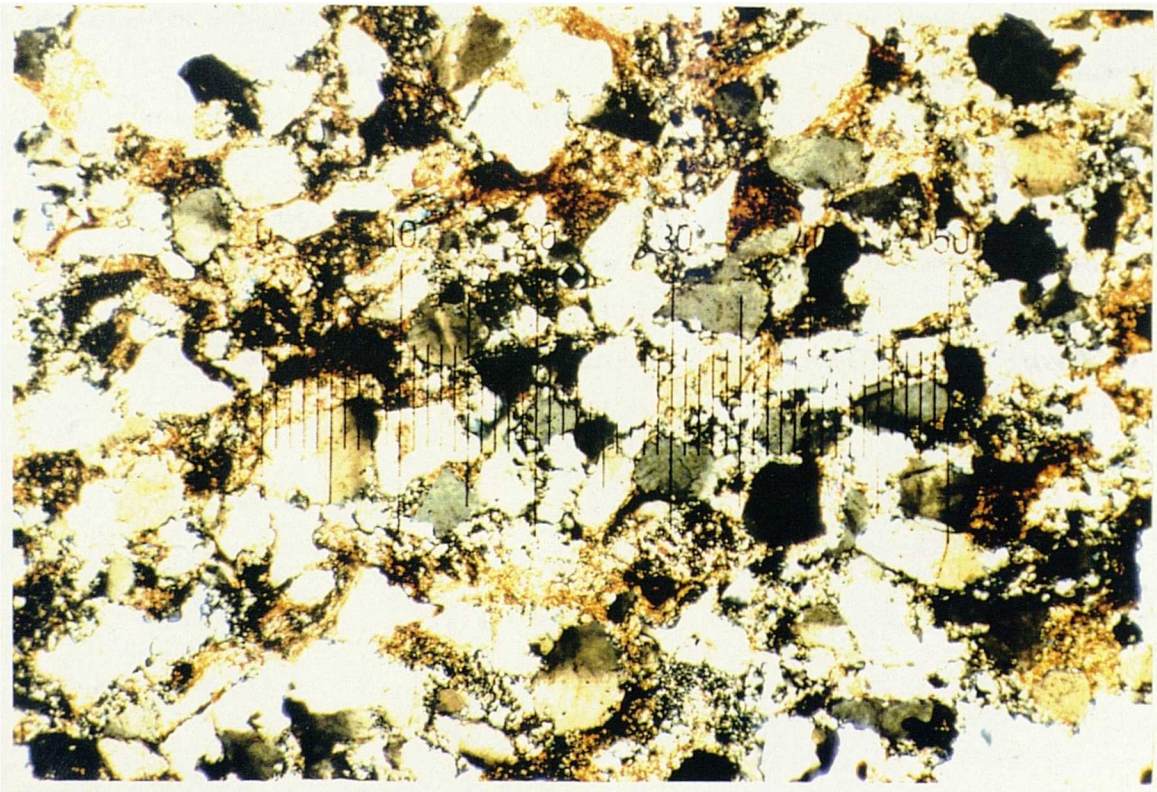

Plate 3.48 Pennant (type D). Section perpendicular to bedding under crossed polars. Sutured contacts are abundant and clay minerals have been recrystallized.
Scale 50 divisions : 1.25mm.

23. Pennant - Type D (PnD)

Mineralogy:	%
Quartz	47.3
Quartz cement	1.7
Alkali feldspar	1.0
Plagioclase feldspar	0.0
SRF's	5.3
MRF's	14.7
IRF's	2.3
Muscovite	0.7
Clays	17.3
Calcite cement	7.7
Pores	2.0

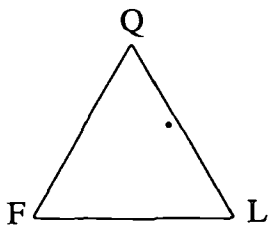

The detrital framework grains are cemented by quartz, calcite and clay minerals. The calcite and clays are porefilling and post-date the quartz. The clays are rich in sericite and chlorite and may have originated from detrital sedimentary rock fragments. In plane polarised light many of the the feldspar grains show a brown discoloration produced by serpentinisation. Abundant silt-sized grains and rounded siltstone fragments are present.

Grain size: The sandstone is poorly sorted, with a modal size range of 0.08 to 0.3mm, (very fine to fine sand).

Grain shape: Angular and of low sphericity.

Packing density: Vertical: 64.2 %
Horizontal: 61.4 %

Contacts: Abundant sutured contacts. Many quartz grains show corrosion.

Grain orientation: No preferential grain alignment.

Classification: *Lithic wacke.*

Plate 3.49 Annan Sandstone. Section perpendicular to bedding in plane polarized light. Alkali feldspars and lithic rock fragments are abundant. Porosity is relatively high. Scale 50 divisions : 1.25mm.

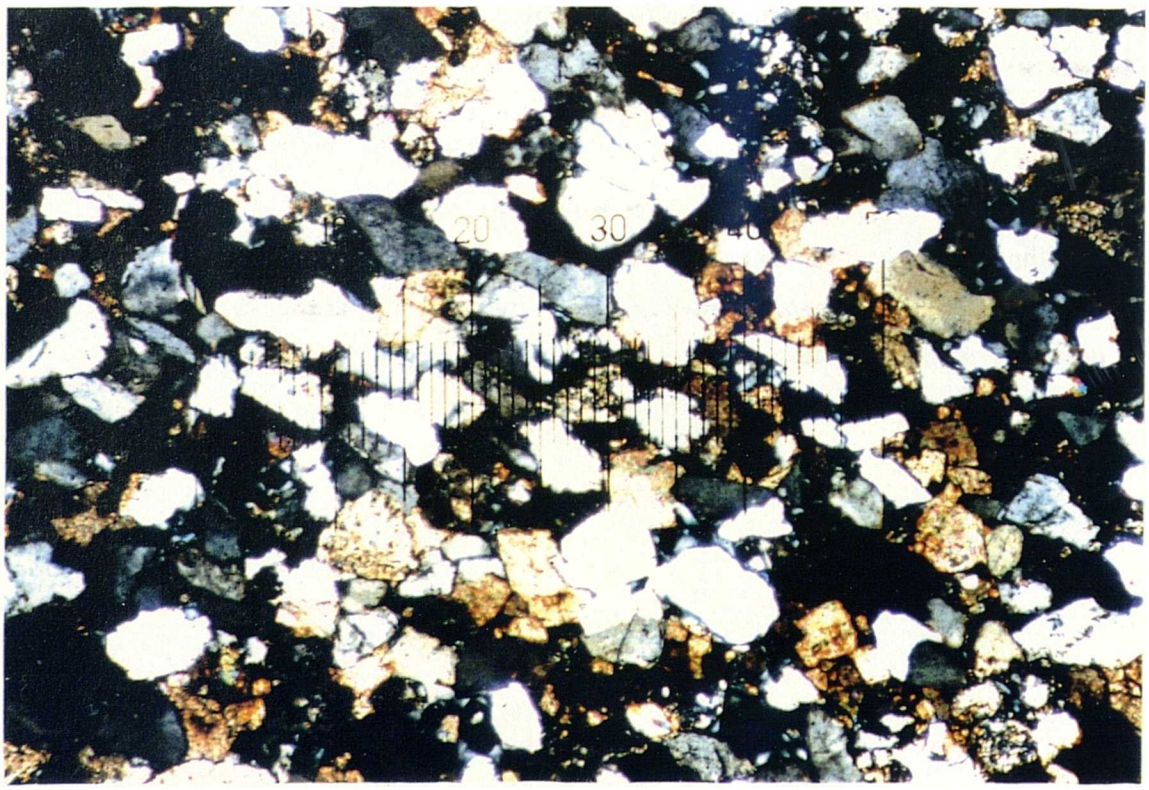

Plate 3.50 Annan Sandstone. Section perpendicular to bedding under crossed polars. CRF's are abundant; many show recrystallization to produce a calcite cement. Scale 50 divisions : 1.25mm.

24. Annan Sandtone (An)

Mineralogy:	%
Quartz	47.3
Alkali feldspar	4.7
Plagioclase feldspar	1.0
SRF's	8.3
MRF's	5.0
IRF's	1.3
CRF's	3.7
Calcite cement	6.7
Haematite	9.7
Opaques	1.3
Clays	6.0
Pores	5.0

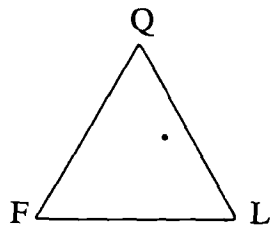

The sandstone is mineralogically and texturally immature, with abundant rock fragments and clays. Carbonate rock fragments are also relatively abundant, some of which may have been dissloved to produce a calcite cement. The grains are also cemented by quartz, haematite and clay minerals.

Grain size: Modal size range is 0.06 to 0.25mm , (very fine to fine sand).

Grain shape: Angular to subangular and of low sphericity.

Packing density: Vertical: 69.5 %

Horizontal: 57.6 % - Due to calcite cement.

Contacts: Concavo-convex and point contacts.

Grain orientation: Alignment of high aspect ratio grains parallel to bedding.

Classification: *Sedarenite.*

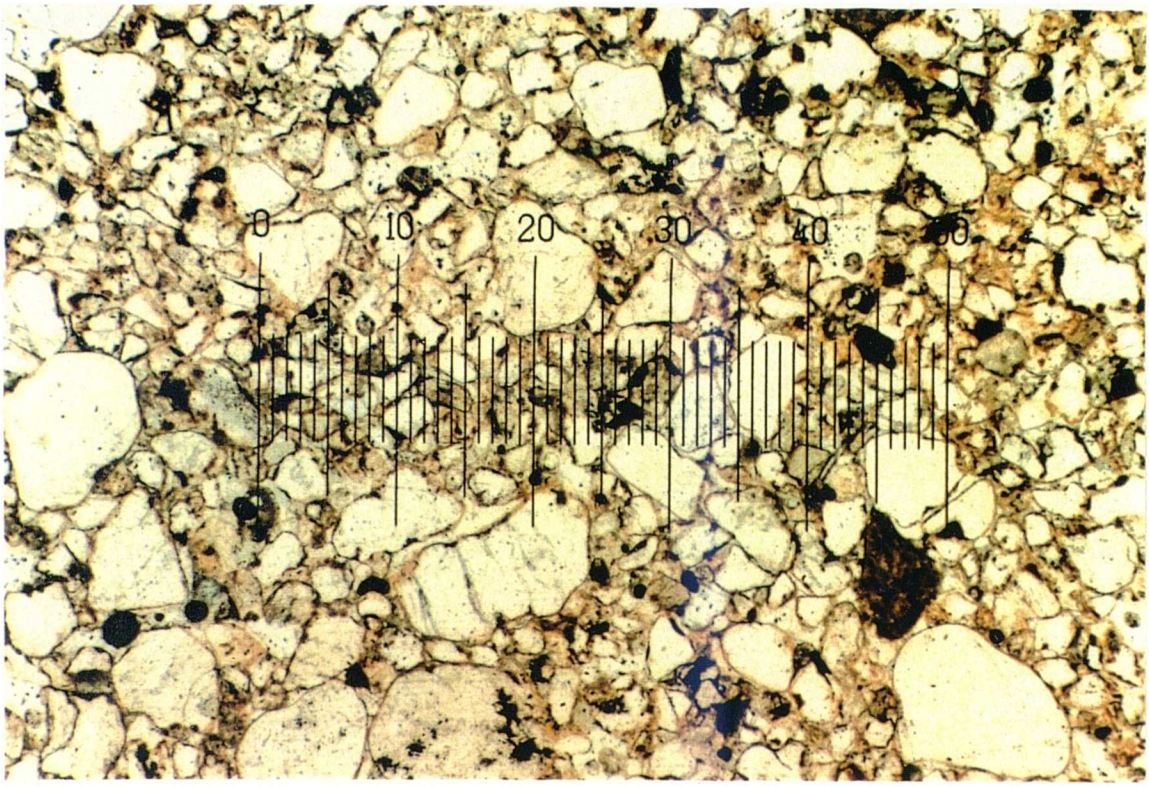

Plate 3.51 Penrith Sandstone (type A). Section perpendicular to bedding in plane polarized light showing poor sorting of detrital grains.
Scale 50 divisions : 2.5mm.

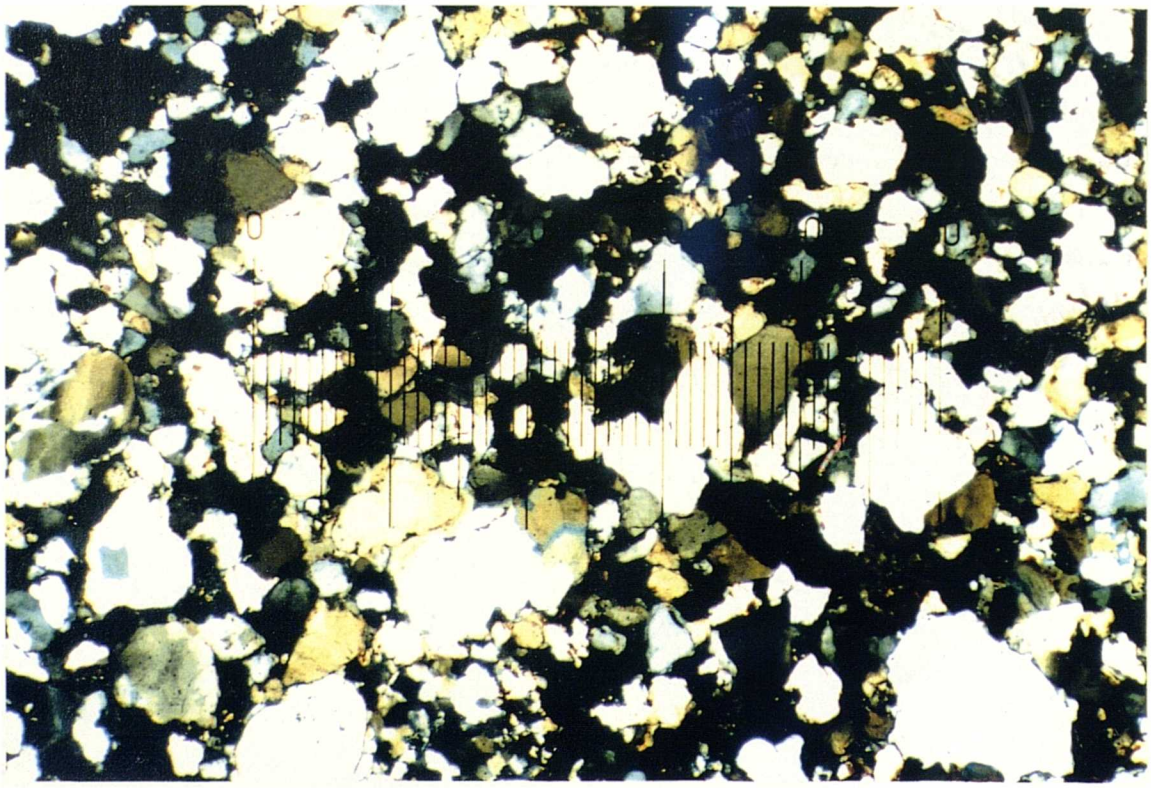

Plate 3.52 Penrith Sandstone (type A). Section perpendicular to bedding under crossed polars. Authigenic quartz overgrowths are abundant on many of the grains.
Scale 50 divisions : 2.5mm.

25. Penrith Sandstone - Type A (PrA)

Mineralogy:	%
Quartz	49.3
Quartz overgrowths	5.0
Alkali feldspar	9.7
Plagioclase feldspar	3.3
SRF's	3.7
MRF'S	0.7
IRF's	5.3
Haematite	12.3
Opaques	0.7
Clays	1.7
Pores	8.3

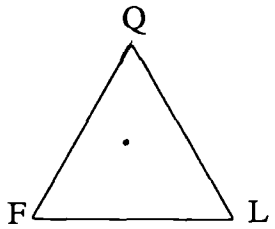

The rock is cemented by quartz and haematite, with quartz overgrowths sporadically developed. Many of the feldspars show a high degree of alteration.

Grain size: Poorly sorted, with a size range of 0.05 to 0.8mm, (fine to coarse sand).

Grain shape: Rounded to subrounded and of low to intermediate sphericity.

Packing density: Vertical: 79.0 %
Horizontal: 71.0 %:

Contacts: Concavo-convex and point contacts.

Grain orientation: High aspect ratio grains are aligned approximately parallel to bedding.

Classification: *Subarkose.*

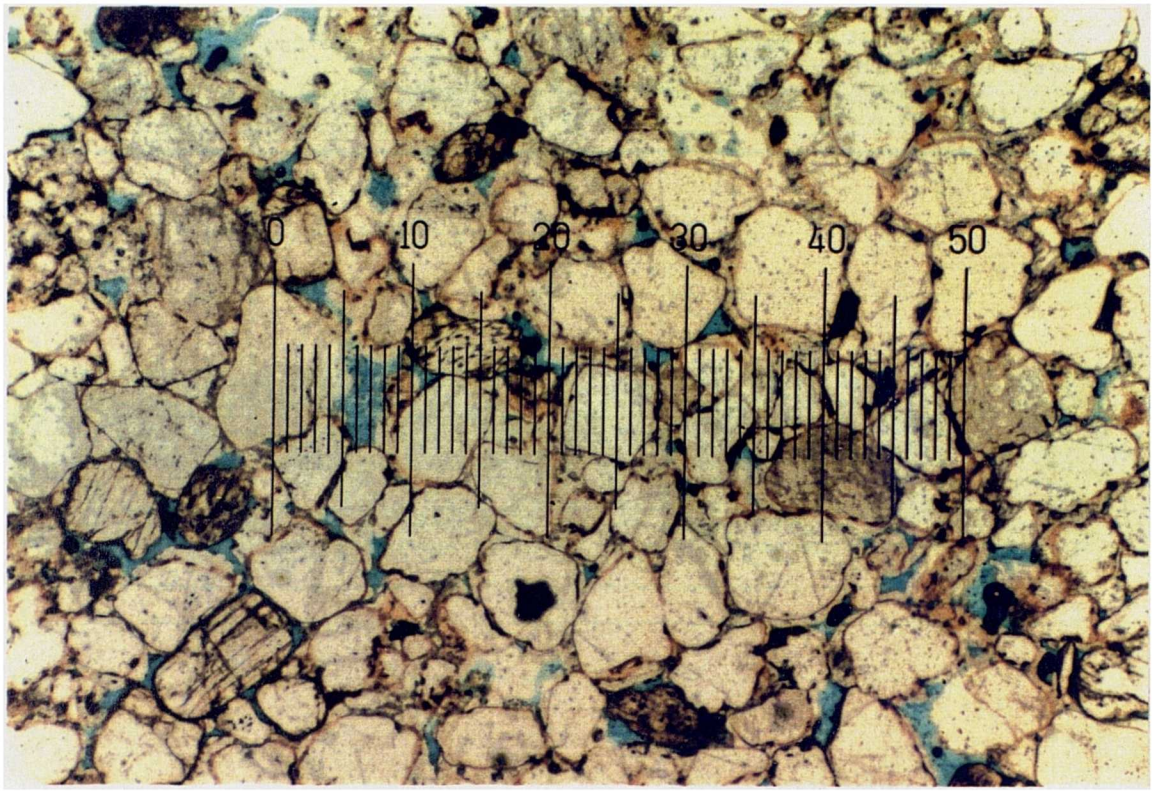

Plate 3.53 Penrith Sandstone (type B). Section parallel to bedding in plane polarized light. Quartz and feldspar grains are well sorted and little matrix material is present. Porosity is high. Scale 50 divisions : 2.5mm.

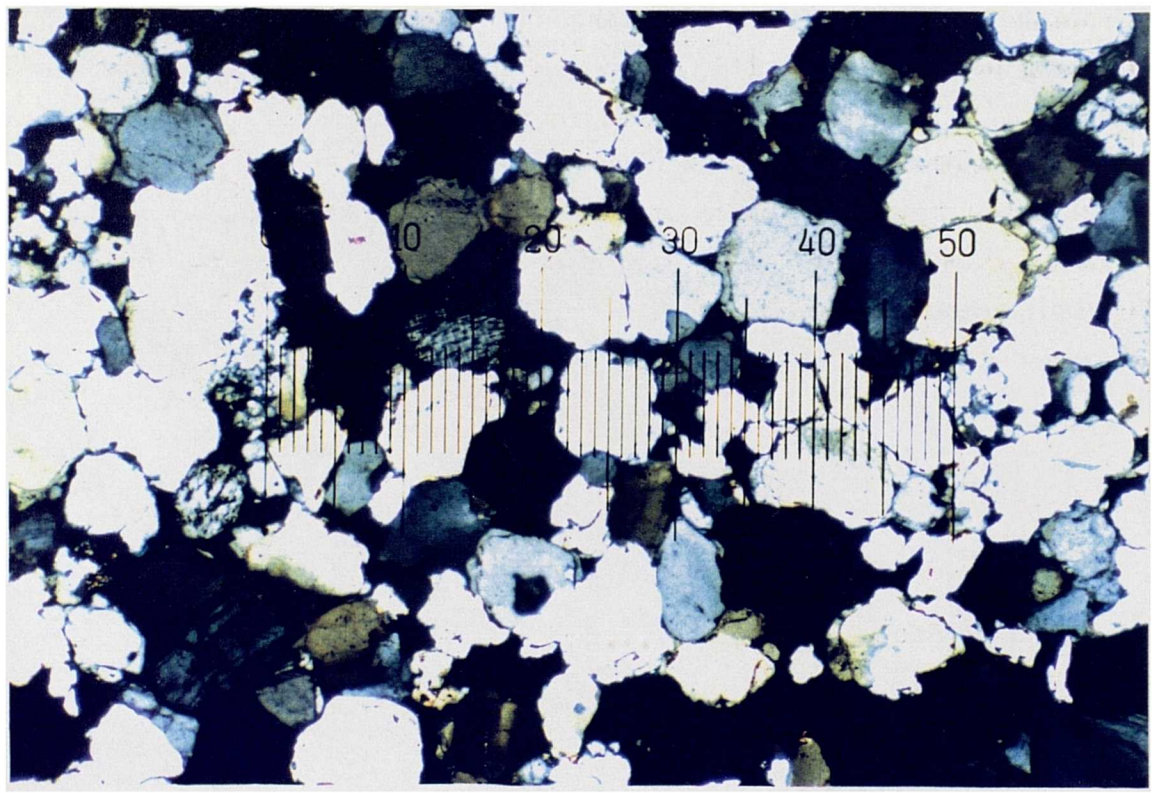

Plate 3.54 Penrith Sandstone (type B). Section parallel to bedding under crossed polars. Authigenic overgrowths are present on all the quartz grains and occur on some feldspar grains. Scale 50 divisions : 2.5mm.

26. Penrith Sandstone -Type B (PrB)

Mineralogy:	%
Quartz	57.3
Quartz overgrowths	18.7
Alkali feldspar	4.0
Plagioclase feldspar	0.0
SRF's	0.3
MRF's	1.7
Haematite	7.0
Opaques	1.3
Clays	2.0
Pores	7.7

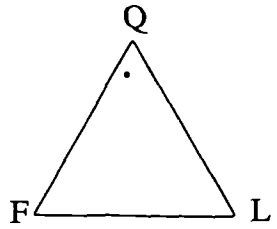

Quartz overgrowths are extremely well developed and weld the detrital grains together. Haematite ghost outlines clearly show the former grain surfaces. Porosity is high in areas where authigenic overgrowths are not well developed. High magnification shows secondary intragranular solution and fracture porosity within many of the feldspar grains.

Grain size: Modal size range is 0.3 to 0.5mm, (medium sand).

Grain shape: All grains are well rounded and of medium to high sphericity. Feldspar grains generally show high sphericity.

Packing density: Vertical: 83.2 %
Horizontal: 70.2 %

Contacts: Original grain contacts are point type but overgrowths have produced straight and concavo-convex contacts.

Grain orientation: No preferential grain alignment.

Classification: *Subarkose.*

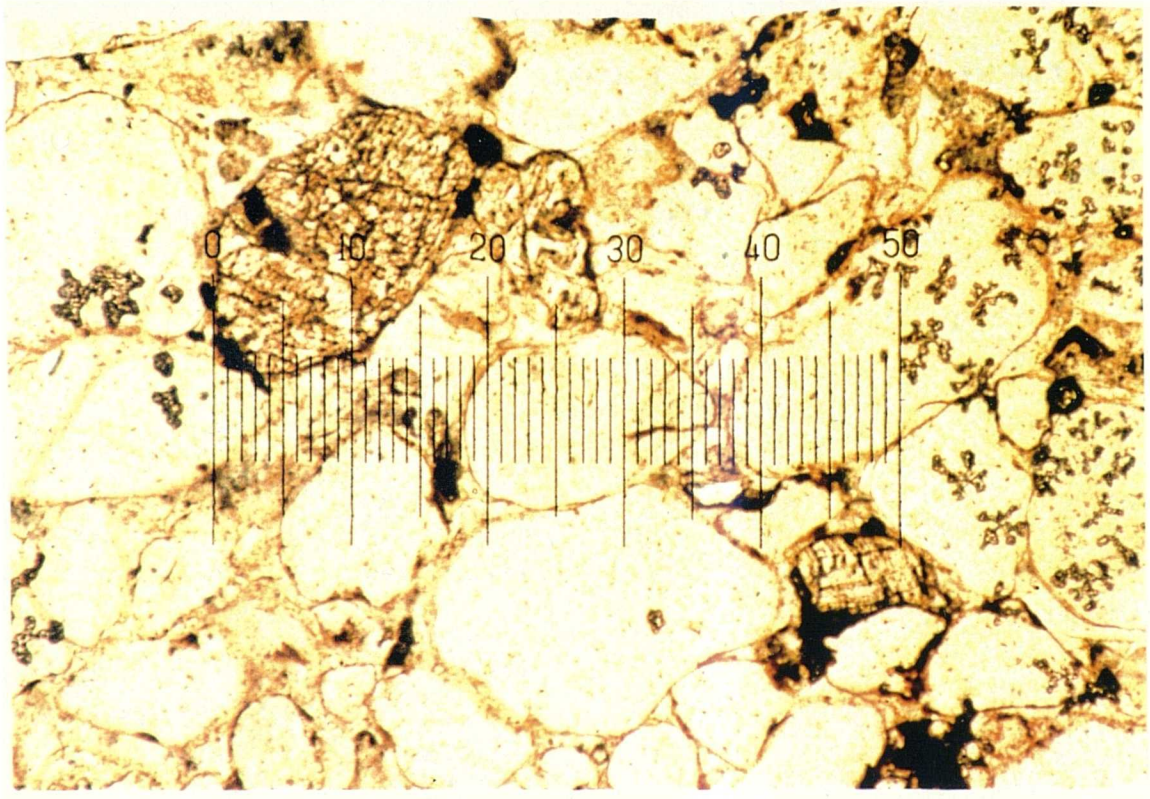

Plate 3.55 Penrith Sandstone (type C). Section perpendicular to bedding in plane polarized light. Packing density is high with many of the grains showing concavo-convex contacts. Scale 50 divisions : 1.25mm.

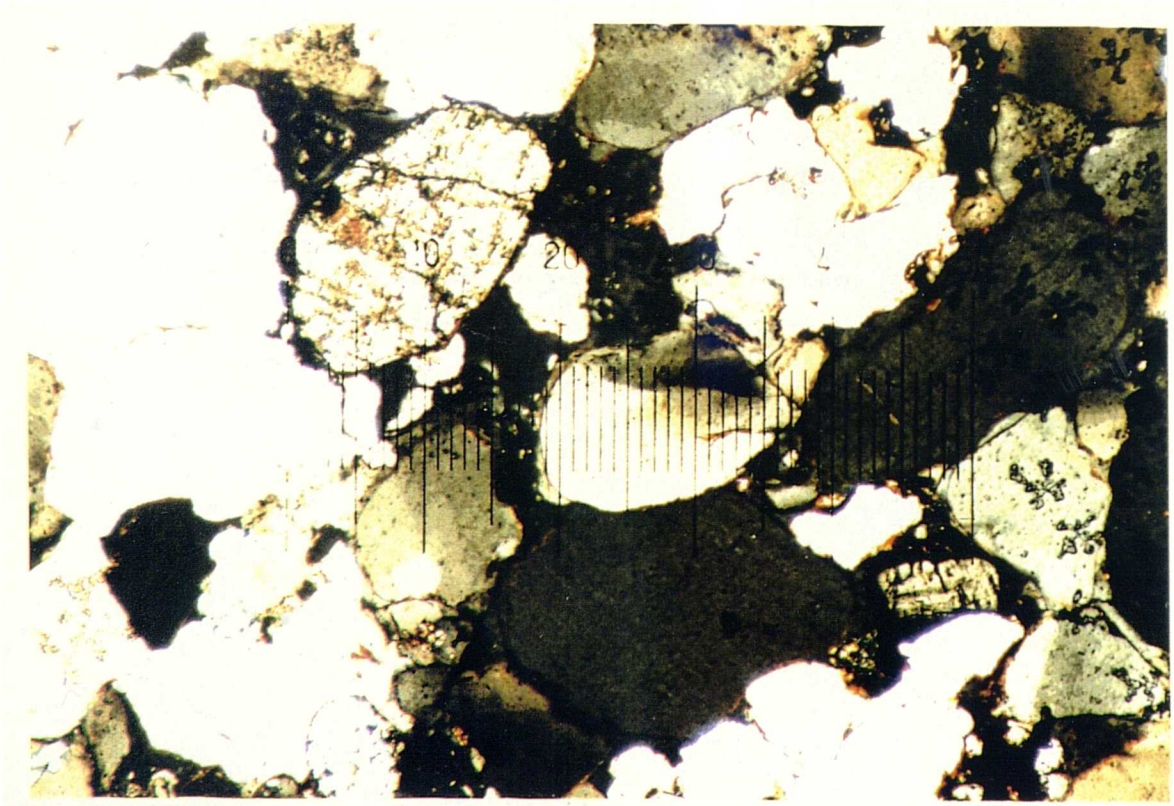

Plate 3.56 Penrith Sandstone (type C). Section perpendicular to bedding under crossed polars. Quartz overgrowths are poorly developed due to original low porosity. Scale 50 divisions : 1.25mm.

27. Penrith Sandstone - Type C (PrC)

Mineralogy:	%
Quartz	51.3
Quartz overgrowths	25.3
Alkali feldspar	4.0
SRF's	2.3
MRF's	9.7
Haematite	5.7
Clays	0.7
Opaques	1.0
Pores	2.7

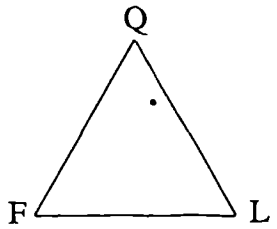

This variety has a lower porosity than any of the other samples collected due to quartz overgrowths and poor sorting of detrital material. Composition is similar to types A and B.

Grain size: The rock is very poorly sorted, with alternating layers of coarse and fine material; all show overgrowths. Size range is from 0.1 to 0.8mm. Most of the detrital grains fall in the coarse sand range.

Grain shape: Well rounded to rounded and of high sphericity.

Packing density: Vertical: 92.5 %
Horizontal: 82.5 %

Contacts: Originally point contacts with some concavo-convex but overgrowths have produced abundant concavo-convex and straight contacts.

Grain orientation: No preferential grain alignment.

Classification: *Sublitharenite.*

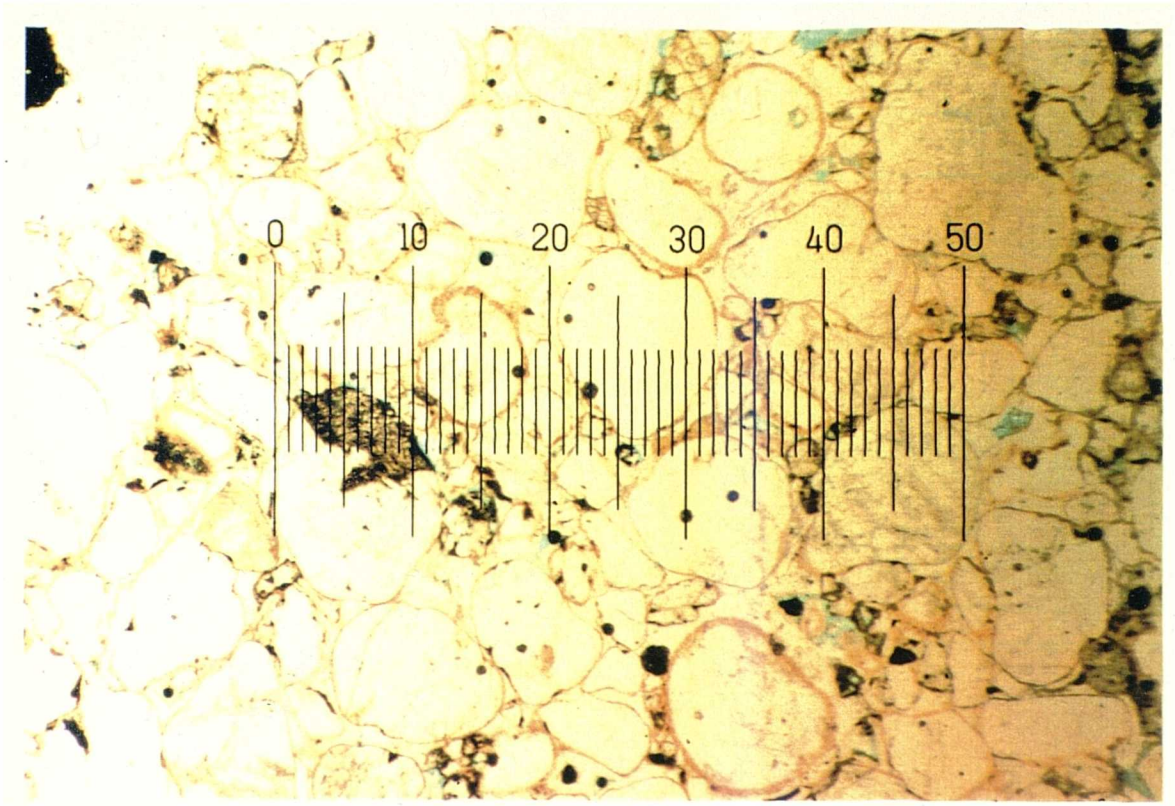

Plate 3.57 Penrith Sandstone (type D). Section parallel to bedding in plane polarized light. Original porosity was extremely high with many grains showing point contacts. Blue epoxy resin shows the remaining pores.
Scale 50 divisions : 2.5mm.

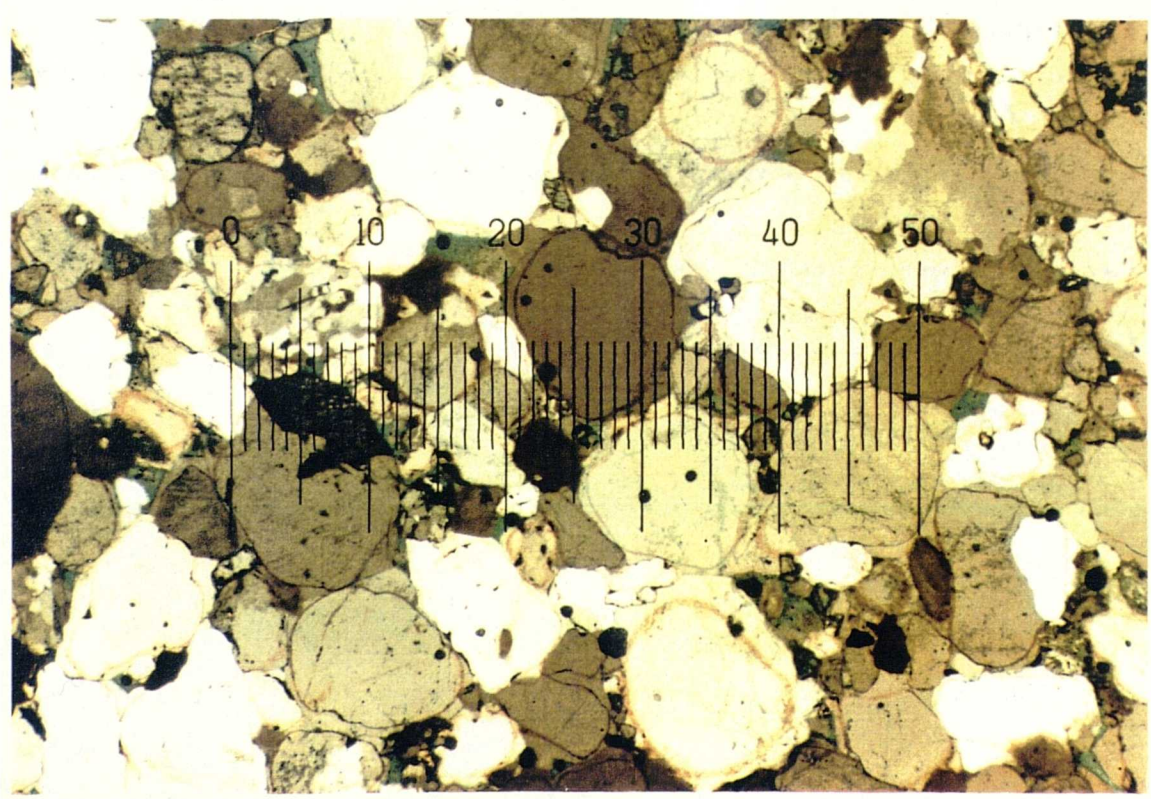

Plate 3.58 Penrith Sandstone (type D). Section parallel to bedding under crossed polars with P/A angle = 70°. Authigenic quartz overgrowths can clearly be seen growing in optical continuity with the detrital grains.
Scale 50 divisions : 2.5mm.

28. Penrith Sandstone - Type D (PrD)

Mineralogy:	%
Quartz	56.7
Quartz overgrowths	9.0
Alkali feldspar	3.0
Plagioclase feldspar	0.0
SRF's	3.7
MRF's	3.3
IRF's	3.0
Haematite	12.3
Chlorite	5.0
Opaques	0.7
Pores	3.3

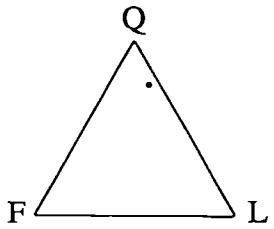

Highly mature sandstone with well developed quartz overgrowths on both mono- and polycrystalline quartz grains. These overgrowths weld the grains together and occlude porosity. Remaining porosity is generally intergranular with some secondary intragranular porosity in the feldspar grains. Plagioclases are rare and occur only as leached remnants.

Grain size: Moderately sorted. Modal size range from 0.25 to 0.7mm, (medium to coarse sand).

Grain shape: Original grains are rounded to well rounded and of high to intermediate sphericity.

Packing density: Vertical: 81.4 %
Horizontal: 80.7 %

Contacts: Original contacts are point and concavo-convex but overgrowths have produced abundant concavo-convex and straight contacts with occasional sutured contacts.

Grain orientation: Some high aspect ratio grains are aligned parallel to bedding.

Classification: *Sublitharenite.*

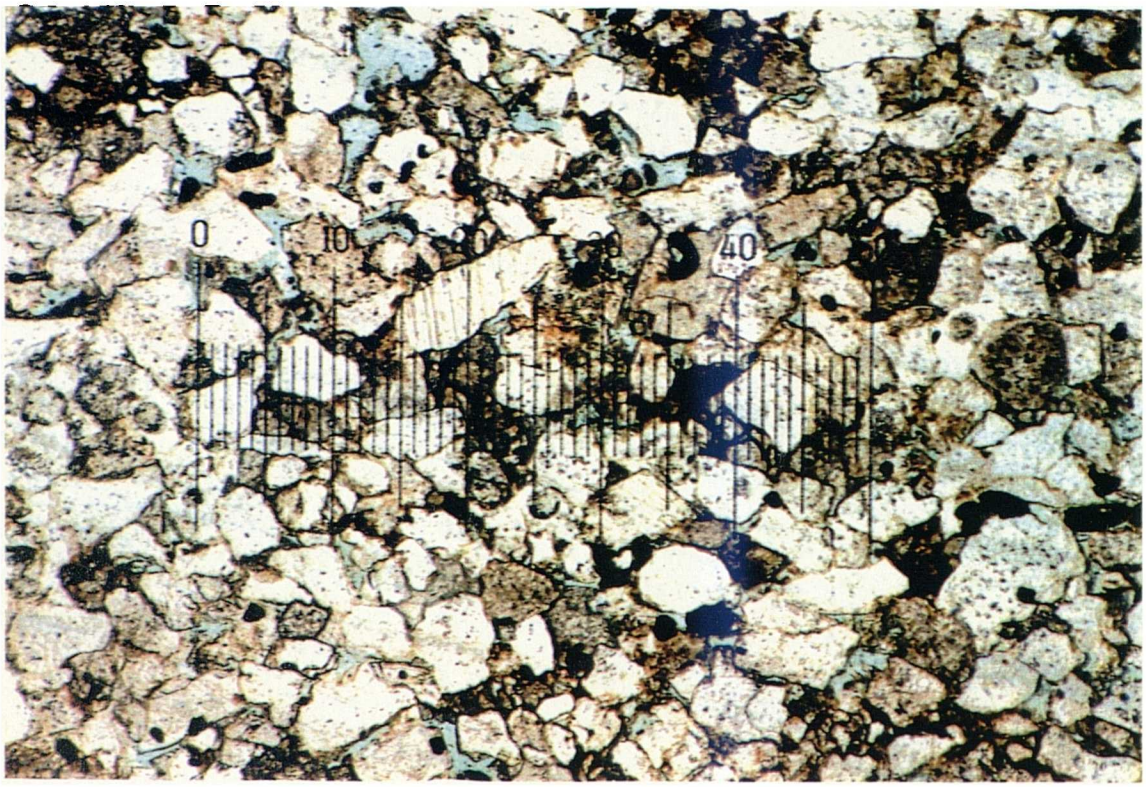

Plate 3.59 Penrith Sandstone (type E). Section parallel to bedding in plane polarized light. This variety is mineralogically and texurally less mature than the other samples with feldspars and rock fragments being abundant.
Scale 50 divisions : 1.25mm.

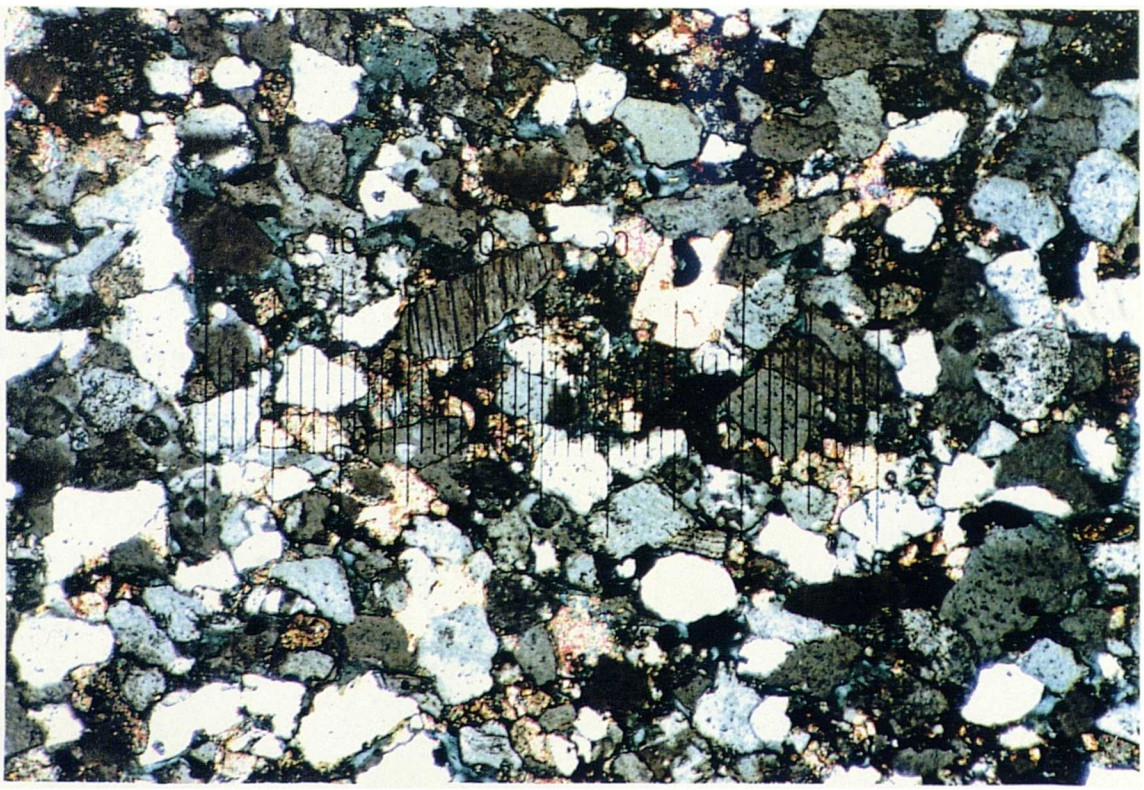

Plate 3.60 Penrith Sandstone (type E). Section parallel to bedding under crossed polars with P/A angle = 70°. Calcite cement is abundant.
Scale 50 divisions : 1.25mm.

29. Penrith Sandstone - Type E (PrE)

Mineralogy:	%
Quartz	45.7
Alkali feldspar	4.3
Plagioclase feldspar	2.7
SRF's	4.7
MRF's	4.3
Haematite	9.0
Opaques	1.7
Clays	5.3
Calcite cement	8.3
Pores	14.0

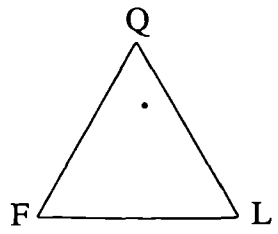

This type of the Penrith Sandstone is much less mature than any other samples collected. Feldspars are abundant and quartz overgrowths are limited. The detrital grains are predominantly quartz cement with secondary calcite. Some of the pore spaces are completely filled with calcite. Haematite coats most of the grains and is also concentrated in sedimentary rock fragments. A high proportion of the original porosity remains.

Grain size: Modal size range is 0.07 to 0.25mm, (*very fine to fine sand*).

Grain shape: Angular to subangular and of low to intermediate sphericity.

Packing density: Vertical: 72.0 %
Horizontal: 71.2 %

Contacts: All types of contact depending on the variable packing density. Occasional sutured contacts occur.

Grain orientation: Internal cross-bedding has aligned high aspect ratio grains.

Classification: *Sublitharenite.*

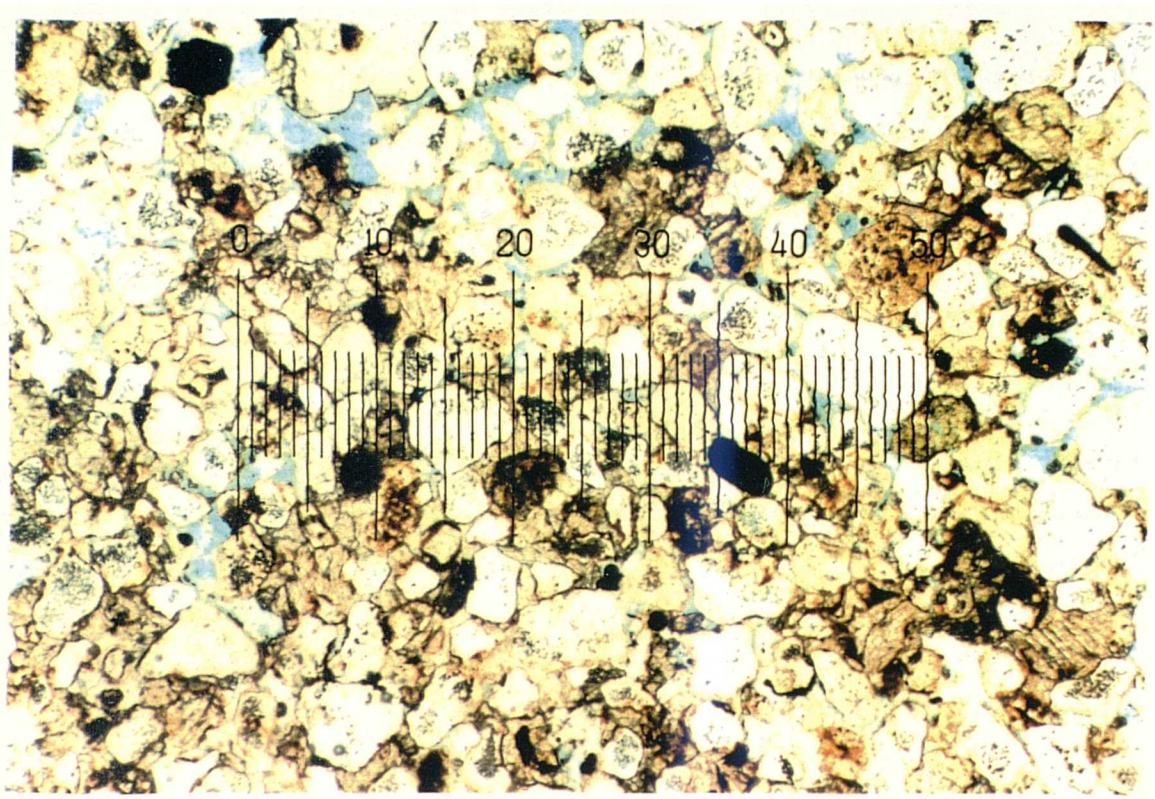

Plate 3.61 Redcliffe Sandstone. Section parallel to bedding in plane polarized light. Porosity is high in areas where cement is poorly developed. Scale 50 divisions : 2.5mm.

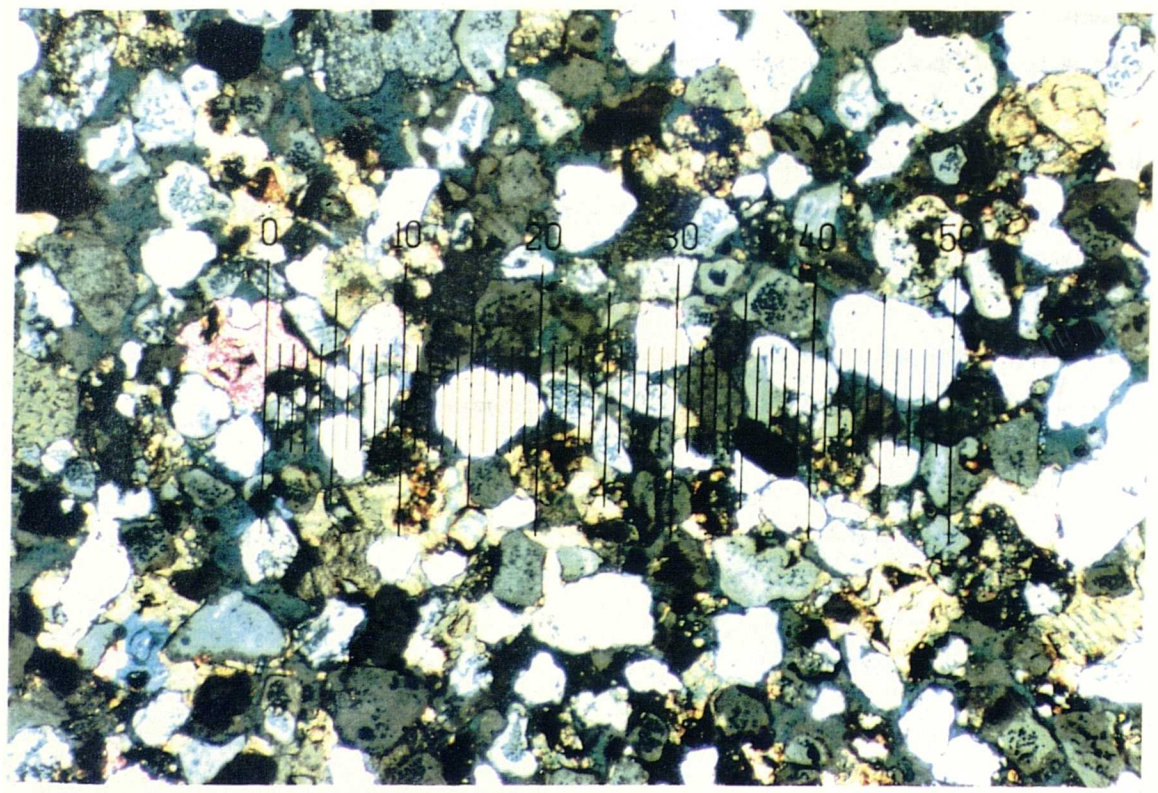

Plate 3.62 Redcliffe Sandstone. Section parallel to bedding under crossed polars with P/A angle = 70°. Calcite cement is abundant, forming a poikilitic texture in some areas. Scale 50 divisions : 2.5mm.

30. Redcliffe Sandstone (R)

Mineralogy:	%
Quartz	41.3
Alkali feldspar	1.3
SRF's	5.0
MRF's	5.7
CRF's	5.3
Muscovite	0.7
Haematite	5.7
Calcite cement	24.3
Clays	3.0
Opaques	1.0
Pores	6.7

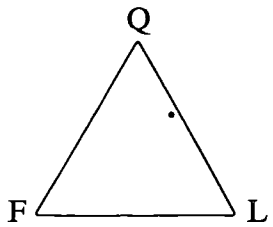

Many detrital grains are coated with haematite. The abundant calcite cement is due to the dissolution of original carbonate rock fragments followed by subsequent recrystallization of the $CaCO_3$ from solution. The former abundance of carbonate rock fragments is seen by the presence of haematite ghost outlines 'floating' in sparry calcite cement. This calcite cement forms large crystals which engulf a number of grains and give the rock a poikilitic texture. Porosity is high.

Grain size: The rock is moderately to poorly sorted with a size range of 0.15 to 0.4mm, (fine to medium sand).

Grain shape: Subrounded to subangular and of low sphericity.

Packing density: Vertical: 65.0 %
Horizontal: 63.1 %

Contacts: Point and concavo-convex contacts.

Grain orientation: No preferential grain alignment.

Classification: *Lithic arenite.*

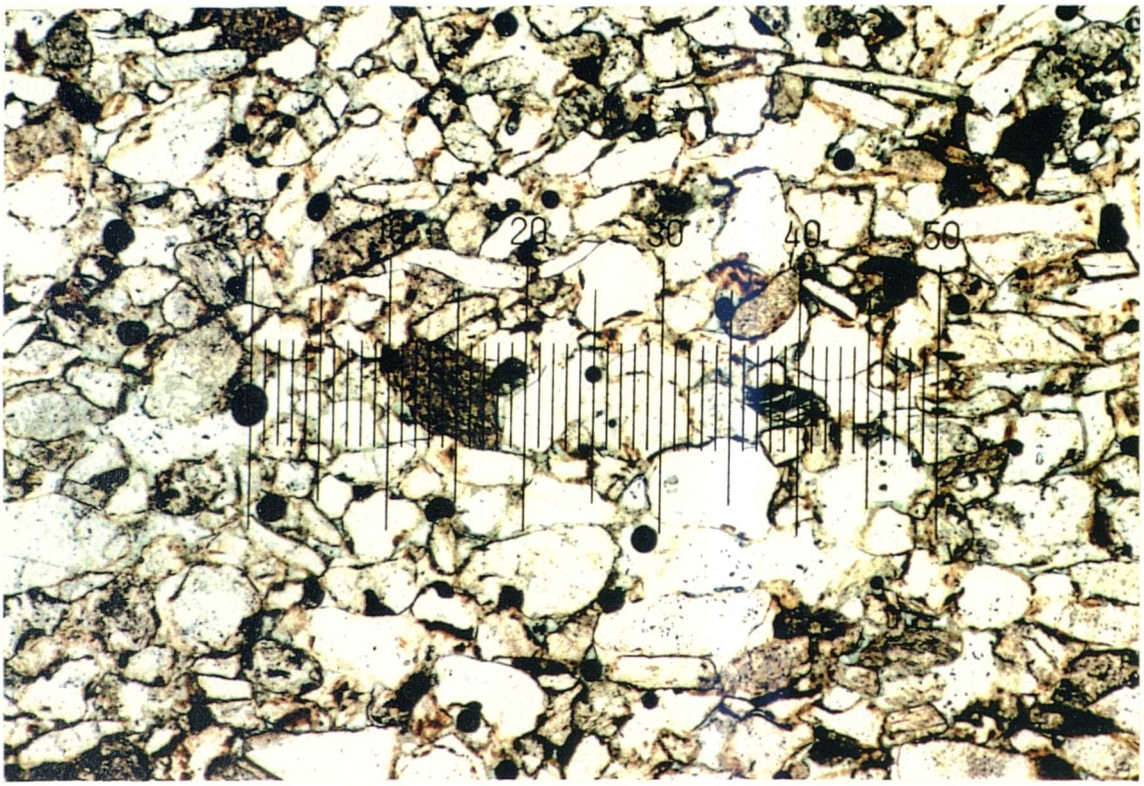

Plate 3.63 St. Bees Sandstone (sample 4v). Section perpendicular to bedding in plane polarized light. Muscovite flakes and elongated grains are aligned parallel to bedding Scale 50 divisions : 1.25mm.

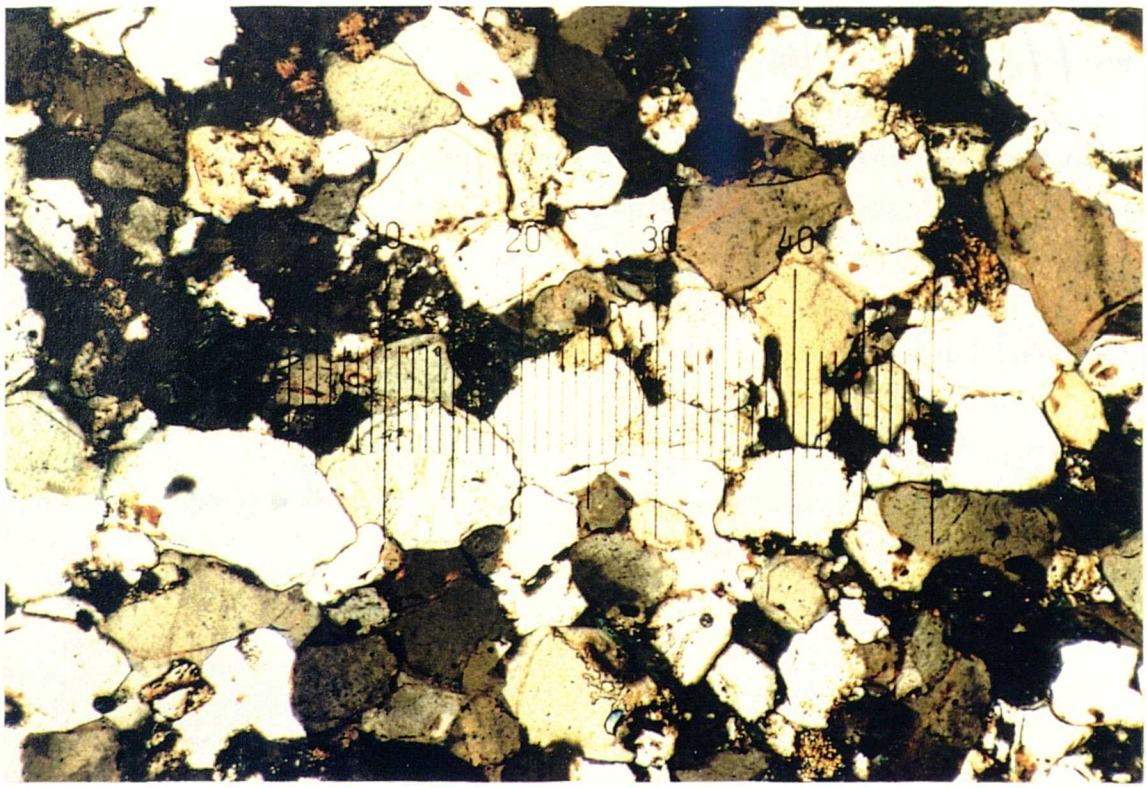

Plate 3.64 St. Bees Sandstone (sample 6v). Section perpendicular to bedding under crossed polars with P/A angle = 70°. Quartz overgrowths are well developed. Many of the feldspar grains show solution porosity.
Scale 50 divisions : 1.25mm.

31. St. Bees Sandstone (StB)

The St. Bees Sandstone samples were collected from borehole cores taken during a site investigation at Sellafield Nuclear Reprocessing Plant. In order to demonstrate variation in the mineralogy and texture down the borehole, a number of samples are described and compared below:

Mineralogy:

	StB 4v	StB 6v	StB 16v
Quartz	55.3	46.3	51.7
Quartz overgrowths	6.7	19.3	9.0
Alkali feldspar	4.7	4.7	2.7
Plagioclase feldspar	1.0	3.0	0.0
SRF's	3.7	5.7	2.3
MRF's	3.0	4.7	15.3
Muscovite	2.3	0.0	0.0
Haematite	9.3	7.0	9.7
Opaques	1.0	1.0	2.3
Clays	4.3	0.0	0.7
Pores	8.7	8.3	6.3

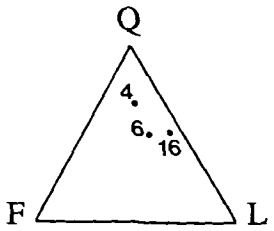

StB 4v

The rock is highly immature. Overgrowths occur on some quartz grains but are not well developed. Porosity is relatively low due to occlusion by overgrowths and fines.

Grain size: Modal size range is 0.1 to 0.3mm, (fine to medium sand).

Grain shape: Original detrital grains are angular to subrounded and of low sphericity.

Packing density: Vertical: 78.0 %
Horizontal: 75.7 %

Contacts: Straight and concavo-convex.

Grain orientation: Strong preferential alignment of high aspect ratio grains parallel to bedding.

Classification: *Sublitharenite.*

StB 6v

This sample is much more mature than StB 4v. Quartz overgrowths are well developed and have markedly reduced an originally high porosity. Labile constituents may have been removed during weathering; some feldspars show a high intragranular porosity.

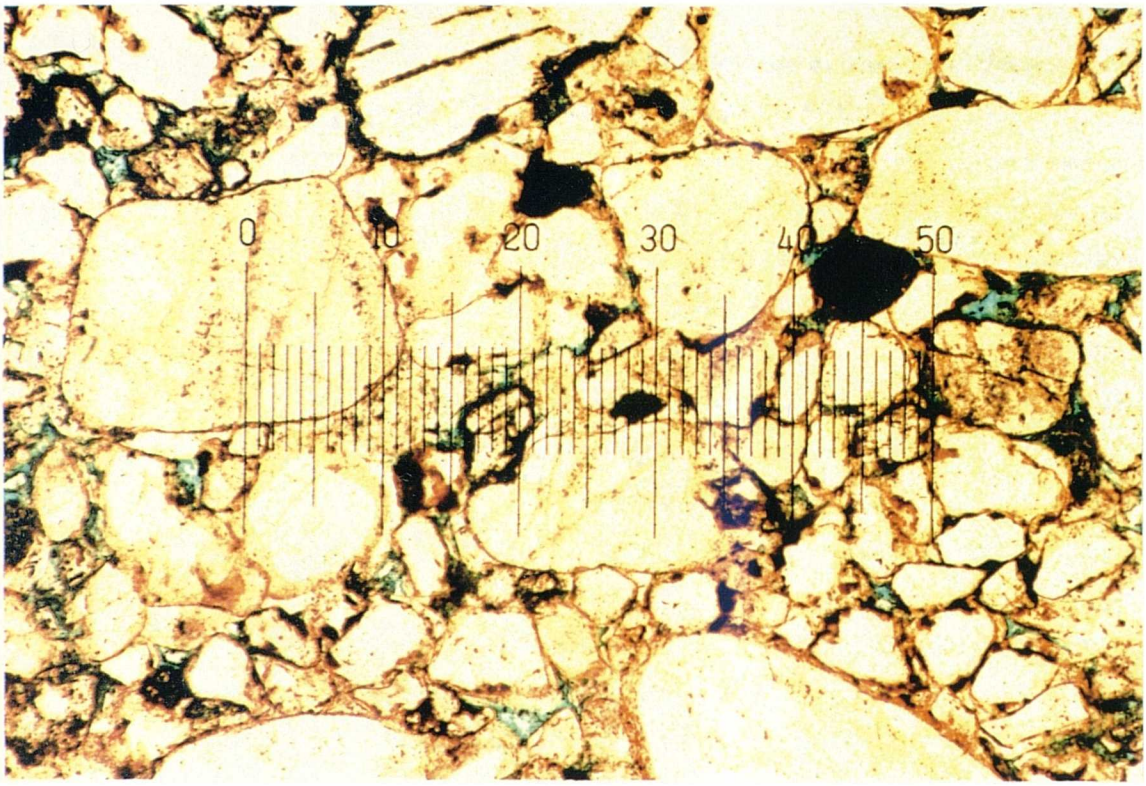

Plate 3.65 St. Bees Sandstone (sample 16v). Section perpendicular to bedding in plane polarized light. The rock is poorly sorted and grain shape is highly variable. Scale 50 divisions : 1.25mm.

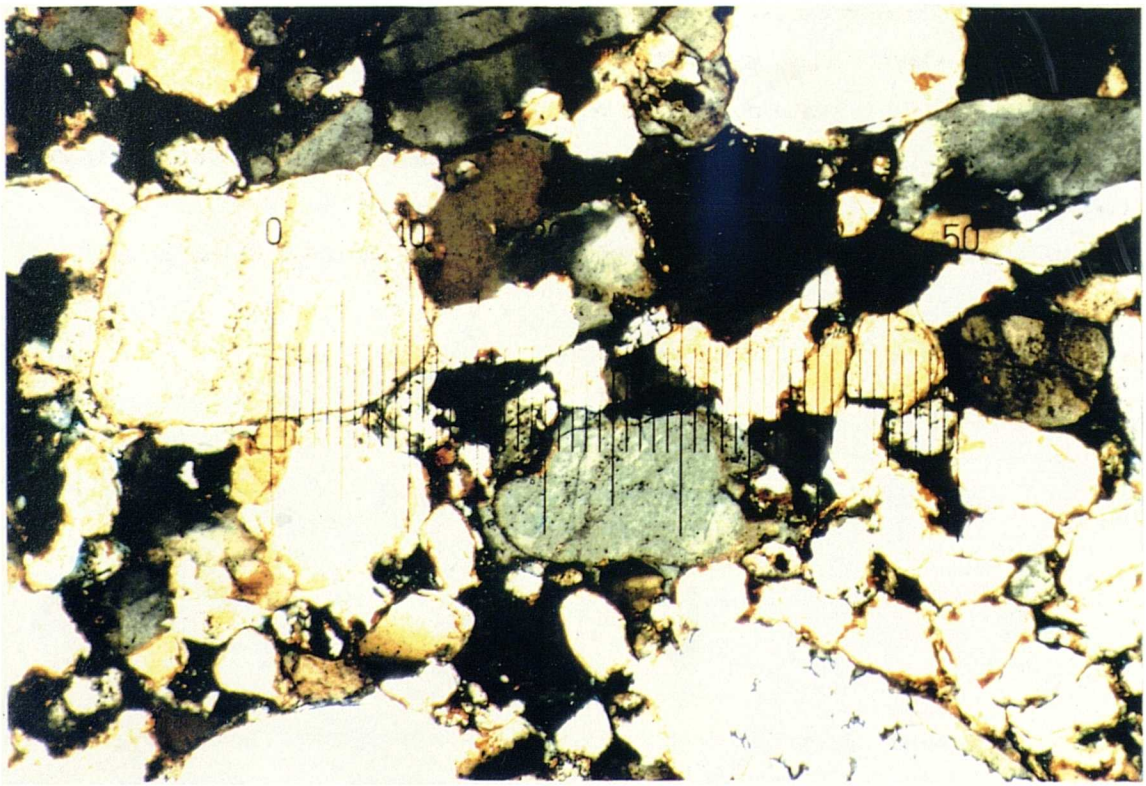

Plate 3.66 St. Bees Sandstone (sample 16v). Section perpendicular to bedding under crossed polars with P/A angle = 70°. Quartz overgrowths are well developed. A large MRF is present to bottom right of plate.
Scale 50 divisions : 1.25mm.

Grain size: The rock is well sorted with a modal size range of 0.15 to 0.40, (fine to medium sand).

Grain shape: Original grains are rounded to subrounded and of high to intermediate sphericity.

Packing density: Vertical: 79.8 %
Horizontal: 79.4 %

Contacts: Point contacts predominated prior to overgrowth formation, but these have produced straight, concavo-convex and undulating contacts.

Grain orientation: No preferential grain alignment.

Classification: *Sublitharenite.*

StB 16v

All the quartz grains are coated with haematite. Overgrowths are well developed and weld the rock framework. Pores are larger but less numerous in the coarse layers than in the finer laminae. The 'well graded' texture has produced an overall porosity lower than other samples.

Grain size: The rock is poorly sorted due to the deposition of alternating coarse and fine laminae which have intergraded during diagenesis. The size range is 0.1 to 0.6mm, (fine to coarse sand), with some quartz grains up to 0.9mm long.

Grain shape: Large grains are subrounded to well rounded while smaller grains are subangular to subrounded. All are of low to intermediate sphericity.

Packing density: Vertical: 76.3 %
Horizontal: 74.2 %

Contacts: Original point contacts with overgrowths producing straight and concavo-convex contacts.

Grain orientation: Partial alignment of elongated grains parallel to bedding.

Classification: *Sublitharenite.*

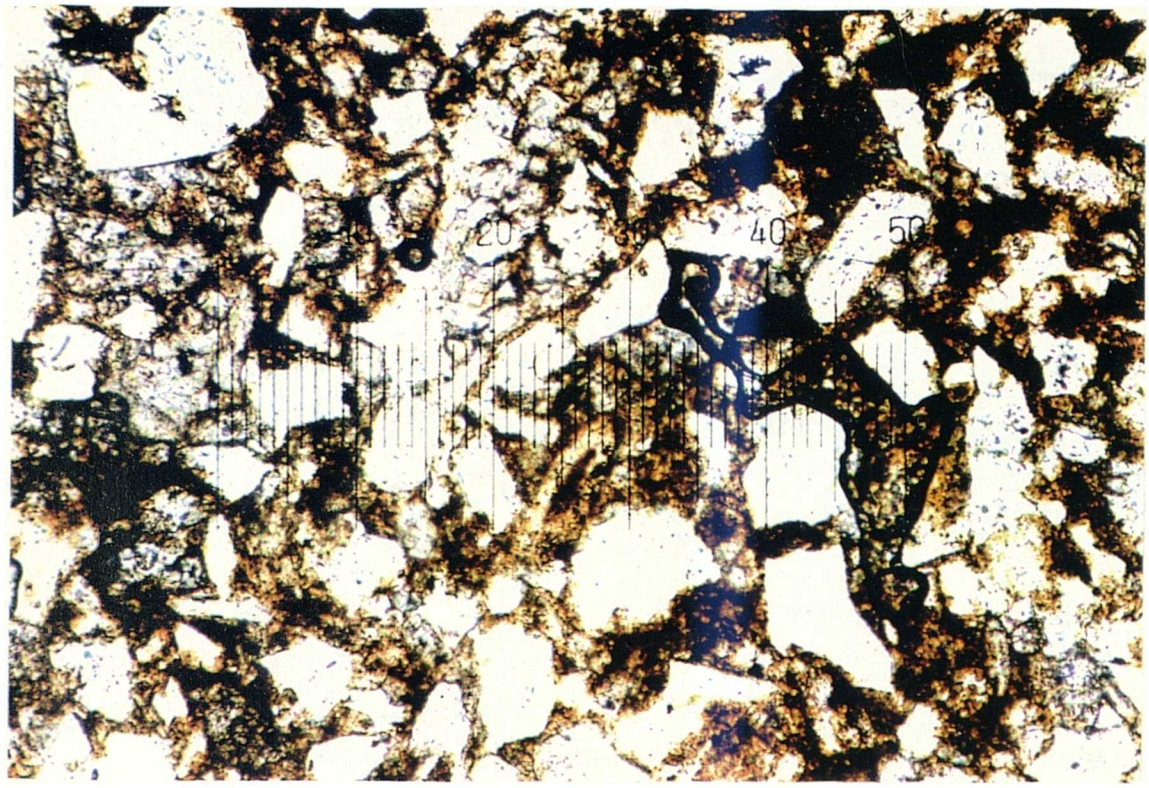

Plate 3.67 Midford Sands. Section perpendicular to bedding in plane polarized light. Most grains are highly angular and are supported in a clay and haematite-rich matrix. Scale 50 divisions : 0.5mm.

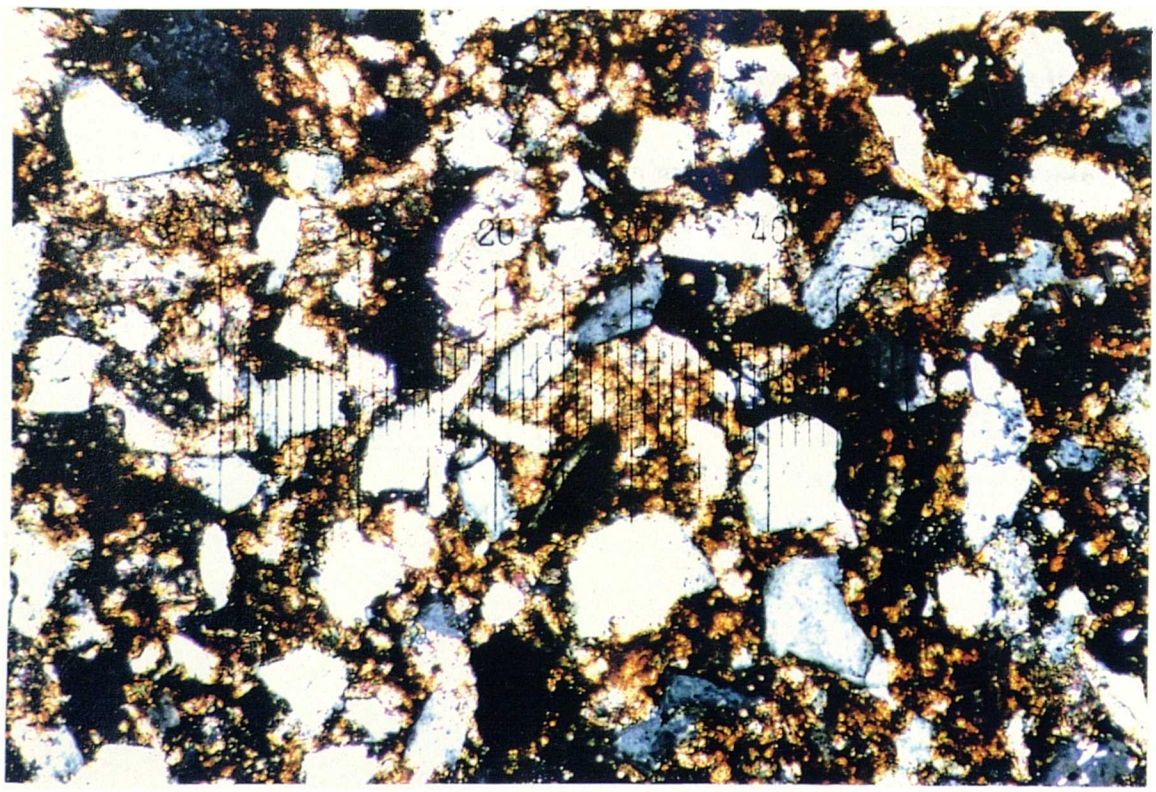

Plate 3.68 Midford Sands. Section perpendicular to bedding under crossed polars. Matrix contains abundant microcrystalline calcite. Some sparry calcite cement has formed in pore spaces. Scale 50 divisions : 0.5mm.

32. Midford Sands (MS)

Mineralogy:	%
Quartz	38.3
Alkali feldspar	0.7
SRF's	1.0
MRF's	0.7
CRF's	6.3
Muscovite	0.7
Carbonate mud	27.3
Calcite	3.3
Haematite	8.3
Clays	11.7
Opaques	1.7
Pores	0.0

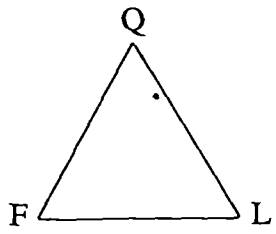

The detrital quartz and rock fragments are matrix supported by a calcite mud, (micrite). Haematite is abundant throughout this matrix forming a haematite/calcite cement. Large calcite crystals include a number of detrital grains and give the rock a sporadically developed poikilitic texture. Shell fragments are also present within the sediment.

Grain size: Modal size range is 0.2 to 0.3mm.

Grain shape: Subangular to angular and of low to intermediate sphericity.

Packing density: Vertical: 45.7
Horizontal: 46.2

Contacts: Majority of grains are matrix supported but occasionally point and concavo-convex contacts occur.

Grain orientation: No preferential grain alignment.

Classification: *Lithic wacke.*

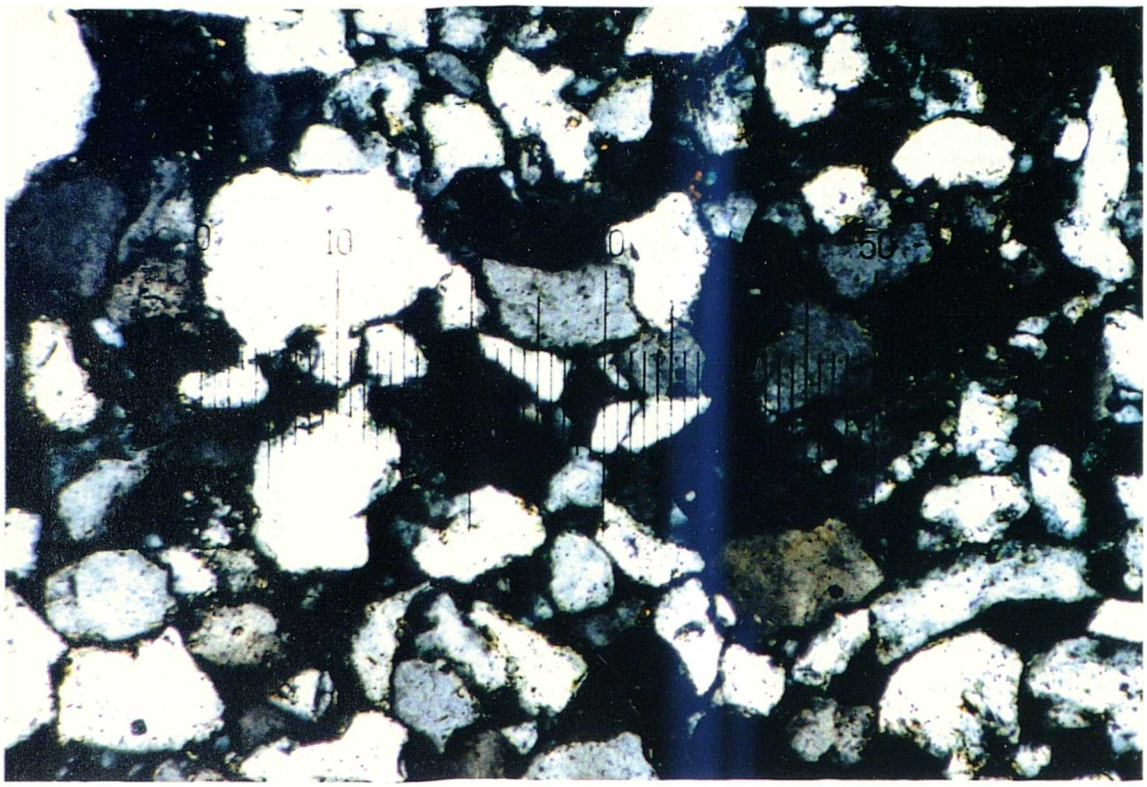

Plate 3.69 Ardingly Sandstone (type A). Section perpendicular to bedding under crossed polars showing predominance of quartz with little intergranular matrix. Scale 50 divisions : 0.5mm.

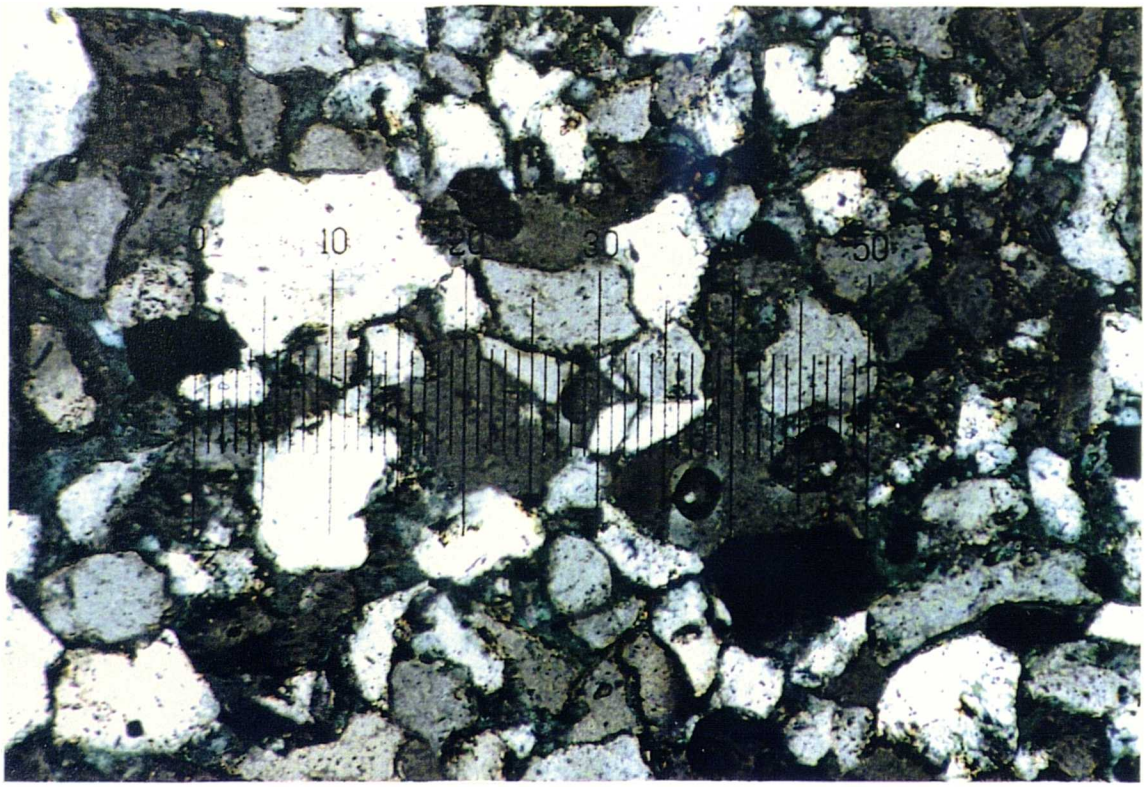

Plate 3.70 Ardingly Sandstone (type A). Section perpendicular to bedding under crossed polars with P/A angle = 70°. The rock shows abundant concavo-convex contacts and a high intergranular porosity.
Scale 50 divisions : 0.5mm.

33. Ardingly Sandstone - Type A (ArdA)

Mineralogy:	%
Quartz	58.3
Alkali feldspar	1.7
SRF's	3.0
Detrital glauconite	2.0
Authigenic glauconite	8.0
Clays	4.0
Haematite	1.3
Opaques	1.7
Heavy minerals	2.0
Pores	18.0

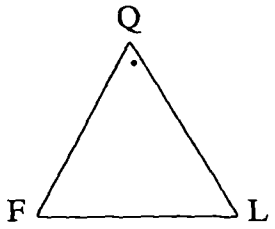

Detrital framework grains are predominantly quartz with occasional mudstone fragments. The areas around these sedimentary rock fragments have a markedly reduced porosity where clays have been squeezed into surrounding pore spaces. In the rest of the rock however, the porosity is generally high with glauconite and clays coating most pores and cementing the framework grains. Clays totally fill some of the smaller pore spaces.

Grain size: The rock is moderately well sorted with a size range of 0.05 to 0.13mm, (very fine to fine sand).

Grain shape: Quartz grains are subrounded to subangular and of high to intermediate sphericity but detrital glauconite grains are well rounded and of high sphericity.

Packing density: Vertical: 65.0 %
Horizontal: 65.1 %

Contacts: Generally point and concavo-convex contacts.

Grain orientation: No preferential grain alignment.

Classification: *Quartz arenite.*

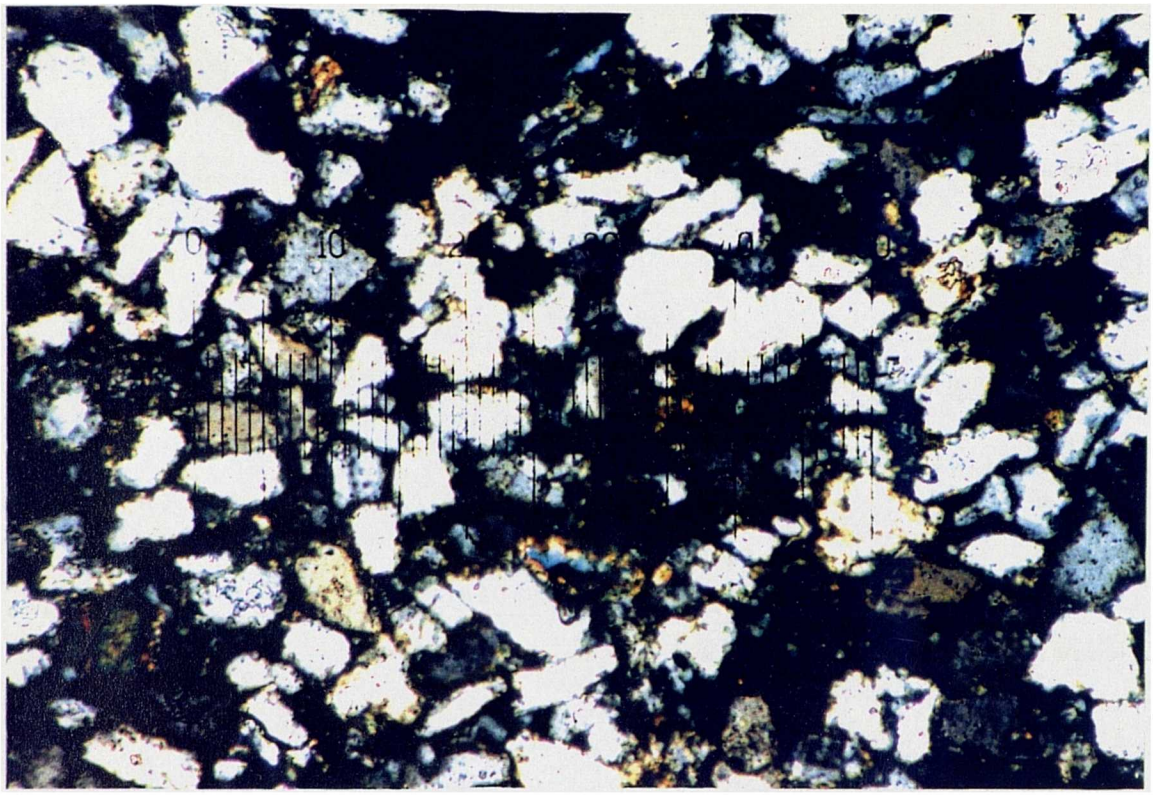

Plate 3.71 Ardingly Sandstone (type B). Section perpendicular to bedding under crossed polars showing finer grain size than type A.
Scale 50 divisions : 0.5mm.

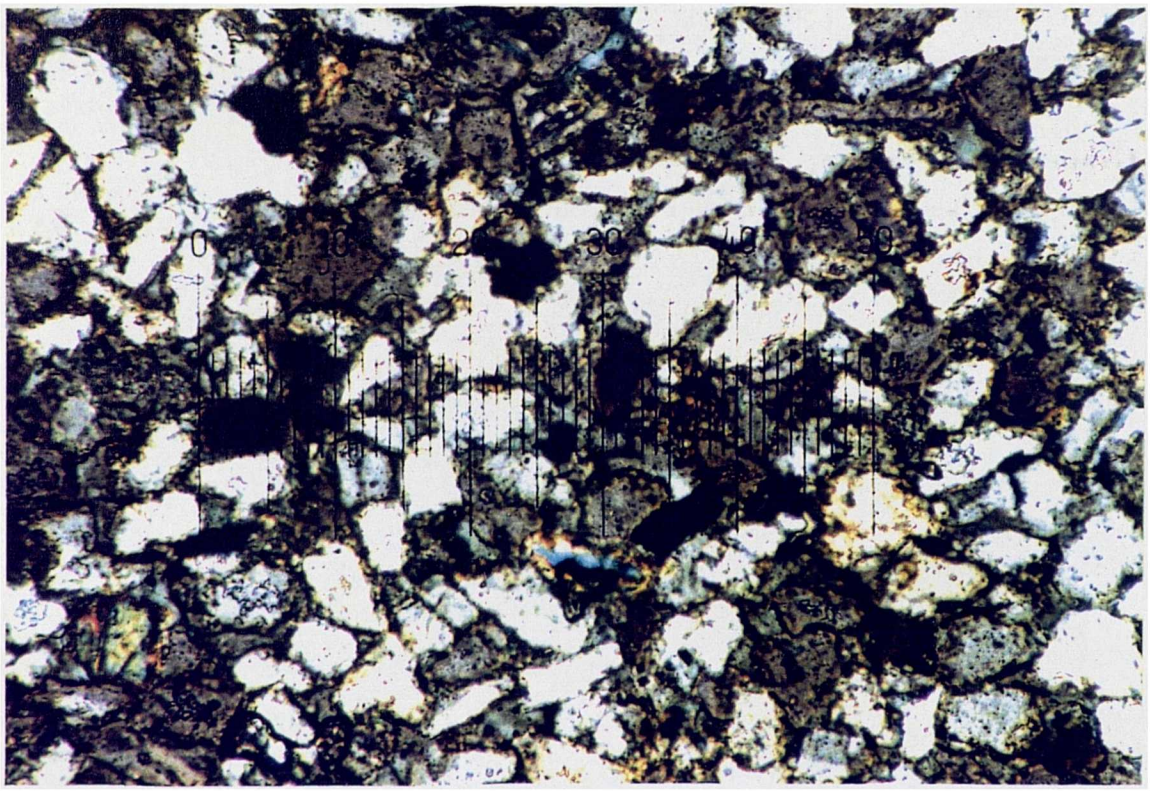

Plate 3.72 Ardingly Sandstone (type B). Section perpendicular to bedding under crossed polars with P/A angle = 70°. Porosity is lower than type A and quartz cement is more abundant. Scale 50 divisions : 0.5mm.

34. Ardingly Sandstone - Type B (ArdB)

Mineralogy:	%
Quartz	57.7
Alkali feldspar	3.3
SRF's	0.0
Detrital glauconite	3.7
Authigenic glauconite	12.3
Clays	7.7
Haematite	0.0
Opaques	1.3
Heavy minerals	0.7
Pores	13.3

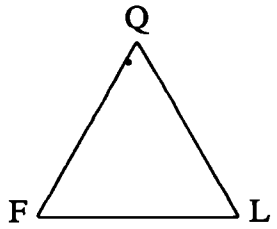

Many of the quartz grains are fractured and strained, (prior to deposition). These detrital grains are again cemented by a glauconite and clay coating. Glauconite also occurs as detrital pellets. Porosity is lower and more occluded by clay minerals than in Type A.

Grain size: Modal size range is lower than Type A - 0.03 to 0.1, (very fine sand).

Grain shape: Subangular to subrounded and of high to intermediate sphericity.

Packing density: Vertical: 65.4 %
Horizontal: 65.3 %

Contacts: Concavo-convex and point contacts.

Grain orientation: No preferential grain alignment.

Classification: *Subarkose.*

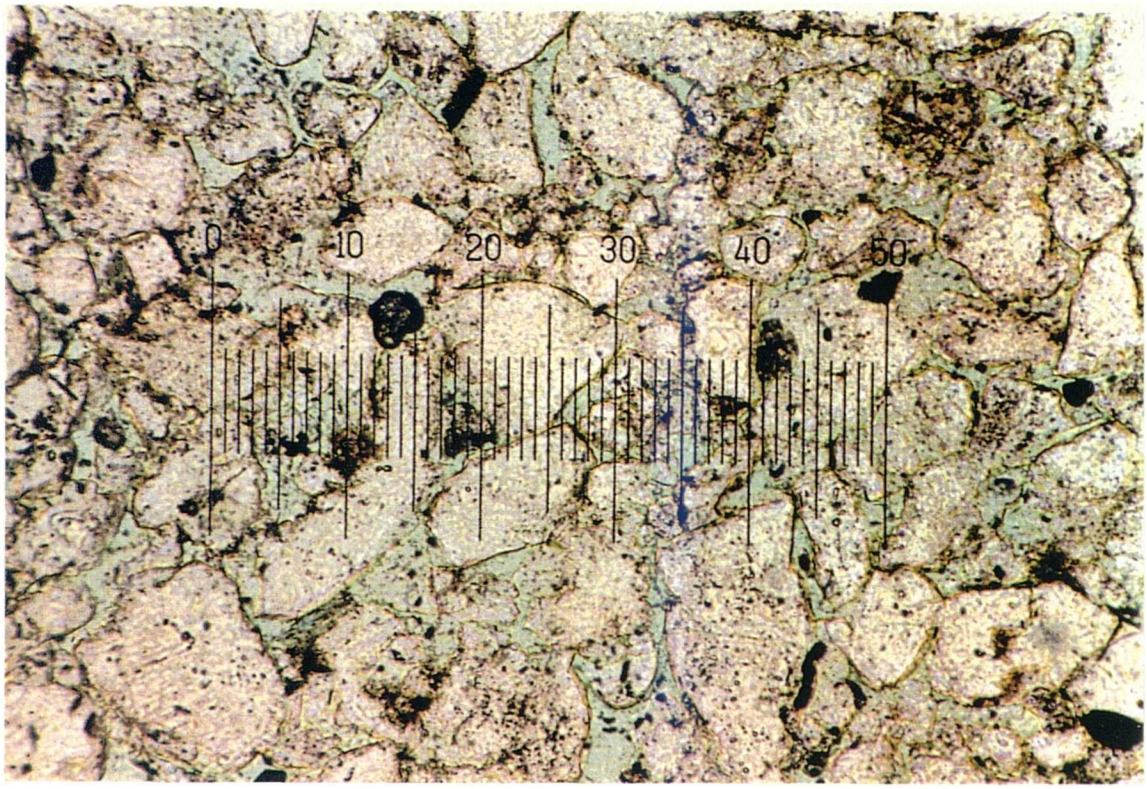

Plate 3.73 Ashdown Sandstone. Section perpendicular to bedding in plane polarized light. Little cement or matrix is present apart from a thin glauconitic coating on the quartz grains. Porosity is therefore high.
Scale 50 divisions : 0.5mm.

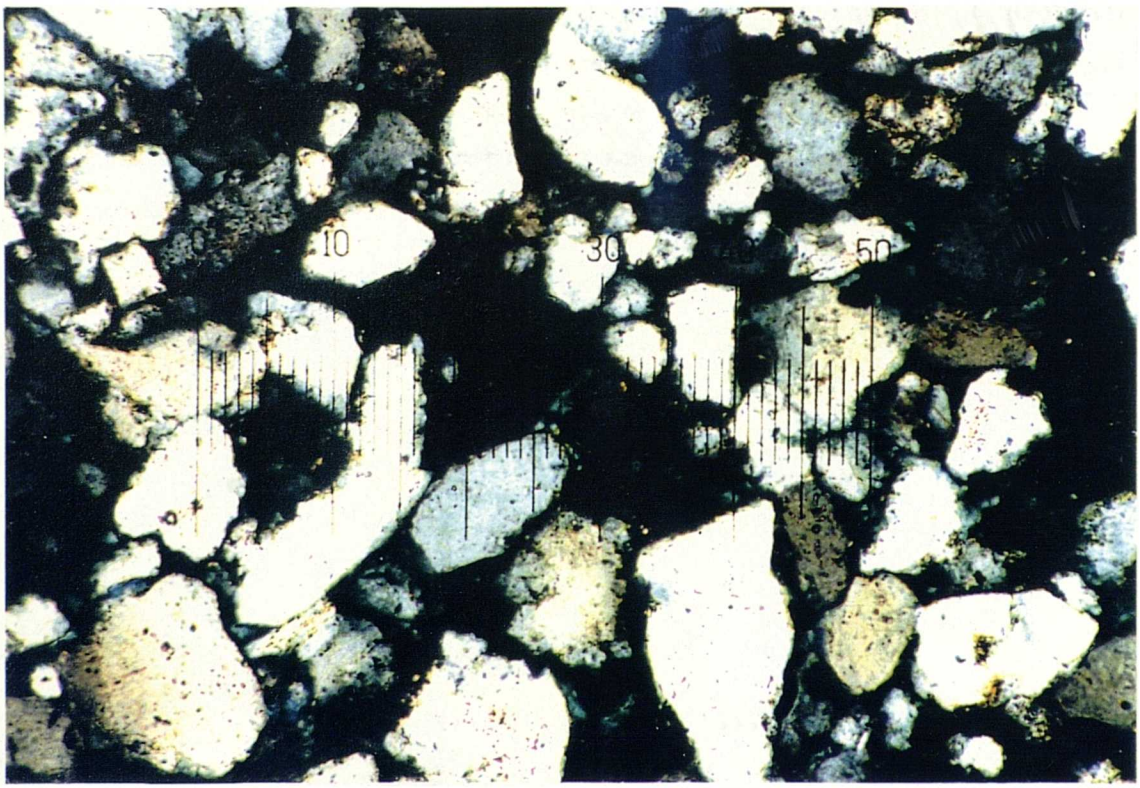

Plate 3.74 Ashdown Sandstone. Section perpendicular to bedding under crossed polars. The rock shows an interlocking texture with some of the grains showing overgrowths. Scale 50 divisions : 0.5mm.

35. Ashdown Sandstone (AS)

Mineralogy:	%
Quartz	63.7
Alkali feldspar	3.0
SRF's	1.0
Detrital glauconite	3.0
Authigenic glauconite	7.7
Clays	0.3
Opaques	1.3
Heavy minerals	1.0
Pores	19.0

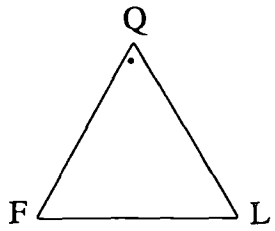

The sandstone possesses little intergranular matrix or cement with a resulting high porosity. The authigenic glauconite forms a sporadically developed coating on the detrital quartz grains.

Grain size: Moderately to well sorted, with a modal size range of 0.07 to 0.17mm, (very fine to fine sand).

Grain shape: Subangular to subrounded and of high to intermediate sphericity.

Packing density: Vertical: 76.7 %
Horizontal: 62.8 %

Contacts: Generally point contacts with some concavo-convex.

Grain orientation: No preferential grain alignment.

Classification: *Quartz arenite.*

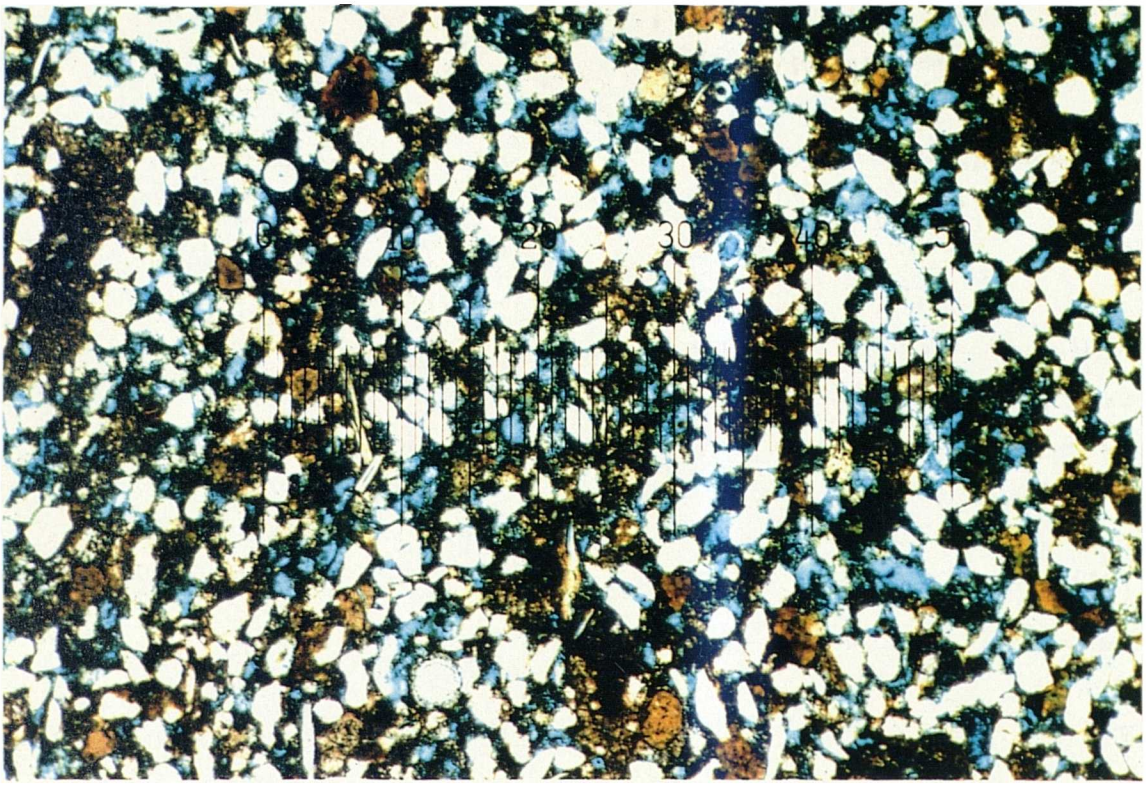

Plate 3.75 Greensand (type A). Section perpendicular to bedding in plane polarized light. Glauconitic, clay-rich matrix is abundant with the result that many of the quartz grains are 'floating'. Scale 50 divisions : 1.25mm.

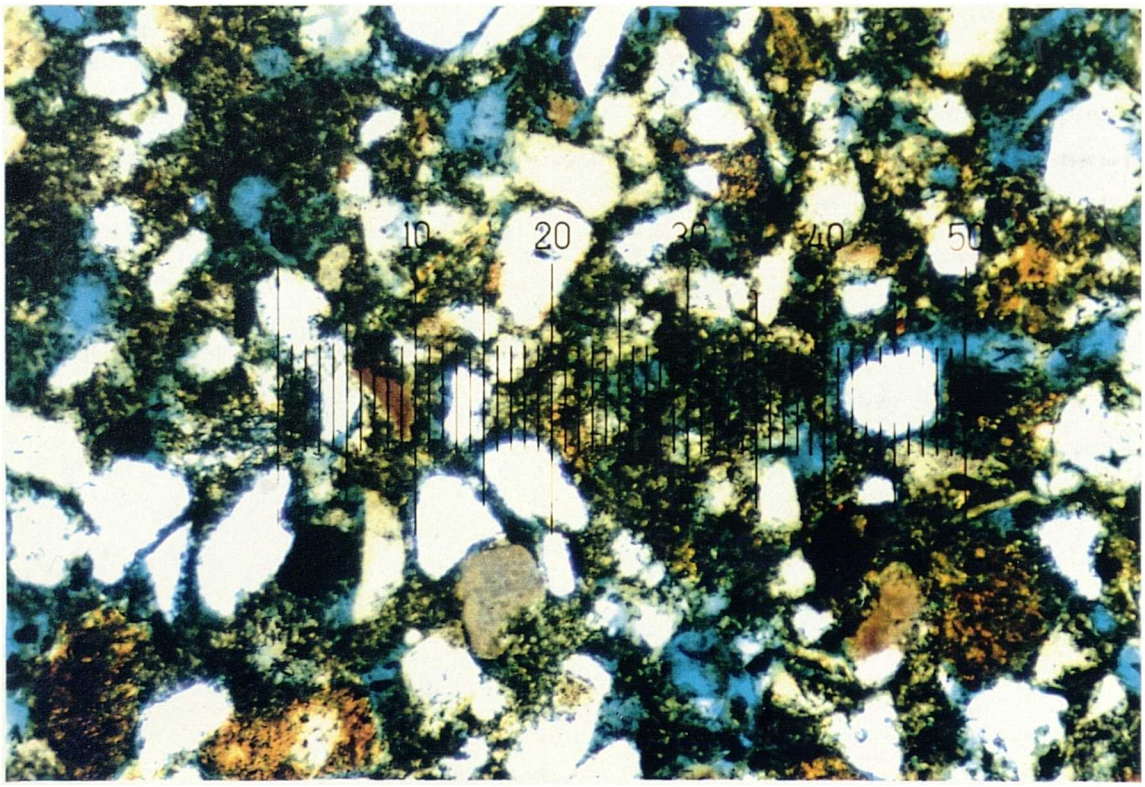

Plate 3.76 Greensand (type A). Section perpendicular to bedding in plane polarized light. At higher magnifications the degree of secondary solution porosity is evident. In addition to matrix, glauconite also occurs as greenish brown detrital grains. Scale 50 divisions : 0.5mm.

36. Greensand - Type A (G)

Mineralogy:	%
Quartz	25.0
Alkali feldspar	0.0
Plagioclase feldspar	0.0
Detrital glauconite	6.3
Authigenic glauconite	1.7
Muscovite	2.3
Microfossils	1.3
Clay matrix	39.3
Calcite mud	1.7
Opaques	0.0
Pores	22.3

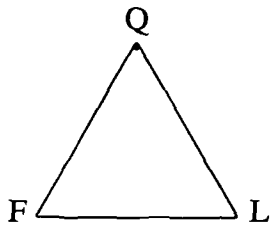

The mineralogy of this sandstone is dominated by the abundance of clay matrix. The high porosity visible under the microscope by the blue impregnation is practically all secondary porosity formed by the dissolution and migration of calcite from fossil material, carbonate rock fragments and calcite mud. The quartz grains show a high degree of corrosion.

Grain size: The framework grains are well sorted - modal size range is 0.06 to 0.09, (very fine sand)

Grain shape: Quartz grains are rounded to subrounded and of high to intermediate sphericity while glauconite pellets are well rounded and of high sphericity.

Packing density: Vertical: 31.0 %
Horizontal: 29.9 %

Contacts: The majority of the grains are matrix supported, but some show point contact with other grains.

Grain orientation: Slight preferential grain orientation parallel to bedding.

Classification: *Quartz wacke.*

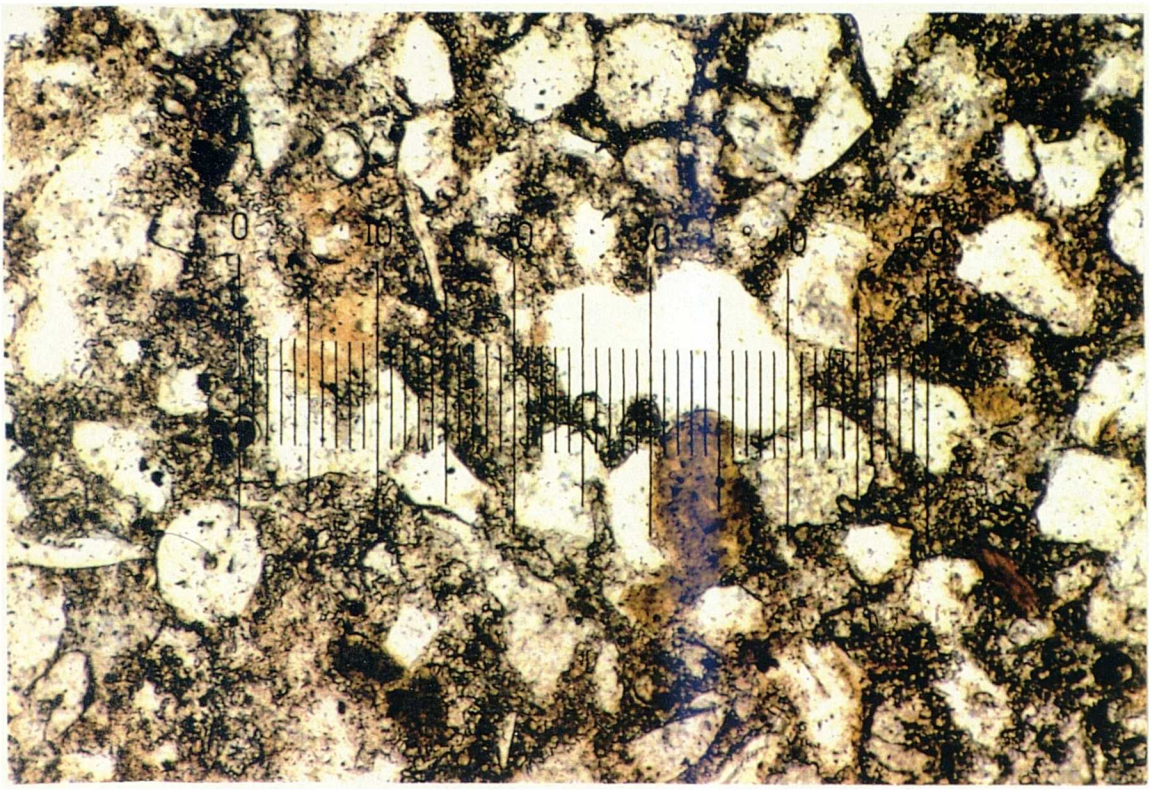

Plate 3.77 Greensand (type B, dogger). Section perpendicular to bedding in plane polarized light. Porosity is much lower than in the normal Greensand but the textural properties of the detrital grains are similar.
Scale 50 divisions : 0.5mm.

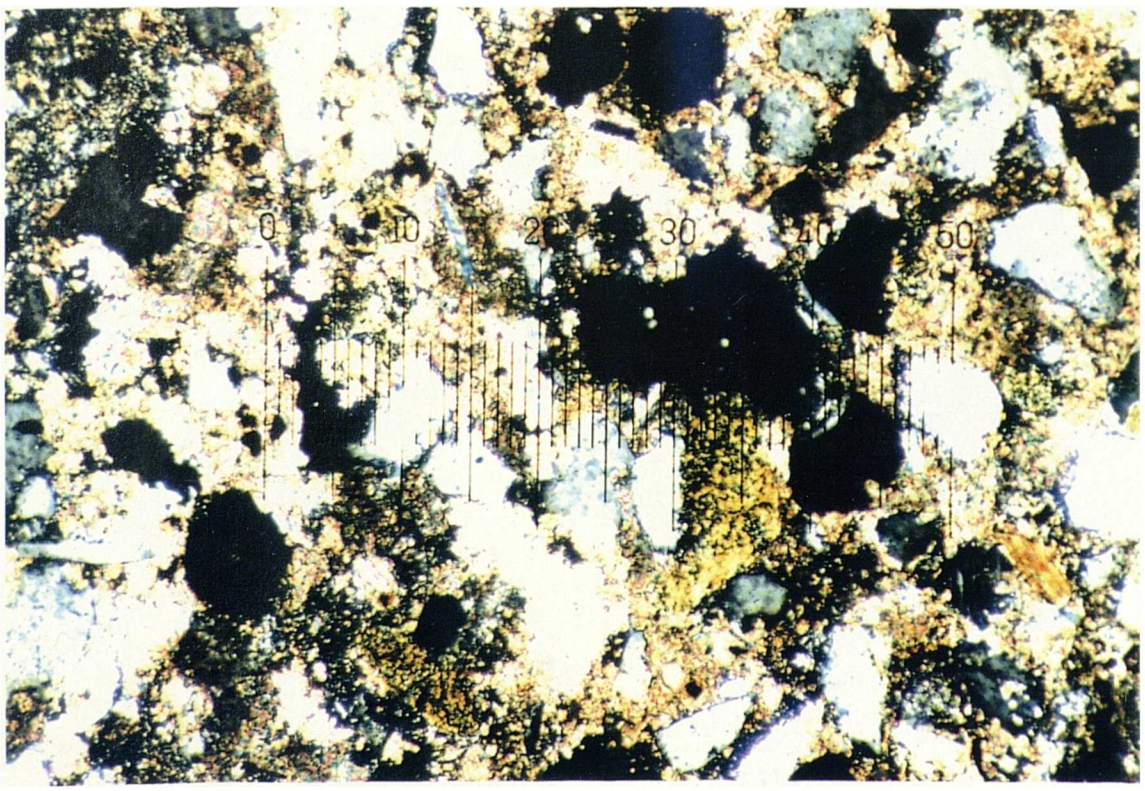

Plate 3.78 Greensand (type B, dogger). Section perpendicular to bedding under crossed polars. Calcite has impregnated the pores and clay minerals giving the rock a micritic matrix. Scale 50 divisions : 0.5mm.

37. Greensand - Type B (D)

Mineralogy:	%
Quartz	29.7
Alkali feldspar	1.7
Plagioclase feldspar	3.7
Detrital glauconite	10.0
Authigenic glauconite	0.0
Muscovite	0.7
Microfossils	2.0
Clay matrix	16.3
Calcite cement	31.3
Opaques	1.3
Pores	3.3

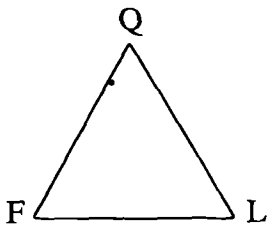

The migration of $CaCO_3$ from the surrounding sediment to these concretionary nodules has had the effect of occluding much of the porosity and of preserving many of the labile constituents. The calcite has impregnated the microporous clay matrix and created a microcrystalline calcite cement.

Grain size: Modal size range is similar to that of Type A - 0.06 to 0.09mm, (very fine sand). Occasionally quartz grains are up to 0.18mm long.

Grain shape: Subrounded to subangular and of high to intermediate sphericity.

Packing density: Vertical: 28.0 %
Horizontal: 27.8 %

Contacts: Grains are generally matrix supported with occasional point contacts.

Grain orientation: Slight preferential grain alignment parallel to bedding.

Classification: *Arkosic wacke.*

3.1.1 Discussion

All the sandstones studied are plotted on a Q-F-L diagram in Figure 3.1. The majority show high quartz percentages with only varieties rich in feldspars or lithic rock fragments plotting below the subarkose or sublitharenite fields. Figure 3.2 shows the different sandstones classified into arenites and wackes, (i.e. those containing <15% and >15% matrix respectively). The division of the different types on the basis of the Dott-Folk classification is as follows:

Quartz arenite	5
Lithic arenite	7
Sublitharenite	6
Arkose	1
Subarkose	10
Quartz wacke	1
Lithic wacke	5
Arkosic wacke	2

It becomes clear that the genetic mineralogical classification proposed by Dott, (1964) and later modified by Folk, (1968), bears little relevance to any rock mechanics properties of the rocks which it groups together. For example, the Donegal Quartzite and the Ashdown Sandstone are both classified as quartz arenites. Even a simple examination in hand specimen will show that the two deposits are totally different in density, porosity and degree of induration and will hence have very different geomechanical properties. Clearly, any rock mechanics classification for sandstones must take mineralogy into account but lean more towards the identification and quantification of the intergranular bonding materials and their strengths rather than the nature of the framework grains. This will be discussed in a later chapter.

The different sandstone varieties show a high degree of mineralogical and textural variation. Quartz is overall the most common framework constituent but many of the sandstones show predominances of feldspars or rock fragments such as the Applecross Sandstone and Pennant respectively. In addition to the framework constituents, the cementing materials are also variable; the more mature and well compacted sandstones show quartz cementation by overgrowths, point contact welding and suturing. Less mature varieties with higher porosity show cementation by calcite and iron oxides. Immature wackes are bonded by clay-matrix. Plate 3.79 (a) - (f) shows a number of scanning electron photomicrographs which indicate the three dimensional morphology of some of the intergranular bonding materials.

Occasionally arenites occur which are mineralogically and texturally mature but

1.	Applecross	A
2.	Donegal Quartzite	DQ
3.	Basal Quartzite	BQ
4.	Brownstones	LORS
5.	Pilton (Type A)	PiA
6.	Pilton (Type B)	PiB
7.	Upper Cromhall	UCS
8.	Millstone Grit (Type A)	MGA
9.	Millstone Grit (Type B)	MGB
10.	Millstone Grit (Type C)	MGC
11.	Millstone Grit (Type D)	MGD
12.	Holcombe Brook Grit (Type A)	HBGA
13.	Holcombe Brook Grit (Type B)	HBGB
14.	Siliceous Sandstone	SS
15.	Elland Flags	EF
16.	Thornhill Rock (Type A)	TRA
17.	Thornhill Rock (Type B)	TRB
18.	Middle Coal Measures	MCM
19.	Crackington Formation	CF
20.	Pennant ((Type A)	PnA
21.	Pennant (Type B)	PnB
22.	Pennant (Type C)	PnC
23.	Pennant (Type D)	PnD
24.	Annan Sandstone	An
25.	Penrith (Type A)	PrA
26.	Penrith (Type B)	PrB
27.	Penrith (Type C)	PrC
28.	Penrith (Type D)	PrD
29.	Penrith (Type E)	PrE
30.	Redcliffe	R
31.	St. Bees	StB
32.	Midford Sands	MS
33.	Ardingly Sandstone (Type A)	ArdA
34.	Ardingly Sandstone (Type B)	ArdB
35.	Ashdown Sands	AS
36.	Greensand (Type A)	G
37.	Greensand (Type B - Dogger)	D

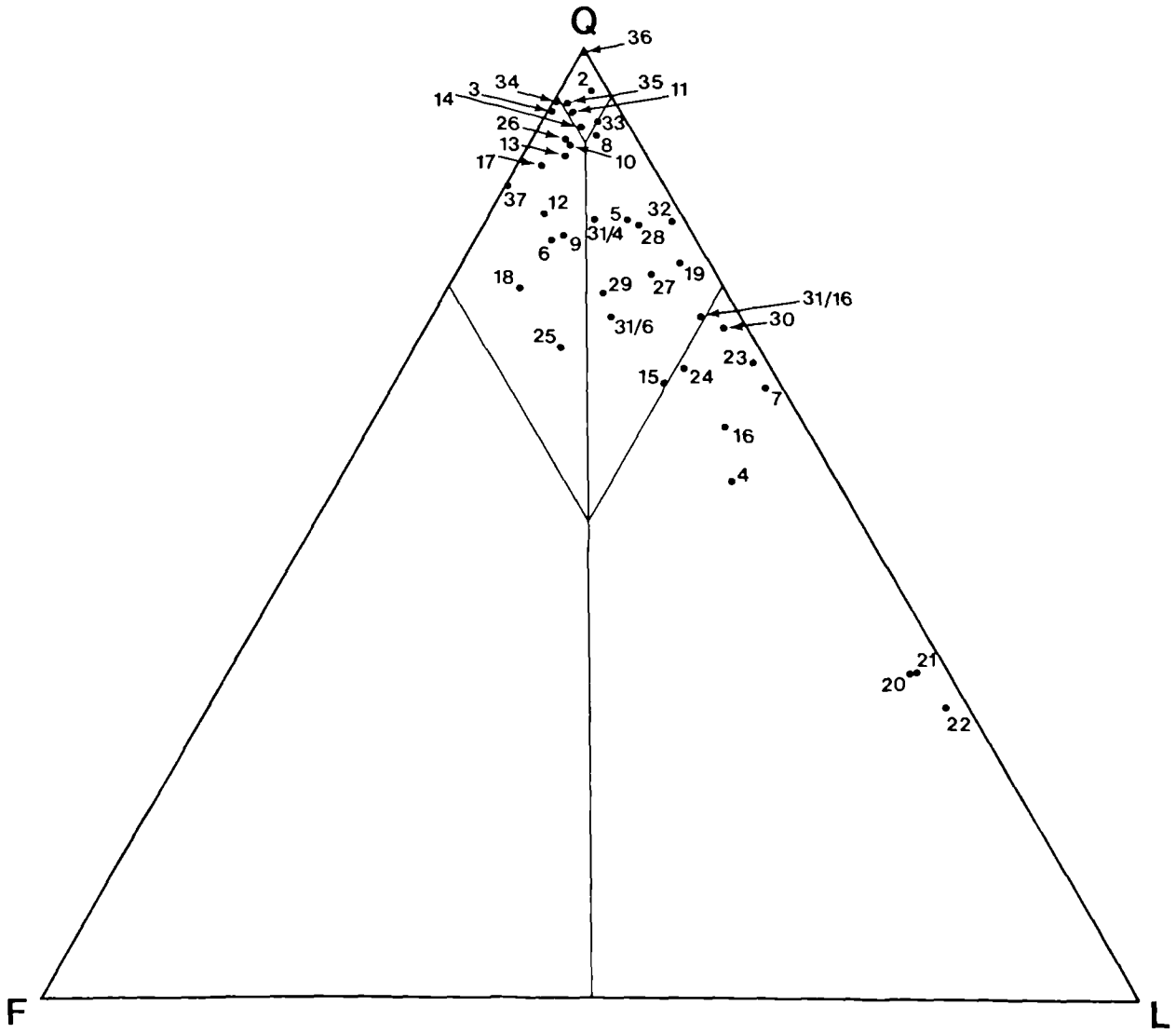

Figure 3.1 Quartz-Feldspar-Lithic rock fragment ternary diagram showing positions of all sandstones studied.

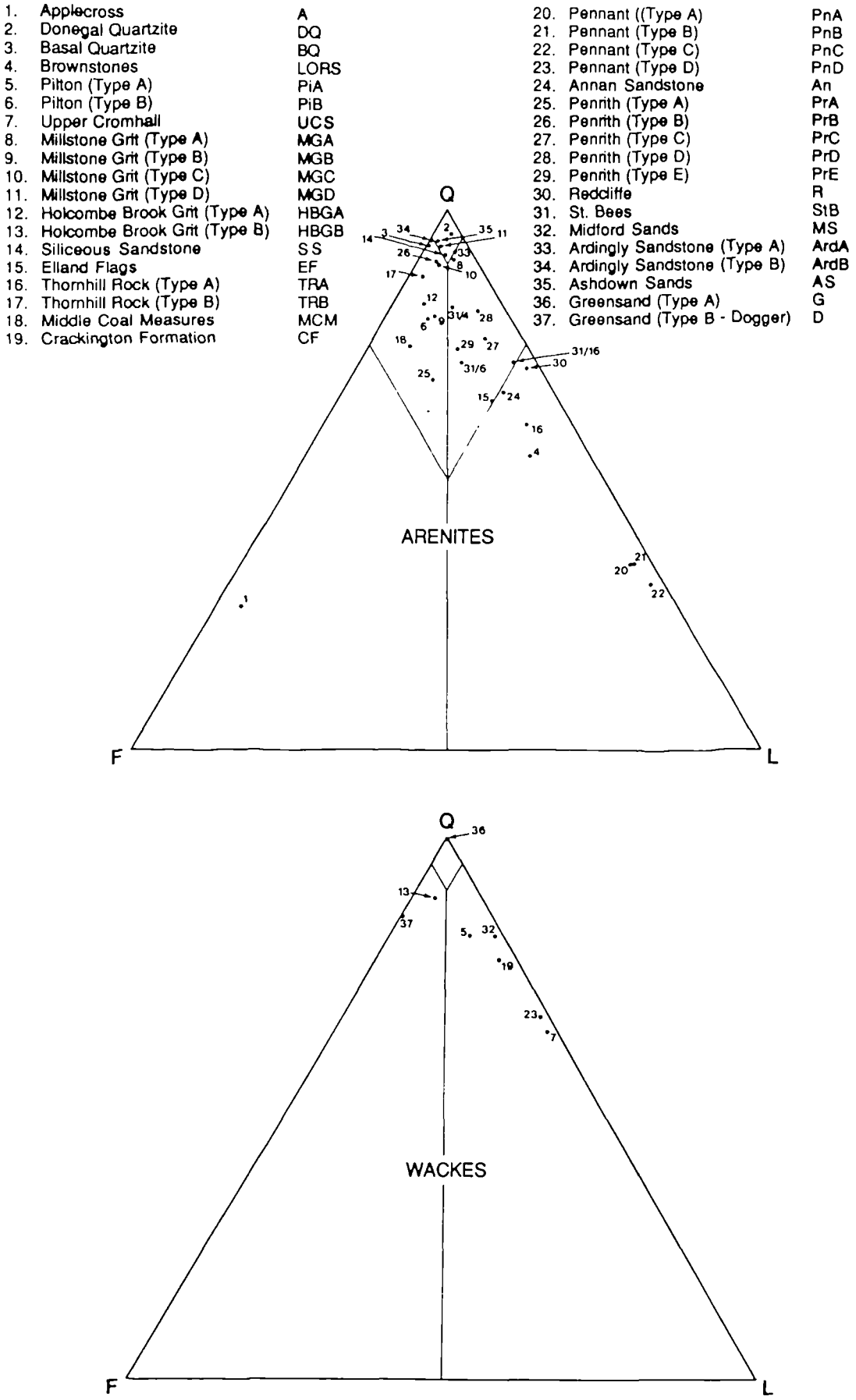

Figure 3.2 Plots of sandstones separated into arenites and wackes on the basis of the Dott-Folk classification.

Plate 3.79(a-h) Some mineralogical and textural variations revealed using SEM.

(a) Pennant Sandstone (type D), showing quartz overgrowths and illite/smectite matrix.

(b) Holcombe Brook Grit (type B) with kaolinite forming characteristic stacks.

(c) Penrith (type C). Porosity is visible but has largely been occluded by overgrowths on most grains.

(d) Well developed euhedral quartz overgrowth in Millstone Grit (type C).

(e) Authigenic chlorite clusters growing in secondary pore space in Greensand.

(f) High porosity and clay cementation in Middle Coal Measures.

(g) High magnification of chlorite clusters in Greensand.

(h) Midford Sands showing abundance of clay minerals coating all the detrital grains.

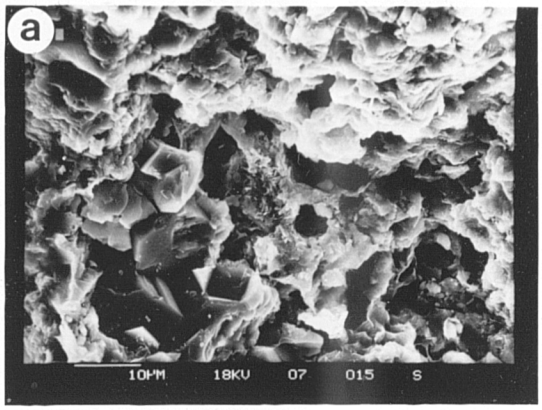
a
10µM 18KV 07 015 S

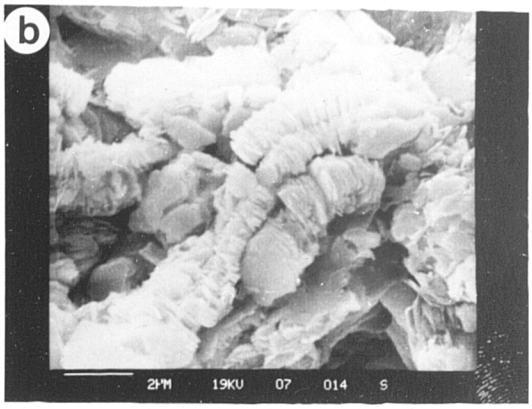
b
2µM 19KV 07 014 S

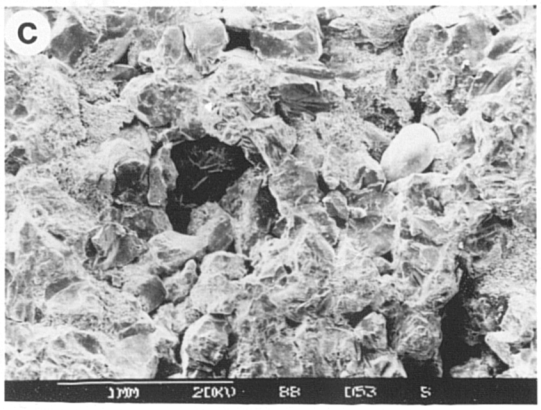
c
1µM 20KV 88 053 S

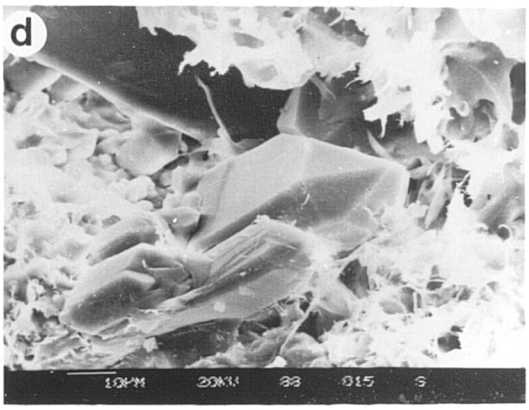
d
10µM 20KV 88 015 S

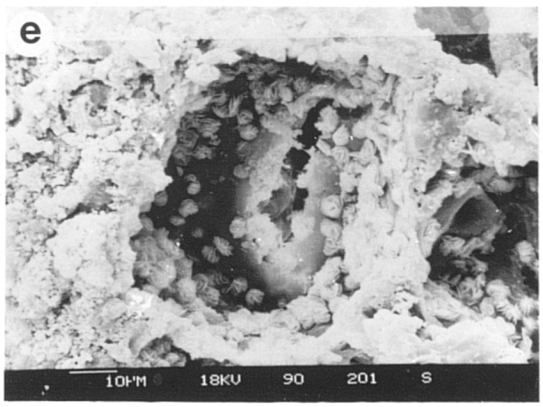
e
10µM 18KV 90 201 S

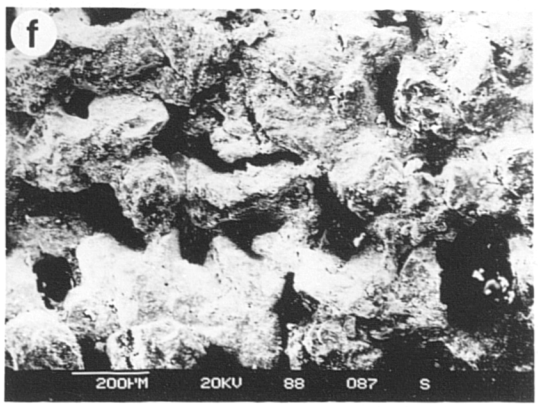
f
200µM 20KV 88 087 S

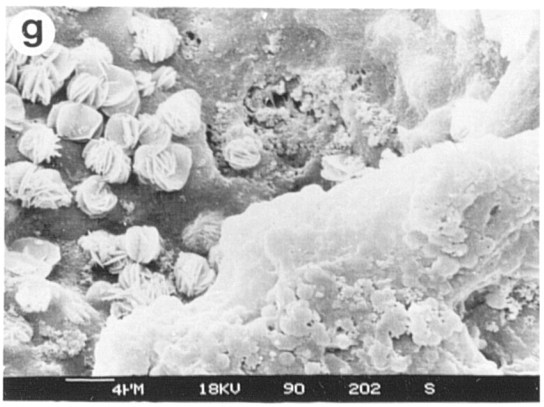
g
4µM 18KV 90 202 S

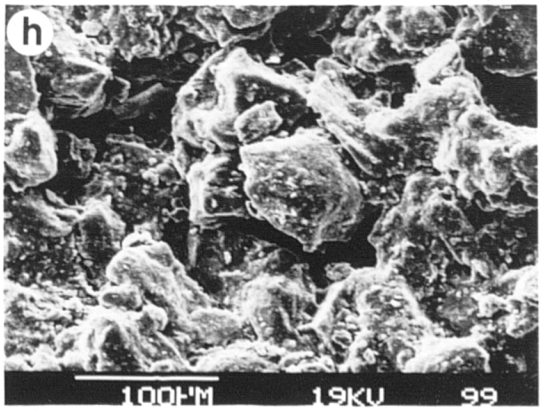
h
100µM 19KV 99

lack strong intergranular bonding materials and are cemented by thin layers of clay, glauconite or haematite. e.g. The Ashdown Sandstone

The Q-F-L diagram shown in Figure 3.2 for the wackes groups a number of very different rock types together. For example Pilton Sandstone (No.5) and Ardingly Sandstone (No.32) plot close together on the basis of their framework grain composition and amount of matrix. The classification does not account for the degree of diagenesis to which the rock has been subjected - in many of the sandstones studied such as the Pilton, Crackington and Pennant (type D) the clays have actually been recrystallized. This phenomenon tends to occur together with textural indications of strong diagenetic alteration such as grain suturing.

Textural variations are most apparent in grain size and grain shape. The research has included very fine varieties such as the Pilton Sandstone to very coarse varieties such as the Millstone Grit from Co. Durham. Sandstones with well rounded grains of high sphericity are usually rich in quartz and generally develop authigenic overgrowths. Mineralogical immaturity is normally evident in sandstones which contain low sphericity, angular grains such as the Pennant deposits of the Forest of Dean.

The parameter which showed an unexpectedly low degree of variation was packing density. The textural end members of the sandstones studied - the Donegal Quartzite and the Greensand showed the expected high and low packing density values but the intermediate deposits which were clearly texturally quite different under the microscope did not show great variation. The definition of packing density as defined by Kahn, (1956) is the ratio of the total cross-sectional length of grains occurring in a thin section traverse. This describes the aggregate properties of the packing but gives no indication of what is between the grains. The reason therefore, for similarity in the packing density values is that two sandstones could have the same packing density but the intergranular spaces can contain either cement, matrix or pores. The occurrence of these three constituents will undoubtedly have a significant influence on the geomechanical rock properties. This will be discussed in Chapter 7.

Finally, some of the rock types show a higher packing value in the horizontal direction than in the vertical direction. This is not what would be expected since the greatest stresses during diagenesis are generally vertical. It is suggested that this is due to the preferential intersection of different grain axes in the two planes. In the vertical profile, the grain intersections are more random and grain lengths appear shorter since in general the cross-sectional length will be close to the c-axis of grains. In the horizontal profile however, the a or b-axes are intersected or almost intersected, (unless the grains are highly deformed or rotated or the rock contains internal sedimentary structures). This means that in a horizontal traverse, the grains appear

longer and therefore spaces form a lower percentage of any given traverse. Thus horizontal packing density could appear higher in a horizontal traverse than in a vertical one. Packing proximity, (Kahn 1956) might be a more suitable parameter since it describes the number of grain to grain contacts as a percentage of the total number of contacts.

3.2 Density.

Dry bulk density and saturated bulk density were measured for each of the sandstone types using the methods described in Chapter 2. The results are presented in Tables 3.1 and 3.2. Densities of specimens taken from blocks showed a high degree of uniformity with low standard deviations. Specimens taken from boreholes show a much wider range in both dry and saturated bulk densities.

Highest values of dry density were measured in rocks which combined high grain density with low porosity, such as the Pilton and Crackington Sandstones. Grain densities were calculated using formula 2.14 and are included in Table 3.2. Highest grain densities were observed in the calcite and iron-rich sandstone varieties. The most quartz-rich sandstones did not show high grain density values.

3.3 Porosity

Table 3.2 includes the results of effective porosity measurements for a number of the prepared core specimens of each sandstone type. When compared with values of porosity measured using the mercury porometer method, it is clear that the latter gives results closer to the value of the rock's total porosity. Extremely low values of porosity, in the region of 1% were measured in the Pilton and Crackington Sandstones while the Greensand showed a porosity of 42%. This high value is due to the formation of secondary porosity by the dissolution of calcium carbonate. In general, good agreement was observed between dry bulk density and porosity.

In addition to measuring porosity, a qualitative technique was used to show the variation in pore morphology within the various sandstone types. This technique is termed pore casting, (Pittman and Duschatco, 1970) and involves the impregnation of the rock with epoxy resin followed by dissolution of the grains and matrix. The rock is dissolved using concentrated hydrofluoric acid, (HF) which leaves a honeycomb network of interconnecting pores. A number of scanning electron photomicrographs of the remaining pore networks are shown in Plate 3.80(a) - (h).

Sandstone Type	No. of samples	DRY BULK DENSITY (g/cc)			Standard Deviation.
		Max.	Min.	Mean	
A	8	2.480	2.462	2.475	6.550×10^{-3}
DQ	10	2.600	2.599	2.600	0.002×10^{-3}
BQ	7	2.610	2.605	2.608	3.626×10^{-3}
LORS	22	2.500	2.431	2.460	0.207
PiA	8	2.811	2.728	2.768	0.054
PiB	8	2.723	2.706	2.712	5.972×10^{-3}
UCS	12	2.720	2.609	2.634	0.033
MGA	9	2.150	2.149	2.149	5.780×10^{-3}
MGB	8	2.209	2.193	2.199	6.025×10^{-3}
MGC	16	2.294	2.284	2.291	3.674×10^{-3}
MGD	8	2.288	2.276	2.283	4.106×10^{-3}
HBGA	14	2.302	2.279	2.286	7.440×10^{-3}
HBGB	14	2.313	2.291	2.302	6.802×10^{-3}
SS	10	2.534	2.529	2.532	3.536×10^{-3}
EF	7	2.240	2.226	2.232	6.021×10^{-3}
TRA	16	2.252	2.194	2.229	0.019×10^{-3}
TRB	9	2.263	2.260	2.261	1.732×10^{-3}
MCM	10	2.090	2.070	2.081	0.010×10^{-3}
CF	12	2.673	2.651	2.653	7.560×10^{-3}
PnA	13	2.472	2.441	2.459	9.962×10^{-3}
PnB	31	2.495	2.453	2.466	0.0153
PnC	21	2.490	2.464	2.477	8.554×10^{-3}
PnD	22	2.593	2.502	2.569	0.194
Du	9	2.123	2.108	2.117	6.432×10^{-3}
PrA	10	2.382	2.333	2.368	0.0155
PrB	19	2.211	2.167	2.183	0.0125
PrC	25	2.450	2.422	2.428	8.367×10^{-3}
PrD	10	2.456	2.421	2.442	0.0127
PrE	9	2.181	2.139	2.163	0.018
R	12	2.290	2.263	2.270	0.013
StB	16	2.281	1.902	2.126	0.106
MS	12	1.782	1.750	1.767	0.011
ArdA	10	1.940	1.927	1.933	6.658×10^{-3}
ArdB	9	1.922	1.916	1.918	2.884×10^{-3}
AS	7	1.899	1.870	1.886	0.012×10^{-3}
G	10	1.553	1.522	1.531	0.014
D	11	2.219	2.113	2.156	0.029

Table 3.1 Dry bulk density measurements for the thirty-seven sandstone varieties.

Sandstone Type	Mean Sat. Bulk Density (g/cc)	Mean Grain Density (g/cc)	Effective Porosity %	Porometer Porosity %
A	2.526	2.639	5.372	6.219
DQ	2.612	2.668	1.294	2.541
BQ	2.615	2.636	0.715	1.060
LORS	2.514	2.765	6.764	11.023
PiA	2.775	2.791	0.702	0.809
PiB	2.719	2.757	0.651	1.632
UCS	2.681	2.779	4.609	5.211
MGA	2.267	2.476	11.741	13.204
MGB	2.313	2.517	11.443	12.648
MGC	2.374	2.602	8.059	11.948
MGD	2.381	2.646	9,214	13.734
HBGA	2.379	2.616	10.112	12.630
HBGB	2.400	2.642	10.297	12.860
SS	2.544	2.580	1.197	1.854
EF	2.353	2.586	12.366	13.698
TRA	2.352	2.561	12.034	12.957
TRB	2.385	2.573	11.920	12.122
MCM	2.219	2.603	12.919	20.043
CF	2.673	2.691	1.973	1.416
PnA	2.532	2.693	7.253	8.629
PnB	2.535	2.775	6.874	11.128
PnC	2.557	2.766	8.208	10.434
PnD	-	-	-	-
Du	2.256	2.626	13.490	19.377
PrA	2.443	2.633	7.603	10.052
PrB	2.304	2.609	12.174	16.320
PrC	2.484	2.661	5.531	8.751
PrD	2.488	2.612	4.698	6.051
PrE	2.296	2.589	11.538	16.462
R	2.443	2.775	17.273	18.199
StB	-	-	-	-
MS	1.989	2.354	22.517	24.923
ArdA	2.120	2.641	18.855	26.804
ArdB	2.085	2.590	17.092	25.954
AS	2.088	2.673	19.861	29.435
G	1.914	2.670	38.332	42.650
D	2.310	2.781	15.589	22.483

Table 3.2 Average saturated bulk densities, grain densities and porosities for the sandstones studied.

Plate 3.80(a-h) SEM photomicrographs of sandstone pore casts. Pore size and geometry are revealed by impregnating the specimens and dissolving the rock grains with acid.

(a) Greensand (type A)

(b) Ashdown Sandstone

(c) Penrith (type D)

(d) Penrith (type C)

(e) Penrith (typeB)

(f) Elland Flags

(g) Holcombe Brook Grit (type A)

(h) Donegal Quartzite

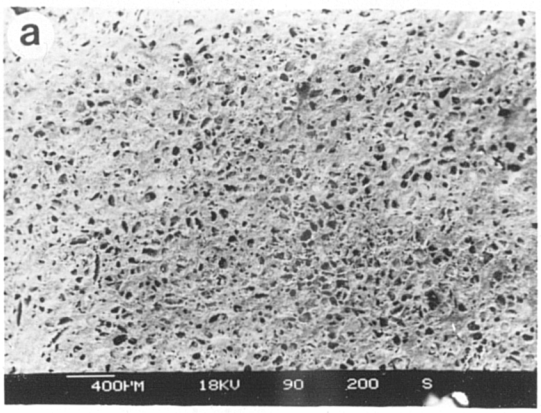
a
400µM 18KV 90 200 S

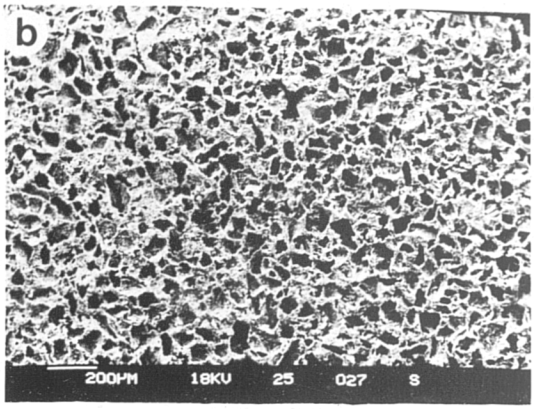
b
200µM 18KV 25 027 S

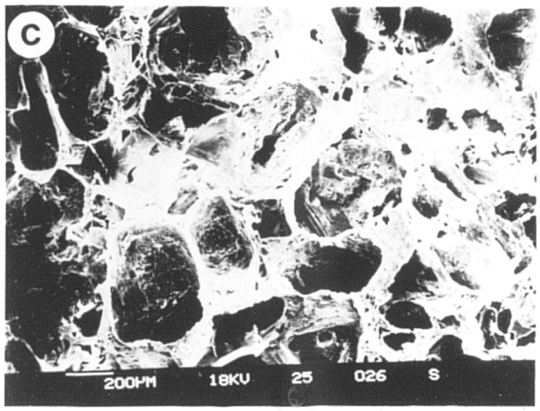
c
200µM 18KV 25 026 S

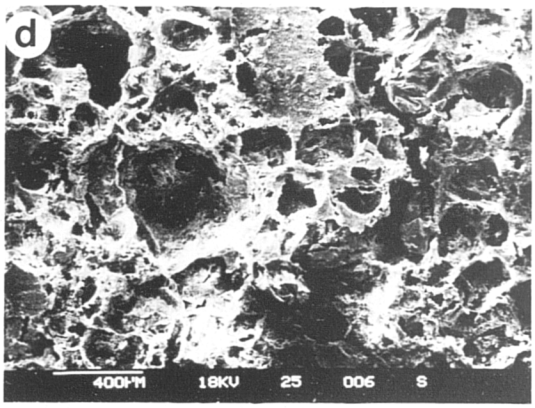
d
400µM 18KV 25 006 S

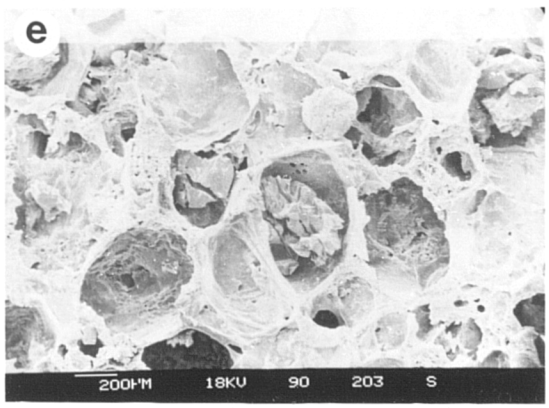
e
200µM 18KV 90 203 S

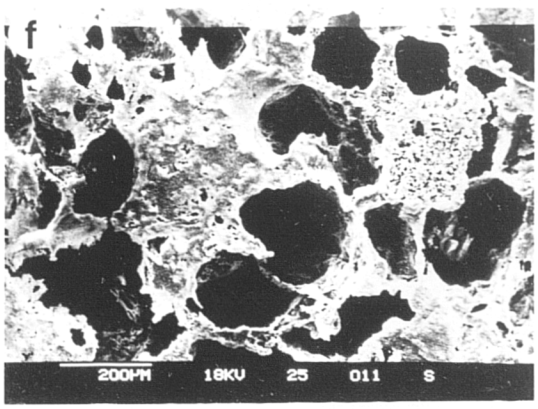
f
200µM 18KV 25 011 S

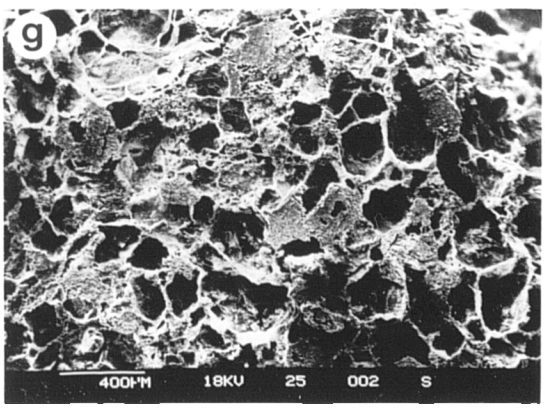
g
400µM 18KV 25 002 S

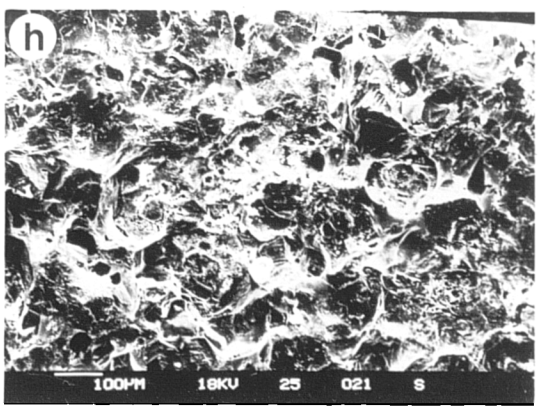
h
100µM 18KV 25 021 S

CHAPTER 4

UNIAXIAL COMPRESSIVE STRENGTH TESTING

4.1 Introduction

In the laboratory study of rock mechanics, engineers are primarily concerned with two aspects of rock behaviour, namely those of strength and deformability. Strength concerns the ability of a material to resist failure under load and incorporates the often violent collapse of a structure which is unable to support the loads for which it has been designed. Deformability concerns the relationship between stresses and strains applied to and occurring within a material, which usually involves some degree of permanent deformation but which may or may not involve failure or collapse.

Two general classes of theory, elasticity and plasticity, have been developed to describe the behaviour of a wide range of engineering materials, particularly metals, and have been applied in a similar fashion for developing theoretical models for rocks and soils. Elasticity is used to relate stresses and strains in regions where application and reversal of a finite stress or strain increment leaves the state of the material unchanged. Plasticity concerns the behaviour of a material when the application and reversal of a stress or strain increment leaves the state of the material with some permanent deformation. A third class of theory, viscosity, has also been developed to describe the time dependent aspect of material behaviour.

The term strength has variable definitions depending on the method used for its determination. Many such methods exist and include:

1) Uniaxial compression test
2) Triaxial test
3) Direct shear test
4) Tensile test
5) Point load test
6) Schmidt hammer test
7) Indentation test
8) Flexural test

The two methods regarded as the best indicators of rock performance are uniaxial and triaxial compression tests. Point load testing as introduced by Broch and Franklin, (1972) is a commonly used index test for producing approximate values of rock strength but results are not regarded as being as reliable as uniaxial compression testing. A number of workers have produced conversion factors for estimating UCS

from point load values, notably Bieniawski, (1975), Carter and Sneddon, (1977) and Hawkins and Olver, (1984). These conversion factors vary from 16, (Anon, 1972) to 28.5, (Carter and Sneddon), depending on the rock type and it is known that the conversion factor can vary even within the same rock type. It is considered that the use of a conversion factor for point load diametral testing of sandstone core would be even more variable, due to the development of incipient bedding within different types.

The uniaxial compression test is generally known to be one of the most rigorous and most frequently used strength tests in rock mechanics. It is considered therefore that for this research it is the best single method for determining which factors ultimately control rock behaviour. Uniaxial compressive strength is defined as the maximum stress which a sample can support as a function of strain during compression. It is calculated as:

$$\sigma_c = \frac{\text{Maximum load applied}}{\text{Original cross section}} \qquad (\text{MN/m}^2 \text{ or MPa}) \qquad (4.1)$$

During compressive testing both the length and cross-sectional dimensions change, therefore the original cross-sectional area is used in the equation. Unlike concrete testing, where cubes are used, rock mechanics normally employs cylindrical specimens.

Of equal importance to the ultimate uniaxial strength is the relationship between stress and strain for a particular rock type. Strain is measured in two directions for uniaxial testing - axially and circumferentially. Axial strain is a measure of the amount of specimen shortening during testing while circumferential strain indicates the degree of lateral expansion.

Figure 4.1 shows an idealised stress-strain diagram for a ductile material. In this diagram it can be seen that up to a certain magnitude of the externally applied stress, (at the proportional limit, point P.L.) a linear relationship exists between stress and strain. In other words the stress σ (or $\Delta\sigma$) is proportional to strain ε (or $\Delta\varepsilon$) by Hooke's Law, "ut tensio sic vis":

$$\sigma = E.\varepsilon \qquad (4.2)$$

$$\Delta\sigma = E.\Delta\varepsilon \qquad (4.3)$$

where $E = \sigma/\varepsilon$ = Hooke's coefficient of proportionality, known as Young's Modulus of elasticity, defined for uniaxial stress; the modulus of elasticity, E represents the stiffness of the material.

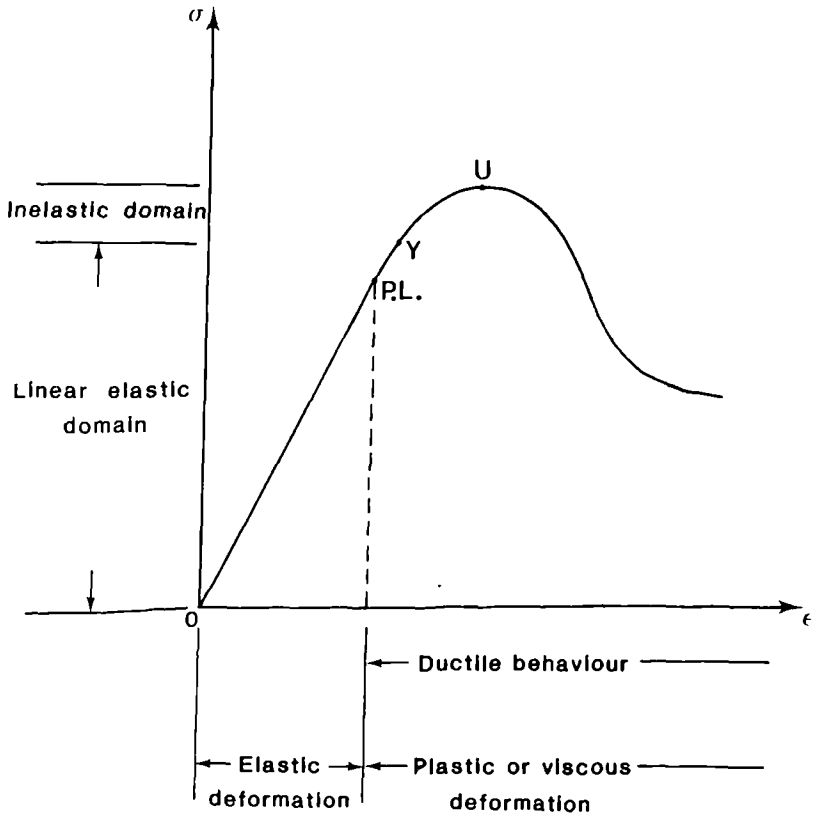

Figure 4.1 Idealised stress-strain diagram for ductile materials.
(After Jumikis 1983)

In Figure 4.1 the point Y, (yield point) is shown along the stress-strain curve from point P.L. The yield point is where the transition from elastic to ductile behaviour occurs. It must be noted however, that for most materials, including rocks, the proportional limit practically coincides with the yield point. The stress region between point P.L. and Y is termed the elastic-plastic domain and is generally extremely small for rocks. for this reason, in rock mechanics the proportional limit and yield point are taken as being the same and the term yield point is used. For most rocks, the stress-strain, (σ–ε) curves take an approximately linear course, ending abruptly in failure just beyond the yield point at the ultimate stress, (U). This is termed brittle deformation; i.e. no plastic deformation occurs prior to failure. Rocks which deform appreciably, (plastically) before failure are referred to as ductile and do not undergo subsequent brittle fracture but fail by ductile rupture. Generally only at high temperatures and pressures does ductile deformation occur in rocks, but such conditions are rarely encountered in engineering practice and are therefore not of great interest in normal rock mechanics. Figure 4.2(a-f) shows various types of σ–ε diagrams encountered in rock mechanics, (Farmer 1968).

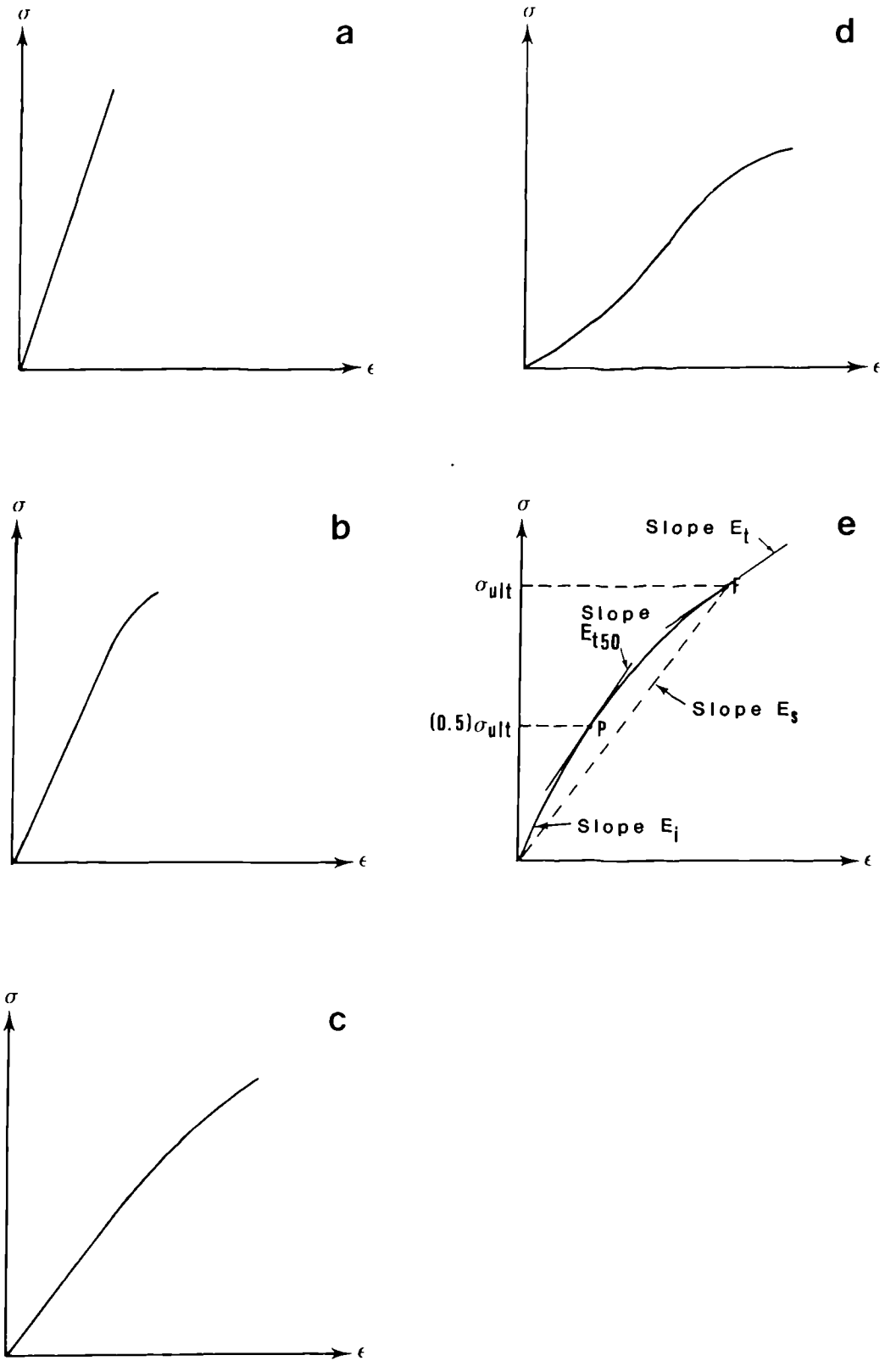

Figure 4.2 Various stress-strain diagrams for rocks, (after Farmer, 1968 and Jumikis, 1983).
(a) Linearly elastic rock.
(b) Quasi-elastic rock.
(c) Semi-elastic rock.
(d) Non-elastic rock.
(e) Generalised stress-strain diagram for rock.

Figure 4.2(a) describes a perfectly elastic material where stress is proportional to strain and where there is no yield point, ending abruptly in failure at point F on the diagram.

Figure 4.2(b) shows the σ–ε curve for what is termed a quasi-elastic rock. These rocks approximate a brittle elastic material with a nearly linear relationship to the point of failure.

In Figure 4.2(c) the slope decreases as the stress increases. Termed semi-elastic, these rocks represent the less elastic, coarser grained igneous and fine-grained, low porosity sediments with a reasonable amount of cohesion.

Figure 4.2(d) represents a non-elastic rock such as a less cohesive and weak sedimentary rock with large void spaces.

Shown in Figure 4.2(e) is the generalised σ–ε diagram for rock. As can be seen, rocks do not exhibit an exactly linear σ–ε behaviour and therefore do not possess a unique modulus of elasticity. Young's modulus is a function of stress and being different for loading and unloading cycles, it must be specified exactly in order to study its variation between different rock types under different loading conditions. Figure 4.2(e) shows three kinds of modulus of elasticity:

1) Ei - the initial tangent modulus
2) Et - the tangent modulus at point F, (also shown is the 50% tangent at point P), and
3) Es - the secant modulus for point F.

The tangent Young's modulus and Secant Young's modulus are defined below in order to study the change in elastic modulus with change in stress. (Lama and Vutukuri, 1978):

$$\text{tangent Young's modulus} = \frac{\text{Incremental axial stress}}{\text{Incremental axial strain}} \tag{4.4}$$

$$\text{secant Young's modulus} = \frac{\text{Total axial stress}}{\text{Total axial strain}} \tag{4.5}$$

In order to define tan E, the stress level (σ) and the stress range ($\Delta\sigma$) must be specified. Normally, Young's modulus without any specification denotes the tan E at 50% of the ultimate load bearing capacity of the rock specimen.

The other elasticity constant used in the strength analysis of elastic materials is Poisson's Ratio, μ:

$$\mu = \frac{1}{m} = \frac{\varepsilon_r}{\varepsilon_l} \tag{4.6}$$

where $m = 1/\mu$ = Poisson's number

ε_r = radial strain

ε_l = longitudinal strain

Poisson's Ratio unspecified is the ratio of the total circumferential strain to the total axial strain at 50% of the ultimate stress. (Hawkes and Mellor, 1970). Like the Young's modulus, tangent and secant Poisson's Ratio can be defined as follows:

$$\tan \mu = \frac{\text{Incremental circumferential strain}}{\text{Incremental axial strain}} \tag{4.7}$$

$$\sec \mu = \frac{\text{Total circumferential strain}}{\text{Total axial strain}} \tag{4.8}$$

In a laboratory test, it is impossible to simulate exactly, the behaviour of a rock mass under stress due to the comparatively small size and homogeneity of the specimen tested. Invaluable information on the strength and deformability of the intact rock can however be obtained from such tests.

The deformational behaviour of rock in uniaxial compression is influenced by a number of factors:

1) The static properties of the rock sample being tested, as defined in Chapters 2 and 3,
2) The sample characteristics; i.e. size, shape (aspect ratio) and standards of preparation, and
3) The test environment; i.e. moisture content, pore pressure, temperature, humidity and chemical conditions.

In order to study the relationship between a particular rock property and the stress-strain characteristics, it is important that the other factors likely to affect the results are kept constant throughout a series of tests. This means that for example to study the effect of moisture content on the strength of a particular sandstone type, specimens should be prepared from the same parent block. In this way sample variation can be kept to a minimum and strength changes can be related directly to the changing external variable.

The remainder of this chapter describes the experimental procedure used during the research for the uniaxial compressive testing of sandstones.

4.2 Specimen Preparation for Laboratory Strength Tests

The sampling and preparation techniques used are of fundamental importance in rock testing since they influence the quality of the results and their applicability to the behaviour of the rock mass from which samples were extracted. The techniques used during the research are outlined in this section.

4.2.1 Sampling

Rock masses, in general, are non-homogeneous and the properties of the samples taken from one portion of the rock mass may be markedly different from those taken elsewhere. This is particularly true for sandstones which can vary over short distances in terms of their mineralogy, porosity and density. Where a rock type was sampled during this research, an effort was made to take representative samples or if a major variation was noted within the outcrop, each lithological unit was sampled. Very often, changes in colour and texture allow the delineation of regions which differ markedly in their lithological nature.

Samples of fresh sandstone are only available when an underground excavation or boring occurs or if a surface excavation is sufficient to remove the overburden and weathered material. During this research, samples were collected from the following sources:

i) Working quarries
ii) Tunnel drives
iii) Recent road cuttings
iv) Site investigation boreholes
v) Deep trial pits
vi) Caves

Block and core samples were collected which contained no obvious bedding planes or structural discontinuities. In each case, an effort was made to obtain fresh samples - falling within Grade 1 of the BS 5930: (1981) weathering classification. Grade 1 specifies, "No visible sign of rock weathering; perhaps slight discoloration on major discontinuity surfaces". The mode of winning of the material was also taken into consideration since blocks obtained in quarries by means of blasting may have been subjected to high intensity stress waves producing incipient microfractures or opening pre-existing ones.

In the case of some of the weaker argillaceous sandstones collected from hand-worked tunnel faces, the weaker portions tend to break into smaller fragments. As a result care must be taken to ensure that the samples collected include not only the non-

representative stronger material but also the weaker material which must be carefully removed from the face.

The quality of samples taken from borehole cores normally depends on the strength of the rock material but is influenced by the skill of the driller. For example, boreholes sunk in the St. Bees Sandtone during a site investigation at Sellafield produced variable quality cores due to the weaker beds being abraided by "wander" of the barrel and the effects of too high a flush pressure. In addition, as discussed in Section 4.1 borehole samples have limited use in quantitative comparisons since only one sample is available at each level.

4.2.2 Sample Geometry

With the exception of the point load 'lump' test, the laboratory testing of intact geomaterials normally involves the preparation of geometrical specimens. Compression tests usually involve the preparation of either cylindrical or cubic specimens, with the latter being the predominant type in concrete testing.

The preparation of cubic specimens in concrete testing is relatively easy since concrete can be moulded into any shape. The normal dimensions of the cubes used are 150mm x 150mm x 150mm, (Neville 1987). Preparation of cubes for rock testing would be a complicated process, especially from originally irregular blocks, since it involves cutting six orthogonal faces. In addition, a very large compression machine would be required to fail 150mm cubes of many rock types. For this reason, rock specimens are normally prepared as cylinders. Additionally, for the purposes of quantifying stress and strain, the stress pattern within a cylinder is much simpler than that produced in a cube since cylinders contain no vertical edges which could produce high stress concentrations.

The size and length-to-diameter, (or aspect ratio) of the cylindrical samples used in strength testing has been the source of much debate. Figure 4.3 shows the relationship established between diameter of specimen tested and the resultant strength for various rock types, (Hoek and Brown, 1982). Only samples from the Lower Old Red Sandstone of The Forest of Dean have been tested at different diameters during this research; the results plotted on Figure 4.3 indicate general agreement with the established trend for other rock types.

Hawkes and Mellor, (1970) suggested that the diameter of the specimen should be at least ten times the size of the largest contained grain. For sandstones, this means that in theory, a core diameter of 20mm would be adequate. ISRM - (Suggested methods for Determining the Uniaxial Compressive Strength and Deformability of Rock Materials, 1981) supports this recommendation but states that specimen diameter should not be less than NX size (54.75mm).

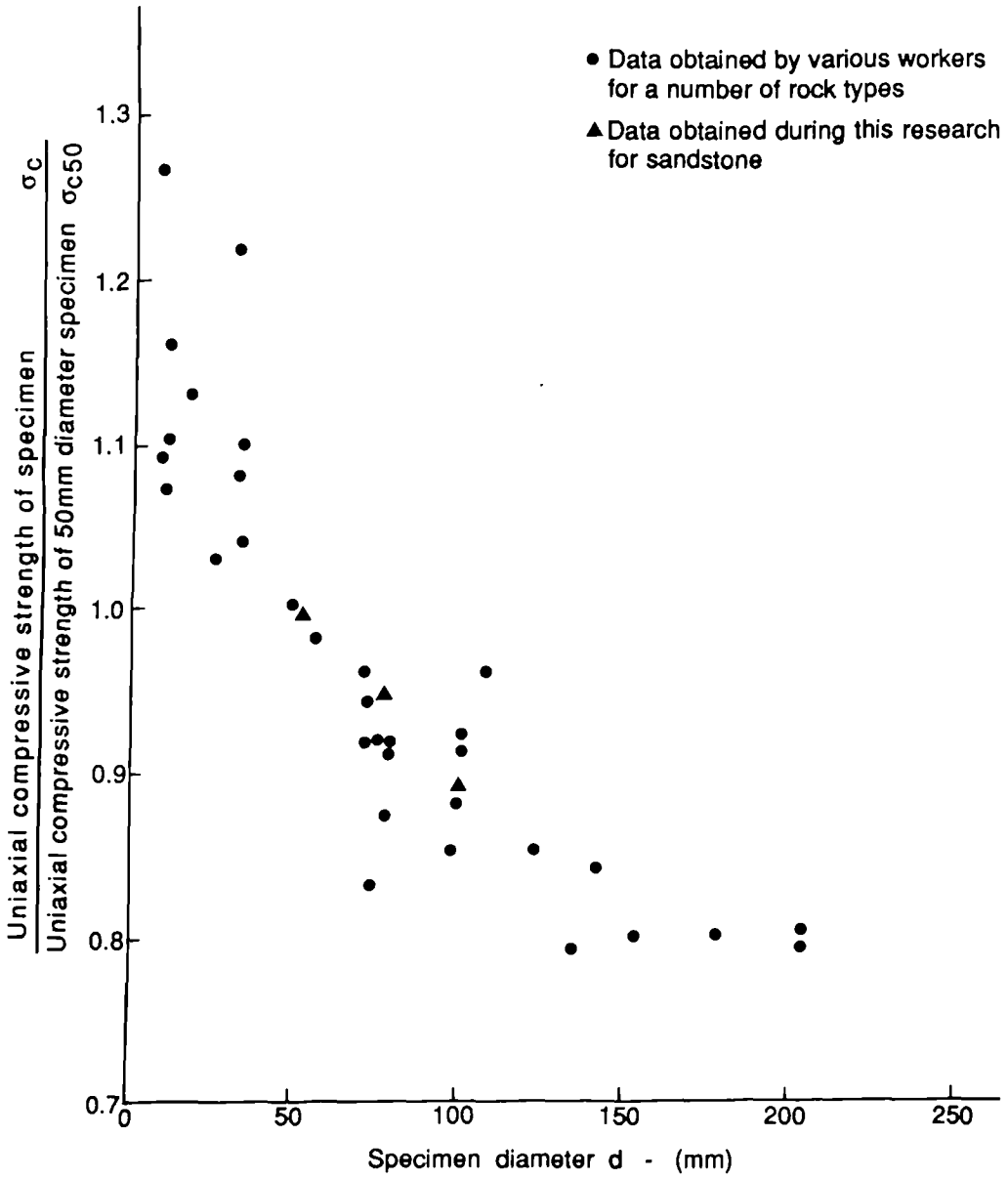

Figure 4.3 Influence of specimen size on the strength of intact rock. (Modified after Hoek and Brown, 1982)

For this research, it was decided that NX sized cores would be used for the majority of the testing program since that size:

i) fulfills the diameter to grain size recommendation,
ii) does not require the high loads needed to fracture larger diameter specimens, so reducing the risk of damage to monitoring equipment,
iii) keeps the length requirement to a minimum so reducing the thickness of bed from which samples can be taken,
iv) provides a large number of cores from conveniently sized blocks
v) is commonly produced from site investigations which could provide some of the individual samples for testing.

The aspect ratio of specimens tested in uniaxial compression has been shown to have a marked effect on stress and strain results. The normal aspect ratio used in rock mechanics is between 2.5:1 and 3.0:1 as recommended by Hawkes and Mellor, (1970) and ISRM, (1981). The aspect ratio used in soil mechanics testing is 2.0:1 and a few workers have suggested that the same be applied to rock mechanics for the purposes of standardising the technique, (Hawkins, 1986). There are however a number of reasons why the aspect ratio must fall within the guidelines of the ISRM:
i) rock specimens failed in uniaxial compression often form cone shaped fragments at the top and bottom. If the aspect ratio is less than 2.5:1 the end cones will meet and the failure mode is therefore controlled by the specimen length rather than the rock properties, (Hawkes and Mellor,1970).
ii) it has been shown that Poissons ratio calculated using radial strains measured at mid-specimen height where aspect ratio is greater than 2.5:1, are close to the Poissons ratio of the rock measured using other methods, (Wawersik, 1975).
iii) aspect ratios of greater than 3.0:1 produce specimens which possess elastic instability during testing, (Wawersik, 1975).

4.2.3 Sample Preparation

NX diameter cores were cut from the samples collected using an ELE. core drill. The machine comprises a Milwaukee 240V AC motorised power unit capable of drill speeds of 450 and 900 rpm. A swivel head is attached to allow the entry of water coolant into the inside of the core barrel. (Plate 4.1)

Plate 4.1 Core drill fitted with rock holding fixture being used to core sandstone specimens.

Plate 4.2 Preparation of a number of specimens for uniaxial testing.

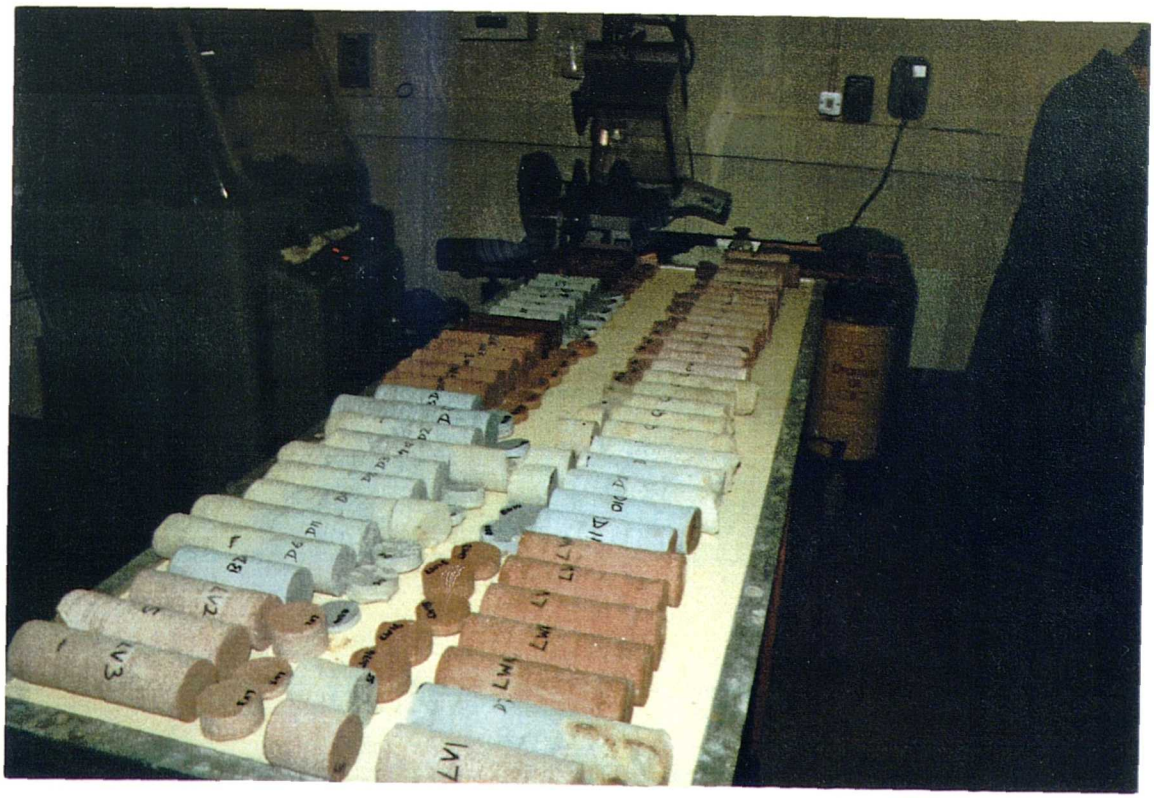

The drill is mounted on a vertical column and this in turn is attached to a cast metal base. A special rock holding fixture was designed and constructed in the departmental workshop and fitted to the drill base. It was fabricated as follows:

i) 2 No. 1070 x 38 x 50 mm BMS slides spaced at 260mm centres bolted to the drill base,
ii) 1 No. fixed and 1 No. adjustable fabricated steel jaw unit in 15mm BMS 320 x 265mm, attached to the base slides,
iii) a clamping mechanism attached to the adjustable jaw.

The adjustable jaw could be rotated to accommadate different shaped rock specimens up to a maximum of 440 x 750 x 400mm.

The thin-walled core barrel allowed the maximum number of cores to be taken from each block sample. It was found that the greater of the two rotational speeds (900rpm) produced higher quality cores with straighter, smoother sides. The huge variation in density and strength of the sandstones studied meant that penetration rates ranged from 19.5 mm/min to 66.0 mm/min. The stronger sandstones tended to produce high quality cores despite slow penetration rates. Alternatively, it was found that the directional stability of the core barrel decreased in the weaker rocks and it was therefore necessary to increase the feed rate to the maximum in order to maintain core quality.

The core sticks were then cut to length using a Mayer and Berger QS2 diamond rock saw. Originally it was intended that the specimens would be cut to 1mm longer than the required 136.875mm and subsequently squared off in a special grinder. However, with the use of a magnetic V-block carefully positioned in the rock saw, a face parallel tolerance of 0.05mm was achieved. Although this is slightly in excess of the 0.02 mm recommended by ISRM, (1981), it was considered acceptable for this research.

In order to maintain uniform length of specimens, one end of each core stick was cut square and a stop attached to the machine table. All the cores could then be slid into the V-block and butted against the stop, ensuring reproducible length dimensions. If the original cores were of sufficient length, prior to squaring the first end, 15mm discs were cut off to provide specimens for thin sections, (Plate 4.2). It was found that if the offcuts were substantial, they occasionally tended to break off prior to the saw blade passing totally through the core specimen. To prevent this, an adjustable support was placed below the core end. It is noteworthy that overbreak tended to occur, not in the weakest rocks but in samples such as the Penrith Sandstone with its

UNIAXIAL COMPRESSION TEST No.											
Sample No.		Lithology		Sampling Locality							
Length: 1	2	Diameter: 1	2	3	4	5	6				
Average L:		Average D:		Core extraction: Ex. Block Ex. Borehole							
Desired moisture content and weight:				Saturation fluid:							
Length of period of saturation:				Period in controlled humidity:							
Sat. Wt.	Dry Wt.	Weight during test.		Moisture content.							
Bedding thickness.	Dip.	Discontinuities.		Veining.		Grain size.					
Offcut:		Porosity		Thin section		SEM					
Fractured specimen:											
Failure Mechanism.		Failure load (kN)		Stress (MPa)							
Angle of shear plane and sketch.				Photographed: Y N Exposure No.							
Notes:											

Figure 4.4 Log sheet used for recording details of each uniaxial compression test.

saccaroidal texture and lack of intergranular cement and thus may be a function of the tensile strength of the rock. This will be discussed in Chapter 5.

The core ends were finally face polished using a diamond lap to remove any small irregularities or sawing marks. The final dimensions of each core were then measured using a Vernier caliper. The average diameter was determined by measuring specimens in two orthogonal directions at two ends and at the middle. The length was measured at four points, (the ends of two orthogonal diameters). Cores whose sides departed from parallelism by greater than 0.25mm were excluded from the strength testing programme and used for porosity and permeability tests. The offcuts produced during dimensioning were trimmed and used for thin section, XRD and SEM analyses.

Fig 4.4 shows the log sheet used for each uniaxial compression test. The specimen details are recorded including dry and saturated bulk masses, length, diameter, macroscale sedimentary features and details of other tests carried out on the fractured specimens after strength testing. The ultimate stress and failure mechanism details can also be noted as well as details of any photographs taken.

Examples of each sandstone type were photographed prior to testing, to record any special features of interest.

4.3 Loading System

4.3.1 Uniaxial compression machine

A 2000 kN compression machine, produced by ELE was used for the strength testing programme. (Plate 4.3). The capacity of the machine was well within that required to fail any sandstone sample with a diameter of 55mm. Hudson et al (1972) reviewed the various testing machines available with reference to rock failure and the amount of information which can be obtained from the tests.

Force has traditionally been regarded as the independent variable in materials testing but the inevitable outcome of a rock mechanics test with a constant loading rate is violent, uncontrolled failure at the peak of the force-displacement curve. The reason for the uncontrolled failure is that as the ultimate strength of the rock specimen is reached, the stresses within the machine decrease rapidly, transferring the energy to the deforming specimen. (Jensen, 1943).

Subsequent work by Broch (1962) and Wawersik and Fairhurst, (1970) showed that the complete failure curve, as shown in Fig 4.5, could be achieved by increasing the stiffness of the machine. In essence, a machine consists of a loading frame with fixed cross-heads and a hydraulic loading mechanism. In rock testing it is common practise to add one or more metal platens or spacers between the cross-heads,

Plate 4.3 Uniaxial compression machine, strain monitoring apparatus and computer system used for testing sandstone specimens.

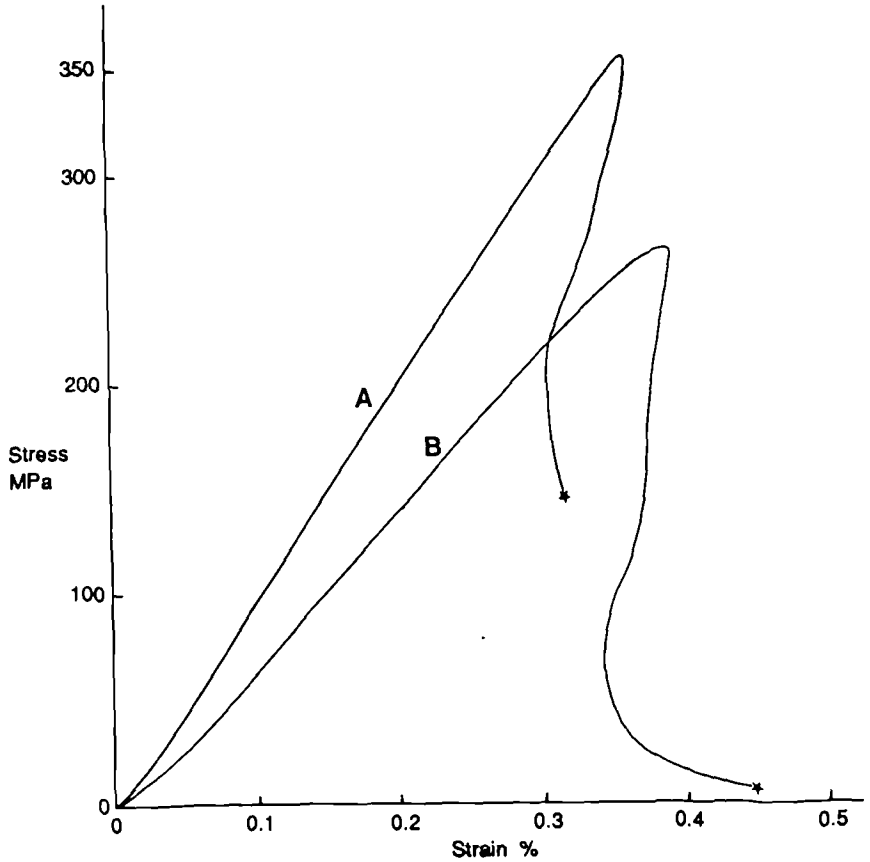

Figure 4.5 Complete stress-strain curve for basalt, (A) and Granite, (B). (After Wawersik and Fairhurst, 1970).

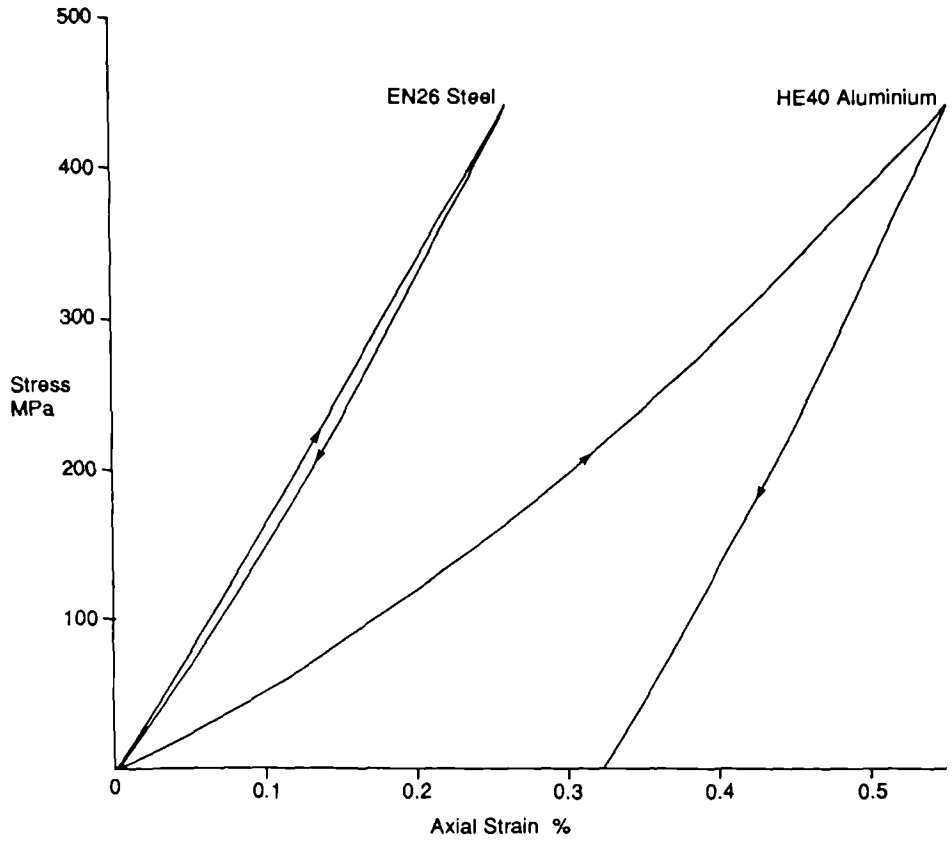

Figure 4.6 Effects of cyclic loading tests up to 440MPa on steel and aluminium platens.

depending on the type of test. The net effect of the platens is to reduce the overall stiffness of the testing system. The composite stiffness, therefore of the machine is the sum of the stiffnesses of the component parts:

$$\left[\sum_{i=1}^{N} \frac{1}{k_i}\right]^{-1} \tag{4.9}$$

where km = the machine stiffness

N = the number of component loaded parts

k_i = stiffness of individual parts

The composite stiffness can be improved by increasing the cross-sectional area or the modulus of elasticity or decreasing the length of the columns or frame.

When a rock specimen is strained until its continued deformation is accompanied by a decrease in load, the machine-specimen system is stable or unstable depending on whether the stiffness of the machine is greater or less than that of the specimen. If km > ks then the system is stable.

Rock specimen stiffness varies throughout its complete range of displacement. In particular, the stiffness becomes negative, (that is the force decreases with increasing displacement) at some point and it is the value of this negative stiffness which controls specimen failure.

Specimen stiffness is given by:

$$Ks = \frac{\pi}{4} \cdot D\left(\frac{L}{D}\right)^{-1} \cdot \frac{d\sigma}{d\varepsilon} \tag{4.10}$$

Since L and D were constant throughout the testing programme, specimen stiffness is proportional to the Young's Modulus of the rock. It was found during testing, that sandstones with a uniaxial compressive strength of less than approximately 15MPa failed passively without any appreciable explosive disintegration.

The other method of preventing violent specimen collapse is by the use of a servo-controlled machine which can be programmed to decrease the load rate and hence the load immediately any strain increment occurs. This has the effect of decreasing the stress within the load frame as the sample's ability to support load decreases. Unfortunately, such a machine was not available for this research; however

it was possible to determine part of the post-peak σ–ε curve by manually decreasing the load as the sample began to fail. This will be discussed in the next chapter.

4.3.2 Load Transfer

The compression machine possesses a lower square platen, which travels vertically and an upper stationary platen with a spherical ball seating to accommadate any slight discrepancies of specimen ends. Both are composed of hardened steel and the lower platen has concentric grooves for centering specimens.

It has been shown by Hawkes and Mellor, (1970) that contact between the specimen ends and the platens produces restraining end effects on the rock during compression testing. They found that by producing platens of the same diameter as the specimens, they could reduce these end effects since relatively small platens will strain radially much more than the large flat types found on most machines.

Ideally the process of platen matching would use platens composed of materials with similar elastic properties to those of the rock. It is impossible, however, to find, for a given rock type, a platen with a suitable E/μ ratio which will not yield under the highest stresses likely to be imposed by the test. The ratio E/μ for typical rocks lies in the range 27 GPa to 270 GPa; these values are not easy to match with materials of sufficient strength, particularly at the low end of the rock range.

Table 4.1 lists E/μ ratios for some common materials which might be considered as platen materials.

Material	E/μ GPa
Carbon Steel	710.16
Cast iron	441.27
Brass, phosphor bronze	310.27
Aluminium alloys	220.63
Magnesium alloys	131.00

Table 4.1 E/μ ratios (after Hawkes and Mellor, 1970)

Aluminium alloy, (HE30 TE) was used to produce a pair of strong platens which would strain radially with the rock. They were machined to a diameter of 54.75mm (NX) and surface ground to a face parallel tolerance of $\pm$0.002mm.
In order to test the performance of the aluminium, they were repeatedly loaded to various stresses of up to 600MPa. The aluminium behaved approximately elastically up to a stress of 30MPa but beyond this they suffered excessive permanent axial shortening. Figure 4.6 shows the performance of the two platen types after loading to

a stress of 440 MPa. The use of aluminium platens would render any rock strain measurements invalid.

Mild steel has similar elastic properties to those of HE30 TE aluminium, so it was considered necessary to use high tensile steel, (EN26). Two platens were machined in the same way and tested. They revealed little axial deformation up to the required stress levels. Despite possessing a low radial strain, it was considered that they would produce less end effects than by mounting the rock on the large platens.

4.3.3 Load Rate

The load rate is the rate at which the load on the rock specimen increases. Kobayashi, (1970) showed that increase in loading rate increased the compressive strength of the specimens. Alesekeev et al, (1970) reported a different relationship. Their results indicated a decrease in strength with increase in load rate. It can be concluded from the literature to date that load rate has variable effect on the compressive strength. For static purposes, the rate of loading is restricted to certain limits so that the time required for conducting tests is reasonable. The following load rates have been recommended:

	NX (54.75mm)	61mm	74mm
British Standards	0.471-0.942	0.202-2.01	0.3-3.02
I.S.R.M.	1.177-2.354	1.41-2.82	2.11-4.23
A.S.T.M.	0.33-0.80	0.58-1.169	0.88-1.75

Table 4.2 Various recommended load rates in kN/sec.

A load rate of 1.1kN/sec was chosen for the compression tests on NX cores as a compromise between the low recommended rates of the British Standards Institute and A.S.T.M. and the higher values of the I.S.R.M.

The compression machine used possesses a built in pacing mechanism which indicates whether the sample is being loaded at the correct rate, as selected by the operator, throughout the duration of the test. If the rate deviates from the set value, the operator can then adjust the control valve to keep the pointer within the tolerance marks of the pacer. e.g. if the load rate drops towards the end of a test.

4.4 Stress and Strain Monitoring

4.4.1 Alternative methods available

The measurement of stress and strain for compression testing of rocks is accepted as routine laboratory procedure. The Young's modulus, E is easily found as the slope of the axial stress-strain curve, the axial strain being determined from measurements of gross axial displacement of the rock sample. Poisson's ratio is calculated as the ratio of the radial to axial strains, the radial strain measured as the lateral expansion of the specimen during testing.

Details of the failure process can be determined from the stress and strain records throughout the test and provided sufficient data is available, conclusions drawn on processes of crack initiation and extension. Brace et al, (1966) have suggested that in laboratory testing, an axial stress - volumetric strain curve is the most sensitive indicator of initiation and subsequent growth of cracks.

At the beginning of this research, a number of important requirements were outlined to assist in the choice of a suitable stress - strain monitoring system. The system was required to:

i) Record time from start of test until failure and the time of any pre- failure events. e.g. onset of radial strain or onset of plastic deformation,

ii) Record load imposed on the sample during the test. i.e. axial stress,

iii) Record the axial strain during the test at small time intervals,

iv) Record the radial or circumferential strain of the sample at small time intervals.

Most uniaxial compression machines display the stress during a test either digitally or by means of a dial gauge. The machine used during this research digitally displays the load in kN with the peak value remaining on the readout for fifteen minutes to allow the noting of final results. The stress on a sample is easily calculated by dividing the load by the cross-sectional area of the specimen. For the purposes of determining the stress - strain curve, incremental values of stress would have to be noted during the test, simultaneous with strain readings.

However, the machine used possesses a 25-pin plug from which a continuous analogue signal is available. This analogue output is proportional to the load on the

specimen; 1mV per kN of load, and can be utilised by connection to a data logging system to give a detailed stress record for any test.

The recording of rock strain is much more difficult. Traditional methods involve the use of dial test indicators, (DTI's) and resistance strain gauges attached to the rock surface. Dial test indicators display displacement in fractions of a millimeter on a dial gauge and have mainly been used in the past to show the displacement between the platens, (axial strain). They require, however, the continuous manual reading of values and it would be extremely difficult to take readings at a frequency greater than every ten seconds.

Resistance strain gauges have been widely used in rock mechanics. They are glued to the rock surface and orientated in the direction of the strain to be measured. They work on a Wheatstone Bridge principle whereby the resistance to an electric current changes as the host specimen and the strain gauge deform. The values of resistance and hence strain can be recorded using a data logger.

The use of strain gauges means that strain is measured over only a very limited area of the rock specimen's surface. It has been shown that the stresses and resultant strains within a specimen in uniaxial compression are non-uniform and can result in localised failure, (Crouch, 1970). Strain gauges mounted in such zones would therefore give higher values than the average strain for that rock type and could lead to miscalculation of rock parameters. Accurate determination of strain would require an impractical large number of strain gauges attached to each specimen. Additionally, if the strain gauge is attached to the sample over an inhomogeneity or flaw in the rock structure, and the size of the flaw is large relative to the gauge length, then the strains measured will be strongly influenced by the properties and presence of the inhomogeneity or flaw. Also if the material to which the strain gauge is attached has a highly porous structure as in the case of many sandstones, the strains measured will not only represent the displacements of the pseudo-skeletal structure, but will also include a component measuring the properties of the adhesive resin that will have filled the pores adjacent to the strain gauge.

Linear Variable Differential Transformers, (LVDT's) are widely used for measuring small-scale linear displacements in laboratory work. It was proposed that transducers of this type would be used to monitor the axial and circumferential strains produced during uniaxial testing. The transducer consists of a primary iron-cored inductance coil and two secondary coils. The primary coil is excited by an input voltage of approximately ten volts DC. The two secondary coils work on a "push-pull" principle whereby a ferromagnetic armature connected to the transducer arm moves between the coils in an axial direction and produces an output voltage proportional to its displacement. These two output windings are connected to produce zero output at

the middle position of the armature.

The output voltage is normally less than 2 volts from each transducer and can be recorded on a data logging system at time intervals dependent on the capability of the recording system. Provided the transducers are calibrated properly, these voltage values can then be converted into displacements and strain calculated.

4.4.2 The Strain monitoring System

As discussed earlier, axial and radial strains were monitored during the testing program. The measurement of the axial rock strain is relatively simple since it can be determined by measuring the change in distance between the upper and lower platens. An LVDT was mounted vertically, (parallel to σ_1) in a universal magnetic clamp attached to the lower platen with the end of the transducer arm in contact with the upper platen. The small strains taking place in the NX platens, (as determined in Section 4.3.2), were accounted for in the processing of the data.

Circumferential, or radial strain is more difficult to determine since it involves the non-uniform lateral expansion of a specimen. Radial strains are normally measured at mid-specimen height and as mentioned earlier, provided the aspect ratio is 2.5:1 or greater, this measured strain gives a Poisson's ratio equivalent to the true value for a particular rock; (Wawersik, 1975). Priest and Selvakumar (1982), produced a wrap-around device incorporating an LVDT. The instrument consisted of a series of 8mm x 25mm long cylinders connected by a steel band which was placed around the specimens at mid-height. It was used with some success as the data-producing element in the feed-back loop for servo-controlled testing. Such a device was not suitable for this research, however, since it was not robust enough to withstand the often violent specimen collapse experienced during non-servo-controlled testing. It is also considered that the device may have produced a slight confining stress on the rock specimen.

For this research it was necessary to design a device which would fulfill the following criteria:

i) Be sensitive enough to measure the radial strain via an LVDT,

ii) Measure radial strain around much of the sample circumference rather than at isolated areas

iii) Be strong enough to withstand violent collapse,

iv) Have a low friction coefficient to prevent imposition of a

confining pressure on the specimen, and

v) Protect the LVDT's.

Plates 4.4 and 4.5 show the apparatus which was designed and fabricated for monitoring radial strain. It comprises a hinged cylinder which totally surrounds the core sample to be tested. The two blocks, a and b shown in Figure 4.7 are mounted on the inside of the cylinder and contact the NX specimen about two quadrants of its circumference. This contact occurs at mid-point along the specimen length, i.e. where maximum radial strain is expected.

An LVDT is mounted on the outside of the cylinder at a distance from the hinge of 2.8 times the distance between the hinge and the core centre. (This distance was dictated by the maximum convenient size of the cell). Using this principle, the small radial expansion of the core is exaggerated by a factor of 2.8, producing a more detailed record of the failure behaviour.

In addition to adhering to standard mechanical engineering tolerances throughout the manufacture of the cell, the design and construction of the hinging mechanism for the two cell wings received special attention.The hinge consists at each end of a screw-adjustable bearing with a 1° positive differential. This achieves good locating accuracy with minimal friction and enables accurate alignment of both cell winges to the basal platen.

The problem of the apparatus imposing a possible confining pressure on the rock was overcome by establishing an equilibrium situation between the cell and the basal platen, with only slight pressure required to open the cylinder. Four self lubricating, carbon-filled PTFE studs were fitted on the base of the cylinder to lower the friction against the polished platen. A number of helical extension springs of different strength were tested to produce a force just capable of overcoming the opening force of the transducer shaft. A spring of 0.218 kg force was found to close the blocks tight against the rock without imposing any significant force on it.

The radial strain monitoring apparatus was used during a number of trial tests on low porosity Millstone Grit sandstone and compared to values of radial strain produced by a series of strain gauges connected to the specimen surface. The outputs from these strain gauges were recorded using a Tinsley strain meter. The cell was found to give results consistent with those produced by the strain gauges. The apparatus assumes, however that any strain will be uniform around the sample circumference. If any anisotropy existed between the x and y-strain directions then the original cylinder design would not be able to detect it.

In order to determine whether anisotropic strain was taking place during

Plate 4.4 Original radial strain cell in position prior to specimen failure.

Plate 4.5 Radial strain cell after failure. Disintegration after peak stress has opened cell beyond measurement range of transducer.

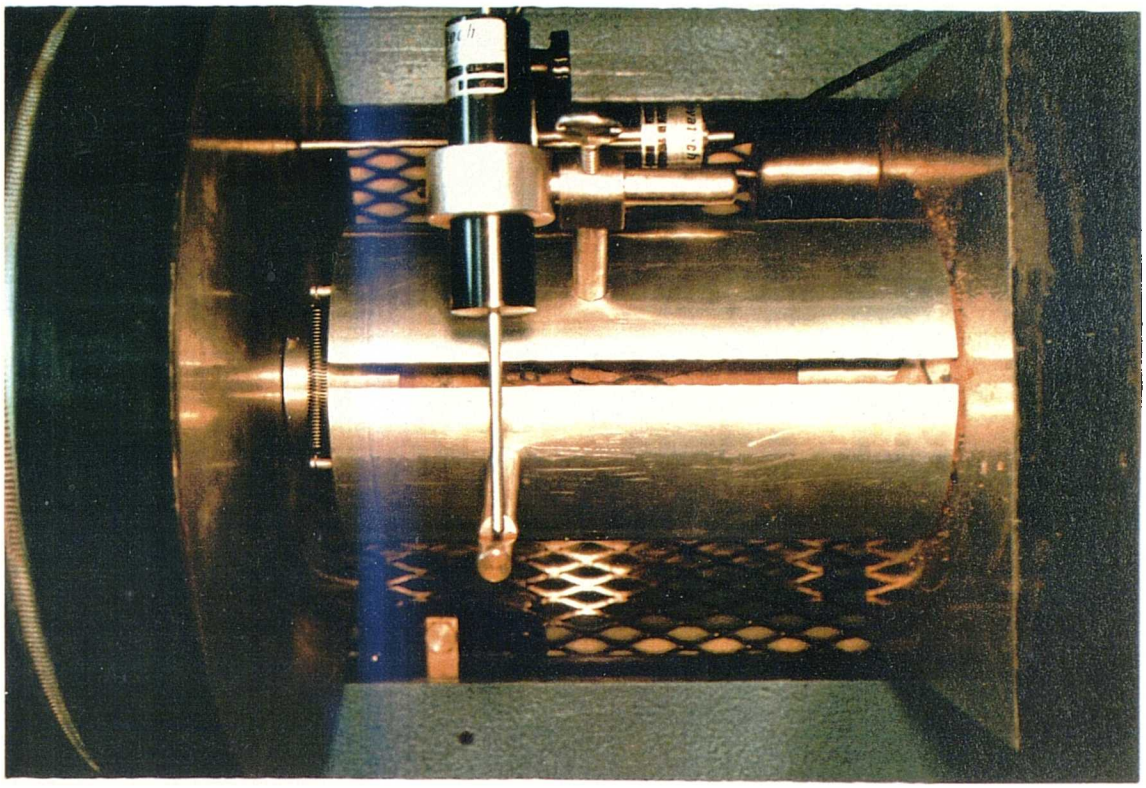

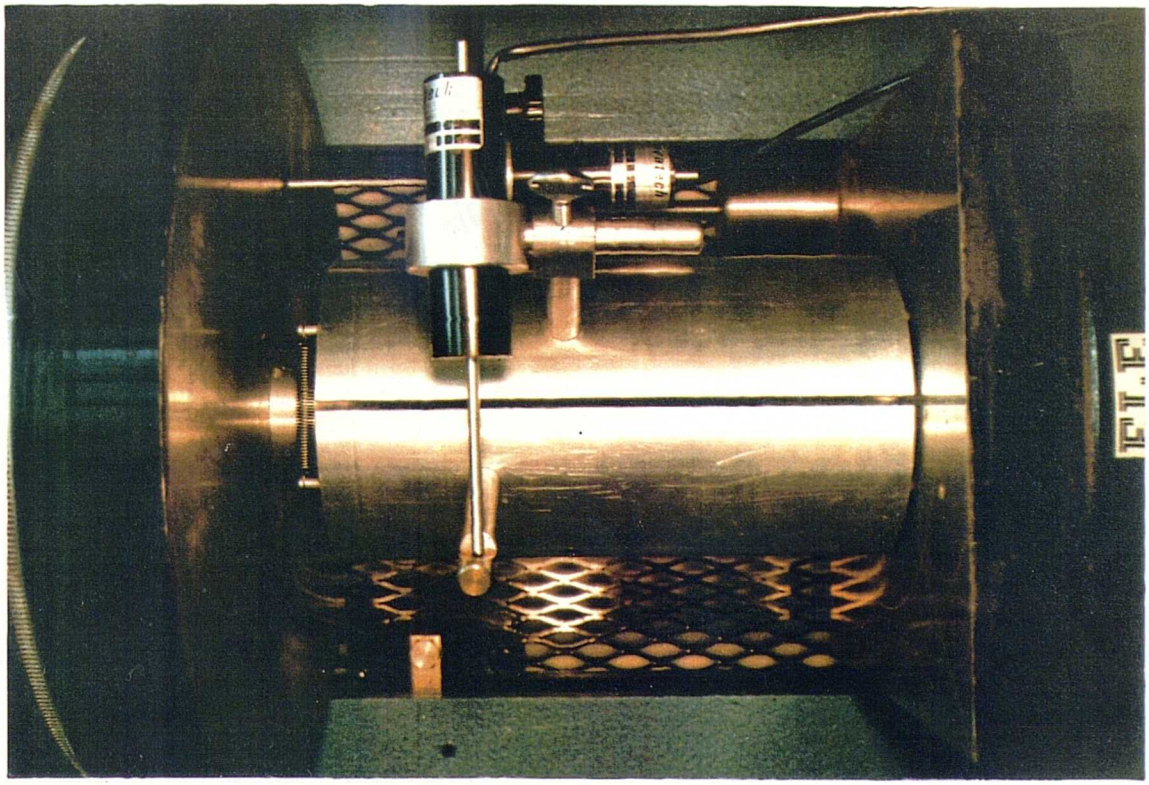

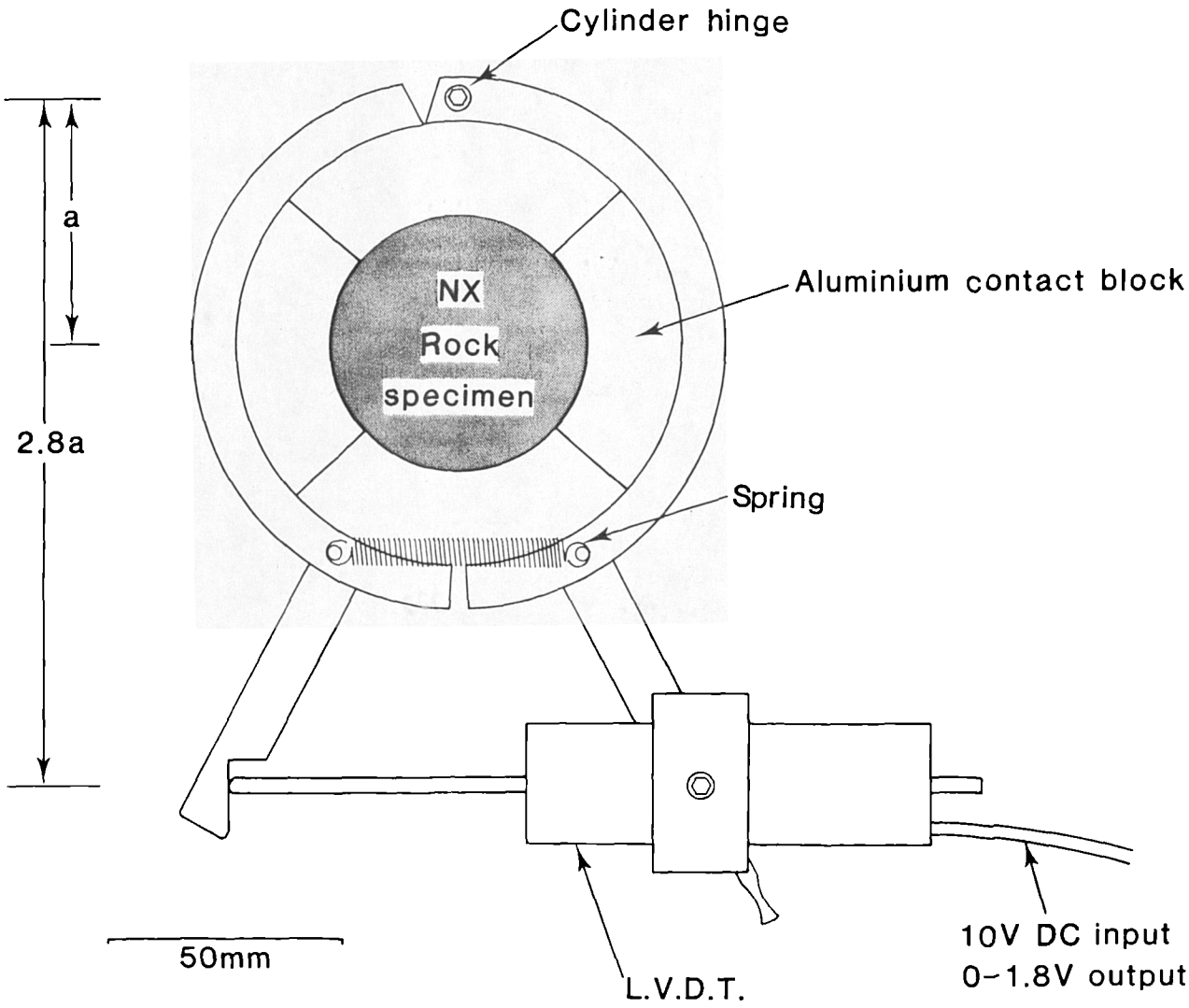

Figure 4.7 Radial strain measurement cell. (Plan view).

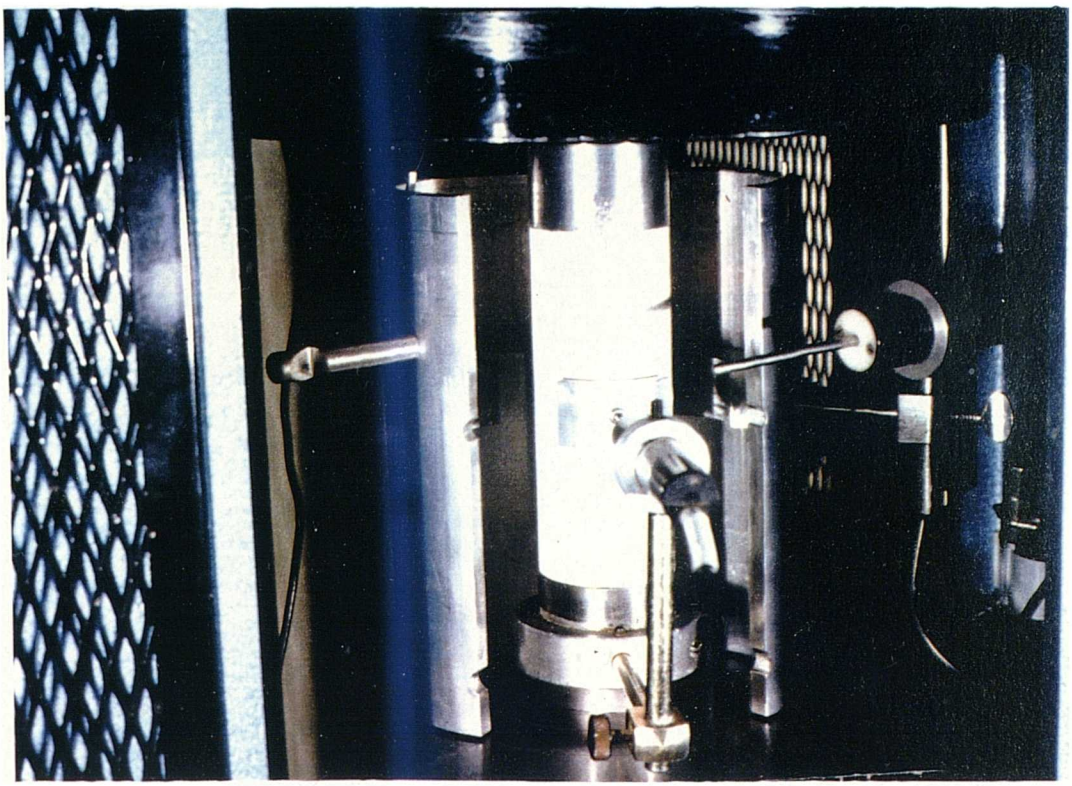

Plate 4.6 y-direction radial strain measuring transducer in contact with rock specimen prior to closure of cell.

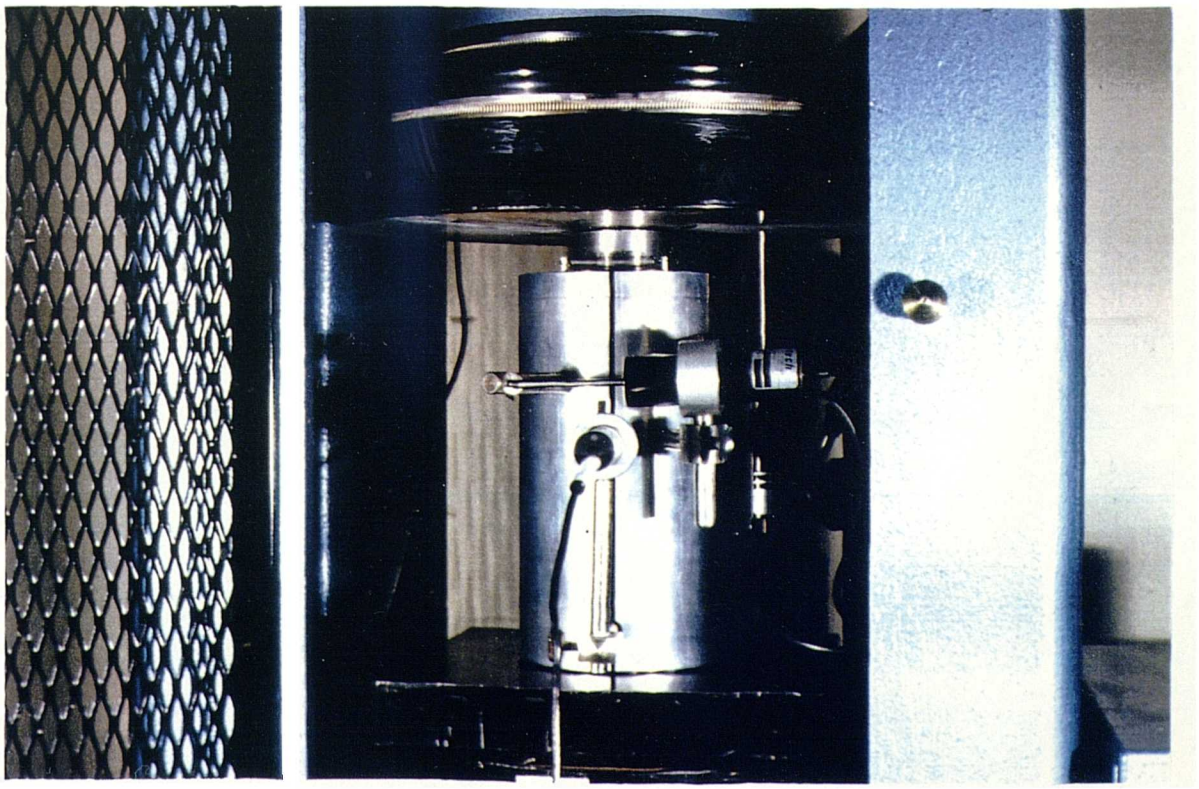

Plate 4.7 Complete apparatus in position prior to testing.

testing, it was decided to measure strain in the y-direction as well. The device designed for determining the y-strain is shown in Plate 4.6. A small aluminium plate machined to fit NX cores is connected to the end of the transducer arm. The transducer arm passes through the cylinder via a small hole at the joint and contacts the specimen between the two blocks inside the cylinder. In order to keep the LVDT stable relative to the rock specimen, it is mounted on an arm which passes through the cell via a second opening and is attached by means of a circular clamp to the basal NX platen.

Since the y-radial strain is only measured on one side of the sample during testing, the values must be multiplied by a factor of two before they can be compared to or averaged with the x-direction strain.

The procedure for using the strain measuring apparatus was as follows:

i) Place basal NX platen with y-direction LVDT attached, on the machine platen,

ii) Mount rock specimen onto NX platen and ensure good alignment between curved specimen surface and y-direction contact piece,

iii) Place top NX platen onto specimen,

iv) Slide cell around specimen but do not close,

v) Start machine and raise the lower platen until no daylight is visible at the top of the upper NX platen and the specimen is held in place by a load no greater than 0.5kN,

vi) Close the x-direction cell around the specimen ensuring a tight fit. Place spring onto the two spuds at the top of the cell,

vii) Swing axial strain transducer to a position as close as possible to the specimen,

viii) Check final position of transducers,

ix) Commence loading.

Plate 4.7 shows the complete appartus in position prior to testing.

4.4.3 Data Aquisition

The BBC microcomputer is ideal for the small scale aquisition of data since it is capable of recording four voltage channels via its analogue port. Each channel can receive a voltage in the range 0-1.8V DC which is converted by the computer to a proportional digital value. The computer also has a built in timing device which can be initiated at the start of a test and allows data readings to be taken at set time intervals, dependent on the controlling program. The transducers and uniaxial load output were connected to the BBC using fine core electrical cable via the analogue port at the rear of the computer. All four available channels were used for monitoring the tests.

A computer program was compiled for the purpose of reading and recording the output voltages from the transducers and uniaxial machine. A listing of the program is shown in Figure 4.8. Part A of the program is a routine which reads only the load value until it reaches 3.0 kN and then initiates the additional recording of the other channels. Simultaneously, the built-in timer is started. In this way the computer program can be set to run prior to the commencement of the test but recording of the data does not start until the specimen begins to take up the load.

Part B reads each of the voltage channels for time, load, axial strain and radial strain and stores the digital equivalents in the computer's memory.

A simultaneous plot is produced by part C on the VDU to give an indication of how the test is proceeding. A typical plot for a moderately weak, dry sandstone is shown in Figure 4.9. The digital values from the voltage channels are displayed at the top of the screen and plotted against time as shown. The line representing load versus time, (i.e.load rate) shows an approximately uniform gradient. Any minor fluctuations in load rate are corrected by the machine's built-in pacing mechanism. Larger variations in load rate can however occur during a test, especially towards failure. These are displayed in the simultaneous plot and the deviation can be corrected by the operator using the manual controls.

The other major advantage with this system is that if any malfunction occurs in the transducers or other equipment, it can be detected at an early stage and remedied without the loss of valuable data.

The maximum number of readings possible is 550 on each channel- a total of 2200 readings per test. The maximum duration for a test is limited by the computer memory to 4 minutes 41 seconds. If a test goes over this time the computer sends the information already in the memory to disc and records another 2200 readings.

When the sample fails, the maximum load is recorded and the data stored on disc by the subroutine in part D of the program shown in Figure 4.8. If the load or strains begin to decrease, they are also recorded by the program; this software was

```
 10REM ************************
 20REM NAME    :- UNIAX.PROG
 30REM DATE    :- 19/6/86
 40REM DATE OF FINAL REVISION:-23/8/86
 50REM ************************
 60MODE4
 70DIMD(550,4)
 80PROCadc
 90PROCsave
100END
110REM Read channels, convert & store
120:
130DEFPROCadc
140CLS:MOVE0,0:DRAW1279,0:DRAW1279,1023:DRAW0,1023:DRAW0,0
150X=50:VDU23;8202;0;0;0;
160W1=0:X1=0:Y1=0:Z1=0
170count=0
180REPEAT:Z=ADVAL(2) DIV 16:UNTIL Z>15
190REPEAT
A 200A=0:B=0:C=0:D=0:WW=0:YY=0:ZZ=0:UU=0:AA=0:BB=0:CC=0:DA=0:DDA=0
210count=count+1
220X=X+2
230REPEAT
240D=D+1
250A=ADVAL(3):W=A DIV 250
260B=ADVAL(1):Y=B DIV 200
B 270C=ADVAL(2):Z=C DIV 16
280 DA=ADVAL(4):U=DA DIV 200
290AA=AA+A:BB=BB+B:CC=CC+C:DDA=DDA+DA
300WW=WW+W:YY=YY+Y:ZZ=ZZ+Z:UU=UU+U
310UNTIL D=6
320T=INKEY(25)
330IFcount=1 THEN X1=X:W1=WW:Y1=YY:Z1=ZZ:U1=UU
340PRINTTAB(1,1);count
350PRINTTAB(1,2);"RADIAL"TAB(15);"AXIAL";TAB(27);"LOAD"
C 360PRINTTAB(1,3);STRING$(30," ")
370PRINTTAB(1,3);AA/6;TAB(14)BB/6;TAB(26)CC/6
380 PRINT TAB(2,10);DDA/6
390MOVEX1,Y1:DRAWX,YY:Y1=YY
400MOVEX1,Z1:DRAWX,ZZ:Z1=ZZ
410 MOVEX1,U1:DRAWX,UU:U1=UU
420MOVEX1,W1:DRAWX,WW:X1=X:W1=WW
430D(count,0)=TIME:D(count,1)=BB/6:D(count,2)=CC/6
440D(count,3)=AA/6:D(count,4)=DDA/6
450UNTIL count=550
460ENDPROC
D 470REM Save data to a named file
480DEFPROCsave
490 *.
500INPUT"Samples Filename ";fn$:IFfn$="" OR LEN(fn$)>8 THEN 500
510X=OPENOUT(fn$):FORT=1TO550
520PRINT£X,D(T,0),D(T,1),D(T,2),D(T,3),D(T,4)
530NEXT
540CLOSE£X:ENDPROC
```

Figure 4.8 Listing of program used to read and display data from uniaxial compression machine and strain monitoring apparatus.

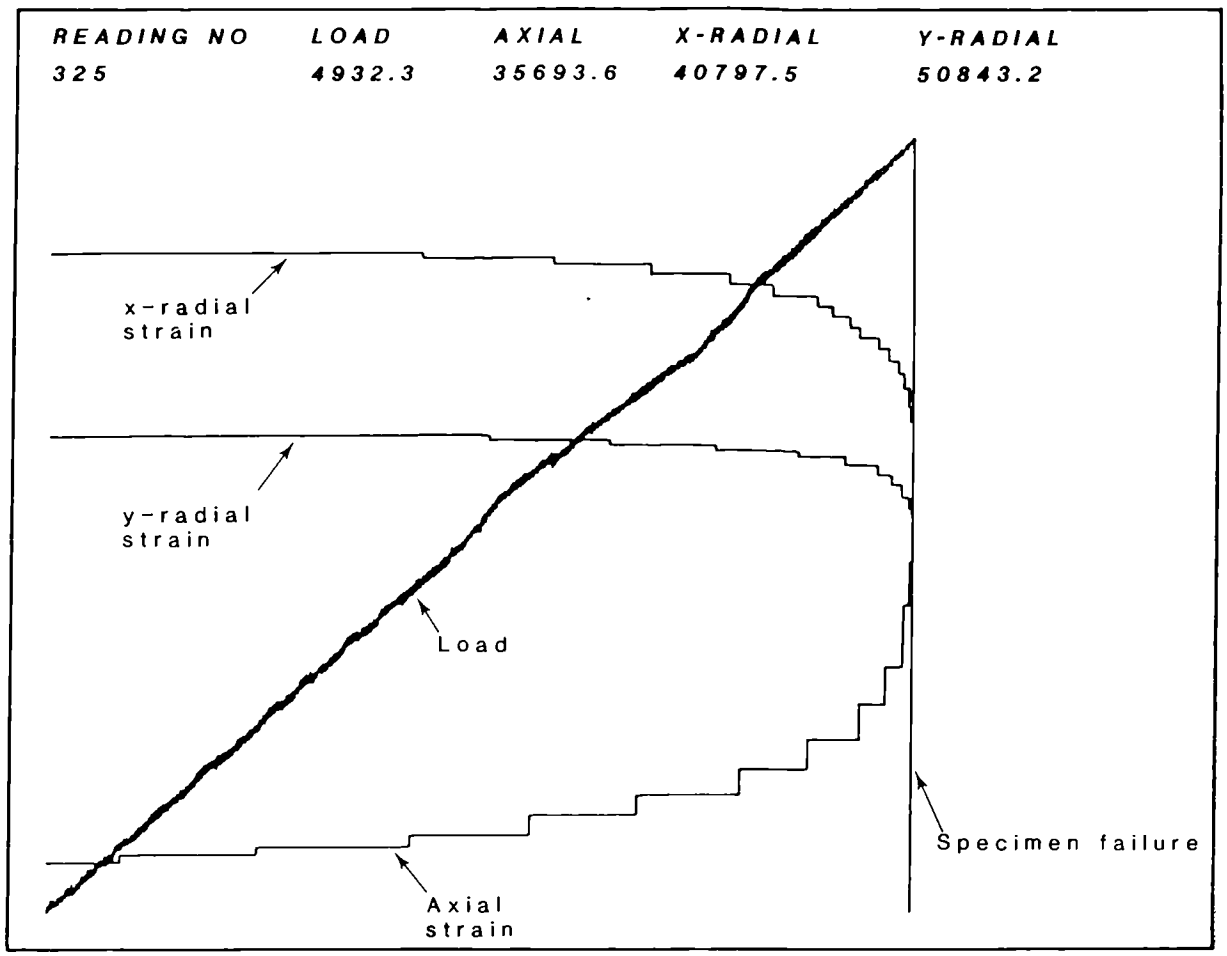

Figure 4.9 Typical plot produced during uniaxial compressive test on a dry sample of Penrith Sandstone.

used successfully during reloading tests.

Each test produces 2750 data points which is the equivalent of 20K of computer memory. Each 3" compact disc has a capacity of 100K on each side and allows the storage of data from eight tests and their modified files. Hence over 50 discs were required for the testing program.

4.4.4 Data Processing and Presentation

Each test produces a file on disc containing 2750 data points, 550 for each of time, load, axial strain, x-direction radial strain and y-direction strain.

This data is in the form of 'raw' digitised values created by the computer and proportional to the voltage values read from each channel. The processing of this data involved the conversion into units of time, load, and percentage strains by means of a second computer program.

The first stage involved the calibration of the transducers in order to match the voltage output with a distance displacement. This was carried out by mounting each transducer in a special calibration unit consisting of a highly accurate micrometer screw. The transducer was then connected to the computer and a preliminary program used to indicate the digitised values produced for different displacements at increments of 0.01mm. This process was repeated several times for each LVDT in both directions of transducer arm travel. During this calibration, it was noted that the transducers produced different results within the first thirty minutes of being energised from those after this period. This was equated to a stabilisation period during which the transducer "warmed up" and output values reached a maximum constant value for any particular displacement. It was decided therefore that transducers would be switched on one hour before any testing would take place.

Since slight variations were likely to occur in the specimen dimensions, the transducers could not be assumed to start from the same position for each test. For this reason the conversion program was designed to record the first value from each channel and subtract it from successive values. In this way the transducers could be positioned quickly.

The program is listed in Fig 4.10. Voltage fluctuations are smoothed by averaging every five values - this gives readings for time and strains every 2.5 seconds.

Any non-linearity in the displacement-output voltage relationship for any transducer is accounted for in the program and is ammended accordingly.

```
 10REM ******************
 20REM NAME : MODIFY.PROG
 30REM DATE 22/6/86
 40REM DATE OF FINAL REVISION 23/8/86
 60REM******************
 70DIMD(181)
 80T=1:Q=OPENIN("KCAL"):REPEAT:INPUT£Q,AA,BB:D(T)=BB:PRINTT,D(T):
 85T=T+1:UNTIL EOF£Q:CLOSE£Q
 90INPUT"WHAT IS THE FILENAME";fn$
100Y=OPENIN(fn$)
102 A$="B"
103 C$=fn$+A$
104 FG=OPENOUT(C$)
110@%=&20209
120 REM VDU2
130 PRINT
140 PRINT;fn$
150 PRINT
160 PRINT
170 PRINT;"TIME";TAB(14)"AXIAL";TAB(23)"LOAD";TAB(31)"RADIAL"
180 PRINT;"(SECS)";TAB(14)"(mm)";TAB(23)"(kN)";TAB(31)"(mm/100)"
190T=0:REPEAT:T=T+1
200 P=0:BI=0:Z=0:W=0:EXX=0:REPEAT:P=P+1
210INPUT£Y,A,B,C,D,EX
220 IF T=1 AND P=1 THEN E=A
230 IF P=1 THEN AI=A
235 IF T=1 THEN FR=FR+EX
236 EXX=EXX+EX
240 IF C<237 THEN J=64
250 IF C>=237 AND C<256 THEN J=60
260 IF C>=256 AND C<354 THEN J=50.5
270 IF C>=354 AND C<529 THEN J=45
280 IF C>=529 AND C<652 THEN J=43
290 IF C>=652 AND C<826 THEN J=41
300 IF C>=826 AND C<1131 THEN J=40
301 IF C>=1131  AND C<1578 THEN J=39
302 IF C>=1578 AND C<3041 THEN J=38
310 IF C>=3041 AND C<4400 THEN J=37
311 IF C>=4400 AND C<6500 THEN J=37
312 IF C>=6500 AND C<8000 THEN J=36.6
313 IF C>=8000 AND C<9136 THEN J=36.6
320 IF C>=9136 THEN J=36.6
350 BI=BI+(C/J)
360 IF B>=3400 AND B<3570 THEN K=120000000
370 IF B>=3570 AND B<3580 THEN K=120000
380 IF B>=3580 AND B<4157 THEN K=45000
390 IF B>=4157 AND B<4717 THEN K=35000
400 IF B>=4717 AND B<5349 THEN K=25000
410 IF B>=5349 AND B<5904 THEN K=20000
420 IF B>=5904 AND B<5941 THEN K=18200
421 IF B>=5941 AND B<6501 THEN K=16500
422 IF B>=6501 AND B<6522 THEN K=15100
423 IF B>=6522 AND B<7712 THEN K=14500
424 IF B>=7712 AND B<7722 THEN K=13000
425 IF B>=7722 AND B<8869 THEN K=12600
426 IF B>=8869 AND B<10709 THEN K=11200
427 IF B>=10709 AND B<11000  THEN K=10192
428 IF B>=11000 AND B<12500 THEN K=9895
430 IF B>=12500 AND B<13600 THEN K=9338
440 IF B>=13600 AND B<20840 THEN K=9338
520 IF B>=20840 AND B<23000 THEN K=8957
530 IF B>=23000 THEN K=8290
700 IF T=1 AND P=1 THEN F=B:IF T=1 AND P=1 THEN X=K
710 Z=Z+(B/K)-(F/X)
720 TT=1:TX=1
730 REPEAT
740 IF D(TX-1)>D AND D(TX)<=D THEN TT=180
750 TT=TT+1:TX=TX+1
760 UNTILTT>180
770 TX=TX-1
780 int=((TX-(TX-1))*(D-D(TX-1)))/(D(TX)-D(TX-1))+TX-1
790 IF T=1 AND P=1 THEN FF=int
800 W=W+int
801 IF T=1 THEN FF=W/5
810 UNTIL P=5
820 REM VDU2
830 @%=&20209
840PRINT;(AI-E)/100,;:@%=&20307:PRINT;TAB(14);(Z/5),;
845@%=&20209
846PRINT;TAB(23);BI/5;TAB(31);(W/5)-FF;TAB(40);((EXX-FR)/5)/38.50
850 VDU3
855 PRINT£FG,(AI-E)/100,(Z/5),BI/5,(W/5)-FF,((EXX-FR)/5)/38.50
860UNTIL EOF£Y
870 CLOSE£Q
880END
```

Figure 4.10 Listing of program used to process 'raw' data from compression tests.

Program	Max. Stress Plotted	Strain Details	Max. Strain
Plot 7	80 Mpa	Axial. x-radial only.	1.5%
Plot 8	80 MPa	Axial. Average of x & y radial.	1.5%
Plot 9	100 MPa	Axial. x-radial only.	1.5%
Plot 10	100 MPa	Axial. Average of x & y radial.	1.5%
Plot 11	200 MPa	Axial. x-radial only.	1.5%
Plot 12	200 MPa	Axial. Average of x & y radial.	1.5%
Plot 13	300 MPa	Axial. x-radial only.	1.5%
Plot 14	400 Mpa	Axial. Average of x & y radial.	1.5%

Table 4.3 Details of plotting programs for stress-strain curves.

The final subroutine of the program prints the converted values on the VDU and to a file on disc under the following headings:

Time in seconds from start of test
Load in kN
Axial strain in mm
x-direction radial strain in mm/100
y-direction radial strain in mm/100

The program processes all the original data including those values produced after failure of the rock specimen. The total number of data points stored in the new

'B' files is 550. (110 x 5).

The plotting of 550 points to produce the stress-strain curves for each test was considered to be a time consuming operation and it was decided to write software capable of reading the information direct from disc and plotting it onto a printer.

Eight programs in total were compiled for this purpose. Each program converts the loads in kN to stress in MPa for NX sized cores and displacements in mm to strains as percentages. Their details are listed in Table 4.3.

A subroutine was added to each of the programs to calculate the densities, effective porosity and moisture content, from the measurements taken prior to testing. The results are then printed out below the stress-strain graph.

4.5 The Testing Programme

4.5.1 Pre-test Specimen Treatment

Prior to testing, the effective porosity, dry bulk density and saturated bulk density were determined for each specimen. The procedures involved, including details of apparatus developed for saturation, are described in Chapter 2.

In addition to the above, the program involved the testing of rock samples at dry and saturated conditions and also at varying intermediate moisture contents. For the preparation of dry specimens, an oven was used to remove all the moisture. Work by Pinches, (1986) has suggested that the temperature of 105°C recommended by ISRM and BS 1377 may cause irreversible chemical and physical changes in clay minerals. A lower temperature of 50°C was therefore chosen as a suitable drying temperature. Comparison between samples dried at 105° and 50° indicates that the lower temperature value is sufficient for the complete removal of moisture, provided samples are dried for a sufficiently long time period. The specimens were removed from the oven after 2 weeks and placed in a dessicator to cool. The resulting weight was then taken as the datum weight to which all subsequent weight changes were related. i.e. those induced by the various treatments to obtain different moisture contents.

Colback and Wiid, (1965) took their datum weight as that established in samples after being stored in a laboratory at room temperature and a relative humidity of 40-50%. Such a process does not standardise the conditions since different rock types would establish varied moisture contents after the allocated, time depending on their permeabilities. Also, the present research has shown that a moisture content of up to 0.5% can be established by storing samples in a laboratory and that such a moisture content can decrease the rock strength from the peak in the totally dry state.

The saturation of specimens for testing was achieved by using the special pressure cell described in Chapter 2. The saturated specimens were removed from the cell, excess water wiped from the surface using a cloth with low capillary suction, weighed and tested within one minute to maintain the high moisture content.

The intermediate moisture content levels in the specimens were obtained by placing them in controlled atmospheric environments of known relative humidity.

Relative humidity is the ratio of water vapour in an atmosphere to the quantity which would saturate at a given temperature. The conditions of controlled relative humidity were achieved by using saturated salt solutions in air-tight containers. Saturated salt solutions produce well defined humidities at a given temperature in a confined atmosphere. (Winston and Bates, 1960). If porous media are placed within these controlled humidity conditions, a low moisture content is developed within the specimen.

Provided the solution is saturated, then slight changes in the relative humidity will cause either precipitation or solution to take place and maintain the equilibrium between the vapour and liquid phases. Some of the common solutions and their resulting relative humidities are shown in Table 4.4.

Specimens from each rock type were placed in sealed containers with the saturated solutions and left for one month to ensure maximum possible moisture penetration. Humidity was monitored throughout the period using a hygrometer.

Saturated Solution	Temperature(°C)	Resulting R.H.(%)
$Pb(NO_5)_2$	20	98.0
K_2SO_4	30	96.5
NH_4Cl	20	79.5
$NaNO_2$	20	63.0
$NH_4NO_3 + NaNO_3$	30	47.0
KNO_2	20	45.0
$CaCl_2.6H_2O$	20	32.3
$LiCl.H_2O$	30	11.5
CaCl	dessicator	totally dry

Table 4.4 Relative humidities produced by various salt solutions

4.5.2 Testing Procedure

Approximately four hundred sandstone specimens were tested uniaxially at varying degrees of moisture content from totally dry to saturated. In addition, a number were tested when saturated in other chemicals to determine the effects on

strength.

The stresses and strains were monitored using the appartus described in Section 4.4 and the results are discussed in Chapter 5. The cell designed for measuring strain was used throughout the program and withstood the large number of explosive impacts even for the strongest and most brittle specimens. It was considered that heavy impacts might cause some damage but regular checks throughout the testing program revealed no such effects. The only damage after four hundred tests were a number of impact marks on the inside of the cell where rock fragments had struck it. The PTFE studs on the base of the apparatus were renewed every fifty tests and the hinge oiled and tightened. The alignment of the hinge was also checked.

Following the failure of each specimen, the relevant details were noted on the log sheet and included failure mechanism, violence of fracture, fracture pattern and details of any photgraphs. A number of failed specimens were selected for microfracture analysis using SEM.

In addition to the normal uniaxial compressive tests, a number of additional special tests were carried out and are detailed in Chapters 5 and 6.

CHAPTER 5

EXPERIMENTAL RESULTS

This chapter presents and discusses the results of over 150 uniaxial compression tests on dry specimens prepared from the thirty-seven sandstone varieties. Tests on specimens at other moisture contents are discussed in the next chapter.

5.1 Dry Strength

The dry strengths for the various sandstone types are presented in Figure 5.1. The range of strength values determined for each type is represented by horizontal bar plots and the number of specimens tested is also indicated. The strongest sandstone tested was from the Upper Carboniferous Crackington Formation of north Devon, with a maximum stress at failure of 298 MPa. The weakest variety was the Upper Greensand of Cretaceous age from Wiltshire which failed at stresses of 7 to 12 MPa in the dry condition. Strength values obtained from specimens which failed along pre-existing fractures are not included within this data since they do not represent the true properties of the intact rock. Sandstones whose specimens were prepared from block samples showed a good uniformity in strength results with an average range of 4.75 MPa. The most highly indurated arenites showed the least variation in strength within the block while the many weakly cemented lithologies with high porosities showed higher deviation due to the variable presence of clays and variation in degree of cementation. The strength ranges of core samples obtained from boreholes are also indicated in Figure 5.1. The results show a greater range of strengths than obtained from block samples - examples referred to are the Upper Cromhall Sandstone, Pennant, Redcliffe and St. Bees sandstones. The greater scatter of results obtained from borehole samples are useful in that they demonstrate the advantages in research of coring specimens from individual blocks, therefore maintaining as near as possible an identical lithology. In addition they emphasise the variation in geomechanical properties through a rock mass. In many cases the degree of variation can be related to the environment of deposition, e.g. the Pennant Sandstone is probably one of the most variable arenaceous sequences in Britain due to its deposition in a delta/shallow marine environment.

The strength values quoted are the peak values, i.e. the maximum stress which the sample could support during the test, as defined by ISRM, (1972). In some cases axial splitting or lateral bursting of small fragments occurred prior to complete failure but in all cases loading was continued until a peak value was obtained. It is important

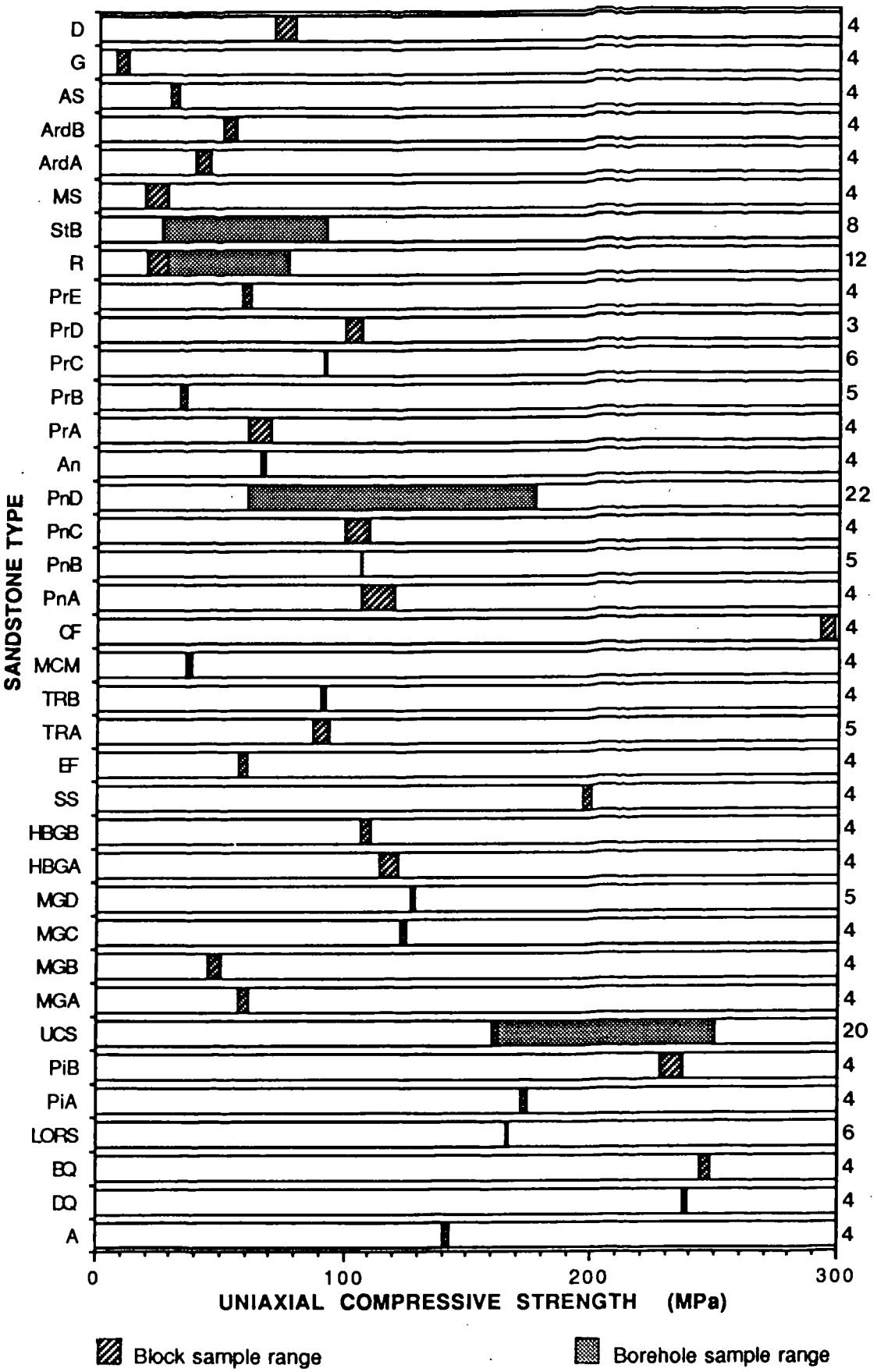

Figure 5.1 Range of uniaxial compressive strength values obtained for the sandstones studied.

to make this distinction since some workers, especially commercial testing laboratories, when dealing with particularly brittle rock types, quote the uniaxial compressive strength as the stress at which the first major macroscopic failure takes place. This can give highly misleading information as to the strength of the intact rock.

The average dry strength results for each lithology are plotted against dry bulk density in Figure 5.2(a) and (b). A number of best-fit curves were attempted using computer based numerical analysis. Figure 5.2(a) shows a linear simple regression curve through the points. The equation for this line is:

$$\sigma_c = -368.552 + 205.113 \,.\, DBD \qquad (5.1)$$

$r = 0.81$

The 'goodness of fit' is given by the value of the correlation coefficient, (the r-value). Values of greater than 0.6 are normally considered to represent a good relationship in rock mechanics. Although the r-value for this best-fit line is well above the critical value suggested by Judd, (1971) to show a good relationship in rock mechanics, the points at the higher and lower ends of the dry bulk density range are not explained.

A logarithmic best-fit curve is shown in Figure 5.2(b). The equation for the curve is:

$$\sigma_c = 1.1 \,.\, DBD^{5.2517} \qquad (5.2)$$

$r = 0.91$

The relationship between dry bulk density and strength is a logarithmic one and equation 5.2 gives an extremely high r-value indicating a strong relationship. The results presented in Figure 5.2 are those obtained from specimens prepared from blocks. In order to test if this relationship holds true for individual samples, results of tests on samples from borehole cores are plotted in Figure 5.3. A best fit logarithmic curve gives the equation:

$$\sigma_c = 0.9009 \,.\, DBD^{5.0652} \qquad (5.3)$$

$r = 0.72$

The relationship is strong but the r-value is not as high as for the results from block samples. It is suggested that this spread of results is due to the variation in diameter of the cores tested from boreholes, since it has been shown that apparent uniaxial compressive strength is affected by diameter of specimen. (Hoek and Brown,

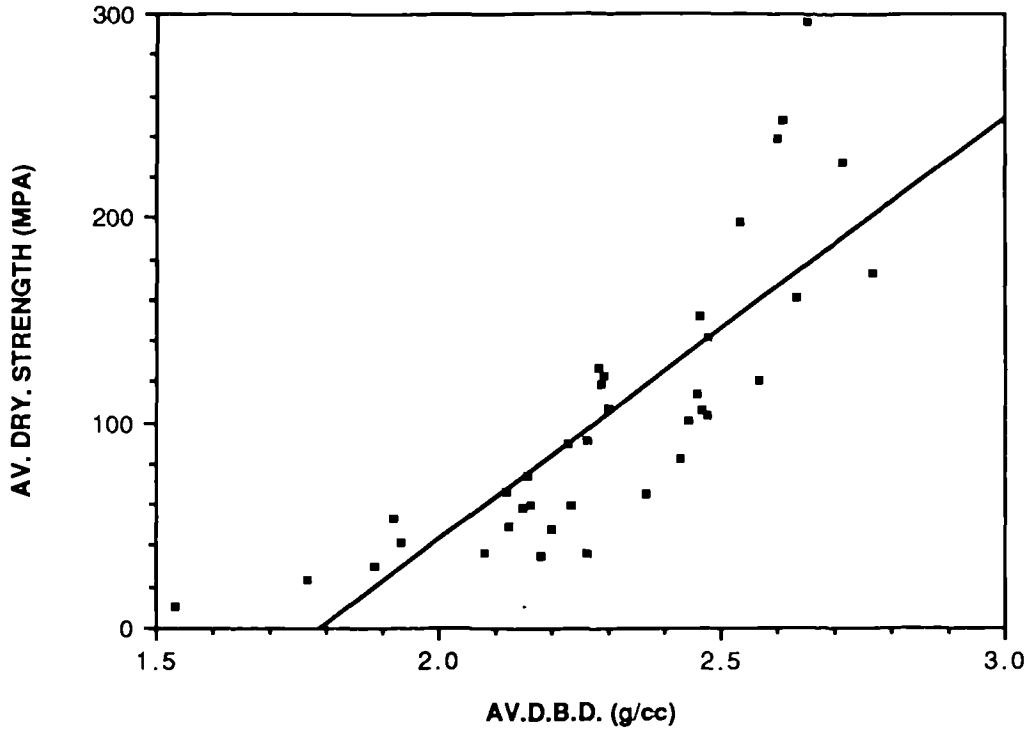

Figure 5.2(a) Uniaxial compressive strength vs. dry bulk density for specimens prepared from blocks, (Linear best-fit).

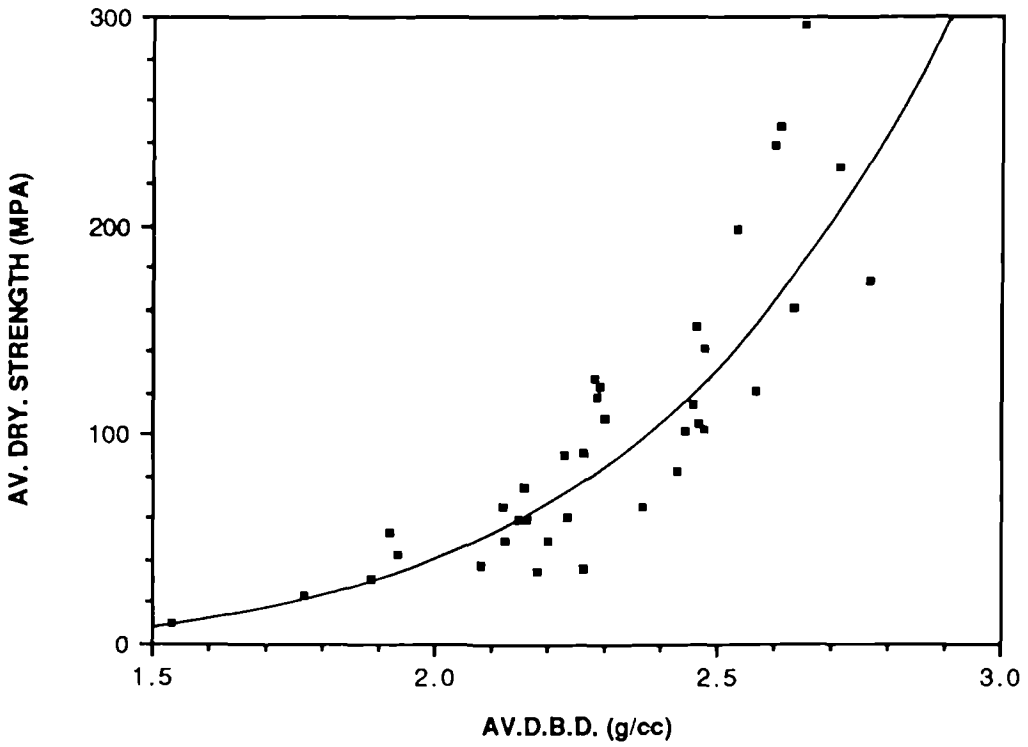

Figure 5.2(b) Uniaxial compressive strength vs. dry bulk density for specimens prepared from blocks, (Log best-fit).

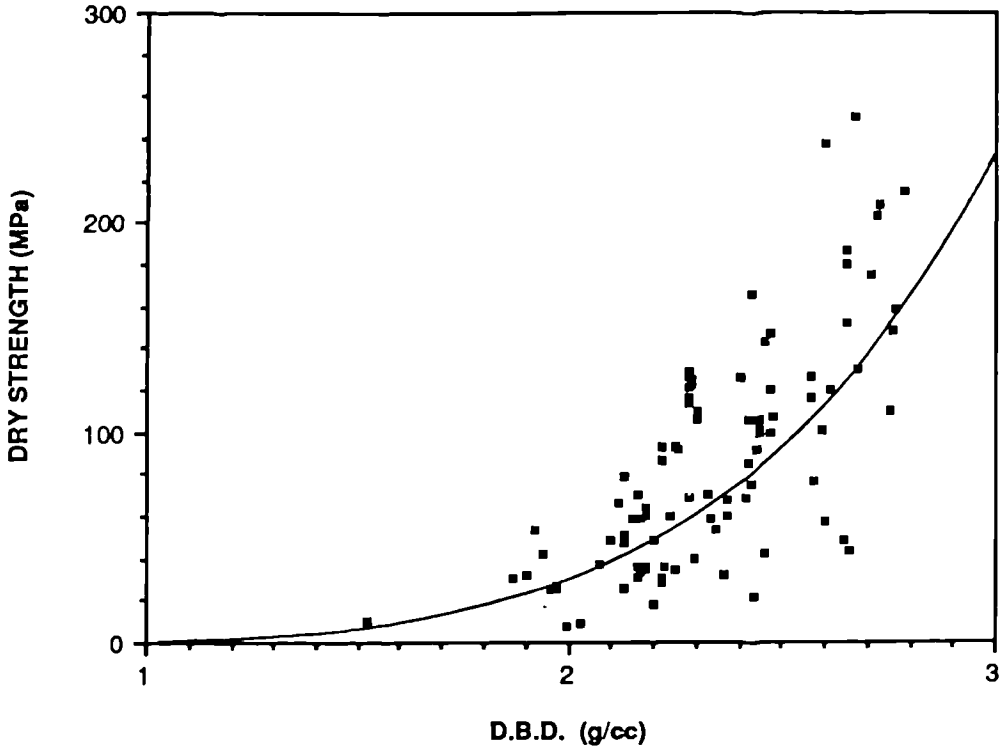

Figure 5.3 Uniaxial compressive strength vs. dry bulk density for borehole specimens.

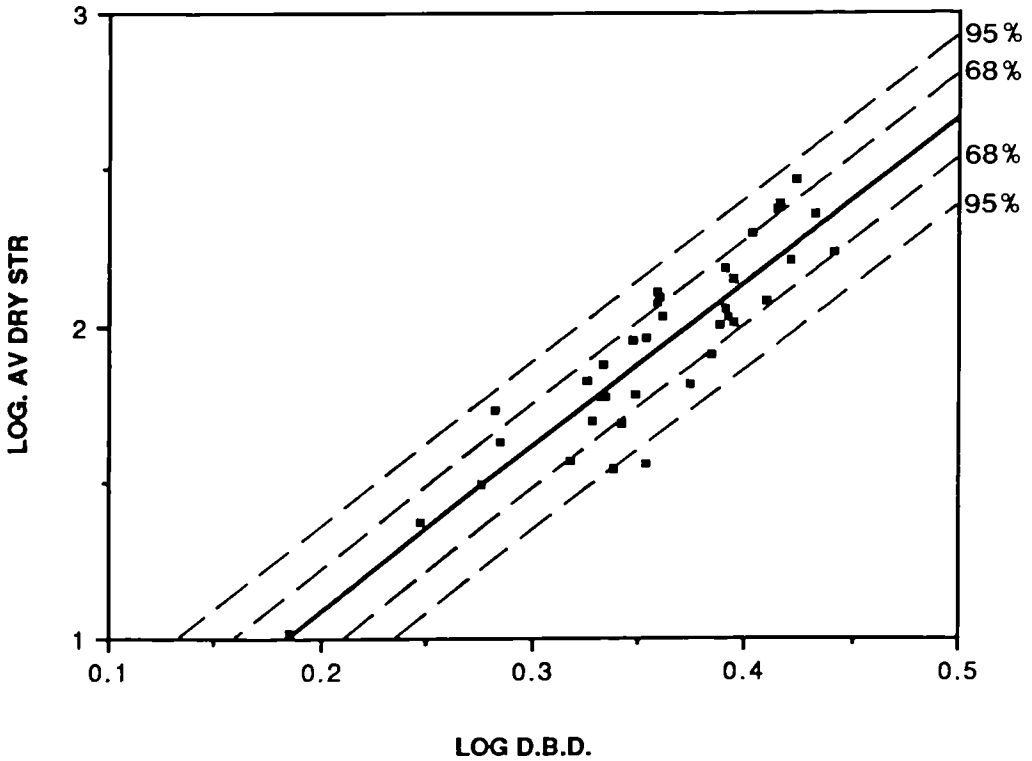

Figure 5.4 Log/Log plot of uniaxial compressive strength vs. dry bulk density with confidence limits shown.

1982).

For the higher strength sandstones the computer generated best fit line does not correspond with that which would be produced manually. The line created by mathematical principles, however provides an equation from which the strengths of sandstones could be predicted.

The good relationship between strength and density for sandstones has apparently not been previously reported. Many authors such as Brace et al, (1966) and Crouch, (1970) have studied the geomechanical properties of a number of different rock types but this research, restricted to sandstones, has been able to demonstrate a clearly valuable relationship. In their original paper, Broch and Franklin, (1972) demonstrated a correlation coefficient of 0.88 between point load index (corrected to a standard diameter of 50mm) and uniaxial compressive strength for a number of different rock types. Figure 5.2(b) and equation 5.2 have shown that dry bulk densities of sandstone samples with the same diameter can predict uniaxial compressive strength with a correlation of 0.91. Figure 5.4 shows dry strength plotted against dry bulk density on logarithmic scales with the 68 and 95% confidence limits superimposed. The fact that a straight line is produced demonstrates that the relationship is log-log. Using standard error principles, Figure 5.4 shows the range of strength values which fall within the 95% confidence limits of the predictive equation. It is therefore suggested that dry bulk density could be a better index test for sandstone strength since the point load test is strongly influenced by internal bedding.

As discussed in Chapter 3, the densities of the main constituent minerals of sandstones fall in the range 2.54 to 3.10g/cc. Matrix-forming minerals, (i.e. clays) have densities of 2.55 to 2.63g/cc. This means that as percentage pores or clay minerals increase, the density and strength decrease. Clearly as shown in Figure 5.2 a number of the density measurements are greater than would be expected if the specimen was composed completely of quartz. This is due to the presence of denser minerals than quartz which although usually much less abundant, have the effect of producing high grain densities. (See section 2.4.3 for definition). Such minerals include plagioclases, micas, some rock fragments, calcite and iron ores.

The spread of points around the best-fit line indicates the subtle differences in strengths of cementing materials with approximately the same density. Figure 5.5 shows the same plot as Figure 5.2(b) but some of the major variations in mineralogy have been indicated. Above approximately 100MPa, quartz cemented sandstones plot above the line; i.e. with higher strengths than would be predicted from the dry bulk densities. Below 100 MPa however, quartz-cemented sandstones plot below the best-fit line indicating a lower strength than would be expected. These varieties include the Penrith Sandstone samples and a number of types of the Millstone Grit, all of which

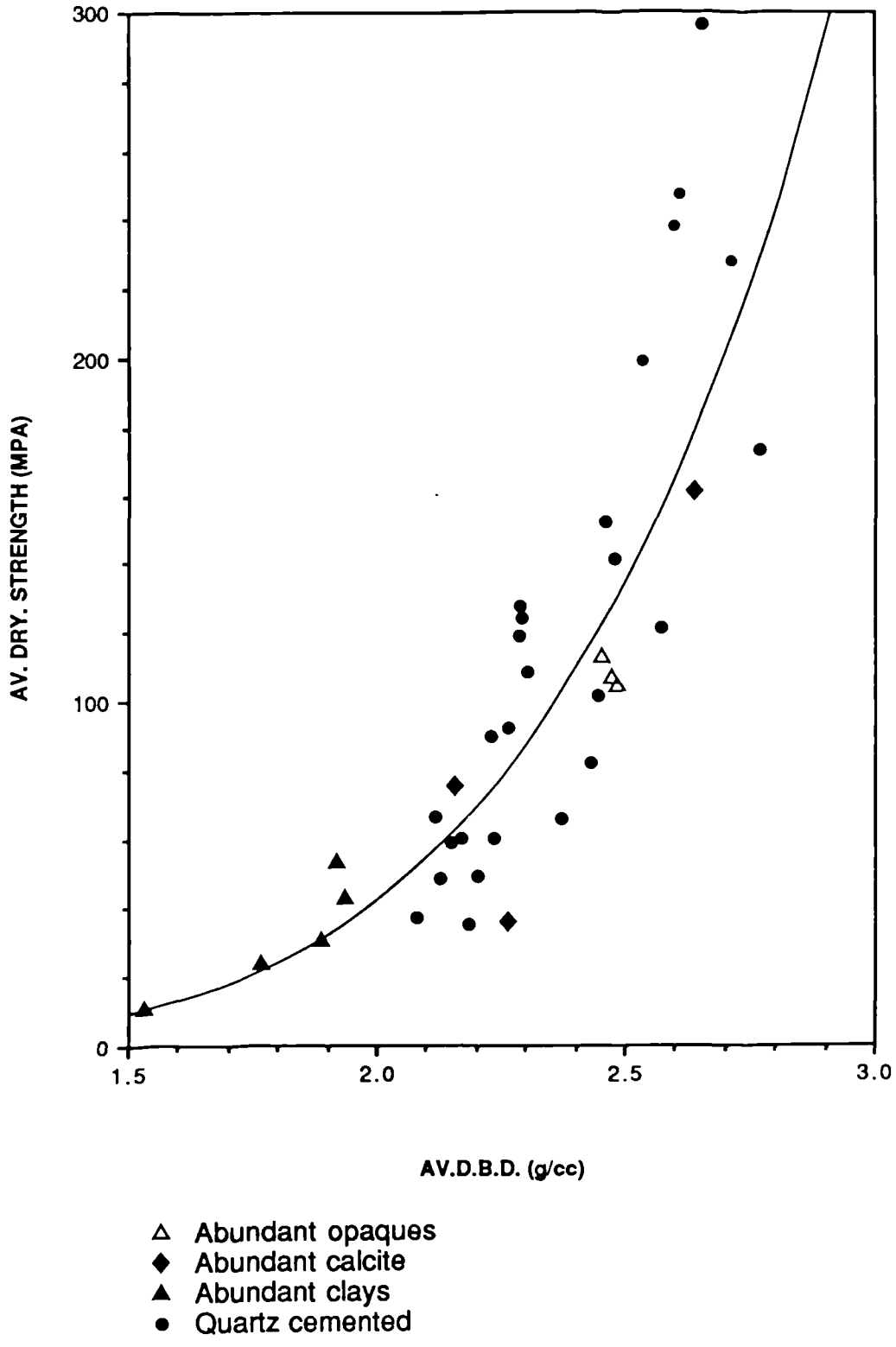

Figure 5.5 Uniaxial compressive strength vs. dry bulk density with major variations in mineralogy shown.

show well developed authigenic quartz overgrowths. This indicates that quartz-cemented sandstones can be divided into two groups:

a) Those cemented by quartz which has recrystallized at grain contacts.

b) Those cemented by quartz which has been introduced authigenically.

The difference between these two classes can be quantified by the packing density or packing proximity, (Kahn 1956) which will be controlled by the degree of grain interaction.

Although the number of data points on calcarenites is low, they generally tend to plot below the line indicating that the presence of calcite produces high density values but lower strength values than would be predicted from the log curve.

Sandstones such as the Pennant varieties from the Forest of Dean which are rich in detrital and authigenic iron oxides plot to the right of the line due to the high density of these constituents.

Two quartz-cemented sandstones with uniaxial compressive strengths greater than 100MPa plot below the line. These are the Pennant (type D) and Pilton (type A) sandstones and their anomalous positions may be due to the presence of dense minerals such as plagioclase, dense sedimentary and metamorphic rock fragments, opaques and micas. It is noteworthy that the quartz-rich sandstones which fall below the line are generally post-Variscan and therefore have probably not suffered the same degree of tectonically related lithification.

In order to produce an equation which could predict sandstone strength from dry bulk density, with a higher degree of accuracy, other textural and mineralogical properties will need to be taken into account. This will be discussed in Chapter 7.

Having looked at the relationship between dry strength and dry bulk density, Figures 5.6 and 5.7 show dry strengths against saturated bulk density and effective porosity. The relationship between dry strength and saturated bulk density can be represented by:

$$\sigma_c = 0.138 \,.\, SBD^{7.3418} \qquad (5.4)$$

$r = 0.88$

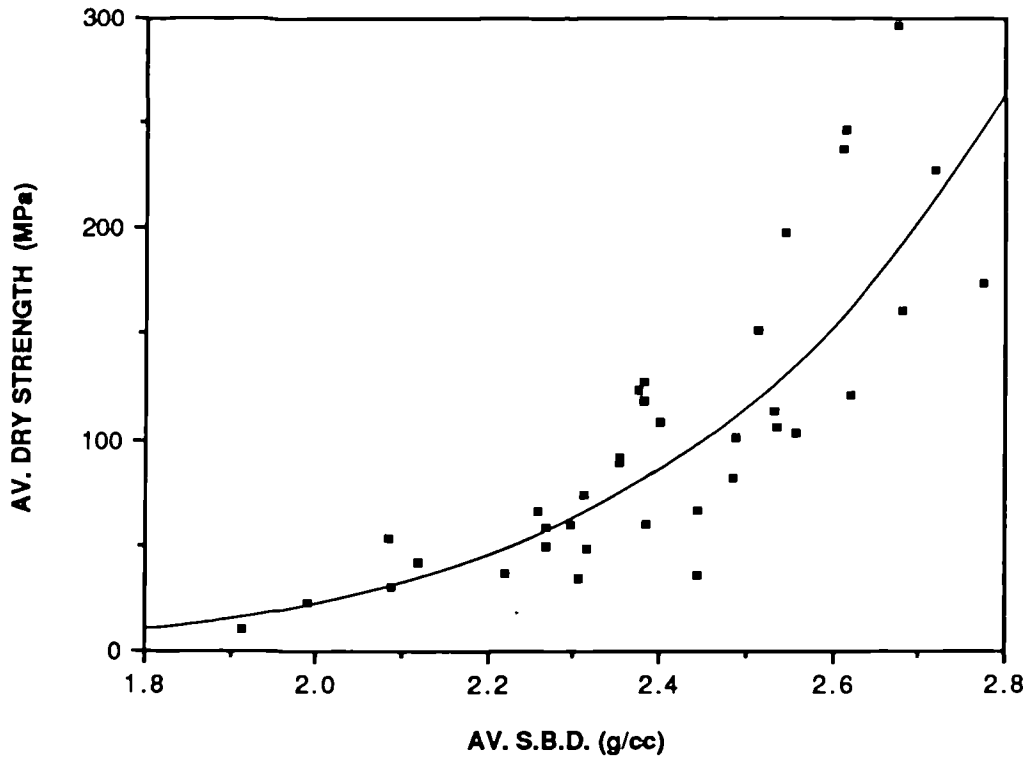

Figure 5.6 Uniaxial compressive strength vs. saturated bulk density, (Log best-fit).

The equation for effective porosity,n versus dry strength is:

$$\sigma_c = 273.5 \cdot n^{-0.5986} \qquad (5.5)$$

r = 0.83

Comparing the results of Figures 5.2(b), 5.6 and 5.7, it is clear that dry bulk density correlates better with dry strength than either saturated bulk density or effective porosity. Saturated bulk density depends on two rock parameters, namely dry bulk density and effective porosity. Thus the correlation for saturated bulk density with strength is decreased by errors in the degree of saturation or the mutiplication of non-correlation of the two parameters dry bulk density and effective porosity with strength. Hence as seen in Figure 5.6 the greater spread of results compared to dry bulk density.

Dobereiner, (1984) proposed the use of vacuum saturated moisture content as an index for strength of weak sandstones, (i.e. those with a uniaxial compressive strength of less than 20 MPa as defined by ISRM). It has been shown that Dobereiner's proposal is not applicable to sandstones of all strengths since many highly indurated sandstones are difficult to saturate, with many of the pores isolated from others. In these cases it is easier to remove all the water from the samples in the vapour phase by drying than to attempt to fill all the pore spaces with water in the liquid phase by saturation. In addition, the term moisture content depends on the mass of the sample since it is calculated as the mass of contained water divided by the mass of the dry sample. It has been shown that the dry mass of different sandstones is highly variable, depending on the respective grain density value; thus two sandstones containing the same volume/mass of water could have different moisture contents. Hence dry bulk density is a better index for estimating the uniaxial compressive strength of all sandstone types.

In theory, a closer inverse relationship should exist between total porosity and rock strength rather than effective porosity since the former is a measure of the lack of rock framework - any void whether connected or unconnected will not support load. Figure 5.8 shows the results of porosity data measured using a mercury porometer, (which is a closer approximation to total porosity), plotted against strength. The best fit logarithmic equation is:

$$\sigma_c = 334.0 \cdot \theta^{-0.6121} \qquad (5.6)$$

r = 0.82

The correlation coefficient is slightly lower than that for effective porosity, but both values are high, indicating that total porosity is important in controlling strength.

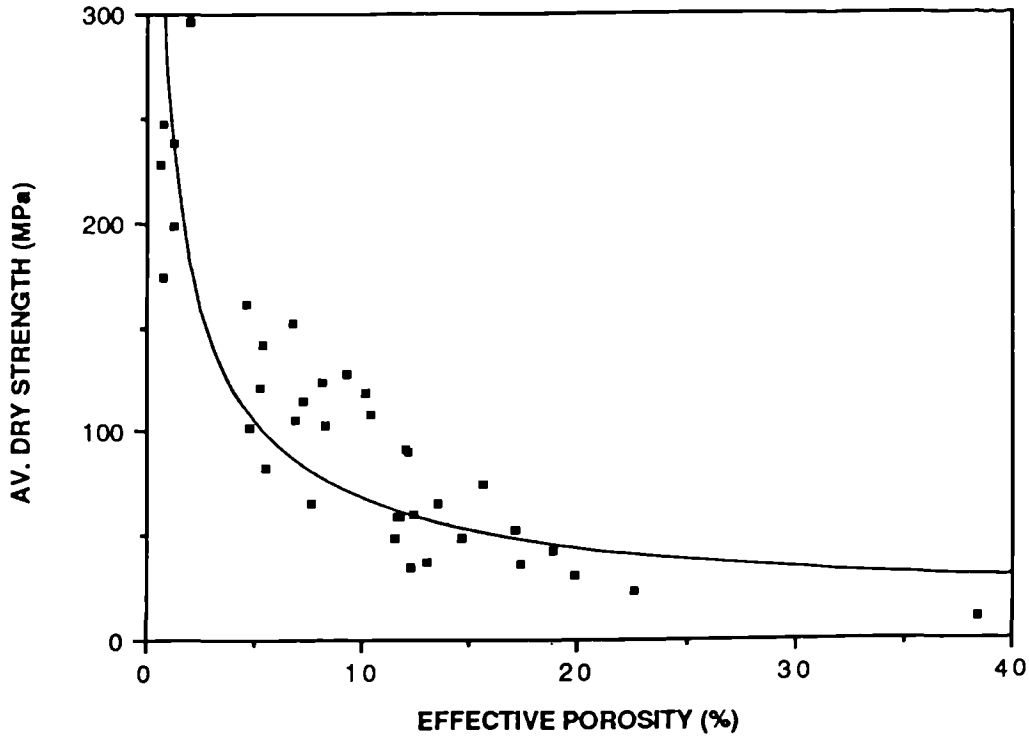

Figure 5.7 Uniaxial compressive strength vs. effective porosity. (Log best-fit).

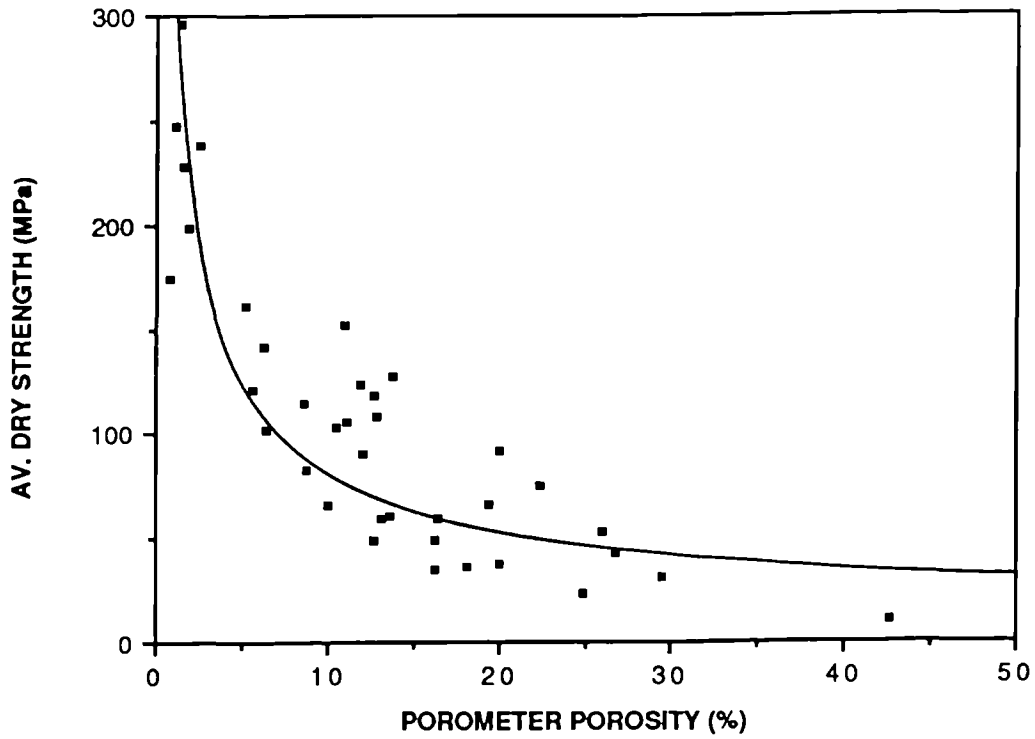

Figure 5.8 Uniaxial compressive strength vs. porosity measured by porometer. (Log best-fit).

5.2 Macroscopic Failure Modes

In all discussions of brittle fracture, the nature and description of the failure surface is of great importance. Three broad modes of failure were observed in the uniaxial compressive testing of sandstones. These failure modes agree approximately with those described by Hawkes and Mellor, (1970) although a number of variations were identified.

A. Cataclasis. Figure 5.9(a). Plate 5.1(a and b)

A general internal crumbling by the formation of multiple macroscopic fractures in the direction of the axial load and at acute angles to it; when specimen collapse occurs conical end fragments are left, together with irregular fragments of rock from the centre and vertical sides of the specimen.

B. Shear. Figure 5.9(b). Plates 5.2(a and b); Plate 5.3(a and b)

The specimen shears along a single oblique shear fracture analagous to faulting on a geological scale. Elongate shards often form along the shear surface in the direction of the applied load. The formation of end cones often occurs in shear failure with the central area of the specimen forming large elongate fragments.

Shear surfaces often develop in two directions with one fracture forming earlier than the other. This produces an effect similar to conjugate faulting on a geological scale with one surface being displaced by the other, (Plate 5.2b). The occurrence of shear failure in sandstones is often evident by extensive grain crushing on the shear surface when the rock is strongly cemented, (Plate 5.3a) and by a zone of grain rolling when weakly cemented, (Plate 5.3b).

C. Axial Cleavage. Figure 5.9(c). Plate 5.3(c and d)

Axial cleavage or vertical splitting where one or more cracks split the specimen along the loading direction. These occur as single discrete splits passing from one end to the other or alternatively as a number of vertical cracks radiating out from the centre of the specimen. Failure results from horizontal tensile stresses.

In some cases it is difficult to distinguish these different modes in a failed specimen and often two or three of the failure modes appear to be present.

Following the testing of each specimen, a photograph was taken for the purposes of measuring shear angles and classifying failure mode. The three modes - cataclasis, shear and axial cleavage are plotted on a bar histogram in Figure 5.10 to

MODE A CATACLASIS

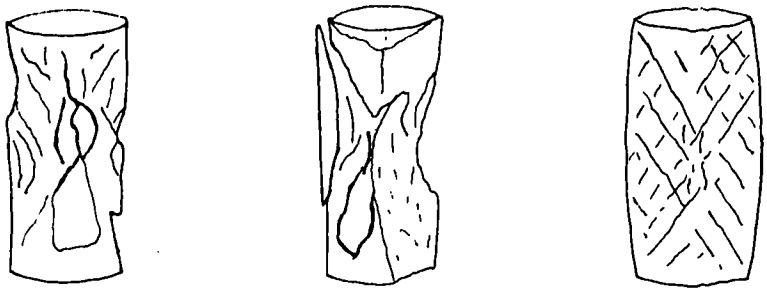

MODE B SHEAR

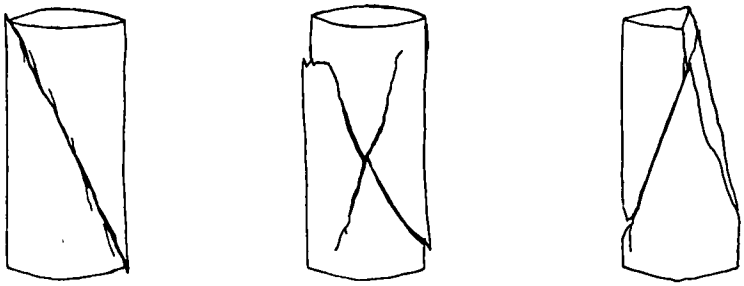

MODE C AXIAL CLEAVAGE

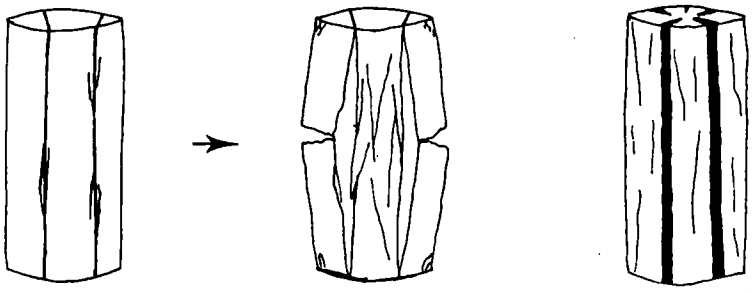

Figure 5.9 Major macroscopic failure modes observed in uniaxial compressive testing.

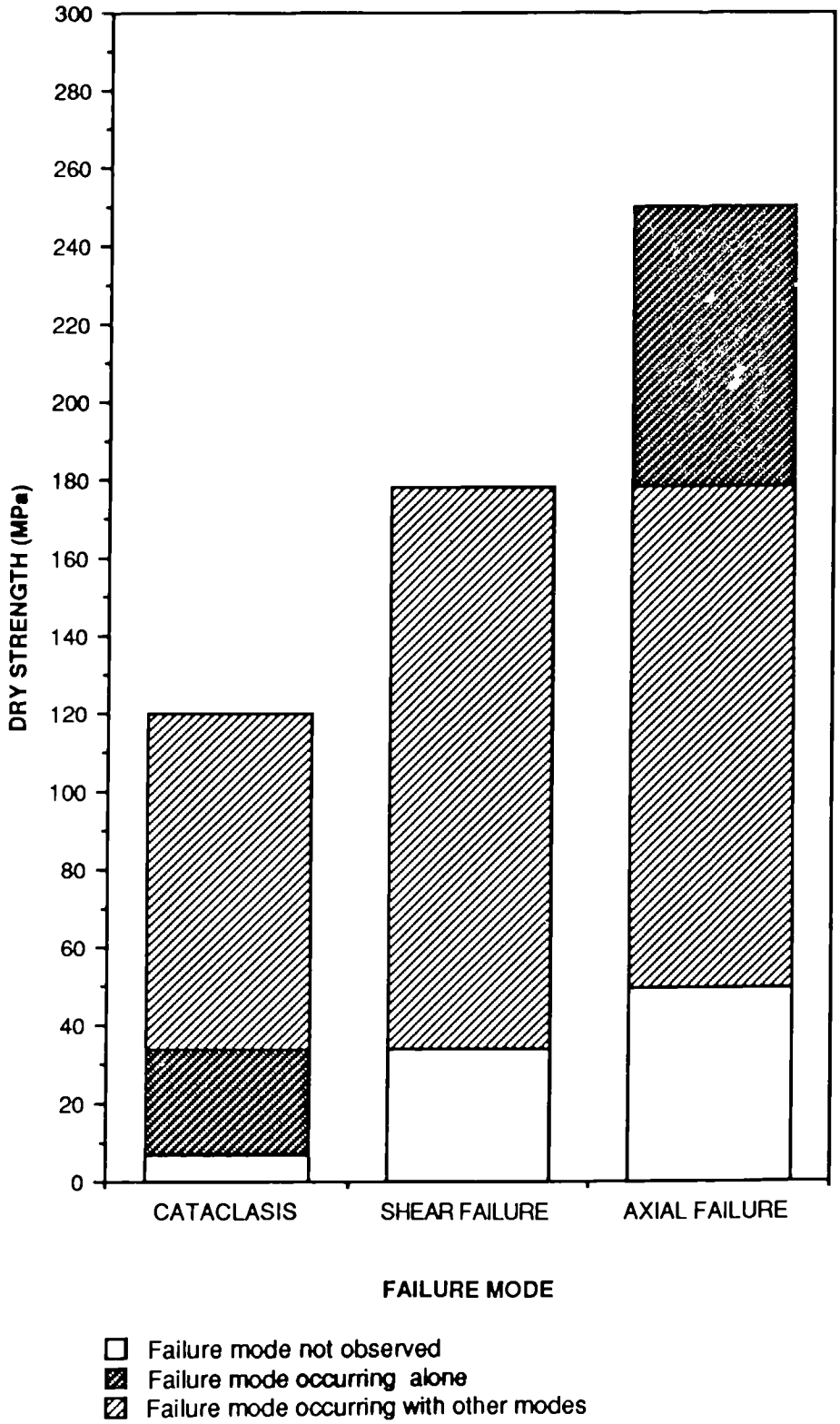

Figure 5.10 Occurrence of the three major failure modes.

Plate 5.1(a) Ardingly Sandstone (type A) - cataclastic failure.

Plate 5.1(b) Greensand (type A) - cataclastic failure.

Plate 5.2 (a) Penrith Sandstone (type C) - shear failure.

Plate 5.2(b) St. Bees Sandstone - conjugate shear failure.

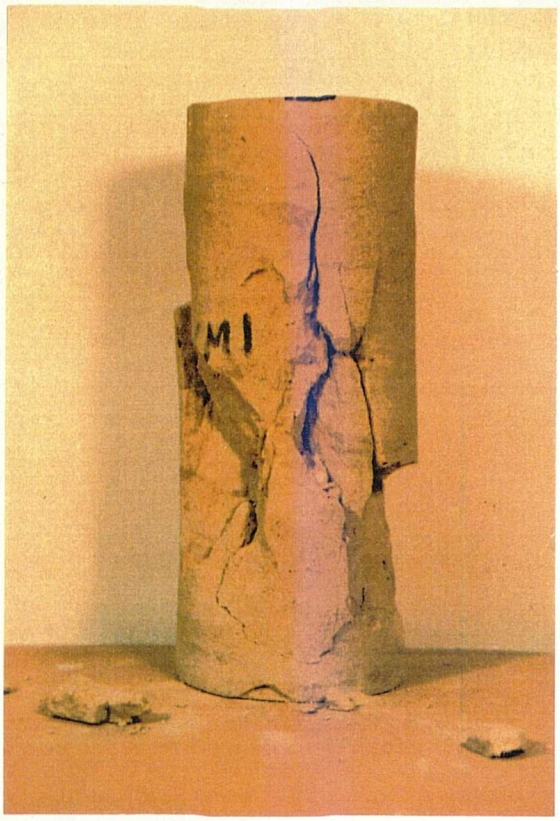
M1

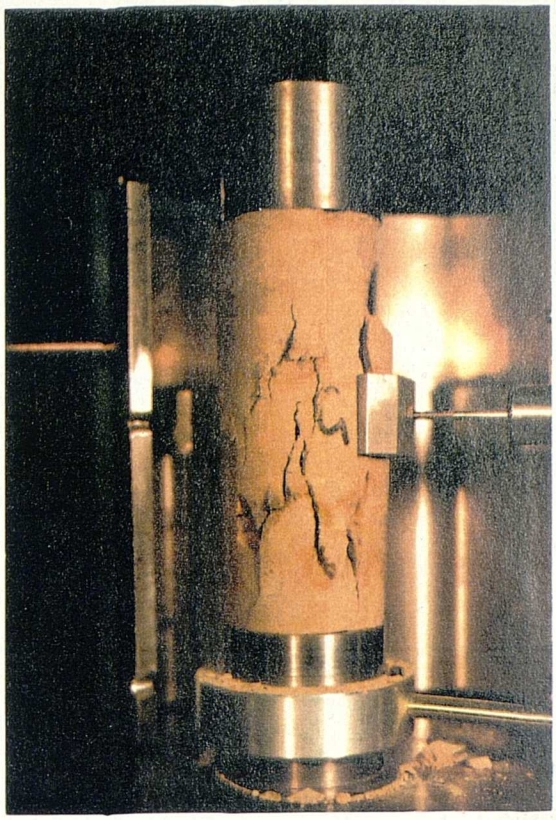

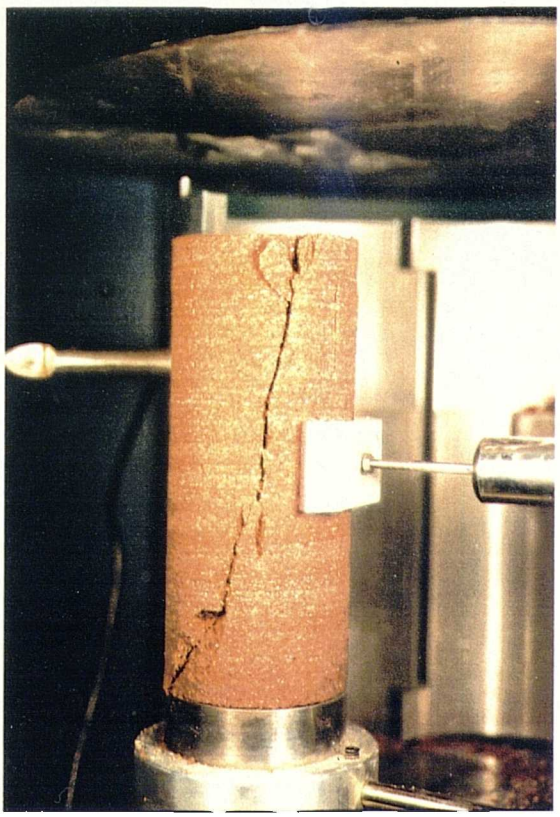

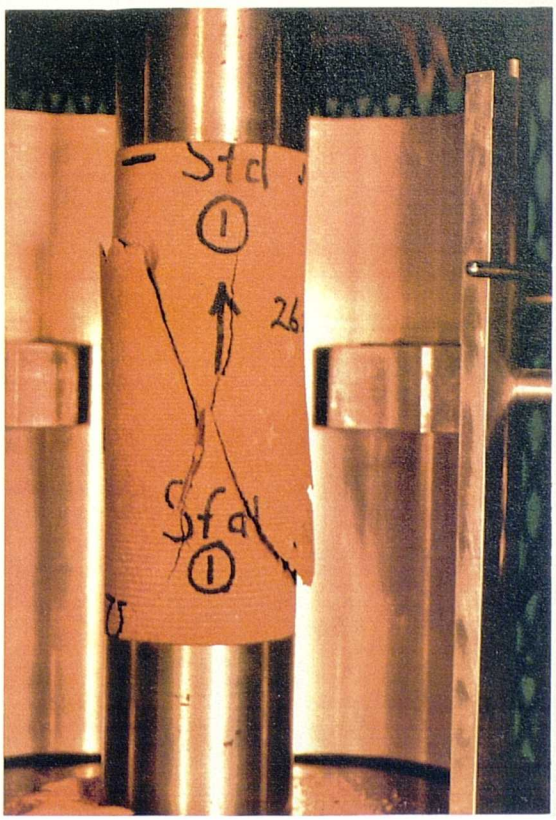
Std
1
26
Std
1

Plate 5.3 (a) Penrith Sandstone (type C) - shear failure with grain crushing.

Plate 5.3(b) Penrith Sandstone (type B) - shear failure with grain rolling.

Plate 5.3(c) Brownstones (LORS) - axial cleavage.

Plate 5.3(d) Donegal Quartzite - axial cleavage.

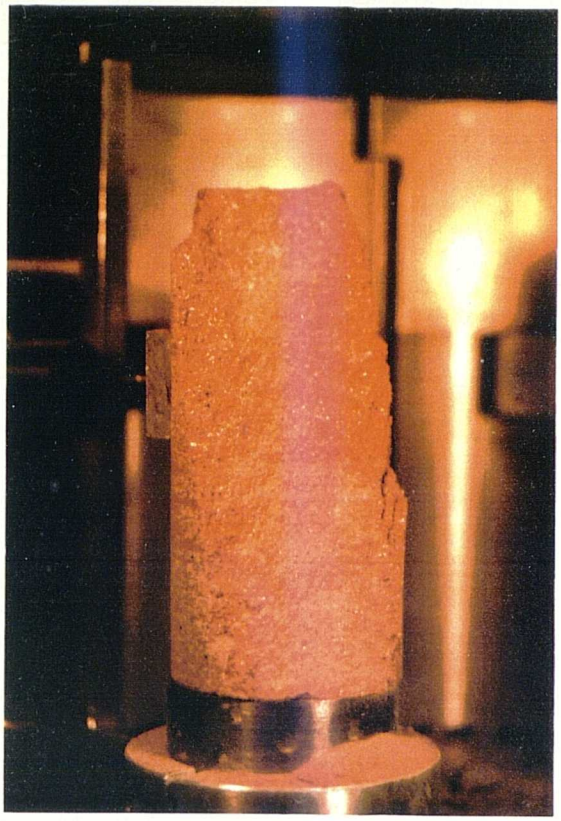

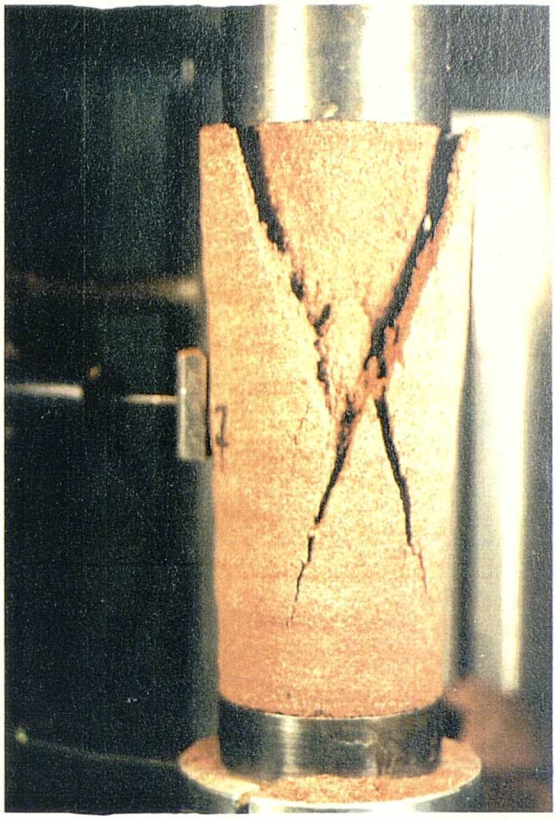

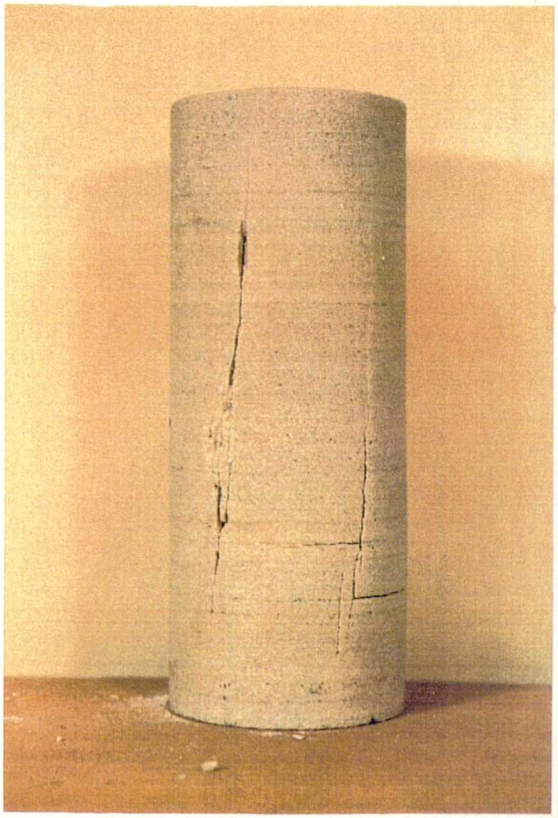

demonstrate the range of dry strengths over which they occur. In many cases more than one failure mode was identified with the result that the classes overlap. Axial failure occurs in the strongest and least deformable varieties often at less than the peak strength value followed by fracture of the specimen into vertical fragments bounded by axial splits. Axial failure has not been observed in sandstones with strength under 50 MPa; below 178 MPa it occurs in conjunction with other modes of failure. Sandstones stronger than 178 MPa always fail by a process of axial cleavage.

Shear failure is the most common observed failure mode in sandstones, occasionally producing a single shear surface. Alternatively however, it can occur in conjunction with axial fracture, (Plate 5.4) or cataclasis, (Plate 5.5). Shearing deformation was only observed on its own in three samples at strengths of 59 and 65 MPa but occurred together with the other modes in sandstones from 34 to 178 MPa.

Cataclastic failure is best seen in the lowest strength sandstones - less than 34 MPa but occurs in stronger varieties together with shear failure up to 120 MPa. Its occurrence in strong sandstones is probably due to the elastic rebound at failure when axial or sheared fragments are flexed and subsequently fracture into a number of smaller fragments. A form of cataclastic deformation is observed during ductile deformation at high confining pressures in triaxial testing when a network of shear fractures occur, (Jaeger and Cook, 1976). This suggests that the formation of cataclastic fractures in weak sandstones is indicative of an approximation to ductile behaviour.

It is important at this stage to address the variation in failure mode in the context of the stresses which occur in a cylindrical specimen during uniaxial loading. Peng, (1971) calculated the internal stress distribution by experimental and theoretical analysis. The stress contour maps for a specimen of 2:1 aspect ratio are shown in Figure 5.11. At the axial plane all the radial stresses are tensile with a maximum value of -0.06 at the centre. Maximum compressive stresses are concentrated at the corners of the specimen which try to rotate as the specimen expands laterally at the mid height.

Bordia, (1971) developed a stress concentration model for finite rock specimens and his solution is given in Figure 5.12. The specimen is divided into three main regions; two containing dominantly compressional stresses adjacent to each metal platen and one containing dominantly tensile stresses perpendicular to the specimen axis. The compressive stresses induce a strengthening effect, while the tensile stresses have a weakening effect on the specimen.

From the stress models described above, it is evident that the end cones which often form in uniaxial compressive testing are related to the compression zones which form due to platen end effects. Tensional stresses in the areas between these zones of

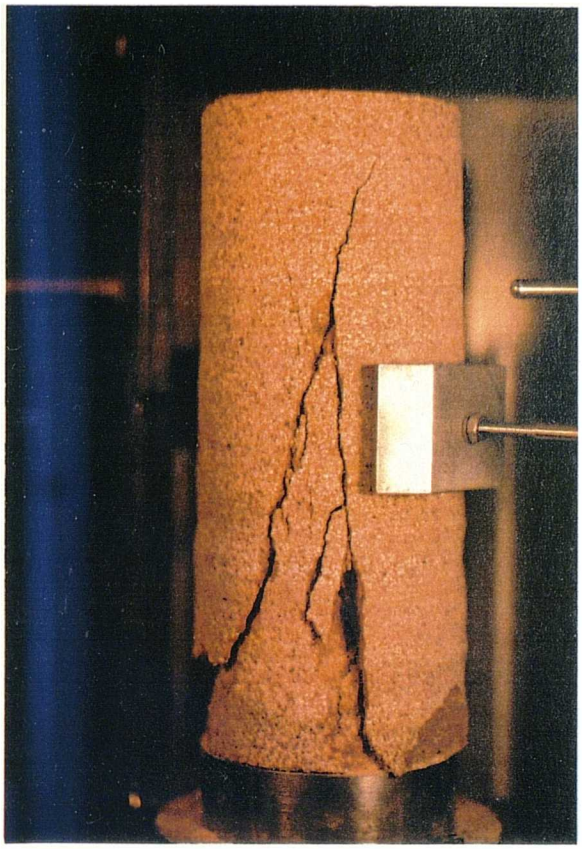

Plate 5.4 Shear failure and axial cleavage ocurring together in Annan Sandstone.

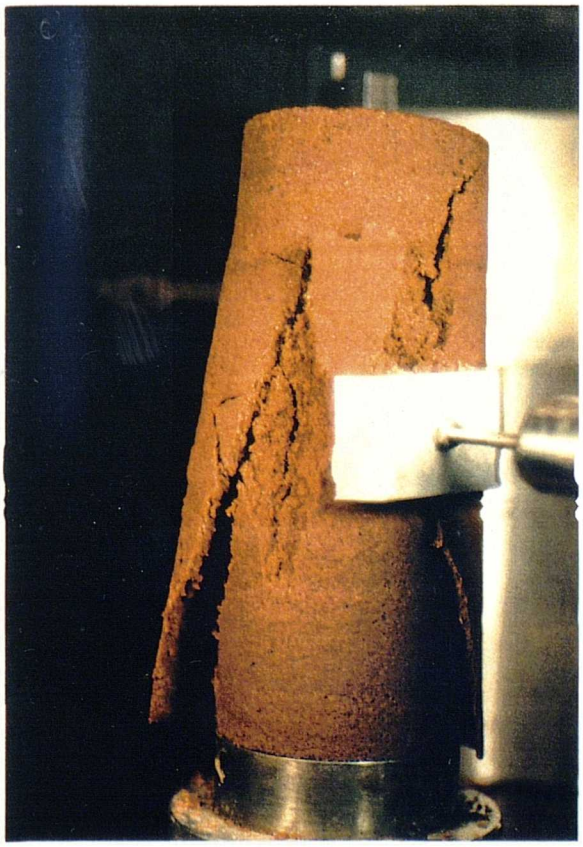

Plate 5.5 Shear failure and cataclasis occurring together in Penrith Sandstone (type A)

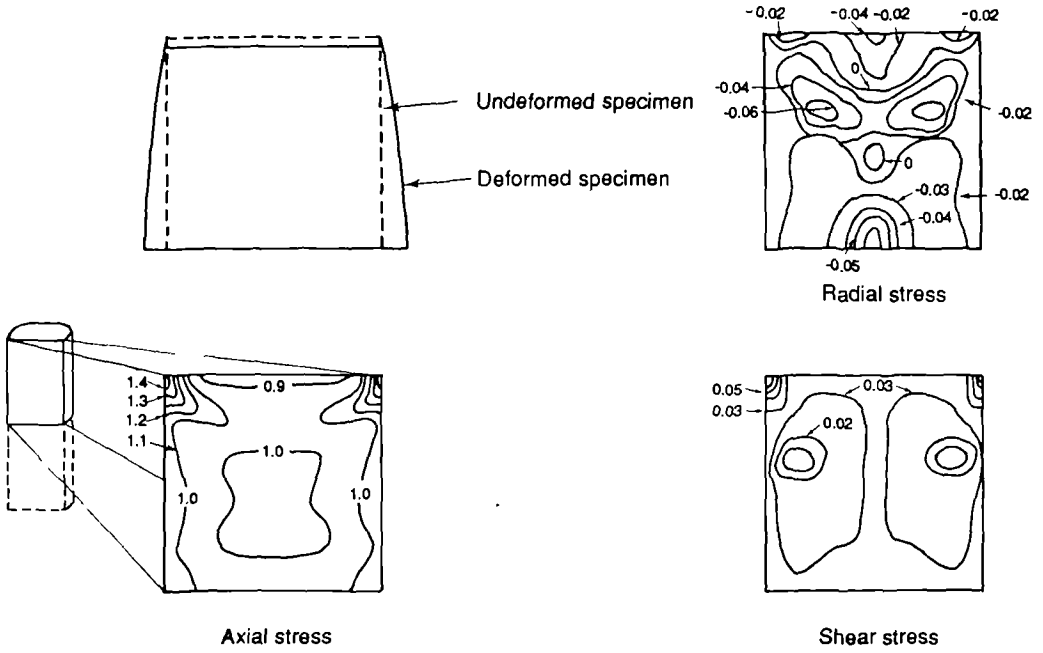

Figure 5.11 Stress-contour map for specimen loaded in uniaxial compression (after Peng, 1971).

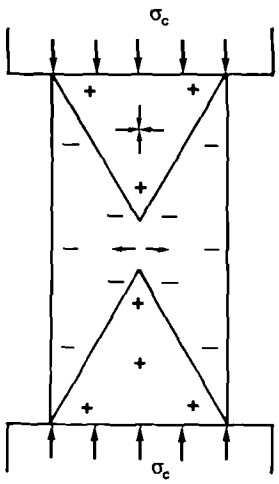

Figure 5.12 Stress concentration model for specimen loaded in uniaxial compression (after Bordia, 1971).

compression cause axial splitting which initiates from the central region of the specimen. In strong sandstones, the tensional stresses at failure in the centre of the specimen are so great as to cause axial splits to propagate through the zones of compression, producing complete axial failure.

Shear failure is related to the boundaries between the zones of compression and tension. In many cases the shear failure is non-planar and follows the curvature of the compression cones.

Cataclasis occurs in weaker rocks where the zones of compression, tension and shear are less well defined and their interaction produces a random orientation of fractures.

5.3 Stress and Strain Records

Representative stress - strain curves for the sandstones studied are included in the Appendix. A typical plot is shown in Figure 5.13. In this case the peak stress is 60.1MPa. Axial and radial strains are denoted by the letters 'A' and 'R' at the terminations of the axial and radial stress-strain curves. These plots are drawn by computer using the data recorded on disc during each compression test. The vertical scales used have been chosen to give the maximum detail for rocks of different strengths. They are 0-80, 0-100, 0-200 and 0-400 MPa. Young's modulus, (E) was calculated from the σ–ε curves using formula 4.4. The value normally used is the tangent Young's modulus at 50% of the peak stress as shown in Figure 4.2. The term Young's modulus was originated to describe the stiffness of truely elastic materials and can thus be applied unqualified to rocks which behave in an elastic manner since E does not change during the course of a loading test. It has been long understood however, that many rock types do not undergo true elastic deformation. The axial stress-strain curves established for the sandstones studied in this research demonstrate elastic, quasi-elastic, semi-elastic and non-elastic deformation, as defined by Farmer, (1975). It is questionable whether there is any usefulness in comparing a standard tangent Young's modulus between rock types which behave in markedly different ways. An example to illustrate this is shown in Figure 5.14; tangent E measured at 50 % for a quasi-elastic sandstone (5.14a) is the same as that measured for a non-elastic sandstone, (5.14b). These values of Young's modulus would indicate that the two arenites behave in the same way despite sandstone (b) showing a much higher axial strain to failure and a non-elastic deformation.

It is therefore proposed that the Young's modulus should indicate the total strain experienced by a specimen. The sec E at the failure point will give a better overall indication of the deformation behaviour. Weak to extremely strong rocks can

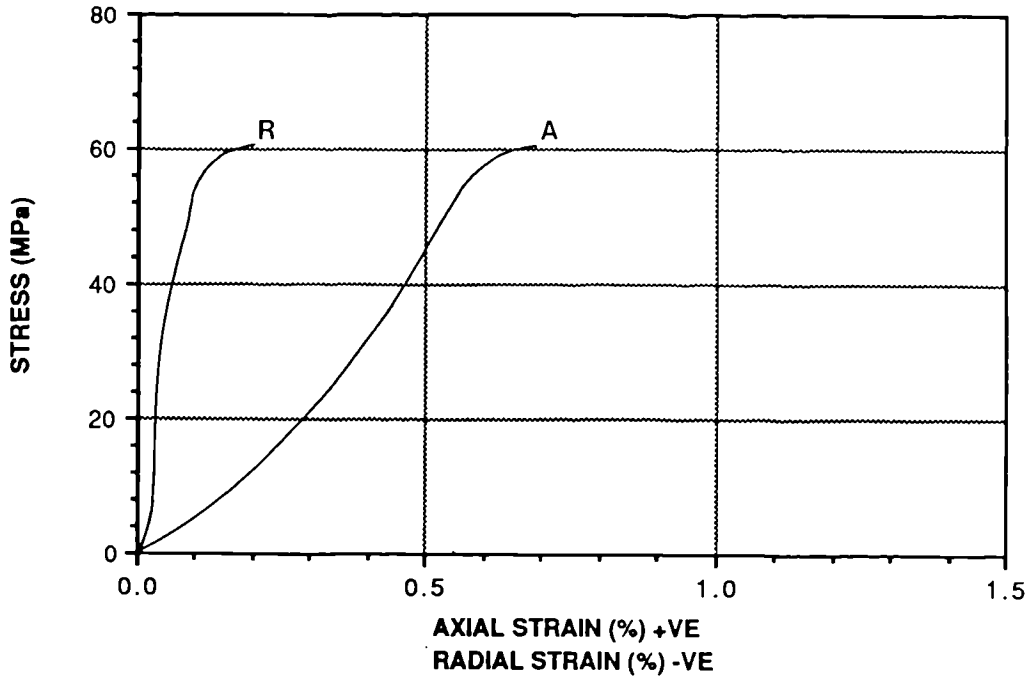

Figure 5.13 Typical stress-strain plot produced by computer monitoring of uniaxial compression tests.

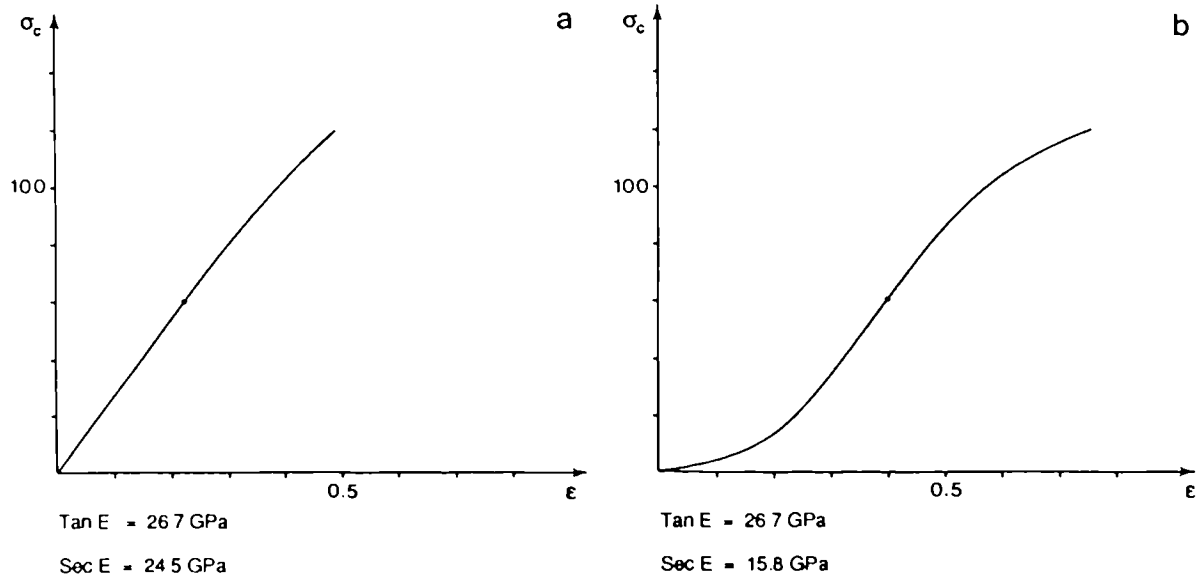

Figure 5.14 Comparison of methods of Young's modulus measurements between two different sandstone types.

therefore be compared with some degree of confidence. It is important however that the tan E at 50% of the ultimate stress is also considered since the difference between tan and sec E will indicate the degree of non-elasticity of the rock type being considered.

Although minor variations occur in samples from blocks, each rock type shows a characteristic deformation pattern. These σ–ε profiles for the thirty-seven sandstone types in the dry state are compared in Figure 5.15. When plotted on the same scale, the variation in σ–ε profile becomes apparent. A number of types show similar tan E values at 50% but very different sec E values. As shown, the latter give a better indication of the rocks' deformation to failure. Few sandstones, even the strongest varieties, behave in an elastic manner - the majority demonstrate an 'S-shaped' profile with an elastic or near-elastic central zone. The curve morphologies have been assigned a degree of elasticity on the basis of a scale from 1 to 10, (10 being perfectly elastic). This was achieved by estimating the departure of each curve from linearity. Degree of elasticity is plotted against dry strength in Figure 5.16. No definite relationship exists between sandstone strength and degree of elasticity of the respective σ–ε curves. The plot can however be divided into three main regions: above approximately 160 MPa sandstones deform with a degree of elasticity greater than 7 (semi-elastic to elastic deformation); below 160 MPa sandstones show curves between 2 and 7, (non-elastic to semi-elastic); and a group of very low strength arenites with apparently high degrees of elasticity. This apparent elasticity is due to the mode of cataclastic deformation which takes place in the weaker sandstones such as the Greensand.

The tangent and sec E for each sandstone type were measured from the σ–ε curves shown in the Appendix. These are listed in Table 5.1. Certain sandstones show marked variation between tan E (50%) and sec E - notably those with a well developed 'S-shaped' profile. The higher the elasticity of deformation, the greater the correspondence between the two measures of Young's modulus.

Tan E is plotted against sec E in Figure 5.17. A linear relationship exists but it is not a 1:1 relationship. For example, from Figure 5.17, the sec E corresponding to a tan E of 10 GPa is 7.47 GPa, (74.7%). At a tan E of 30 GPa the sec E is 24.52 GPa, (81.76%). The correspondence increases at higher Young's modulus values.

When plotted against strength as in Figure 5.18(a) & (b) the tan E and sec E show general linear relationships. Despite the r-value for tan E being higher than that for sec E, it is considered that sec E will give a better representation of the sandstones' total deformation to failure.

Poisson's ratio, (μ) was measured as the sec value at 50% of the peak stress as defined in equation 4.8. Radial strain was measured in two orthogonal directions using

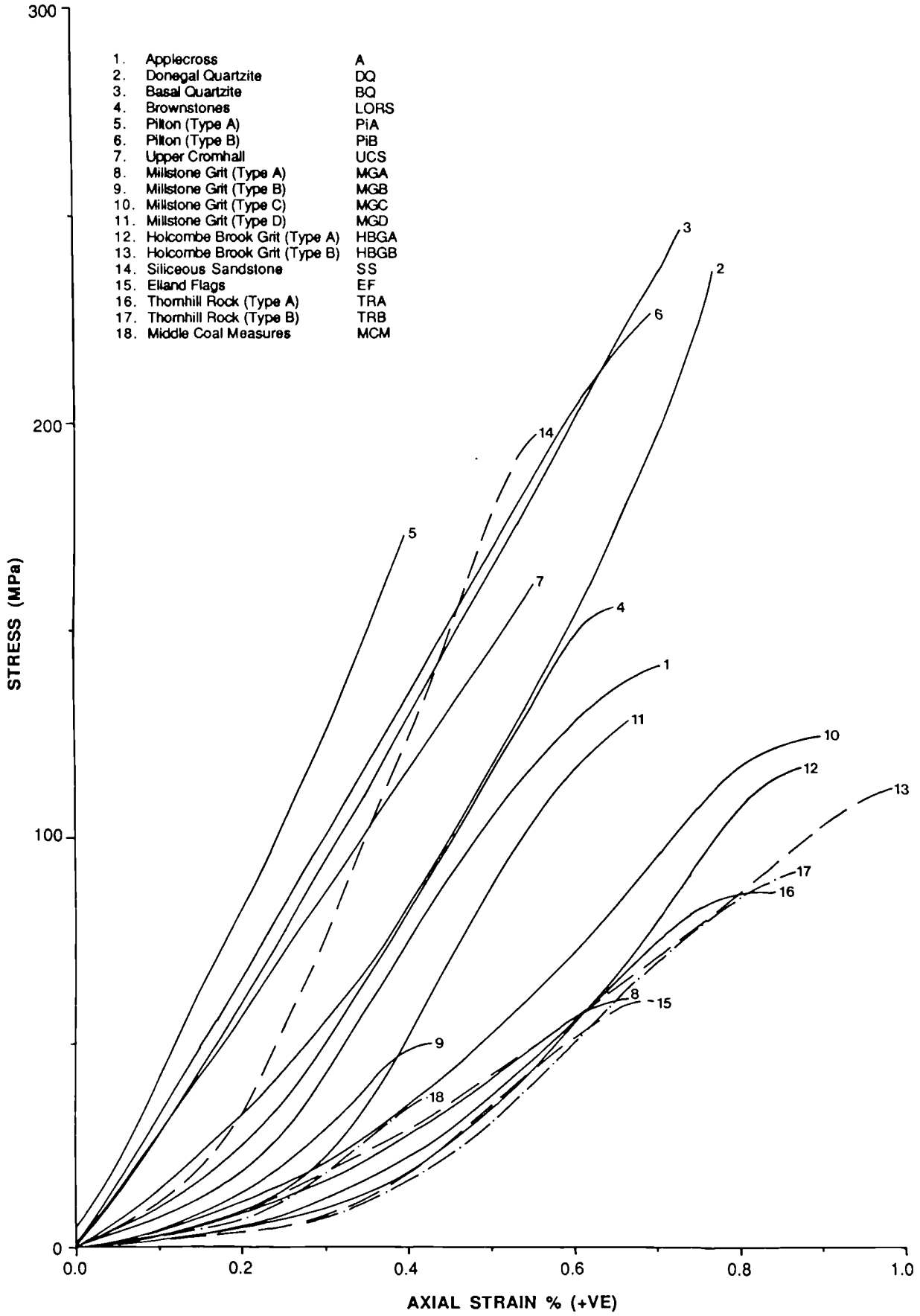

Figure 5.15 (a) Comparison of axial stress-strain curves for the sandstones studied.

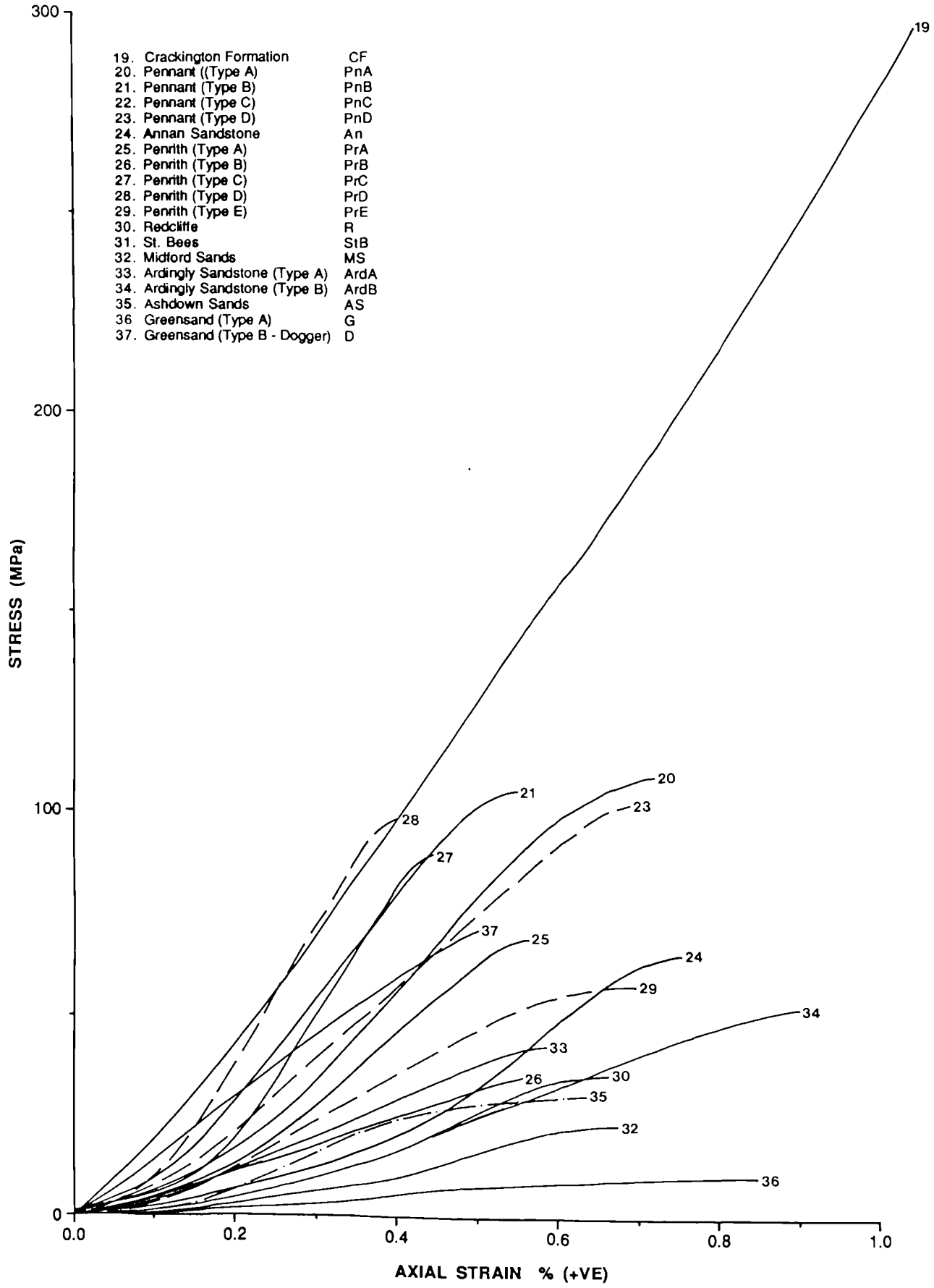

Figure 5.15 (b) Comparison of axial stress-strain curves for the sandstones studied.

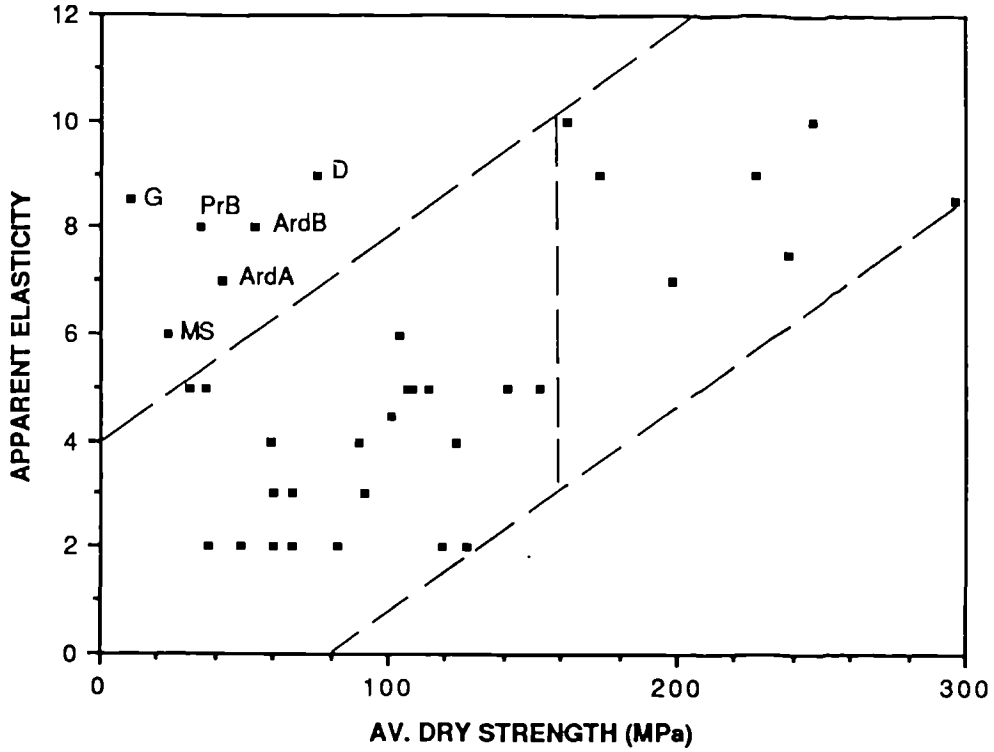

Figure 5.16 Uniaxial compressive strength vs. estimated elasticity of stress-strain curve.

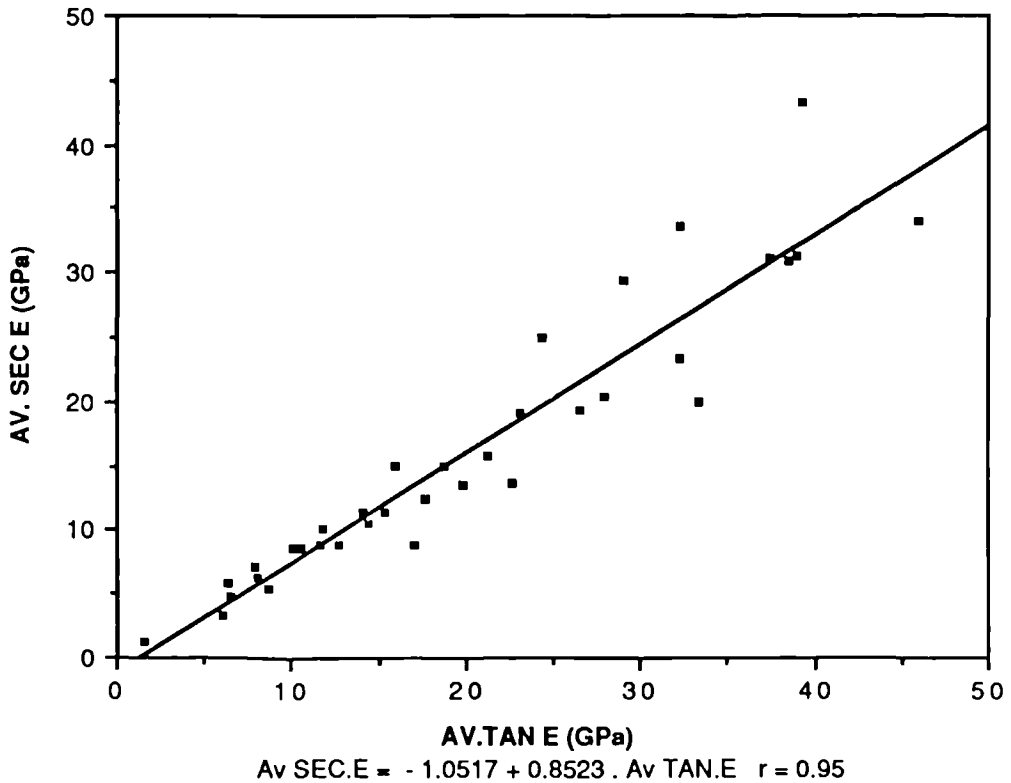

Figure 5.17 Tangent Young's modulus at 50% of ultimate stress vs. secant Young's modulus at failure (Linear best-fit).

Sst Type	UCS	TAN E	SEC E	Poisson's R
A	141.32	33.33	19.90	0.168
DQ	237.86	38.46	30.81	0.208
BQ	247.00	32.32	33.61	0.197
LORS	152.03	32.27	23.39	0.147
PiA	173.28	39.29	43.32	0.093
PiB	227.29	39.02	31.21	0.090
UCS	161.37	28.99	29.34	0.159
MGA	59.33	12.80	8.86	0.346
MGB	49.03	15.38	11.40	0.044
MGC	123.36	22.62	13.71	0.171
MGD	127.50	23.08	19.03	0.150
HBGA	119.08	19.86	13.53	0.030
HBGB	108.06	14.08	11.37	0.262
SS	198.36	45.98	34.04	0.043
BF	59.94	10.60	8.56	0.092
TRA	89.94	14.49	10.58	0.188
TRB	91.84	11.78	9.98	0.140
MCM	37.08	11.59	8.72	0.216
CF	298.18	36.38	30.04	0.172
PnA	114.18	21.21	15.86	0.191
PnB	106.15	26.63	19.30	0.255
PnC	103.38	18.86	14.98	0.181
An	66.28	17.02	8.84	0.237
PrA	65.96	17.70	12.39	0.074
PrB	34.77	8.05	6.36	0.239
PrC	81.99	27.97	20.36	0.221
PrD	101.16	24.39	24.98	0.100
PrE	59.72	10.08	8.53	0.303
R	36.05	8.76	5.42	0.322
MS	23.20	6.06	3.44	0.342
ArdA	42.15	7.92	7.14	0.379
ArdB	53.35	6.30	5.93	0.143
AS	30.58	6.45	4.78	0.917
G	10.45	1.56	1.23	0.125
D	74.51	16.00	14.90	0.279

Table 5.1 Average values of uniaxial compressive strength, tan E, sec E and Poisson's ratio for sandstones tested in the dry state.

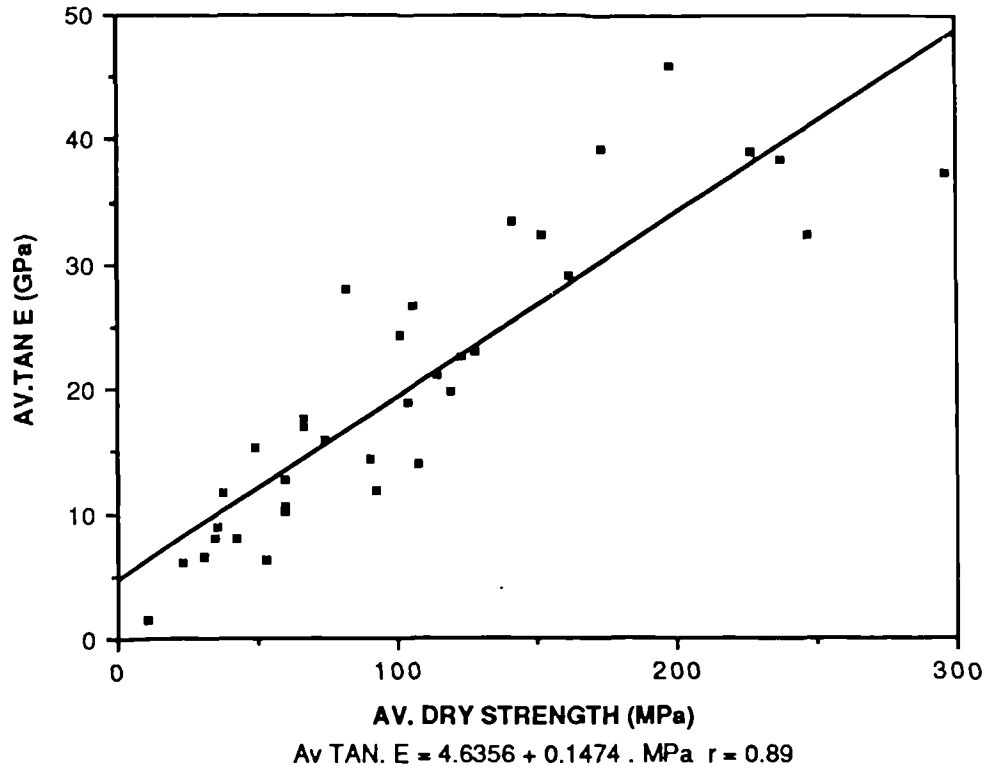

Figure 5.18(a) Uniaxial compressive strength vs. tangent Young's modulus at 50% of ultimate stress (Linear best-fit).

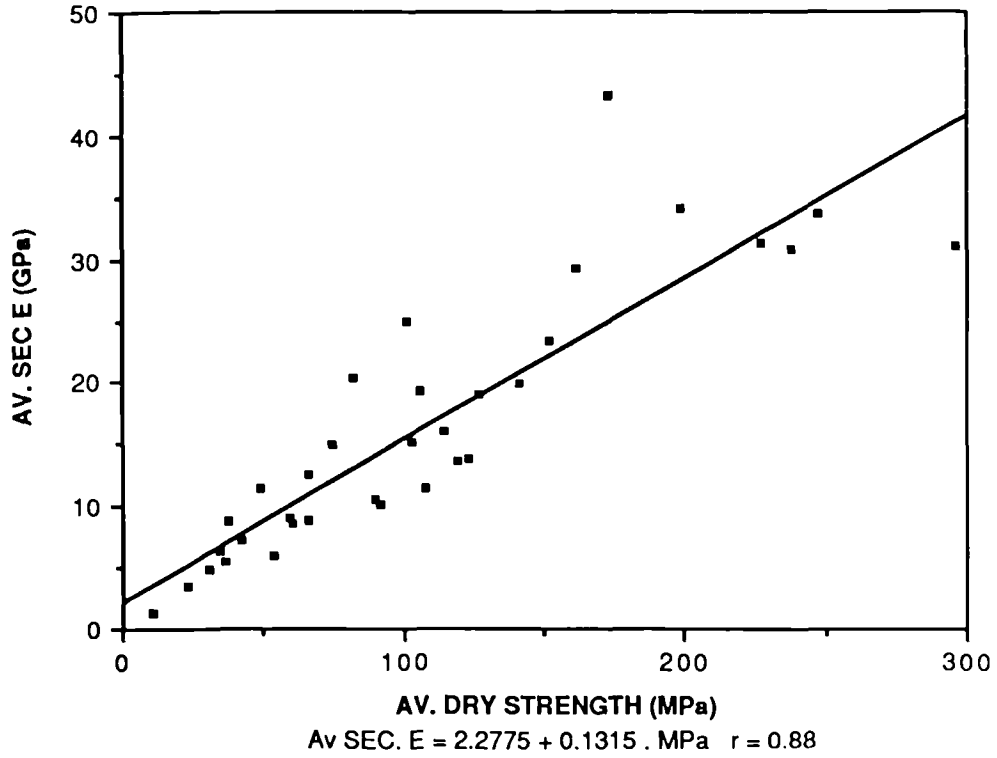

Figure 5.18(b) Uniaxial compressive strength vs. secant Young's modulus at failure (Linear best-fit).

the apparatus described in Chapter 4. Good agreement was generally observed between the two directions and the values were averaged to produce a representative Poisson's ratio for each sandstone type. Some major differences did occur however in a number of the weaker sandstones, between the two recorded values of radial strain as failure was approached. This was due to higher degrees of deformation taking place in specific zones along which subsequent failure planes formed.

The values of sec μ are listed in Table 5.1. The observed values of Poisson's ratio are generally higher in the weaker sandstones although the relationship is unclear, (Figure 5.19). A number of interesting values were obtained: In the quartzites the Poisson's ratios tend to be low; tests on the Siliceous Sandstone and Basal Quartzite produced values of 0.043 and 0.087 respectively. The Donegal Quartzite however, produced much higher values, in the region 0.2. This may be due to the high degree of alignment of muscovite grains parallel to bedding, (perpendicular to loading). These muscovite-rich planes, (Plates 3.3 and 3.4) would provide potential slip surfaces in response to lateral tensile stresses produced during the loading process. A similar spread of results is observed when plotted against tan and sec E as shown in Figure 5.20(a) and (b). It is considered that Poisson's ratio is strongly influenced by textural factors which do not affect strength or Young's modulus in the same way. This will be discussed in Chapter 7.

5.4 Sandstone Deformation and Microscopic Failure Mechanisms

Sandstones which behave elastically or semi-elastically generally show an approximately uniform Young's modulus up to the yield point. Beyond the yield point failure of the rock specimen occurs and the Young's modulus decreases to the failure point. In strong, highly brittle rocks the yield point and the failure point coincide or are extremely close together.

Figure 5.21 shows a loading cycle for a sandstone sample taken from the Crackington Formation. As can be seen from Figure 5.15, this sandstone behaves quasi-elastically, where the Young's modulus remains approximately constant to the yield point. In this test the specimen was loaded to a stress value of 66% of the ultimate stress and then unloaded. As can be seen, the axial strain value decreases almost to the origin with little permanent deformation of the specimen. The Crackington Sandstone can therefore be described as 'elastic with hysteris' - i.e. the axial strain value decreases to zero following a loading and unloading cycle but the unloading σ–ε curve does not follow the same path as the loading curve.

Figure 5.22 represents a 'non-elastic' sandstone, the Holcombe Brook Grit,

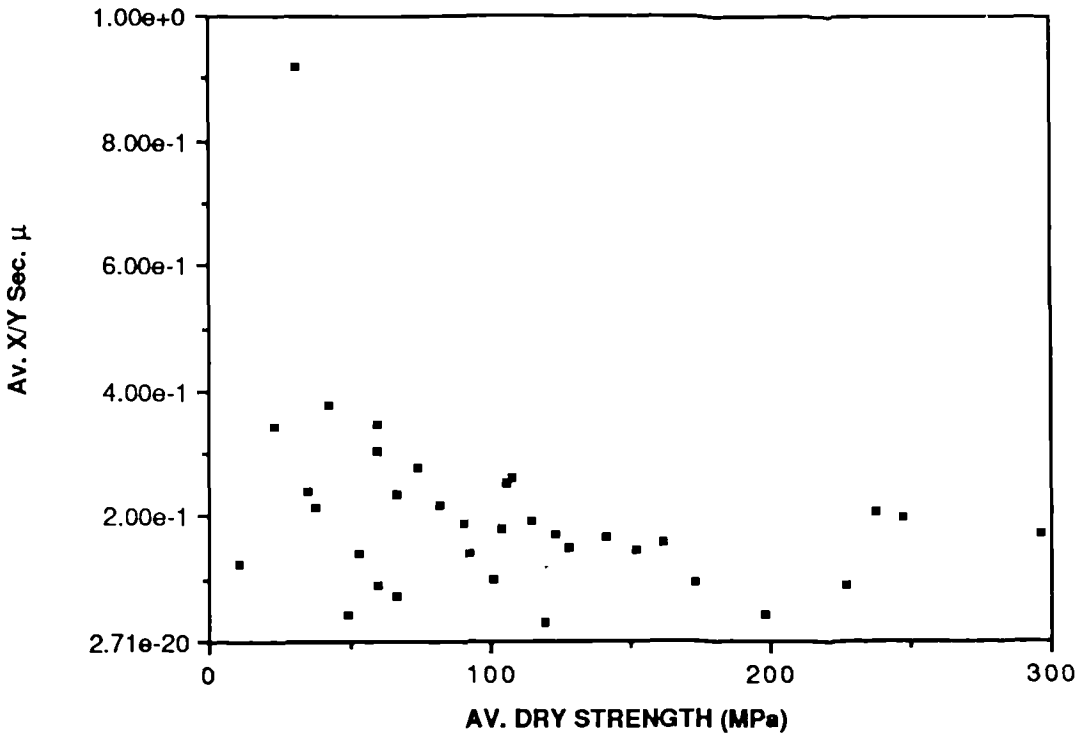

Figure 5.19 Uniaxial compressive strength vs. secant Poisson's ratio at 50% of ultimate stress.

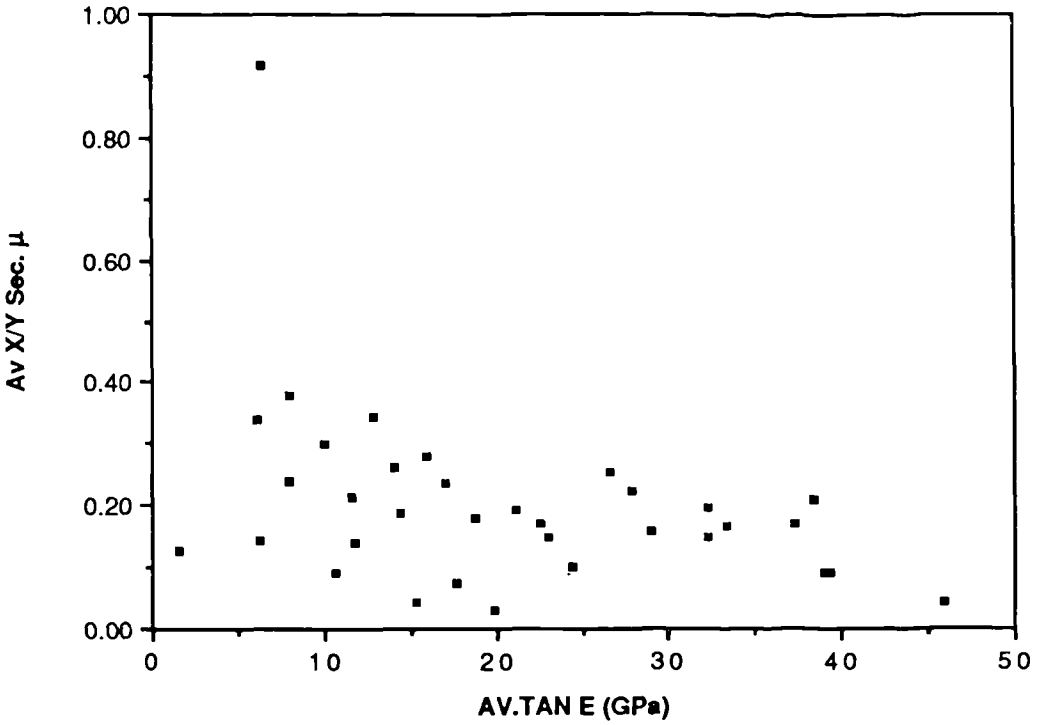

Figure 5.20(a) Poisson's ratio vs. tangent Young's modulus.

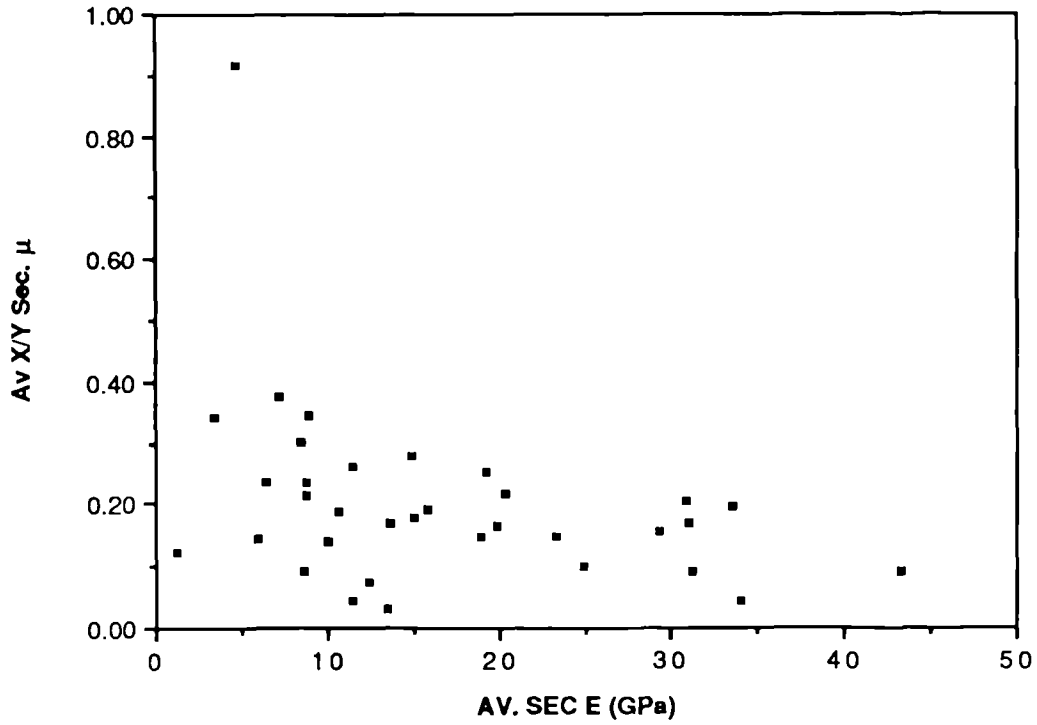

Figure 5.20(b) Poisson's ratio vs. secant Young's modulus.

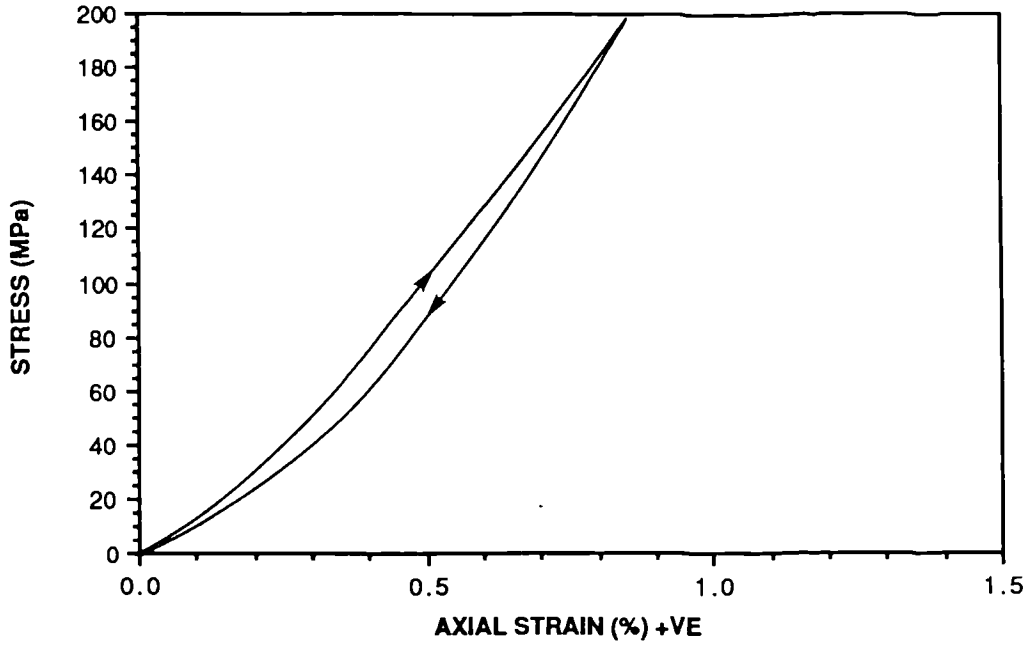

Figure 5.21 Stress-axial strain diagram for loading cycle on Crackington Sandstone to 200 MPa.

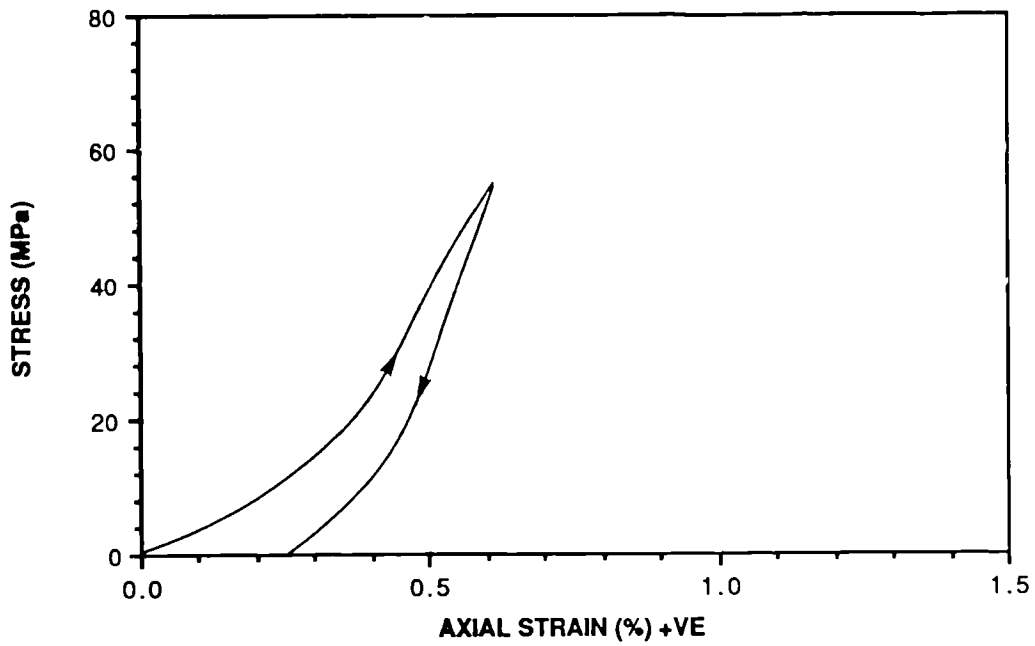

Figure 5.22 Stress-axial strain diagram for loading cycle on Holcombe Brook Grit to 56 MPa.

(type B), whose σ–ε curve shows increasing E with increasing stress. A cyclic loading test to only 50% of the ultimate stress shows a marked permanent axial strain after unloading. This phenomenon is attributed to microscopic failure processes which take place in the rock specimen prior to the main deformation at the yield point and is termed microfracturing, (Brace et al, 1966). These processes involve the interaction between pre-existing natural and stress induced microfractures.

5.4.1 Natural microcavities.

Natural microcavities exist in all rocks in the form of pores, solution hollows, mineral cleavages and at grain boundaries. These are especially common in sandstones where grains, cement and matrix are not bonded together as strongly as crystalline igneous or metamorphic rocks. Lindqvist et al, (1984) identified two main types of microcavities in rock - cracks with an aspect ratio of less than 10^{-1} which were termed low aspect ratio cavities, (LARC's); and those with an aspect ratio of greater than 10^{-1}, high aspect ratio cavities, (HARC's). Plates 5.6(a-h) show natural cavities within sandstones which have been filled with araldite and had the surrounding grains dissolved away. The orientation and arrangement of these natural pores are generally random with grain boundaries being preferred sites for intergranular LARC's.

In the more porous sandstones such as the Cretaceous Ashdown Sandstone and the Ardingly Sandstone, (Plates 5.6 a and b), the grain boundaries are in many cases HARC's. With increasing diagenesis these grain boundaries become much narrower until in theory no space is left between grains when a high degree of recrystallization has taken place.

In thin section, this appears to be the case; pore casting however, can indicate the presence of even the finest pores and cavities - Plate 5.6(h) shows the Donegal Quartzite which possesses numerous thin cavities indicating that even at high degrees of diagenesis, low aspect ratio cavities remain.

Unlike the less indurated specimens, where two or three LARC's meet, they do not form large pore spaces.

The total porosity in any sandstone is composed of pores, (normally HARC's), open grain boundaries, (normally LARC's), intragranular fractures (LARC's), intergranular fractures (LARC's) and solution voids (LARC's or HARC's depending on the form of the originally dissolved grains). The percentage of LARC's to HARC's depends ultimately on the diagenetic and tectonic histories of the deposit. For example Penrith Sandstone Type A, (Plate 5.6c) shows large HARC's in the form of pores with subsidiary LARC's along the grain boundaries. Quartzite on the other hand, (Plate 5.6h) shows a fairly continuous system of very fine cracks. Clearly, the

Plate 5.6 SEM photomicrographs of pore casted sandstones showing morphology of grain boundary cavities and pores.

(a) Ashdown Sandstone

(b) Ardingly Sandstone (type A)

(c) Penrith Sandstone (type B)

(d) Penrith Sandstone (type A)

(e) Pennant (type C)

(f) Holcombe Brook Grit (type A)

(g) Brownstones (LORS)

(h) Donegal Quartzite

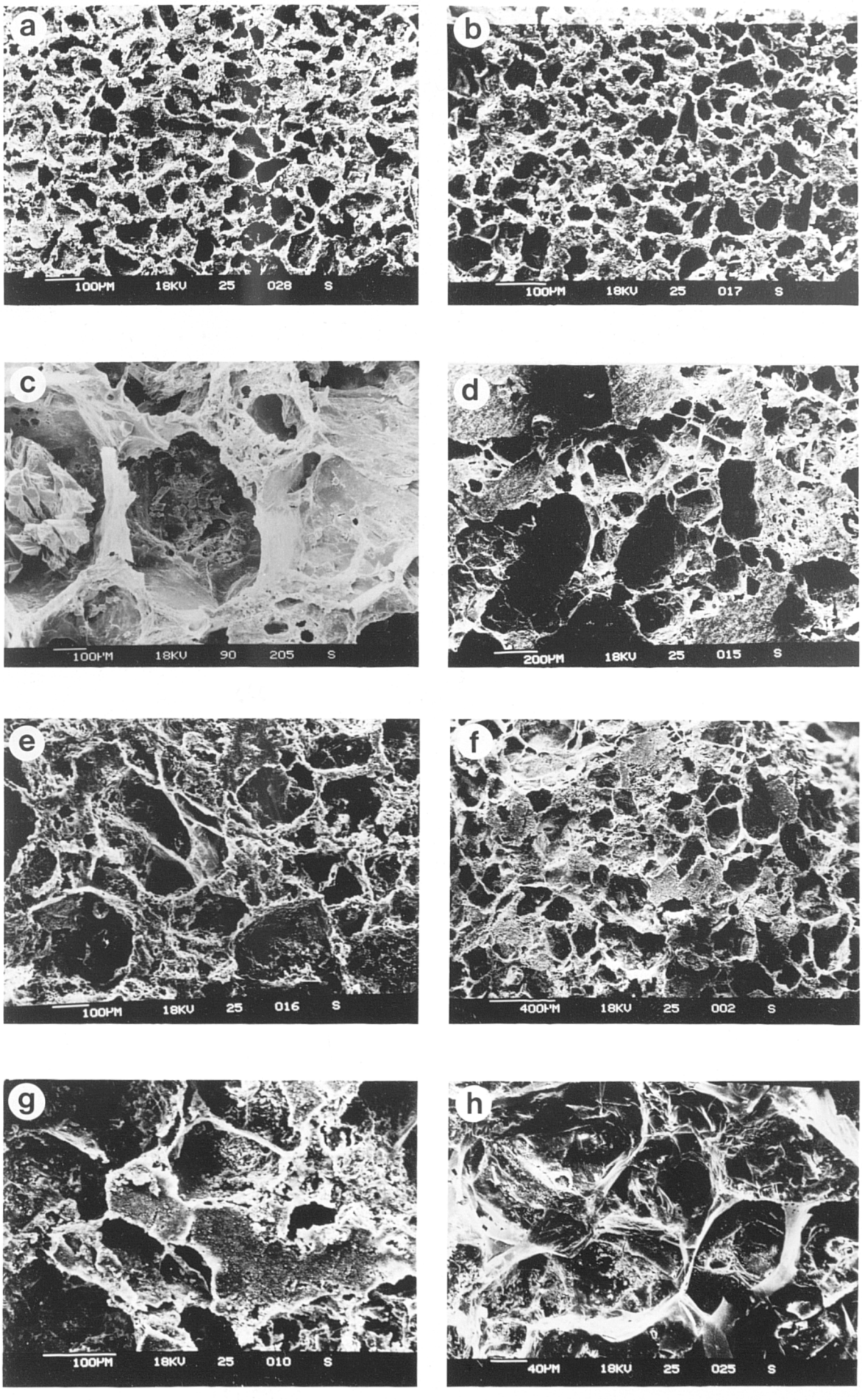
a
100µM 18KV 25 028 S
b
100µM 18KV 25 017 S
c
100µM 18KV 90 205 S
d
200µM 18KV 25 015 S
e
100µM 18KV 25 016 S
f
400µM 18KV 25 002 S
g
100µM 18KV 25 010 S
h
40µM 18KV 25 025 S

presence of pre-existing cavities in the rock will influence the initiation and behaviour of mechanically induced cracks.

5.4.2 The role of stress-induced microfractures

Microfracturing was first detected indirectly by Obert and Duval, (1942) who found that small noises were emitted from rock during loading in compression. Since then many papers have been published on the formation and role of microfracturing in the brittle failure of different rock types. {Brace et al, (1966), Scholz, (1968) and Wawersik and Fairhurst, (1970)}.

Brittle fracture occurs by the separation of the deformed material into parts. Early work showed however that any direct calculation of the forces necessary to break atomic bonds in a crystalline solid gives values for the strength orders of magnitude greater than the strengths observed.

In his classic work, Griffith, (1924) resolved this problem by assuming that defects exist in all brittle materials in the form of narrow cracks which can produce stress concentrations during loading. He proposed that fracture initiates when the stress at the tip of the crack with the highest stress concentration exceeds the stress required to break atomic bonds. This crack will then propagate unstably through the body, causing fracture. Using mathematical solutions for stress around an isolated crack in an elastic homogeneous body, he then calculated a failure criteria based on this model. According to Griffith's model, a brittle material should behave elastically until the most highly stressed crack propagates and the sample fractures.

Scholz, (1968) proposed that in rocks, 'small-scale' fracturing begins at about half the fracture stress and accelerates steadily until a point a few percent below the fracture stress when a rapid increase occurs immediately prior to total failure. He concluded that the 'Griffith' criterion of brittle fracture is not applicable to rock because the inhomogeneity inherent in rock will produce fluctuations in the stress field sufficient to arrest cracks shortly after they have been initiated.

Research carried out by a number of workers on compression of rock has detected stable crack growth prior to total failure. Acoustic, microseismic and direct observation techniques have shown that many thousands of cracking events can be detected before fracture, (Scholz, 1968, 1970; Cook et al 1984). This work supports Scholz's original theory that the Griffith criterion cannot be applied to sandstones.

Brace et al, (1966) first outlined the theory on dilatancy - i.e. the increase in volumetric strain relative to the increase that would be expected if the material were linearly elastic. In a linearly elastic material the volumetric strain is a straight line with a positive slope, that is the value decreases with increasing compression because $\varepsilon_1 > |2.\varepsilon r|$. The volumetric strain is given by:

$$\frac{\Delta V}{Vo} = \varepsilon_l + 2\varepsilon_r \qquad (5.7)$$

where ΔV = change in volume of specimen

Vo = original volume of specimen

ε_l = longitudinal strain (shortening positive)

ε_r = radial strain (expansion negative)

Figure 5.23(a) shows the stress-strain curves for Pennant Sandstone (type B) tested during this research. As can be seen, the Young's modulus changes significantly throughout the test, indicating the inelastic nature of the rock. The curve 'A' is the axial strain, 'R' is the radial strain and 'V' is the volumetric strain. The volumetric strain begins to deviate from the straight line of an elastic material when the stress reaches a value of about 1/2 the strength, and the deviation from this straight line becomes so great near specimen failure that the volume of the rock at this stage of compression exceeds its original volume. This deviation represents an increase in volume with compression relative to the behaviour of a linear elastic material, that is a relative negative volumetric strain with compression, (dilatancy). To account for this dilatancy, the sum of the lateral strains of the specimen near failure must exceed its axial strain, that is $|2\varepsilon_r|>\varepsilon_l$. It follows that Poisson's ratio for different rock specimens in such compresssion tests is far from constant. By testing specimens of rock in the form of thick-walled tubes Cook, (1970) showed that dilatancy is a pervasive volumetric phenomenon, because both the external and internal diameters of the specimens increased in the same proportions during compression.

On the basis of dilatancy behaviour, Brace et al ,(1966) found that the stress-strain curves of different rock types could be divided into four parts, each of which is characterised by a different stage in the microfracturing process.

The four stages proposed by Brace et al, (1966) are shown schematically in Figure 5.23(b). The behaviour of the rock during these four stages is explained as follows:

STAGE I - the σ–ε curve is concave upwards, indicating that the modulus is increasing. At the same time, volumetric strain indicates that the sample is decreasing in volume faster than expected from linear elasticity, as indicated by the dashed line. It has been proposed that this stage results from the closure of pre-existing cracks and pores by the applied stress.

Axial and volumetric strain versus stress in STAGE II are quite linear and

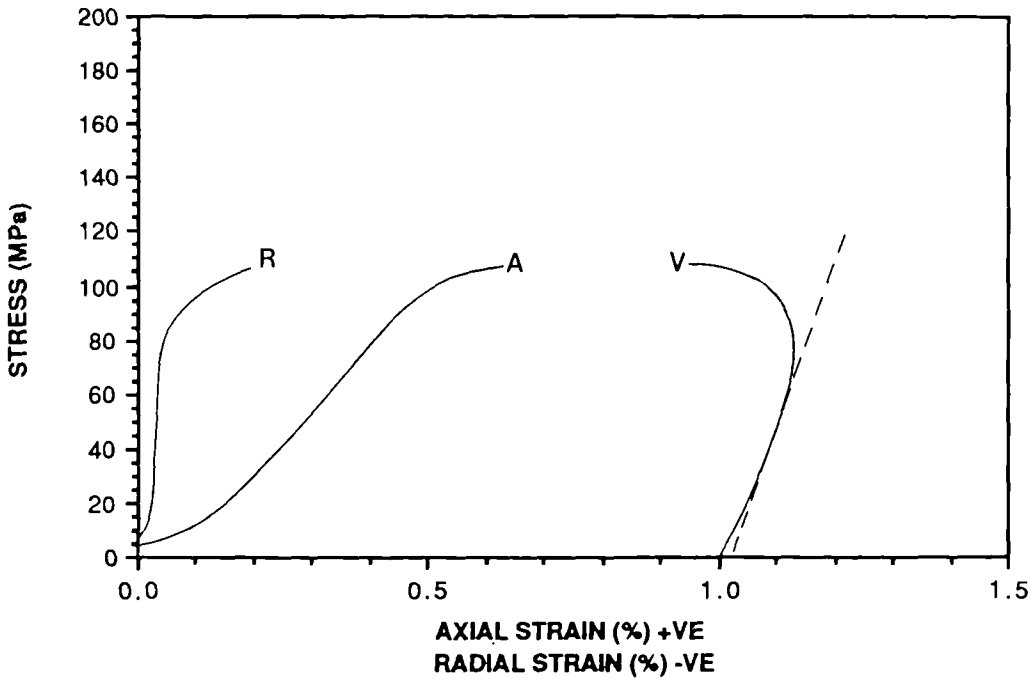

Figure 5.23(a) Stress-strain diagram for Pennant Sandstone (type B) with volumetric strain shown.

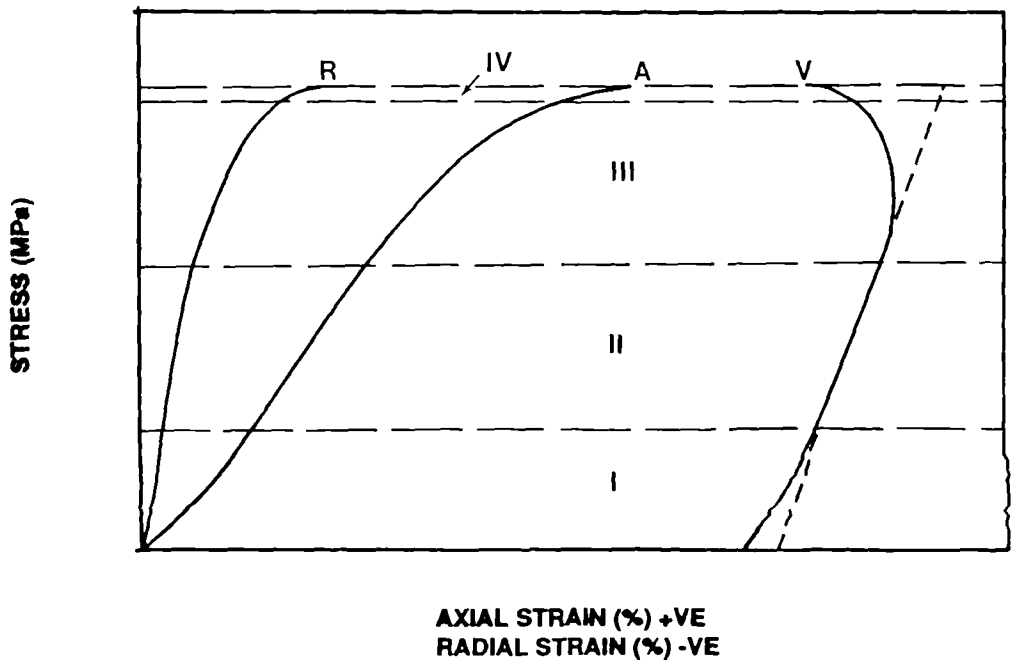

Figure 5.23(b) Generalised stress-strain curve for rock with four stages of deformation as defined by Brace et al, (1966).

provide the gradient for the standard calculation of tan E at 50% of the ultimate stress. Deformation is thus considered to be linearly elastic or nearly so in this region.

In STAGE III on the other hand, the modulus begins to decrease and dilatancy begins to occur, as shown by the volumetric strain curve. Brace et al attributed these effects to the opening of new cracks i.e. microfracturing. It is assumed that if dilatancy is proportional to the number of microfractures formed, then microfracturing begins at low stress levels and continually accelerates as higher stress levels are reached.

STAGE IV which occurs at roughly 95 % of the fracture strength, is typified by a greatly increased dilatancy and has been suggested to represent the region in which microfractures coalesced to form the macroscopic fracture along which failure occurs.

Bieniawski, (1967a,b,c) made a subsequent study along the same lines and although he recognised the same four stages, he chose to interpret them somewhat differently. He suggested that cracks propagated stably, with low velocity in Stage III and unstably with high velocity in Stage IV. He suggested that the onset of Stage III occurred when the Griffith (1924) criterion was reached.

If the theory, which is now generally accepted, that existing cavities within the rock specimen close during Stage I is true, then the amount of change of Young's modulus from Stage I to Stage II might be expected to be related to the original rock porosity. The change in E from Stage I to Stage II was measured for all the sandstones and plotted as a percentage change against effective porosity in Figure 5.24.

The relationship between porosity and change in Young's modulus is unclear and it can be concluded that the non-elastic behaviour which takes place during the deformation of many sandstones is due only in part to the closure of pores and cavities. It is more likely that the behaviour is related to a combination of closure of cavities and the compression and straining of existing cements or matrix. The relative positions of the grain boundaries between stages and the role of these stages is highly variable between different sandstone types.

A simple model for StageI/StageII deformation of different porosity sandstones is given below:

i) Very low porosity sandstones. <2 %

As the axial load increases from zero, stresses are concentrated first on any contained intergranular matrix causing it to deform. If the rock possesses LARC's along grain boundaries these will close during Stage I. If little or no matrix or LARC's exist then the stresses are immediately transferred to the cement or grain to grain contacts and the rock behaves approximately elastically, with negligible change in Young's modulus from I to II.

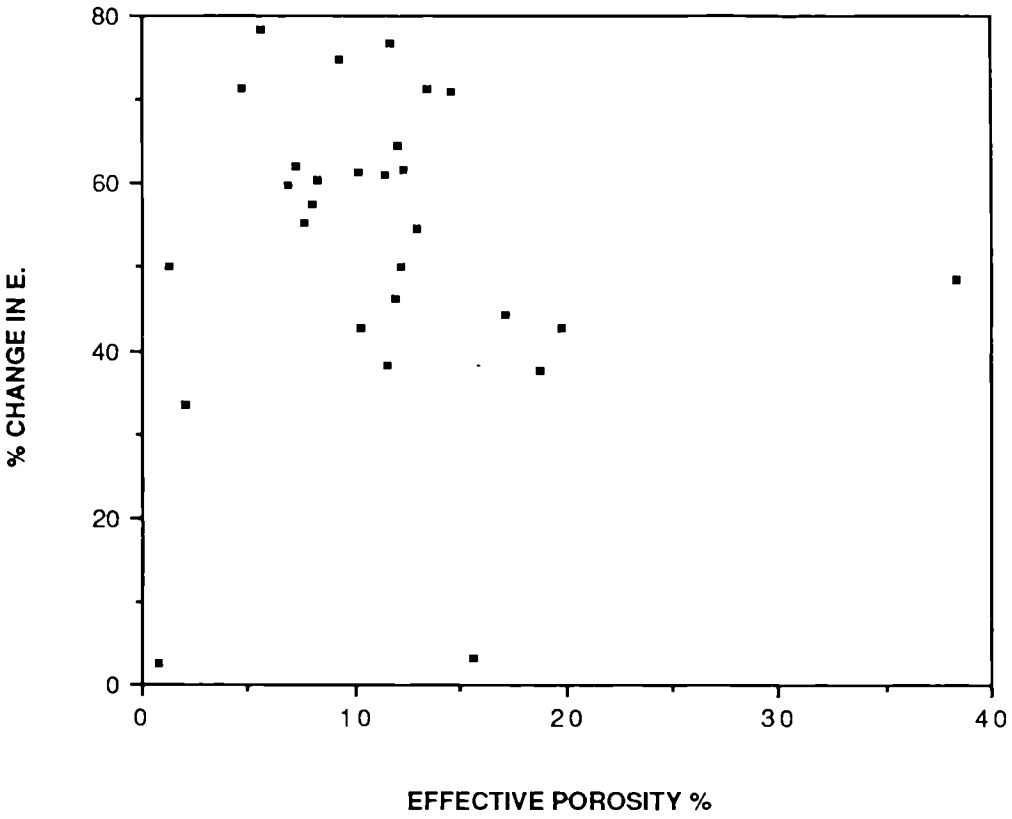

Figure 5.24 Percentage change in Young's modulus from Stage I to Stage II plotted against effective porosity.

Studying the thin section photomicrographs of the Donegal Quartzite, one would expect elastic deformation under uniaxial load. This is not the case however, since the σ–ε curves show a steady increase in E from Stage I to Stage II as in Figure 5.15. Linqvist et al, (1984) identified a greater degree of microfracturing in quartz when surrounded by mica grains and it can be concluded that the phenomenon identified in the Donegal Quartzite is partly due to an elastic mismatch between the muscovite mica and the predominant quartz grains. In this case Stage I is produced by the attainment of a critical stress in the mica which produces preferential fracturing. The onset of Stage II deformation occurs when these microfractures attempt to propagate into the adjacent quartz grains but are arrested due to the higher strength of quartz. Such a change in Young's modulus was not identified in the Basal Quartzite from Skye which has a total quartz content of 93.3% and no muscovite mica. The presence of thin cavities along grain boundaries as discussed previously also has an effect on the shape of the σ–ε curve.

ii) Intermediate porosity sandstones. 2-19 %

As stresses within the specimen increase from zero, partial closure of pores occurs with a high degree of closure of LARC's, probably until packing proximity reaches a critical value. If the sandstone contains matrix, it will deform into pores and vertical and horizontal packing will increase. [This type of deformation is not considered to take place in triaxial compression tests under moderate confining pressures, (Scholz, 1970)]. At the onset of Stage II deformation, one or both of two processes will occur: i) matrix deformation and packing density increase until packing proximity reaches a critical value and stresses are transferred to the framework grains; ii) in well cemented, low matrix content sandstones such as the Penrith (type A), stresses are concentrated along the boundaries of interlocking grains. These stresses result in the straining of individual overgrowths and some degree of microfracturing of highly stressed areas. The change in Young's modulus from Stage I to Stage II is produced by the 'locking- up' of these euhedral and subhedral welded overgrowths.

It is noteworthy that authigenic quartz overgrowths generally develop in sandstones with high porosities. Stresses imposed on such rocks will produce higher intergranular stresses along overgrowth junctions than those which would be developed in more tightly packed quartzites for instance. This may explain the unexpectedly lower strengths for sandstones which show well developed overgrowths than would be predicted from the dry bulk density. (see Figure 5.5)

iii) High porosity sandstones. 20-40 %

This group of sandstones generally has a low cement content although

abundant clay-rich matrix is often present. e.g. the Greensand. Deformation of such rock types normally shows an initial low E since the stress is supported at an early stage by the weak cement/matrix. The stresses concentrated within the matrix are sufficient to cause it to fail and because of low packing density, the matrix continues to deform and stresses are not taken up by the floating grains. This means that the Young's modulus for Stage II does not increase from Stage I and the rock appears to deform elastically, (Figure 5.25). This is not however the case since axial shortening is accompanied by a high radial strain. When the volumetric strain is plotted on the graph it becomes clear that volume is increasing from an early stage, therefore dilatancy is occurring at very low stresses.

The same result is true for high porosity sandstones which have no matrix but are weakly cemented by a clay grain coating, e.g. Ashdown Sandstone, (Figure 5.26). In this case Stage II is very short since Stage I represents the fracturing of the weak intergranular cement and Stage III represents the rolling type deformation of the now unconnected grains. This is accompanied by extremely high radial strain.

5.4.3 The interaction of natural microcavities and stress-induced microfractures.

The σ–ε curves for most sandstones indicate a high degree of pore and cavity closure during Stage I deformation. In the majority of cases this closure must be accompanied by the brittle failure of weak matrix or cement; clays for instance are likely to break or 'burst' in areas where stress concentrations are highest in order to allow the increase in packing to occur.

This cement/matrix deformation occurs at relatively low energy levels. The speed and energy of this 'bursting' is not sufficient to produce an acoustic pulse and its description as microfracturing is not applicable. The term *microbursting* is therefore introduced. In crystalline rocks such deformation during Stage I has not been detected; Cook et al, (1984) were unable to detect acoustic events during Stage I/Stage II uniaxial deformation of granite. During this research, a number of sandstone samples were loaded to low stress levels. The specimens were then examined using the SEM, but no discernable changes in the rock microfrabric were observed.

Following the pore closure and increase in packing density during Stage I, the approximate elastic deformation of Stage II takes place. As the load increases, stresses are concentrated around openings within the rock structure. At a critical point in the σ-ε curve, (the yield point) these stresses are sufficient to cause microfracturing of the weakest areas. These microfractures are unstable, (i.e. they propagate without increase in stress) but become stable when they reach areas of low stress. This is due to the inhomogeneity which is inherent in sandstone microfabric; it is this non-uniformity which produces the differences between the deformation observed in most sandstones

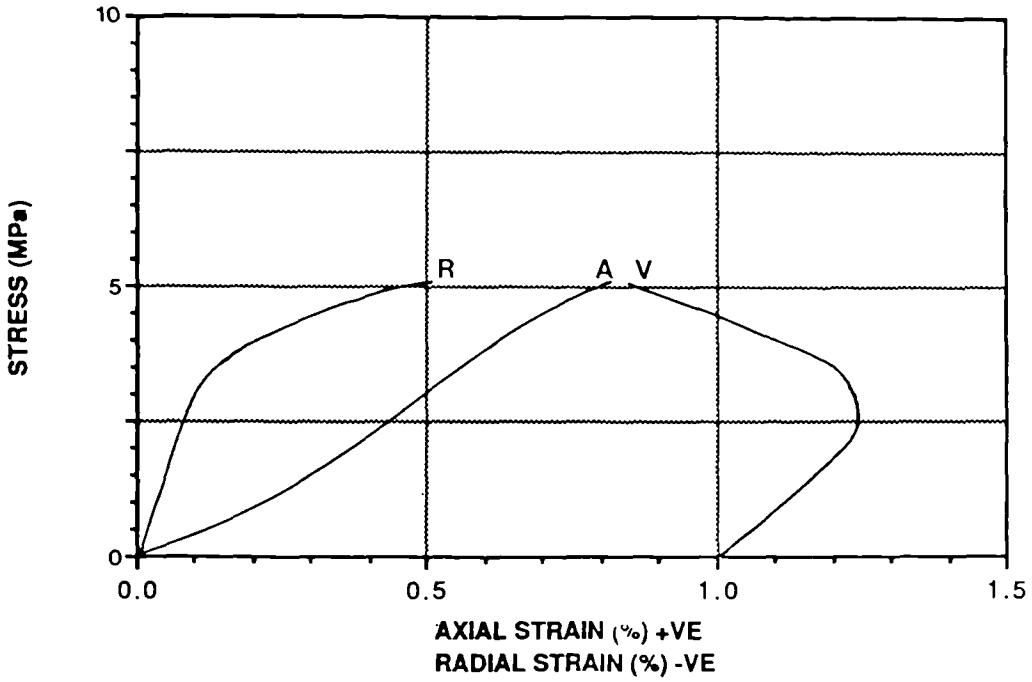

Figure 5.25 Stress-strain diagram for Greensand with volumetric strain shown.

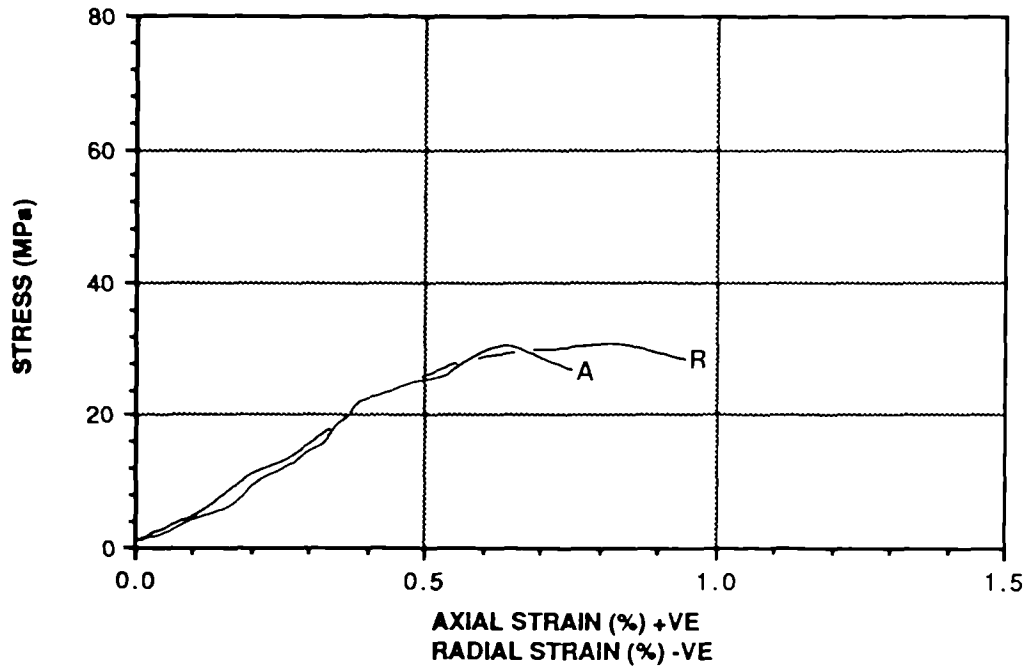

Figure 5.26 Stress-strain diagram for Ashdown Sandstone.

and that observed in igneous and metamorphic rocks where grains are highly interlocked and porosity is extremely low.

The path followed by the microfractures in sandstones is generally around grains but is controlled by the strength differential between the framework grains and the cementing materials. In high porosity sandstones the fractures generally follow grain boundaries and stable microfracturing processes dominate. It has been shown, (Scholz, 1970) that microfractures will tend to align parallel to the maximum stress direction, (in this research, the uniaxial stress). Since stable microfracturing in high porosity rocks tends to follow grain boundaries, their detailed alignment parallel to σ_1 will be poor. This is due to the irregular packing of grains which is observed in all sandstones.

In high porosity rocks, microfractures form a network of non-parallel fractures passing through matrix and cement. The linkage of these microfractures will cause cataclastic deformation where in many cases large volumes of the rock disintegrate into grain-sized fragments. e.g. Midford Sands and Greensand.

In sandstones of slightly higher strength, these microfractures link at high angles to σ_1 and shear localization occurs, the mode of failure depending on the degree of cementation. In the Ardingly Sandstone for example, (Plate 5.7a), a rolling mode of failure results between disaggregated grains. In contrast Plate 5.7(b) shows a shear surface in Millstone Grit (type C) where the unstable macroscale fracture has sheared through grains leaving a relatively flat surface. The degree of shear localization, even in moderately strong sandstones is evident from Plate 5.7(c). The line superimposed on the photomicrograph is 200μm from the macroscale failure plane, (and parallel to it). Little microfracturing is evident beyond this line.

Lower porosity sandstones also show stable microfracturing around framework grains but the cracks are aligned closer to σ_1. The following processes are considered to occur in the intermediate and low porosity sandstones:

i) Microfractures are initiated during Stage III where stress concentrations are high such as around existing pores and cavities within the rock. (Analagous to the stresses around a tunnel through a rock mass.).

ii) Unstable microfractures propagate along grain boundaries tending to align parallel to σ_1.

iii) When these microfractures reach areas of low stress, (e.g. pores or matrix) they will terminate since they have released some of the energy stored within the highly stressed zone.

If a large strength differential exists between grains and cement, the crack will follow grain boundaries. Plates 5.7(d) to (g) show microfractures passing around

Plate 5.7 SEM photomicrographs of microscopic failure modes occurring in sandstones. (See text for descriptions).

(a) Ardingly Sandstone (type A)

(b) Millstone Grit (type C)

(c) Ardingly Sandstone (type A)

(d) Penrith Sandstone (type C)

(e) Penrith Sandstone (type C)

(f) Penrith Sandstone (type D)

(g) Annan Sandstone

(h) Holcombe Brook Grit (type A)

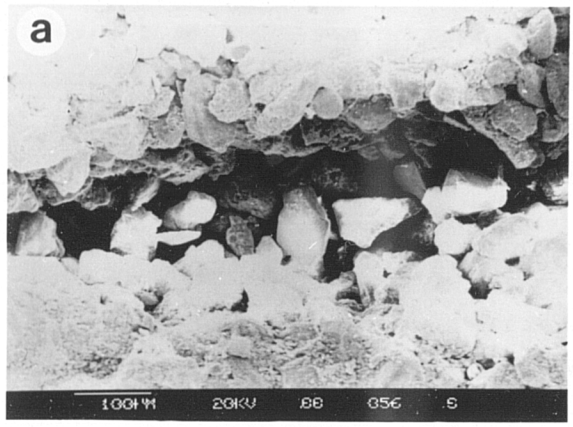
a
100µM 20KV 88 056 S

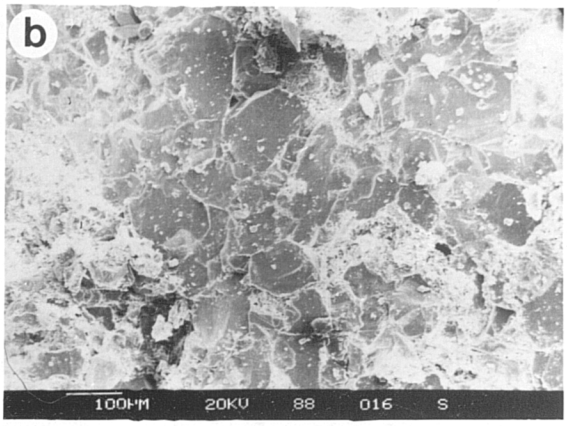
b
100µM 20KV 88 016 S

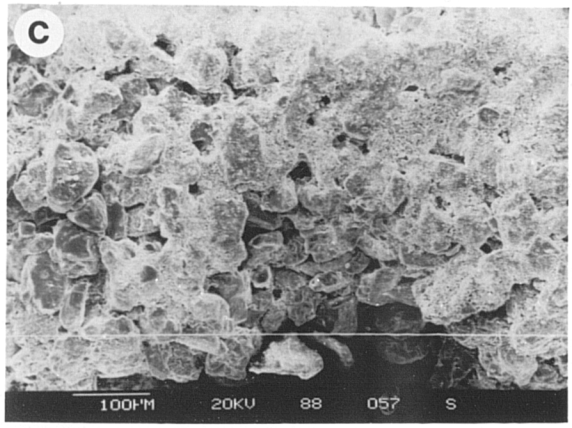
c
100µM 20KV 88 057 S

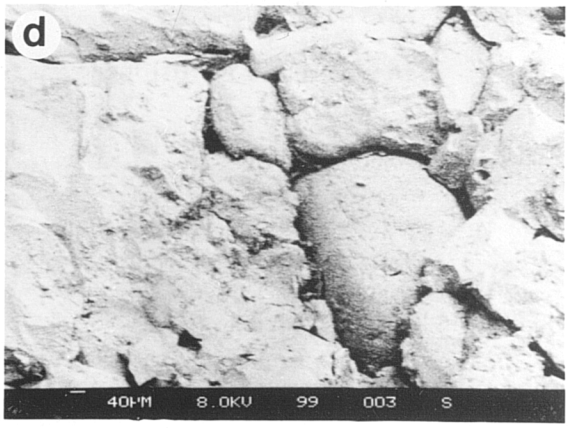
d
40µM 8.0KV 99 003 S

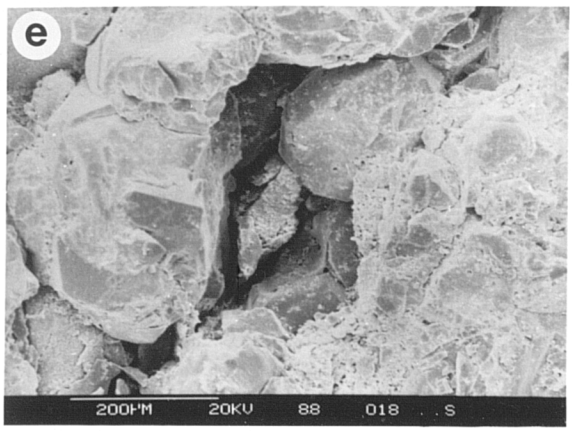
e
200µM 20KV 88 018 S

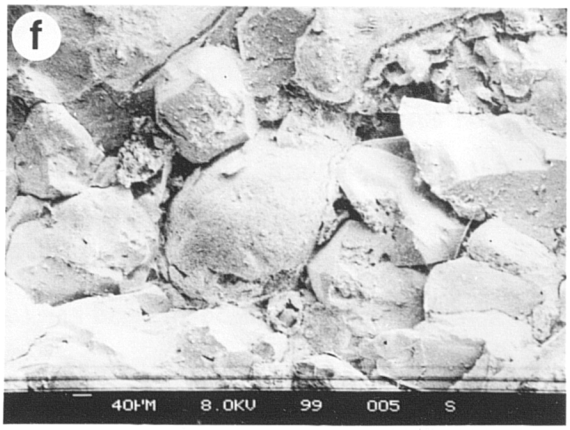
f
40µM 8.0KV 99 005 S

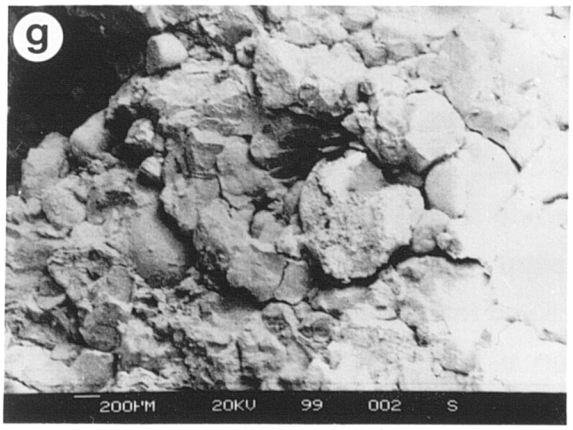
g
200µM 20KV 99 002 S

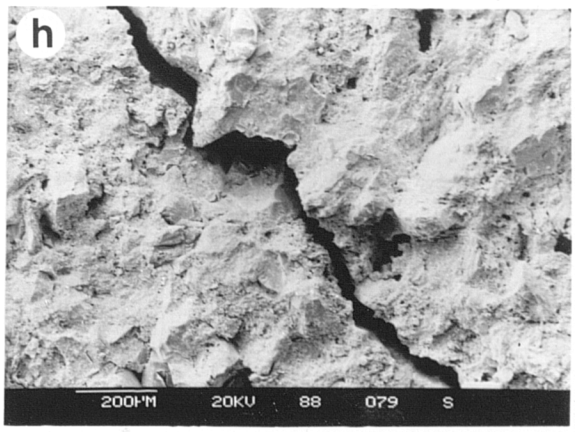
h
200µM 20KV 88 079 S

grains. It is suggested that the ease of propagation of microfractures around grain boundaries also depends on grain roundness, (Plate 5.7h). The presence of highly angular, low sphericity grains will inhibit fracture propagation.

The microfracture path will depend to a large extent on whether it is occurring in a stable or unstable mode. Plate 5.8(a) shows a macroscale fracture which has formed by linkage of both stable and unstable fractures. The failure is characterised by a zone of fracturing with the majority of the microfractures being intergranular. A number of transgranular fractures are evident where the speed of micro-failure has been too rapid for the microfracture to change propagation direction around the grains. SEM examinations indicate that microfractures will be trans- or intergranular depending on a number of factors:

1) Mode of propagation -stable or unstable. Unstable fractures are more likely to pass through grains,
2) The strength differential between grains and cement,
3) The roundness of grains,
4) The angle of incidence of a propagating unstable microfracture with the grain boundary, and
5) Internal grain inhomogeneities such as cleavage.

Plate 5.8(b) shows a high magnification of Plate 5.8(a). In this case the linkage of stable microfractures has ocurred by the unstable fracture propagation during Stage IV to form the macroscale fracture. The propagating microfracture has struck the grain boundary at approximately 90°. At the point of incidence, a fan of fractures have propagated into the grain in a manner analagous to blasting, (Matheson,1983). In this way a large amount of energy is dissipated but one fracture continues to propagate through the grain in the direction of σ_1.

The feldspar grain shown in Plate 5.8(c) has been bisected by a transgranular microfracture along the cleavage while intergranular microfractures have formed in the surrounding area where quartz grains are present. In unstable microfracture formation which dominates when the strength differential is low, (in low porosity sandstones), the propagtion will occur through grains irrespective of shape. When an area of high stress within a specimen contains a number of microfractures, these will interact. Kranz, (1979) considered crack interaction and the influence of the local stress field on the direction of crack propagation. The basic types of interaction are shown in Figure 5.27, uniaxial compression at some distant boundary is assumed. When en echelon crack arrays are directed at an acute angle to the applied stress, shear linkage can be seen. Kranz concluded that dilatant cracks associated with shear failure were rarely observed in crystalline rocks. This is not the case in sandstones where packing

Plate 5.8 SEM photomicrographs of microscopic failure modes occurring in sandstones. (See text for descriptions).

(a) Millstone Grit (type A)

(b) Millstone Grit (type A)

(c) Penrith Sandstone (type C)

(d) Donegal Quartzite

(e) Holcombe Brook Grit (type A)

(f) Donegal Quartzite

(g) Donegal Quartzite

(h) Holcombe Brook Grit (type B)

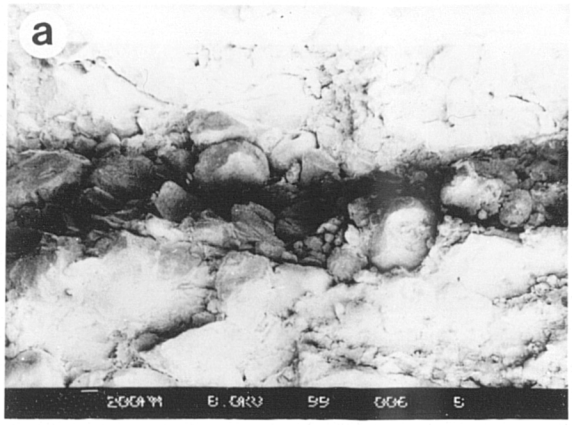
a
20UM 8.0KV 99 006 S

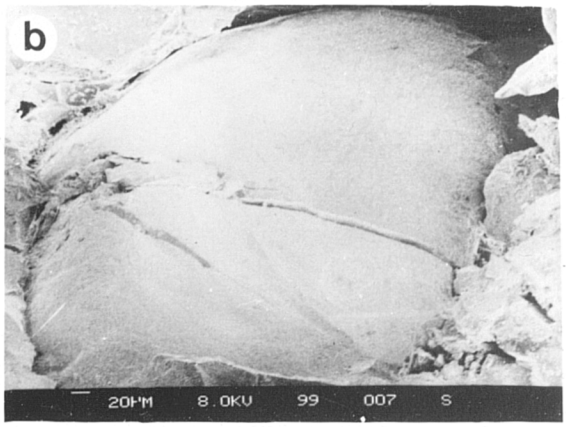
b
20UM 8.0KV 99 007 S

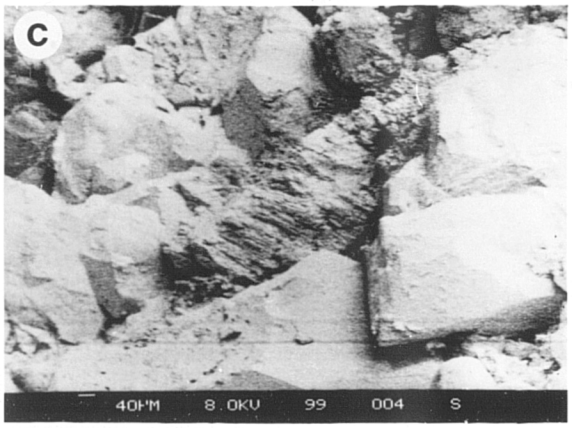
c
40UM 8.0KV 99 004 S

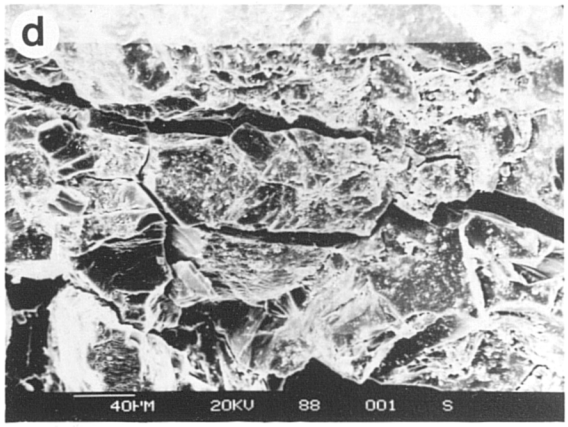
d
40UM 20KV 88 001 S

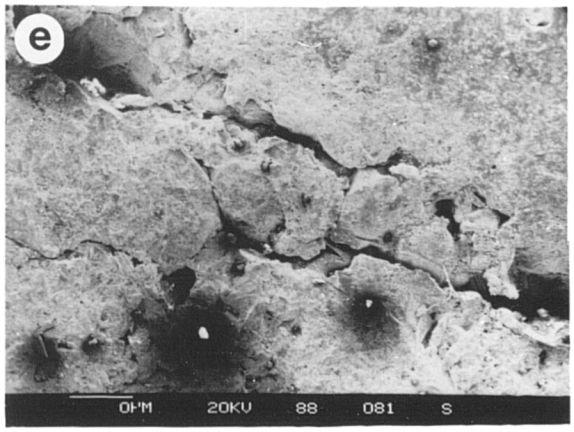
e
0UM 20KV 88 081 S

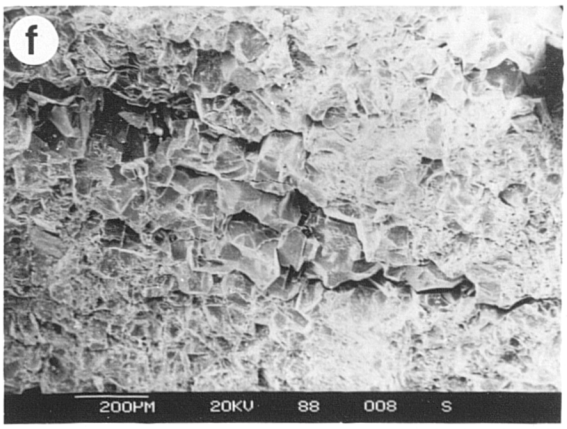
f
200UM 20KV 88 008 S

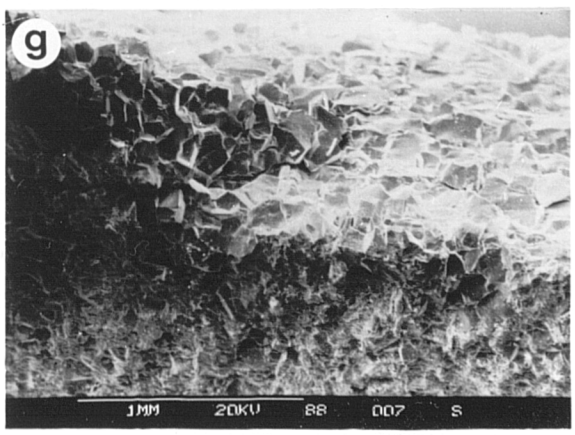
g
1MM 20KV 88 007 S

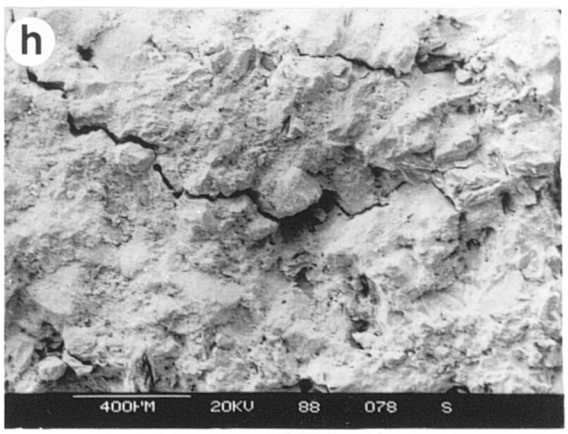
h
400UM 20KV 88 078 S

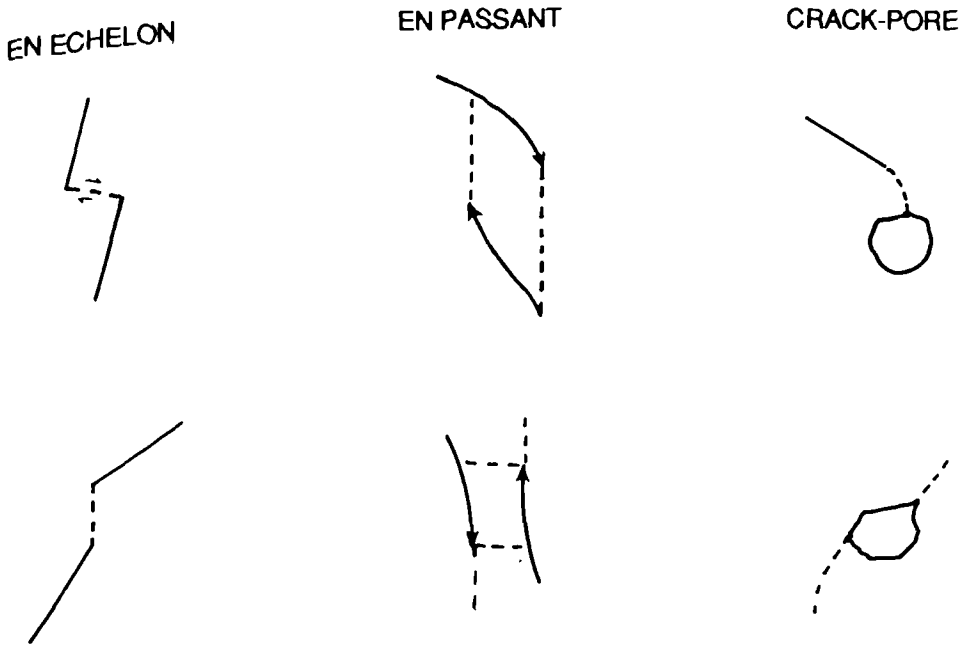

Figure 5.27 Basic types of interactions. Dashed lines indicate extension links or branch paths. (After Kranz, 1979).

geometry dictates that certain grains will be stressed so as to move between adjacent grains and force them apart. This phenomenon which can be termed *microwedging*, must occur for axial strain to take place, the result being that shear failure will take place between grains on a microscopic scale. The lowest porosity sandstones generally have a much more homogeneous structure and therefore stable crack growth is limited - tensile linkage in a vertical or near vertical direction occurs as branch cracks grow towards the maximum stress.

This generally occurs in an unstable fashion with the main formation occurring in Stage IV. During this stage transgranular and intergranular microfractures are present, depending on the degree of inter-grain suturing. The result of this grain interaction means that certain microfractures and macroscale fractures will become abandoned as the main failure passes through the sandstone specimen, (Plates 5.8d to 5.9b).

A number of physical theories have been developed with the aim of determining the σ-ε behaviour of brittle rock in terms of micro-mechanical processes. A group of models, commonly referred to as sliding crack models postulate that frictional sliding along grain boundaries or inclined at high angles to σ_1 pull open other tensile cracks causing the latter to extend parallel to σ_1 and give rise to dilatancy, (Kachanov, 1982; Moss and Gupta, 1982).

On the other hand, Stevens and Holcomb, (1980) argued on the basis of SEM

Plate 5.9 SEM photomicrographs of tensional and shear microfractures in post- and pre-failure samples of sandstones. (See text for descriptions).

(a) Penrith Sandstone (type A)

(b) Millstone Grit (type B)

(c) Siliceous Sandstone

(d) Donegal Quartzite

(e) Basal Quartzite

(f) Penrith Sandstone (type D)

(g) Donegal Quartzite

(h) Donegal Quartzite

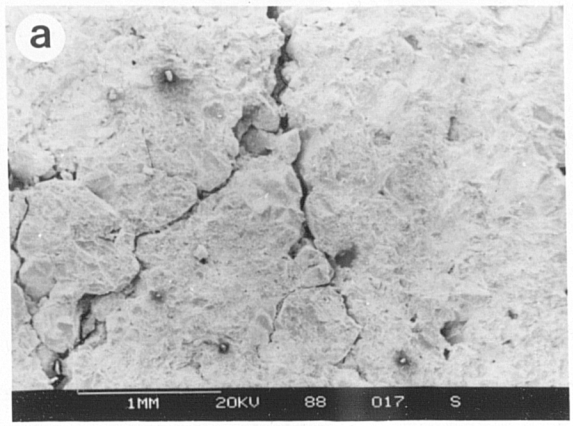
a
1MM 20KV 88 017 S

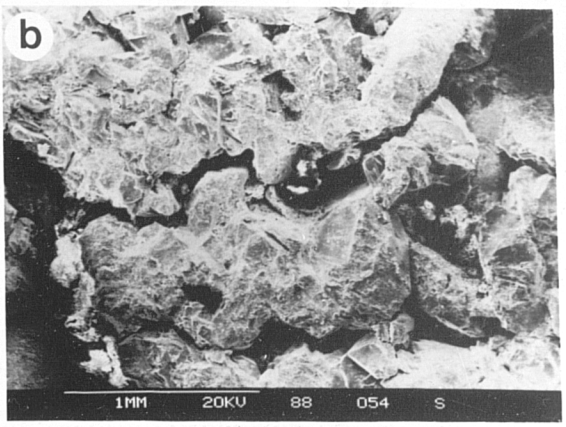
b
1MM 20KV 88 054 S

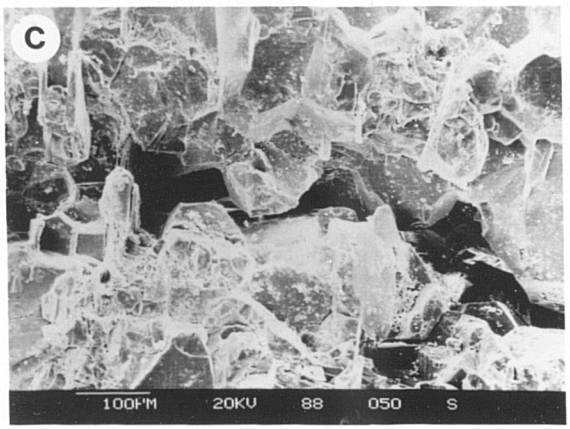
c
100µM 20KV 88 050 S

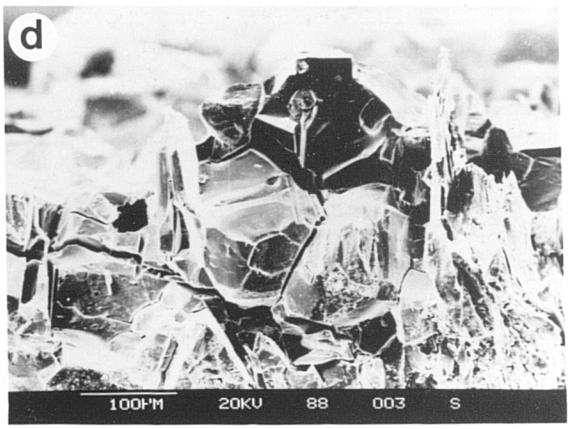
d
100µM 20KV 88 003 S

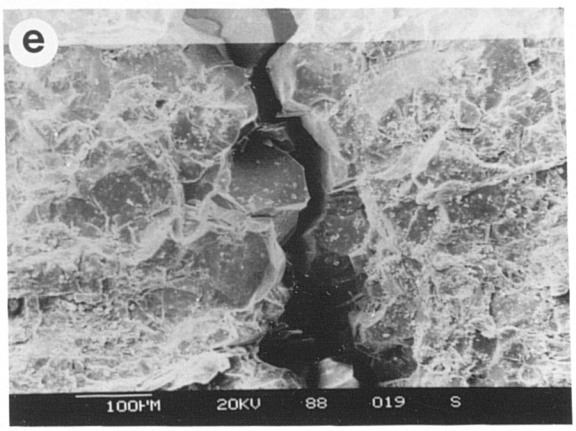
e
100µM 20KV 88 019 S

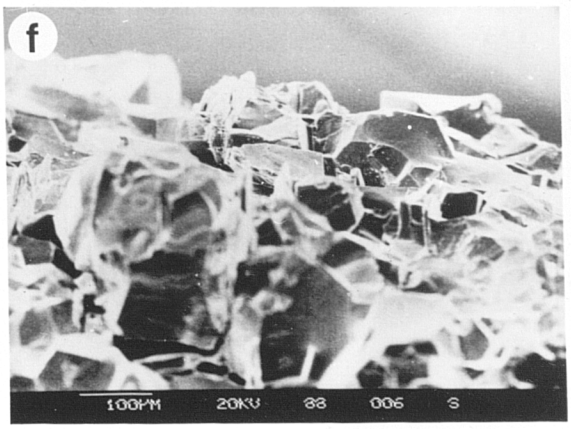
f
100µM 20KV 88 006 S

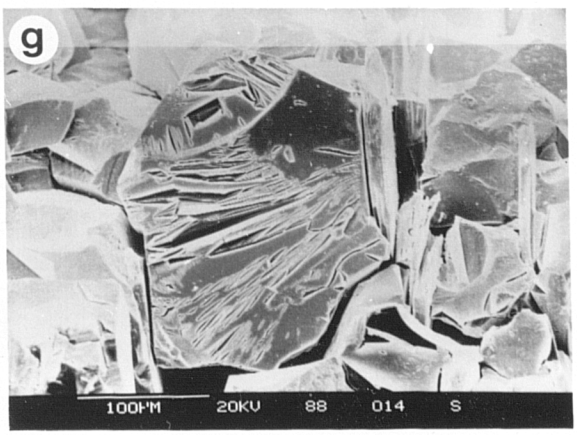
g
100µM 20KV 88 014 S

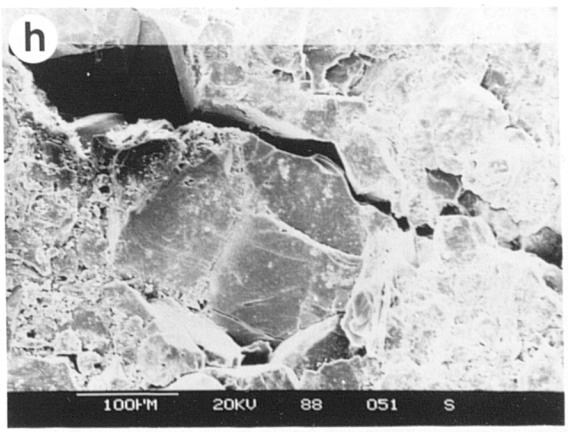
h
100µM 20KV 88 051 S

observations and their own study of hysteresis in stress cycling tests that the 'sliding crack' is unrealistic. SEM studies of Tapponier and Brace, (1976) concluded that dilatancy is primarily a consequence of two types of cracking: (1) widening and extension of pre-existing discontinuities such as grain boundaries cracks and pores; (2) initiation and propagation of cracks at localities with high contrast in elastic moduli such as at transverse grain boundaries between different minerals.

The conclusion of the SEM study carried out during this research is that the stress induced cracks are generally 'mode I' tensile cracks, (i.e. displacement is normal to the crack plane) but that mode II and mode III microfractures do occur due to the process of microwedging. Plates 5.9(c-f) show tensile fracture in post failure specimens of quartz-rich sandstones. Plate 5.9(g) shows indications of shear in prefailure samples of Donegal Quartzite where a rotational moment imposed on a quartz grain has caused internal microfracturing. In Plate 5.9(h), a pore has initiated microfracture propagation at a high angle to σ_1 and shows signs of dextral shear displacement, (mode III). The crack orientation varies widely between different sandstone types depending on whether stable or unstable microfracture formation is predominant during Stage III. SEM studies have shown that microfractures are aligned closer to the direction of σ_1 in prefailure specimens of strong sandstones while the alignment is poor in the weaker varieties. The strong alignment of microfractures parallel to σ_1 or within 15° of σ_1 in the strongest sandstones corresponds with the results of work by Tapponier and Brace, (1976) and Kranz, (1979) on granite.

5.5 Summary

A wide range of strength values has been determined during the testing of dry sandstone specimens. These strength values have been related to a number of static properties and good correlations have been observed, especially with dry bulk density. The detailed monitoring of the axial and radial strains during the loading has revealed interesting deformation patterns between different sandstone types. It can be concluded that with the exception of the strongest varieties, sandstones behave in a non-elastic manner, with dilatancy playing an important role in the deformation process. This dilatancy produces stress-strain curves with a large variation in Young's modulus and for this reason it is important to express E in terms of the sec E at failure as well as the tan E at 50% of the ultimate stress.

The Poisson's ratio values measured during the research have proved to be highly variable and it is suggested that the variation is controlled by textural parameters which do not influence strength or Young's modulus to the same degree.

The macroscale failure modes have been divided into three classes but it has

been shown that they often occur together. Only when failure is examined on a microscale, do the reasons for processes of macroscale failure become apparent.

To summarize the relationship between micro- and macroscale failure, an idealised model is proposed in Figure 5.28. The examples have been chosen as good representations of the main behavioural variations observed from the weakest argillaceous sandstones to the extremely strong wackes and quartzites. Generalised stress-strain curves and the relevant elastic parameters for the sandstone types are included to show how the deformation is controlled by the microscale processes. The relative positions of the onset of Stage II and the onset of dilatancy are also shown.

Figure 5.28 Idealised model for sandstone failure in uniaxial compression. Four examples are shown to illustrate the variation in macro- and micro-scale failure. Unstable microfractures are shown by branching cracks propagating through grains. Onset of Stage II and onset of dilatancy are shown and expressed as a percentage of the total stress at failure.

ONSET OF STAGE II AND DILATANCY	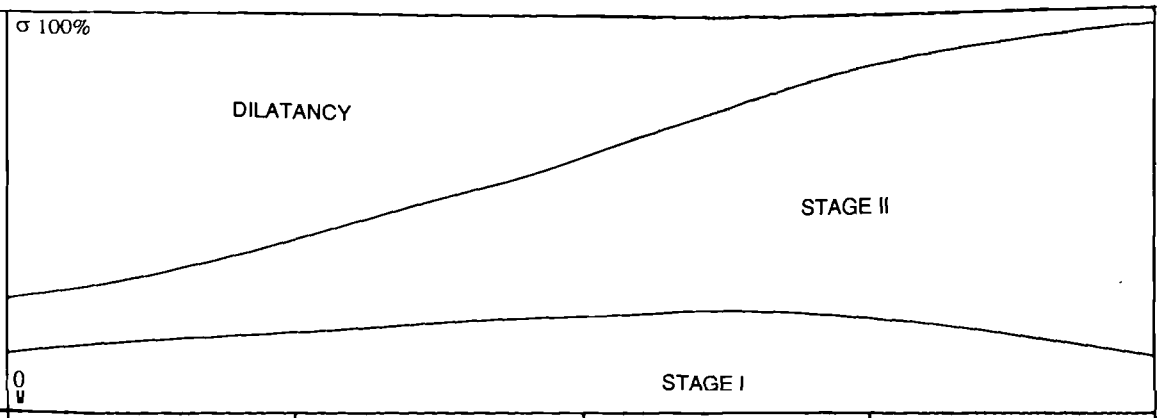			
e.g.	Ardingly Sst	Pennant (type B)	Brownstones	Crackington
STATIC PROPERTIES	D.B.D. 1.933 S.B.D. 2.120 n 18.855	D.B.D. 2.466 S.B.D. 2.535 n 6.874	D.B.D. 2.460 S.B.D. 2.514 n 6.764	D.B.D. 2.653 S.B.D. 2.673 n 1.973
ELASTIC PARAMETERS	Tan E 7.92 Sec E 7.14 Sec μ 0.379	Tan E 26.63 Sec E 19.30 Sec μ 0.225	Tan E 32.27 Sec E 23.39 Sec μ 0.147	Tan E 36.38 Sec E 30.04 Sec μ 0.172
MICROFAILURE	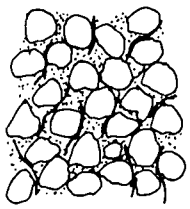	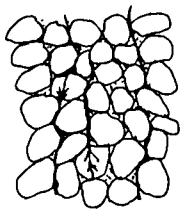	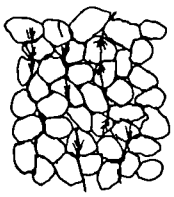	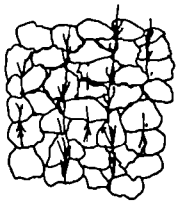
MACRO-FAILURE	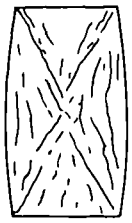	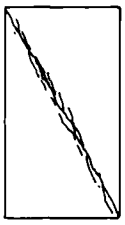	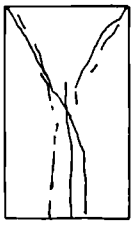	
STRESS-STRAIN CURVE	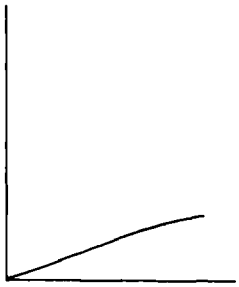		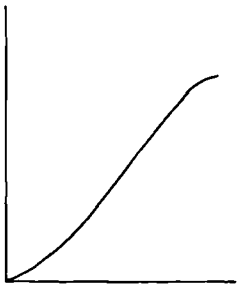	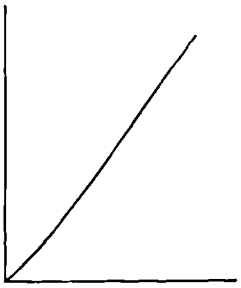

CHAPTER 6

THE EFFECTS OF MOISTURE CONTENT ON THE STRENGTH AND DEFORMABILITY OF SANDSTONES

6.1 Introduction

The effects of water on the strength and deformability of many rock types, (especially sedimentary varieties) have been reported for many years. Colback and Wiid, (1965) demonstrated a 50% loss in strength for a quartzitic shale and a quartzitic sandstone tested in submerged conditions compared with testing in the dry condition. Burstein, (1968) studied the effect of moisture on the strength and deformability of some Russian sedimentary rock types including a quartz arenite and clay-rich sandstone. He found that with an increase in moisture content from 0 to 4 %, the quartz arenite lost half of its compressive strength and that an increase in moisture content in the 'argillite' from 0 to 1.5% reduced the compressive strength to one third of its initial value. In addition, Burstein found that tensile strength and modulus of deformation were both sensitive to moisture content for the two sedimentary rocks studied. Van Eeckhout and Peng, (1975) studied the effect of humidity on the strength and elastic properties of a number of coal mine shales. Using relative humidities of 0, 48 and 100%, their results showed a reduction in strength with increased moisture and associated decrease in Young's modulus and increase in Poisson's ratio.

Previous research clearly shows that rock is weaker when tested in a wet condition than when dry. However, with the exception of work by Priest and Selvakumar, (1982) who studied five different British rock types, no real relation between uniaxial compressive strength and moisture content has been established for any specific rock type. Generally in the past rock mechanics studies have only tested samples in the fully saturated and dry conditions with no consideration of the intermediate moisture levels; i.e. the levels generally occurring in rocks which are stressed during engineering construction. e.g. tunnels both above and below the water table.

6.2 Existing theories

There appears to be no generally accepted explanation for the influence of moisture on rock strength, although several mechanisms have been suggested such as: (1) fracture energy reduction; (2) capillary tension decrease; (3) pore pressure increase; (4) frictional reduction and (5) chemical and physical deterioration. None of these

mechanisms can be discounted outright but some are more likely than others for certain rock types and conditions. In order to attempt to determine the processes involved in sandstone strength reduction, it is important to outline the various theories which have been proposed.

6.2.1 Fracture energy reduction

Fracture energy reduction is the mechanism predominantly used to explain the effects of moisture on rock strength. Essentially it uses the Griffith fracture criterion for a continuous material with a crack of unit thickness, which states that:

$$\sigma_t = \left(\frac{2E\gamma}{\pi C_o}\right)^{1/2} \qquad (6.1)$$

where σ_t = tensile strength necessary to cause crack growth.

E = Young's Modulus

γ = surface energy, and

C_o = one-half the initial flaw or crack length.

Although the equation is defined for tensile stress situations, experimental observations suggest that strength in uniaxial compression is affected by tensile brittle cracking, (Peng and Johnson, 1972). If it is assumed that an equation of the form $\sigma=k(E\gamma/C_o)^{1/2}$ holds, where γ is the energy required per unit advance of the crack and C_o is some measure of a critical flaw length, then if γ is lowered with the absorption of water, the fracture strength will be lowered and hence the intact rock strength.

Hammond and Ravitz, (1963) studied the effects of environment on the brittle fracture of silica. They show that for silica glass rods in different saturated vapours, the strength is lowered according to Griffith's criterion and they use an expression for surface energy reduction based on the vapour pressure, molecular weight and the surface free energy of the solid. They noted a general reduction of strength with surface energy reduction.

Colback and Wiid, (1965) showed that the uniaxial compressive strength of a sandstone was reduced in a linear fashion when immersed in liquids of increasing surface tension* and concluded that the reduction in strength is predominantly due to the reduction of the surface free energy of quartz. They noted a difference in rate of

* surface tension is the phenomenon occurring between two fluids (in this case water and air) due to molecular attractions which appear to rise from a tension in the surface of separation. It is expressed in dynes per cm.

strength reduction with increasing moisture for a shale and a sandstone and suggested that it was possibly due to a difference in porosities, (0.28% for the shale vs. 15% for the sandstone).

Wiid, (1967) expanded this discussion to include four sandstones and a quartzite. The quartzite had a porosity of 1% while the sandstones had values of 20% or greater. The lowering of uniaxial compressive strength which he observed for these samples is shown in Figure 6.1. (Sample 1001 is the quartzite). He also found that the apparent tensile strength reduction in the Brazilian test for sandstone 1005 was very similar to the trend shown in Figure 6.1. Despite major discrepancies between theoretically calculated values and observed values, he established a strength dependency on surface energy for sandstones of greater than 20% porosity.

Using thermodynamic theory, Segall, (1984) has shown that the equilibrium fracture surface energy of quartz in a given chemical environment can set lower limits for the crack extension force above which a tensile crack can grow.

6.2.2 Capillary tension decrease.

Rocks which contain expandable clay minerals, (particularly the montmorillonite group) expand when water is introduced by adding interlayer water molecules into their structure, which although itself is a reversible process, disintegrates the rock due to unequal local pressures.

Expansion can however occur in rocks which do not contain expandable clays, (Duncan, 1968) and in this situation is generally attributed to capillary action, (Van Eeckhout, 1976). Capillary tensions have an effect on the amount of moisture present in a rock, especially those rocks exposed to air. The actual tension present is a function of the vapour pressure in equilibrium with capillary water. The meniscus thus created - which is idealised in Figure 6.2, with r_c as the radius of curvature of the crack tip and r_w as the radius of curvature of the meniscus, is governed by the Kelvin equation, (Thomson, 1871):

$$\ln\frac{pr}{po} = -2\Gamma V/rwRT \qquad (6.2)$$

where po = water vapour pressure over water with no curvature
pr = water vapour pressure over water of curvature r_w
Γ = surface tension of water (0.072 J/m^2)
V = molar volume of water (0.018m^3/kg/m-mole)
R = gas constant
T = absolute temperature

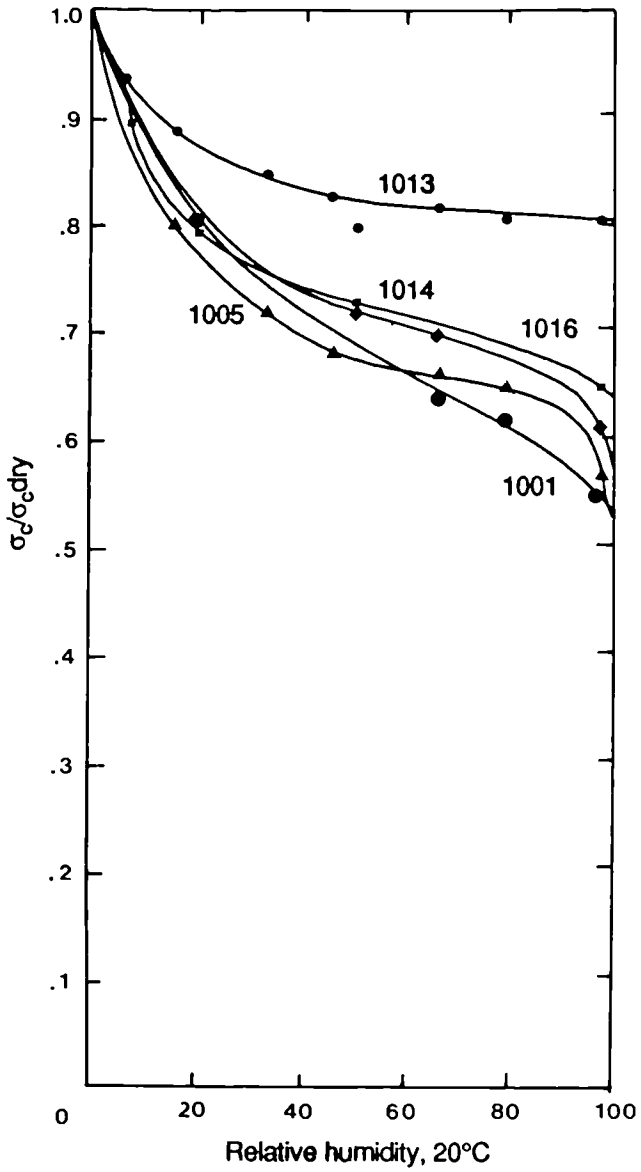

Figure 6.1 Effect of various relative humidities on uniaxial compressive strength of various rock types. (After Wiid, 1967).

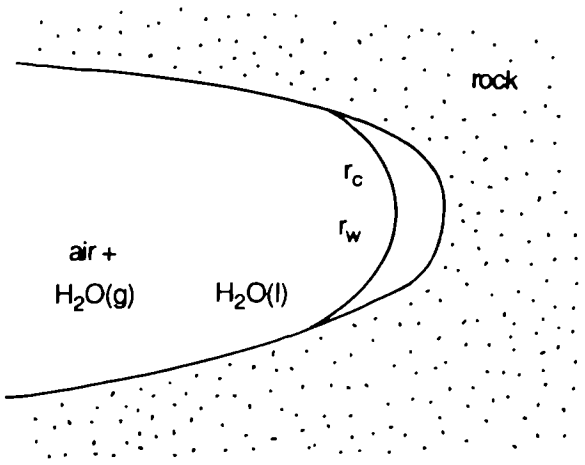

Figure 6.2 Schematic diagram of a water pocket at a crack tip. (After Wiederhorn, 1967).

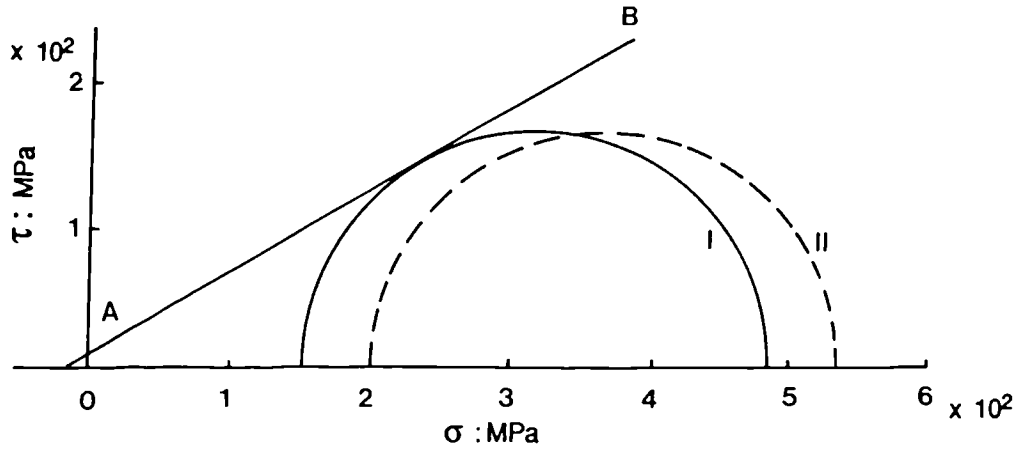

Figure 6.3 The effect of pore pressure on failure. AB is the Mohr envelope. Curve I: Mohr circle for effective stresses. Curve II: Mohr circle for actual stresses.

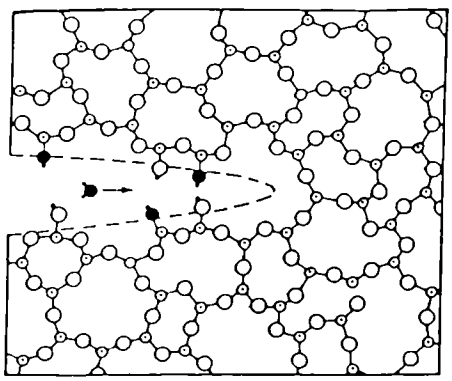

Figure 6.4 2-D representation of water-induced bond rupture of silica glass. Large circles: oxygen, intermediate circles: silicon, small circles: hydrogen. Solid circles denote species originally from the environment. (after Lawn & Wilshaw, 1975).

This means that if the gas-water vapour pressure is greater than the meniscus water vapour pressure, the water pocket will grow until equilibrium is reached, and visa versa. Van Eeckhout states that if a solute is added to pore water, it will lower the equilibrium water vapour pressure. This solute lowering of the water vapour pressure is basic to the use of salt solutions in dessicators to simulate the desired humidity. Since most in situ water has some impurities, one expects some variation from the pure water situation. Chenevert, (1970) suggested that in saturated, low porosity rocks such as shales where little or no air is present, voids are not dilated due to vapour pressure instability.

Where air and water are present within a rock pore system, capillary tensions are created. This process has been used to explain slaking; in an originally dry rock dessication produces high suctions which have the effect of increasing the strength. On subsequent rapid immersion in water the entrapped air becomes pressurized by the capillary pressures developed in the outer pores. Failure of the mineral skeleton then occurs exposing a fresh surface which subsequently undergoes a repeat cycle. The process can be seen to occur in abandoned mine pillars where the removal of rock by this process reduces pillar cross-sectional area and decreases mine stability, e.g. the Bath Stone mines.

This process is also dependent on the surface tension of the fluid present in the pores but differs from fracture energy reduction in that it takes place prior to increased stress. i.e. wetting the rock produces capillary pressures which work to force the rock framework apart. Burstein, (1968) showed that repeated cycles of wetting and drying have a marked detrimental effect on the strength and elastic properties.

6.2.3 Pore pressure increase

In general all rocks at normal pressures contain a proportion of voids, some of which may be interconnected to form passages through which fluids can penetrate - the effective porosity. Clastic sedimentary rocks are therefore normally considered as a solid framework with a fine network of capillaries composed of pores and cracks; in lower porosity sandstones the voids are normally only grain boundary cracks, (LARC's).

The most familiar effect of pore fluid in rock is to reduce the effective value of the mean normal compressive stress. This effect is usually expressed in terms of the so-called effective stress laws. The concept of effective stress was proposed in 1923 by Terzaghi on experimental grounds and has been subsequently been shown to be sufficiently accurate for engineering purposes, (Skempton, 1960). The basic principle is given by the equation:

$$\sigma = \sigma' + \mu \qquad (6.3)$$

where σ = total stress

σ'= effective stress

μ = pore pressure

The theory was originally proposed for soils but Terzaghi, (1945) later suggested that his definition of effective stress may be incorrect for low porosity materials such as rock, and that the effective stress governing the behaviour of the material should be written:

$$\sigma' = \sigma - (1\text{-}nb)\mu \qquad (6.4)$$

where nb was termed the boundary porosity. Many authors have argued strongly that the original expression is correct for rocks, while others argue equally strongly that it does not apply.

Hoek and Brown, (1982) consider that the original definition is applicable to rock provided that the pore structure of the rock is sufficiently interconnected and the loading rate sufficiently slow to permit internal fluid pressure to equalise during testing. Handin et al, (1963) suggest that in porous rocks such as sandstones, the loading rate required to satisfy effective stress conditions appears to be within the range of normal laboratory testing and that the original definition of effective stress applies. The way in which pore pressure affects failure may be seen from Figure 6.3 for Handin's results on sandstones. Here AB is the experimental Mohr envelope for zero pore pressure. Curve 1 for p=50MPa corresponds to failure with σ_1=540MPa and σ_3=200MPa so that σ_1'=490MPa, σ_3'=150MPa and the Mohr circle is seen to touch AB. Curve II shows the Mohr circle for σ_1=540MPa and σ_3=200MPa with zero pore pressure which is seen to lie within the Mohr envelope. As the pore pressure is increased, this curve is moved to the left until it touches the Mohr envelope and failure can take place.

Obert and Duval, (1967) postulated that the moisture within a rock may be unable to migrate freely, (within the time limit of the test) and hence the pore fluids will be pressurised. They concluded that if the pore fluids are pressurised as the rock is compressed, an outward pressure gradient will be created, so lowering the strength. Szabo, (1966) suggested that if no change in Young's modulus was found between the dry and wet situation, it was unlikely that the pores are being pressurised.

Brace and Martin, (1968) noted an increase in strength (at some constant pore pressure) with increased strain rate. This effect was attributed to increasing porosity (dilatancy) as failure was approached. Consequently, internal pore pressures lagged

behind those measured externally, leading to a strengthening effect.

6.2.4 Frictional reduction

Reduction of the coefficient of friction due to moisture has been studied by a number of workers. Walsh, (1965) developed a theoretical expression relating elastic moduli and the coefficient of sliding cracks. Wiid (1967) applied this relationship to the rocks which he was studying and found little effect on the coefficient of friction with different moisture levels. However if Young's modulus is affected by moisture, then perhaps the coefficient of friction is also affected.

6.2.5 Chemical and physical deterioration

If some of the constituent minerals in a rock change due to either solution or softening in the presence of water, then the overall strength of the rock will decrease. The problem of softening is particularly important if clay minerals are abundant, especially expandable clays. Under normal conditions the constituent minerals of sandstones can be regarded as insoluble (labile constituents are removed during transport). However, solubility can increase with stress as reported by Atkinson, (1979). This process is known as stress corrosion and involves the hydrolysis of strong Si-O-Si bridges at crack tips where proton and electron transfers from the highly polarized water molecules facilitate the reaction. This reduces the periodic activation barrier to crack growth by replacing the strong Si-O-Si bridges by weak hydrogen bonds across the hydrolysed bridge. The reaction has been summarized by Lawn and Wilshaw, (1975) as:

$$(\text{-Si-O-Si-}) + (\text{H-O-H}) = (\text{-Si-OH-HO-Si-})$$

The basic crack tip reaction is illustrated two dimensionally in Figure 6.4. The influence of stress corrosion on crack growth is illustrated in Figure 6.5. As water concentration and/or pressure increases, crack propagation on quartz grains should increase considerably. The stress factor K_I used in Figure 6.5 is suggested to give a measure of the intensity of loading of the crack tip, (Paterson, 1978). K_{IC} is the critical stress intensity factor below which no crack growth can occur. In region 1, the crack velocity is apparently controlled by the rate of stress corrosion reactions at the crack tip. In region 2, the rate of transport of reactive substances to the crack tip is believed to exert overall control on the crack velocity. Crack velocity in region 3 is considered to be controlled by some poorly understood thermally activated process that is comparatively insensitive to the chemical environment. Atkinson, (1979) has suggested that crack velocity is considerably increased in the presence of moisture.

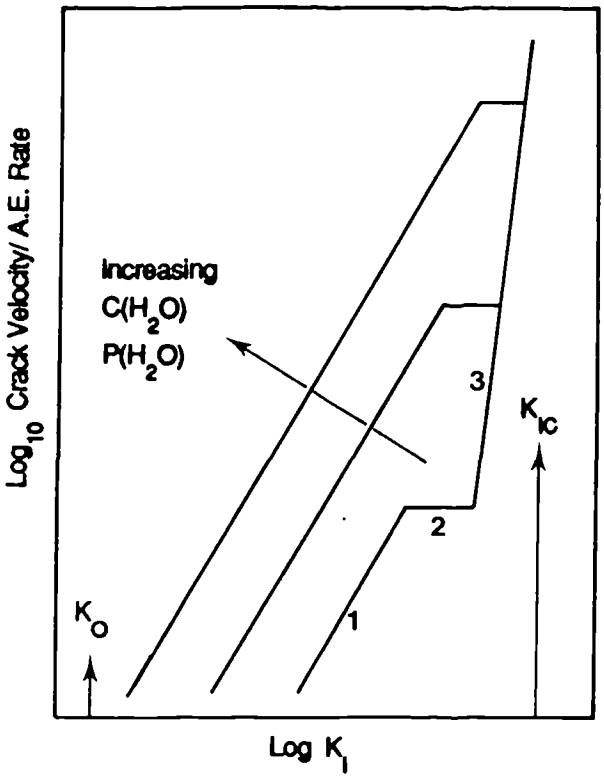

Figure 6.5 Schematic stress intensity factor versus crack velocity curves (Atkinson 1982).

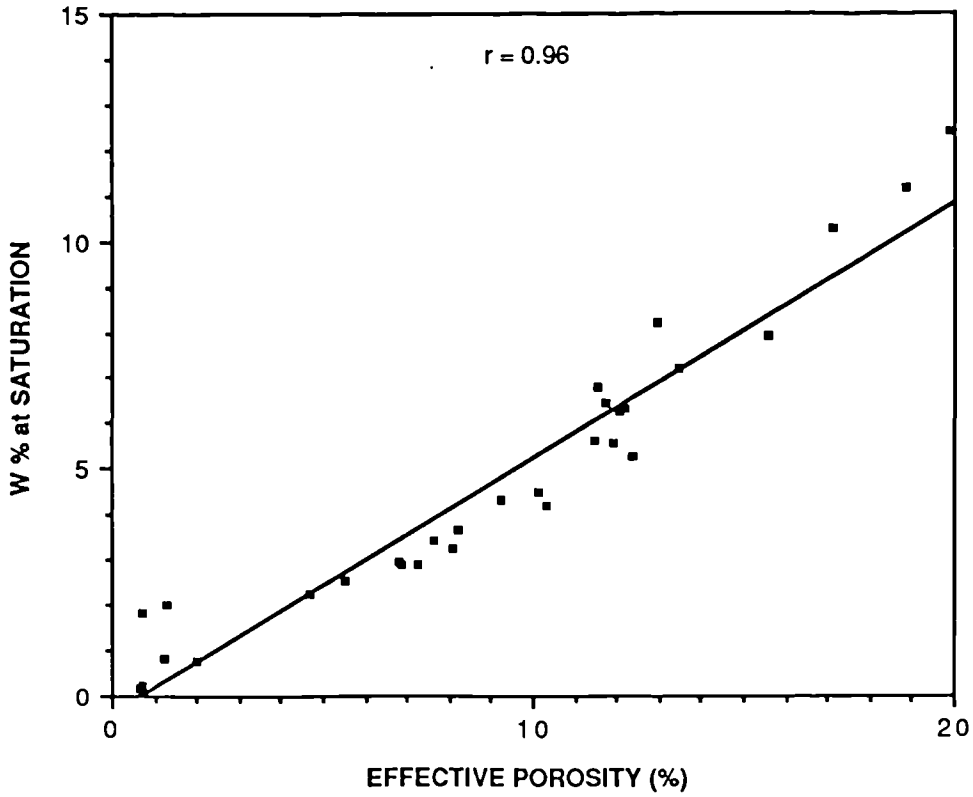

Figure 6.6 Moisture content at saturation versus effective porosity for the sandstones studied.

Dunning et al, (1984) however dispute this process in rocks in normal geological environments since solution at the crack tip has only been shown to occur in the presence of highly acidic and basic environments.

6.3 Experimental procedure

Extensive work was carried out during this research to quantify the strength loss in a number of sandstone types due to changes in moisture content and to attempt to elucidate the processes involved. All of the thirty-five sandstone type specimens prepared from blocks were tested in both completely dry and saturated states. In addition, fifteen of these varieties were tested at intermediate moisture contents to establish the relationship between strength and moisture content for a number of texturally and mineralogically different arenites.

Saturated specimens were obtained using the specially designed pressure cell as described in section 2.3.5. The percentage moisture content by weight at saturation for the different rock types varied depending on the effective porosity. Highest moisture contents were achieved in the Greensand - 26.7%, (38.33% porosity) while the Crackington sandstone contained only 0.75% moisture at saturation, (porosity of 1.97%). Moisture content is plotted against effective porosity in Figure 6.6. As expected, a good relationship exists between the two variables and is given by the equation shown. The reason for the spread of points is that effective porosity is a volumetric measure while moisture content is related to the mass of the specimen.

$$n = \frac{dw \,.\, w\%}{V} \qquad (6.5)$$

where n = effective porosity
dw = dry weight
V = volume
w% = moisture content

The relationship is non-proportional since the dry weight varies between sandstone types due to different grain densities.

Specimens at intermediate moisture contents were obtained by storing in different relative humidity conditions as described in Chapter 4. In certain low to intermediate porosity sandstones, moisture contents just below the saturation value could not be achieved using saturated solution techniques. In these cases samples were first saturated and subsequently allowed to lose moisture at a slow rate in a high

relative humidity environment. When the desired degree of wetting was achieved, the specimens were tested and monitored for stress and strain in the normal way.

As discussed earlier, a number of theories have been proposed relating to the chemical effects of water on the rock framework cement. In order to test these theories, specimens of a number of sandstone types were tested after soaking in fluids of different chemical properties to those of water. The chemicals used and their respective relevant properties are listed in Table 6.1. Saturation of specimens with these chemicals was achieved in the normal way using the pressure cell. When using liquids with a low boiling point such as methanol it was necessary to prevent moisture loss by coating the specimen sides with cling film and testing as quickly as was practical. For example, methanol, which has a boiling point of 65°C was found to evaporate from a saturated specimen of Pennant Sandstone at a rate of 0.4g per minute.

In order to test the effects of pore water pressure on the strength of sandstones it was decided to determine whether pore pressures occur on a microscopic scale in uniaxial testing to a large enough degree to influence failure strength. Constant pore pressure apparatus was used in an attempt to measure pore pressures within saturated core specimens. The apparatus was connected to the centre of the core specimens by means of special inserts as shown in Figure 6.7. These inserts were machined from brass to an external diameter of 4mm with a 1.5mm internal conduit. These were inserted into a 6mm diameter hole drilled a distance of 31.5mm into the rock specimen at mid-height. The tube was not fully inserted into the hole so that a void was left at the centre of the specimen measuring 4mm long by 6mm diameter, to allow the measurement of fluid pressure within a number of pores. The inserts were sealed into the sandstones using an elastic epoxy resin to reduce their influence during the deformation process. The resin was also chosen on the basis of its viscosity - a non-viscous glue would tend to impregnate many of the pores and hence invalidate pore pressure readings. Care was taken not to allow resin to reach the void at the centre of the specimen. When the resin had hardened, the samples were saturated.

A number of preliminary tests indicated that the apparatus was not sensitive enough to detect the small pore pressures, if any, which formed within the rock. It was decided to develop an inexpensive semi-quantitative manometer for the detection of these small pore pressures. The apparatus was manufactured by a glass blower in the University and is shown in Figure 6.8. It consists of a capillary u-tube with a 0.2mm internal diameter and a valve for de-airing the system. A bead of mercury was placed in the tube and changes in pore pressure were indicated by displacement of the mercury along the capillary. The manometer was connected to the inserts using transparent tube as shown in Plate 6.1. The non-quantitative nature of this apparatus was fully

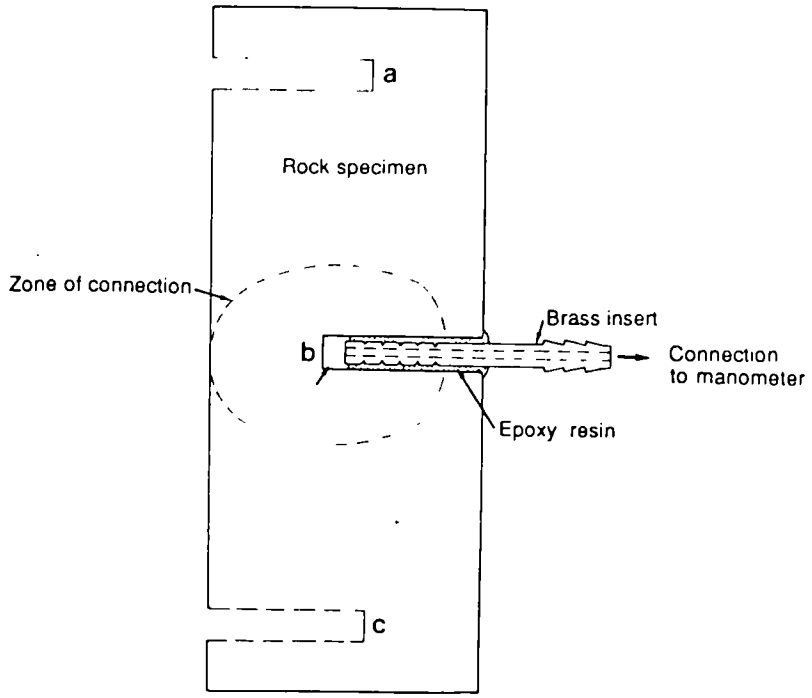

Figure 6.7 Cross-section through sandstone specimen showing pore pressure insert and positions of additional inserts.

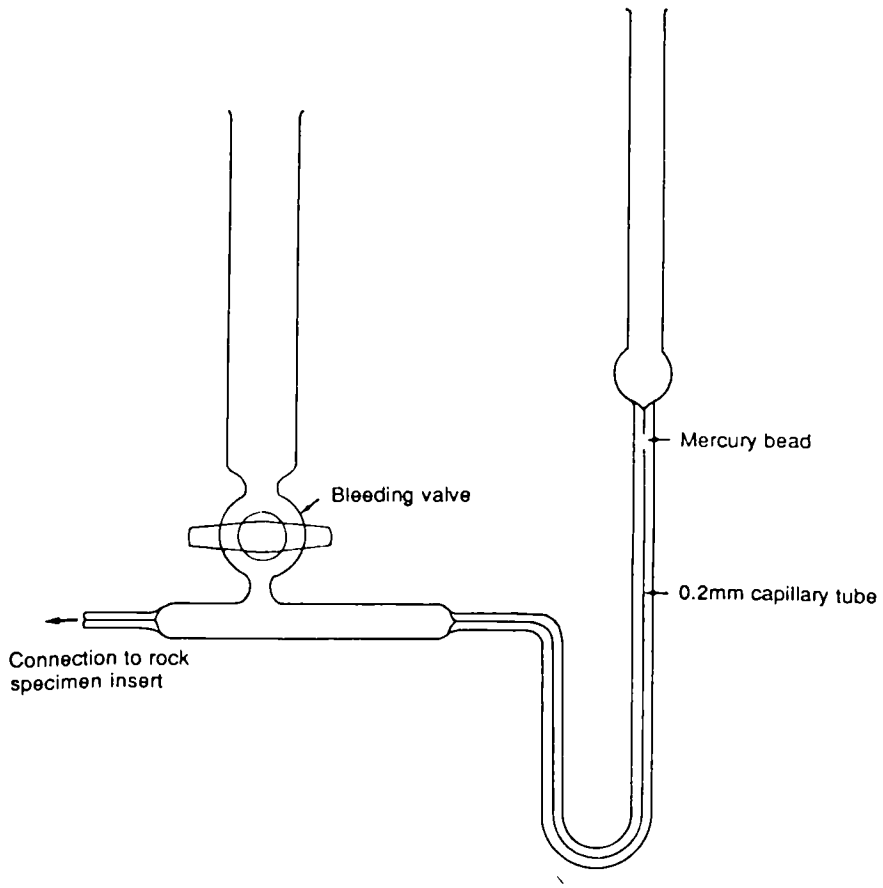

Figure 6.8 Manometer used for pore pressure monitoring. (apparatus is 200mm tall).

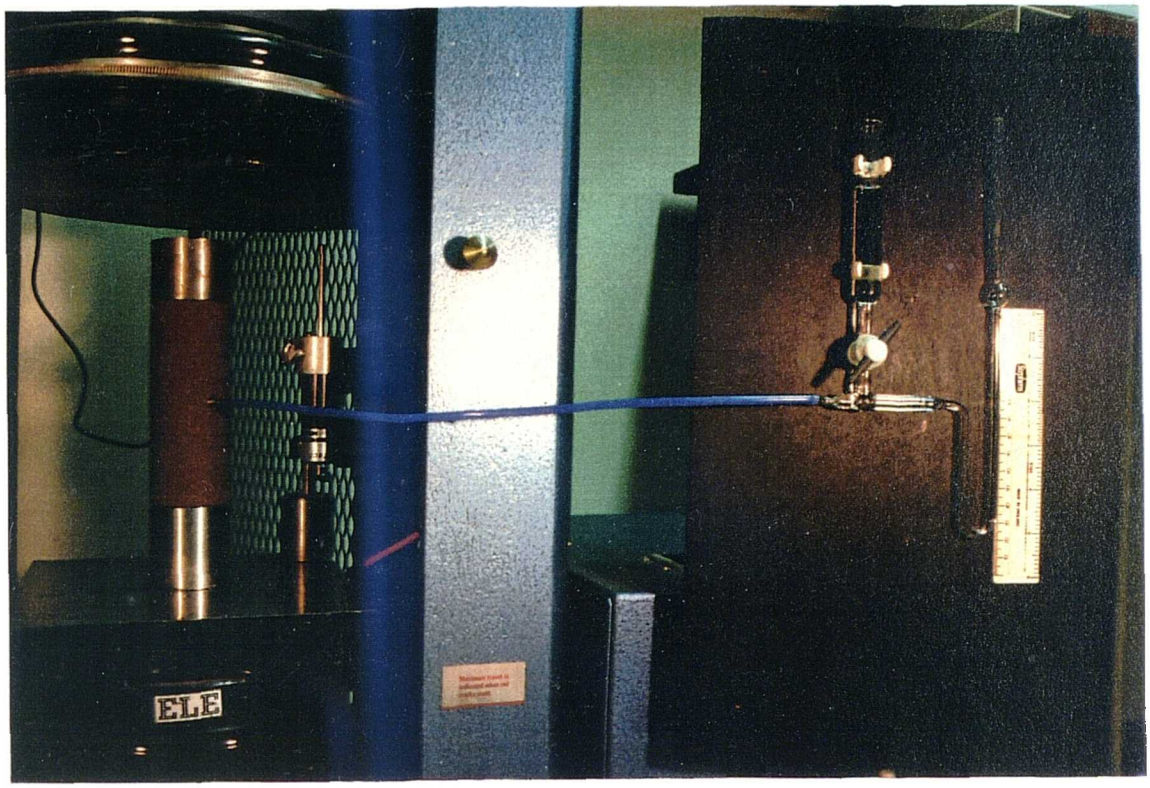

Plate 6.1 Manometer connected to rock specimen prior to testing.

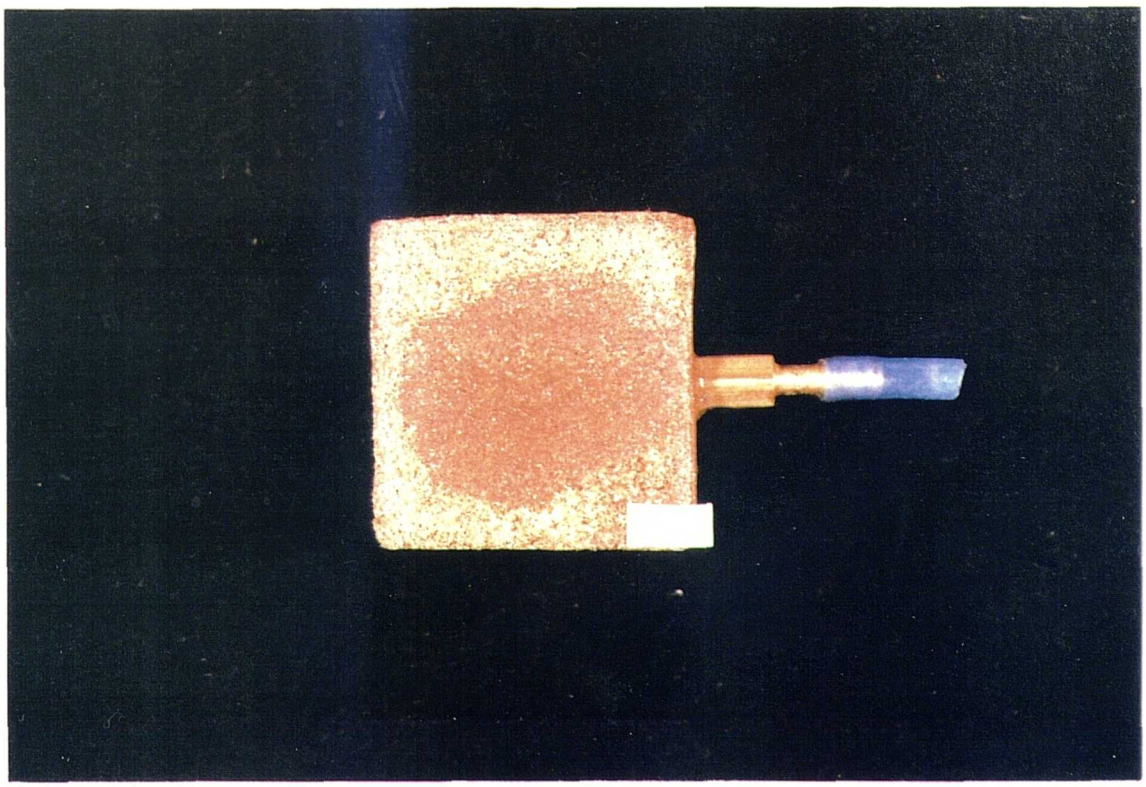

Plate 6.2 Zone of interconnection of pores shown by epoxy impregnation indicating large volume of influence for pore pressure measurement.

	pH	Density	Surface tension
Water	7.0	1.000	72.75 at 18°C
HCL (0.1N)	1.1	1.097	72.55 at 18°C
H2SO4 (0.1N)	1.2	1.066	72.21 at 18°C
Carbonic Acid	3.8	1.021	73.18 at 18°C
H2S (0.1N)	4.1	1.539	72.58 at 18°C
CaCO3 (sat)	9.4	1.217	73.45 at 18°C
NaCl (sat)	6.5	1.025	82.55 at 18°C
Ammonia solution	10.5	1.092	71.65 at 18°C
Methanol	6.8	0.791	22.61 at 20°C
NaNO3	7.9	1.239	87.05 at 20°C
n-Hexane	3.3	0.660	18.43 at 20°C

Table 6.1 Some chemical and physical properties of the liquids used for saturation of sandstone specimens.

appreciated since accurate pore pressure measurements require a closed system. It was considered however that the manometer would give a semi-quantitative indication of the pressures forming within the rock during uniaxial loading. Calibration of the apparatus showed that a displacement of the mercury by 5.70mm represented a pore pressure change of approximately $1kN/m^2$.

In addition to these single tests, a number were carried out using two other identical manometers connected to the rock specimens near the top and bottom at positions (a) and (c) as shown in Figure 6.7.

The sandstones which were tested in these experiments were Crackington sandstone, three varieties of the Penrith Sandstone and the two varieties of the Greensand. These were chosen from the range of sandstones to represent strong, intermediate and weak varieties.

6.4 Results and discussion.

6.4.1 Effects of moisture content on strength

In most cases a substantial decrease in uniaxial compressive strength occurred on saturation. Average dry strengths, average strengths at saturation and degree of strength loss are listed for each sandstone in Table 6.2. Maximum loss of strength was observed in the Greensand, (77.8% of original dry strength) while the minimum value of 8.1% reduction occurred in the Siliceous Sandstone from Bristol. In the Ashdown Sandstone the uniaxial compressive strength actually increased on saturation by an average of 5.7% from the dry state. This was the only sandstone variety tested which showed an increase in strength from the dry state. The great degree of variation in the change of strength on wetting indicates that the strength reduction processes involved are different from one sandstone variety to another. The predominances of these processes must be controlled by the mineralogy and texture of the rock in which they take place. For example the presence of abundant clay minerals may lead to softening and possible expansion of the rock framework.

In order to examine the controlling factors on the degree of moisture content related strength reduction, (MCRSR) it is desirable to attempt to correlate certain textural and mineralogical parameters with the degree of strength loss. Figure 6.9 shows the relationship between effective porosity and strength loss. The relationship is poor but an approximate trend exists, indicating that the higher the porosity, the greater is the loss in strength. The strength loss could however occur in higher porosity sandstones due either to an increased pore pressure or due to a greater total area of contact between water and grains or cement which would allow a chemical process to be more effective. It is clear that porosity is an indirect control on the degree of strength loss since it provides access for fluids to reach the rock framework and cements. Of the five theories described above it is possible that a number are occurring simultaneously, to varying degrees in different sandstones.

The stresses at failure are plotted against moisture content for each sandstone which was tested at intermediate moisture values between dry and saturated, Figures 6.10(a) to (o). The single points at zero moisture content represent the average of a number of tests on dry specimens. As can be seen, the decrease in uniaxial compressive strength from dry to fully saturated is not a gradual one. The plots generally show a sharp loss in strength at low moisture contents followed by a decreased rate of strength loss at higher moisture contents. In the majority of cases, most of the strength loss occurs during the increase from zero to 1.0% moisture content with only 5 to 10% of the compressive strength reduction occurring with an increase of moisture above 1%. The major exception to this general rule is the

Sandstone Type	Av. Dry Strength (MPa)	Av. Sat. Strength (MPa)	Loss (MPa)	(%)
1. Applecross A	141.32	99.28	42.04	29.7
2. Donegal Quartzite DQ	237.86	183.97	53.89	22.7
3. Basal Quartzite BQ	247.00	202.05	44.95	18.2
4. Brownstones LORS	152.03	107.35	44.68	29.4
5. Pilton (Type A) PiA	173.28	152.19	21.09	12.2
6. Pilton (Type B) PiB	227.29	208.40	18.89	8.3
7. Upper Cromhall UCS	161.37	143.92	17.45	10.8
8. Millstone Grit (Type A) MGA	59.33	39.61	19.72	33.2
9. Millstone Grit (Type B) MGB	49.03	40.15	8.88	18.1
10. Millstone Grit (Type C) MGC	123.36	72.05	51.31	71.2
11. Millstone Grit (Type D) MGD	127.50	98.58	29.92	23.5
12. Holcombe Brook Grit HBGA	119.08	49.03	70.05	58.9
13. Holcombe Brook Grit HBGB	108.06	48.63	59.43	55.0
14. Siliceous Sandstone SS	198.36	182.23	16.13	8.1
15. Elland Flags EF	59.94	31.40	28.54	47.6
16. Thornhill Rock (Type A) TRA	89.94	38.42	51.52	57.3
17. Thornhill Rock (Type B) TRB	91.84	46.68	45.16	49.2
18. Middle Coal Measures MCM	37.08	25.31	11.77	31.7
19. Crackington Formation CF	298.18	232.25	64.03	21.6
20. Pennant (TypeB) PnA	114.18	50.03	64.15	56.2
21. Pennant (Type B) PnB	106.15	52.64	53.51	50.4
22. Pennant (Type C) PnC	103.38	47.04	56.34	54.5
23. Pennant (Type D) PnD	121.00	-	-	-
24. Annan Sandstone An	66.28	43.57	22.71	34.3
25. Penrith (Type A) PrA	65.96	53.14	12.82	19.4
26. Penrith (Type B) PrB	34.77	29.39	5.38	15.5
27. Penrith (Type C) PrC	81.99	72.75	9.24	11.3
28. Penrith (Type D) PrD	101.16	87.90	13.26	13.1
29. Penrith (Type E) PrE	59.72	40.77	18.95	31.7
30. Redcliffe R	36.05	22.43	13.62	17.3
31. St. Bees StB	49.31	-	-	-
32. Midford Sands MS	23.20	14.58	8.62	37.2
33. Ardingly Sandstone (Type A) ArdA	42.15	36.90	5.25	12.5
34. Ardingly Sandstone (Type B) ArdB	53.35	47.57	5.78	10.8
35. Ashdown Sands AS	30.58	32.31	-1.73	-5.7
36. Greensand (Type A) G	10.45	2.32	8.13	77.8
37. Greensand (Type B - Dogger) D	74.51	46.66	27.85	37.4

Table 6.2 Dry and saturated strength values and degree moisture content related strength reduction.

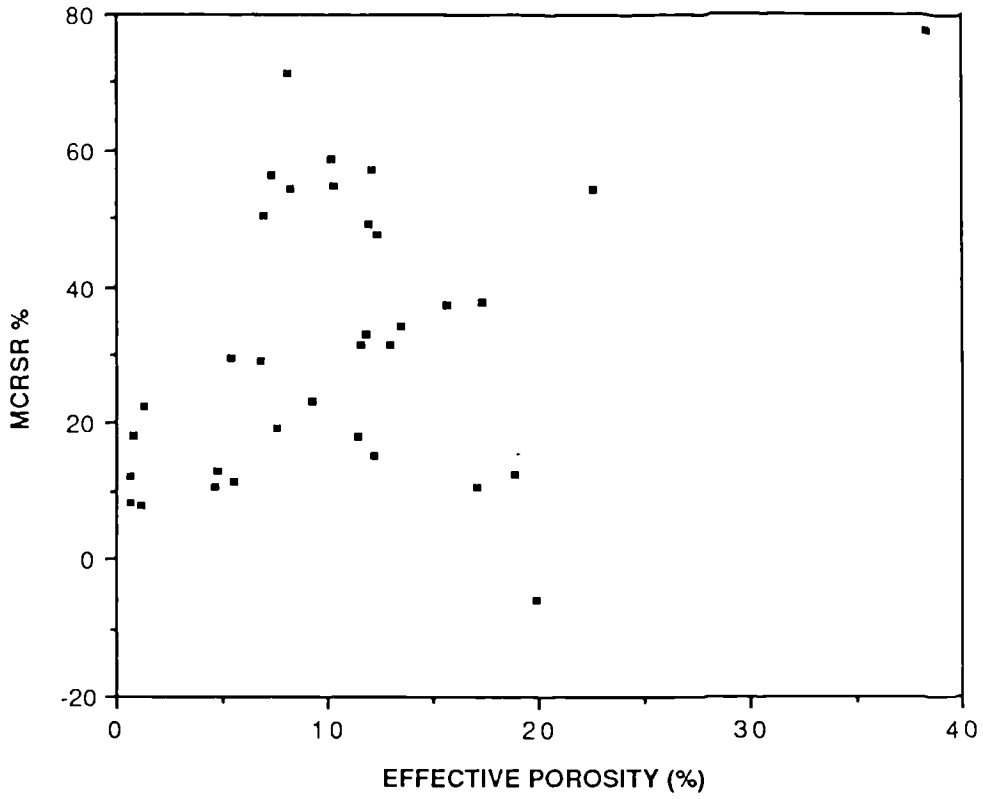

Figure 6.9 MCRSR% versus effective porosity (n).

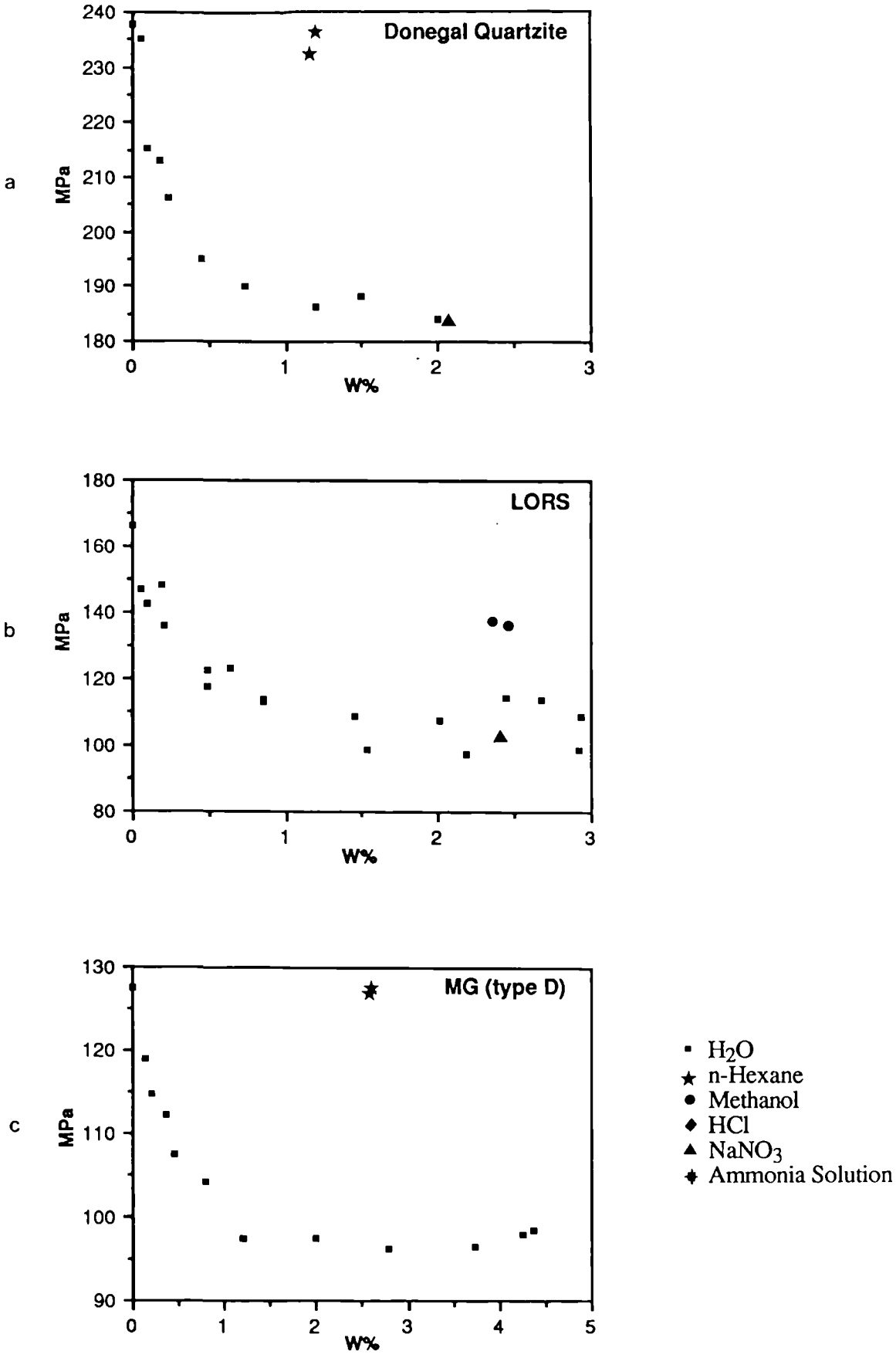

Figure 6.10 - Various plots of UCS versus moisture content for different sandstones.

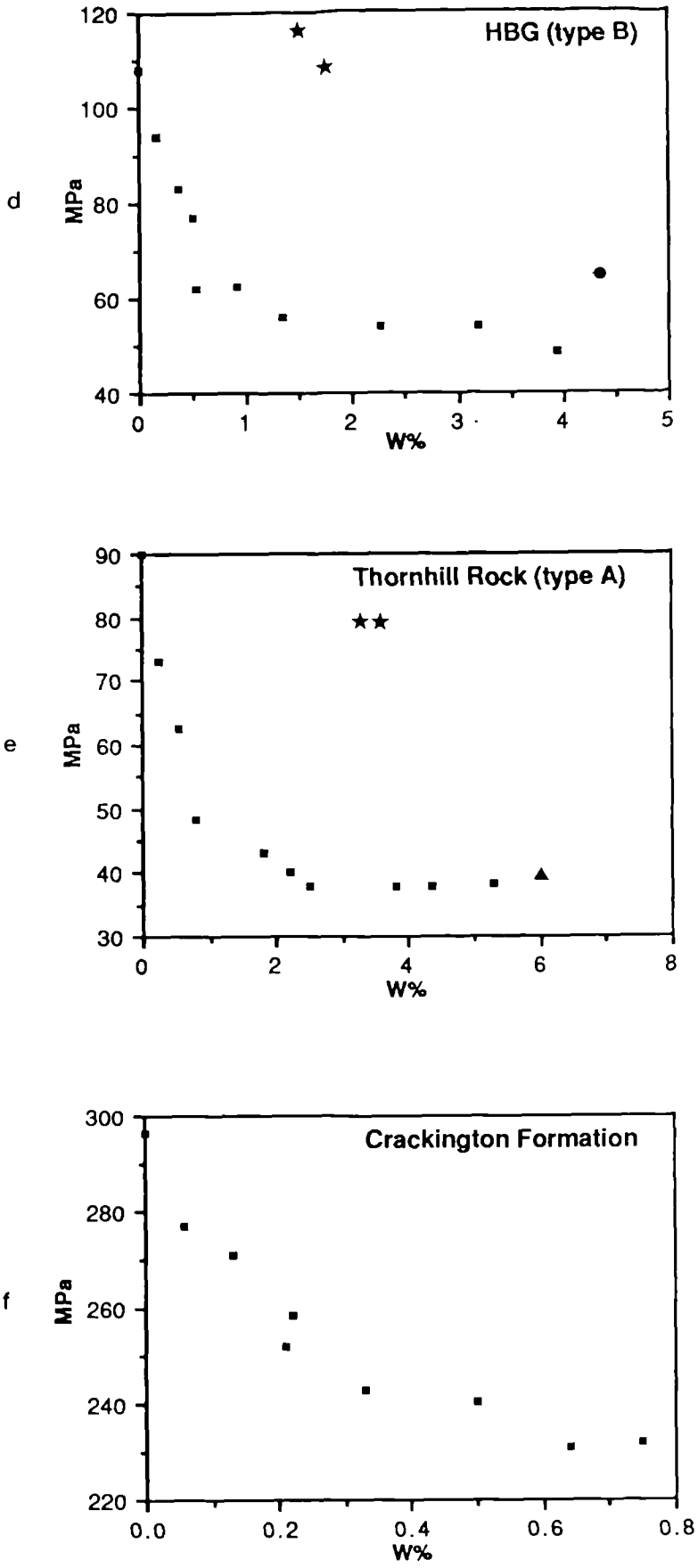

Figure 6.10 - Various plots of UCS versus moisture content for different sandstones.

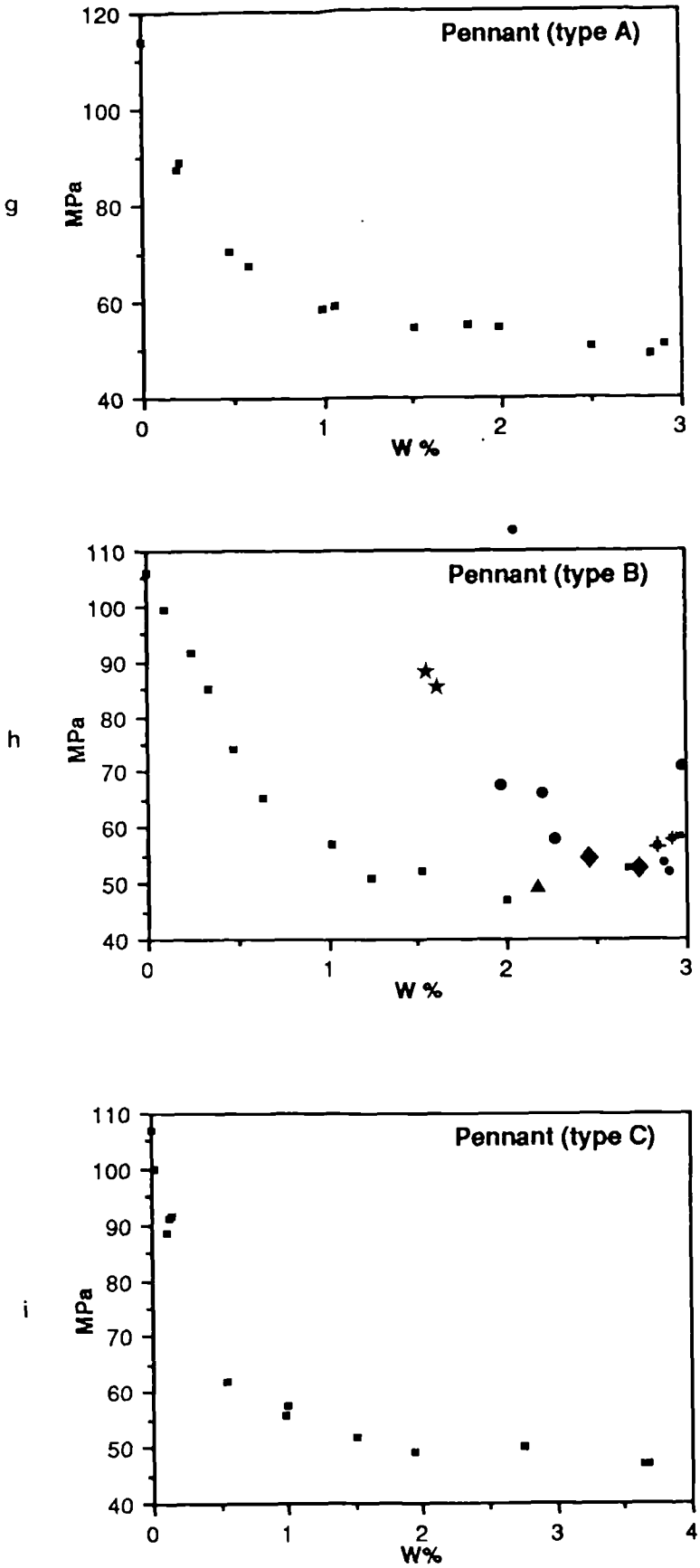

Figure 6.10 - Various plots of UCS versus moisture content for different sandstones.

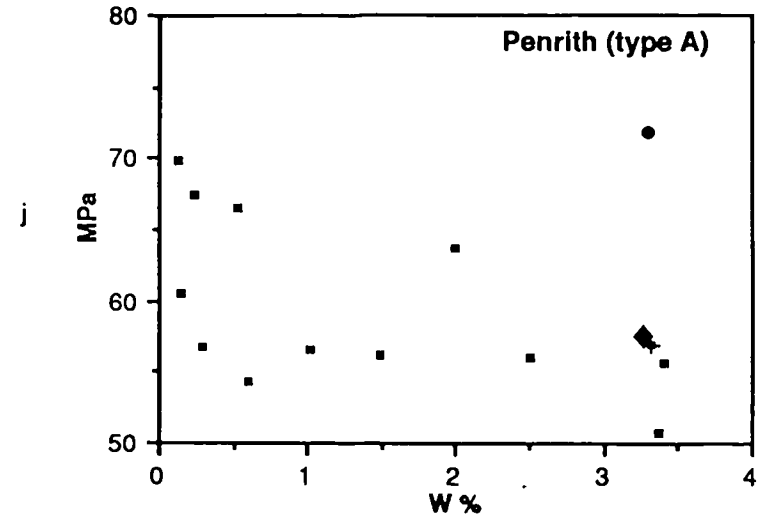

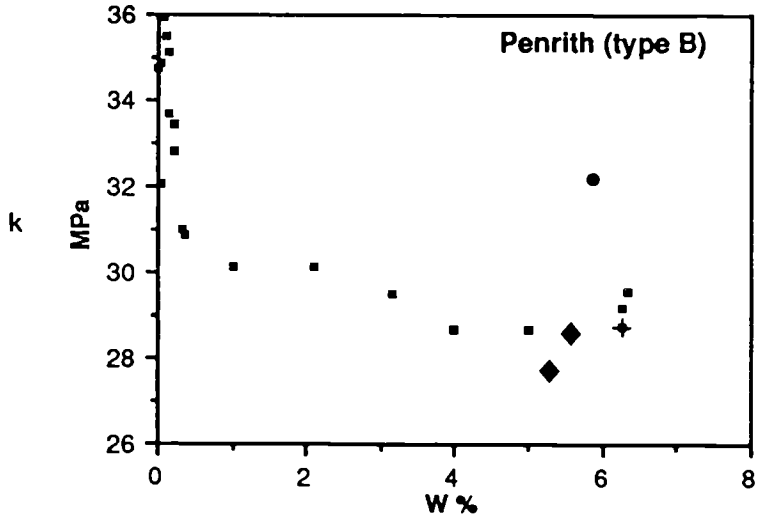

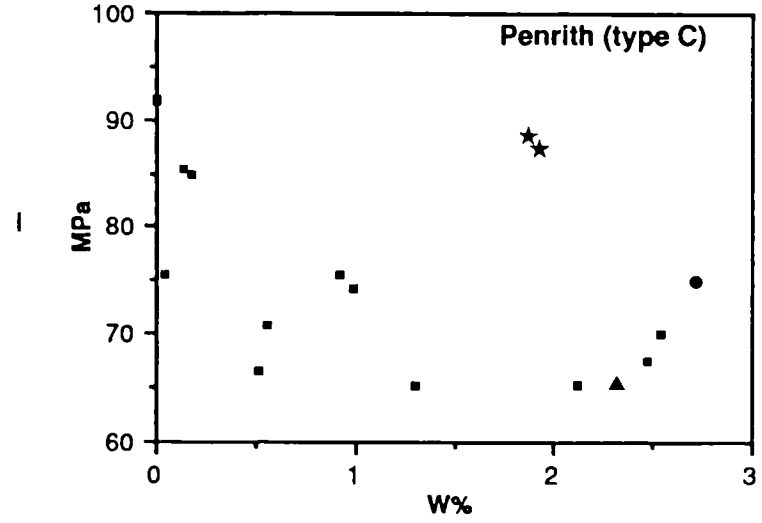

Figure 6.10 - Various plots of UCS versus moisture content for different sandstones.

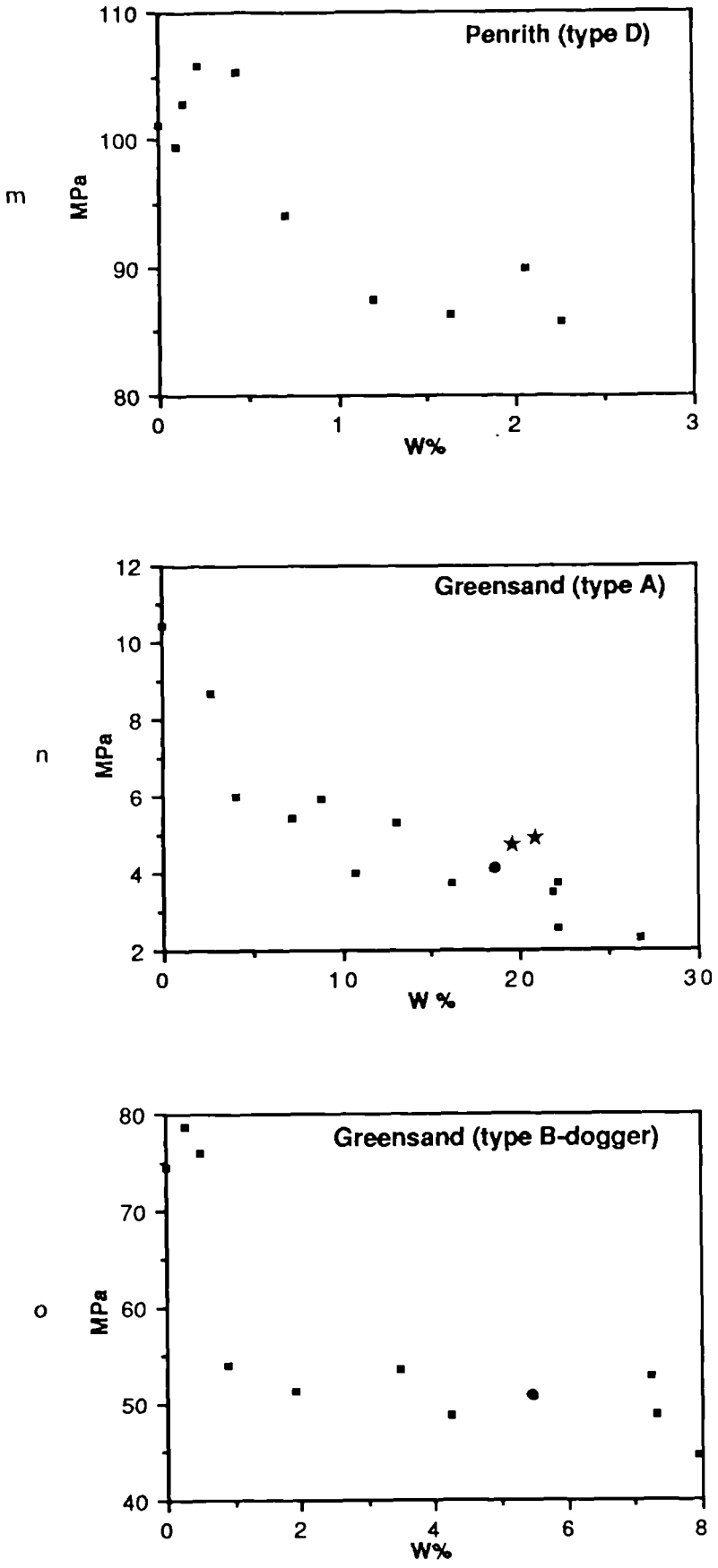

Figure 6.10 - Various plots of UCS versus moisture content for different sandstones.

Greensand where the bulk of the MCRSR has occurred by 15% moisture content. Since porosity (and density) are variable between sandstone types, the estimated moisture content at which the bulk of the strength loss has occurred can be expressed as a percentage of the moisture content at saturation. From the data presented in Table 6.3 it can be shown that 80-90% of the MCRSR occurs by an average of 31.2% of the moisture content at saturation.

Sandstone	Moisture Content %	% of moisture content at saturation
DQ	0.5	25
LORS	1.0	33
MGD	1.0	22
HBGB	1.0	25
TRA	1.5	28
CF	0.4	53
PnA	0.75	25
PnB	0.8	30
PnC	1.0	27
PrA	1.0	29
PrB	2.0	33
PrC	0.75	29
PrD	1.0	43
G	15.0	53
D	1.0	12.5

Table 6.3 Strength vs. w% inflexion points expressed as moisture contents and as percentages of saturation moisture contents.

These results agree approximately with those of Priest and Selvakumar, (1982) and less closely with those of Burstein, (1968). The relatively sudden decrease in strength at low moisture content values, (well before saturation) indicates that pore pressure is not a major controlling factor.

Priest and Selvakumar stated that...

> "If the pore pressure build-up is the main cause of strength reduction due to moisture increase, then one might expect a gradual decrease in strength until it reaches a minimum at the fully saturated moisture state....."

The results of this research indicate that the majority of the MCRSR occurs when the pores and microcavities within the rock are only partially filled with water.

Since the remainder of the pore space would be filled with air, which can be regarded essentially as infinitely compressible, it is highly unlikely that significant pore pressures develop and cause loss in strength.

When the pores are completely filled, i.e. at saturation, one might expect a significant decrease in strength if the theory of Obert and Duval (1967) were valid. This is not the case; many of the sandstones show slight increases in the expected strength values at saturation - examples are LORS, MGD PnB and two varieties of the Penrith Sandstone. This would indicate that in some cases, at total saturation, pore pressures develop which reduce the stress on the rock framework, obeying Terzaghi's equation and give the rock an apparently higher strength.

Below total saturation: σ_c at failure = σ_c on framework

At saturation: σ_c at failure = (σ_1 on framework) + pore pressure

This is supported by the results of the pore pressure tests which are presented in Figure 6.11. As shown, the pore pressure results are plotted using the same stress axis as the axial stress-strain curves. Of the six tests carried out, one sandstone type, (the strongest) did not develop positive pore pressure during loading, while the others showed only very small increases in pore pressure. Following the tests, low viscosity epoxy resin was injected into the inserts under low pressure to examine the zone of connection over which pore pressure had been measured. Plate 6.2 shows a sample of Penrith sandstone (type C). The ellipsoid of connection with its long axis parallel to bedding is shown by the impregnation which indicates that any pore pressures measured were created by the deformation of a large number of pores.

The maximum value recorded was 1.32kN/m^2 which occurred in the Greensand indicating a high degree of pore closure and collapse as suggested in Chapter 5. The other sandstones showed values ranging from 0.08kN/m^2 to 0.7kN/m^2. In most cases, slightly higher pore pressures were recorded in the end zones indicating a higher degree of compression in these areas. This supports the stress distribution model proposed by Bordia, (1971) who states that the end cones are zones of compression while the centre of the specimens is a zone of tension.

In all the pore pressure tests, relatively high negative pore pressures, (vacuums) were recorded towards specimen failure. When plotted with the σ-ε curves as in Figure 6.11 it is clear that the pore pressure curves change from +ve to -ve gradients at stresses close to or at the yield point. This can be attributed to the formation of microfractures and subsequent dilation of the rock. The highest -ve pore

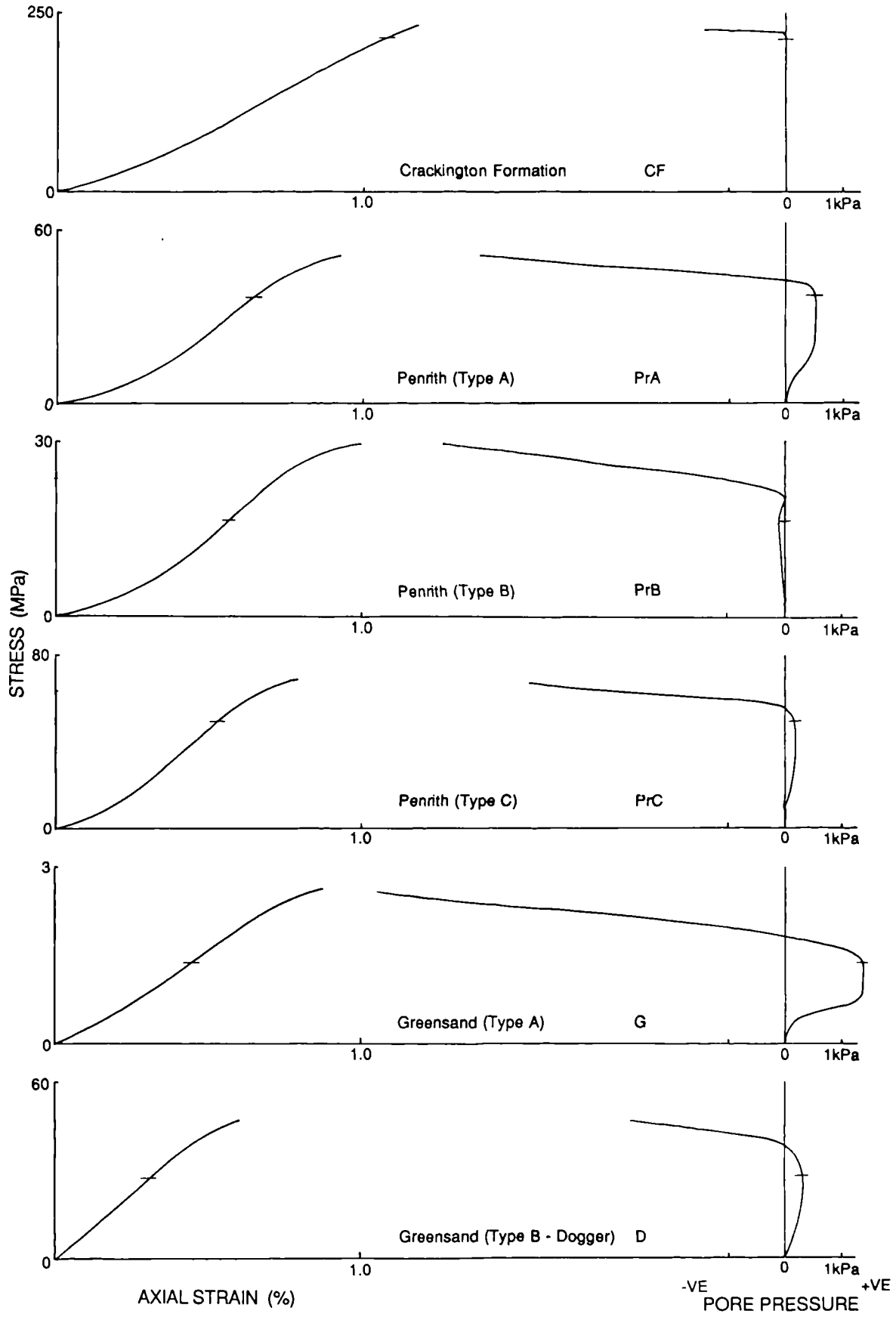

Figure 6.11 Results of pore pressure tests on various sandstones.

pressures were detected in the central area of the specimen.

The effect of the small +ve pore pressure is relatively insignificant, generally only causing a slight increase in strength at complete saturation in some sandstones. It can be concluded that minor pore pressure increases will occur only in sandstones with a sufficiently high porosity for water storage but of low to intermediate permeability to prevent dissipation within the duration of the test. The result is a slight strengthening of the rock rather than a weakening effect.

Handin et al , (1963) have illustrated that pore pressure significantly influences rock strength in triaxial testing. Their tests however introduce high pore pressures which are produced externally and not by the rock specimen itself. This means that these high pore pressures reduce the values of σ_1, σ_2 and σ_3 such that:

$$\sigma'_1 = \sigma_1 - p, \quad \sigma'_2 = \sigma_2 - p \quad \text{and} \quad \sigma'_3 = \sigma_3 - p$$

Since σ_2 and σ_3 are much smaller than σ_1, they are lowered by a disproportionate amount. The result is that the effective confining stress is markedly reduced and fracturing is promoted. (The Mohr circle meets the failure envelope as shown in Figure 6.3).

In uniaxial testing where a significant MCRSR occurs, the rock specimen itself does not create high pore pressures. If high pore pressures were developed by pore and cavity closure, then σ_2/σ_3, (equal to zero) would be reduced, resulting in tensile stresses, and hydraulic fracturing would occur. This research has shown that negligible pore pressures develop in uniaxial tesing and it can be concluded that the observed MCRSR is due to factors other than pore pressure.

The plots of uniaxial compressive strength against w% shown in Figure 6.10(a-o), show definite trends which can be summarised by best-fit experimental curves. A more useful representation however, is a mathematical best-fit applied to each data set. A number of curve fits were attempted and it was found that the relationships are best described by a negative exponential function of the form:

$$\sigma_c = ae^{-bw} + c \qquad (6.6)$$

where σ_c = uniaxial compressive strength (MPa)

w = moisture content (%)

a,b,c = constants

As defined by Priest and Selvakumar, (1982), the strength at zero moisture content is given by (a+c). The strength at saturation is given by c, and the parameter b is a dimensionless constant that defines the rate of strength loss with increasing

moisture content.

The constants a,b and c and the correlation coefficients, r, obtained for each sandstone type are listed in Table 6.4.

Sandstone	a	b	c	r-value
DQ	39.03	1.9601	184.23	0.93
LORS	29.34	0.7646	105.23	0.78
MGD	12.30	0.6821	96.27	0.71
HBGB	36.13	0.7794	48.65	0.88
TRA	45.73	1.5942	40.29	0.97
CF	84.01	6.4167	230.98	0.91
PnA	83.76	0.2306	51.02	0.86
PnB	28.81	0.5506	49.37	0.62
PnC	47.12	1.5439	47.65	0.95
PrA	7.0562	0.0752	56.3	0.70
PrB	4.1604	0.4061	28.90	0.87
PrC	17.271	1.0675	67.75	0.85
PrD	20.37	1.2629	87.29	0.88
G	6.1386	0.1104	2.97	0.93
D	19.12	0.2567	45.79	0.77

Table 6.4 Numerical values of constants a,b and c and respective r-values for best-fit exponential equations.

The correspondence between the empirical and experimental curves will not be exact but the equations give an idealised mathematical relation which could be used for prediction. All the r-values for the models are greater than 0.62 with the majority of curve fits showing r-values in excess of 0.85. (All are greater than 0.6 as suggested by Judd, (1971) to show a reasonable correlation in rock mechanics). The scatter graphs for Penrith (type D) and Greensand (type B) show slight increases in strength from the dry state at low moisture contents, in the region of 0.2%. Barton, (1974) observed such a phenomenon in weak sandstones and attributed it to the moisture content reaching an optimum for 'stress-induced' cohesion. No explanations for this limited phenomenon became apparent during this research.

Superimposed on the plots of strength vs moisture content (Figure 6.10) are a number of points representing specimens saturated in the other chemicals. As can be seen, there is a slight disparity between the aqueous solutions and the specimens saturated in water. The most interesting result however, is that samples tested in

methanol do not show the same degree of strength loss.

Of the five hypotheses outlined in Section 6.2, a number can be tentatively discounted from the evidence seen so far. Pore pressures do not appear to play a significant role in strength reduction. It is unlikely that methanol will be subjected to different pore pressures from those of water if pore closure and confinement take place; therefore the change in strength for saturation in methanol is not related to a change in pore pressure.

It is considered that frictional reduction, (hypothesis No.4) is controlled on a microscopic scale by the ease of fracturing of framework grains or cement/matrix. Thus any change in the coefficient of friction is a modification subsequent to fracture energy reduction or chemical/physical deterioration.

This essentially narrows the important processes down to three:

1. fracture energy reduction
2. capillary tension decrease
3. chemical and physical deterioration

With reference to process three, chemical deterioration will take place in the presence of chemically aggressive fluids. Work on weathering by Mason, (1966) has shown that most silicate minerals are essentially insoluble except at high pHs. Figure 6.12 demonstrates that only at pH values of greater than 10 does the solubility of quartz increase markedly. During this research, samples were placed in ammonia solution, (pH 11) for in excess of one month and subsequently pressurised; these samples did not show a substantial decrease in strength compared to those saturated in water, Figure 6.10(h), (j) and (k). In addition, low pH solutions such as HCl and H_2SO_4 do not have marked effect on strength except in sandstones which contain abundant calcite cement or carbonate rock fragments, the degree of the effect being time dependant. Ollier, (1984) states that the solubility of iron is 100,000 times greater at pH 6 than at pH 8.5. Even in the iron-rich Pennant varieties however, there is no indication of strength reduction in the lower pH solutions - in many cases the reverse is true.

It is likely that low and high pHs will affect rock strength if they are allowed to act over a sufficiently long time. The research has shown however that such solutions do not have an effect on the apparently instantaneous loss of strength observed in water saturated samples. It can be concluded that chemical dissolution of sandstone constituents prior to deformation is not an important process in MCRSR.

The other possibility is the physical, as opposed to chemical deterioration of sandstone constituents - the main type being clay minerals. The physical softening of clay minerals by the uptake of absorbed and interlattice water is well documented, e.g.

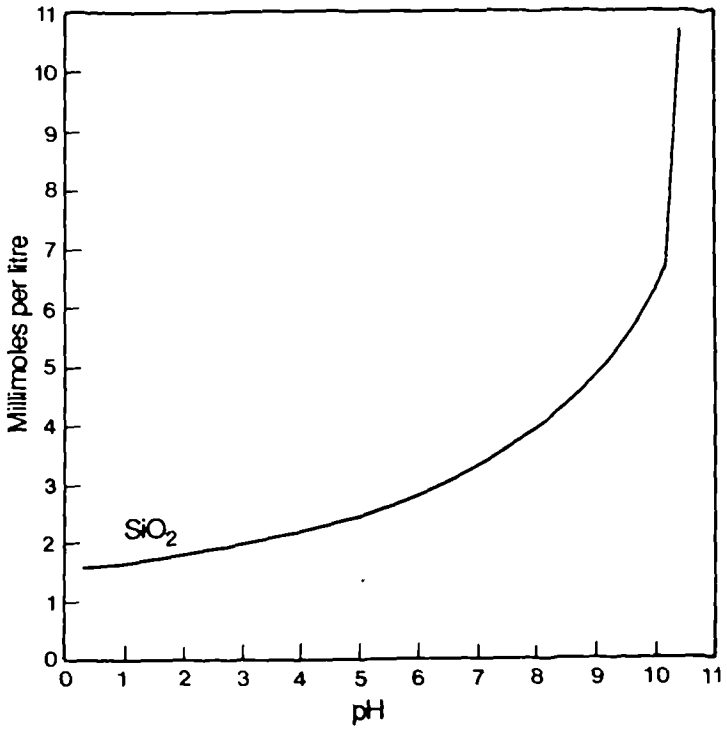

Figure 6.12 The solubility of silica and alumina as a function of pH (from: Mason, 1966).

Skempton and Northey, (1952). It is considered that the process will take place in porous rocks which contain a significant proportion of clay minerals or soft sedimentary rock fragments. Using the point counting data presented in Chapter 3, clay content is plotted against MCRSR in Figure 6.13(a). The correlation between the two variables is poor but a definite trend exists; hence clay content does have a significant effect on the MCRSR.

Figure 6.13(b) and (c) show MCRSR plotted against clays + phyllitic rock fragments, (PRF's) and clays + phyllitic rock fragments + sedimentary rock fragments, (SRF's). For these plots the total contents of PRF's and SRF's were not used but an estimate of the 'active' clay ingredient of these grains; 20% and 10% respectively. The correlation coefficients show marked improvement when the PRF's and SRF's are included in the clay content values.

This reinforces the theory that clays play a significant role in MCRSR but it underlines the fact that softening of clay minerals is not the only process involved. This is evident in sandstones which contain little or no clays or SRF's such as quartzites but show substantial decrease in strength on wetting.

A control experiment was carried out to ensure that the low sensitivity of sandstones to methanol saturation was not due to an effect on the clay softening process, i.e if methanol does not cause the same softening effect as water, then this would explain the higher uniaxial compressive strength on saturation with low surface tension liquids. Plastic limit Atterberg tests, (BS 1377, 1975) were carried out on two samples of the same clay using water and methanol. The respective 'moisture contents' for the two liquids at the same degree of softening were 48.75% (water) and 38.8% (methanol). Recalculation of these values as volumes, (to account for the low density of methanol) demonstrated that the degree of softening for the two liqiuds is practically identical.

With respect to fracture energy reduction and capillary tension decrease, it has been suggested that these processes are controlled by the high surface tension of water (75 dynes/cm). The results obtained by saturation in methanol which has a surface tension of only 22.61 dynes/cm, indicate that one or both of these processes are involved. It is considered unlikely that the low density of methanol would affect the related strength reduction. If either or both of the theories involving fracture energy reduction or capillary tension are valid then it is the low surface tension of methanol which causes the higher strengths. To test this supposition, a number of sandstones were tested in two additional chemicals, n-hexane and sodium nitrate solution. These were chosen for their respective low and high surface tension values in contact with air. n-Hexane has a surface tension of 18.43d/cm at 20°C which would be expected to give a low strength loss, while 47% $NaNO_3$ solution has a surface tension of

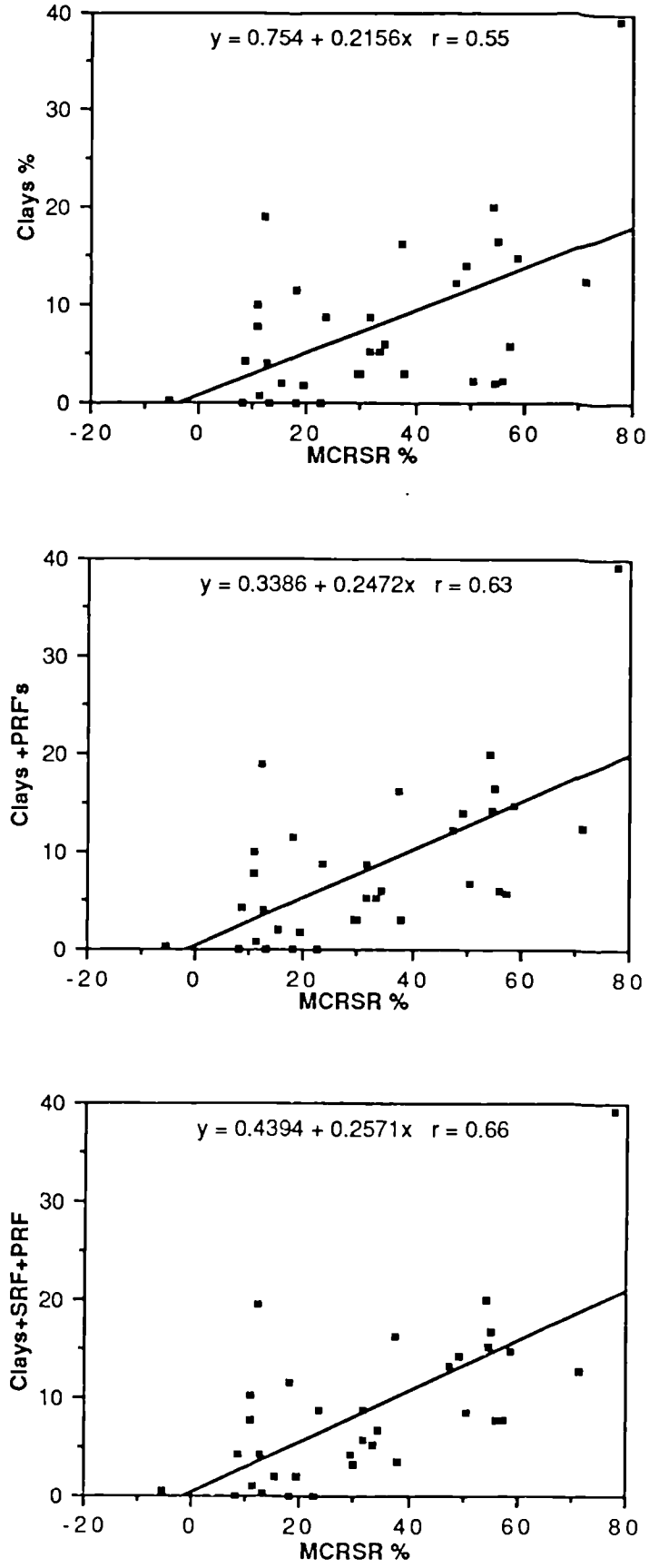

Figure 6.13 a) Clay content versus MCRSR.
b) Clays and Phyllitic RF's versus MCRSR.
c) Clays and PRF's and SRF's versus MCRSR.

87.05d/cm. This extremely high surface tension should give a greater strength loss than when saturated in water. These tests were carried out on Donegal Quartzite, Millstone Grit (type D), Holcombe Brook Grit (type B), Thornhill Rock (type A), Pennant (type B) and Penrith (typeC); the results are included in Figure 6.10.

Saturation in $NaNO_3$ gave low strength values but in the majority of cases did not give values below those obtained by saturation with water. Saturation of specimens with n-hexane however, produced high strength values. In a number of cases the values achieved were similar to, or slightly greater than those measured in completely dry tests. In sandstones which contain high percentages of clay minerals n-hexane did not produce high strength values (i.e. comparable to dry tests).

6.4.2 Effects of moisture on elasticity of deformation

Average tangent and secant Young's modulus and Poisson's ratio for saturated specimens are listed in Table 6.5. Representative stress-strain curves for sandstones tested at dry and saturated conditions are shown in Figure 6.14. In all cases the tan and sec E decrease from the dry state - in many cases the sec value shows a greater change than the tan E indicating a less elastic mode of deformation. Many of the curves display a more well developed Stage I deformation when saturated. This indicates that the process or processes leading to strength reduction cause a weakening of the framework and hence a higher degree of pore closure and cement deformation at low stresses.

Sandstones which showed a high degree of elasticity in the dry state, despite experiencing marked decreases in Young's moduli on saturation did not show significant change in the shape of the σ–ε profile. e.g. the Cambrian Basal Quartzite.

Figure 6.15 shows the sequential σ–ε curves for Lower Old Red Sandstone and Pennant (type A) tested at intermediate moisture contents. These examples demonstrate how the profile changes as moisture content increases. The most obvious change is the increased 's-shape' of the σ-ε curve which can be seen to develop at low moisture contents. The result of this change of profile is that sec E decreases substantially while tan E does not show the same modification. The two diagrams demonstrate the need to measure sec E as well as tan E, since sec E gives an indication of the behaviour in Stages I, III and IV. It is noteworthy that these are the areas of the σ-ε diagram which are most important in engineering, where low loads are imposed, (Stage I) and where failure occurs, (stage IV).

The variation in tan and sec E for these sandstones is plotted against moisture content in Figure 6.16. Sec and tan E show similar trends to those produced by plotting strength against moisture content. Values generally decrease sharply with increase in moisture content but above approximately 1% show little change. Sec E appears to show a more uniform relationship with moisture content than does tan E. It

Sst Type	TAN E	SEC E	Poisson's R.
A	23.52	12.40	0.195
DQ	24.02	22.30	0.219
BQ	29.95	28.92	0.214
LORS	26.19	18.89	0.162
PiA	38.23	37.54	0.158
PiB	33.42	28.03	0.173
UCS	22.19	22.54	0.179
MGA	11.68	6.93	0.491
MGB	17.40	9.125	0.221
MGC	17.02	11.44	0.167
MGD	16.37	13.88	0.358
HBGA	7.58	5.51	0.114
HBGB	9.03	7.06	0.144
SS	37.55	29.36	0.098
BF	5.80	5.3	0.176
TRA	5.92	5.26	0.237
TRB	6.72	5.53	0.149
MCM	5.81	5.63	0.602
CF	19.9	18.47	0.193
PnA	12.21	15.68	0.085
PnB	15.21	12.18	0.437
PnC	13.27	9.97	0.378
An	5.07	6.82	0.258
PrA	15.38	9.93	0.127
PrB	7.95	5.82	0.270
PrC	16.23	14.60	0.327
PrD	33.33	24.32	0.465
PrE	7.81	6.80	0.237
R	5.34	3.95	0.427
MS	5.11	2.76	0.521
ArdA	8.62	7.38	0.222
ArdB	5.92	5.44	0.147
AS	5.70	4.68	0.286
G	0.909	0.761	0.637
D	15.39	11.25	0.529

Table 6.5 Average values of tan E, sec E and Poisson's ratio for sandstones tested in the saturated state.

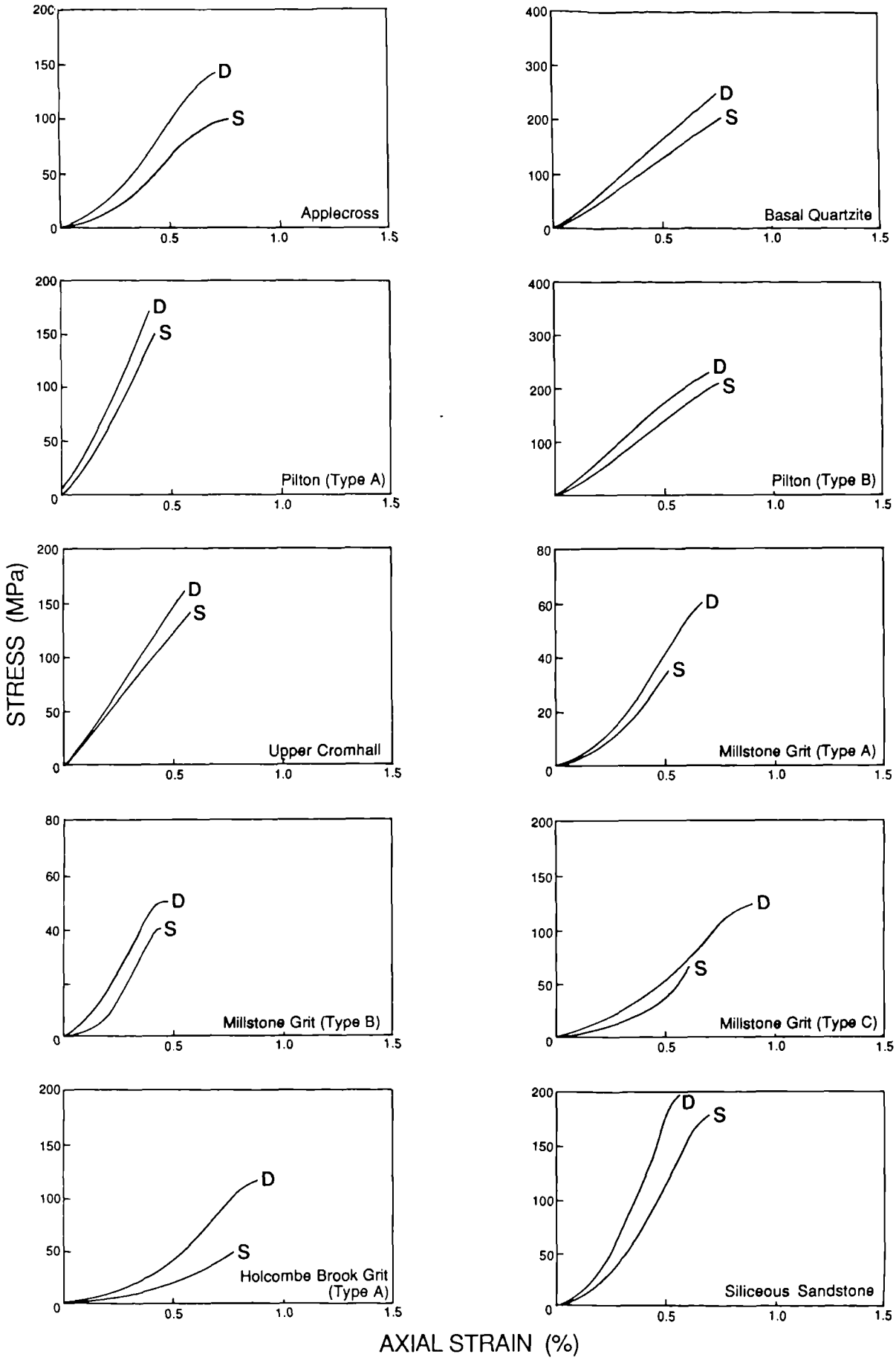

Figure 6.14a Stress-strain curves for each sandstone tested in dry and saturated state.

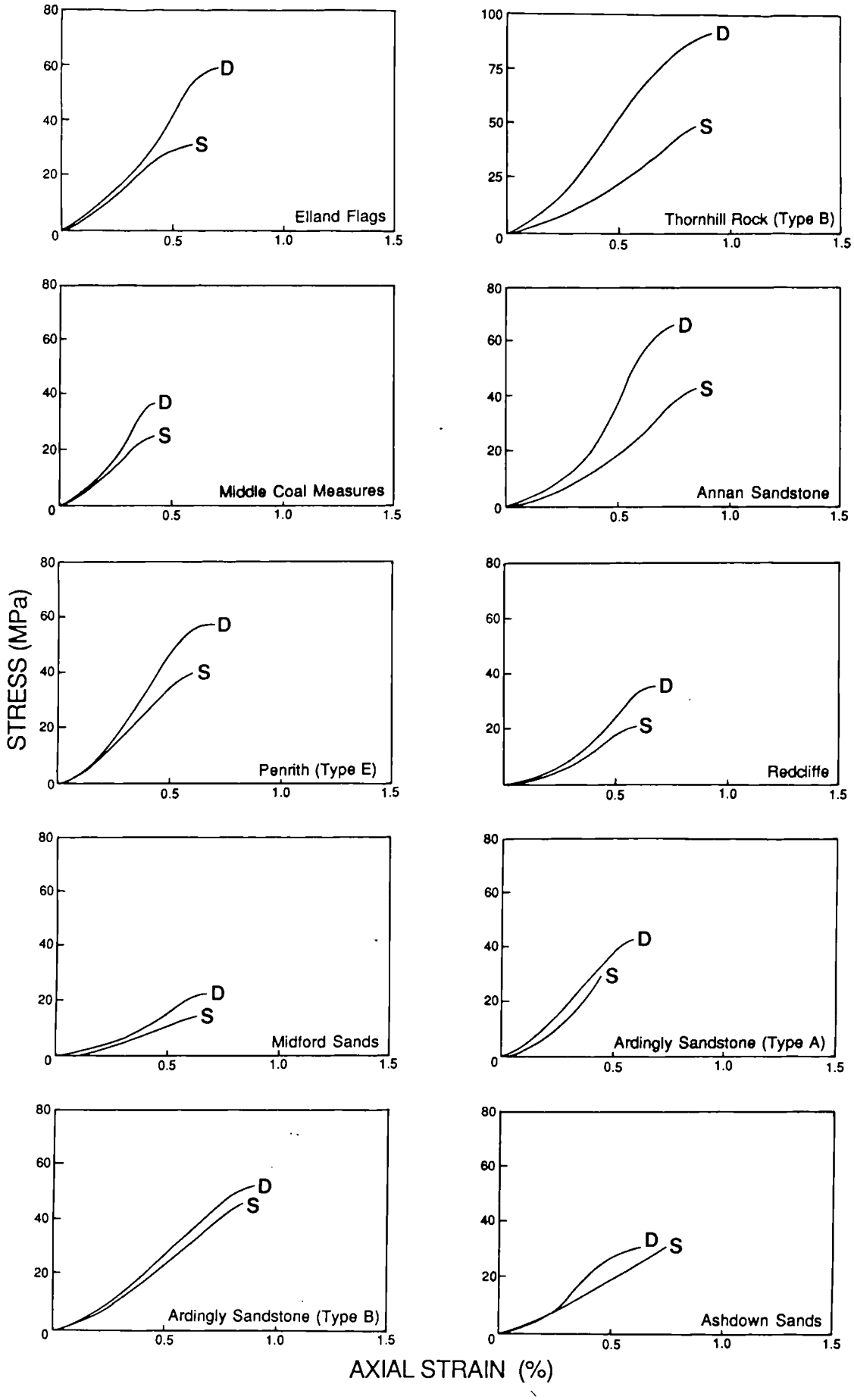

Figure 6.14b Stress-strain curves for each sandstone tested in dry and saturated state.

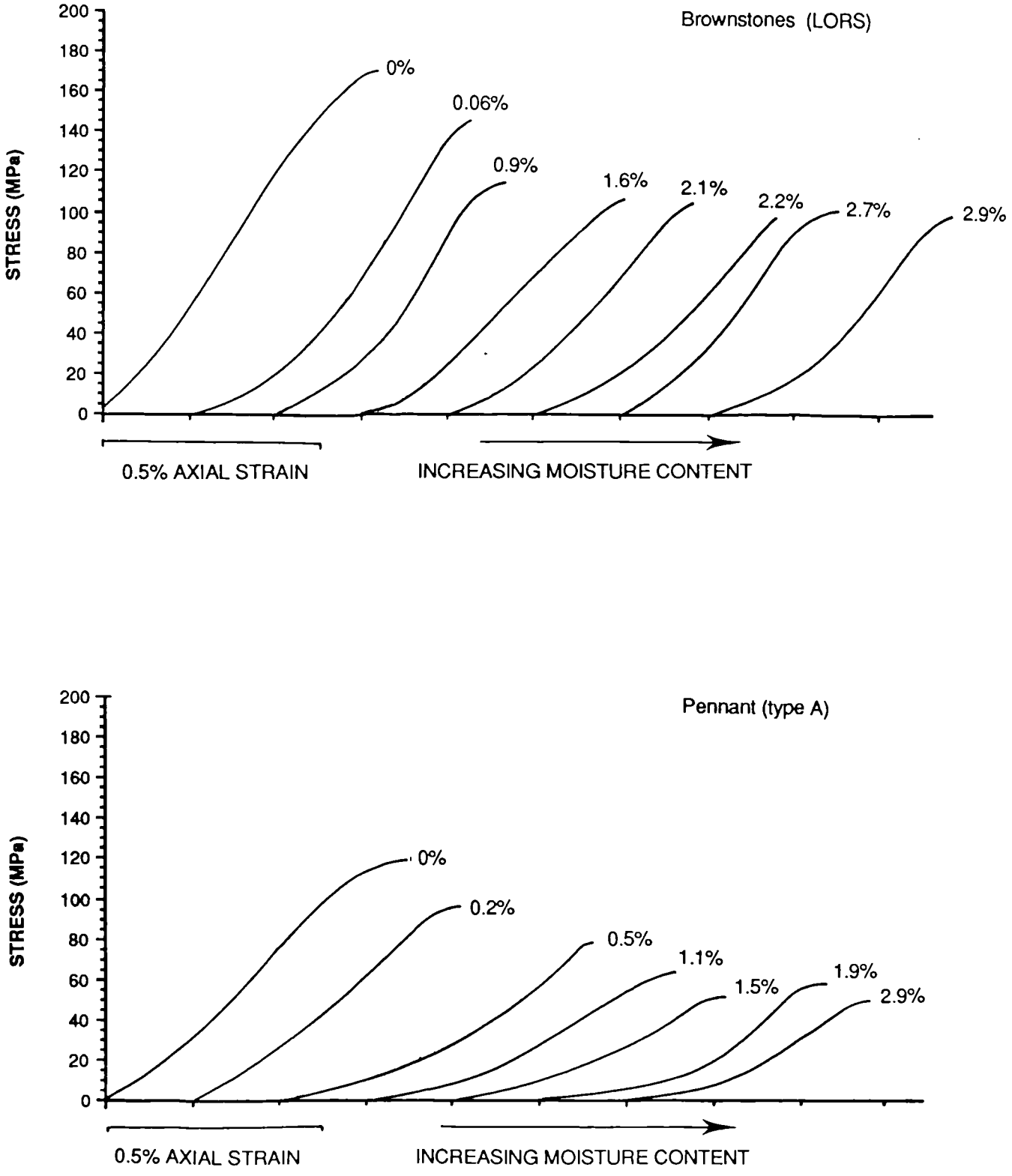

Figure 6.15 Sequential stress-strain curves at various moisture contents.

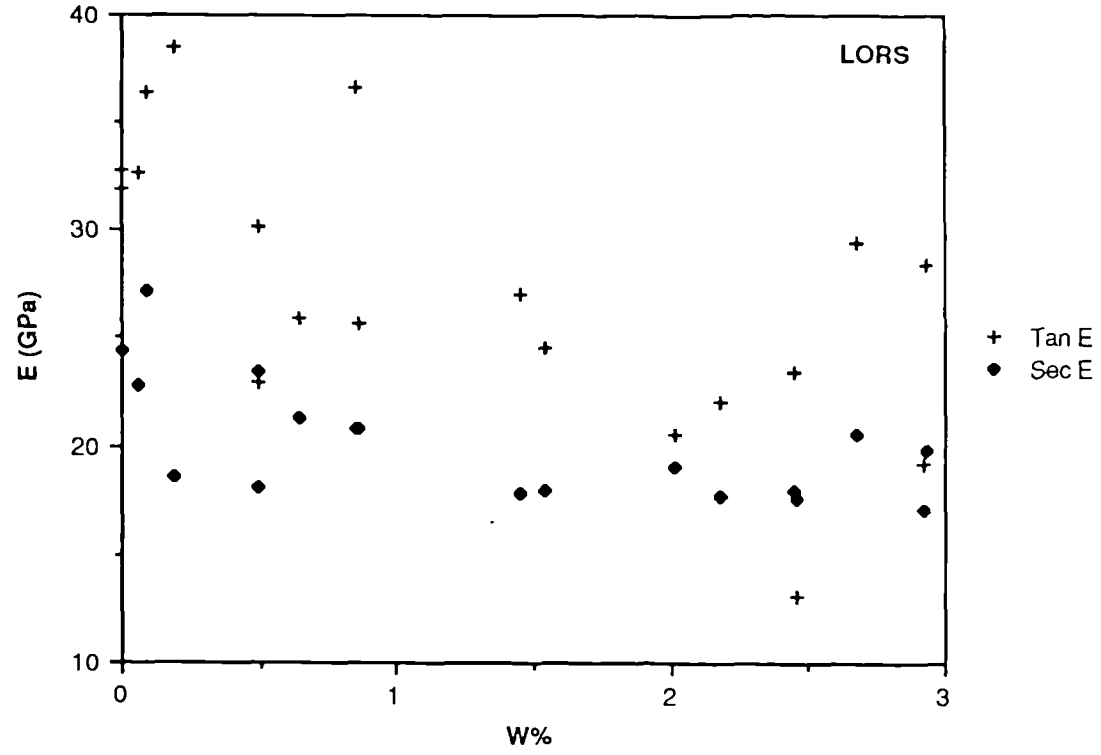

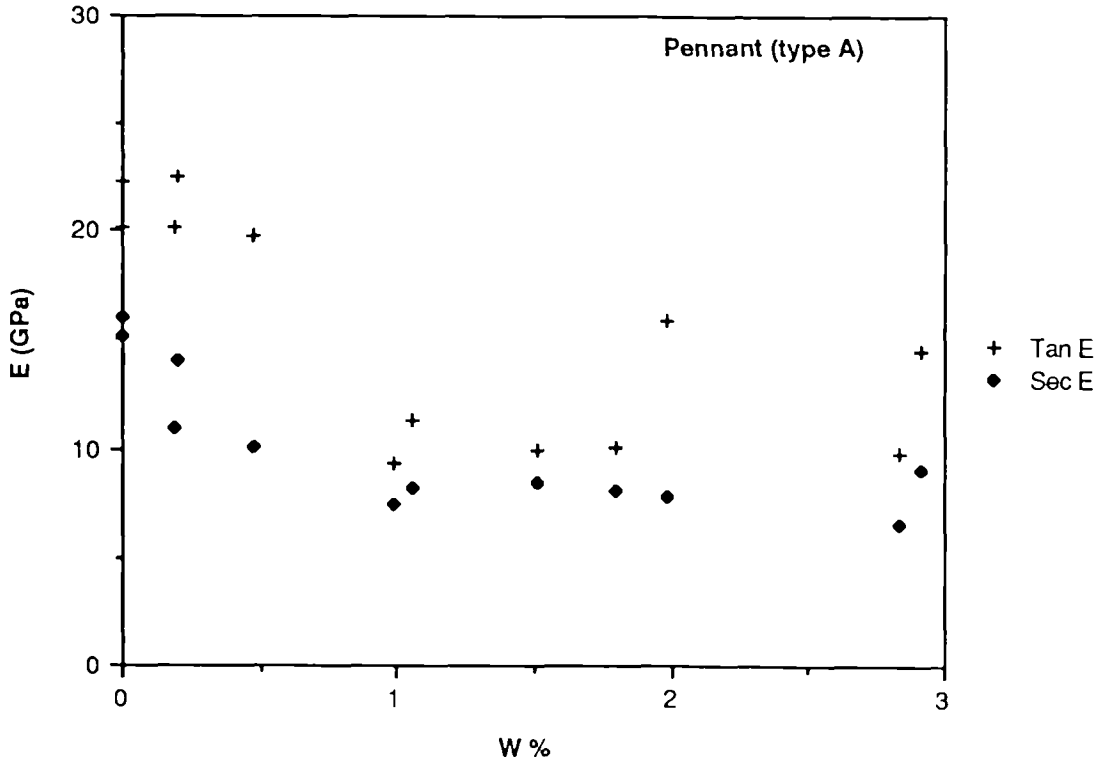

Figure 6.16 Moisture content versus tan E and sec E for Brownstones and Pennant Type A.

was observed for many sandstones that tan E showed a slight increase from the dry state at low moisture contents. This may be attributed to the development of a more s-shaped profile at low moisture contents, without substantial increase in axial strain to failure.

Figure 6.17 shows Poisson's ratio plotted against moisture content. Moisture generally causes an increase in Poisson's ratio but the effect is less well defined than with uniaxial compressive strength and Young's modulus.

A number of sandstones, (including LORS and PnA) showed slight decreases in Poisson's ratio at low moisture contents followed by a general increase. These results are similar to those shown by Priest and Selvakumar, (1982).

The positions of points which do not fit the trend described above may be due to high radial strains occurring over relatively small areas. This could be due to an increased degree of localisation of deformation in the presence of moisture.

6.4.3 Effects of moisture on the mode of deformation.

As discussed in Chapter 5, the mode of deformation observed in uniaxial compression testing is influenced to a large extent by the strength of the specimen. The strongest varieties fail by axial cleavage while the weakest types fail by cataclasis with shear failure being the most common failure mode. During the testing of wet samples in this research, the mode of deformation was described and the failed sample photographed. Plates 6.3 to 6.6 show examples of the change in failure mode due to wetting in some of the sandstone types.

Despite extensive overlap of failure modes, in general, wetting of the specimens caused a weaker mode of deformation to occur. For example sandstones deforming totally by axial cleavage in the dry state showed shear failure and/or a combination of shear and axial cleavage. Similarly in weaker varieties, where shear failure is the dry failure mode, a combination of shear and cataclasis took place on saturation. The change in style of deformation was normally observed at low moisture content values and although no clear pattern has been recognised, it is likely that the changes take place during the period of major strength reduction, i.e. less than 1% moisture.

On a microscopic scale the failure planes often showed a higher degree of disaggregation leading to a rolling mode of failure. This demonstrates the weakening effect of moisture on the cement/matrix causing microfractures to form around grains to a higher degree than in the dry state. The main effect of this type of microfracturing is to produce a much more passive mode of failure.

This passive failure in moist samples was extremely evident in all sandstones tested. The reduction in the explosive energy dissipated at failure is to a certain extent a

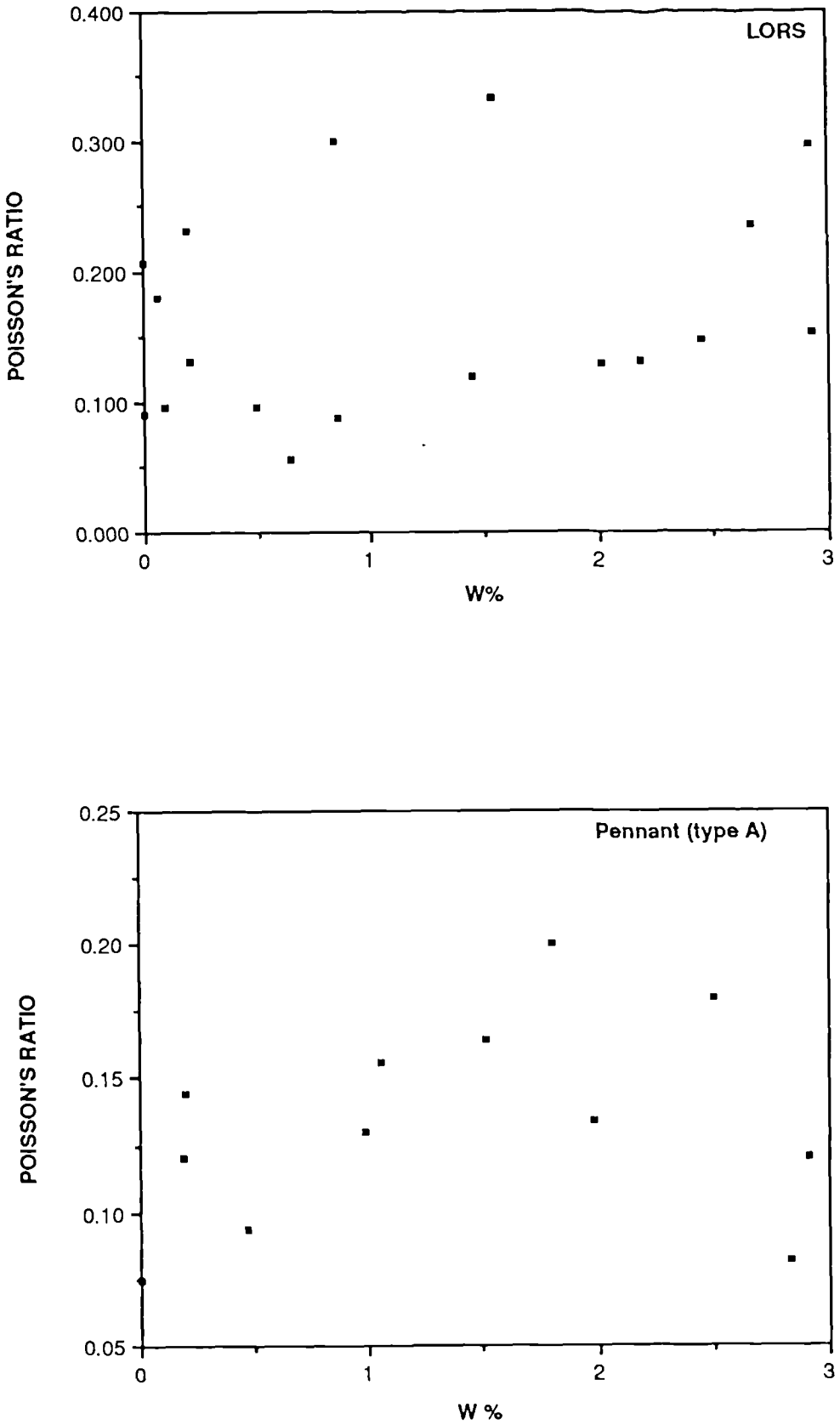

Figure 6.17 Moisture content versus Poisson's ratio for Brownstones and Pennant Type A.

Plate 6.3 Penrith Sandstone (type B) deforming by conjugate shear failure in dry state.

Plate 6.4 Penrith Sandstone (type B) deforming by cataclasis in saturated state.

Plate 6.5 Greensand (type B) deforming by shear failure in dry state.

Plate 6.6 Greensand (type B) deforming by cataclasis in saturated state.

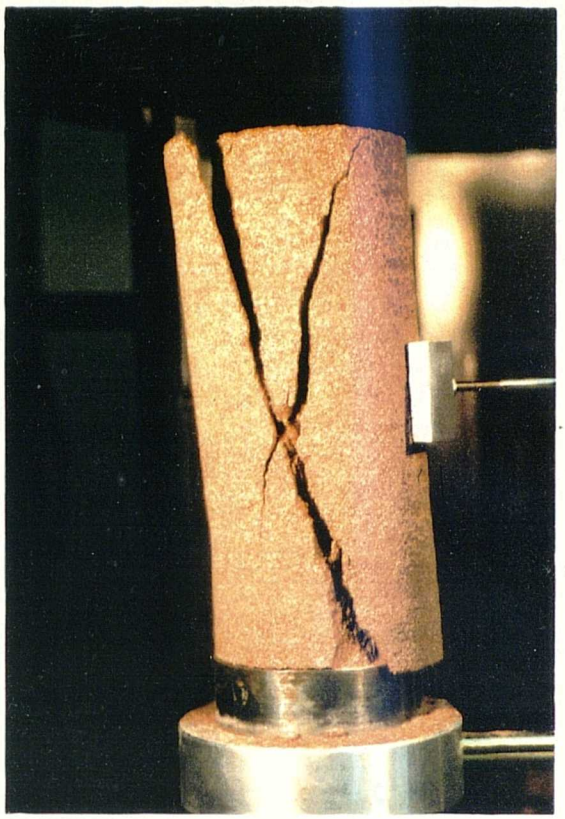

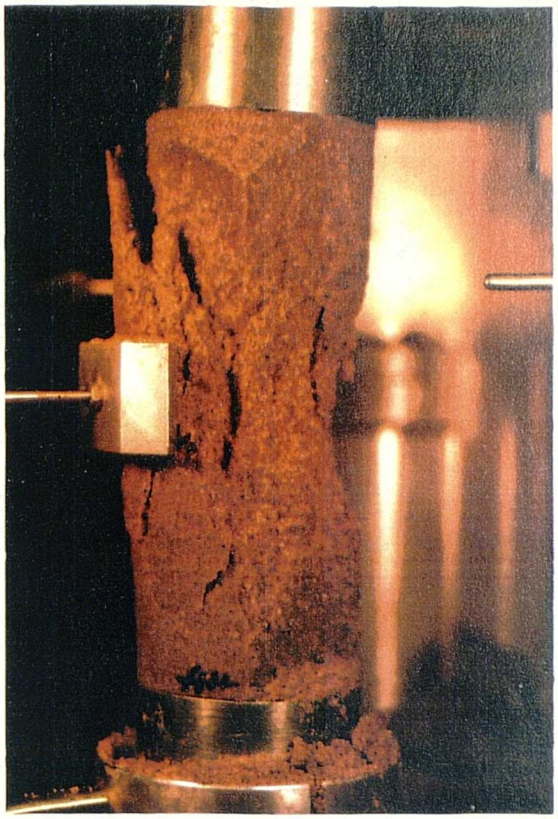

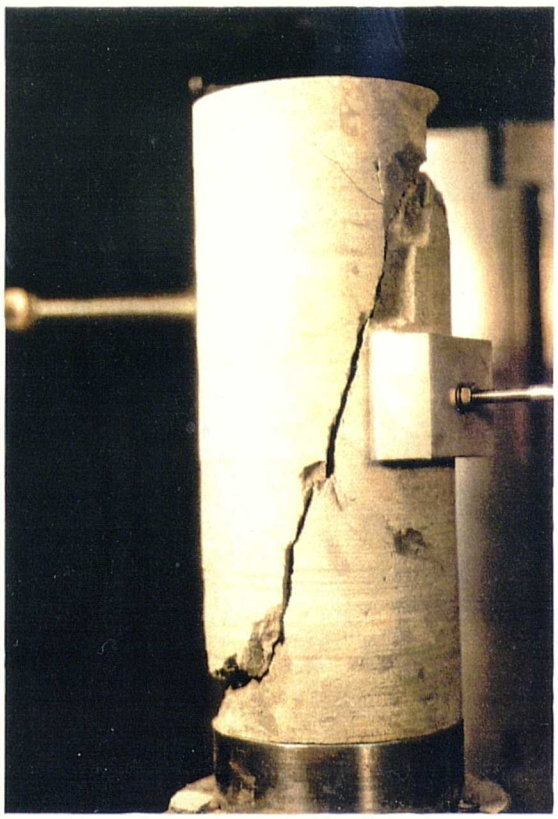

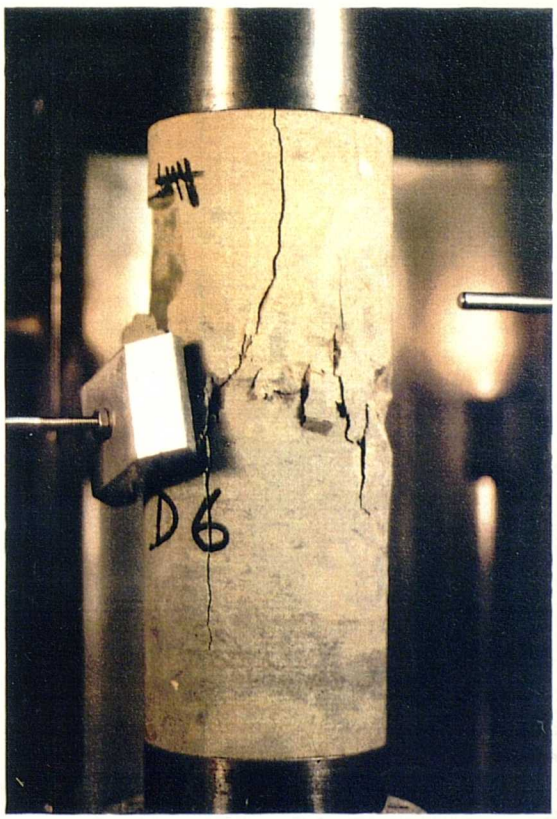
D6

result of the lower stresses built up within the machine; in addition however, it is suggested the overall brittleness of the rock is substantially reduced by wetting. Hudson and Morgan, (1975) defined a Brittleness Index which could be determined from the complete stress-strain curve for rocks tested in a servo-controlled machine. Unfortunately, the Brittleness Index could not be calculated during this research. Priest and Selvakumar, (1982) however, obtained brittleness values for Bunter and Carboniferous sandstones at various moisture content levels and found that a sharp drop in brittleness occurs form zero to 1% moisture content paralleling the drop in strength. They also found that in some cases the brittleness increased gradually above 1% but were unable to explain the phenomenon.

As mentioned earlier, one effect of water is to cause a higher degree of microfracturing around grains leading to rock disaggregation. An exception to this rule was the Ashdown Sandstone which showed up to 70% disaggregation in the dry state. When studied under the binocular microscope, it was apparent that the fragments consisted of complete grains with little or no signs of fracturing. Testing in the saturated condition however caused the rock to remain more intact, indicating that the vacuum theory for strength increase is correct.

The major problem in studying failure mode is that the macroscale process occurs so fast that only the end product of failure can be observed. High speed photography was therefore undertaken to observe the failure mechanism occurring towards the peak stress of a typical sandstone type.

6.5 High Speed Photography of Rock Failure.

Failure of sandstones of strength greater than 50 MPa is normally highly explosive and apparently instantaneous in a normal testing machine. Fracture propagation occurs extremely rapidly - Atkinson, (1975) reported crack velocities for quartz in the range 10^{-4} to 10^{-10} ms^{-1}. This section describes the attempts made to observe fracture processes in a dry and a saturated state.

6.5.1 Apparatus.

High speed photography is normally taken as faster than 10 frames per second, (fps). Modern, and extremely expensive cameras are capable of photographing very high speed action such as bullet trajectories at rates of up to twenty million fps. The Department of Zoology at Bristol posseses a camera capable of filming at speeds of 1000 to 3000 fps. This apparatus was used to record a number of cores being fractured and at the early stages it was not certain whether useful results would be obtained. A

number of problems were foreseen:

i) high speed photography requires high levels of light to expose the film used over the extremely short period of time during which it passes in front of the lens.

ii) switching the camera on would have to be synchronised with failure. If this was done too early, film would be wasted, (approximately 5.6m per second) while switching on too late could miss the action completely. This problem is compounded by the need to allow the camera 1.25 seconds to achieve full filming speed.

iii) protecting the camera from any fast moving fragments of rock produced during the explosive failure of the specimen.

The high speed camera uses 16mm continuous cine film. In order to achieve the film rotation speed necessary for the camera to operate properly, a 30 Amp surcharge is required; a special electricity supply was fitted in the laboratory for this purpose.

Plate 6.7 shows the camera mounted on a plinth at the correct height for viewing into the compression machine aperture. Lighting is provided by two 1000 W fluorescent lamps mounted on stands and directed from close range onto the rock subject. In retrospect, the degree of lighting could ideally have been higher but resources did not allow a repeat exercise.

In order to film the specimens during failure, it was not possible to use the radial strain cell. However, axial and y-direction radial strains were recorded in the normal way. The use of the two transducers and the subsequent simultaneous plot were considered to be of use in synchronising start of filming with the visible rock failure since it has been recognised from past tests that failure can be predicted by the increased curvature of the axial and radial strain curves after the rock's yield point.

Protection of the camera from flying rock fragments was carried out by placing a sheet of plywood between the camera and the compression machine, with the camera lens projecting through an aperture in the sheet. The lamps were also protected by wire mesh which did not impair the degree of illumination.

6.5.2 Test Procedure

The rock chosen for the tests was a variety of the Millstone Grit from west Yorkshire - the Holcombe Brook Grit, (See section 3.2 for petrography etc). Eleven samples cored from the same block were used for the experiments with three actually being filmed during failure. Six samples were oven dried and six saturated using the saturation cell at a pressure of 500kN/m^2. Four samples were tested in the dry state

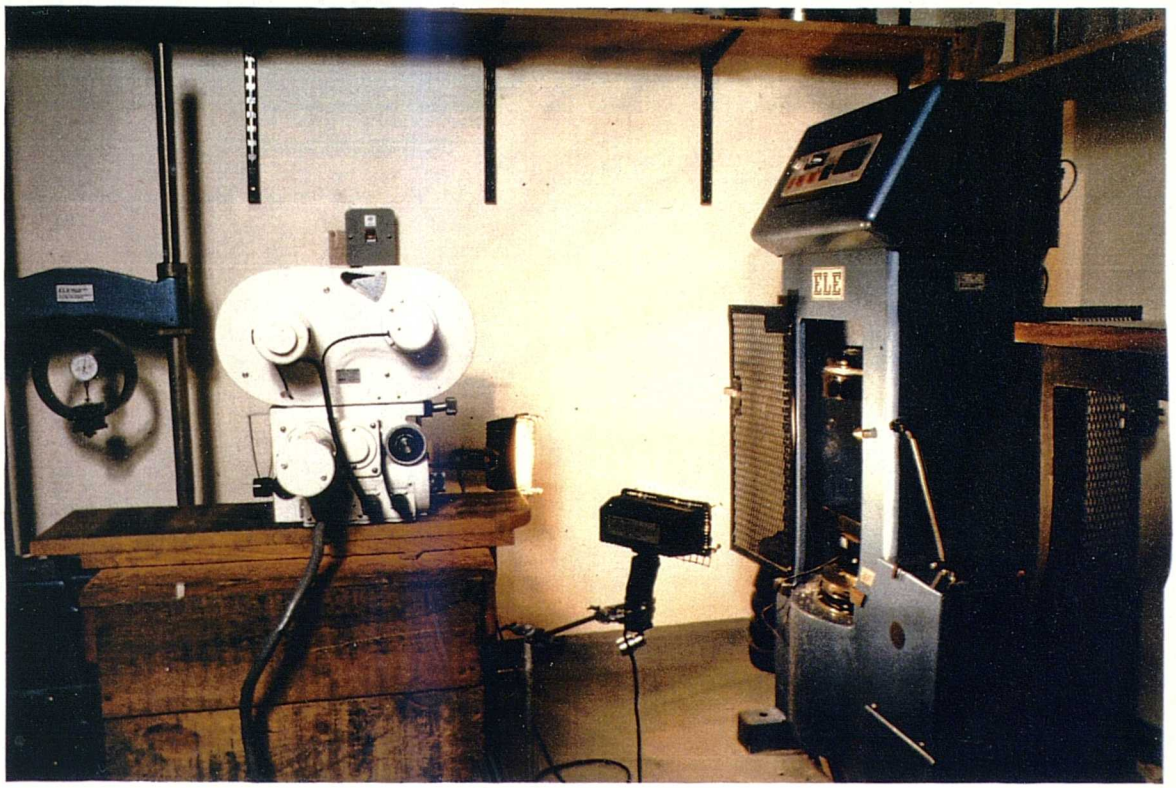

Plate 6.7 High speed camera mounted on plinth viewing into uniaxial machine aperture. Lighting is by two 1000W lamps.

and four in the saturated state using the complete strain measuring apparatus. The results of these preliminary tests are shown in Table 6.6. The average failure stress was 116.9MPa for the dry and 49.03MPa for the saturated tests. In addition to the stress-strain values, the shape of the simultaneous time-strain plots were studied to determine the characteristic profile for this rock type.

Specimen No.	w%	Mpa	
HBGA1	0.00	116.31	
HBGA2	0.00	121.84	
HBGA3	0.00	118.93	
HBGA4	0.00	119.12	
HBGA5	4.10	53.65	
HBGA9	3.64	46.92	
HBGA10	3.76	46.32	
HBGA11	3.92	49.22	
HBGA6	0.00	118.69	(FILMED)
HBGA7	3.64	46.83	(FILMED -unsuccessful)
HBGA8	3.64	46.63	(FILMED)

Table 6.6 Results of preliminary and filmed tests on Holcombe Brook Grit (type A).

The camera posseses an automatic switch which can be triggered by an electronic signal from a transducer output. For such a device to be used during this work, it would have to be capable of detecting the final stages of failure, e.g an acoustic or accelerometer type transducer. Unfortunately, electronic equipment for predicting total failure was not available and it was decided that the camera could be switched on manually when the average strength value for that rock type was approached, if accompanied by a typical deflection in the strain curves.

The three tests used a total of approximately 125m of film. Two of the tests were successfully recorded on film while for one test the camera was switched on too late and the fracturing process missed. The film was sent to a specialist developing firm who produced a continuous 16mm negative and a continuous 16mm print. This print was then played on a standard cine projector at speeds of 28 and 22 fps. The results were good but the quality of the projection was poor; even at 22 fps the action was too fast to delineate sequential stages in the fracture process.

The 16mm cine film was taken to a film editor with the objective of converting

it to a video which could be played at a slower speed or paused using a good video player. The capabilities of the editing machinery were greater than expected in that the print could be projected onto a screen while being recorded on video, the action speeded up, slowed down or stopped. In addition a time count related to frame number could be superimposed in the corner of the image.

Using this equipment, the action was effectively slowed down at important points to show the development of fractures without losing any of the high picture quality. The action for each test which was recorded on video consisted of playing the film at 18 fps, reversing it (the result is effectively sticking the rock back together again) and playing the film again at very slow speeds, (0.1 to 5 fps) to study the fracture propagation rates.

6.5.4 Results

The end product of the work was a video showing two tests on Holcombe Brook Grit - one completely dry and one saturated. The picture quality for the dry test is better than that for the wet one but both clearly show the propagation of the main fracture and the subsequent explosive disintegration of the rock specimen. By superimposing the frame count onto the video, the timing of any given event can be calculated. The times quoted below in milliseconds are taken as the time interval from the first sign of macroscopic failure. The relevant data for the tests is given in Tables 6.6 to 6.8. The stress-strain curves for the two tests are shown in Figure 6.18.

Time (milliseconds)	Plate	Action
0.000	6.8(b)	Slight bulging of sample just above y-direction transducer.
1.000		White dust spots appear on specimen surface. Due to collapse of pores.
1.500		White dust spots disappear.
2.000		No visible change.
2.900	6.8(d)	First stage of fracture process in top left quadrant of specimen lateral bursting out under tension
2.925		Similar 60° split failure at mid specimen height on right hand side.
2.950		Two main fractures meet in middle of specimen at mid height.
3.000		Lateral bursting of small fragments just below convergence of two fractures.
3.350		Explosive bursting of fragments and dust from left hand fracture. Expulsion of dust only from right hand fracture.
3.400		New fracture propagating downwards from point of convergence of two initial fractures.
3.500		Vertical fracture opening.
3.550	6.8(e)	Fracture has reached lower end of specimen.
4.000	6.8(f)	Specimen disintegrating into multiple fragments. Long top end cone and short basal end cone. Axial side splitting of elongate fragments on right hand side.
8.000	6.8(h)	Initially horizontal tracjectories of two main side fragments indicating tensional failure.
11.000	6.8(k)	Extremely violent collapse of specimen with small fragments flying in every direction.
11.500	6.8(j)	Large fragment on right impacts axial strain transducer.
32.000	6.8(i)	Top end cone drops vertically onto lower cone and rests there momentarily before toppling over.

Table 6.7 Sequence and timing of events observed during tesing of *dry* specimen.

Time (milliseconds)	Plate	Action
0.000	6.9(b)	First sign of macroscopic failure. 60° fracture surface forms within sample just to right of y-direction transducer.
3.500		No change in position or extent of fracture.
10.000	6.9(c)	Fracture propagates upwards by 15mm but stops.
41.000	6.9(d)	Fracture propagates to left hand side of specimen accompanied by expulsion of dust at point of emergence.
44.500	6.9(f)	Fracture has propagated to top of specimen. Single shear failure is complete.
45.500	6.9(g)	Two parts of specimen sliding past each other- definite shear failure.
51.000	6.9(k)	Lower fragment tilting over and rotating.

Table 6.8 Sequence and timing of events observed during testing of *saturated* specimen.

The high speed photography of the two samples revealed a number of interesting aspects of the failure of dry and saturated sandstones:

1. The dry specimen behaved in a much more brittle manner, with the specimen disintegrating into multiple fragments.
2. Maximum expansion of specimens does not necessarily occur at mid-height towards failure.
3. The period of time from the first signs of macroscopic failure to disintegration of the specimen is much shorter in the dry specimen, (3.55ms) than in the saturated one, (44.5ms).
4. Propagation of individual fractures occurs at much higher velocities in the dry specimen: 9×10^{-2} ms^{-1} in the dry specimen and 1.7×10^{-2} in the saturated specimen. This disagrees with Atkinson, (1979) who states that fracture propagation is accelerated in the presence of moisture.
5. Saturation increases the degree of shear localisation. This could explain the poor relationship between moisture content and Poisson's ratio measured at mid height.
6. There is some evidence that fracture propagation is much more stable in the presence of moisture. The fracture observed in Plate 6.9 actually terminates temporarily and propagates in the opposite direction before reactivating upwards.

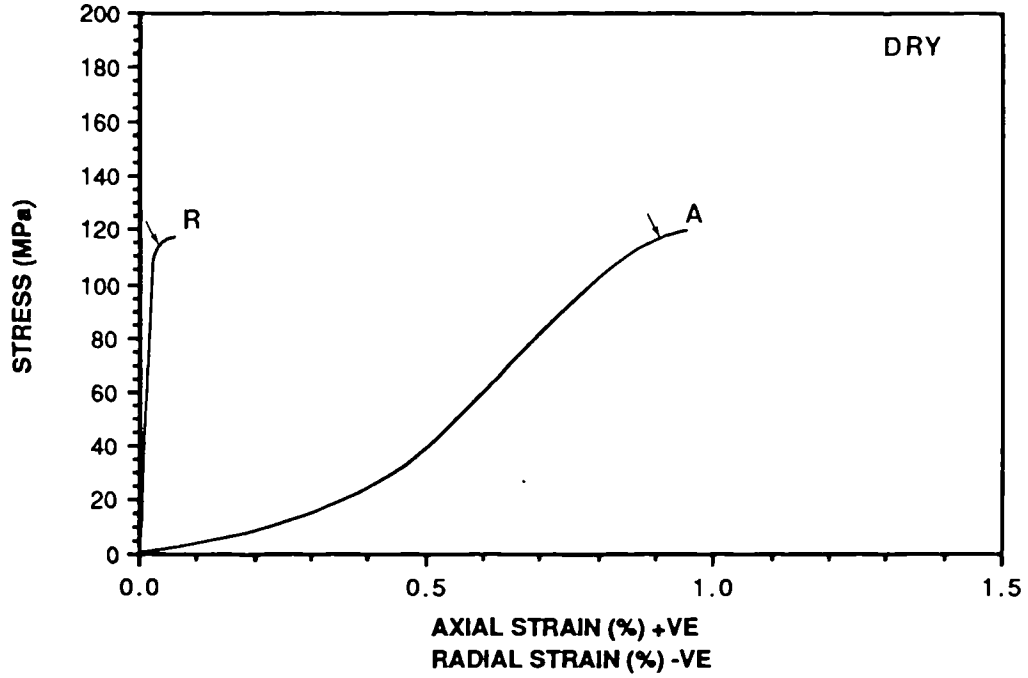

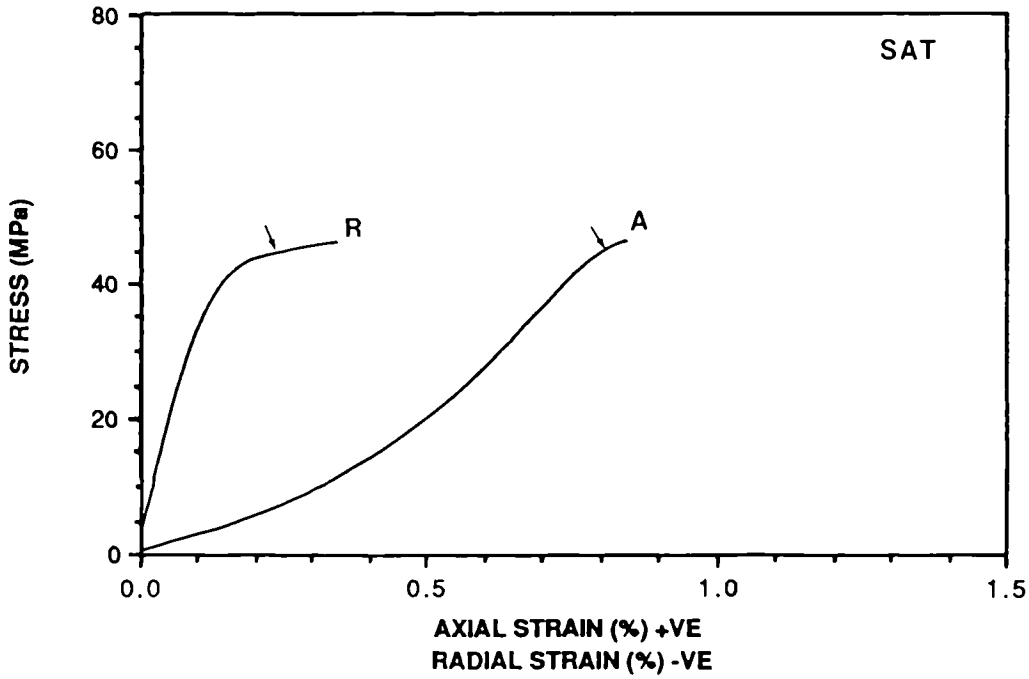

Figure 6.18 Axial and radial stress-strain diagrams for Holcombe Brook Grit samples used in high speed photography.

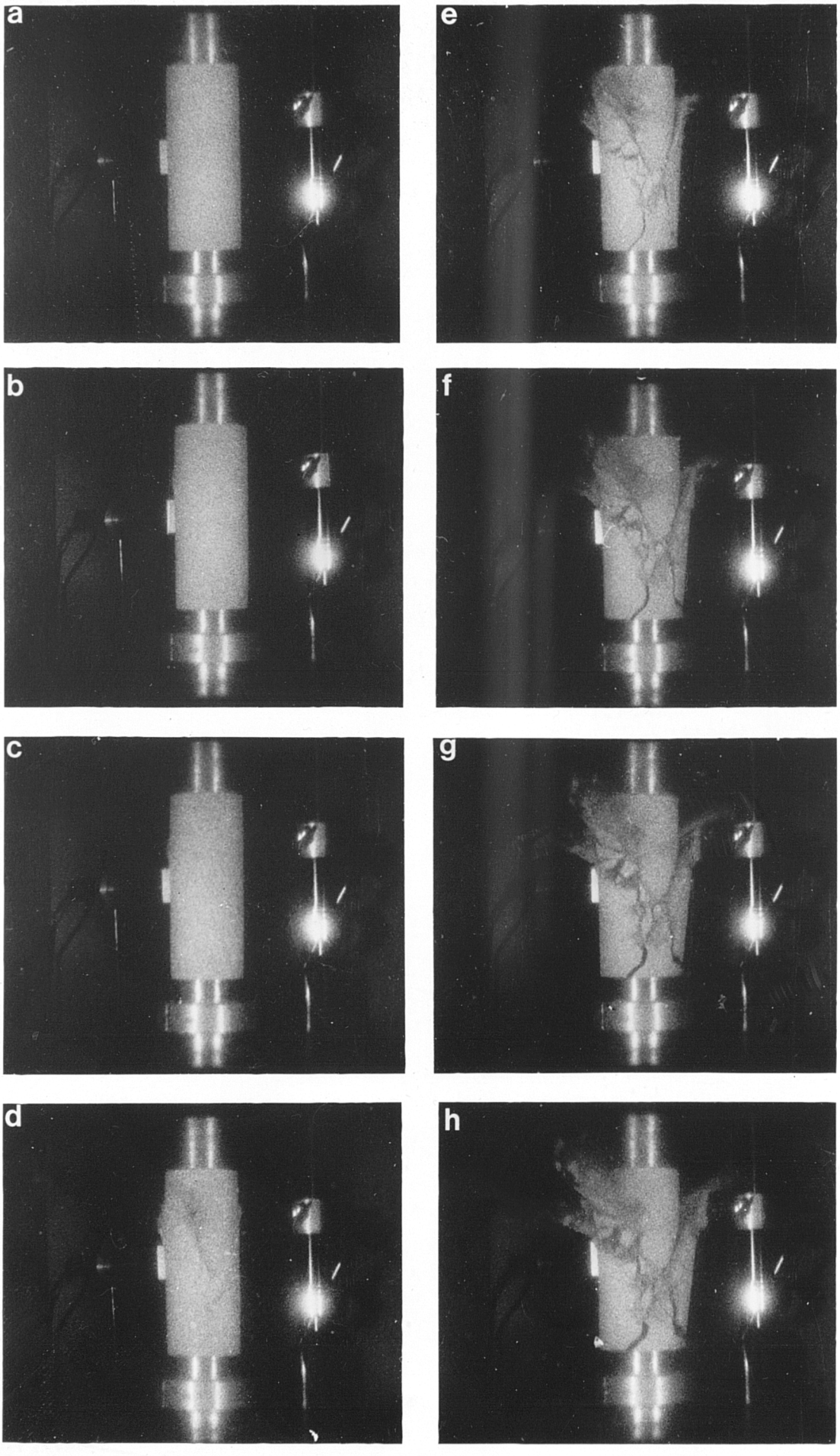
a
e
b
f
c
g
d
h

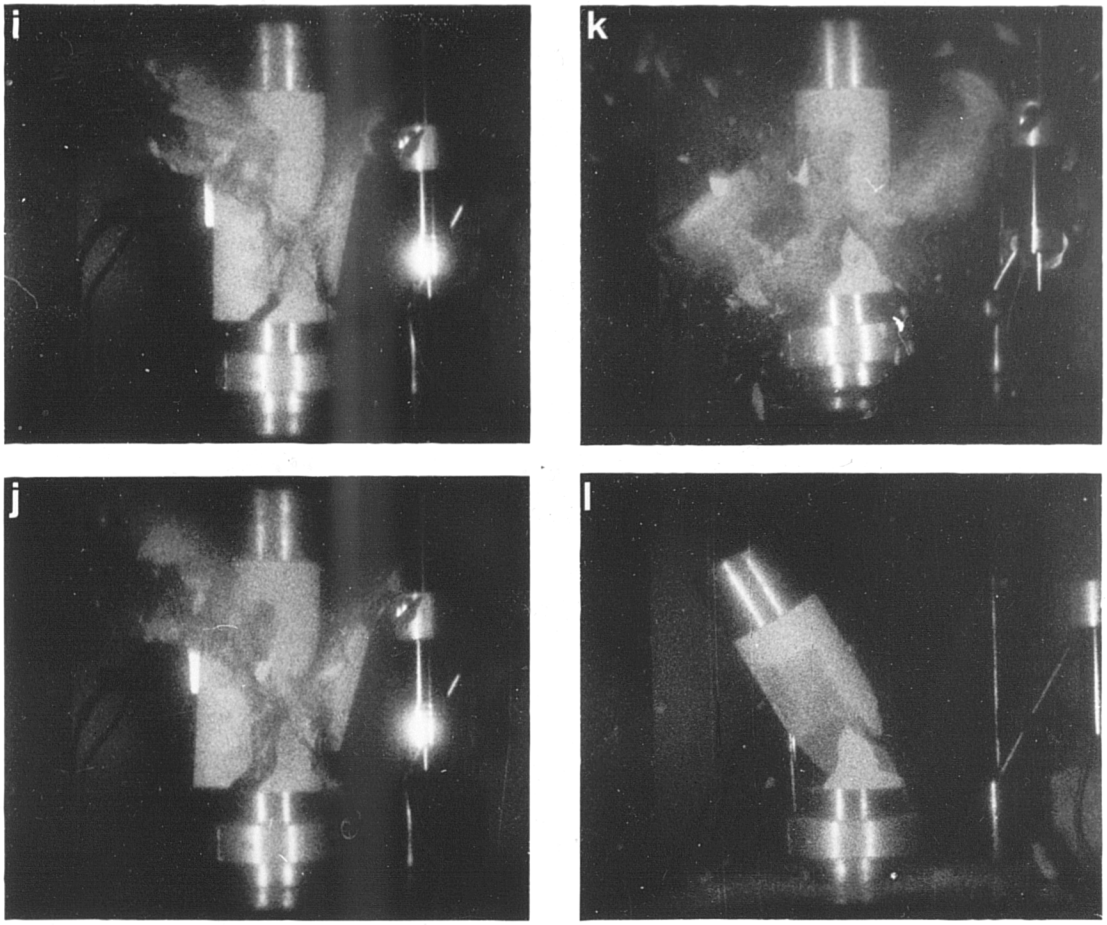

Plate 6.8 (a - l) Sequential stages in fracture process of a dry specimen of Holcombe Brook Grit loaded in uniaxial compression.
Specimen size: 136.9mm x 54.75mm.

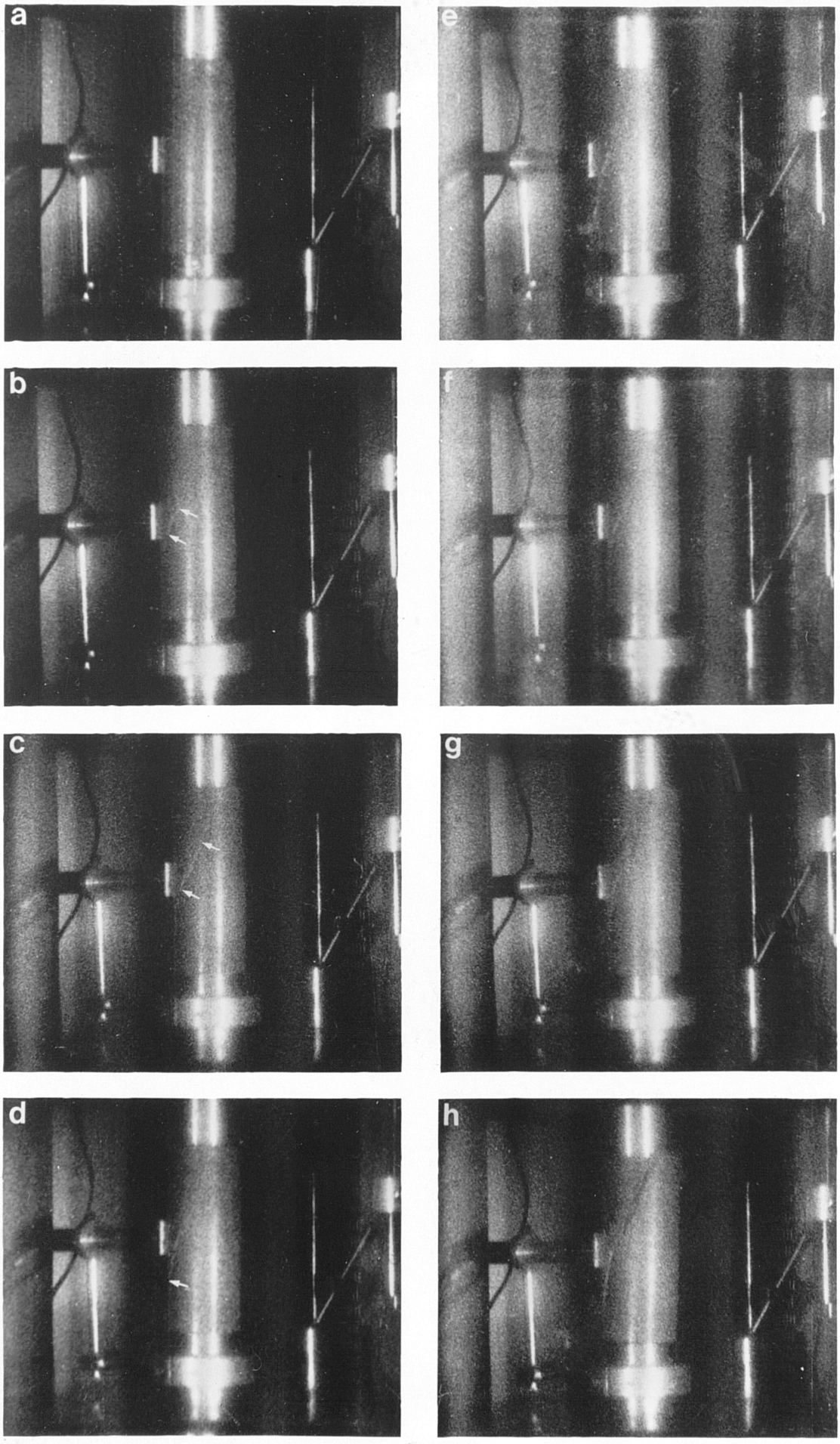
a
b
c
d
e
f
g
h

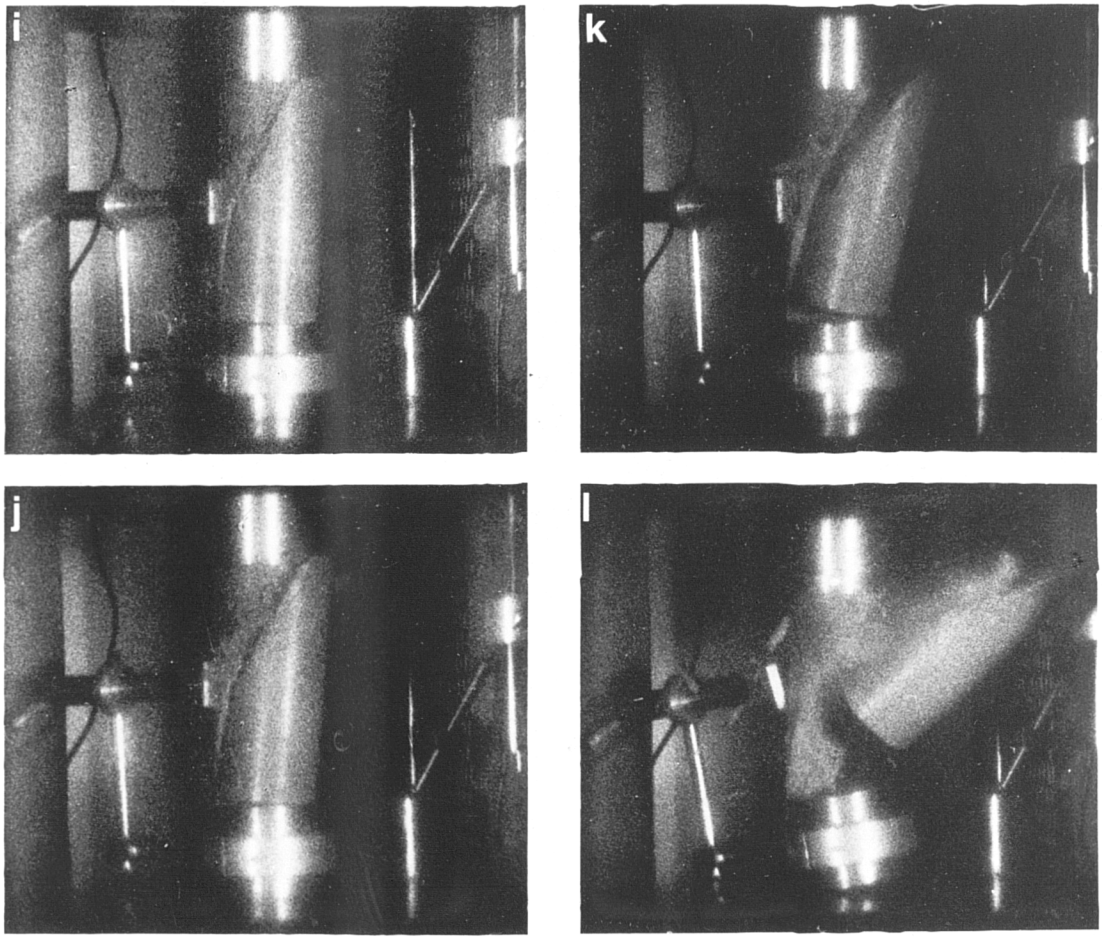

Plate 6.9 (a - l) Sequential stages in fracture process of a saturated specimen of Holcombe Brook Grit loaded in uniaxial compression.
Specimen size: 136.9mm x 54.75mm.

6.6 Summary and Conclusions.

Moisture content is an important factor in controlling strength and failure mechanisms in sandstones. Degree of strength reduction varied between different varieties, dependent on the mineralogy of the specific types. The bulk of the moisture content related strength reduction, (MCRSR) occurs at low moisture contents; at an average of 31.2% of the moisture content at saturation. The relationship between strength and moisture content for a specific sandstone can be described in terms of a negative exponential function. Using such an equation, the strength at certain moisture contents could be predicted from other values.

The presence of moisture has a similar effect on the Young's modulus. Sec E shows a clear relationship with moisture content while tan E shows a greater spread of results. This is due to the development of a more s-shaped σ-ε curve in the presence of moisture. Stages I,III and IV type deformation are thus more significant, indicating that:

1. pore closure and collapse are more intense in the presence of moisture, and

2. stable microfracturing occurs earlier and to a greater degree towards failure.

Intergranular microfracturing is more intense in wet rocks, resulting in the rolling of grains along failure planes as opposed to fracturing through the grains.

As outlined in section 6.2, the processes involved in MCRSR have been the subjects of much discussion. This research has shown that two main processes are prevalent. These are: 1) Physical deterioration of clay constituents, and 2) fracture energy reduction.

Sandstones which contain abundant clay minerals or sedimentary rock fragments show the greatest degree of strength reduction. This process occurs prior to increased stress and in the weakest varieties may cause slight expansion of the rock. It is not considered however, that expansion induced by capillary tensions is important since huge pressures would be required to occur instantaneously within each pore, to cause the MCRSR recorded in the strongest sandstone varieties.

Correlation between clay/SRF/PRF content indicates that clay softening is an important process but it cannot explain the loss of competence in the pure quartzites. Saturation of specimens in liquids of varying pHs and surface tensions has shown that chemical deterioration is not an important process on the time scale involved in MCRSR. Surface tension of the saturating liquid does however have a profound influence on sandstone strength; the process of change in surface energy outlined by

Rehinder and Gichtman, (1957) appears to be correct. The process of stress corrosion as described by Atkinson, (1975) may play a subsidiary role but it is difficult to explain why the theory of increased crack velocity in the presence of moisture contradicts the crack velocity recorded from high speed photography.

Fracture energy reduction occurs mostly during the latter part of Stage II and during stages III and IV, when microfracturing is occurring. The overall effect is to lower the fracture propagation energy , resulting in lower strengths, greater strains to failure and less brittle deformation.

The research has shown that the development of pore pressures does not occur to any great degree and hence is not a contributing factor in MCRSR. The only effect of pore pressure occurs at total saturation where a number of sandstones show a slight increase in strength from the value produced by fracture energy reduction and clay softening. This occurs only when the pores are filled or almost filled with water and the recorded stress at failure is given by equation 6.3.

CHAPTER 7

A QUANTITATIVE ASSESSMENT OF SANDSTONE MICROFABRIC RELATIVE TO STRENGTH AND DEFORMABILITY

7.1 Introduction

The research described so far has indicated that sandstone strength is controlled to a large extent by dry bulk density and effective porosity. The relationships are not clearly defined however since density, strength and porosity are controlled ultimately by the mineralogy and texture which are highly variable between different sandstone types.

Griffiths, (1952) proposed that any property of a sediment, P, can be thought of as a function of the size, shape, orientation, mineral composition and packing of the sediment. i.e. P=f(s,sh,o,mc,p). In the past a number of workers have attempted to relate physical properties such as permeability and tensile strength to grain size. (Krumbein and Graybill, 1965; Davis, 1986; Till, 1974). These attempts have usually proved to be moderately successful, but problems have arisen because the relationship between any aggregate physical property and the mineralogical/textural variables is extremely complicated.

In order to relate strength and deformability to microfabric, it is necessary to:

1) Quantify the mineralogy and texture in terms of a number of variables.
2) Use a statistical procedure which can determine the most important parameters in controlling sandstone strength while indicating the degree of interdependency of these variables.

This chapter outlines the attempts made during the research to quantify mineralogy and texture and to relate these to the deformational behaviour.

7.2 A Quantitative Microfabric Analysis.

Chapter 3 describes the static properties of the sandstones studied, including mineralogy, porosity, packing density and a qualitative assessment of grain contact types. A quantitative microfabric analysis, (QMA) requires the choice of a number of variables which can numerically describe the mineralogy and texture of different sandstone types with a high degree of confidence. The proposed QMA is based on the

following parameters, some of which have been discussed in Chapter 3:

1. Framework mineralogy
2. Cement/matrix mineralogy
3. Packing density
4. Porosity
5. Degree of interlocking
6. Grain size
7. Grain shape
8. Grain orientation

7.2.1 Framework mineralogy

The 1980's have seen the development of computer based image analysis for the determination of rock mineralogy. The work has been used mostly by the oil and gas industry on sandstones, (Dilks and Graham, 1985; Ehrlich et al, 1984). The method is based on the image analysis of back scattered electron (BSE) images. Mineral phases are differentiated by their 'grey levels' which has led to problems of mineral identification since certain species such as quartz and feldspars can have very similar grey levels to each other in optical or electron-optical images.

If the researcher is interested only in the porosity or in total grain counts independent of composition, then a fully automatic computer-based system is useful. Schafer and Teyssen, (1987) reviewed the available methods and concluded that the skill of an experienced geologist was far superior to a fully automatic system for the identification and detailed description of mineralogy.

The mineralogical data and descriptions presented in Chapter 3 are considered to be reliable enough for use in the QMA. The numerical representation of mineralogy is based on the percentage of each of the following mineral species:

1. Quartz
2. Alkali feldspars
3. Plagioclase feldspars
4. Sedimentary and Phyllitic rock fragments
5. Metamorphic rock fragments
6. Igneous rock fragments
7. Carbonate rock fragments
8. Haematite
9. Clays
10. Opaques
11. Glauconite
12. Biotite and muscovite

13. Heavy minerals
14. Sparry calcite
15. Micrite

It is likely that certain minerals can be grouped together on the basis of their similarity in strengths; this grouping can be carried out if any relationship is proved. Conflicting reports exist on the relationship between mineralogy and mechanical properties. Bell, (1978) reported that the quartz content of Fell Sandstone had no influence on the UCS while Gunsallus and Kulhawy, (1984) found a definite relationship between quartz content and strength properties. Plotting the mineralogy on a QFL diagram as in Figure 3.1, sandstones which plot in the quartz arenite field can show appreciably different strength properties. One hypothesis at this stage is that strength is controlled by the percentage of framework mineralogy which is converted to cement, rather than the overall grain mineralogy. This will be tested in the statistical analysis.

7.2.2 Cement/matrix mineralogy

The mineralogy of the cements and matrices vary widely within the thirty-seven sandstone types studied. Figure 5.5 shows dry bulk density plotted against dry strength. The results indicate that the cementing materials have a strong influence on the strength properties of sandstones. For this reason, the term 'cement index' is introduced to describe the sandstone cement in terms of mineralogy, abundance and strength properties.

The abundance of the cement/matrix minerals can be expressed as a percentage of the total mineralogy. These values can easily be recalculated from the point counting data presented in Chapter 3. Table 7.4 includes the mineralogy values recalculated to 100% after the removal of the pore counts. Point counting however does not identify the proportions of framework grains which are acting as cements. For example, authigenic quartz overgrowths are easily identified in thin section but where quartz welding has occurred, a certain percentage of the detrital quartz grains will have undergone pressure solution and acted as cements. For this reason, where quartz cementing has occurred, a percentage of the total quartz population is counted as active cement. The value of this active cement is estimated as 10% of the cross-sectional area. A value of 3% is used for metamorphic rock fragments which can show quartz cementation between grains. In addition, for sedimentary rock fragments, a value of 10% is taken as clay cement since SRF's are generally rich in clays and are deformed around more competent grains.

Normally the term cement refers to minerals which form authigenically and bond the framework grains together but excludes the fine grained detrital matrix which also acts to cement the rock. For the purposes of a cement index, matrix can be regarded as an abundant clay cement since it acts as a weak framework grain bonding agent.

The variation in the strength properties of the various cement types must be taken into account in the cement index. The most commonly used index of mineral strength is its hardness. Moh's, (1773-1839) scale of hardness is useful for the qualitative comparison of mineral species but could not be used for quantitative assessment since the scale is non-linear. It was originally developed to denote minerals which could scratch the next lowest mineral in the list. This means that the differences in absolute strength between the different minerals in the scale are not equal. More scientific hardness tests have however been devised; one example is the Knoop indentation test which uses a small diamond point pressed by machine into a prepared specimen surface. The results are considered to give an absolute scale of hardness (strength) which is represented in Figure 7.1 where Knoop values are plotted against Moh's scale. Hardness is affected to a high degree by structural weaknesses within minerals. Accurate hardness values however, account to a large extent for variations in presence of cleavage and it is therefore considered unnecessary to allow for structural inhomogeneity in the cement index.

The cement index must therefore include information on the percentage of cements/matrix present and their respective absolute hardness. Table 7.1 shows the Knoop numbers and active cementing percentages of the various cements present in the sandstones studied. The cement index is calculated by:

$$C.I.= \sum_{i=1}^{n} \left[\frac{ac.p}{n} \cdot \frac{Kn}{100} \right] \qquad (7.1)$$

where Kn = Knoop number

n = number of cements present

ac = active cementing percentage, and p = point count.

Using this system, the different cement types are weighted to account for variations in strength. The index also accounts for the presence of more than one type of cement.

Bell, (1978) suggested that an inverse relationship exists between percentage cement and uniaxial compressive strength. He explained this correlation by an increase in cement content as the void content increased; however this deduction only applies to

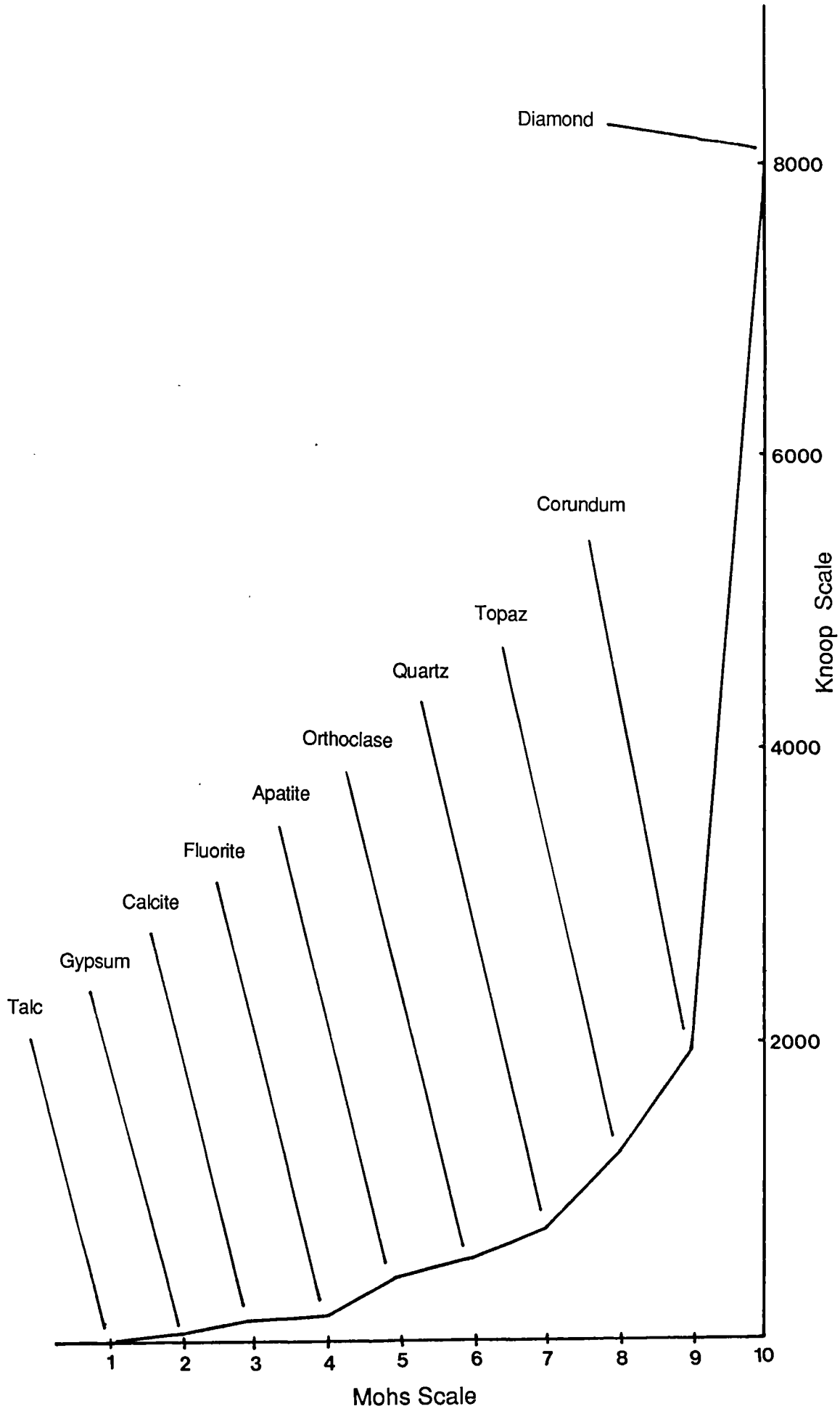

Figure 7.1 Mineral hardness: Mohs vs Knoop numbers.

Cement Type	Mohs Scale	Knoop No.	Active Cementing %
Quartz	7.0	750	100
Feldspar	6.0	550	100
Calcite	3.0	150	100
Haematite	6.0	550	100
Clays	2.25	100	100
Recrystallized clays	-	350	100
Glauconite	2.0	60	100
Mica	2.75	140	100
Quartz (quartz grains)	7.0	750	10
Quartz (MRF's)	7.0	750	5
Clays (SRF's)	2.25	100	10
Chlorite	2.25	100	100
Calcite (CRF's)		150	10

Table 7.1 Knoop numbers and active cementing values used in the QMA.

sandstones cemented by authigenic quartz overgrowths. It is suggested that the unlikely relationship proposed by Bell is due to the non-weighting of the data on cement type e.g. 10% quartz will impose a greater strength on framework grains than 15% calcareous cement. This underlines the importance of not only quantifying cement type but of also weighting it on the basis of its strength.

The calculated cement indices are given in Table 7.4.

7.2.3 Packing Density

Packing Density is defined by Kahn, (1956) as:

$$Pd = m \frac{\sum_{i=1}^{n} gi}{t} \times 100 \qquad (7.2)$$

where n = the total number of grains in a given traverse
gi = the grain intercept size of the ith grain in the traverse
m = a magnification constant, and
t = the length of the traverse

The results of packing density measurements in both vertical and horizontal directions are included in Chapter 3. In addition, computer based image analysis was used to measure the two dimensional packing density of all the sandstone types. It is given by:

$$\text{2-D P.D.} = \frac{\text{Total area of study}}{\text{Total area of framework grains}} \times 100 \qquad (7.3)$$

This involves the following process:

1. Colour photomicrographs similar to those shown in Chapter 3 were enlarged to A4 size. The exact size of any feature on the photocopy can be determined from the superimposed scale.
2. Transparent acetate sheets were then laid over the photomicrographs and the outlines of all the framework grains manually traced.
3. These grain outline maps were then digitised by tracing the outlines with a

mouse on a digitising tablet. The data was then stored on computer.

The work is extremely time consuming but the high workload is counterbalanced by the reliability of results. Fully automatic methods have been used for such fabric studies but grain shape resolution has proved to be problematical when for example rock fragments with polycrystalline quartz are dispersed in a quartzose matrix or when monocrystalline quartz grains are overgrown by authigenic quartz, (Schafer and Teyssen, 1987).

The digitising process yields useful data which includes the total area studied and the total area of framework grains. An example of an enlarged photomicrograph and an acetate overlay is shown in Plate 7.1 and Figure 7.2.

Bell, (1978) showed that as packing density increased in the Fell Sandstone of Northumberland, so did the uniaxial compressive strength, tensile strength and Young's modulus. The correlation coefficients were 0.675, 0.742 and 0.582 respectively.

In addition to packing density, Kahn defined the term packing proximity to describe the number of grain to grain contacts (irrespective of type) as a percentage of the total number of grain boundaries in a traverse. Packing proximity is given by:

$$Pp = \frac{q}{n} \times 100 \qquad (7.4)$$

where q = number of grain to grain contacts

n = total number of contacts

Packing proximity was calculated for each sandstone type in a direction parallel to loading. The results are included in Table 7.4.

7.2.4 Porosity

Porosity is important in any quantification of microfabric. The results presented in Chapter 5 demonstrate a good relationship between porosity and strength and would suggest that porosity could form the basis for a QMA of sandstones. Porosity data can be determined as a percentage number of pores from point counting as presented in Chapter 3. The percentage porosity determined by this method is invariably lower than true porosity and is generally unreliable since it is impossible to detect the smallest pores and cracks, (described by Halley, 1976 as submicroscopic porosity) using normal petrographic techniques.

Plate 7.1 Example of an enlarged thin section photomicrograph for digitising microfabric.

Figure 7.2 Acetate overlay for digitising microfabric.

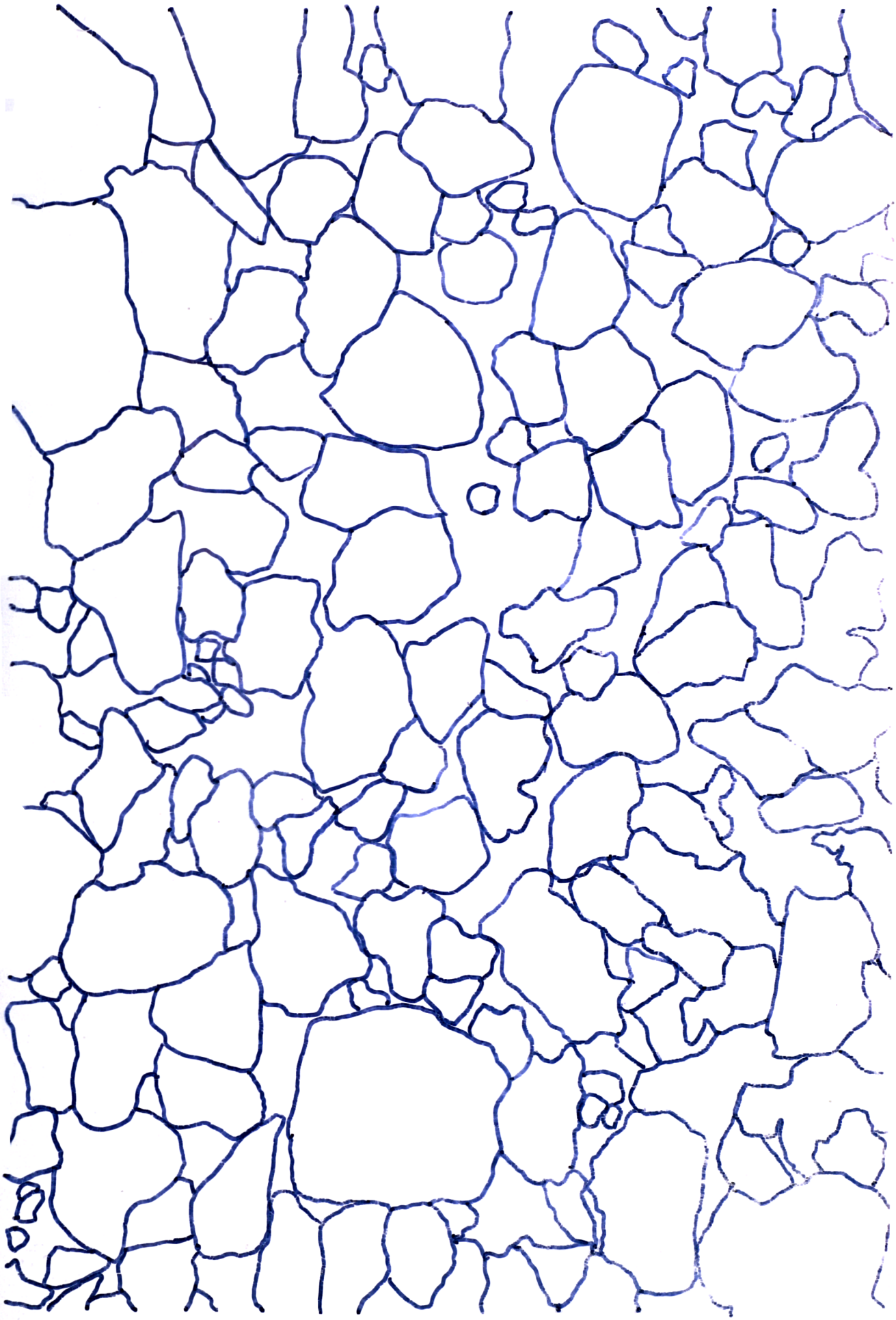

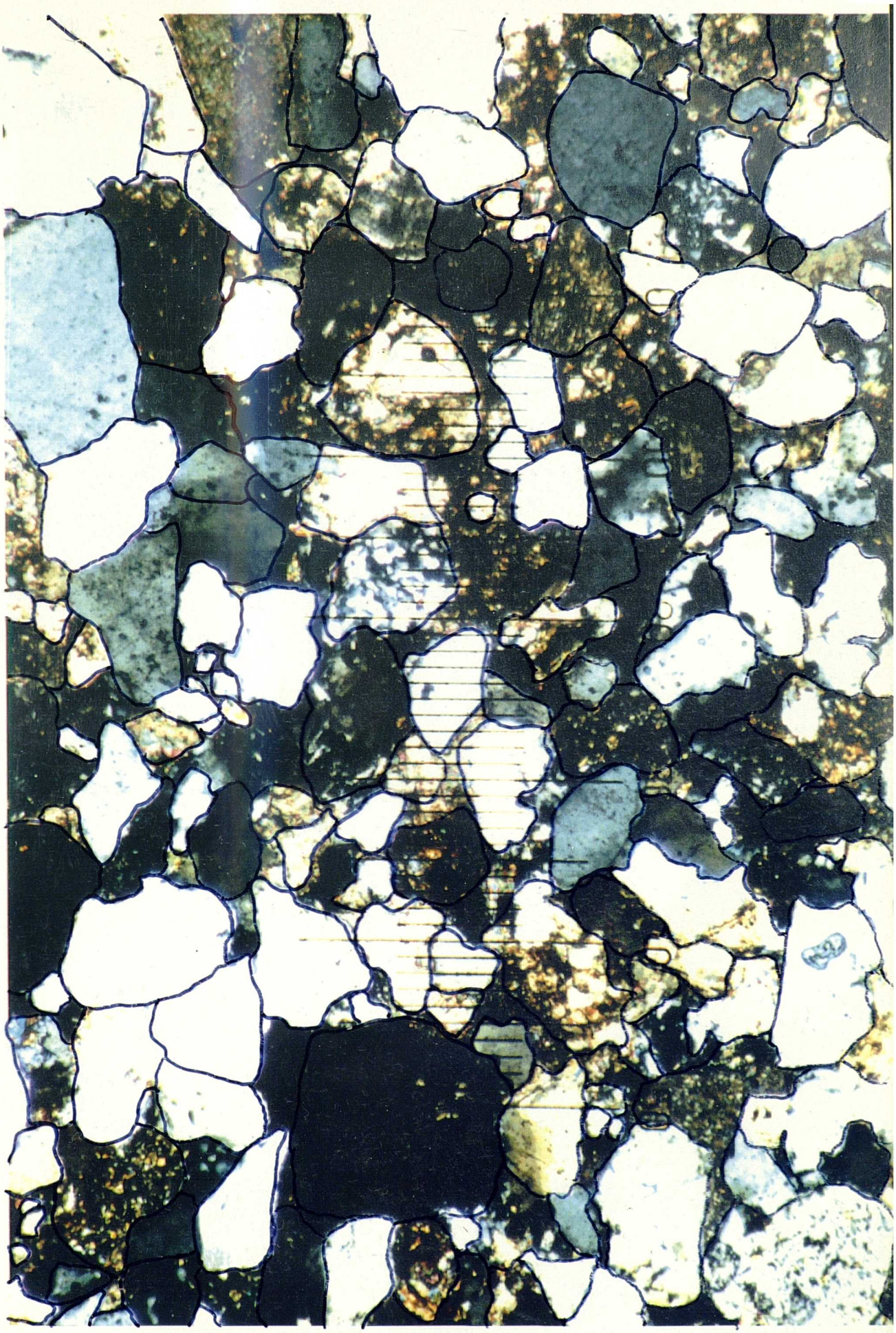

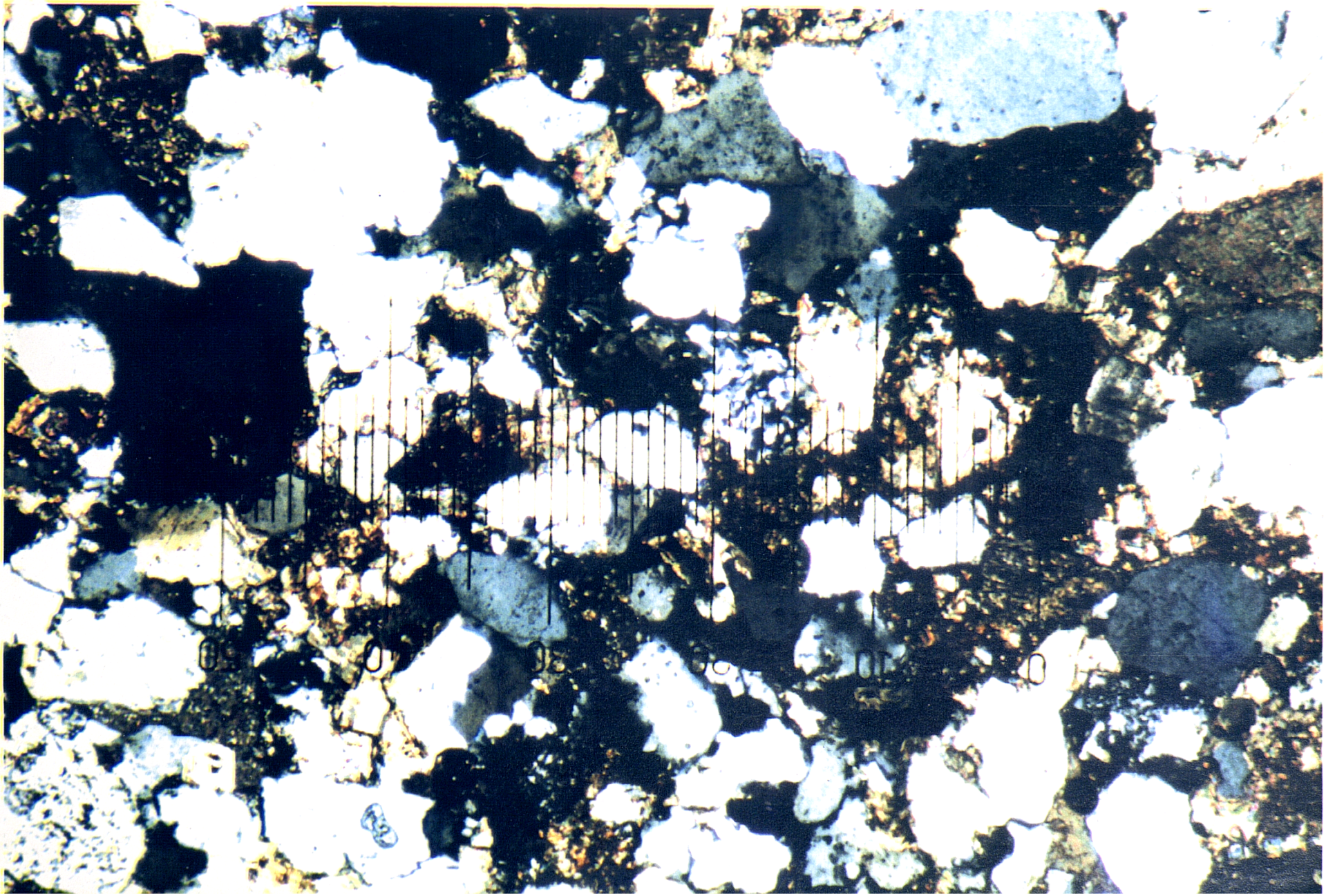

It is suggested that porosity measured by porometer should be used in this work since it showed a good correlation with UCS, (r=0.83) and gives values close to the total porosity of the rock. Figure 5.8. It is noteworthy that porosity will include pre-existing, tectonically formed microfractures within rock specimens, which can cause a decrease in strength.

7.2.5 Degree of interlocking

The load bearing capacity of any rock type will be influenced by the degree of interlocking of the constituent particles. Hoek, (1965) suggested that in igneous and metamorphosed sedimentary rocks, in which grains have been tightly packed and recemented, severe interlocking of the grains can occur which causes a considerable increase in the applied stress required to propagate grain boundary cracks. The same principle is true, but to a lesser degree, in sandstones, where diagenesis increases packing, number of grain contacts and degree of interlocking.

In order to quantify the degree of interlocking, the frequency and type of grain contact per 100 grains must be determined. The proposed Interlocking Index is thus given by:

$$\text{I.I.} = \frac{\Sigma\ (F\ .\ wf)}{N} \times\ 100 \qquad (7.5)$$

where F = frequency of each contact type
wf = weighting factor
N = number of grains

The different types of grain contact and their respective weighting factors are outlined in Table 7.2. The weighting factors have been chosen on the basis of the degree of diagenetic compaction indicated by the presence of each contact type. An acetate trace is made of the vertical thin section and each contact type is counted and the number of each type multiplied by the weighting factor. In some cases no contact appeared to occur between grains but the boundaries were close together and parallel. This is due to the corpuscle effect and indicates sectioning just above or below a contact. These were not counted as grain to grain contacts for the purposes of the QMA.

Contact Type	Weighting Factor
Point contact	1
Straight contact	2
Concavo-convex	3
Triple point	4
Sutured contact	5

Table 7.2 Weighting factors used in the calculation of the interlocking index for sandstones.

7.2.6 Grain size

As discussed in Chapters 1 and 2, grain size within sandstones is highly variable. A number of workers have reported that the yield stress increases when the mean grain size decreases, (e.g. Hugman and Friedman, 1979). Bell, (1978) however, found that no relationship existed between grain size and strength variations within the one sandstone type tested.

Area equivalent diameter, (AED) is regarded as being one of the most truely representative measures of grain size since it takes some account of the variations in volume of differently shaped grains with the same long axis dimension. AED is determined by measuring the area of each grain in a thin section and calculating the diameter of a circle of equivalent area. The grain areas were calculated by digitising photomicrographs of each sandstone.

Grain size measurements made from thin sections always possess a certain error since section diameters of randomly orientated grains are recorded rather than the maximum equatorial diameter. The reason for this bias is the corpuscle effect, (Burger and Skala, 1973 and 1974). The diameter measured in the thin section may either be correct (i.e. in the correct grain size class) or too small. As diameters can never be too large, the thin section derived grain size distribution curve is always slightly biased towards its finer tail. Computer programs have been developed, (e.g. Schafer and Teyssen, 1987) which perform a stochastic Monte Carlo simulation for correction of grain size analyses from thin section. The effect of the process is to increase the apparent sorting and decrease the standard deviation of the results.

During this research it was considered unnecessary to carry out such a modification of the data since the errors are relatively small and, provided all the sandstones are measured in the same way, the effect will be minimal.

Grain size data was collected for 300 grains from both horizontal and vertical sections and input into a grain size analysis program which calculates the statistical measures of grain size. The following statistical parameters were used from the grain size analyses:

Mean grain size
Standard deviation
Folk mean
Folk sorting
Folk kurtosis
Folk skewness

The results are included in Table 7.4. Hamilton, (1988 pers. comm) states that the Folk measures are the most statistically valid grain size parameters. Folk skewness

is an indication of how much the distribution is weighted in the direction of either the coarse or the fine fraction, Figure 7.3(a). Folk kurtosis is a measure of the spread of the distribution about the mean. Figure 7.3(b).

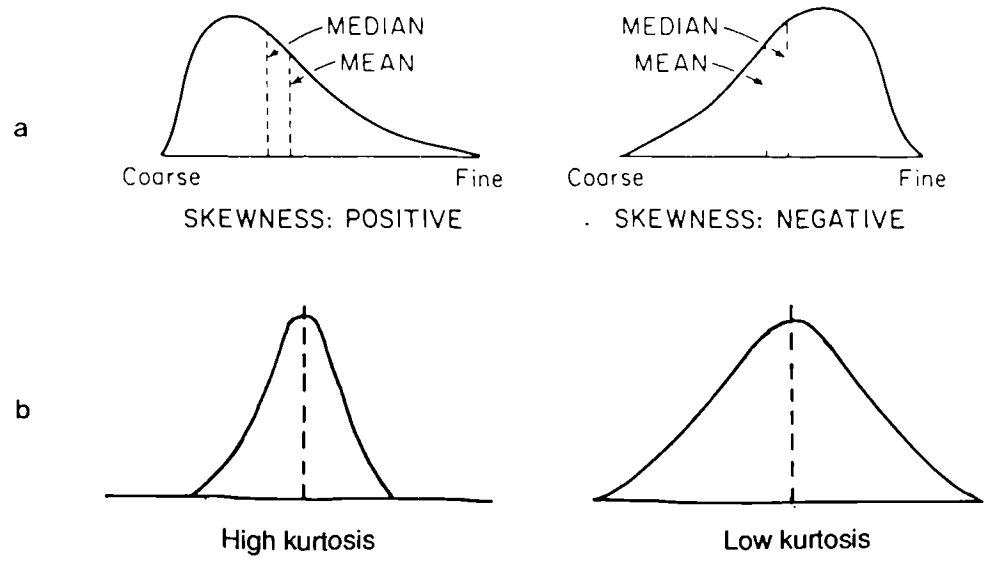

Figure 7.3 Definitions of (a) skewness and (b) kurtosis.

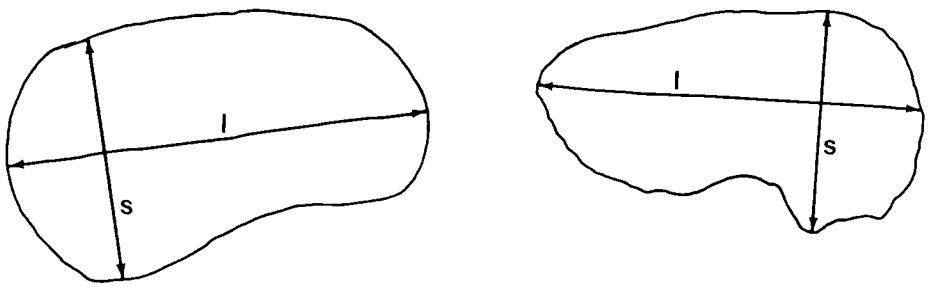

Figure 7.4 Method of measurement of long and short grain axes in thin section.

7.2.7 Grain shape

Howarth and Rowland, (1986) state that minor changes in grain shape occur during loading. Clearly the effect increases at higher stresses. This leads to the question, is there an ideal shape which inhibits fracture propagation and thus increases strength? SEM studies described in Chapter 5 have indicated that stable microfracturing occurs more readily in sandstones containing well-rounded and high sphericity grains.

As discussed in Chapter 2, grain shape is defined by a number of different terms, such as sphericity, form and roundness. Since form is to a large extent explained by sphericity or elongation, it is considered that for the purposes of a QMA, only sphericity and roundness will be used. Leader, (1982) states that in thin section, sphericity is assessed as elongation, i.e. the ratio of length to width of a grain. For the QMA, sphericity, roundness and elongation factor have been used for correlation.

Elongation factor is calculated as the maximum long axis of a grain divided by the maximum orthogonal width as shown in Figure 7.4. Since particular grain axes are normally observed in thin section, elongation was measured over 100 grains from sections cut parallel to bedding and the results averaged.

Both sphericity and roundness have been defined mathematically as described in Section 2.3.2. However, to calculate these parameters from first principles for a large number of grains and sandstone types would be an extremely time consuming operation. A number of two-dimensional images have been created by workers such as Powers, (1953), Krumbein and Sloss, (1963) and Pettijohn et al, (1973). They allow the rapid visual estimation of roundness and sphericity and have been shown to give results which correspond well with calculated values. For the purposes of a QMA the system of Krumbein and Sloss is the most useful since it gives four numerical classes for each parameter. The modified version of Krumbein and Sloss's system which was used in this research is shown in Figure 7.5.

Sphericity and roundness were measured using this system for 100 grains in both vertical and horizontal sections. The measurements were then averaged to give a value for roundness and sphericity for each sandstone. The results are included in Table 7.4.

7.2.8 Grain orientation

Rock mechanics studies on sedimentary rocks have indicated that UCS values are lower when specimens are tested parallel to bedding, (Dobereiner, 1984; Al-Jassar, 1979). This strength decrease has been attributed to the alignment of individual grains in the direction of loading.

Angular orientation of grains has been quantified by the development of an angle factor by Howarth and Rowlands, (1986). This factor was only calculated for elongated grains, i.e. those with an aspect ratio greater than 2.0. It is given by the equation:

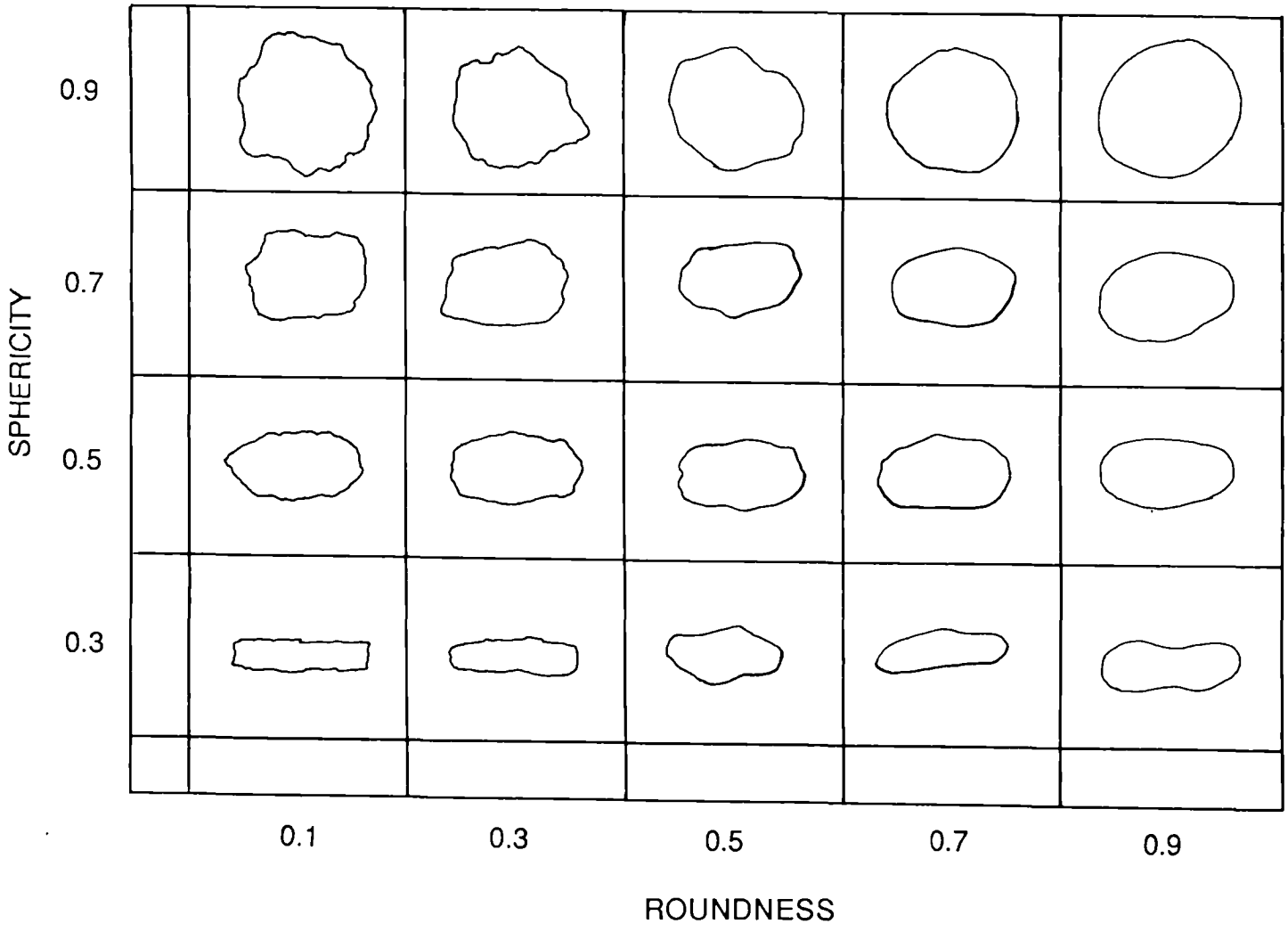

Figure 7.5 Roundness and Sphericity chart

$$\text{Angle Factor} = \sum_{i=1}^{9} \left[\frac{xi}{\frac{N(N-1)}{2}} \right] \times i \qquad (7.6)$$

where N = total number of elongated grains

xi = number of angular differences in each class

It is calculated by a class weighted system applied to the absolute, acute angular differences, (0 to 90°) between each and every elongated grain. The angular differences are then separated into nine classes, each of which are weighted.

This system will give a good indication of the degree of preferential alignment of grains within a rock but does not indicate how this alignment is related to any imposed stress. Since microfractures form in uniaxial compression, generally parallel to the direction of the applied stress, it is likely that alignment of the long axis of grains close to this direction will promote microfracture formation. It was therefore decided that a 'σ_1 alignment factor' should be used to indicate the degree of alignment of elongate grains parallel to σ_1. The formula is a modified version of the Howarth and Rowland angle factor. It is given by:

$$\sigma_1 \text{ Alignment Factor} = \frac{N}{T} \sum_{i=1}^{9} \left[\frac{xi}{N} \right] \times wi \qquad (7.7)$$

where xi = number of grains in each class

wi = weighting factor for each class

N = number of elongated grains

T = total number of grains

The nine classes and their respective weighting factors are given in Table 7.3. The weighting factors have been selected so that when all the grains are elongate and within 0-10° of the σ_1 direction, the alignment factor approaches 1. As the number of high sphericity grains increases or the number of grains at high angles to σ_1 increases, then the alignment factor approaches 0. Elongated grains were regarded as those of aspect ratio greater than 2.0. The inclusion of the fraction N/T in the equation accounts

Classes	Weightings
$\theta<10°$	0.9
$10<\theta<20°$	0.8
$20<\theta<30$	0.7
$30<\theta<40$	0.6
$40<\theta<50$	0.5
$50<\theta<60$	0.4
$60<\theta<70$	0.3
$70<\theta<80$	0.2
$80<\theta<90$	0.1

Table 7.3 Angle classes and weighting factors used for calculation of σ_1 alignment factor.

for the number of elongated grains in the total grain population studied. This is because the alignment of elongated grains parallel to σ_1 will have a negligible effect if they form only a small proportion of the total number of grains.

7.2.9 Summary

The data collected from each sandstone type was processed by computer and the relevant parameters calculated. It would be impossible to present all the data collected for each grain but the relevant parameters used in the statistical analysis are included in Table 7.4

SANDSTONE REGRESSION DATA

	Sst Type	UCS	TAN E	SECE	Poisson's R	MCRSR %
1	A	141.32	33.33	19.90	0.168	29.7
2	DQ	237.86	38.46	30.81	0.208	22.7
3	BQ	247.00	32.32	33.61	0.197	18.2
4	LORS	152.03	32.27	23.39	0.147	29.4
5	PiA	173.28	39.29	43.32	0.093	12.17
6	PiB	227.29	39.02	31.21	0.090	8.31
7	UCS	161.37	28.99	29.34	0.159	10.81
8	MGA	59.33	12.80	8.86	0.346	33.2
9	MGB	49.03	15.38	11.40	0.044	18.1
10	MGC	123.36	22.62	13.71	0.171	71.2
11	MGD	127.50	23.08	19.03	0.150	23.5
12	HBGA	119.08	19.86	13.53	0.030	58.8
13	HBGB	108.06	14.08	11.37	0.262	55.0
14	SS	198.36	45.98	34.04	0.043	8.1
15	EF	59.94	10.60	8.56	0.092	47.6
16	TRA	89.94	14.49	10.58	0.188	57.3
17	TRB	91.84	11.78	9.98	0.140	49.2
18	MCM	37.08	11.59	8.72	0.216	31.7
19	CF	298.18	36.38	30.04	0.172	20.0
20	PnA	114.18	21.21	15.86	0.191	56.2
21	PnB	106.15	26.63	19.30	0.255	50.4
22	PnC	103.38	18.86	14.98	0.181	54.5
23	An	66.28	17.02	8.84	0.237	34.3
24	PrA	65.96	17.70	12.39	0.074	19.4
25	PrB	34.77	8.05	6.36	0.239	15.5
26	PrC	81.99	27.97	20.36	0.221	11.3
27	PrD	101.16	24.39	24.98	0.100	13.1
28	PrE	59.72	10.08	8.53	0.303	31.7
29	R	36.05	8.76	5.42	0.322	37.8
30	MS	23.20	6.06	3.44	0.342	37.2
31	ArdA	42.15	7.92	7.14	0.379	12.5
32	ArdB	53.35	6.30	5.93	0.143	10.8
33	AS	30.58	6.45	4.78	0.917	-5.7
34	G	10.45	1.56	1.23	0.125	77.8
35	D	74.51	16.00	14.90	0.279	37.4
36						

Table 7.4 Data used in regression analysis. (Pages 270-276).

SANDSTONE REGRESSION DATA

	DBD	n	Poro.	Porosity	2-D. P.D.	VERT. P.D.	HORIZ P.D.
1	2.475	5.372		6.219	83.2	87.2	83.0
2	2.600	1.294		2.541	99.5	99.0	98.0
3	2.608	0.715		1.060	99.8	95.0	93.0
4	2.460	6.764		11.023	77.2	84.0	83.1
5	2.768	0.702		0.809	68.7	85.2	85.1
6	2.712	0.651		1.632	69.7	87.6	82.1
7	2.634	4.609		5.293	45.5	63.9	62.4
8	2.149	11.74		13.20	74.2	81.0	79.7
9	2.199	11.44		12.65	70.3	79.1	87.1
10	2.291	8.06		11.95	74.3	82.1	75.2
11	2.283	9.21		13.73	77.7	81.4	80.8
12	2.286	10.11		12.63	75.3	83.9	82.7
13	2.302	10.30		12.86	74.0	85.7	85.0
14	2.532	1.20		1.85	90.2	91.5	91.2
15	2.232	12.37		13.70	73.2	78.9	83.1
16	2.229	12.03		12.01	80.1	83.1	85.2
17	2.261	11.92		20.04	80.5	71.9	83.4
18	2.081	12.92		20.04	65.9	71.9	78.1
19	2.653	1.97		1.42	96.5	81.1	83.6
20	2.459	7.25		8.63	76.3	91.8	90.7
21	2.466	6.87		11.13	75.0	89.7	85.0
22	2.477	8.21		10.43	79.5	86.2	86.8
23	2.117	13.49		19.38	62.7	69.5	57.6
24	2.368	7.60		10.05	65.6	79.0	71.0
25	2.183	12.17		16.32	36.33	83.2	70.2
26	2.428	5.531		8.75	80.25	92.5	82.5
27	2.442	4.70		6.50	71.0	81.4	80.7
28	2.163	11.54		16.46	64.8	72.0	71.2
29	2.270	17.27		18.20	66.25	65.0	63.1
30	1.767	22.52		24.92	49.8	45.7	46.2
31	1.993	18.86		26.80	58.9	65.0	65.1
32	1.918	17.09		25.95	61.3	65.4	65.3
33	1.886	19.86		29.44	63.5	76.7	62.8
34	1.531	38.33		42.65	38.1	31.0	29.9
35	2.156	15.589		22.48	38.4	28.0	27.8
36							

SANDSTONE REGRESSION DATA

	Roundness	Sphericity	Interlocking	Alignment F.	Packing Prox.	% Quartz
1	0.36	0.53	3.05	0.0015	20	20
2	0.31	0.52	6.37	0.008	100	88.7
3	0.13	0.47	9.28	0.015	100	94.3
4	0.30	0.55	2.86	0.0095	70	40.9
5	0.12	0.40	4.92	0.007	65	63.3
6	0.28	0.35	5.24	0.008	85	61.3
7	0.48	0.69	1.59	0.085	10	37.0
8	0.52	0.81	3.89	0.007	55	74.6
9	0.57	0.79	4.57	0.004	55	69.0
10	0.34	0.53	5.74	0.004	75	74.2
11	0.53	0.51	5.80	0.009	55	79.9
12	0.41	0.69	5.12	0.010	65	67.5
13	0.19	0.54	5.20	0.009	60	71.7
14	0.22	0.73	7.19	0.001	90	84.7
15	0.35	0.75	4.59	0.012	55	53.9
16	0.31	0.67	5.36	0.005	80	55.2
17	0.32	0.60	5.29	0.004	60	72.9
18	0.54	0.69	3.57	0.014	45	64.0
19	0.21	0.52	7.21	0.001	75	62.3
20	0.48	0.52	6.26	0.019	75	28.3
21	0.42	0.71	6.20	0.023	85	31.2
22	0.35	0.53	6.51	0.009	75	29.6
23	0.30	0.53	3.63	0.013	60	49.8
24	0.62	0.74	1.68	0.015	70	59.2
25	0.67	0.81	1.40	0.007	25	82.4
26	0.73	0.73	3.30	0.017	60	76.6
27	0.75	0.82	1.45	0.007	45	67.9
28	0.42	0.54	3.32	0.019	40	53.1
29	0.68	0.79	2.91	0.006	30	44.3
30	0.21	0.67	1.30	0.013	20	38.3
31	0.32	0.70	2.32	0.002	15	71.2
32	0.49	0.51	2.10	0.005	20	66.6
33	0.30	0.55	2.53	0.077	5	78.6
34	0.51	0.54	1.07	0.093	0	32.2
35	0.50	0.54	1.25	0.087	20	30.7
36						

SANDSTONE REGRESSION DATA

	% Alk Feld.	% Plag Feld.	% SRF's	% PRF's	% MRF's	% IRF's
1	44.3	8.0	1.3	0	1.0	0
2	0.5	1.0	0	0	2.5	0
3	4.7	1.0	0	0	0	0
4	5.1	2.0	13.3	0	5.1	2.4
5	3.7	0.3	4.0	0	6.0	0
6	6.7	3.3	0.7	0	4.7	0
7	1.0	0.0	3.0	0	4.0	5.3
8	2.4	0.3	0.7	0	3.9	0
9	9.2	1.1	1.4	0	5.3	0
10	5.3	0	2.0	1.0	0	0
11	2.4	1.1	1.8	0	0.3	0
12	8.0	2.1	1.8	0	2.4	0
13	2.0	4.1	3.1	0	0	0
14	2.7	1.0	1.0	0	3.3	0
15	5.1	3.4	8.5	0	10.2	0.7
16	4.8	2.1	21.9	0	6.9	0
17	8.6	0.0	2.1	0	0	0
18	13.3	1.4	1.1	0	1.1	2.9
19	2.0	0	9.7	0	6.3	0
20	3.0	0	18.7	7.3	25.0	0
21	2.1	0.7	18.2	9.3	29.2	0
22	2.0	0.0	8.8	24.9	30.3	0
23	4.9	1.1	8.7	0	5.3	1.4
24	10.5	3.6	4.0	0	0.8	5.8
25	4.3	0	0.3	0	1.8	0
26	4.1	0	2.1	0	9.6	0
27	3.1	0	3.8	0	3.4	3.1
28	5.0	3.1	5.5	0	5.0	0
29	1.4	0	5.4	0	6.1	0
30	0.7	0	1.0	0	0.7	0
31	2.1	0	3.7	0	0	0
32	3.8	0	0	0	0	0
33	3.7	0	1.2	0	0	0
34	0.0	0	0	0	0	0
35	1.8	3.8	0	0	0	0
36						

SANDSTONE REGRESSION DATA

	% CRF's	% Haematite	% Opaques	% Clays	% Chlorite	% Glauconite
1	0	13.3	0	3.0	8.0	0
2	0	0	0	0	0	0
3	0	0	0	0	0	0
4	6.1	13.0	2.0	3.1	0	0
5	0	0	3.7	16.0	0	0
6	0	9.7	0	4.3	0	0
7	7.4	0	0.3	0	0	0
8	0	0	2.1	13.9	0	0
9	0	0	1.1	12.0	0	0
10	0	0	0.7	12.7	0	0
11	0	3.5	0.7	9.2	0	0
12	0	0	1.0	15.2	0	0
13	0	0	0.3	16.7	0	0
14	0	0.7	2.7	3.0	0	0
15	0	2.0	0.7	12.6	0	0
16	0	0	2.4	5.9	0	0
17	0	0	0.7	14.4	0	0
18	0	2.5	2.9	9.4	0	0
19	0	1.0	0	15.3	0	0
20	0	3.0	11.7	2.3	0	0
21	0	0	1.3	7.9	0	0
22	0	0	1.3	2.0	0	0
23	3.9	10.2	1.4	6.3	0	0
24	0	13.4	0.8	1.9	0	0
25	0	7.6	1.4	2.2	0	0
26	0	5.9	1.0	0.7	5.2	0
27	0	12.7	0.7	0.1	0	0
28	0	10.5	2.0	6.2	0	0
29	5.7	6.1	1.1	3.2	0	0
30	6.3	18.3	1.7	1.7	0	0
31	0	1.6	2.1	4.9	0	12.3
32	0	0	1.5	8.9	0	18.5
33	0	0	1.6	0.4	0	13.2
34	1.7	0	0	50.5	0	10.3
35	2.1	0	1.3	16.9	0	10.3
36						

SANDSTONE REGRESSION DATA

	% Spry. Calcite	% Micrite	% Micas	% Hvy.	Cement Index	Elongation
1	0	0	0	0	31.9	1.21
2	0	0	7.3	0	75.0	1.62
3	0	0	0	0	75.0	1.35
4	4.4	0	1.4	1.0	39.6	1.42
5	0	0	3.0	0	48.2	1.56
6	5.3	0	4.0	0	72.9	1.57
7	10.7	31.3	0	0	33.2	1.27
8	0	0	2.1	0	33.0	1.09
9	0	0	1.1	0	34.1	1.12
10	2.7	0	1.0	0.3	31.6	1.33
11	0	0	1.1	0	41.3	1.35
12	0	0	2.1	1.0	30.1	1.40
13	0	0	2.0	0	29.3	1.41
14	0	0	0.3	0.7	75.0	1.30
15	0	0	3.0	0	31.0	1.42
16	0	0	0.7	0	38.8	1.31
17	0	0	1.3	0	31.7	1.28
18	0	0	1.4	0	37.5	1.13
19	2.0	0	0.7	0.7	83.5	1.22
20	0	0	0.7	0	44.7	1.75
21	0	0	1.0	0	31.2	1.37
22	0	0	1.0	0	40.8	1.69
23	7.1	0	0	0	42.5	1.60
24	0	0	0	0	60.3	1.43
25	0	0	0	0	35.2	1.19
26	0	0	0	0	43.1	1.48
27	0	0	0	0	56.9	1.32
28	9.7	0	0	0	36.6	1.55
29	26.0	0	0	0	25.9	1.22
30	3.3	27.3	0.7	0	24.5	1.42
31	0	0	0	2.1	31.2	1.54
32	0	0	0	0.8	23.2	1.56
33	0	0	0	1.2	6.12	1.53
34	2.3	0	3.0	0	9.5	1.47
35	0	32.4	0.7	0	12.0	1.44
36						

SANDSTONE REGRESSION DATA

	Mean G. Size	Std. Deviation	Folk Mean	Folk Sorting	F. Kurtosis	F. Skewness
1	2.91	0.93	2.88	0.95	2.40	0.09
2	3.00	0.88	3.42	0.24	3.57	0.69
3	1.72	1.33	1.74	1.24	2.53	0.43
4	2.92	1.33	2.85	1.17	2.29	0.35
5	3.48	0.88	3.99	2.24	3.58	0.69
6	2.94	1.06	2.92	0.58	1.17	-0.05
7	2.63	0.83	2.57	0.77	1.02	0.06
8	2.36	0.59	2.46	0.40	1.39	-0.33
9	0.74	1.36	0.74	1.60	2.21	0.92
10	3.13	0.87	3.13	0.82	1.93	-0.06
11	3.28	0.53	3.26	0.69	1.33	0.32
12	2.45	0.67	2.46	1.24	1.53	0.38
13	2.46	0.66	2.46	1.25	1.47	0.39
14	3.09	0.15	3.11	1.53	1.09	0.10
15	2.31	0.73	2.33	0.87	3.21	0.43
16	3.25	0.62	3.27	1.21	2.39	0.03
17	3.26	0.58	3.26	1.11	2.30	0.05
18	2.00	0.43	2.09	0.49	1.23	-0.34
19	3.90	0.94	5.44	3.10	1.11	0.81
20	1.73	0.95	1.65	0.63	1.29	0.13
21	2.43	0.87	2.39	0.85	0.88	0.08
22	2.25	1.14	2.23	0.93	0.95	0.13
23	2.74	0.83	2.70	1.54	1.33	-0.43
24	3.19	1.18	3.14	0.67	1.55	0.11
25	2.26	1.73	2.30	0.92	0.70	-0.29
26	2.18	0.81	2.20	0.85	0.91	-0.07
27	2.09	0.82	2.07	0.84	0.85	-0.04
28	3.13	0.93	3.06	0.87	0.84	0.42
29	4.36	1.17	6.70	3.58	0.70	0.45
30	4.50	0.84	7.36	3.58	0.64	0.23
31	3.76	0.99	6.79	1.24	1.04	0.32
32	4.26	0.83	6.23	1.09	0.93	0.37
33	3.62	0.73	6.72	0.93	0.88	0.53
34	4.35	0.91	6.89	3.66	0.74	0.37
35	4.29	0.85	6.54	3.51	0.67	0.54
36						

7.3 A Sandstone Performance Regression Model.

7.3.1 The principles of multiple regression analysis.

Simple regression has been used in this research to study the correlation between certain static properties and strength properties. Scatter diagrams have been used to represent relationships between two numerical variables; where an association has been discerned it has been summarised with greater or lesser accuracy by the equation of a trend curve passing through the cloud of points. The position of the line is chosen to minimise the sum of squares of the residuals or differences between observed and predicted y values for each observed x value. A measure of the goodness of fit of a least squares simple regression is given by the correlation coefficient, r-value or more precisely its square. When r=1 or -1 there is no scatter and every point lies on the trend line.

Simple regression assumes that differences in a dependent variable are accounted for partly by the linear effect of a single explanatory variable and partly by a disturbance term that lumps together individuality, measurement error and the effects of relevant but unconsidered variables. In order to determine the true controls on some dependent variable, it is desirable to reduce the residual scatter as far as possible towards zero. Nothing can be done about genuinely unique individual circumstances and it may be impracticable to obtain more accurate measurements. Therefore the main scope for improvement usually lies in separating out from the disturbance term other relevant explanatory variables and incorporating them explicitly in a multi-variable or multiple regression model.

Multiple regression is one of the most widely used statistical tools for analysing multifactor data where several conflicting or reinforcing effects are at work and the variables responsible are themselves interrelated. Since such a statistical procedure involves the processing of a large amount of data, computers are ideally suited for the purpose. Although highly sophisticated software is available, computers are blind to any anomalies or any expected relationships in the data which would be obvious to the researcher with a knowledge of the problem. The raw data should therefore be studied initially to discover any interesting relationships, unusual behaviour or exceptional points, as a key to understanding difficulties which may arise during fitting and diagnostic stages. After fitting a linear model to a given body of data, an assessment is made of the adequacy of fit - the square of the multiple correlation coefficient, i.e. R-squared. This denotes the proportion of total variability explained by the regression equation, in the range of 0-100%. When the model fits well, the R-squared will be close to 100%. However, a high R-squared value does not necessarily mean that the

data has been well fitted by the model.

There are four assumptions of multiple regression vital to the Ordinary Least Squares, (OLS) estimates and inferential tests:

1) linearity

2) constant error variance, (heteroskedasticity);

3) lack of spatial autocorrelation, and

4) no severe multicollinearity.

At the initial stage calculation and inspection of a correlation matrix between all independent and dependent variables is important. It serves to identify:

a) high pairwise correlation between the response and particular variables, and

b) patterns of correlation between independent variables. This is critical to the process of multiple regression modelling.

The main guide to the importance of variables in the regression model is the significance of the associated t-statistic. However graphical methods also need to be used. The importance of graphics was noted by Chambers, (1983); "Graphical methodology is a powerful tool for conveying properties of the fitted regression, assessing the adequacy of fit and suggesting improvements". The use of scatter plots for each variable can however be misleading and partial regression plots or adjusted variable plots are used instead. By using this method the influence of the other explanatory variables are accounted for or 'removed' in a manner that permits the plot to be interpreted in many of the ways appropriate in the simple regression situation. Partial regression plots allow tests for linearity, outliers and heteroskedasticity.

Homoskedasticity is defined as a constant degree of scatter about the population rather than local regions of high or low scatter. If this condition is violated, then heteroskedasticity is occurring, i.e. a condition of non-constant scatter. If OLS is applied, ignoring heteroskedasticity, the estimated coefficient is still unbiased, but is no longer the best in the sense of precision. The problem is detected by a wedge shaped plot in the partial regression diagram. If heteroskedasticity is detected without corrective action being taken and OLS is applied to the raw data, the resulting estimated coefficients lack precision and the estimated standard errors of the regression coefficient are often understated giving a false sense of precision. Heteroskedasticity is dealt with using Weighted Least Squares, (WLS), which weights each observation. This is obtained by minimising weighted sum-of-squares residuals, where the weights are inversely proportional to the variance of errors. Once transformed, errors should show no structure and are therefore homoskedastic and the standard assumption of the Least Squares theory holds.

Lack of multicollinearity is the implicit assumption that the independent variables are not strongly interrelated. In complete absence of a linear relationship

between them, variables are orthogonal, but in most regression applications, explanatory variables are non-orthogonal, (or show severe multicollinearity). Although difficult to detect, it is important to realise that it exists since any conclusions based on regression analysis in the presence on multicollinearity are often doubtful. Regression analysis fails due to multicollinearity because there are not separate variables but effectively one.

The presence of multicollinearity is indicated by the size of the correlation coefficient existing among explanatory variables, but this only accounts for pairwise correlations. A more subtle test is that of the R-squared partial regression test, (Rj^2), when Xj is regressed as the dependent variable against all other variables. If Rj^2 is greater than R^2 then problems exist. If multicollinearity is identified between two variables, deletion of one of these variables will have little effect on the model, and in many cases will in fact improve it.

The aim is to progressively improve the model to the point where it is deemed to be highly successful, trying to choose the least number of independent variables that explain the most substantial part of the variation in the dependent variable. Only a total comprehensive analysis will provide an adequate selection of variables and a useful regression equation.

7.3.2 Processing the Data.

The data which was used in the regression analysis is shown in Table 7.4. A total of 41 variables were used and are listed in Table 7.5. These consist of five dependent and 36 independent variables. The data was processed using a Minitab statistics package capable of performing complex manipulation of data at high speeds. All the variables were fed manually into the computer to create a matrix of 41 columns by 35 rows. A printout of the data was then created and the values checked.

7.3.3 Results

The first stage in the regression analysis was to produce a correlation matrix of the 5 dependent variables against the independent values. This matrix serves to identify at an early stage, any variables which are strongly correlated. high r-values, (correlation coefficients) obtained from a correlation matrix will however only indicate linear relationships. The r-values may be low therefore, even if a strong log relationship exists, as seen earlier in the research.

Table 7.6 lists part of the correlation matrix for all the sandstone data. The 'C' values correspond to the variables in the original data matrix. The strongest r-values for the 5 independent variables are indicated. It is obvious that with the exception of the cement index, which shows a high r-value, the strength and elastic properties are

C1	Dry Strength
C2	Tan E
C3	Sec E
C4	Sec m
C5	Saturation Decrease
C6	DBD
C7	n
C8	Poro porosity
C9	2D P.D.
C10	Vertical P.D.
C11	Horizontal P.D.
C12	Roundness
C13	Sphericity
C14	Interlocking Index
C15	sc alignment factor
C16	Packing proximity
C17	Quartz
C18	Alkali feldspar
C19	Plagioclase feldspar
C20	SRF's
C21	PhRF's
C22	MRF's
C23	IRF's
C24	CRF's
C25	Haematite
C26	Opaques
C27	Clay minerals
C28	Chlorite
C29	Glauconite
C30	Calcite cement
C31	Micrite
C32	Muscovite
C33	Heavy minerals
C34	Cement Index (iii)
C35	Elongation Factor
C36	Mean Grain Size
C37	Std Deviation
C38	Folk Mean
C39	Folk sorting
C40	Folk Kurtosis
C41	Folk Skewness

Table 7.5 Dependent and independent variables used. (C1-C5 are the dependent variables).

	C1	C2	C3	C4	C5
C2	0.887				
C3	0.877	0.945			
C4	0.343	0.403	-0.384		
C5	-0.226	-0.322	-0.396	-0.217	
C6	0.816	0.871	0.870	-0.407	-0.259
C7	-0.781	-0.849	-0.825	0.360	0.364
C8	0.796	0.856	-0.833	0.435	0.280
C9	0.668	0.606	0.512	-0.201	-0.041
C10	0.529	0.584	0.502	-0.169	-0.207
C11	0.550	0.564	0.510	-0.303	-0.123
C12	-0.508	-0.346	-0.358	-0.075	-0.054
C13	-0.478	-0.326	-0.354	-0.013	-0.044
C14	0.673	0.540	0.499	-0.237	0.151
C15	-0.183	-0.215	-0.152	0.206	0.171
C16	0.649	0.636	0.560	-0.412	0.125
C17	0.219	0.132	0.187	0.062	-0.421
C18	0.028	0.153	0.012	-0.142	-0.034
C19	0.098	0.160	0.043	-0.175	0.078
C20	0.058	0.063	0.007	-0.049	0.359
C21	0.002	0.020	-0.003	-0.014	0.312
C22	0.056	0.143	0.100	-0.078	0.284
C23	-0.036	0.065	0.106	-0.195	-0.221
C24	-0.119	-0.082	-0.075	0.084	0.008
C25	-0.146	0.003	-0.087	-0.036	-0.193
C26	-0.124	-0.037	-0.032	0.056	0.123
C27	-0.200	-0.302	-0.255	-0.199	0.542
C28	0.069	0.203	0.134	-0.104	-0.100
C29	-0.360	-0.444	-0.369	0.418	-0.175
C30	-0.097	0.113	-0.117	0.110	0.014
C31	-0.074	-0.073	0.008	0.102	-0.050
C32	0.312	0.248	0.250	-0.209	0.190
C33	-0.003	-0.062	-0.087	0.314	-0.268
C34	0.799	0.755	0.735	-0.432	-0.355
C35	0.054	0.041	0.069	0.120	0.052
C36	-0.116	-0.216	-0.194	0.269	0.025
C37	-0.014	-0.065	-0.024	-0.031	-0.121
C38	-0.258	-0.374	-0.321	0.463	-0.054
C39	-0.018	-0.109	-0.061	0.045	0.167
C40	0.394	0.382	0.407	-0.314	0.052
C41	0.210	0.077	0.145	0.045	-0.103

Table 7.6 Correlation matrix for sandstone properties

controlled primarily by textural rather than mineralogical parameters.

Graphical methods were used to check the plots of dependent against independent variables for any non-linear relationships. A number of these plots are included in Figure 7.6.

The next stage in the analysis involved the regression of each dependent variables against the independent variables. A step-wise procedure was followed whereby a relatively large number of variables were regressed initially and progressively deleted to derive an improved equation. In this way, only variables with a high t-ratio were retained while maintaining a high R2 value for the equation.

When the equation was derived, a number of statistical tests were carried out as described in section 7.3.1.

A. Uniaxial compressive strength.

The uniaxial compressive strength is strongly related to a number of textural variables, notably:

Dry bulk density
Effective porosity
Porometer porosity
Vertical packing density
Horizontal packing density
2-D packing density
Sphericity
Interlocking Index
Packing proximity

Many of these variables are however strongly interrelated, (i.e. they show multicollinearity), and therefore a number must be removed from the regression model. It was decided that dry bulk density would not be used in the model since it describes too much of the bulk characteristics of the rock and is influenced by porosity, mineralogy and textural features. porosity measured by porometer was therefore used as a basis for the model. The final equation for strength is given as :

$$\sigma_c = 193 - 40.5\log\theta + 0.807(2\text{-DPD}) - 125(\text{Sph}) + 0.623(\text{CI})$$

$$R^2 = 87.2\%$$

where σ_c = uniaxial compressive strength

θ= porosity

2-DPD = 2 dimensional packing density
CI = cement index
Sph = sphericity

	t-ratios	significance
logθ	-5.23	99%
2-DPD	2.68	99%
Sph	-2.71	99%
CI	2.12	95%

Cement index and packing density show a certain degree of multicollinearity but it is not sufficient to merit removal of one from the model. The actual numerical values of the equation are not of as much importance as the contained variables:

θ — the high degree of control on strength has been discussed in Chapter 5. The results of the regression analysis indicate that porosity is the single most important variable in controlling rock strength.

2-DP.D. — This variable, as measured by digitising thin sections, has proved to have greatest textural control on strength. The degree of contact of the grains therefore controls the competence of the rock. Other textural packing variables such as interlocking index and packing proximity also showed high correlations but since they are strongly multicollineated with 2-DP.D., they cannot be included in the model.

Sphericity — As indicated from the microscale failure modes, grain sphericity is an important parameter in controlling sandstone strength. This is due to the ease of propagation of stable (and to a certain extent, unstable) microfractures around high sphericity grains as opposed to angular morphologies. Grain roundness does not show the same control.

C.I. — The cement index, as calculated using formula 7.1, proved to be a useful method of indicating the strength of the intergranular cements. The results of the QMA and regression analysis demonstrate the lack of influence of grain mineralogy on sandstone strength. This was indicated by the positions on the QFL diagrams of sandstones which show marked variation in geomechanical properties. It can therefore be concluded that strength is controlled to a large degree by the types of authigenic cements or degree of conversion of grains into cements. Percentage of clay minerals present does have an influence on strength but their presence is taken into account in the cement index.

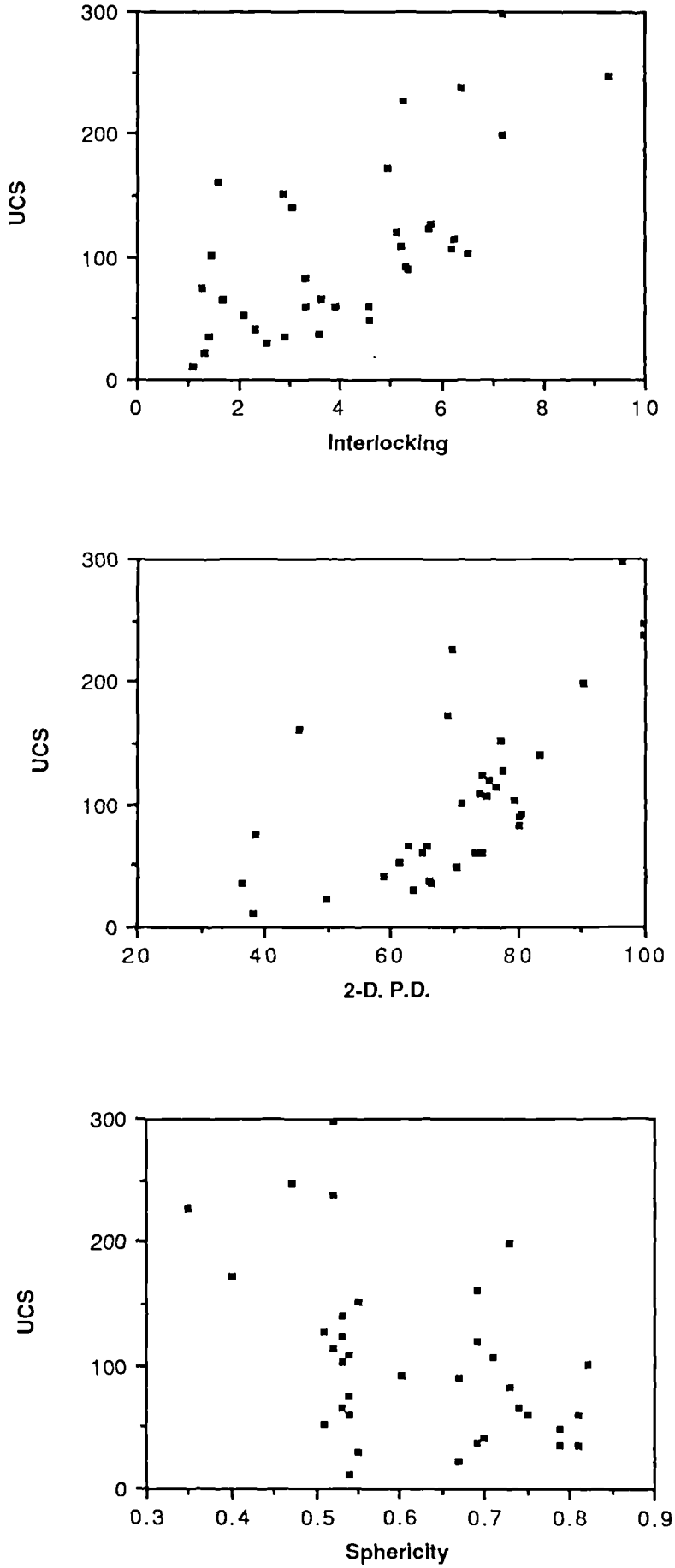

Figure 7.6 A number of linear plots of uniaxial compressive strength vs. textural variables.

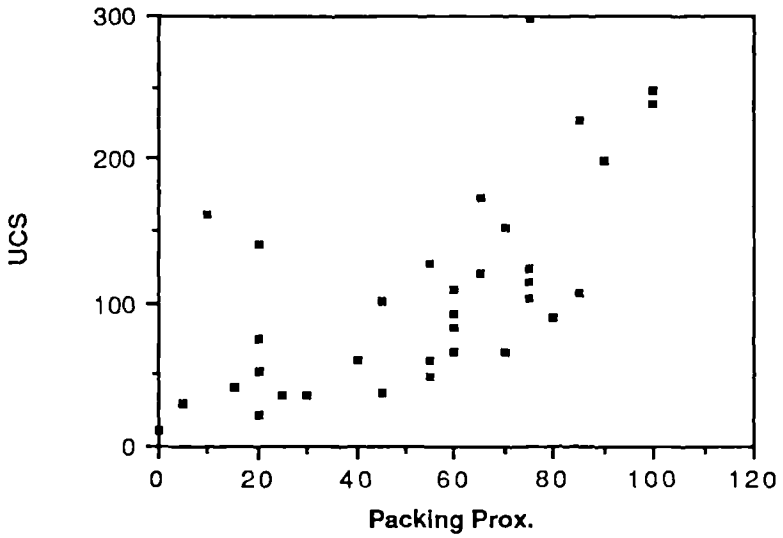

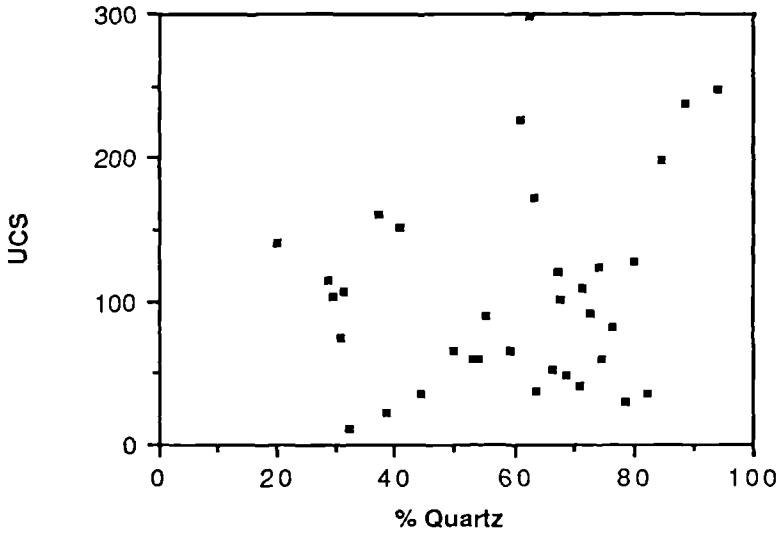

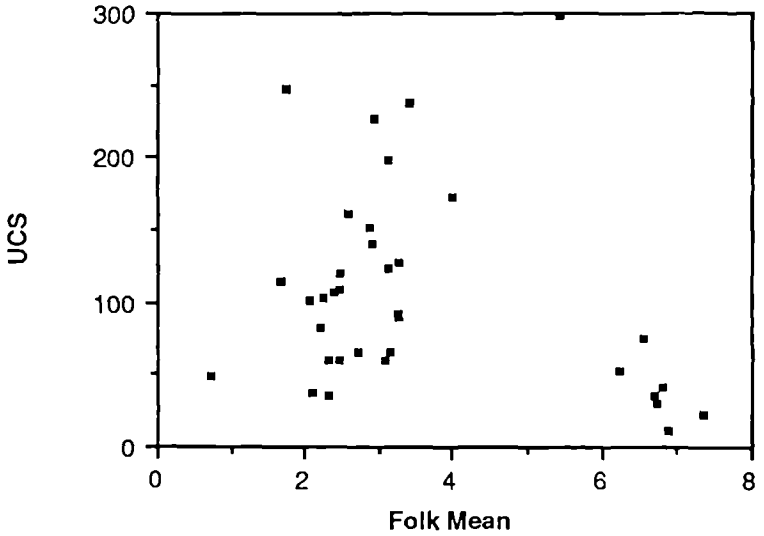

Figure 7.6(cont'd) A number of linear plots of uniaxial compressive strength vs. textural variables.

The two main omissions from the regression model are quartz content and grain size. Both have been suggested to have a controlling influence on strength, (Bell, 1978 and Hugman and Friedman, 1979). Over the whole range of sandstones, the relationship between grain size and uniaxial compressive strength is unclear. However, an interesting trend can be seen in Figure 7.6. The plot divides into 2 regions:

1) where an approximately linear relationship exists between grain size and strength, and
2) where a group of fine grained weak sandstones plot separately.

If the sandstones which plot in zone 2 are removed from the graph, then grain size can be seen to have some influence on strength. It is interesting that these same weak sandstones plot in anomalous positions in Figure 5.10 where their apparent elasticity is described.

B. Tan Young's modulus

Young's modulus is controlled to a high degree by those variables which influence strength. The equation for tan E is:

$$\tan E = 40.1 - 9.71\log\theta + 0.0642(P.P) - 0.033(C.I)$$

$$R2 = 79.9\%$$

	t-ratios	significance
θ	−5.70	99%
P.P.	2.30	95%
C.I.	2.35	95%

The results indicate that tan E is controlled by the three variables listed above, which agree closely with those controlling strength. Packing proximity, (i.e. the number of grain to grain contacts) is important since packing increases or attempts to increase during loading.

C. Sec Young's modulus

$$\sec E = 45.6 - 11.1\log\theta + 0.0736(C.I.) - 0.0.175(2\text{-}DP.D.)$$

$$R2 = 88.1\%$$

	t-ratio	significance
logq	-9.39	99%
C.I.	2.14	95%
2-DP.D.	-2.42	95%

Sec E is controlled by the same general characteristics as tan E but 2-D packing density appears to be more important than packing proximity.

D. Poisson's ratio.

Regression of Poisson's ratio against the textural and mineralogical variables did not produce a statistically valid regression equation. This suggests that radial strain is the property most sensitive to minor changes within a rock. This is especially true in the coarse grained sandstones which can show marked inhomogeneity within specimens. The variation in Poisson's ratio suggests that strain localisation may be taking place even at 50% of the ultimate stress. The correlation matrix indicates that the percentage of clay minerals present has a strong influence on the value of Poisson's ratio.

E. Moisture content-related strength reduction.

The final regression analysis involved moisture content related strength reduction. The final equation is given by:

MCRSR = 43.8 - 0.353(Q%) +1.05(CL%)

R2 = 60.9%

	t-ratio	significance
Q%	-2.58	95%
Cl%	3.54	99%

where Q% = percentage quartz
Cl% = percentage clays

This regression equation reinforces the theories expressed in Chapter 6 on the factors controlling MCRSR. The degree of strength loss is related to the percentage of clay minerals present but is also influence by the percentage quartz. Although the R^2 value is relatively low, indicating that these factors do not explain all the variation, the

levels of significance are high demonstrating the importance of the two variables.

7.4 Summary

The strength and deformability of sandstones are controlled primarily by textural variations. Mineralogy of framework grains does not play such an important role. The QMA devised for the purposes of quantifying mineralogy and texture has produced a number of parameters; regression analysis has revealed that the most important in controlling sandstone response to uniaxial loading are:

1) Porosity

2) 2-dimensional packing density determined from computer digitisation of thin section photomicrographs.

3) Grain sphericity.

4) Interlocking index.

4) Packing proximity (i.e. number of grain to grain contacts as a percentage of total number of contacts per traverse).

5) Cement Index.

CHAPTER 8

SUMMARY

Sandstones constitute between 25 and 30% of the surface outcrop in the British Isles and hence form the founding strata for many engineering structures and the host rocks for tunnels and other underground excavations. Despite the importance of these rocks, there is a general tendency to group all sandstones together under one heading and assume that they will behave in similar ways when subjected to external stresses. This research has examined the variation in the geomechanical behaviour of sandstones and elucidated some of the major controlling factors.

The initial objective of the research was to examine the relationships between the static properties of the sandstones, their moisture content and their geomechanical properties. As a consequence thirty-seven different sandstone varieties have been collected from a number of localities throughout the British Isles. These were chosen to represent a range of ages, compositions and depositional environments from the Precambrian to the Cretaceous.

The geomechanical behaviour of the sandstones was determined using uniaxial compressive testing which is the standard, accepted, and one of the most useful methods for strength testing in rock mechanics. The procedure is regarded as giving a true indication of the rock's behaviour when loaded.

A computer-based monitoring system has been developed specifically for recording stress and strain during uniaxial testing. Linear variable differential transformers were used to measure axial displacements and radial displacements using a specially designed cell. This apparatus was manufactured in the departmental workshop and was found to give reproducible results which agree closely with those obtained by conventional strain gauge methods. Calibration of these transducers allowed the output voltages to be recorded directly onto computer using specially compiled software. The output voltages were then converted to values of time, load, axial and radial strains. For each of the approximately 400 tests carried out during the research, 2750 data points were recorded. This large amount of data produced detailed records of the loading tests, which was then plotted as stress-strain curves by computer, directly from the data files.

The system proved to be considerably faster than any other method of monitoring rock behaviour and hence a large number of tests were possible. In addition, the cell used for measuring radial strains is regarded as giving more representative values of Poisson's ratio since it measures expansion of the rock specimen over a larger area than with the use of normal strain gauges. Further, the

results are not influenced by the strains occurring in the materials used for bonding the strain gauges to the rock surface.

For 35 of the 37 sandstone types studied, specimens were cored from large blocks collected mainly from quarries and engineering projects. Specimens prepared in this way showed a high degree of uniformity in static properties as well as strength and elastic parameters. Four sandstone types were obtained from boreholes and as shown in Figure 5.1 these showed a high degree of variation in strength through the sequence. It is noteworthy that a number of the specimens tested from boreholes were not of the NX size diameter, which was otherwise used throughout the testing program. This may explain some of the observed variation in strength and deformability.

The results of the testing program for dry sandstone specimens are presented in Chapter 5. A high degree of variation in strength and deformability was observed throughout the range of rocks tested, with values of stress at failure ranging from 7MPa in the Upper Cretaceous Greensand of Wiltshire to 298MPa in the Upper Carboniferous Crackington Formation of north Devon.

Three broad modes of failure were recognised during the compression testing; cataclasis, shear failure and axial splitting. These modes were observed to occur either alone or in conjunction. Generally axial failure occurs alone in sandstones which fail at stresses greater than 180MPa, cataclasis occurs alone in sandstones weaker than 37MPa while shear failure is an intermediate mode which often overlaps with the two end members in the series and was observed at strengths from 37-180MPa.

When average dry strength values were plotted against density and porosity, good relationships were observed. Dry bulk density showed the best relationship, producing a linear best-fit with a correlation coefficient of r=0.81. A logarithmic best-fit however, gave a value of 0.91. This is extremely high and far in excess of the standard value of 0.6 generally regarded in rock mechanics as demonstrating a good relationship. The best-fit curve plotted by computer for the data is not the same as that which would be produced manually but the computer derived curve gives a mathematical relationship between the two variables. The equation is given as:

$$\sigma_c = 1.1 \, . \, DBD^{5.25} \qquad (8.1)$$

$r = 0.91$

This clear relationship between dry bulk density and uniaxial compressive strength could form the basis for an index test for sandstones. By plotting the confidence limits for the data obtained during the research, it has been shown that the

equation can predict strength to within an error probably less than or equal to that obtained in commercial testing laboratories. In addition, the estimation of sandstone strength from dry bulk density could be easily performed. The process would involve the drying and subsequent weighing of relatively small, intact rock fragments. The volume of the specimens could then be determined using a volume measuring apparatus and the density easily calculated.

Would such a quick index test be superior to the existing accepted tests such as the point load? A correlation coefficient of 0.88 has been demonstrated by Broch and Franklin, (1972) between point load index (corrected to a standard diameter of 50mm) and uniaxial compressive strength for a number of different rock types. As discussed earlier, the point load test can give misleading strength values in sedimentary rocks where diametral testing produces failure along incipient bedding at low strength values. Measurement of sandstone density would have the advantage of being a non-destructive test, measuring the overall competence of the specimen without being influenced by any existing anisotropy. The good correlation between dry bulk density and uniaxial compressive strength would give representative strength values not requiring corrections for sample geometry or size.

Dobereiner, (1984) suggested vacuum saturated moisture content as an index for strength of weak sandstones and demonstrated reproducible results. The method, however, cannot be applied to sandstones stronger than 20MPa due to the difficulty in saturating specimens of low porosity. In addition 'moisture content' is dependent on the mineral grain density of the rock in which it is measured and grain density has been shown to be highly variable throughout the sandstones tested.

A good relationship was also observed between porosity and strength. The values of porosity determined by the resaturation technique and by the mercury porometer method gave r-values of 0.82 and 0.83 respectively. The difference is negligible but is consistent with the assumption that total rather than effective porosity controls rock strength. Saturation of rock specimens for the calculation of effective porosity was attempted using vacuum apparatus but the process gave poor results, especially in the less porous sandstones. Saturation was achieved using a specially designed pressure cell for NX-sized specimens which imposed a low positive pressure on the samples and drove the air out via a portal in the top of the apparatus. The procedure gave similar or slightly greater values than those produced by soaking specimens at atmospheric pressure for periods of up to two months, without causing any damage to the rock structure.

The detailed monitoring of the axial and radial strains during the uniaxial tests has revealed interesting variations in the deformation suffered by different sandstone types. The comparison of the stress-strain curves demonstrates the variation in the

degree of elasticity of the rocks tested. The strongest varieties behaved elastically or approximately elastically to failure. Below strengths of about 150MPa, deformation is quasi-, semi-elastic or non-elastic with the progressive development of more s-shaped stress-strain curves. The majority of sandstones therefore deform in a non-elastic manner and the stress-strain curves can be divided into four stages as described by Brace et al (1966). The role of natural microcavities is especially important in sandstones since their closure and collapse during loading dictates the shape of the lower (Stage I) part of the stress-strain curve. These microcavities exist as large high aspect ratio pores, (HARC's) and elongate low aspect ratio cavities, (LARC's) usually along grain boundaries. SEM examination of pore casted specimens has revealed that such LARC's exist in even the most indurated sandstones such as the Donegal Quartzite.

A simple model has been proposed to describe the variation in microscopic deformation during Stage I. The processes involved depend on the degree of cementation and packing density of the grains. In low porosity sandstones the stresses are taken up at an early stage at grain contacts and within cements. In intermediate porosity/strength varieties where packing density and/or degree of cementation is not as high, a greater degree of closure of LARC's occurs and cements may undergo some degree of deformation. The term 'microwedging' has been introduced in this thesis to describe the movement of grains resulting from intense intergranular stresses between adjacent particles, causing them to move in a direction perpendicular to the maximum stress direction. High porosity sandstones may undergo relatively passive deformation of weak cements or matrix; since such deformation does merit description as microfracturing, the term 'microbursting' is proposed.

The permanent deformation which takes place at low stress levels in weak sandstones produces stress-strain curves which show a degree of apparent elasticity. This is due to the mode of deformation where the degree of pore closure or straining within the rock never reaches a critical level and a true Stage II type elastic deformation does not occur. In stronger sandstones this permanent deformation occurs at a later stage in the stress-strain curve, termed 'dilatancy' by Brace et al, (1966).

Young's modulus was measured for each sandstone as the tan E at 50% of the ultimate stress and as the sec E at failure. The difference between the two measurements highlights the departure from elasticity of the stress strain curve. Since an elastic and a non-elastic sandstone could have the same tan E it is important to measure the sec value which gives a better indication of the rock's deformation to failure. Although minor variations occurred in specimens prepared from blocks, each rock type shows a characteristic deformation pattern. When plotted on the same scale, the variation in the stress-strain profile becomes apparent. Few sandstones, of even the

strongest varieties behave in an elastic manner. The majority demonstrate an 's-shaped' profile with an elastic or near elastic central zone.

Poisson's ratio values were generally higher in the weaker sandstones, although the relationship proved to be unclear. Good agreement was observed between the radial strains measured up to 50% ultimate stress in the two orthogonal directions but in the weaker sandstones large variations were recorded. The higher radial strain values generally indicated the occurrence of localised zones of deformation as failure was approached. The only value of Poisson's ratio above 0.4 was for the Ashdown Sandstone which revealed a value of over 0.9. The huge radial strains required to produce this value were observed in a number of specimens of the sandstone and are attributed to the relatively cement-free, interlocking microfabric. It is suggested that the rock behaves in a similar manner to locked sands as described by Dusseault and Morgenstern, (1979).

The shape of the upper part of the stress-strain curves and the macroscopic failure modes can be explained in terms of failure mechanisms occurring on a microscopic scale. In weak sandstones stable microfracturing processes dominate, with fractures initiated at grain boundaries and propagating around grains at stresses well below the failure stress. The microfractures therefore show a variable alignment relative to σ_1. Examples of this can be seen in the SEM photographs presented in Chapter 5. The microfractures form a network of interconnecting fractures passing through matrix and cement. The linkage of these microfractures causes the rock to deform by cataclastic deformation, where in many cases large volumes of the rock disintegrate into grain-sized fragments. e.g. the Midford Sands and Greensand.

In slightly stronger sandstones unstable microfractures begin to form at the yield point but become stable when they reach areas of lower stress. As the load increases, these microfractures interact to form the macroscale failure plane. The low porosity sandstones, such as the Crackington Sandstone, do not undergo appreciable stable microfracturing but deform by the instantaneous linkage of unstable σ_1 aligned microfractures. In these sandstones, the stress induced cracks are predominantly mode I tensile cracks, (i.e. displacement is normal to the crack plane). SEM analysis of prefailure specimens has shown that shear can occur parallel to the crack planes due to the process of microwedging. The conclusion of the study is that the macroscale failure can be explained in terms of the microscale activity. To summarise the relationship, an idealised model is proposed in Figure 5.28 with examples chosen to represent the main behavioural variations observed from the weakest argillaceous sandstones to the extremely strong wackes and quartzites.

Extensive work was carried out during the research to quantify the strength loss

in a number of sandstone types due to changes in moisture content and to attempt to elucidate the processes involved. All of the thirty-five sandstone types prepared from blocks were tested in both the completely dry and saturated state. In addition, fifteen of these varieties were tested at intermediate moisture contents to establish the relationship between strength and moisture content for a number of texturally and mineralogically different arenites.

In most cases a substantial decrease in uniaxial compressive strength occurred on saturation, with the greatest losses of strength occurring in the weak, clay-rich sandstones. Sandstones tested at intermediate moisture contents demonstrated a sharp loss in strength at low moisture contents followed by a decrease in rate of strength loss at higher moisture contents. The results presented in Chapter 6 show that 80-90% of the moisture content-related strength reduction occurs at values up to an average of 31.2% of the moisture content at saturation. In most sandstones this represents a value of approximately 1% moisture content.

The general trend observed for the sandstones studied at intermediate moisture content can be summarised by a negative exponential equation of the form:

$$\sigma_c = ae^{-bw} + c \qquad (8.2)$$

where σ_c = uniaxial compressive strength
w = moisture content (%)
a,b,c = constants

In addition to substantially decreasing the strength , moisture content has a marked effect on the elasticity of deformation. In all cases the tan E and sec E decrease from that in the dry state - in many cases the sec value shows a greater change than the tan E, indicating a less elastic mode of deformation. Many of the stress-strain curves showed a more well developed Stage I deformation when saturated.

The effect of moisture content on the stress-strain curve can be demonstrated by plotting sequential stress-strain curves at intermediate moisture contents. The most obvious change is the increased 's-shape' of the curves which can be seen to develop at low moisture contents. The result of this change of profile is that sec E decreases substantially while tan E does not show the the same modification. Moisture generally causes an increase in Poisson's ratio but the effect is less well defined than with uniaxial compressive strength and Young's modulus. This may be due to an increase in the degree of strain localisation in the presence of moisture, producing high radial strain values in certain areas.

Despite extensive overlap of failure modes, in general wetting of specimens

caused a weaker mode of deformation to occur. The failure planes formed at failure of wet specimens often showed a high degree of disaggregation leading to a rolling mode of failure.

In addition to the normal tests on specimens at several moisture contents, a number of tests were carried out on specimens saturated in liquids of different physical and chemical properties. It was found that liquids of different pH did not affect the strength values recorded when saturated in water. Liquids of low surface tension such as methanol and n-hexane did not cause a significant reduction in strength. As a control, tests were carried out on clays, using methanol to ensure that the low surface tension liquids did not produce a different effect from water. No difference in degree of softening was observed.

Pore pressure tests using a specially designed manometer connected to the rock pore framework demonstrated that appreciable pore pressures do not form during uniaxial compression; hence pore pressure increase is not a contributing factor in MCRSR.

High speed photography carried out on dry and saturated specimens has demonstrated a number of interesting differences in the failure characteristics. The most important observation was the variation in speed of fracture propagation. Velocities of 9×10^{-2} ms^{-1} were observed in the dry sample while speeds of only 1.7×10^{-2} occurred in the saturated specimen. These findings do not agree with those of Atkinson (1979) who states that fracture propagation is accelerated in the presence of moisture.

It is concluded that two main processes are active in MCRSR in sandstones:

1) Softening of clay minerals and soft sedimentary rock fragments occurs on wetting prior to any increase in stress.
2) Fracture energy reduction occurs in the presence of moisture and is most active during the latter part of Stage II and during Stages III and IV. The process of stress corrosion may play a subsidiary role, but it is difficult to explain in terms of a theory of increased crack velocity in the presence of moisture, crack velocities observed from high speed photography.

A quantitative microfabric analysis (QMA) has been developed and regression analysis used to elucidate some of the factors controlling sandstone strength and deformability. The results of this work have demonstrated that framework grain mineralogy is not as important as textural parameters and type of intergranular cement. A number of regression equations have been developed which indicate the degree of control of certain variables on the strength, Young's modulus and MCRSR.

The research has shown that future work could profitably be undertaken on the following topics:

a) High speed photography of rock failure should be carried out on both strong and weak sandstones to examine the progressive failure of specimens and to determine crack propagation velocities.

b) Triaxial testing using a cell designed to measure radial strains. This would be used to determine the effects of moisture content and lithological variation on shear strength.

c) Simulation of hydrofracturing of different sandstone types.

CHAPTER 9

CONCLUSIONS

From the previous chapters which describe the research undertaken a number of conclusions can be drawn:

1) A strong relationship has been proved to exist between the uniaxial compressive strength and the dry bulk density for sandstones. This has been shown to have an r-value of 0.91

2) The good correlation would allow the dry bulk density to be used as an index. The fact that this does not involve destruction of the specimen and can assess the intact strength of various shapes and sizes makes it a potentially useful index for estimating sandstone strength.

3) It has been shown that dry sandstone samples have a higher strength than saturated or partially saturated samples; the only exception being the Ashdown Sandstone. The loss in strength was frequently in the 20-50% range, reaching a maximum in the Greensand (type A) of 78%.

4) Detailed testing indicated that the most marked loss in strength occurred between dry samples and those containing 1% moisture. In the case of the weakest sandstones however, the change occurring at low moisture content was less apparent.

5) The regression analysis has indicated that the degree of moisture content related strength reduction in some sandstones is dependent on the percentage of clay minerals in the rock. These exist both in the form of sedimentary rock fragments and as phyllitic rock fragments. The maximum determined proportion of 24% occurred in the Pennant (type C), which showed a 54% moisture content-related strength reduction on saturation.

6) Samples saturated in liquids of low surface tension tended to give higher strength values than those saturated in water. The results indicate that when n-hexane is used in sandstones with low clay percentages, the strengths are similar to those for the dry tests. In sandstones where clay is abundant, such as the Greensand, n-hexane saturation gives strengths similar to saturation in water. Clearly, a process of clay softening is involved.

7) The process of clay softening cannot explain the moisture-content related strength reduction occurring in sandstones with low clay percentages. In these rocks the surface tension of the saturating liquid is important and it is considered that fracture energy reduction is the most important process in these sandstones.

8) High speed photography has shown how fracture propagation varies between dry and saturated samples. A velocity of 9.0×10^{-2} ms^{-1} has been calculated for fracture propagation rate in dry sandstone while a value of only 1.7×10^{-2} ms^{-2} was established for the saturated sample. This contradicts the view put forward by Atkinson, (1979).

9) When pre-failure and post-failure samples were examined under the SEM they revealed variations in fracture morphology. Microfractures have been observed in the pre-failure samples; these can be seen to initiate at pores and to propagate towards other pores or grain/cement contacts.

10) SEM examination indicates that microfractures will be trans- or intergranular depending on a number of factors:

1) Mode of propagation -stable or unstable. Unstable fractures are more likely to pass through grains,
2) The strength differential between grains and cement,
3) The roundness of grains,
4) The angle of incidence of a propagating unstable microfracture with the grain boundary, and
5) Internal grain inhomogeneities such as cleavage.

11) Three major macroscopic modes of failure have been observed. Sandstones which fail at stresses greater than 180MPa always show axial cleavage. Sandstones weaker than 37MPa fail in cataclasis. Shear failure is an intermediate mode which often occurs in conjunction with the two end members.

12) A simple model has been proposed to illustrate how the macroscopic failure mode is controlled by the microscopic deformation prior to and at failure.

13) It has been shown that the majority of sandstones deform in a non-elastic manner, with typical 's-shaped' stress-strain profiles. The main exceptions to this are the strongest and weakest varieties. In the strongest sandstones porosity is low and there is little difference between Young's modulus in Stage I and Stage II. Examination

of pore casts has shown that the Stage I/Stage II change in E is controlled by the aspect ratio of the natural cavities. The weak sandstones show relatively straight and apparently elastic stress-strain curves.

14) In rock types which generally deform non-elastically it is important to measure the sec E at failure in addition to the tan E at 50% of ultimate stress. It is suggested that sec E will give a better indication of the rock's deformation to failure.

15) The results from the cell designed specifically for obtaining the best representation of radial strain were compared to standard strain gauges and were found to be more reproducible, probably as a consequence of the greater measured area and the fact that values are not influenced by strain gauge cements.

16) The Poisson's ratio values obtained during the testing program were generally below 0.4. Of the thirty-seven sandstone types studied, the only exception to this was in the Ashdown Sandstone, which repeatedly gave exceptionally high values in the region of 0.9. Microscopic examination indicates that this sandstone has a microfabric characteristic of a locked sand.

17) A quantitative microfabric analysis and regression model have been developed. Thirty-six mineralogical and textural variables were included in the initial work. The research has indicated that the observed variation in uniaxial compressive strength is mainly a function of the porosity, the 2-dimensional packing density and the Cement Index.

REFERENCES

Adams A.E., Mackenzie W.S. & Guilford C. 1984. *Atlas of sedimentary rocks under the microscope*. Longman.

Al Jassar S.H. 1979. *Geotechnical properties of the Carboniferous limestone of the Bristol area*. Unpubl. Ph.D. Thesis, University of Bristol.

Allen J.R.L. 1962 Petrology, origin and deposition of the highest Lower Old Red sandstone of Shropshire, England. *Jour. Sed. Petrology* **32**, 657-697.

Allen J.R.L. 1974. Sedimentology of the Old Red Sandstone (Siluro-Devonian) of the Clee Hills area , Shropshire, England. *Sedim. Geol.* **12**, 73-167.

Allen P. 1975. Wealden of the Weald: a new model. *Proc. Geol. Ass* . **86** 389-438.

Allen T. 1981. *Particle size measurement*. 3rd Ed., 678p. London: Chapman and Hall.

Allison P. 1988. *The taphonomy of soft-bodied fossil biotas*. Unpubl. Ph.D. Thesis, University of Bristol.

Almon W.R., Fullerton L.B. & Davies D.K. 1976. Pore space reduction in Cretaceous sandstones through chemical precipitation of clay minerals. *Jour. Sed. Petrology*, **46**, 89-96.

American Petroleum Institute. 1956. *Recommended Practice for determining permeability of porous media*. **R.P. 27**. American Petroleum Institute, Dallas, Texas, 55p.

American Petroleum Institute. 1960. *Recommended practice for core analysis procedure*. R.P. 40. American Petroleum Institute, Dallas, Texas, 27p.

Anderton R. 1980. Distinctive pebbles as indicators od Dalradian provenance. *Scott. J. Geol.* **16,** 143-152.

Anon. 1972. The preparation of maps and plans in terms of engineering geology. *Q.J.E.G.* **5**, 293-382.

Atkinson B.K. 1979. A fracture mechanics study of subcritical tensile cracking of quartz in wet environments. *Pure and Applied Geophysics*, **117**, 1011-1024.

Atkinson B.K. 1982. Subcritical crack propagation in rocks: Theory, experimental results and applications. *J. Struct. Geol.*, **4**, 41-56.

Atkinson B.K. 1984. Subcritical crack growth in geological materials. *J. Geophys. Res.*

Atkinson B.K. & Meredith P.G. 1981. Stress corrosion cracking of quartz: A note on the influence of the chemical environment. *Tectonophysics*, **77**, T1-11.

Attewell P.B. & Farmer I.W. 1971. *Principles of engineering geology*. Chapman and Hall.

Aydin A. & Johnson A.M. 1983. Analysis of faulting in porous sandstones. *J. Struct. Geol.*, **5**, 19-31.

Bagnold R.A. The physics of blown sand and desert dunes, 265p. *London: Methuen.*

Barron R.S. 1976. *The Geology of Wiltshire.* Moonraker Press.

Barton M.E. 1974 Soft sandstones: Geotechnical properties and sensitivity to moisture changes. *Prc 2nd Congress of the International Association of Engineering Geologists*, Sao Paulo, Brazil. Theme IV, Paper 7, 6P.

Barton M.E., Palmer S.N. & Wong Y.L. 1986. A geotechnical investigation of two Hampshire Tertiary Sand Beds: are they locked sands? *Q.J.E.G.*, **19**, 399-412.

Barton M.E. & Palmer S.N. 1989. The relative density of geologically aged, British fine and fine-medium sands. *Q.J.E.G.*, **22**, 49-58.

Barton C.C. 1980. Behaviour of rock before and during propagation of opening mode cracks. *EOS*, **61**, p.361.

Bazant Z.P. 1985. *Mechanics of Geomaterials.* John Wiley & Sons.

Beard D.C. & Weyl P.K. 1973. Influence of texture on porosity and permeability of unconsolidated sand. *Bull Am. Assoc. Petrol. Geol.*, **57**, 349-369.

Bell F.G. 1978. Petrographical factors relating to porosity and permeability in the Fell Sandstone. *Q.J.E.G.*, **11**, 113-126.

Berner R.A. 1980. *Early diagenesis*, 241p. Princeton, New Jersey: *Princeton Univ. Press.*

Bieniawski Z.T. 1967. Mechanisms of brittle failure of rocks. *Int. J. Rock Mech. Min. Sci.*, **4**, 395-430.

Bieniawski Z.T. 1975. The point-load test in geotechnical practise. *Engng. Geol.*, **9**, 1-11.

Bieniawski Z.T. 1988. The Rock Mass Rating (RMR) system (geomechanics classification) in engineering practice. *In:* Rock Mass Systems for Engineering Purposes. Louis Kirkaldie (Ed.). *Am. Soc. Test. Mat.* Philadelphia. 167p.

Bjorlykke K. 1984. Formation of secondary porosity : How important is it? In: McDonald D.A. and Surdam R.C. (eds.). Clastic diagenesis. *Mem. Am. Assoc. Petrol. Geol.*, **37**, 277-286.

Blatt H. 1982. *Sedimentary Petrology.* W.H. Freeman and Company, San Fransisco, 564p.

Blatt H., Middleton G.& Murray R. 1980. *Origin of sedimentary Rocks.* Prentice-Hall, Inc., Englewood Cliffs, N.J. 782p.

Bordia S.K. 1971. The effects of size and stress concentration on dilatancy and fracture of rock. *Int. J. Rock Mech. Min. Sci.*, **8**, 629-640.

Boulton R.A. 1951. Permian rocks of the Midlands. *Geol. Mag.*, **88**, 36-40.

Brace W.F., Paulding B.W & Scholz C. 1966. Dilatancy in the fracture of crystalline rocks. *J.Geophys. Res.*, **71**, 3939-3953.

Brace W.F. & Martin R.J. 1968. A test of the law of effective stress for crystalline rocks of low porosity. *Int. J. Rock Mech. and Min. Sci.*, **5**, 415-426.

Brindley G.W. & Brown G. 1980. (Eds.) Crystal structures of clay minerals and their X-ray identification. *Monogr. Mineral. Soc. London.* **5**, 495p.

Broch E. 1974. The influence of water on some rock properties. *Proc. 3rd Int. Conf on Rock Mechanics, ISRM* Denver, **11A**.

Broch E. & Franklin J.A. 1972. The Point Load Strength Test. *Int. J. Rock Mech. Min. Sci.* **9**, 669-697

Brown E.T. (editor) 1981 *Rock Characterisation, Testing and Monitoring-ISRM Suggested Methods.* Oxford, Pergamon Press, 211p.

Brown E.T. & Hudson J.A. 1971. The influence of micro-structure on rock fracture on the laboratory scale. *Proc. Int. Symp. on Rock Mech.*, Nancy, Vol. 11-20.

BS 1377. 1975. *Methods of test for soils for engineering purposes.* British Standards Institution, H.M.S.O., London.

BS 5930. 1981. *Code of practice for site investigations.* British Standards Institution, H.M.S.O., London.

Burland J.B. & Symes M. 1982. A simple axial displacement gauge for use in the triaxial apparatus. Technical note. *Geotechnique*, **32**, 62-65.

Burley S.D. 1984. Patterns of diagenesis in the Sherwood Sandstone Group (Triassic), United Kingdom. *Clay Miner.*, **19**, 403-440.

Burley S.D. 1986. The development and destruction of porosity within Upper Jurassic reservoir sandstones of the Piper and Tartan fields, Outer Moray Firth, North Sea. *Clay Miner.*, **21**, 649-694.

Burley S.D., Kantorowic J.D. & Waugh B. 1985. Clastic diagenesis. In : Brenchley P.J. and Williams B.P.J. (eds). Sedimentology : recent developments and applied aspects. *Spec. Publ. Geol. Soc. London.* **18**, 189-226.

Burst J.F. 1958. "Glauconite" pellets: Their mineral nature and application to stratigraphic problems. *Am Assoc. Petroleum Geologists Bull.* **42**,310-327.

Burstein, L.S. 1968. Effect of moisture on the strength and deformability. 573-576

Byerlee J.D. 1968. Brittle ductile transition in rocks. *J. Geophys. Res.*, **73**, 4741-4750.

Carroll D. 1970. Clay minerals: A guide to their X-ray identification, *Geol. Soc. America Spec. Pub.* **126**, 80p.

Carter P.G. & Sneddon M. 1977. Comparison of Schmidt hammer, point load and unconfined compression tests in Carboniferous strata. *Proc. Conf. on Rock Engng. Newcastle,* U.K., 197-210.

Carver R.E. 1971. *Procedures in Sedimentary Petrology.* Edited by Robert E. Carver. New York Interscience.

Cayeux Lucien. 1906. Structure et origine des gres du Tertiare parisien. Etudes des gites mineraux de la France, 160p. *Paris: Impr. Nationale.*

Chenevert M.E. 1970. Absorptive pore pressure of argillaceous rocks. In: Rock Mechanics Theory and Practice. *Proc 11th Symposium on Rock Mechanics,* 599-628.

Clarke F.W. 1924. The data of geochemistry, 5th Ed., *U.S. Geol Survey Bull.* **770,** 841p.

Coates D.F. 1964. Classification of rocks for rock mechanics. *Int. J. Rock Mech. Min. Sci.*, **1**, 421-429.

Colback P.S.B. & Wiid B.L. 1965. The influence of moisture content on the compressive strength of rock. *Proc. 3rd Can. Symp. Rock Mech.* Toronto Ontario 1965, 65-83.

Colter V.S. & Ebbern J. 1978. The petrography and reservoir properties of some Triassic sandstones of the Northern Irish Sea Basin. *J. Geol Soc. London,* **135**, 57-62.

Cook N.G.W. 1970. An experiment proving that dilatancy is a pervasive volumetric property of brittle rock loaded to failure. *Rock Mech.*, **2**, 181-188.

Cook N.G.W., Hood M. & Tsai F. 1984. Observations of crack growth in hard rock loaded by an indenter. *Int. J. Rock Mech.*, 97-107.

Cook P.J. 1976. Sedimentary phosphate deposits. In: Wolf K.H. (Ed.): *Handbook of strata-bound and stratiform ore deposits,* **7**, 505-535. Amsterdam, Elsevier.

Cook S. & Parker A. 1988. Compositional analysis of sedimentary rocks from SEM/X-Ray imaging of polished thin sections. *Microscopy and Analysis,* **6**, 24-25.

Cowie J.W. 1974. The Cambrian of Spitsbergen and Scotland. In: C.H. Holland (ed.) *Cambrian of the British Isles, Norden and Spitzbergen,* Wiley, London, 123-155.

Craig C.Y. 1965. Permian and Triassic. In: Craig, G.Y. (Ed). *The Geology of Scotland.* Oliver and Boyd, Edinburgh, 383-400.

Craig R.F. 1984. *Soil Mechanics.* Van Nostrand Reinhold (UK) Co.Ltd.

Crouch S.L. 1970. Experimental determination of volumetric strain in failed rock. *Int. J. Rock Mech. Min. Sci.*, **7**, 589-603.

Currey D.T. 1969. Weathering in joint troughs. *Australian Institute of Min. Met. Melbourne. Rock Mechanics Symposium..*

Dapples E.C. 1967. Diagenesis of sandstones. In: Larren G.and Chilingar G.V. (eds.). *Diagenesis in sediments. Developments in Sedimentology*, **8**, Elsevier, Amsterdam, 91-125.

Davis J.C. 1986. *Statistics and data analysis.* 2nd edition, New York, wiley, 646p.

Daw G.P. 1971. A modified Hoek-Franklin Triaxial cell for rock permeability measurements. *Geotechnique*, **21**, 89-91.

Deer W.A. Howie R.A. & Zussman. J. 1982. *An introduction to the rock forming minerals.* Longman. 528p.

Dilks A. & Graham S.C. 1985. Quantitative mineralogical characterisation of sandstones by backscatter electron image analysis. *Jour. Sed. Petrology*, **55**, 347-355.

Dobereiner L. 1984. *Engineering geology of weak sandstones.* Unpublished Ph.D Thesis. University of London , 471p.

Dobereiner L. & De Freitas M.H. 1983. Saturated moisture content as an index for assessing strength. *Proc. Int. Symp. on Engineering geology and Underground .*

Dobereiner L. & De Freitas M.H. 1986. Geotechnical properties of weak sandstones. *Geotechnique* , **36**, 79-94.

Dott R.L., Jr. 1964. Wacke, graywacke and matrix-what approach to immature sandstone classification? *Jour. Sed. Petrology,* **34**, 625-632.

Doyle L.J., Cleary W.J. & Pilkey O.H. 1968.Mica: Its use in determining shelf depositional regimes. *Marine Geol.*, **6**, 381-389.

Dube A.K. & Singh H.B. 1969 Determination of tensile strength of rocks by disc test method. *J. Min. Metall Fuels*, **17**, 305-307.

Duncan N., Dunne M.H. & Petty S. 1968. Swelling characteristics of rock. *Wat. Pwr.* **19**, 185-192.

Dunning J.D., Petrovski d., Schuyler J. & Owens A. 1984. The effects of aqueous chemical environments on crack propagation in quartz. *J. Geophys. Res.*, **89**, 4115-4123.

Dusseault M.B. & Morgenstern N.R. 1979. Locked Sands. *Q.J.E.G.,* **12**, 117-131.

Dusseault M.B. 1980. Itacolumites: the flexible sandstones. *Q.J.E.G.* , **13**, 119-128.

Dumbleton M.J. 1968. The classification and description of soils for engineering purposes: A suggested revision of the British system. *R.R.L.* Report **LR182.**

Edmond J.M. & Paterson M.S. 1972. Volume changes during the deformation of rocks at high pressures. *Int. J. Rock Mech. Min. Sci.*, **9**, 161-182.

Ehrlich R., Kennedy S.K., Crabtree S.J. & Cannon R.L. 1984. Petrographic image analysis, 1.Analysis of pore reservoir complexes, *Jour. Sed. Petrology*, **54**, 1365-1376.

Elliott G.M & Brown E.T. 1986. Technical note: Further development of a plasticity approach to yield in porous rock. *Int. J. Rock Mech. Min. Sci. & Geomech. Abstr.*, **23**, 151-156.

Elliott G.M. & Brown E.T. 1986. Technical Note. Further development of a plasticity approach to yield in porous rock. *Int. J. Rock Mech. Min. Sci. and Geomech. Abstr.*

Farmer I.W. 1968. *Engineering properties of rocks*. 1st edition. London, E. and F.N. Spoon. Ltd.

Farmer I.W. 1975. *Engineering properties of rocks*. 2nd edition. London, E. and F.N. Spoon. Ltd.

Fayed L.A. 1970. The clay minerals of some British coal measure rocks. *Int. J. Rock Mech. Min. Sci.* **7**, 253-256.

Fogler J.N. & Khilar H. 1983. Fluid sensitivity of sandstones. *J. Pet. Eng. Tech*, **23**, 133-142.

Folk R.L. 1968. *Petrology of sedimentary rocks*. 1st edition.Hemphill Publishing company, Austin, Texas, 170p.

Folk R.L. 1974. *Petrology of sedimentary rocks*. 2nd edition. Hemphill Publishing Company, Austin, Texas, 182p.

Folk R.L. 1976. Reddening of desert sands : Simpson Desert, North Territory, Australia. *Jour. Sed. Petrology*, **46**, 604-615.

Folk R.L. 1978. Angularity and silica coatings of Simpson Desert sand grains Northern Territory, Australia. *Jour. Sed. Petrology*, **48**, 611-624.

Franklin J.A. & Hoek E. 1970. Developments in triaxial testing technique. *Rock Mech.*, **2**, 223-228.

Franks S.G. & Forester R.W. 1984. Relationships among secondary porosity, pore-fluid chemistry and carbon dioxide, Texas Gulf Coast. In: McDonald, D.A. and Surdam, R.C. (eds.). Clastic Diagenesis. *Mem. Am. Assoc. Petrol. Geol.*, **37**, 63-79.

Friedman G.M. 1979. Differences in size distributions of populations of particles among sands of various origins. *Sedimentology*, **36**, 3-32.

Frondel C. 1962. *Dana's system of mineralogy*, 7th Ed., 334p. New York: Wiley.

Fuchtbauer H. 1967. Influence of different types of diagenesis on porosity. *Proc. 7th World Petrol. Cong.*, Mexico City, **2**, 353-369.

Fuchtbauer H. 1974. *Sediments and sedimentary rocks I*. Pt. II. 464p. New York: Wislay Halsted Press.

Gaither A. 1953. A study of porosity and grain relationships in experimental sands. *J. Sed. Petrology,* **23**, 180-195.

Galehouse J.S. 1971. Point counting. In: Carver, R.E. (ed) *Procedures in Sedimentary Petrology.* Wiley Interscience.

Gilligan A. 1920. The petrography of the Millstone Grit of Yorkshire. *Geol. Soc. London Quart. Jour.* **75**, 251-294.

Goldring R. 1955. The Upper Devonian and Lower Carboniferous trilobites of the Pilton Beds in north Devon. *Senckenbergiana lethea,* **36**, 27-48.

Goldsmith J.R. Graf D.L. Witters J. & Northdrop D.A. Studies in the system $CaCO_3$-$MgCO_3$-$MnCO_3$-$FeCO_3$. *Jour. Geology,* **70**, 659-688.

Gordon R.B. 1974. Mechanical relaxation spectrum of crystalline rock containing water. *J. Geophys. Res.* **79**, .

Graton L.C. & Fraser H.J. 1935. Systematic packing of spheres with particular relation to porosity and permeability. *Jour. Geology,* **43**, 785-909.

Griffith A.A. 1924. Theory of rupture. *First Int. Congr. Appl. Mech.*,Delft, 56-63.

Guidicini G., Nieble C.M. & Cornides A.T. 1973. Analysis of point load test as a method for preliminary geotechnical classification of rocks. *Bull. Int. Assoc. Engng. Geol.,* **7**, p37-52.

Hadding A. 1932. The pre-Quaternary sedimentary rocks of Sweden: Part III, The Paleozoic and Mesozoic sandstones of Sweden. *Lunds Univ. Arsski., N. K.,Avd. 2,* **25**, 287p.

Hadizadeh J. & Rutter E.H. 1982. Experimental study of cataclastic deformation of a quartzite. In*: Issues in Rock Mechanics. Proc. 23rd Symp. on rock Mech.,* Berkeley, California, 372-379.

Halliday A.N., Graham C.M., Aftalion M. & Dymoke P. 1989. The depositional age of the Dalradian Supergroup: U-Pb and Sm-Nd isotope studies of the Tayvallich Volcanics, Scotland. *Jour. Geol. Society.*, **146**, 3-6.

Halley R.B. 1978. Estimating pore cement volume - thin section. *Jour. Sed. Petrology,* **48**, 642-650.

Hammond M.L.& Ravitz S.F. 1963. Influence of environment on brittle fracture of silica. *J. Am. Ceram. Soc.*, **46**, 329-332.

Hancock J.M. 1975. The petrology of the Chalk. *Proc. Geol. Ass.* **86**, 499-536.

Handin J. & Hager R.V. 1957 Experimental deformation of sedimentary rocks under confining pressure: tests at room temperature on dry samples. *Am. Assoc. Petrol. Geol. Bull.,* **40**, 343-351.

Handin J., Hager R.V., Friedman M. & Feather, J. N. 1963. Experimental deformation of sedimentary rocks under confing pressures: pore pressure effects. *Assoc. Petrol. Geol. Bull.,* **47**, 717-755.

Hardie L.A. 1967. The gypsum-anhydrite equilibrium at atmosphere pressure. *Am. Mineralogist* **52**, 171-200.

Harrell J.A. & Eriksson K.A. 1979. Empirical conversion equations for thin-section and sieve derived size distribution parameters. *Jour. Sed. Petrology* **49**, 273-280.

Harrell J. 1980. Measurement errors in thin-section analysis of 'grain' packing. *Jour. Sed. Petrology*, **51**, 674-676.

Harris A.L., Baldwin C.T., Bradbury H.J., Johnson H.D. & Smith R.A. 1978. Ensialic basin sedimentation: the Dalradian Supergroup. In: Bowes and Leake (eds.) *Crustal evolution in north-western Britain and adjacent regions*, Seel House Press, Liverpool.

Hartley A. 1974. A Review of the Geological Factors influencing the mechanical properties of road surface aggregates. *Q.J.E.G.*, **7**, 66-100.

Hawkes I. & Mellor M. 1970. Uniaxial Testing in Rock Mechanics Laboratories. *Eng. Geol.* **4**, 177-285.

Hawkes J.R. & Hoskins J.R. 1972. 1972. British arenaceous rocks for skid-resistant road surfacings. *Transp. Rd. Res. Lab. Rep.* **No. lr 488.**

Hawkes J.R. & Hosking J.R. 1973. British arenaceous rocks for skid resistant road surfacings. *Quarry Managers Journal, London* , **57**, 39-47.

Hawkins A.B. & Olver J.A.G. 1984. Point load tests: Correlation factor and contractural use. An example from the Corallian at Weymouth. *Eng. Group Geol. Soc. Reg. Conf.* Guilford, 260-264.

Hawkins A.B. 1988. "Unpredictable to the core". *Tunnels and Tunnelling*, 20, 48-49.

Hayes J.B. 1979. Sandstone diagenesis - the whole truth. In: Scholle P.A. and Schluger P.R. (eds.). Aspects of Diagenesis. *Spec. Publ. Soc. Econ. Paleontol. Miner.* **26**, 127-139.

Heald M.T. & Renton J.J. 1966. Experimental study of sandstone cementation. *Jour. Sed. Petrology* , **36**, 977-991.

Hickman A.H. 1975. The stratigraphy of late Precambrian metasediments between Glenroy and Lismore. *Scott. J. Geol.*, **11**, 117-142.

Hiscott R.N. & Middleton C.V. 1980. Fabric of coarse deep water sandstones, Turelle formation, Quebec, Canada. *Jour. Sed. Petrology*, **50**, 703-722.

H.M.S.O. 1975. *British Regional Geology*; South-West England.

H.M.S.O. 1980. *British Regional Geology*; Bristol and Gloucester District.

Hoek E. 1965. Fracture of anisotropic rock. *J. S. Afr. Inst. Min. Metall.*, **64**, 501-518.

Hoek E. & Bray J.W. 1974. *Rock Slope Engineering*. I.M.M., London.

Hoek E. & Brown E.T. 1982. *Underground Excavations in Rock*. I.M.M., London.

Hoshino K. & Koide H. 1970. Process of deformation of the sedimentary rocks. In: *Proc. 2nd CongrInt. Soc. Rock Mech.*, Belgrade, **1**, 353-359.

Hoshimo K. 1974. Effect of porosity on the strength of the clastic sedimentary rocks. *Proc. 3rd Cong. of the Int. Socfor Rock Mech.*, Denver, **IIA**, 511-516.

Houseknecht D.W. 1984. Influence of grain size and temperature on intergranular pressure solution, quartz cementation and porosity in a quartzose sandstone. *Jour. Sed. Petrolology*, **54**, 348-361.

Howarth D.F. & Rowland J.C. 1986. Development of an index to quantify rock texture for qualitative assessment of intact rock properties. *A.S.T.M. Geotechn. Test.*, **9**. 169-179.

Hudson J.A., Brown E.T. & Rummel F. 1972. The Controlled failure of rock discs and rings loaded in diametral compression. *Int. J. Rock Mech. Min. Sci.*. **9**, 241-248.

Hudson J.A., Crouch S.L. & Fairhurst C. 1972. Soft, stiff and servo-controlled testing machines: A review with reference to rock failure. *Engng. Geol.*, **6**, 157-189.

Hudson J.A. & Morgan J.M. 1975. Compressive failure of chalk. *T.R.R.L. Laboratory*, **Report 681**.

Hugman R.H. & Friedman M. 1979. Effects of texture and composition on the mechanical bechaviuor experimentally deformed carbonate rocks. *Am. Assoc. Pet. Geol. Bull.*, **63**, 1478-1489.

Hull E. 1969. The Triassic and Permian rocks of the Midlands Counties of England. *Mem geol. Surv. G.B.*, 127p.

Hurlbut C.S. & Klein G. 1977. *Dana's manual of mineralogy*. 19th edition, New York, Wiley.

Hurst A. & Irwin H. 1982. Geological modelling of clay diagenesis in sandstones. *Clay Miner.*, **17**, 5-22.

Hutchison C.S. 1974. *Laboratory Handbook of Petrographic Techniques*. New York, Wiley, 527p.

I.S.R.M. 1979. Suggested methods for determining water content, porosity, density, absorption and related properties and swelling and slake-durability index properties. *Int. J. Rock Mech. Min. Sci*, **16**, 141-156.

I.S.R.M. 1981. *Suggested methods for rock characterisation, testing and monitoring*. Ed. E.T. Brown, Pergamon Press.

I.S.R.M. 1983. Suggested methods for determining the strength of rock materials in triaxial compression: revised version. *Int. J. Rock. Mech. Min. Sci.*, **20**, 283-290.

Ixer R.A., Turner P & Waugh B. 1979. Authigenic iron and titanium oxides in Triassic red beds (St. Bees Sandstone). Cumbria, Northern England. *Geol. J.*, **14**, 179-192.

Jackson P.D., Smith D.T. & Stanford P.N. Resistivity-porosity-particle shape relationships for marine sands. *Geophysics,* **43**, 1250-1258.

Jaeger J.C. & Cook N.G.W. 1976. *Fundamentals of Rock Mechanics.* 2nd Edition. Chapman and Hall.

Janczuk B. & Bialopiotrowiz T. 1988. Components of surface free energy of some clay minerals. *Clays and Clay Min.*, **36**, 243-248.

Judd W.R. 1971. Strain distribution around underground openings. *Advanced Research Projects Agency, Department of the Defense, U.S.A.*, Tech. Rep. **6**.

Jumikis A.R. 1983. *Rock Mechanics.* Trans Tech Publications.

Kachanov M.L. 1982. Continuum model of medium with cracks. Spec. Iss. *J. Eng. Mech. Div. of ASCE, Mechanics of Heterogeneous Media*, **106**, EMS.

Kahn J.S. 1956. The analysis and distribution of the properties of packing in sand size sediments, 1. On the measurement of packing in sandstones. *Jour. Geol.ogy*, **64**, 385-395.

Kessler L.G. 1978. Diagenetic sequence in ancient sasndstones deposited under desert climatic conditions. *J. geol. Soc. London*, **135**, 41-49.

Kirby S.H. 1984. Introduction and digest to the special edition on chemical effects of water on the deformation and strength of rocks. *J. Geophys. Res.* **89**, 3991-3995.

Kobayashi S. 1970. Fracture criteria for anisotropic rocks. *Mem Fac. Eng. Kyoto Univ.* **32**, 307-333.

Kranz R.L. 1979. Crack/crack and crack/pore interactions in stressed granite. *Int. J. Rock Mech. Min. Sci, & Geomech Abstr.*, **16**, 37-47.

Krynine P.D. 1940. Petrology and genesis of the Third Bradford Sand. *Pennsylvania State College Bull.* **29**, 134p.

Krynine W.C. 1945.Sediments and the search for oil. *Producers Monthly* **9**, 17-22.

Krumbein W.C. 1934. Size frequency distribution of sediments. *Jour. Sed. Petrology* **4**, 65-77.

Krumbein W.C. 1936. Application of logarithmic moments to size frequency distribution of sediments. *Jour. Sed. Petrology,* **6**, 35-47.

Krumbein W.C. & Graybill F.A. 1965. *An introduction to statistical methods in geology.* New York: McGraw-Hill, 475p.

Kuenen Ph.H. 1941. Geochemical calculations concerning total mass of sediments in the earth. *Am. Jour. Science.*, **239**, 161-190.

Lama R.D. & Vutukuri V.S. 1978. *The Handbook on Mechanical Properties of rocks, Vol. II*, Trans. Tech. Publications.

Larese R.E., Haskell N.L., Prezbindowski D.R. & Beju D. 1984. Porosity development in selected Jurassic sandstones from the Norwegian and North Sea, Norway - an overview. In : *Petroleum Geology of the North European Margin.*

Lasaga A.C. 1984. Chemical effects of watre-rock interactions. *J. Geophys. Res.*, **89**, 4009-4025.

Lawn B. & Wilshaw R. 1975. Indentation fracture: principles and application. *J. Mater. Sci.*, **10**, 1049-1081.

Leeder M. 1982. *Sedimentology: processes and products.* George Allen & Unwin, London, 344p.

Leary E. 1986. *The building sandstones of the British Isles.* Building Research Establishment.

Leith C.K. & Mead W.J. *Metamorphic geology.* New York: Henry Holt, 337p.

Lindqvist P.A., Lai H.H. & Alm O. 1984. Indentation fracture development in rock continuously observed with a *Sci. and Geomech. Abstr.* **21**, 165-182.

Loughnan F.C. 1962. Some considerations in the weathering of the silicate minerals. *Jour. Sed. Petrology*, **32**, 284-290.

Mackenzie F.T. & Garrels R.M. 1965. Silicates: Reactivity with sea water. *Science*, **150**, 57-58.

Matheson G.D. 1983. Presplit blasting for highway rock excavations. *TRRL Lab.* **Report 1094.**

McFeat-Smith I. 1982. Logging in tunnel geology. *Tunnels and Tunnelling*, **14**, 20-25.

Meredith P.G. 1983. *A fracture mechanics study of experimentally deformed crustal rocks.* PhD Thesis, Imperial College.

Milner H.B. 1922. *An introduction to sedimentary petrography.* 125p. London: Murby.

Misra B. 1972. *The correlation of Rock Properties with Machine Performance.* Unpub. Ph.D Thesis. University of Leeds.

Mogilevskaya S.E. 1970. Effect of composition, features of structural fabric and water saturation on rock deformability. In: *Proc. 2nd Congr. Int. Soc. Rock. Mech.*, Belgrade, **1**, 353-359.Monicard R.P. 1980. *Properties of Reservoir Rocks. Core Analysis.* Editions Technip.

Morris K.A. & Shepperd C.M. 1982. The role of clay minerals in influencing porosity and permeability characteristics in the Bridport Sands of Wytch Farm, Dorset. *Clay Miner.*, **17**, 41-54.

Nami P. 1976. An exhumed Jurassic meander belt from Yorkshire, England. *Geol. Mag.* **133**, 47-52.

Neville J.J. 1987. *Concrete Technology.* Harlow Longman. Scientific and Technical.

Nickel E. 1978.The present status of cathodoluminesence as a tool in sedimentology. *Minerals Sci. Eng.*, **23**, 73-100.Obert L. & Duval W. 1942. Use of sub-audible noises for prediction of rock bursts, Part II. *U.S. Bur. Min. Rep. Invest.*, **3654**, 22p.

Obert L. & Duval W, 1942. Use of sub-audible noises for prediction of rock bursts, Pt. II. *U.S. Bur. Min. Rep. Invest.*. **3654.**, 22p.

Obert L. & Duval W. 1967. *Rock mechanics and the design of structures in rock.* New York, Wiley.

Odom I.E., Doe T.W. & Dott R.H. 1976. Nature of feldspar-grain size relations in some quartz-rich sandstones. *Jour. Sed. Petrology*, **4**, 862-870.

Okamoto R., Kojima K. & Yoshiaka R. 1981. Distributioin and Engineering properties of weak rocks in Japan. *Proc. Int. Symp. on Weak Rock*, **5**, 89-103.

Okubo S. & Nishimatsu Y. 1986. Computer modelling of stochastic rock failure during uniaxial loading. *Int. J. Rock Mech. Min. Sci.*, **23**, 363-370.

Olivier H.J. 1979. Some aspects of the influence of mineralogy and moisture on the weathering behaviour of mudrocks. *Proc. 4th Congr. Int. Soc Rock Mech.*, Montreux, **3**, 467-474.

Ollier C. 1975. *Weathering.* 2nd ed. Longman Group.

Ollier C. 1984. *Weathering.* 3rd ed. Longman Group.

Pandit B.I. & King M.S. 1979. The variation of elastic wave velocities and quality factor Q of a sandstone with moisture content. *Can. J. Earth Sci.*, **16**, 2187-2195.

Parfenoff A. Pomerol C. and Tourenq J. 1970. *Les mineraux en grains,* 571p. Paris: Masson.

Paterson M.S. 1978. *Experimental Rock Deformation- The Brittle Field.* Publ, Berlin: Springer-Verlag, 254p.

Peck L. 1980. Stress corrosion cracking of quartzite. *EOS*, **61** ,p 361

Peng S.S. 1971. Stresses within elastic circular cylinders loaded uniaxially and triaxially. *Int. J. Rock Mech. Min. Sci.*, **8**, 399-432.

Peng S.S. & Johnson A.M. 1972. Crack growth and faulting in cylindrical specimens of Chelmsford granite. *Int. J. Rock Mech. Min. Sci.*, **9**, 37-86.

Pettijohn F.J. 1972. Sand and sandstone 1st Ed. *Springer Verlag, New York, Inc.*

Pettijohn F.J., Potter P.E. & Siever R. 1987. *Sands and Sandstones.* 3rd edition. Springer- Verlag., New York, Inc.

Pinches G.M. 1986. *Geotechnical implications of weathering of Upper Trias in the Bristol area.* Unpubl. Ph.D. Thesis, University of Bristol. 423p.

Pirson S.J. 1958. *Oil reservoir engineering*, 2nd Ed. New York: McGraw-Hill, 735p.

Pininska J. 1977. Correlation between mechanical and acoustic properties of flysch sandstones. *The Geotechniques of Structurally Complex Foundations*, Capri, 387-394.

Pininska J. 1978. Anisotropy of acoustic properties of sandstones in the northern flysch carpathians. *Proc. 3rd Congress of the International Association of Engineering Geologists*, Madrid, **2**, 76-80.

Pittman E.D. 1972. Diagenesis of quartz in sandstones as revealed by scanning electron microscopy. *Jour. Sed. Petrology*, **42**, 507-519.

Pittman E.D. & Duschatko R.W. 1970. Use of pore casts and scanning electron microscope to study pore geometry. *Jour.Sed.Petrology*, **40**, 1153-1157

Poldervaart A. 1955. Chemistry of earth's crust. In: Poldervaart, A. (Ed). Crust of the earth-a symposium. *Geol. Soc. America Spec. Paper,* **62**, 119-144.

Potter P.E. 1978. Petrology and chemistry of modern big river sands. *Jour. Geology,* **86**, 423-449.

Powers, M.C. 1953. A new roundness scale for sedimentary particles. *Jour.Sed.Petrology*, **23**, 117-119.

Priest S.D. & Selvakumar S. 1982. *The failure characteristics of selected British Rocks.* Transport and Road Research Lab, Report, 189p.

Rittenhouse G. 1971a. Pore-space reduction by solution and cementation. *Bull. Am. Assoc. Petrol. Geol.*, **55**, 80-91.

Rittenhouse G. 1971b. Mechanical compaction of sands containing different percentages of ductile grains : a theoretical approach. *Bull. Am. Assoc. Petrol. Geol.*, **55**, 92-96.

Rogers J.J. & Head W.B. 1961. Relationship between porosity, median size & sorting coefficients of synthetic sands. *Jour. Sed. Petrology*, **31**, 467-470.

Sabins F.F. 1962. Grains of detrital, secondary, and primary dolomite from Cretaceous strata of the western interior. *Geol. Soc. America Bull.* **73**, 1183-1196.

Sasaki T., Kinoshita S. & Ishijima Y. 1981. A study on water-sensitivity of argillaceous rock. *Proc. Int. Symp. on Weak Rock*, **I-2-25**, 143-148.

Savage R.J.G. 1977. *Geological Excursions in the Bristol District.* University of Bristol.

Schafer A. & Teyssen T. 1987. Size, shape and orientation of grains in sands and sandstones - image analysis applied to rock thin sections, *Sedim. Geol.*, **52**, 251-271.

Scheider A.E. 1974. *The physics of flow through porous media*, 3rd edition. University of Toronto Press, Toronto, 353p.

Schmidt V. & McDonald D.A. 1979a. Texture and recognition of secondary porosity in sandstones. In: Scholle, P.A. and Spearing, P.R. (eds.). Aspects of diagenesis. *Spec. Publ. Soc. econ. Paleontol. Miner.*, **26**, 209-225.

Schmidt V. & McDonald D.A. 1979b. The role of secondary porosity in the course of sandstone diagenesis. In: Scholle P.A. and Schluger P.R. (eds.). Aspects of diagenesis. *Spec. Publ. Soc. econ. Paleontol. Miner.*, **26**, 175-207.

Scholle P.A. 1978. A colour illustrated guide to carbonate rock constituents, textures, cements, and porosities. *Am. Assoc. Petroleum Geologists Memoir*, **27**, 241p.

Scholle P.A. 1979. A colour illustrated guide to constituents, textures, cemnets and porosities of sandstones and associated sedimentary rocks. *Am. Assoc. Petroleum Geologists Memoir*, **28**, 201p.

Scholle P.A. & Schluger P.R. (eds.). 1979. Aspects of diagenesis. *Spec. Publ. Soc. econ. Paleontol. Miner.* **26**, 443p.

Scholz C.H. 1968. Microfracturing and the inelastic field of rock in compression. *J. Geophys. Res.*, **73**, 1417-1432.

Scholz C.H. 1970. The role of microfracturing in rock deformation. *J. Geophys. Res.*, **75**, 323-327.

Scholz C.H. & Kranz R., 1974. Notes on dilatancy recovery. *J. Geophys. Res.*, **79**, 2132-2135.

Selley R.C. 1970. *Ancient sedimentary environments*. Chapman and Hall, London.

Shearman D.J. 1978. Evaporites of coastal sabkhas, In: Dean W.E. and Schreiber B.C. (Eds.): Marine evaporites. *S.E.P.M. Short course* **4**, 6-42.

Shiki T. 1959. Studies on sandstone in the Maizuru Zone, southwest Japan, pt. 1, Importance of some relations between mineral composition and grain size. *Mem. Coll. Sci., Univ. Kyoto, Ser. B*, **29**, 291-324.

Shotton F.W. 1956. Some aspects of the New Red Desert in Britain. *Geol. J.*, **1**, 450-465.

Sibley D.F. & Blatt H. 1976. Intergranular pressure solution and cementation of the Tuscarora Orthoquartzite. *Jour. Sed. Petrology*, **46**, 881-896.

Siebert R.M., Moncure G.K. & Lahann R.W. 1984. A theory of framework dissolution in sandstones. In: McDonald, D.A. and Surdam R.C. (eds.). Clastic diagenesis.*Am. Assoc. Petrol. Geol. Mem.*, **37**, 163-175.

Siever R. 1968. Establishment of equilibrium between clays and sea water. *Earth Planet. Sci Letters*, **5**, 106-110.

Siffert B. 1962. Quelques reactions de la silice en solution: la formation des argiles. *Service Carte Geol. Alsace Lorraine Memoirs* **21**, 86p.

Skempton, A.W. 1960. Terzaghi's discovery of effective stress. In: *From theory to prractice in soil mechanics; selections from the writings of Karl Terzaghi.* Bjerrum L., Casagrande A., Peck R.B. & Skempton A.W. (eds). New York, Wiley, 42-53.

Skinner E.H. 1988. A ground support prediction concept: The Rock Structure Ratin, (RSR) model. *In:* Rock Mass Systems for Engineering Purposes. Louis Kirkaldie (Ed.). *Am. Soc. Test. Mat.* Philadelphia. 167p.

Smith J.V. 1974. *Feldspar Minerals, Vols. 1-3.* Berlin-New York: Springer-Verlag.

Smith D.B., Brunston R.G.W., Manning P.I., Simpson S. and Shotton F.W. 1974. A correlation of Permian rocks in the British Isles. *Jour. Geol. Soc. Lond.* **130**, 1-45.

Smoltzyk v & Gartung E. 1979. 1979. Geotechnical properties of a soft Keuper Sandstone. *Proc. 4th Congr. Int. Soc. Rock Mech.*, Montreux, **2**, 639-644.

Sneed E.D. & Folk R.L. Pebbles in the lower Colorado River, Texas, a study in particle morphogenesis. *Jour. Geology,* **66**, 114-150.

Sorby H.C. 1859. On the structure and origin of the Millstone Grit of south Yorkshire. *Proc. West Yorkshire Geol. Soc,* **3**, 669-675.

Stadler P.J. 1973. Influence of crystallographic habit and aggregate structure of authigenic clay minerals on sandstone permeability. *Geol., Mijnbouw*, **52**, 217-219.

Sudo T., Shimoda S., Yotsumoto H. & Aita S. 1981. *Electron micrographs of clay minerals.* New York. Elsevier. 203p.

Surdam R.C., Boese S.W. & Crossley L.J. 1984. The chemistry of secondary porosity. In: McDonald D.A. and Surdam R.C. (eds.). Clastic Diagenesis. *Am. Assoc. Petrol. Geol. Mem.*, **37**, 127-149.

Swett K., Klein G. de V., & Smith D.E. 1971. A Cambrian Tidal sand body - the Eriboll Sandstone of north-west Scotland; An ancient-recent analog. *Jour. Geology,* **79**, 400-415.

Szabo B.A. 1966. Stress concentrations around pores in saturated rocks of low permeability. *Proc. Int. Cong. Rock Mech.*, Lisbon, **2**, 467-472.

Taira A. & Lienert B.R. 1979. The comparative reliability of magnetic, photometric and microscopic methods of determining the orientations of sedimentary grains. *Jour. Sed. Petrology.* **49**, 759-772.

Tapponier P. & Brace W.F. 1976. Development of stress-induced microcracks in Westerley granite. *Int. J. Rock Mech. Min. Sci.,* **13,** 103-112.

Taylor B.J. 1978 *British Regional Geology of Nortern England.* 4th edition. H.M.S.O.

Taylor J.M. 1950. Pore space reduction in sandstones. *Am. Assoc. Petroleum Geol.*ogists *Bull.*, **34**, 701-716.

Terzaghi K.V. 1923. Die Berechung der Durchlassigkeitsziffer des Tones austen Verlauf der hydrodynamischen Spannungserscheinungen. *Sber. Akad. Wiss. Wien*, **132**, 105.

Terzaghi K. 1945. Stress conditions for the failure of saturated concrete and rock. *Proc. Amer. Soc. Testing Materials.*, **45**, 777-792.

Thomson, W. (Lord Kelvin) 1871. Equilibrium vapour at a cyrved surface of liquid. *Phil. Mag.* **42**, 448-452.

Till R. 1974. *Statistical methods for the earth scientist,* New York: Wiley, 154p.

Tomlinson M.J. 1980. *Foundation design and Construction..* 4th edition. Pitman Publishing Ltd, London.

Tomashevskaya I.S. & Volodina S.I. 1976. Deformation of rock samples under uniaxial compression. *Izvestiya Acad. Sci. USSR, Physics of the Solid Earth,* **12**, 348-350.

Trask P.D. 1932. *Origin and environments of source sediments of petroleum.* Houston: Gulf Publ. Co., 321p.

Tucker M.E. 1978. Triassic lacustrine sediments from south Wales: shore zone clastics, evaporites and carbonates. In: *Modern and ancient lake sediments*, A. Matter and M.E. Tucker (Eds.). Oxford: Blackwell Sci. Publications.

Tucker M.E. 1981. *Sedimentary Petrology.* An Introduction. Blackwell Scientific Publications.

Turk N. & Dearman W.R. 1986. A new procedure for determination of point load strength in site investigation. *Geol. Soc., Eng. Geol. Spec. Pub.* **2.**

Turner P. 1980. *Continental red beds. Developments in Sedimentology*, 29, Elsevier, Amsterdam, 562p.

Udden J.A. 1914. Mechanical composition of clastic sediments. *Geol. Soc. America Bull.* **25**, 655-744.

Van Der Plas L. & Tobi A.C. 1965. Achart for judging the reliability of point counting results. *Am. Jour. Science*, **263**, 87-90.

Van Eeckhout E.M. & Peng S.S. 1975. The effect of humidity on the compliance characteristics of coal mine shales. *Int. J. Rock Mech. Min Sci.*, **12**, 335-340.

Van Eeckhout E.M. 1976. The mechanisms of strength reduction due to moisture in coal mine shales. *Int. J. Rock Mech. Min Sci.*, **13**, p.61-67.

Velde B. 1977. *Clays and clay minerals in natural and synthetic systems*, 218p. New York: Elsevier.

Vutukuri V.S. 1974. *Handbook on Mechanical Properties of Rock.*. Trans. Tech. Publ., Claustal, 280p.

Waddel H. 1935. Volume, shape and roundness of rock particles. *Jour. Geology* **40**, 443-451.

Walker T.R. 1967. Formation of red beds in modern and ancient deserts. *Geol. Soc. America Bull.*, **78**, 353-368.

Walker T.R. 1974. Formation of red beds in moist tropical environments: A hypothesis. *Geol. Soc. America Bull.* **85**, 633-638.

Walker T.R. 1979. Red color in dune sand. In: McKee, E.D. (ed.). A study of global sand seas. *Prof. Pap. U.S. geol. Surv.*, **1052**, 61-81.

Walker T.R. Waugh B. & Crone A.J. Diagenesis in first cycle desert aluvium of Cenozoic Age, southwestern United States and northwestern Mexico. *Geol. Soc. America Bull,* **89**, 19-32.

Walsh, J.B. 1965. The effect of cracks on the uniaxial compression of rocks. *J. Geophys. Res.* **70**, 415-426.

Waugh B. 1970. Petrology, provenance and silica diagenesis of the Penrith Sandstone (lLower Permian) of N.W. England. *Jour. Sed. Petrology,* **40**, 1226-1240.

Waugh B. 1978. Authigenic k-feldspar in British Permo-Triassic sandstones. *Jour. Geol. Society London*, **135**, 51-56.

Wawersik W.R. & Fairhurst C. 1970. A study of brittle rock fracture in laboratory compression experiments. *Int. J. Rock Mech. Min. Sci.*, **7**, 561-575.

Wawersik W.R. 1975. Technique and apparatus for strain measurements on rock in constant confining pressure experiments. *Rock Mech.*, **7**, 231-241.

Wentworth C.K. 1929. Method of computing mechanical composition types of sediments. *Geol. Soc. America Bull.* **40**, 771-790.

Wentworth C.K. 1933. Fundamental limits to the sizes of clastic grains, *Science,* **77**, 633-634.

Weyl P.K. 1959. Pressure solution and the force of crystallization- a phenomenological theory. *J. Geophys. Res.*, **64**, 2001-2025.

West G. 1979. Strength properties of Bunter Sandstone. *Tunnels and Tunnelling* Vol.

Wetton J.E. 1984. SEM petrology atlas A.A.P.G. Tulsa. 237p.

Wiid B.L. 1967. *The influence of moisture upon the strength behaviour of rock.* PhD Thesis, University of Witwatersrand, 184p.

Wilkens . H., Simmons ., Wissler . M. & Caruso . 1986. *Int. J. Rock Mech. Min. Sci. and Geomech. Abstr.* **23**, 313-325.

Williams G.E. 1966. Palaeogeography of the Torridonian Applecross Group. *Nature, London.*, **209**, 1303-1306.

Winston P.W. & Bates D.H. 1960. Saturated solutions for the control of humidity in biological research. *Ecology*, **41**, 232-237.

Worthington P.F. & Barker R.D. 1972. A centrifugal technique for rapidly estimating the permeability of a consolidated sandstone. *Geotechnique*, **22**, 521- 524.

Zimmerman R.W. Technical Note: Elastic moduli of a solid with spherical pores: New self-consistent method. *Int. J. Rock Mech. Min. Sci. and Geomech. Abstr.* **21**, 339-343.

APPENDIX

REPRESENTATIVE STRESS-STRAIN CURVES FOR THE SANDSTONES TESTED AT DRY, SATURATED AND INTERMEDIATE MOISTURE CONTENTS.

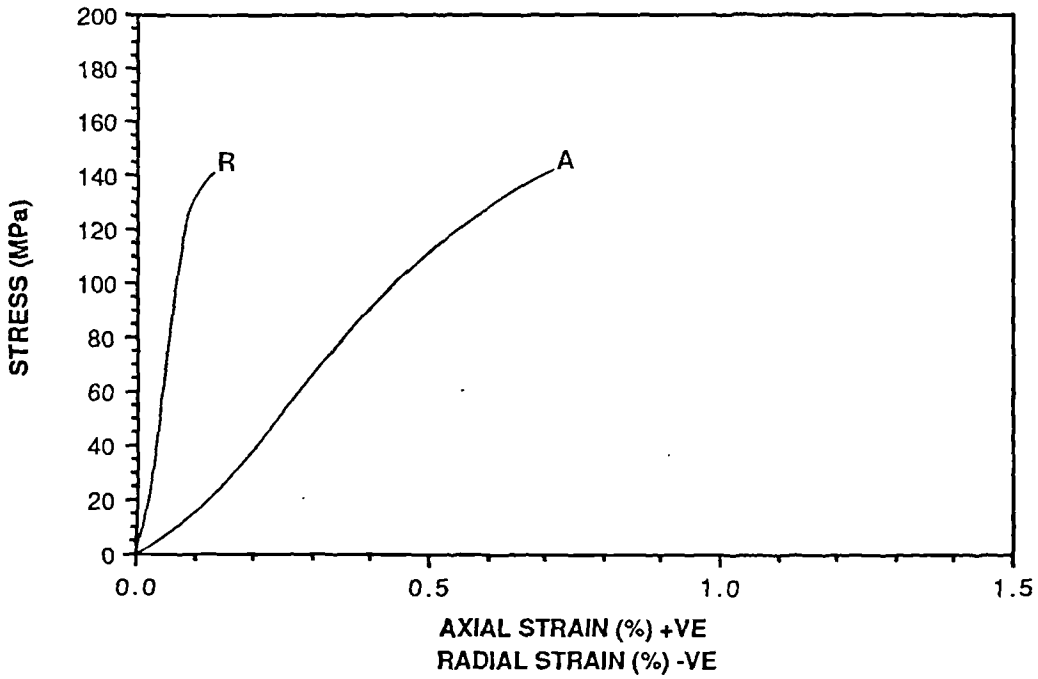

Sample No. A1

w% = 0.00

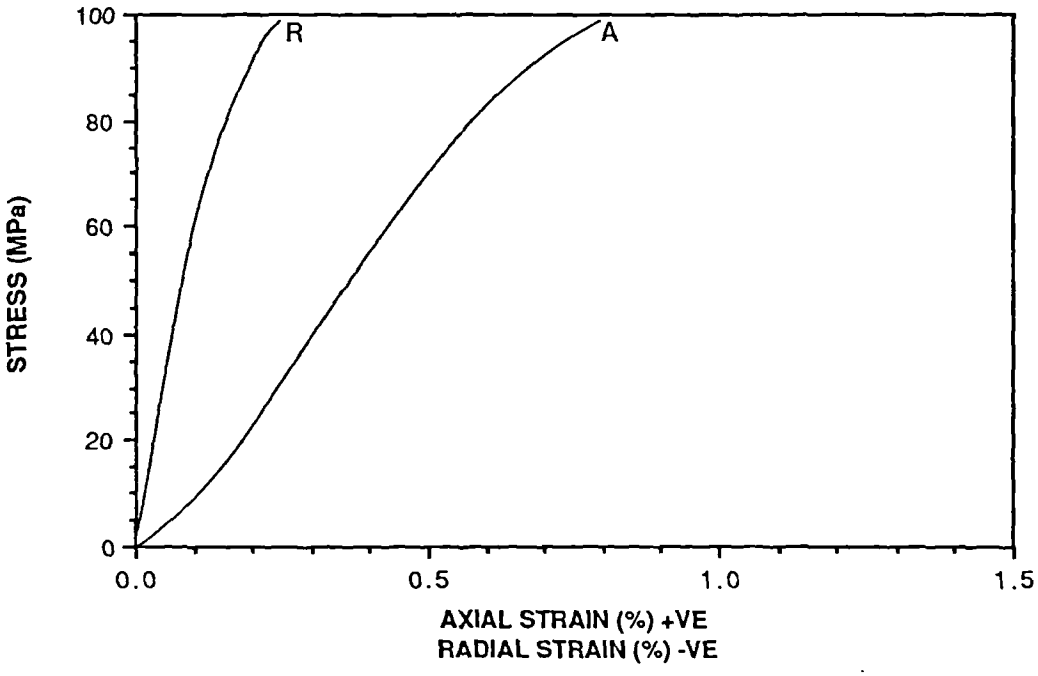

Sample No. A5

w% = SAT

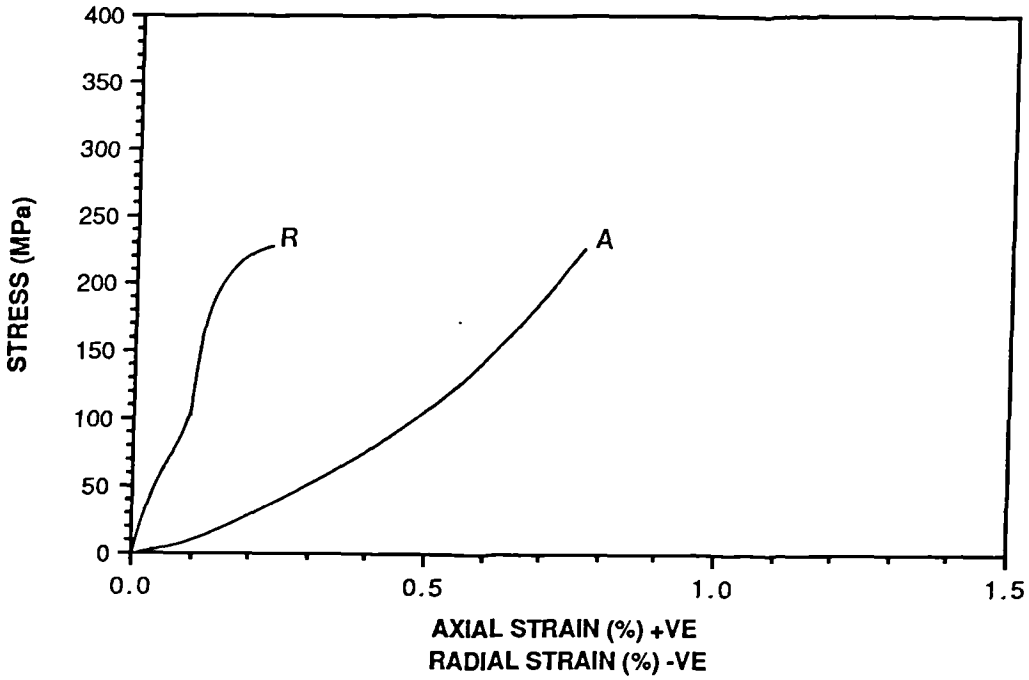

Sample No. DQ 1

w% = 0.00

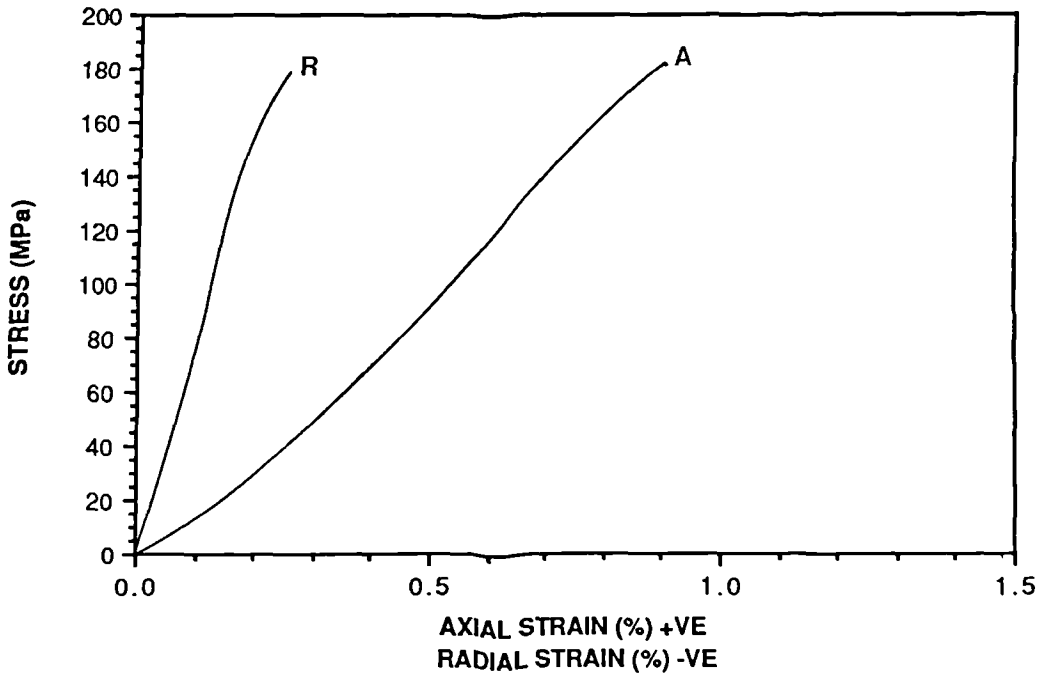

Sample No. DQ 6

w% = SAT

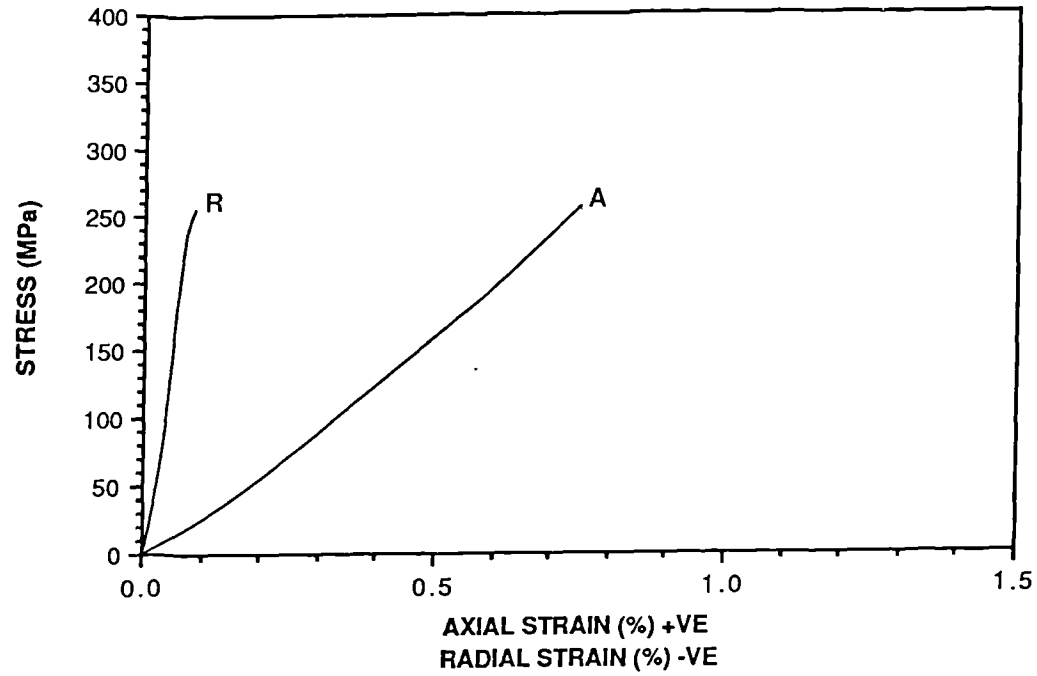

Sample No. BQ 4

w% = 0.00

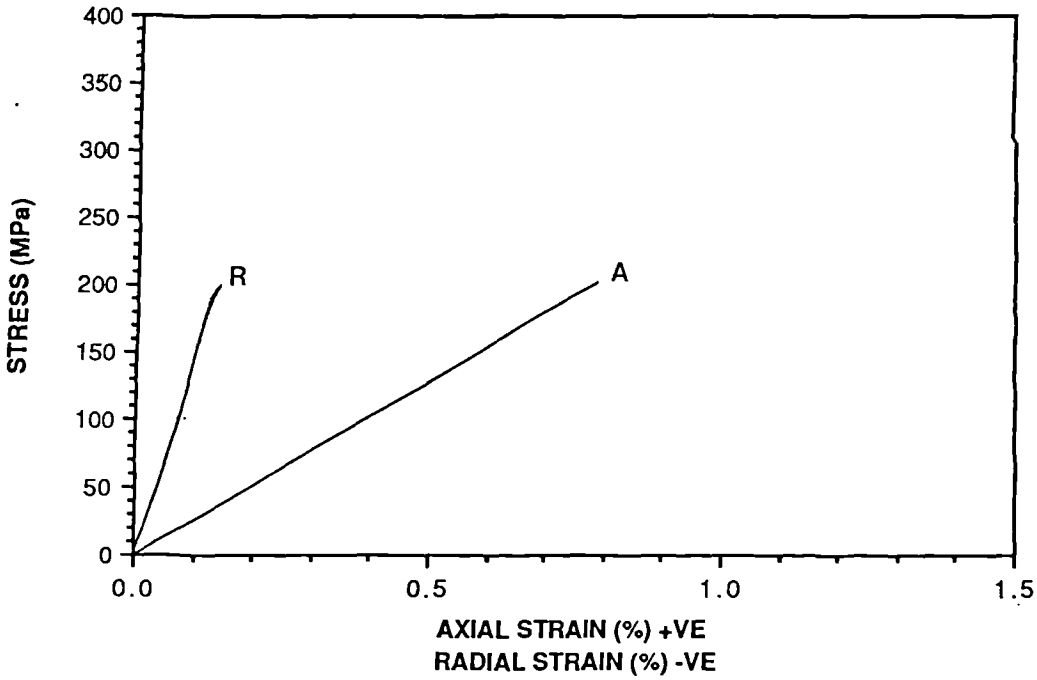

Sample No. BQ 6

w% = SAT.

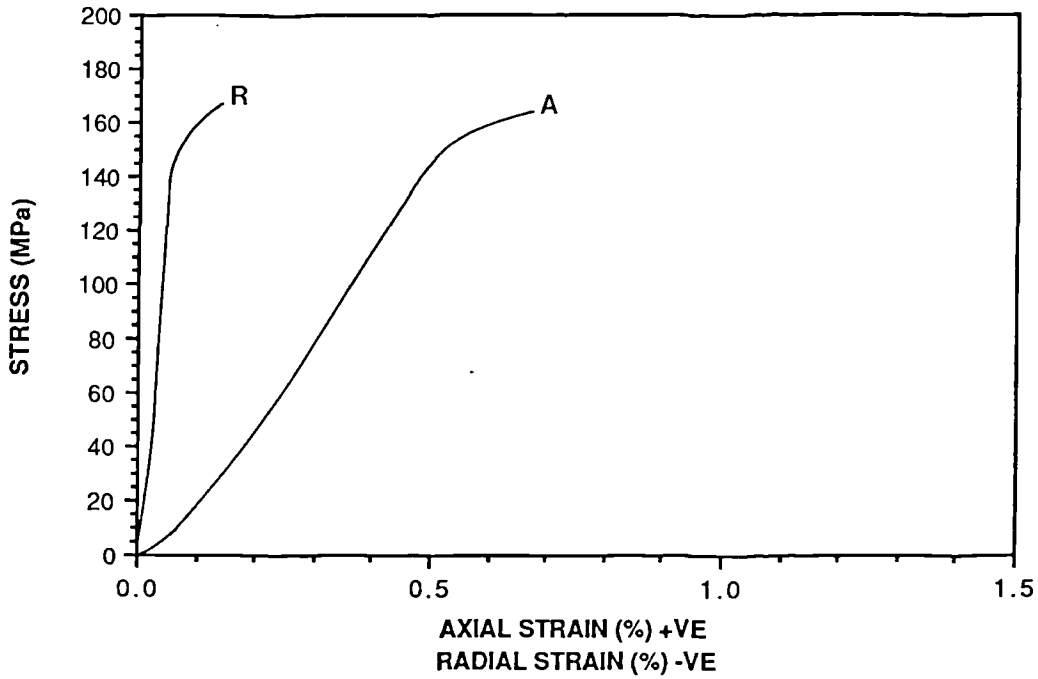

Sample No. LORS 3

w% = 0.00

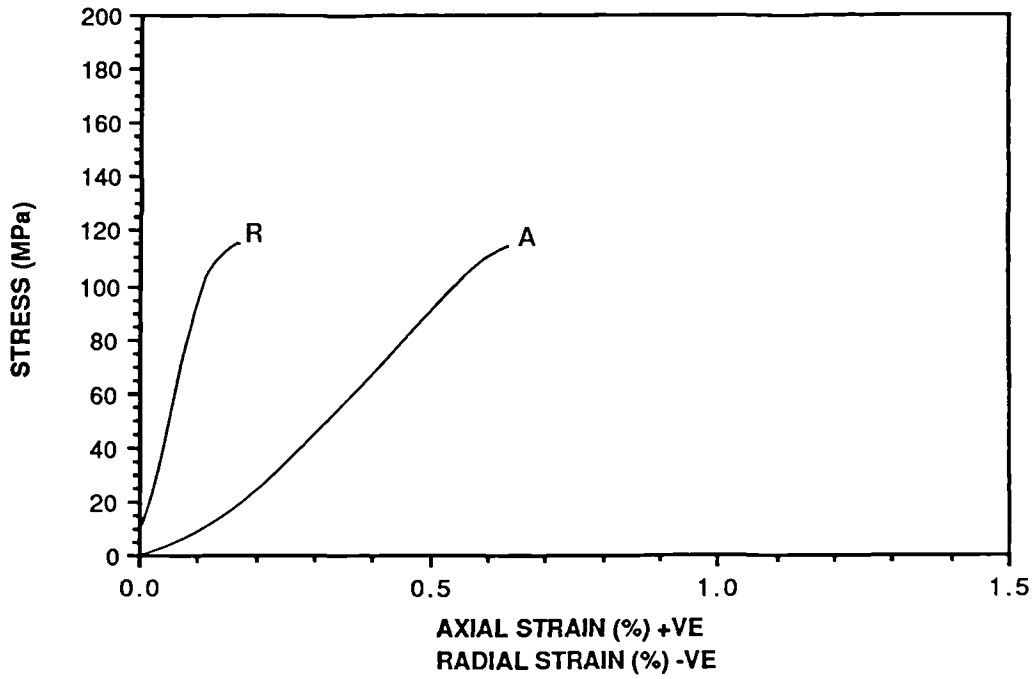

Sample No. LORS 9

w% = SAT.

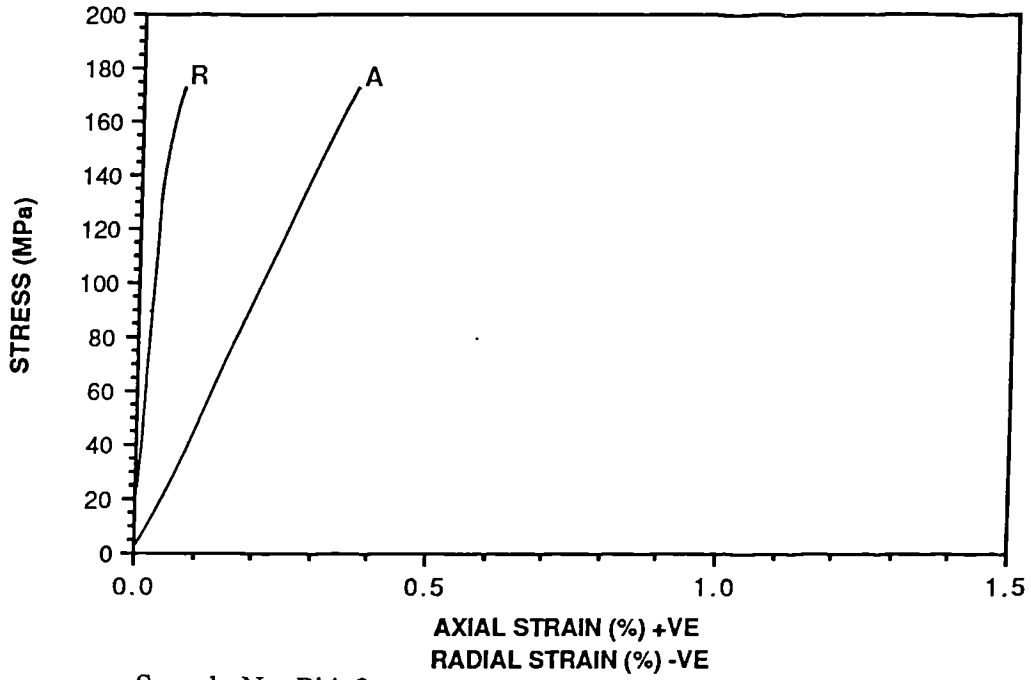

Sample No. PiA 2

w% = 0.00

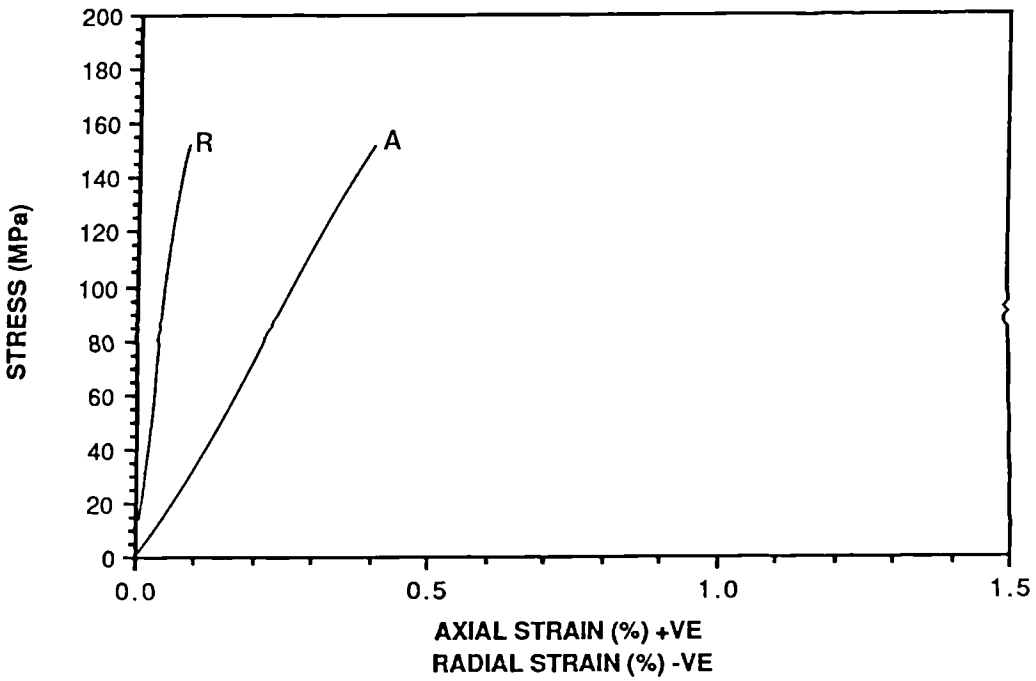

Sample No. PiA 5

w% = SAT.

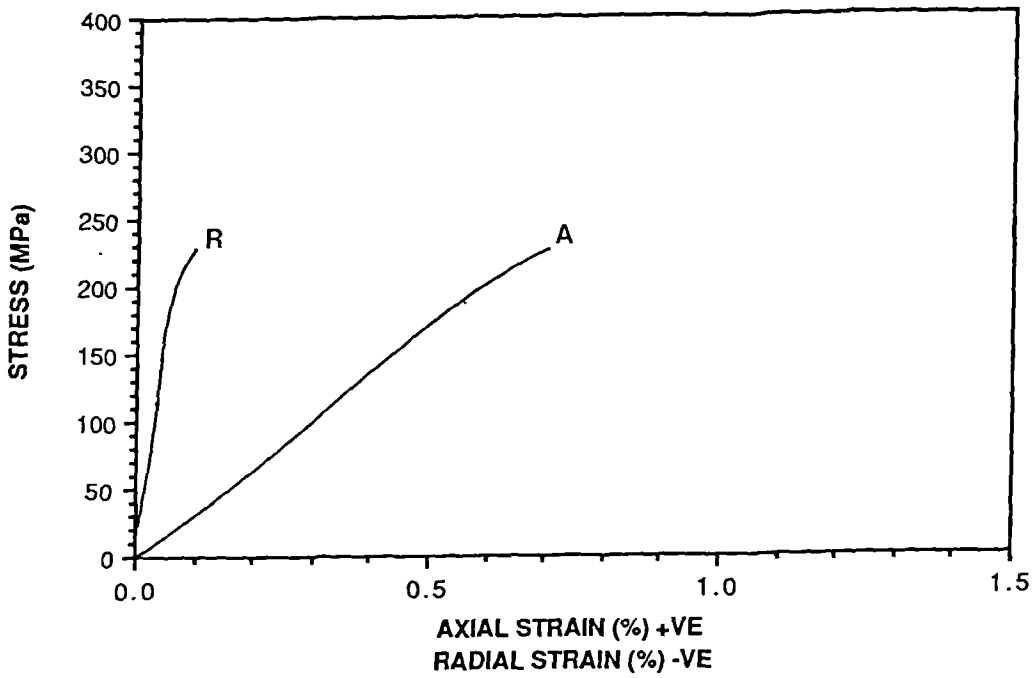

Sample No. PiB 3

w% = 0.00

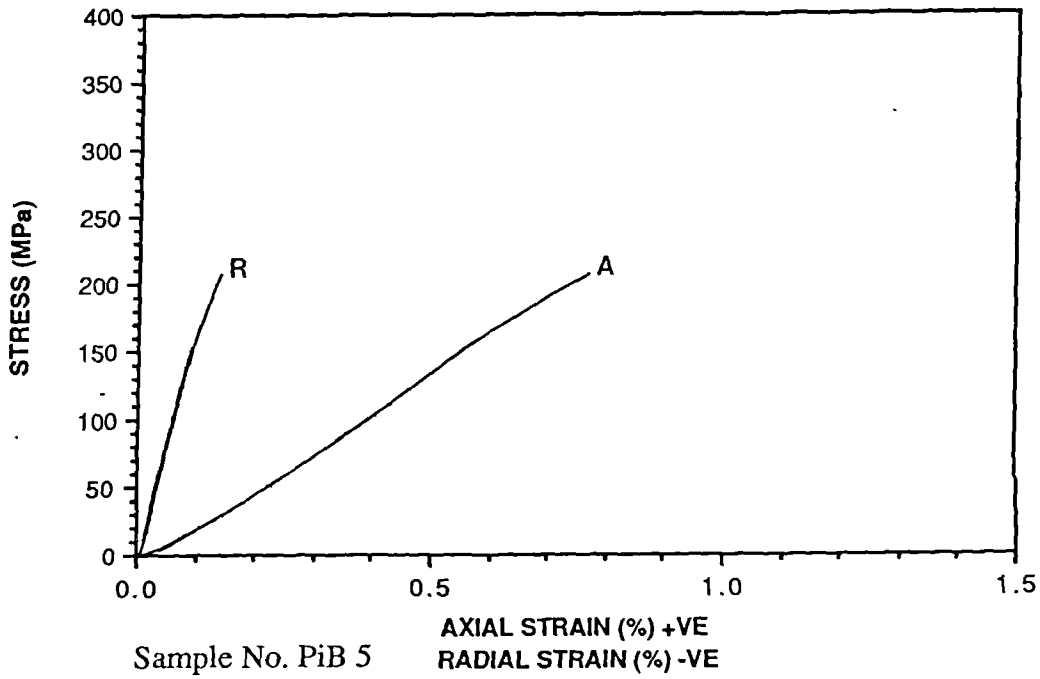

Sample No. PiB 5

w% = SAT.

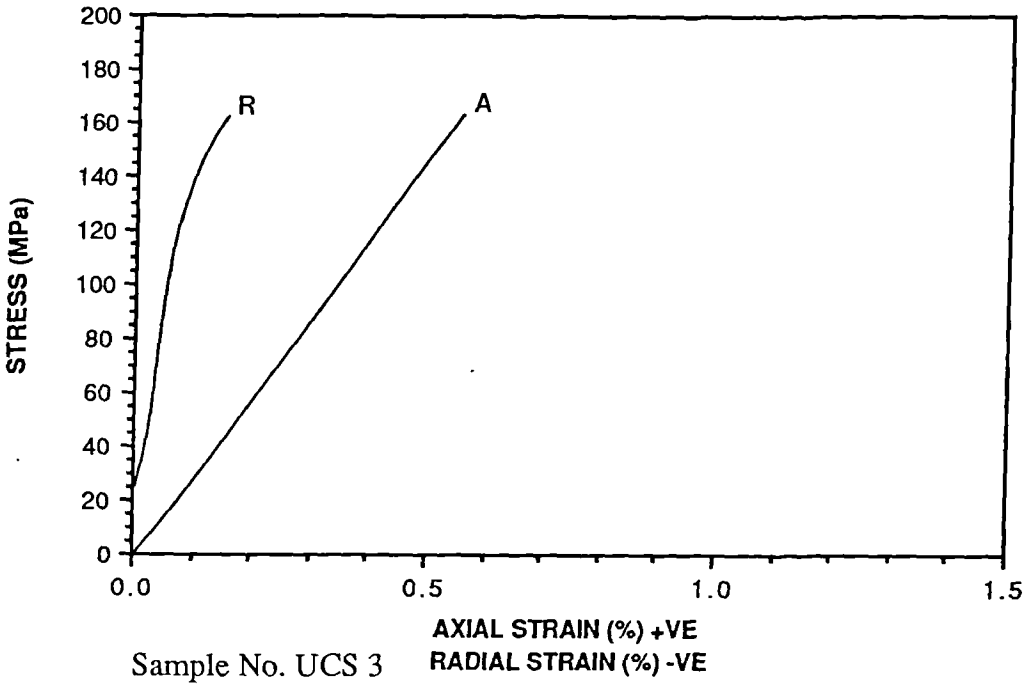

Sample No. UCS 3

w% = 0.00

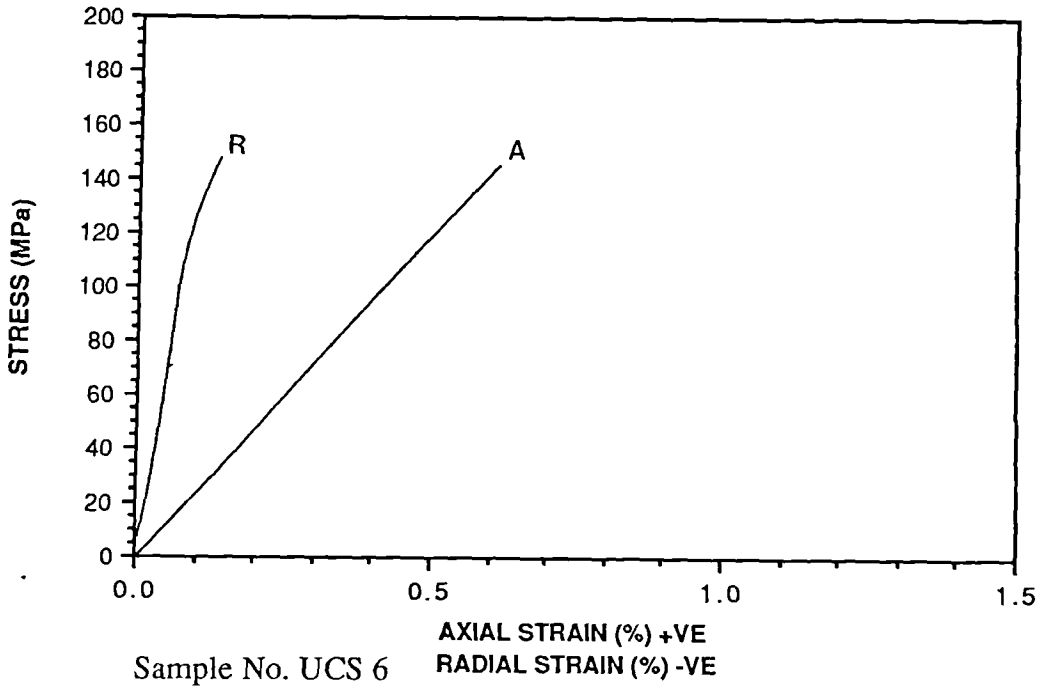

Sample No. UCS 6

w% = SAT.

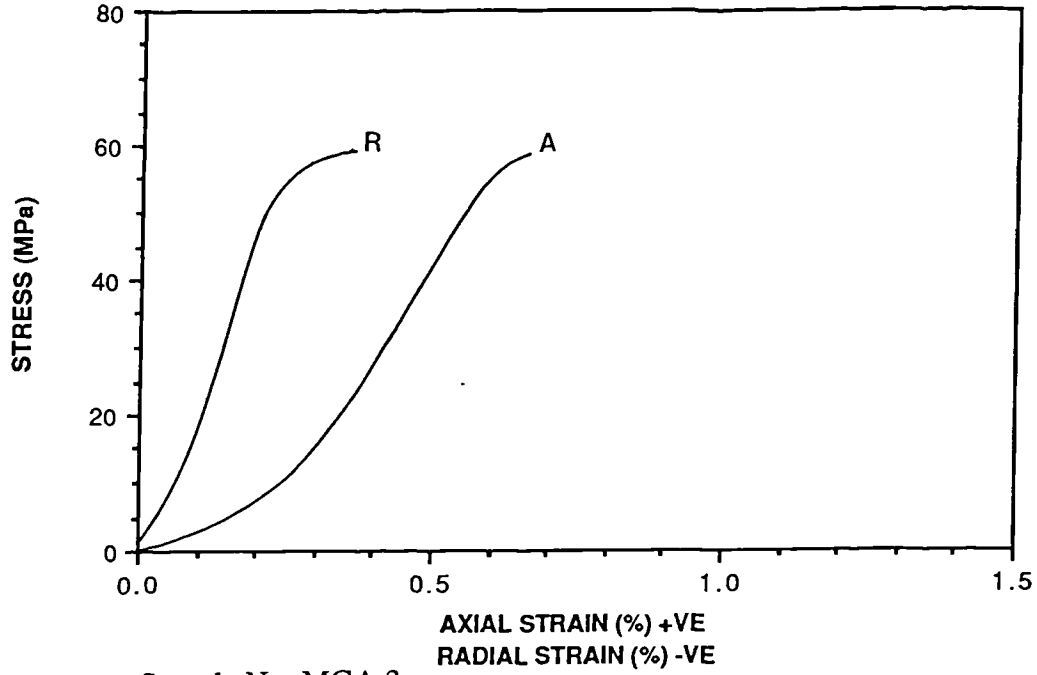

Sample No. MGA 3

w% = 0.00

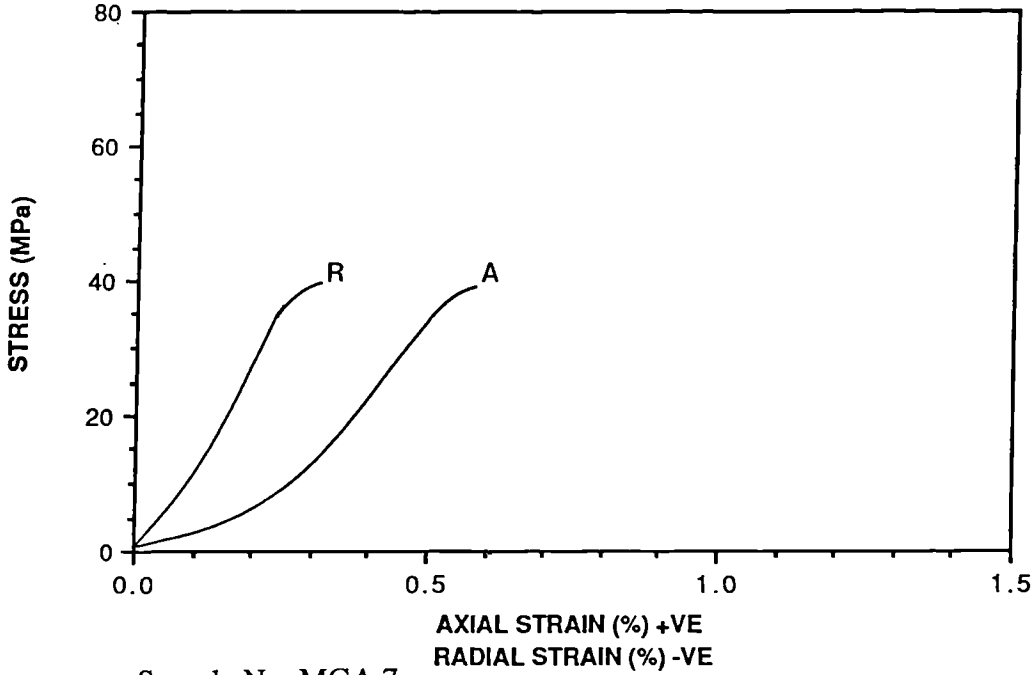

Sample No. MGA 7

w% = SAT.

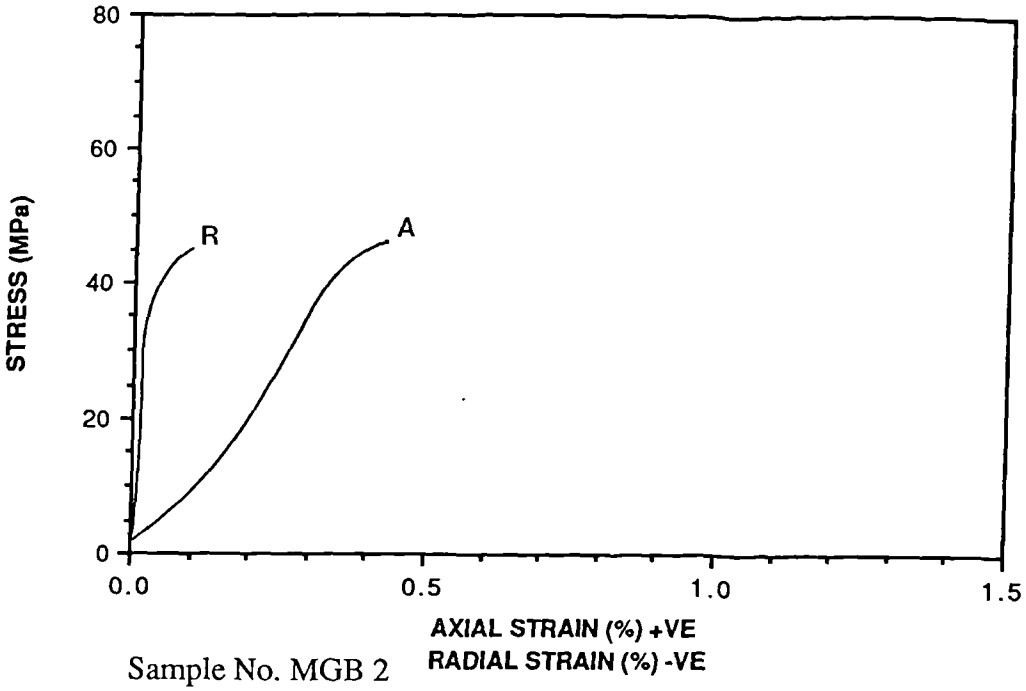

Sample No. MGB 2

w% = 0.00

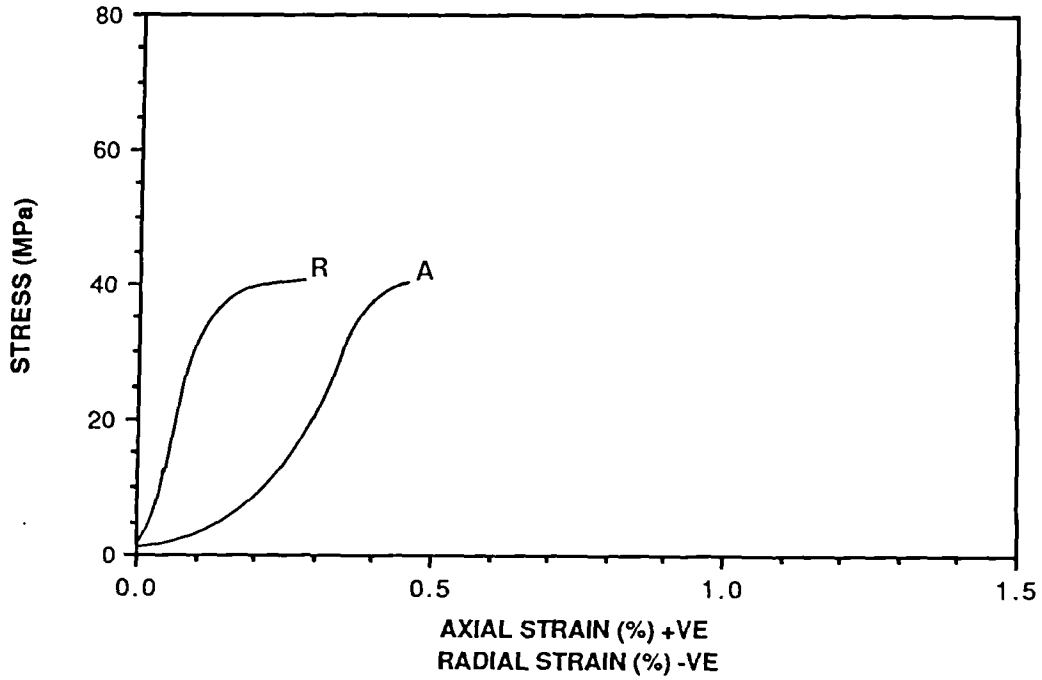

Sample No. MGB 6

w% = SAT.

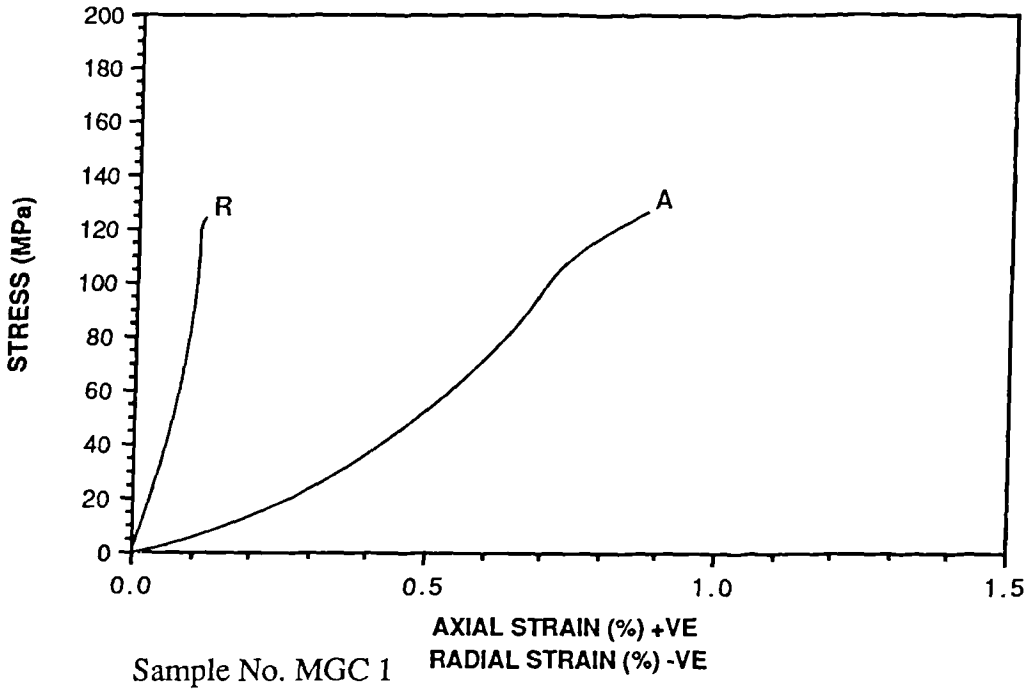

Sample No. MGC 1

w% = 0.00

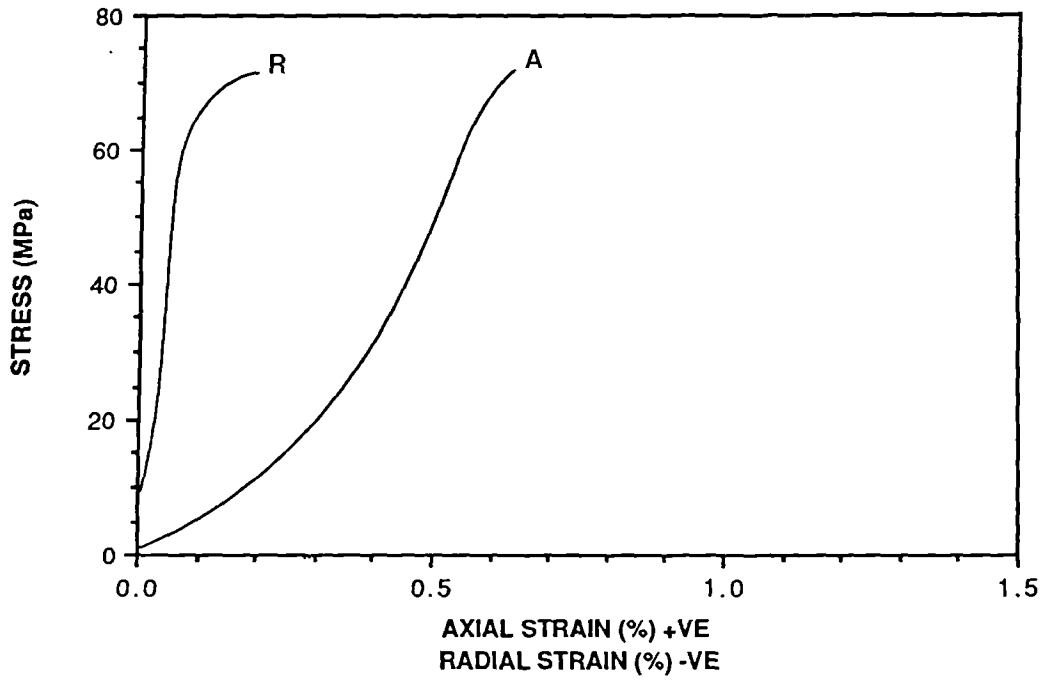

Sample No. MGC 7

w% = SAT.

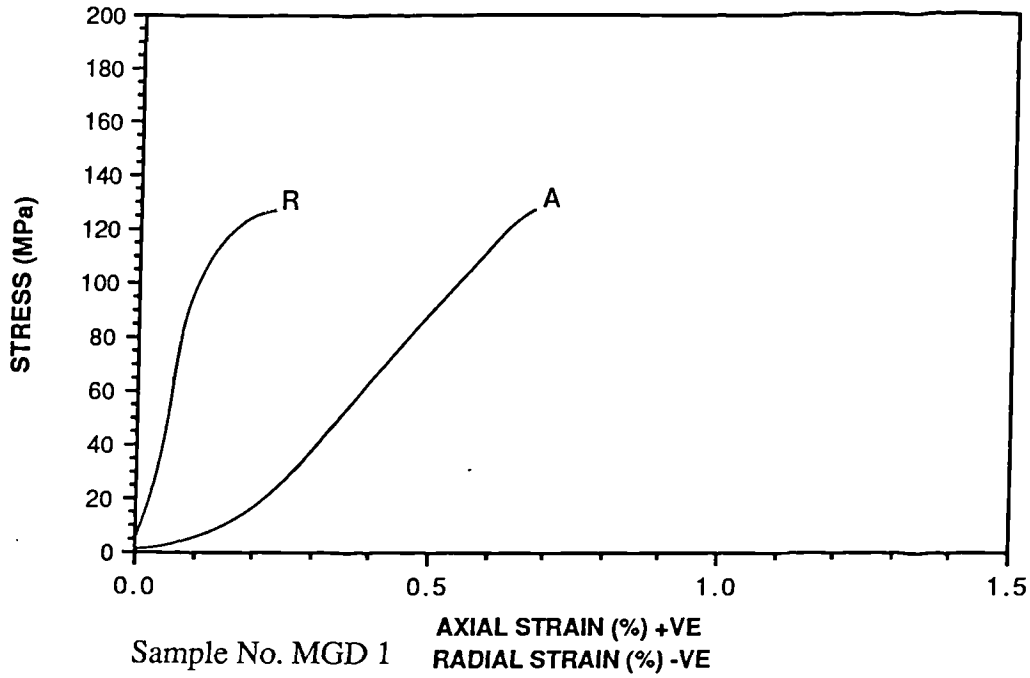

Sample No. MGD 1

w% = 0.00

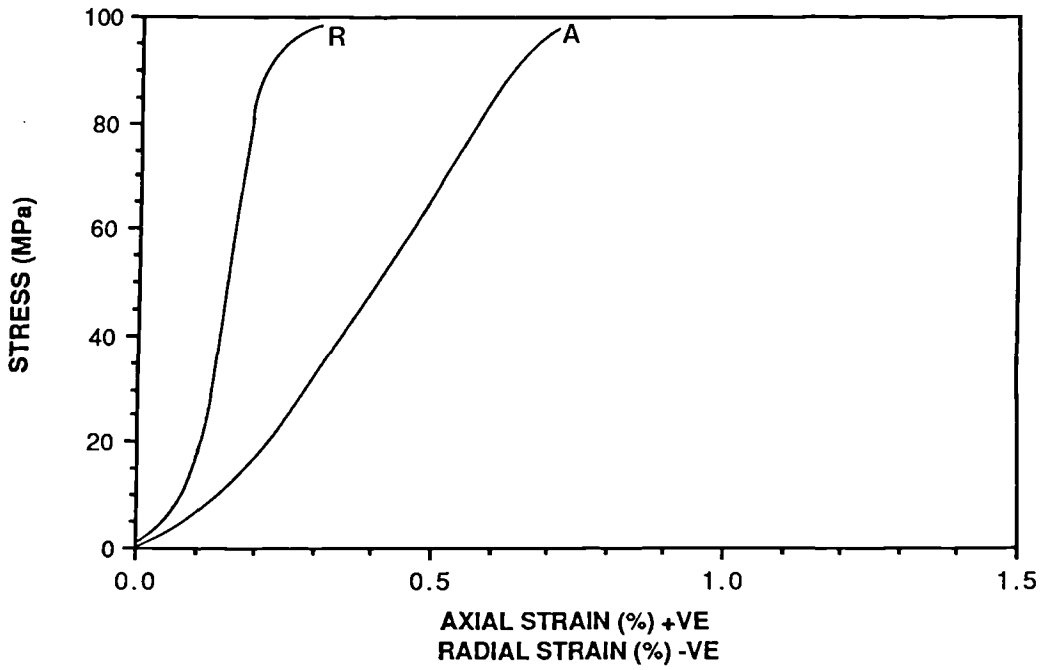

Sample No. MGD 8

w% = SAT.

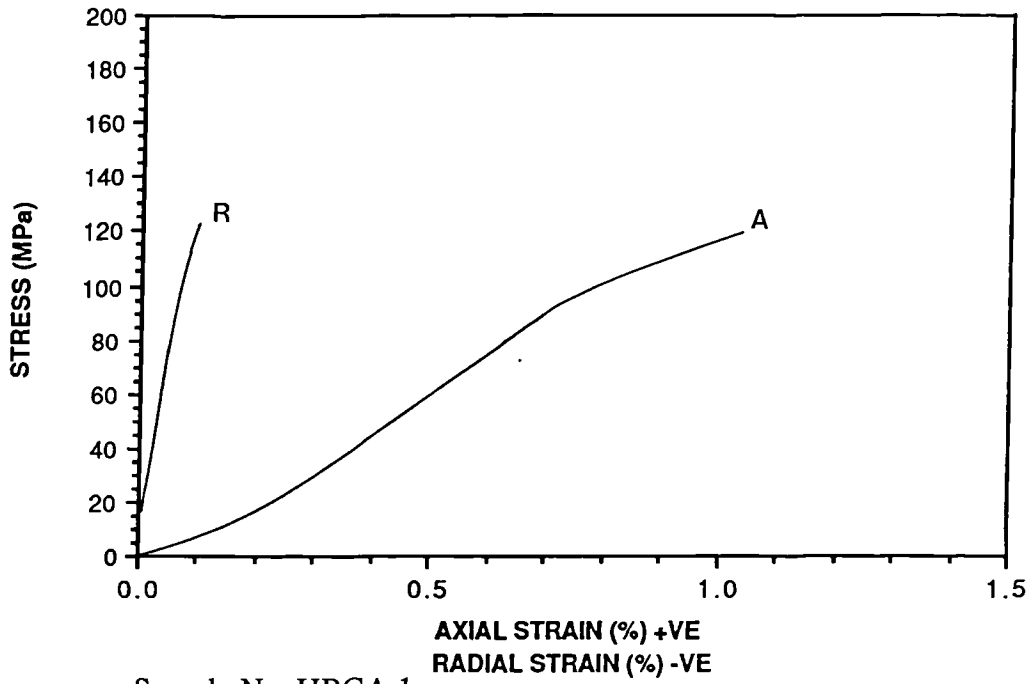

Sample No. HBGA 1

w% = 0.00

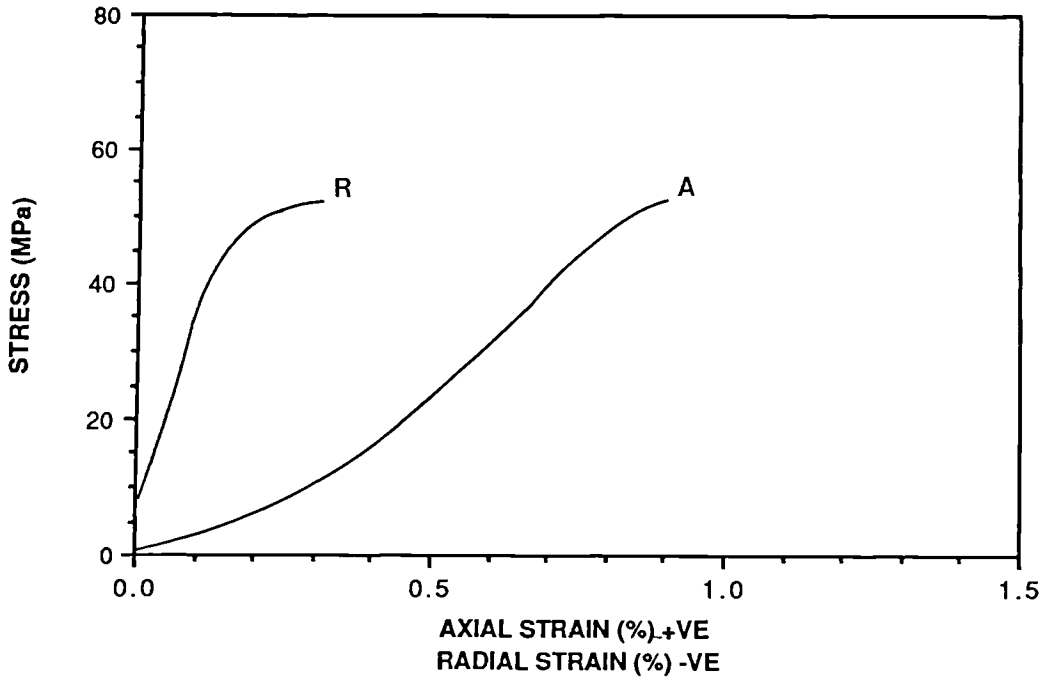

Sample No. HBGA 8

w% = SAT.

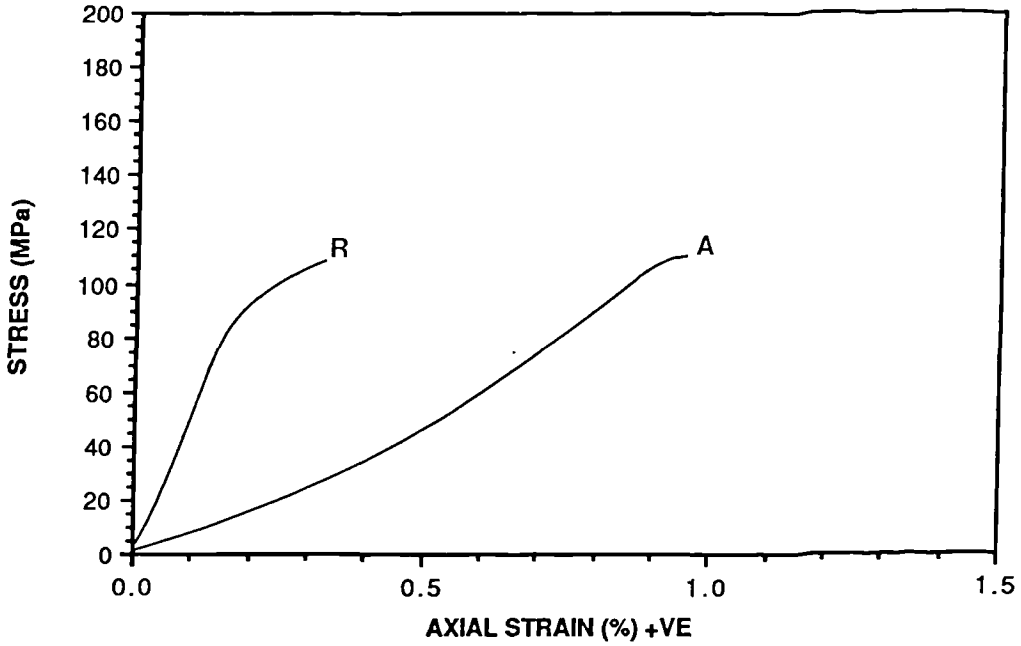

Sample No. HBGB 1

w% = 0.00

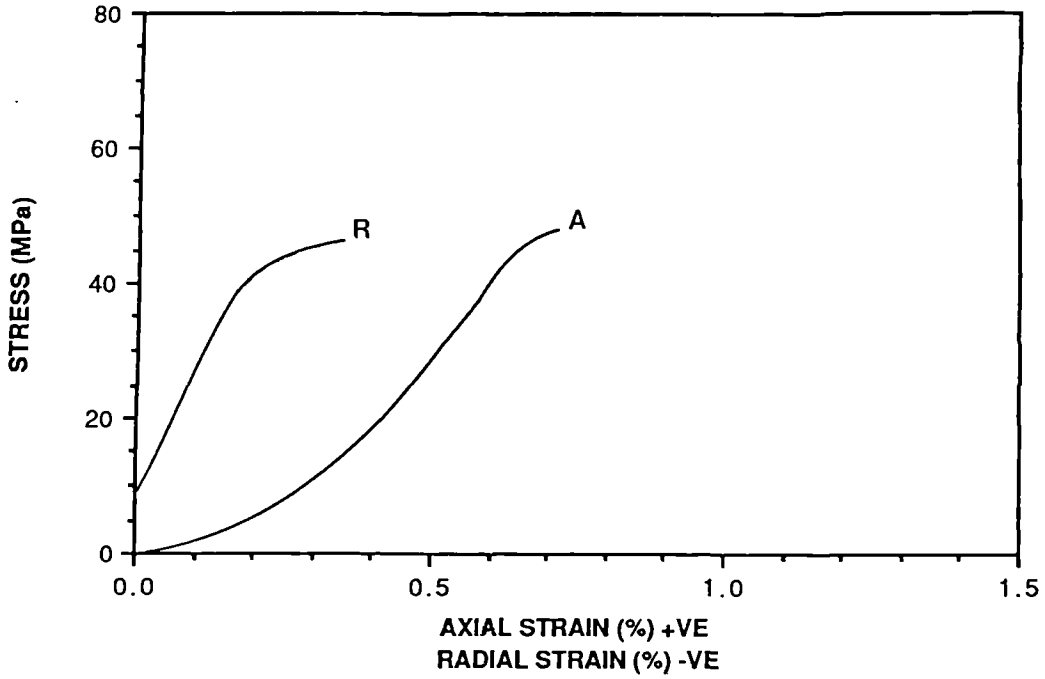

Sample No. HBGB 7

w% = SAT.

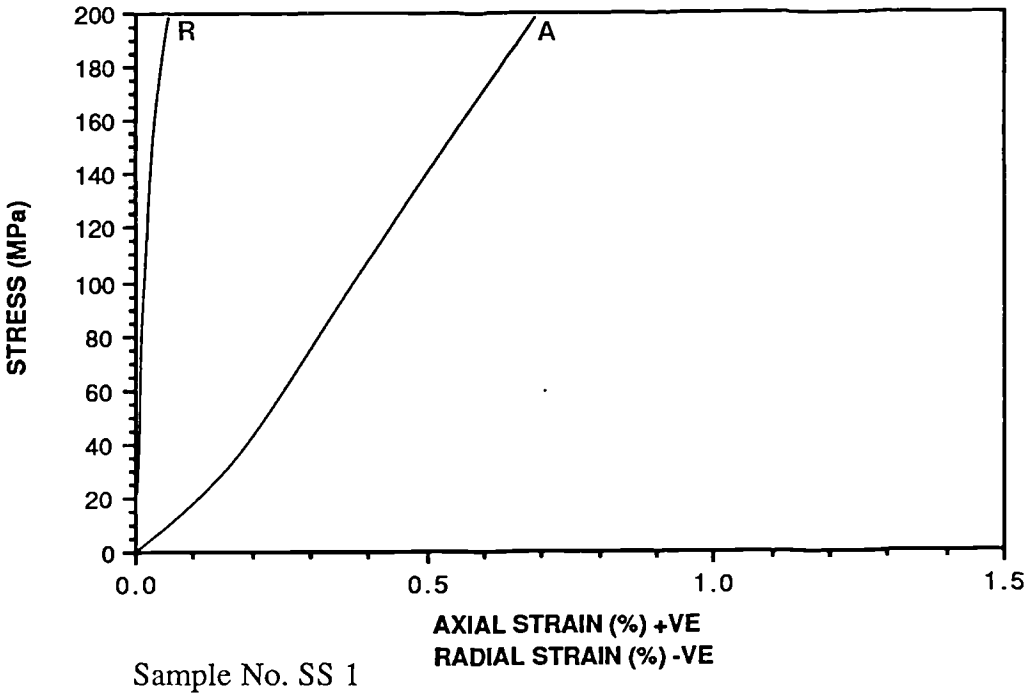

Sample No. SS 1

w% = 0.00

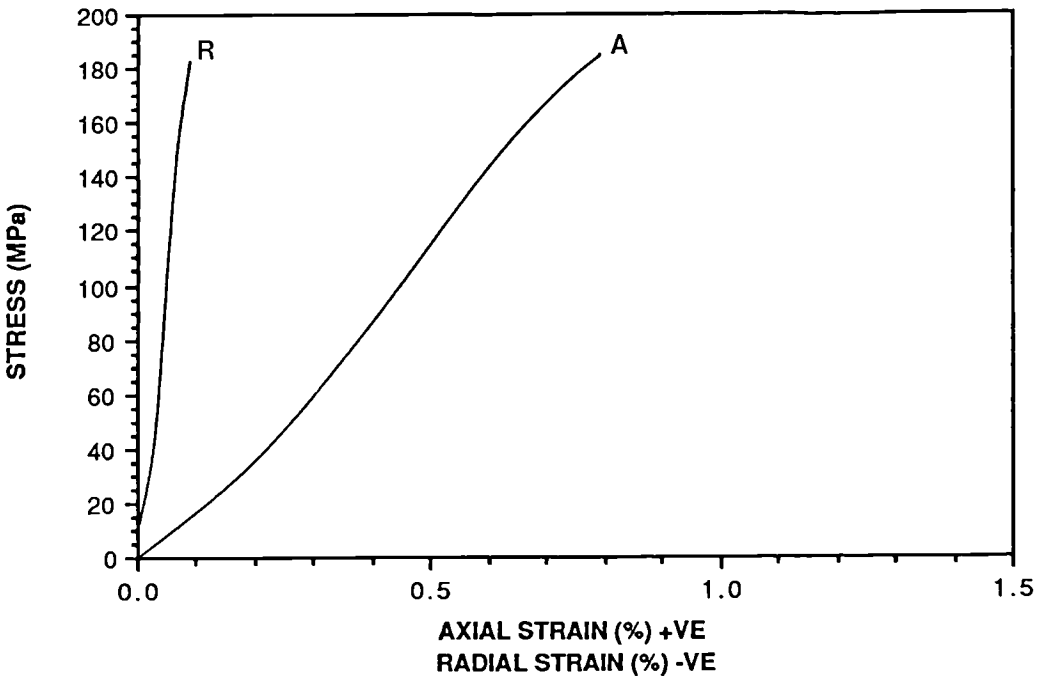

Sample No. SS 4

w% = SAT.

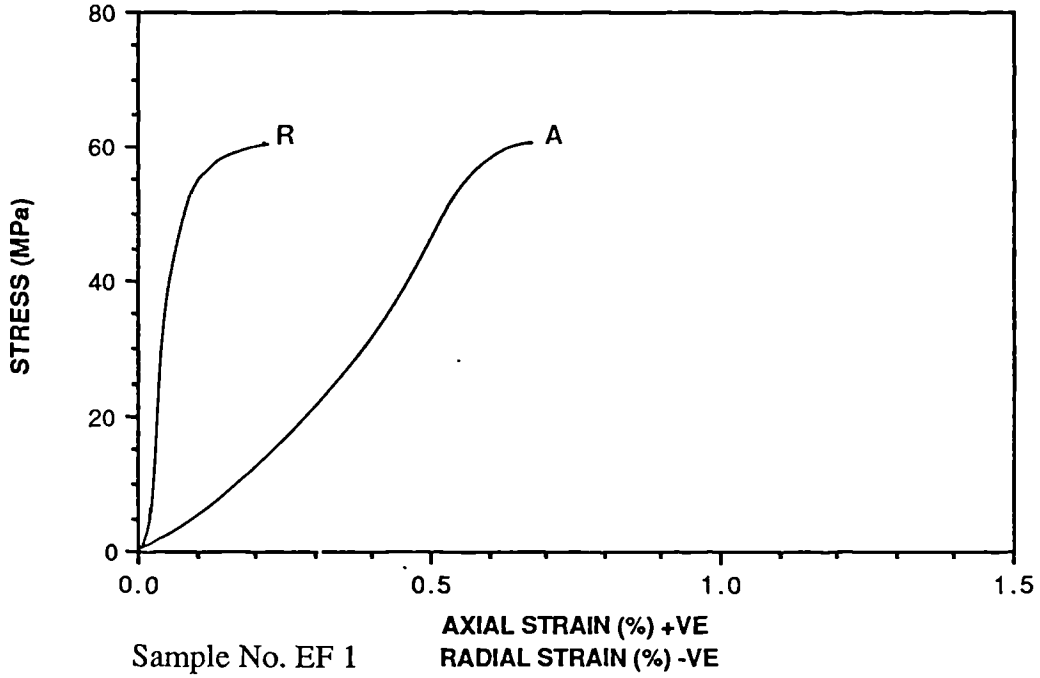

Sample No. EF 1

w% = 0.00

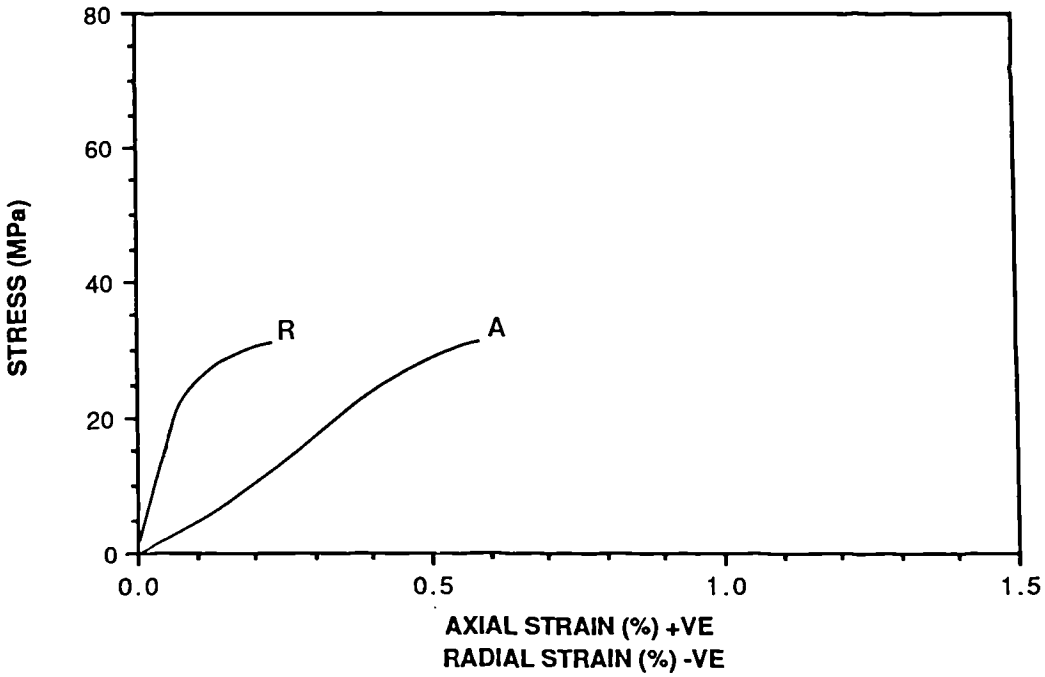

Sample No. EF 7

w% = SAT.

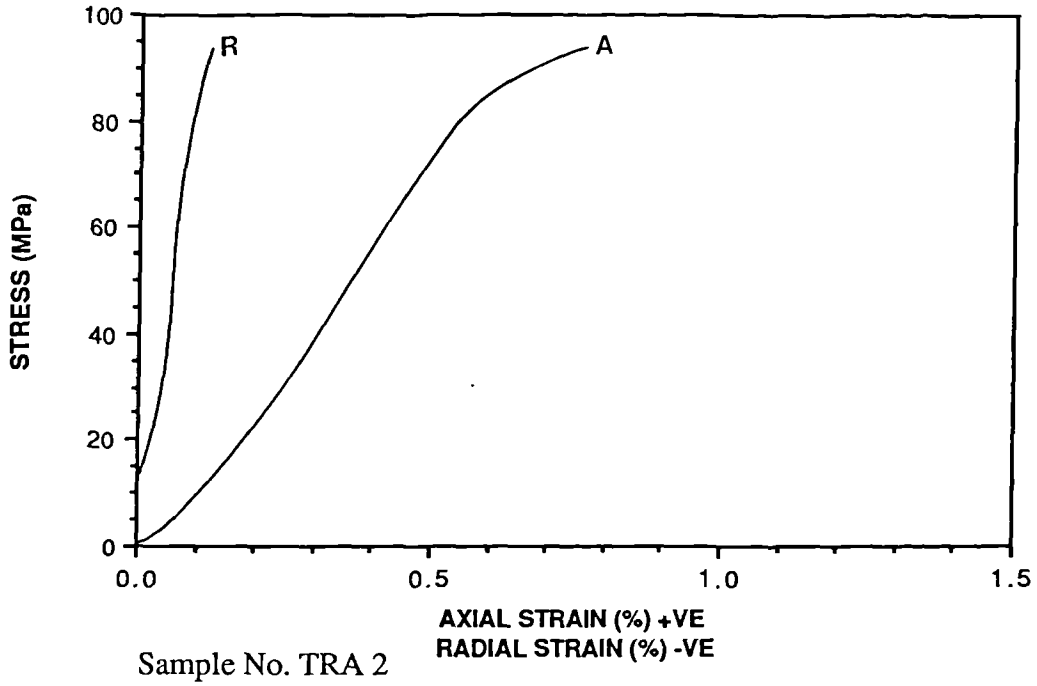

Sample No. TRA 2

w% = 0.00

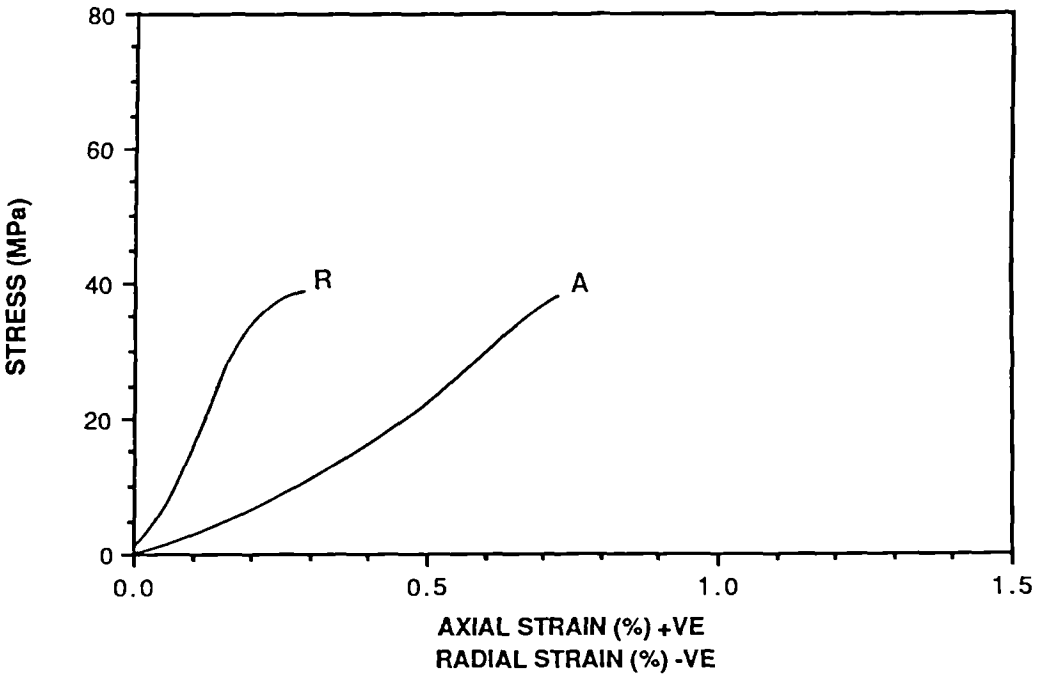

Sample No. TRA 6

w% = SAT.

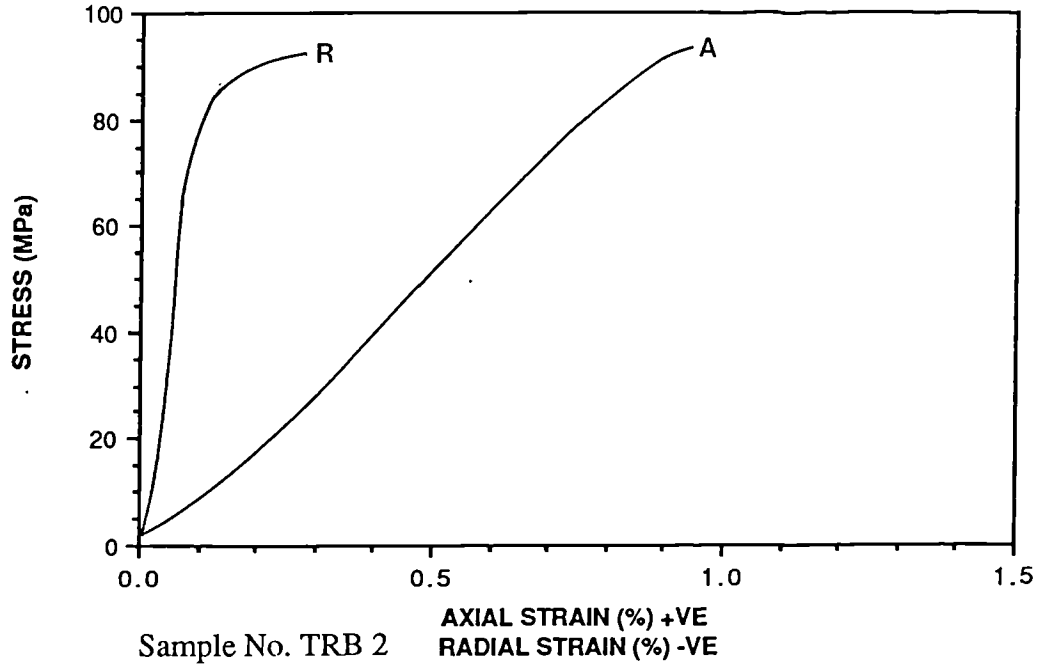

Sample No. TRB 2

w% = 0.00

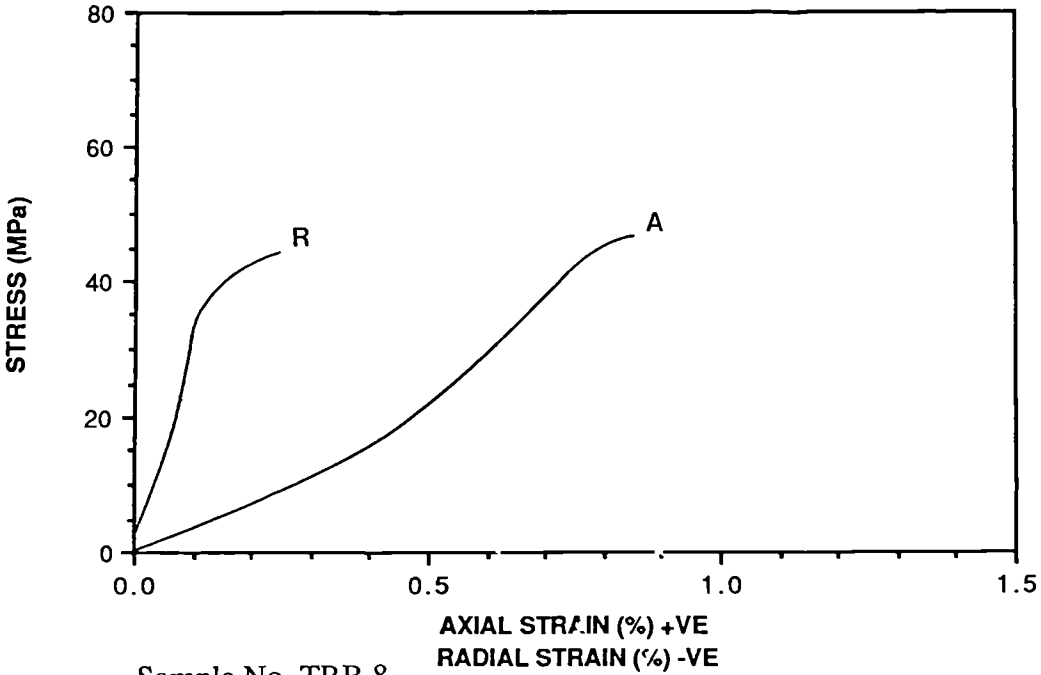

Sample No. TRB 8

w% = SAT.

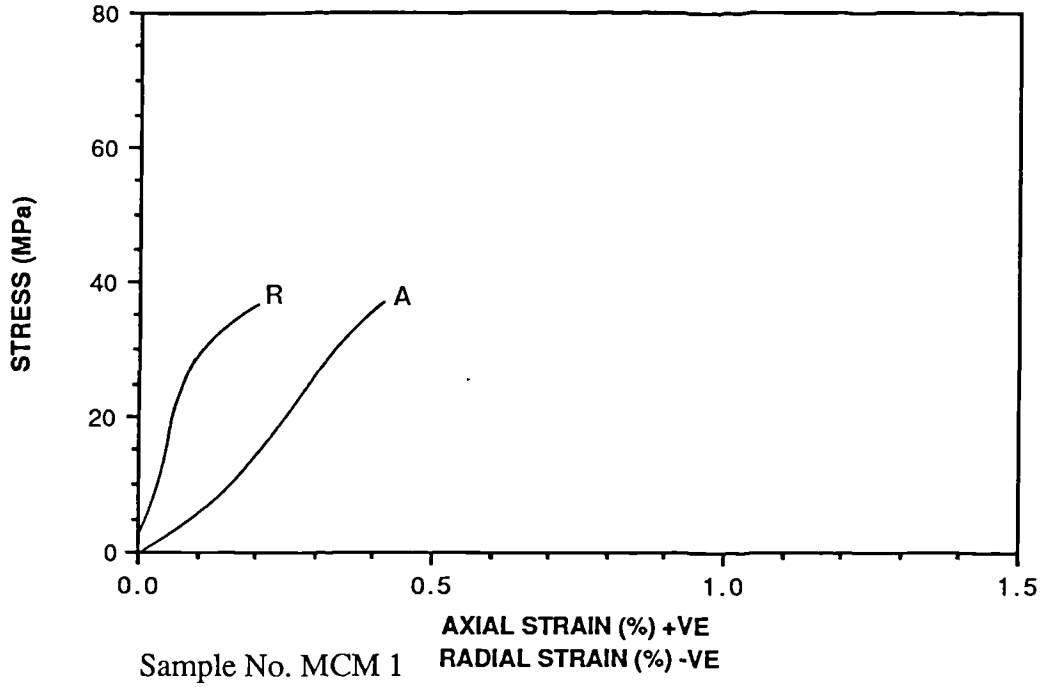

Sample No. MCM 1

w% = 0.00

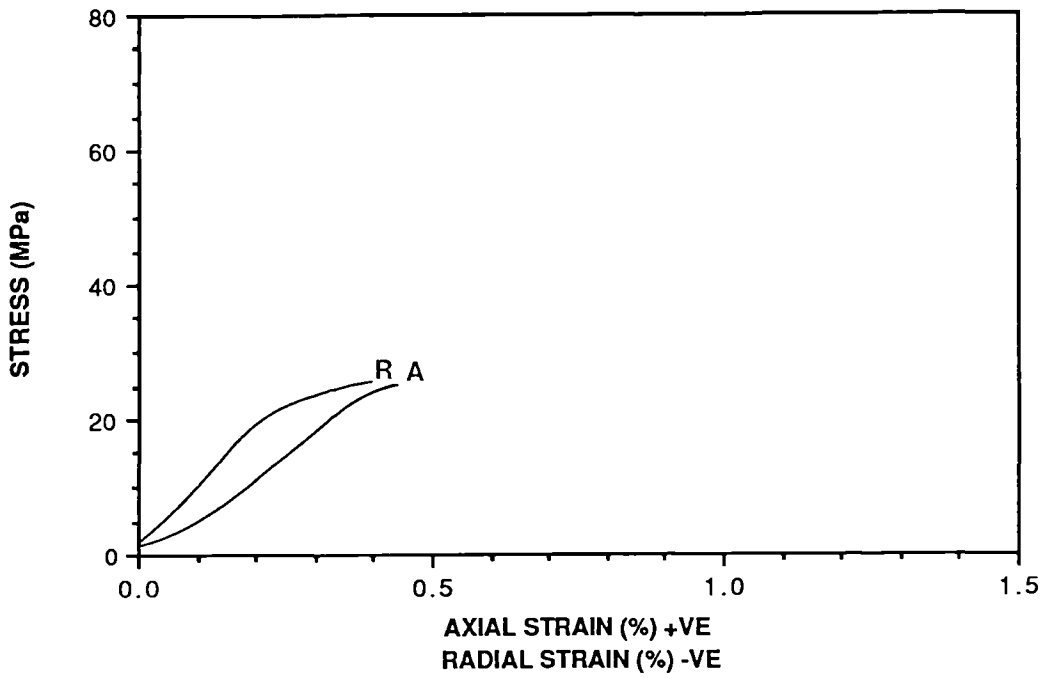

Sample No. MCM 5

w% = SAT.

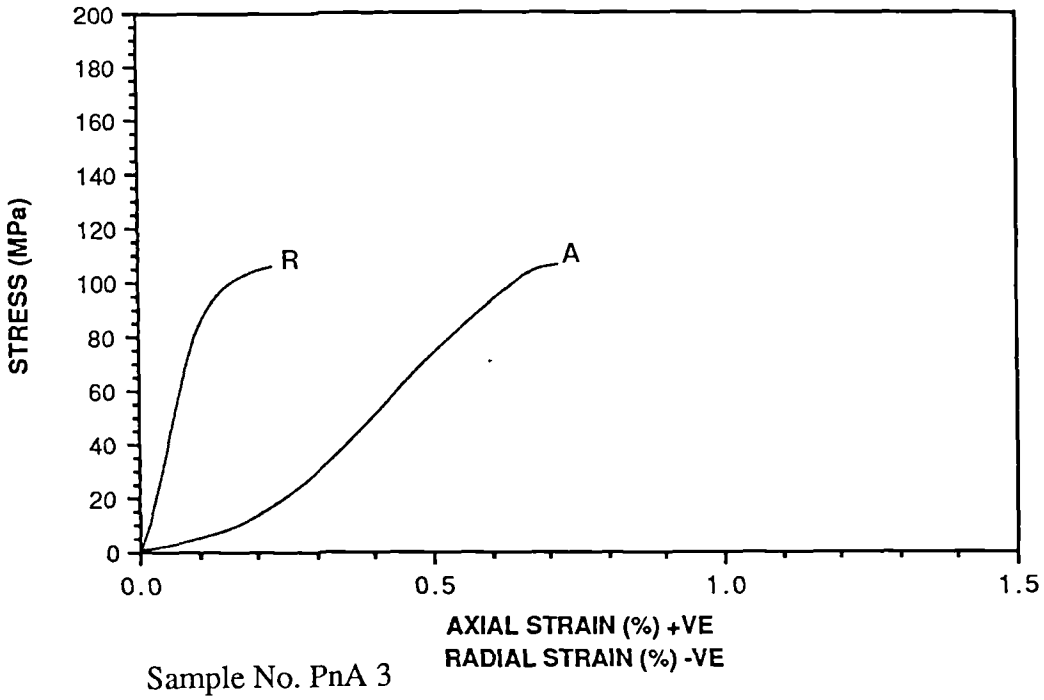

Sample No. PnA 3

w% = 0.00

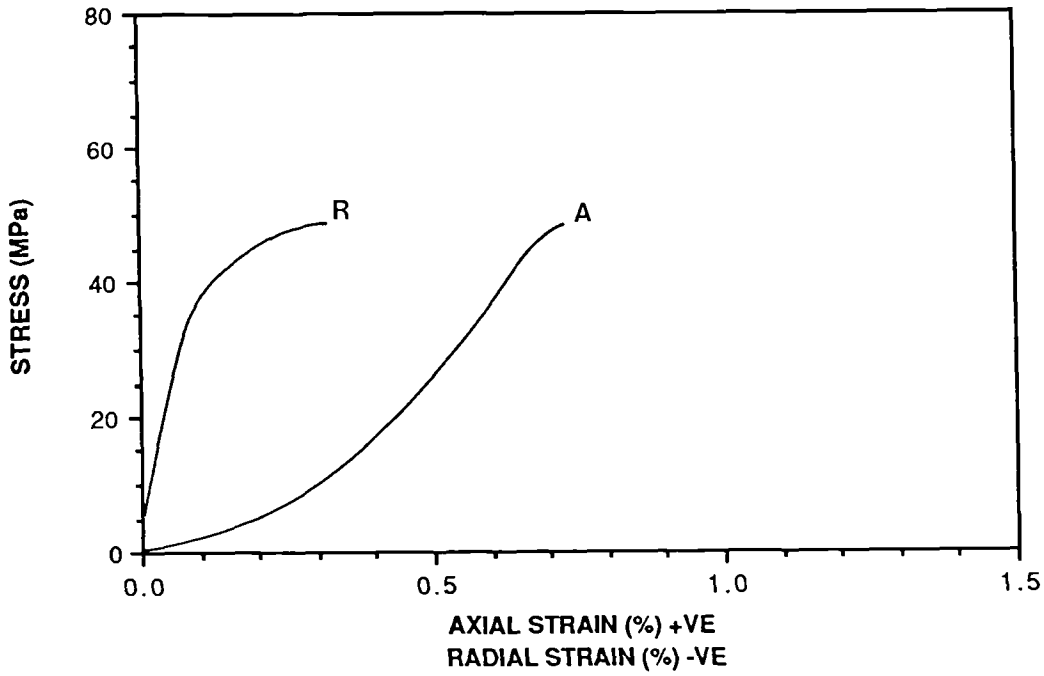

Sample No. PnA 9

w% = SAT.

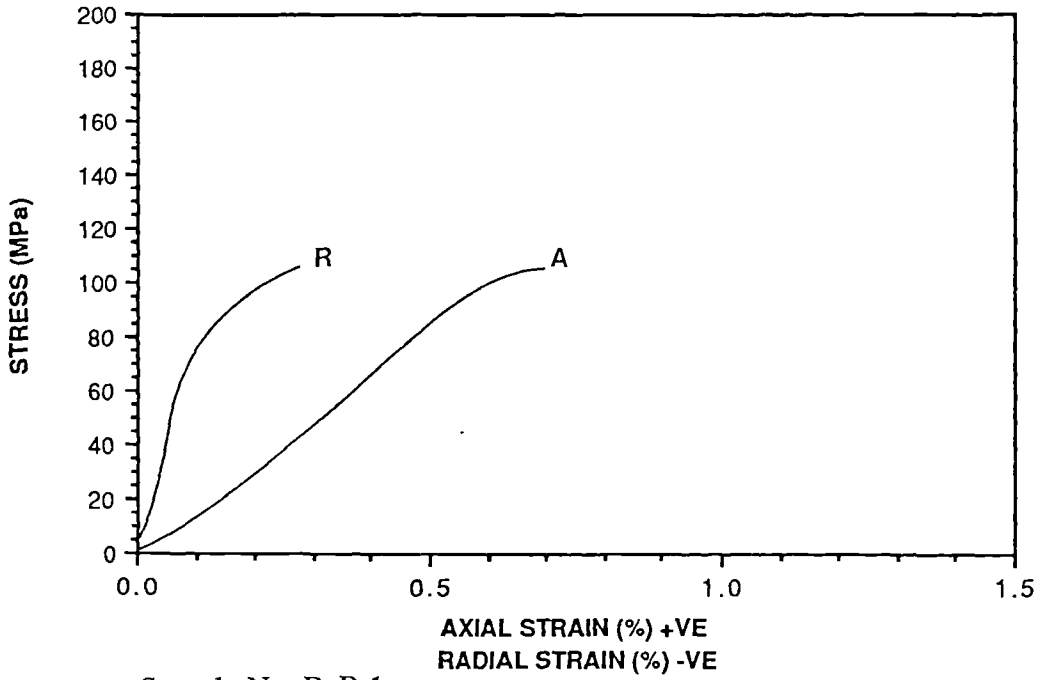

Sample No. PnB 1

w% = 0.00

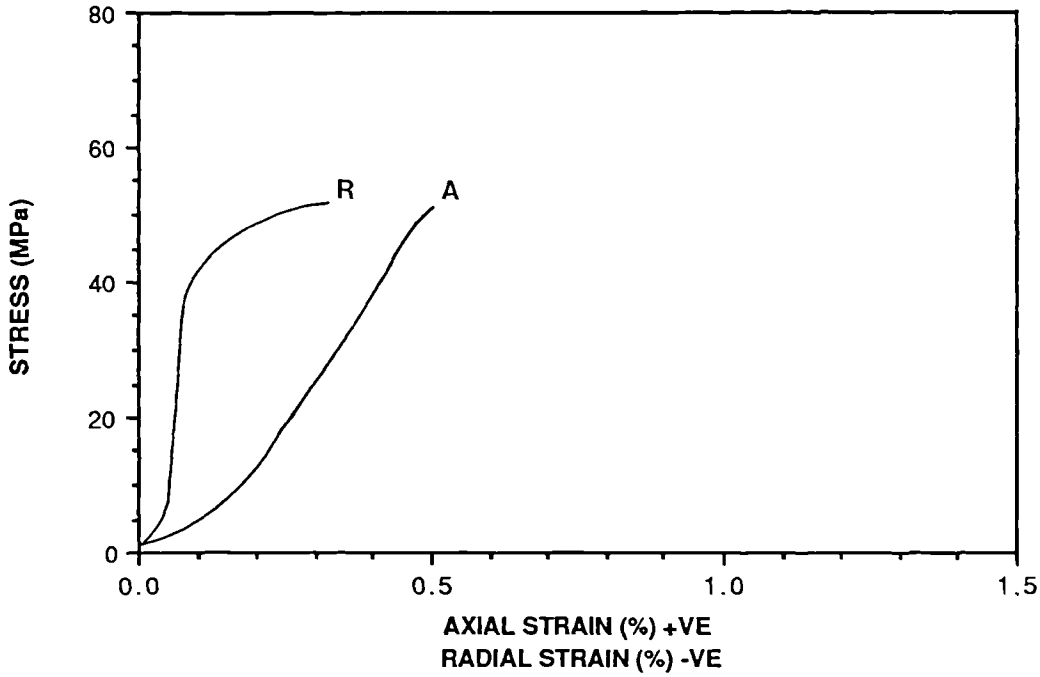

Sample No. PnB 8

w% = SAT.

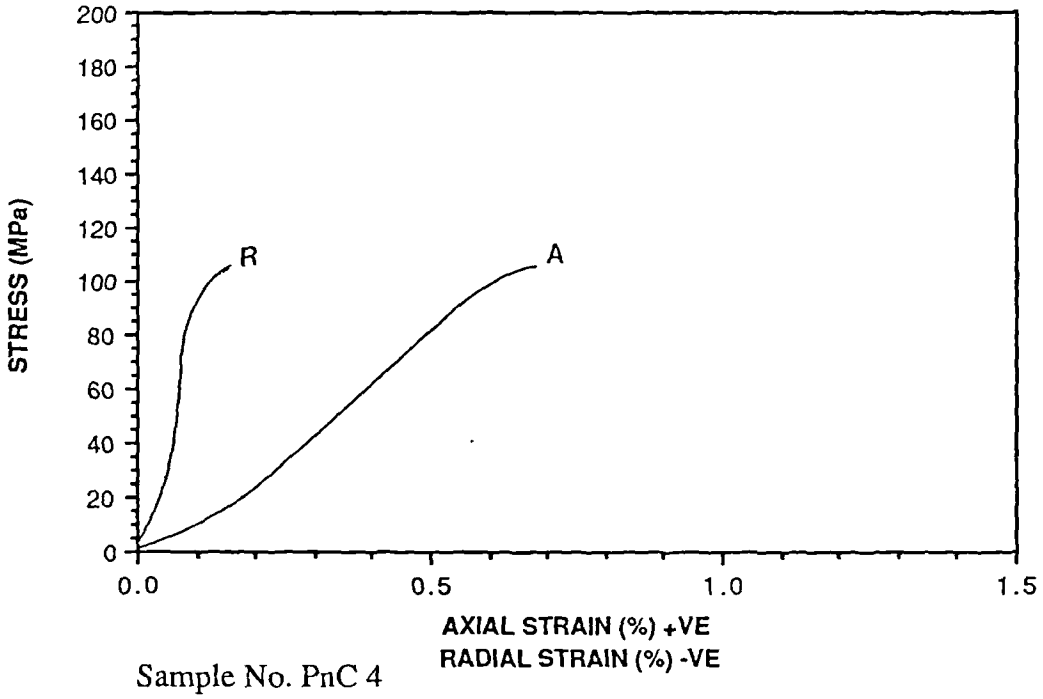

Sample No. PnC 4

w% = 0.00

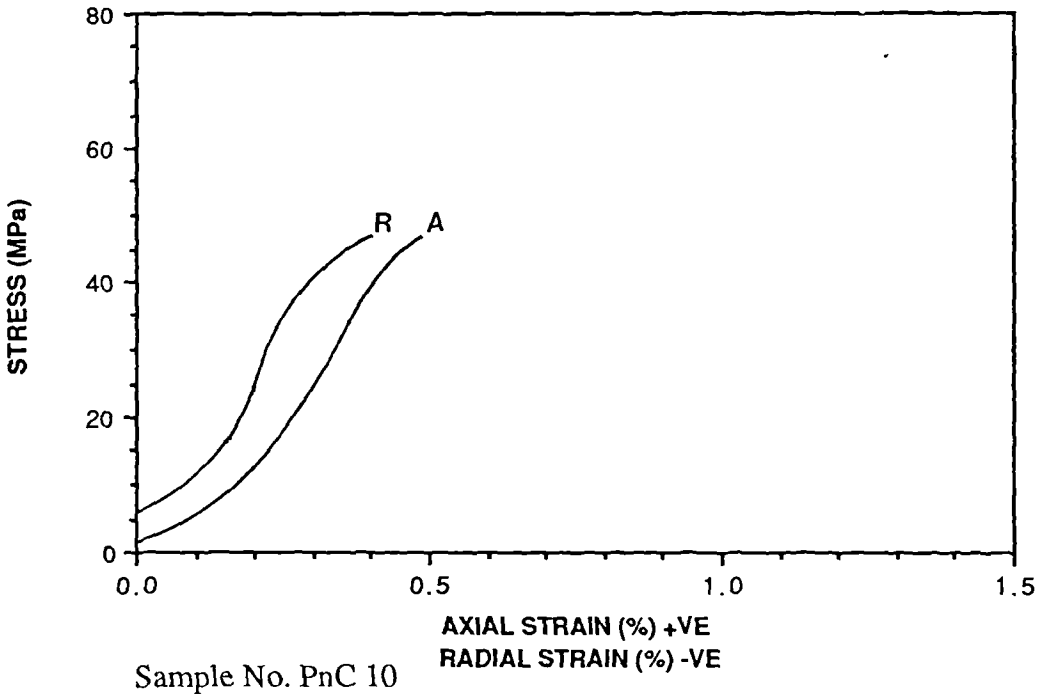

Sample No. PnC 10

w% = SAT.

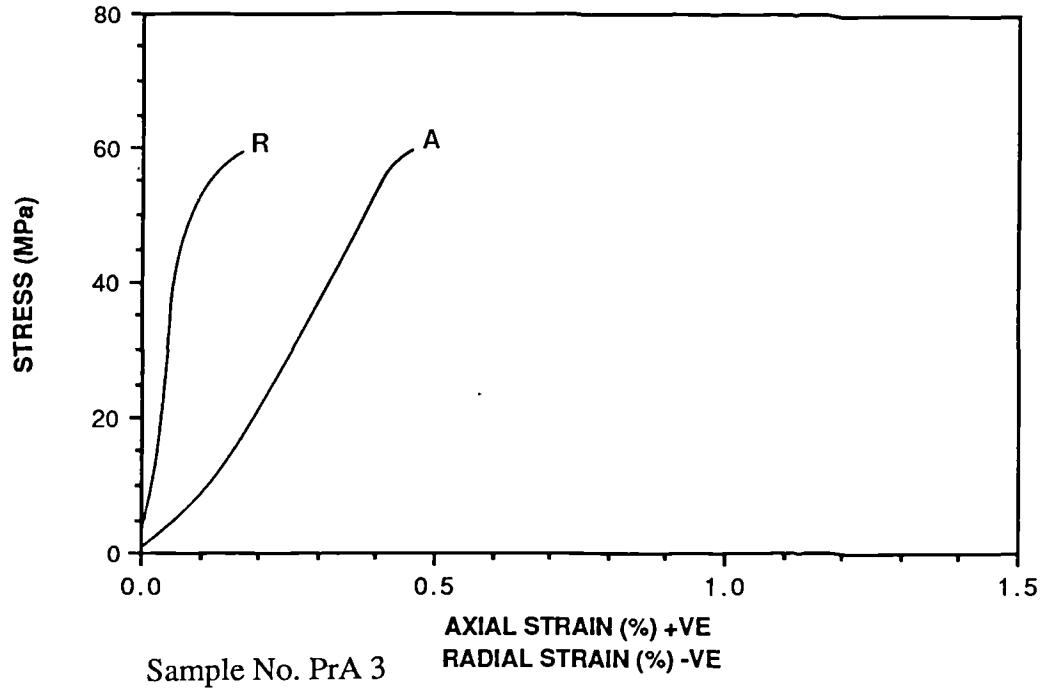

Sample No. PrA 3

w% = 0.00

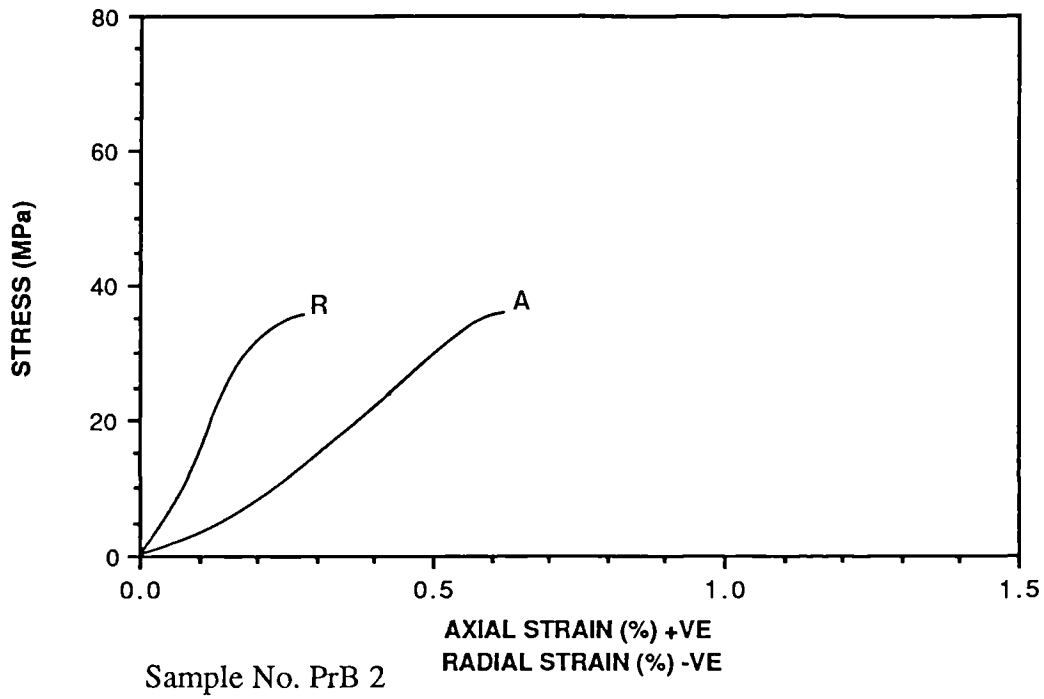

Sample No. PrB 2

w% = 0.00

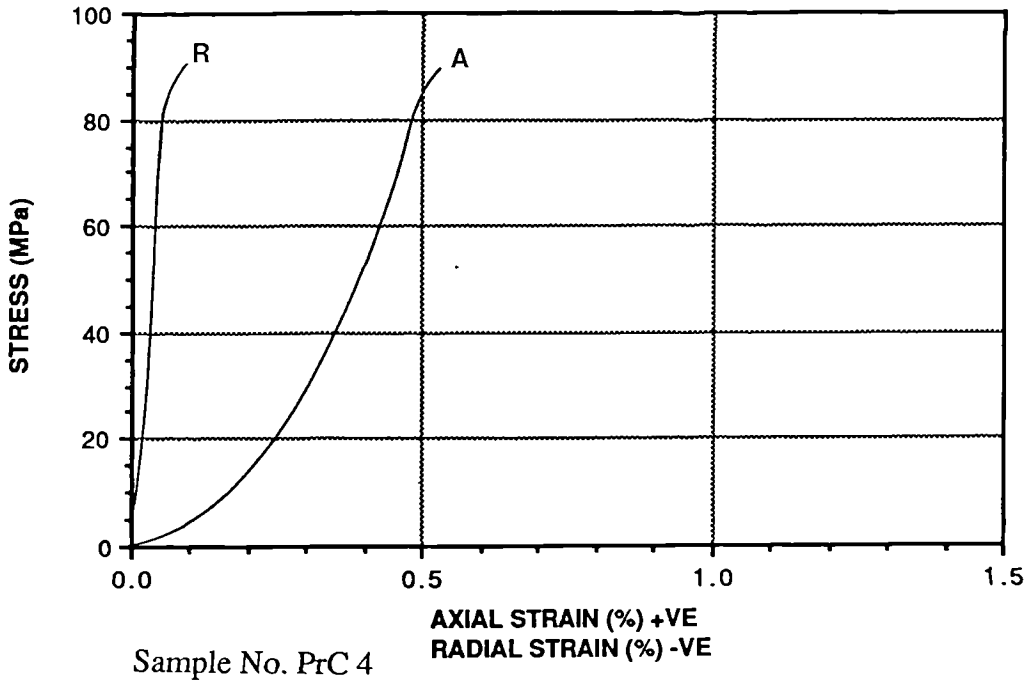

Sample No. PrC 4

w% = 0.00

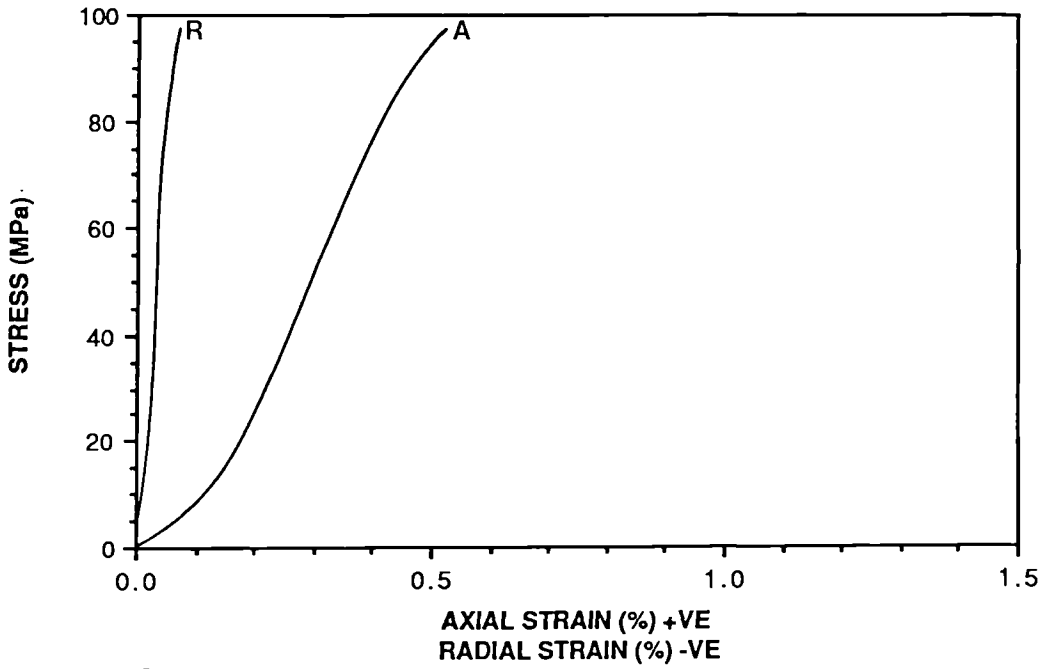

Sample No. PrD 3

w% = 0.00

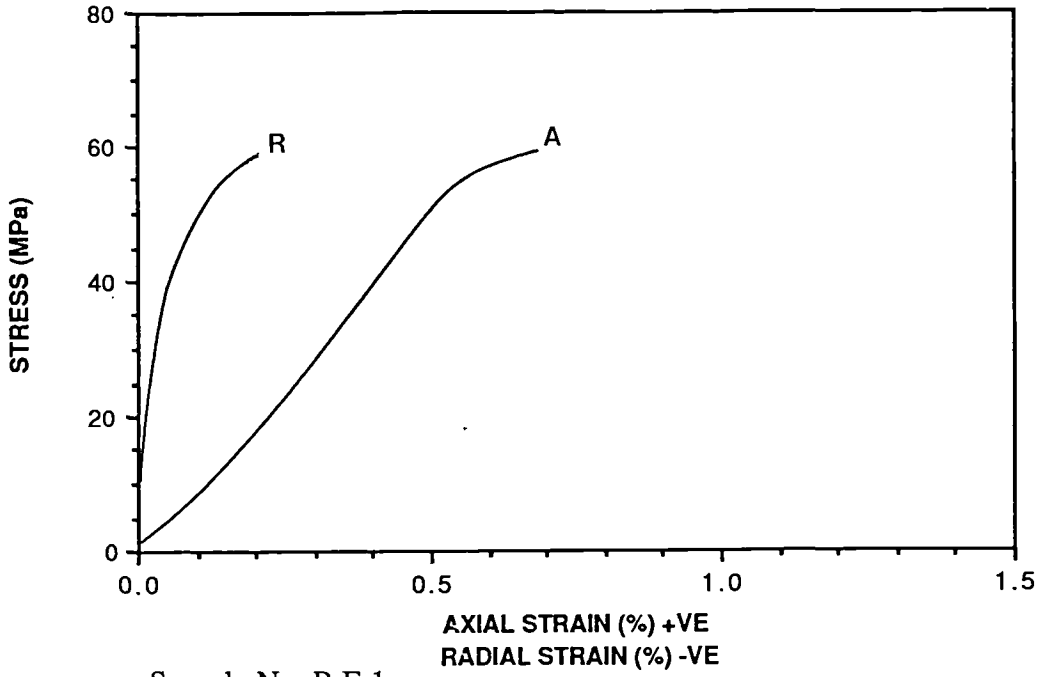

Sample No. PrE 1

w% = 0.00

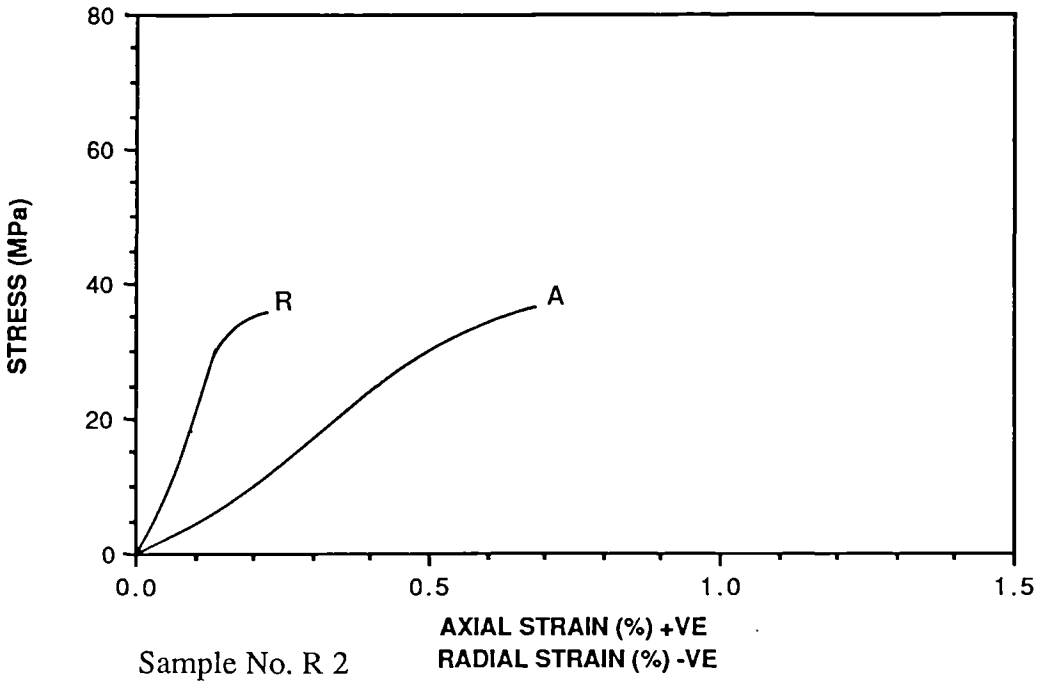

Sample No. R 2

w% = 0.00

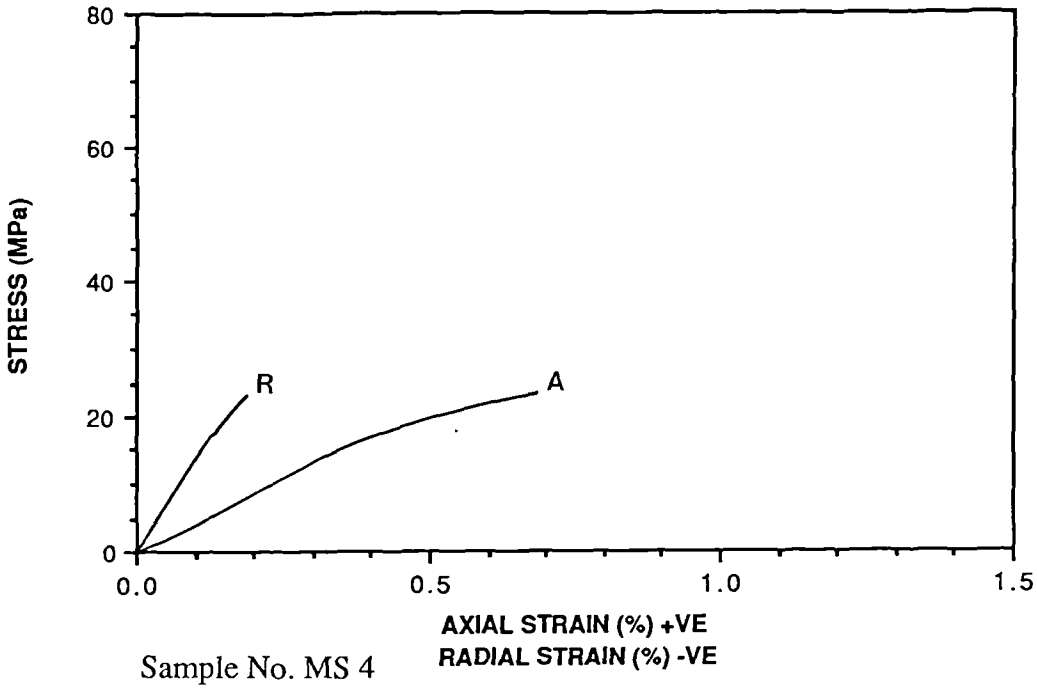

Sample No. MS 4

w% = 0.00

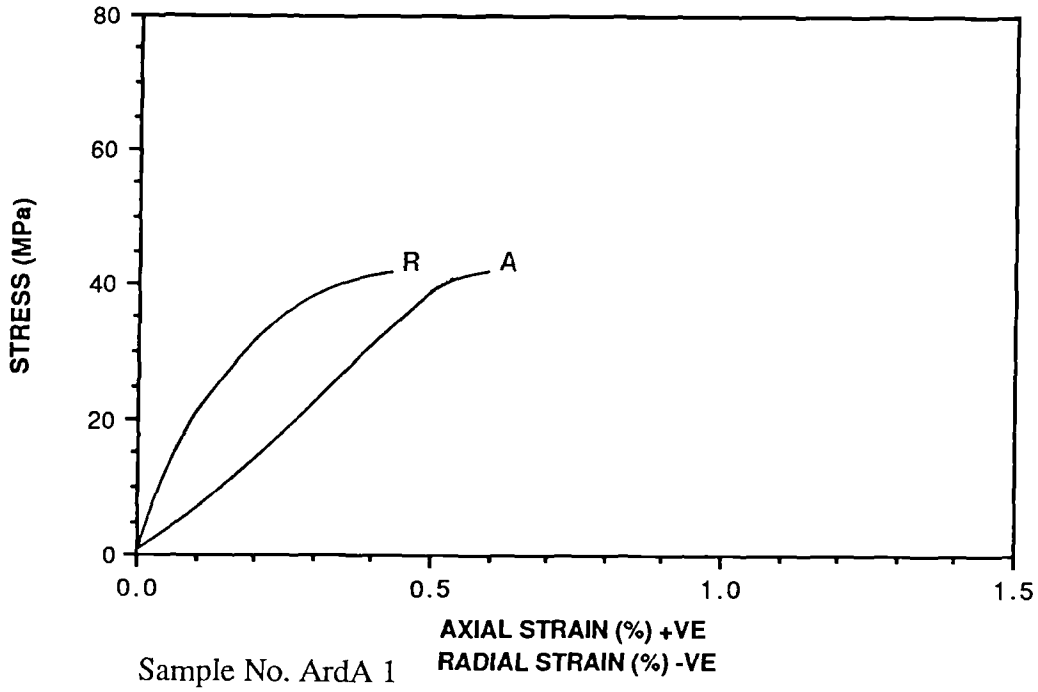

Sample No. ArdA 1

w% = 0.00

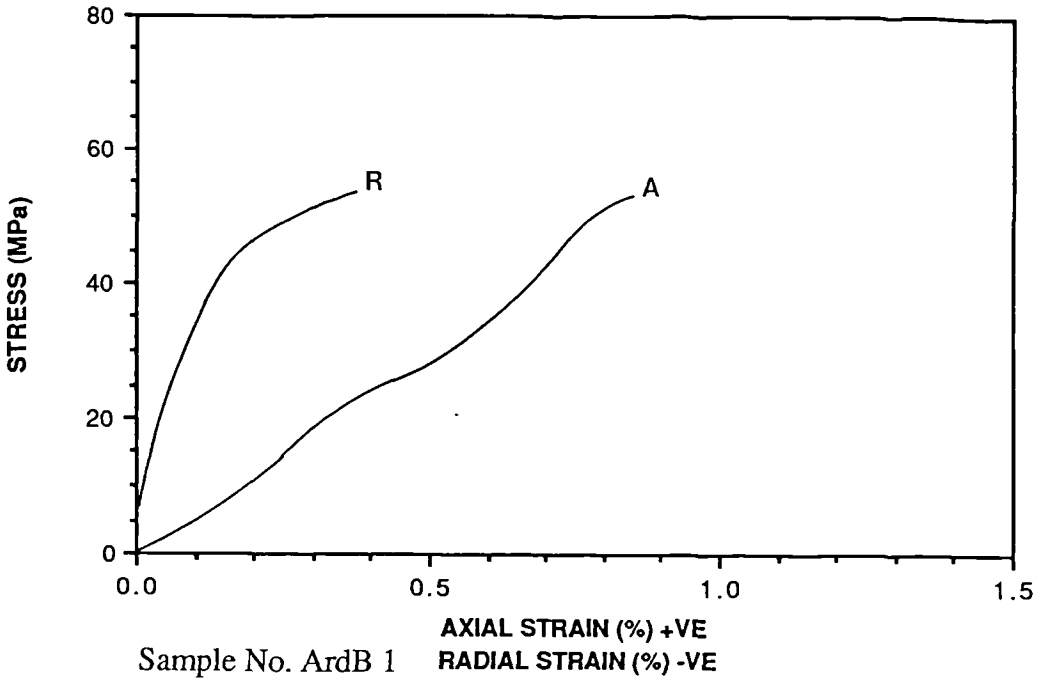

Sample No. ArdB 1

w% = 0.00

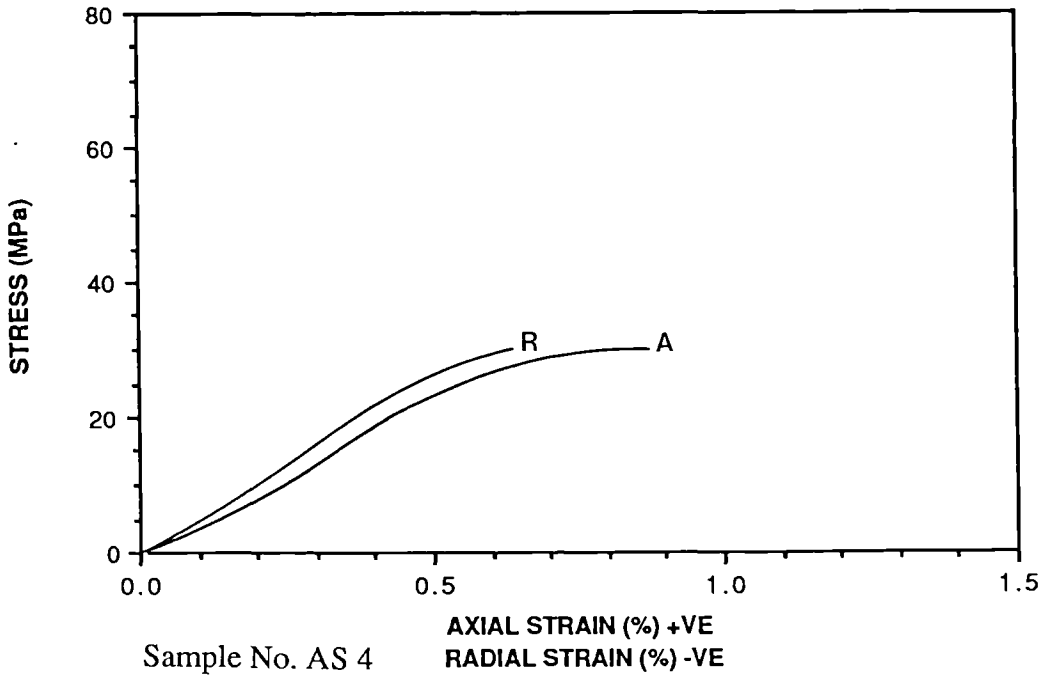

Sample No. AS 4

w% = 0.00

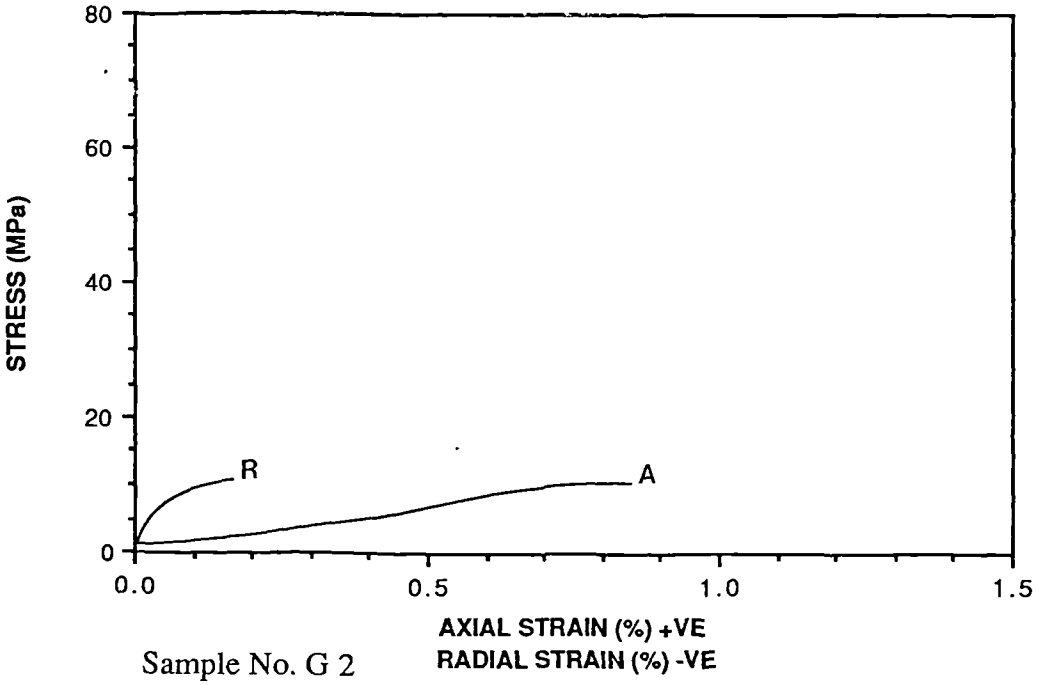

Sample No. G 2

w% = 0.00

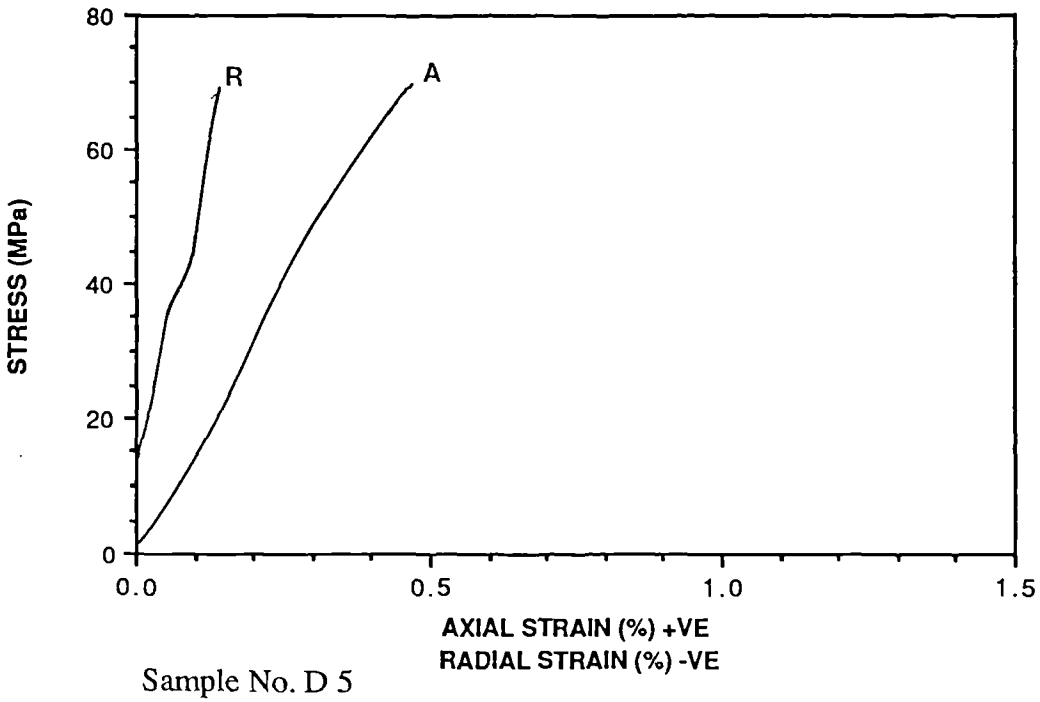

Sample No. D 5

w% = 0.00